3.01 Basic Aspects of Membrane Reactors

J Caro, Leibniz Universität Hannover, Hanover, Germany

3.01.1	**Introduction**	2
3.01.2	**Conversion Enhancement in Extractor-Type Membrane Reactors Operating Thermodynamically under Equilibrium-Controlled Reaction Conditions**	3
3.01.2.1	Boosting of Alkane Dehydrogenation by Hydrogen Removal	3
3.01.2.2	Increasing the Esterification Yield by Water Removal	4
3.01.2.3	Water removal in Knoevenagel condensations in micro reactors	5
3.01.2.4	Hydrogen Production by Water Splitting Using Oxygen-Selective Perovskite Membranes	6
3.01.3	**Selectivity Enhancement in Distributor/Contactor-Type Membrane Reactors Operating under Reaction Kinetics Conditions**	8
3.01.3.1	Partial Oxidation of Hydrocarbons by Nonselective Supply of Oxygen through a Porous Membrane as Reactor Wall	8
3.01.3.2	POM to Synthesis Gas in a Perovskite Hollow-Fiber Membrane Reactor	8
3.01.3.3	Hydrocarbon Partial Oxidation with Selective Oxygen Supply	12
3.01.3.4	*p*-Xylene Oxidation to Terephthalic Acid in a Reactor with a Bifunctional Membrane	14
3.01.3.5	Partial Hydrogenation of Cyclooctadiene to Cyclooctene in a Pore-through-Flow Membrane Reactor	14
3.01.4	**Removal of Oxygen as a Reaction Rate Inhibitor in the NO_x Decomposition in an Extractor-Type Membrane Reactor**	18
3.01.5	**Conclusions**	20
3.01.6	**Acknowledgments**	21
References		21

Glossary

Dense membrane Nonporous layers which can separate highly selective gases such as hydrogen due to atomic transport through Pd alloys or oxygen due ionic transport through oxygen vacancies of a perovskite oxide.

Extractor-type membrane reactor A permselective membrane allows product molecules to leave or educt molecules to enter selectively the reactor.

Ideal separation factor Ratio of the fluxes of the single gases through a membrane.

Membrane reactor Combining a chemical reaction with a selective membrane separation in one device following the concept of process intensification.

Mixture separation factor Ratio of the molar compositions of permeate and retentate, for gases usually determined by gas chromatography.

Molecular sieve membrane Nanoporous layers which can separate molecules due to their shape and size such as zeolite, carbon, or silica films.

Oxygen transporting perovskite membrane Highly selective oxygen separator based on the effect that oxygen is transported as oxygen ion via oxygen ion vacancies in the crystal framework.

Perovskite membrane hollow fiber Fiber obtained by spinning or extrusion of a mixture of a perovskite powder and an organic spinning solvent followed by a subsequent sintering.

Supported membrane A thin membrane layer which is alone mechanically not stable is supported by a mechanically strong macroporous ceramic or metal substrate.

3.01.1 Introduction

The conversion and selectivity of a chemical reaction can be improved when the reaction is performed in a membrane reactor. A membrane reactor is a bifunctional apparatus combining a membrane-based separation with a (catalytic) chemical reaction in one device [1]. There are some recent reviews showing the benefits of a membrane-supported chemical reaction [2–14]. Membrane-supported operations and membrane reactors will play an important role in process intensification; for example, membrane contactors are reactor concepts with a high feasibility [15–17]. Many chemical processes of industrial importance, classically using fixed-, fluidized-, or trickle-bed reactors, involve the combination of high temperature and chemically harsh environment that favor inorganic membranes [14]. However, as yet no inorganic membranes are used in large-scale industrial gas separation and no high-temperature chemical membrane reactor is in operation. On the contrary, in biotechnology, a beginning of the exploitation of both organic and inorganic membrane reactor technology in low-temperature applications can be stated [18–19].

There are numerous concepts to classify membrane reactors following, for example, the reactor design such as extractors, distributors, or contactors, dividing the membrane into inorganic and organic ones or porous and dense ones, using the reaction types such as oxidations, hydrogenations, isomerizations, and esterifications, defining inert or catalytic membrane reactors, or taking as classification principle the position of a catalyst in/near/before/behind a membrane. Different to these sophisticated concepts, in this chapter, a simple classification of membrane reactors into only two groups is used (as shown in **Table 1**):

1. *Conversion enhancement in extractor-type membrane reactors operating thermodynamically near/at reaction equilibrium.* To overcome the equilibrium restriction, the reaction must be sufficiently fast compared to the mass transport through the membrane (kinetic compatibility). A special advantage can be that the removal of one of the products provides an integrated product purification, thus decreasing the number of process units. Besides, selectivity improvements can be found by selectively removing reaction rate inhibitors [20].
2. *Selectivity enhancement in distributor/contactor-type membrane reactors operating under reaction kinetics-controlled conditions.* The desired product is

Table 1 Classification of membrane reactors used in this chapter

Thermodynamically controlled reactions	*Kinetically controlled reactions*
$\Delta_R G^0$ near zero	$\Delta_R G^0$ very negative
$\Delta_R G^0 = -RT \ln K \rightarrow K \approx 1$	$\Delta_R G^0 = -RT \ln K \rightarrow K >> 1$
$A + B \leftrightarrows C + D$	$A + B \rightarrow C + D$
Extractor type membrane reactor Conversion enhancement: 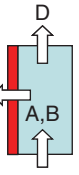 Dehydrogenation Esterification Steam reforming Knoevenagel condensation Water splitting	*Distributor/contactor type membrane reactor* Selectivity enhancement: 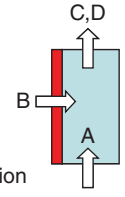 Hydrocarbon oxidation p-Xylene oxidation Methane to synthesis gas Partial hydrogenation

usually an intermediate in a consecutive reaction, or is one of the products in a system of parallel reactions. One should note that in the case of a distributed feed along the reactor, the flow rate downstream usually increases and the residence time at the catalytic sites will be reduced.

Because of the worldwide intense research and development (R&D) on membrane reactors and the corresponding large number of publications and patents, only characteristic examples for the two principles are discussed and emphasis is given to recent literature after 2000. Further, the successful use of an extractor-type membrane reactor in the decomposition of NO_x into the elements N_2 and O_2 is described. Here, the product molecule oxygen acts as a reaction rate inhibitor, which can be *in situ* removed using an oxygen-transporting perovskite membrane.

3.01.2 Conversion Enhancement in Extractor-Type Membrane Reactors Operating Thermodynamically under Equilibrium-Controlled Reaction Conditions

3.01.2.1 Boosting of Alkane Dehydrogenation by Hydrogen Removal

There are numerous examples for the conversion enhancement of an alkane dehydrogenation using porous (zeolite and sol–gel metal oxide) or dense (metal and ceramic) hydrogen-selective membranes. The concept to increase the alkane conversion by selectively removing the hydrogen seems to be simple at first sight; however, there can be a number of implications, such as coking, hydrogenolysis, and cracking [2], in the usual tubular membrane reactors for dehydrogenation (**Figure 1**). Further, if pore membranes are used and a light sweep gas such as He is applied to reduce the hydrogen partial pressure on the permeate side, the crossover of the sweep gas by counter-diffusion from the sweep to the feed side of the membrane must be avoided since the dilution of the alkane on the feed side by the sweep gas also increases the conversion of the alkane dehydrogenation.

On the other hand, it is not compulsory to use narrow-pore membranes with pores only accessible

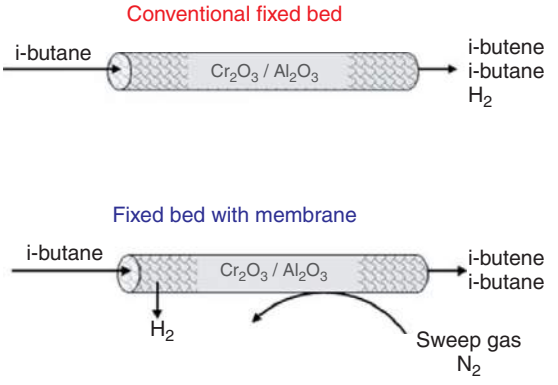

Figure 1 Typical experimental setup used for the membrane-supported dehydrogenation of alkanes using tubular hydrogen-selective membranes. Overlapping processes of dehydrogenation with cracking, coking, hydrogenolysis, and dilution of the feed by the sweep gas can falsify the results (see text).

for hydrogen. In addition, medium-pore zeolite membranes, the pore size of which allows the passage of both hydrogen and the hydrocarbons, can be used successfully in the membrane-supported dehydrogenation. As an example, a MFI zeolite membrane is used in the catalytic dehydrogenations of i-butane. Despite the fact that both H_2 and i-butane can pass the 0.55-nm pores due to their kinetic diameters (0.29 and 0.50 nm, respectively), the interplay of mixture adsorption and mixture diffusion results in a H_2 selectivity at high temperatures (H_2 flux $\approx 1\ m^3\ m^{-2}\ h^{-1}$ with a mixture separation factor α (H_2/i-butane ≈ 70 at 500 °C) and in an i-butane selectivity of the silicalite-1 membrane at low temperatures (i-butane flux $\approx 0.5\ m^3\ m^{-2}\ h^{-1}$ with a mixture separation factor α (i-butane/H_2 ≈ 15 at room temperature) [21]. In the conventional packed-bed experiment, the thermodynamic equilibrium conversion was obtained (**Table 2**). As hydrogen was removed selectively through the silicalite-1 membrane, the i-butane conversion increased by about 15% [21]. The removal of hydrogen leads to hydrogen-depleted conditions, which have two positive effects: (1) the conversion of i-butane is increased as expected due to a lower rate of the reverse reaction and (ii) the selectivity to i-butene is also increased because the hydrogenolysis is suppressed. Therefore, at the beginning of the reaction the i-butene yield in the membrane reactor is higher by about 1/3 than in the conventional packed-bed (**Table 2**). However, because of the hydrogen removal, coking is promoted and after approximately 2 h time on stream the olefin

Table 2 Increase of the i-butane conversion X(i-butane) above the equilibrium limit if hydrogen is removed through a silicalite-1 membrane

	X(i-butane) (%)	
Temperature (°C)	*Classical packed bed*	*Membrane supported packed bed*
510	35	39
540	43	60

Conditions: WHSV = 1 h^{-1}, Cr_2O_3/Al_2O_3-catalyst (Süd-Chemie), membrane area per unit mass of catalyst = 20 $cm^2\,g^{-1}$, data after 20 min time on stream. From Illgen, U., Schäfer, R., Noack, M., Kólsch, P., Kúhnle, A., Caro, J. *Catal. Commun.* **2001**, *2*, 339.

yield of the membrane reactor drops below that of the classical packed bed [22]. However, after an oxidative regeneration, the activity and selectivity are restored completely. Further experimental results for the silicalite-1-assisted dehydrogenation of i-butane can be found, for example, in References 22 and 23.

Future developments of membranes for hydrogen economy could trigger new activities in the membrane-supported dehydrogenation. Most promising seems to be the development of thin (about 1 μm) supported hydrogen-selective zeolite layers on a wide variety of carriers, for example, capillaries, fibers, tubes, or monoliths, such as the synthesis of thin zeolite layers on spun hollow fibers as support [24]. Since Si-rich zeolite membranes are hydrothermally more stable, Corma's full SiO_2 with LTA structure (ITQ 29) [25] would be a promising candidate for a hydrogen-selective membrane development and first attempts can be stated [26]. In addition, the synthesis of one-dimensional (1D) $AlPO_4$-5 membranes with a c-out-of-plane orientation of the parallel AFI pores by tertiary growth, is a pioneering concept for developing 1D membranes for hydrogen sieving [27]. Six-ring zeolite membranes, such as SOD (0.28-nm pore size), and 8-ring zeolite membranes, such as CHA (0.34 nm) and DDR (0.44 nm), will allow the effective separation of hydrogen.

3.01.2.2 Increasing the Esterification Yield by Water Removal

With the availability of water-selective membranes, which are stable in acidic surrounding and organic solvents at elevated temperatures, membrane-supported esterification becomes possible. There are different ways to increase the yield of an esterification. Most frequently, the cheapest educt is present in a surplus concentration or the low boiling ester is removed by reactive distillation. Another concept is to keep the concentration of the product water as low as possible by the use of adsorbents such as LTA zeolites or even by chemical reactions such as the hydrolysis of Al tri-isopropylate, thus consuming water. In the case of the low-temperature esterification of methanol or ethanol with short-chain monovalent hydrocarbon acids, hydrophilic organic polymer membranes can be used for the *in situ* dewatering in a membrane reactor. However, to support esterifications at higher temperatures, hydrophilic inorganic membranes with high stability against strong acids have to be used. ZSM-5-type zeolite membranes are suitable candidates to fulfill these demands. The benefits of a membrane-supported esterification were shown for the reaction of *n*-propanol with propionic acid using a ZSM-5 membrane of the Si/Al = 96. The ester yield can be increased from 52% to 92% by removal of water through the membrane (**Figure 2**). This ZSM-5 membrane is acid stable up to pH = 1; however – due to the low Al-contents – the hydrophilicity is low and, consequently, the resulting water flux of 72 $gm^{-2}\,h^{-1}\,bar^{-1}$ is still much too low for technical applications.

There is ongoing research on novel water selective membranes. A recently developed phillipsite (PHI) membrane with a mixture separation factor $\alpha > 3000$ for a 10 wt.% water/90 wt.% ethanol mixture with water fluxes $> 0.3\,kg\,m^{-2}\,h^{-1}$ looks promising [28]. In another application for the selective removal of water by pervaporation and vapor permeation during an esterification by using hydrophilic ZSM-5 and mordenite (MOR) membranes, almost complete conversion of about 100% was reached within 8 h in the esterification of lactic acid with ethanol [29]. Vapor permeation is also applicable to the *in situ* removal of water in the formation of unsaturated polyesters [29].

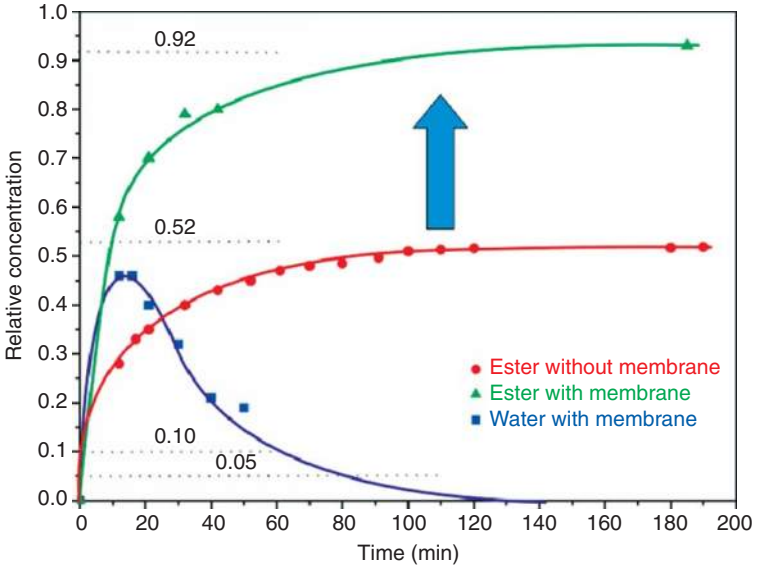

Figure 2 Conversion enhancement by water removal via a hydrophilic ZSM-5 membrane with a Si/Al = 96 in a membrane reactor for the esterification reaction of propionic acid + i-propanol ⇆ ester + water at 70 °C [36].

Conventionally, only hydrophilic membranes are used for dehydration of solvents. Despite its hydrophobic character, the all-silica DDR membrane turns out to be well suited to separate water from organic solvents by molecular sieving due to its small pore size [30]. Excellent performance in the dewatering of ethanol (flux of $2\,kg\,m^{-2}\,h^{-1}$ and $\alpha = 1500$) is observed and the membrane is also able to selectively remove water from methanol (flux of $5\,kg\,m^{-2}\,h^{-1}$ and $\alpha = 9$). Water could also be removed from methanol/ethanol/water mixtures, even at water feed concentrations below 1.5 wt.%. This water removal by DDR membranes is attributed to molecular sieving. Water easily passes through the DDR structure, while the organic molecules experience increasing diffusion hindrance with increasing size.

In the Fischer–Tropsch synthesis, the removal of the by-product water has several advantages on the reactor performance, such as reduced catalyst deactivation and lowered kinetic inhibition. Therefore, it was proposed to use hydrophilic membranes to increase reactor productivity [31]. The *in situ* water removal by a sol–gel silica-based membrane [32] and a ceramic-supported polymer membrane [33] in the presence of a CO/CO_2-shift active Fe-based catalyst resulted in increased total carbon conversion to hydrocarbons. The application of more hydrophilic zeolite membranes than silica or organic polymers with higher selectivity and higher water fluxes, such as LTA [34] and H-SOD [35], for the *in situ* water removal in Fischer–Tropsch synthesis looks promising.

3.01.2.3 Water removal in Knoevenagel condensations in micro reactors

The Knoevenagel condensation is a modification of the aldol condensation named after Emil Knoevenagel. It is a nucleophilic addition of an active hydrogen compound to a carbonyl group followed by a dehydration reaction in which a molecule of water is eliminated (hence condensation). The combination of the concepts of membrane reactor and process miniaturization provides new routes for chemical synthesis that promises to be more efficient, cleaner, and safer [37]. These smart, integrated, microchemical systems are expected to bring into realization a distributed, on-site, and on-demand production for high value-added products in the form of miniature factories and micro-pharmacies [38]. The incorporation of zeolites in microreactors as functional elements, including catalysts [39–41] and membranes, has been reported in previous works [42–44].

A recent example of fine chemical reaction carried out in a membrane microreactor is the Knoevenagel condensation reaction where the selective removal of the by-product water during the reaction led to a 25% improvement in the conversion [45]. The reaction between benzaldehyde and ethyl cyanoacetate to produce ethyl-2-cyano-3-phenylacrylate was

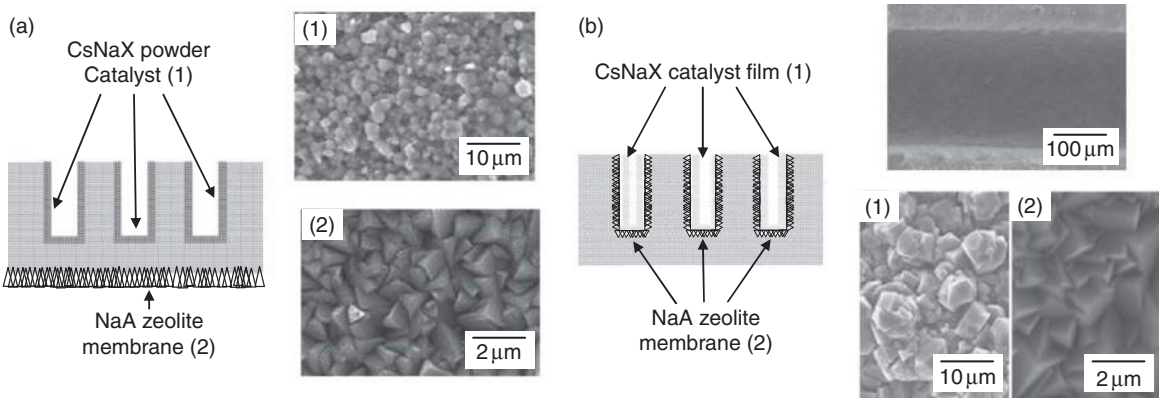

Figure 3 Membrane microreactor for Knoevenagel condensations with water removal [45, 46]: (a) The CsNaX catalyst (1) is deposited as powder on the microchannel wall and the 6-μm-thick NaA membrane (2) is grown on the back of the stainless steel plate. (b) The CsNaX catalyst film (1) is deposited directly on top of the 6.5-μm-thick NaA membrane (2) in the microchannel.

catalyzed by a CsNaX zeolite catalyst deposited on the microchannel and the water was selectively pervaporated across an LTA membrane (**Figure 3(a)**) [46]. All the water produced by the reaction was completely removed and the membrane was operating below its capacity [47]. This means that the performance of the membrane microreactor is limited mainly by the kinetics, that is to say that both thermodynamic and mass transfer constraints were removed. A fourfold increase in reaction conversion was obtained when the improved CsNaX–NH_2 catalyst was used instead of CsNaX [48]. Locating the separation membrane immediately next to the catalyst further improved the membrane microreactor performance (**Figure 3**(**b**)). The selective removal of the by-product water in the membrane microreactors also benefited other Knoevenagel condensation reactions, such as reactions between benzaldehyde and ethyl acetoacetate and diethyl malonate [49].

A multichannel membrane microreactor for the continuous selective oxidation of aniline by hydrogen peroxide on TS-1 nanoparticles was successfully demonstrated. The high surface-area-to-volume ratio that can be attained in the microreactor ($3000\,m^2\,m^{-3}$) facilitates the selective removal of the water by-product, which reduces also the catalyst deactivation during the reaction. An improvement in the product yield and selectivity toward azoxybenzene was also observed. Azobenzene was obtained as by-product and its formation was attributed to the homogeneous reaction of nitrosobenzene with aniline. Increasing temperature was beneficial for both yield and selectivity; however, beyond 67 °C, microreactor operation was ineffective due to bubble formation and hydrogen peroxide decomposition [50, 51].

3.01.2.4 Hydrogen Production by Water Splitting Using Oxygen-Selective Perovskite Membranes

Recently, it was shown that it is possible to produce significant amounts of hydrogen from water splitting at around 900 °C, using a novel $BaCo_xFe_yZr_zO_{3-\delta}$ (BCFZ) oxygen-permeable hollow-fiber membrane [52]. Although water dissociation into oxygen and hydrogen is conceptually simple, efficient hydrogen production from water remains difficult due to the small equilibrium constant of water dissociation $H_2O \rightleftarrows H_2+\frac{1}{2}O_2$. Because of the low $K_p \approx 2\times10^{-8}$ at 900 °C only tiny equilibrium concentrations of $P_{O2} \approx 4.6\times10^{-6}$ bar and $P_{H2} \approx 9.2\times10^{-6}$ bar will be found. However, even these small equilibrium concentrations are sufficient to extract oxygen through an oxygen-selective perovskite membrane.

Early studies demonstrated the possibility of hydrogen production from direct water decomposition using the mixed-conducting oxygen-selective membrane at extremely high temperatures of 1400–1800 °C. Balachandran *et al.* [53] fed hydrogen on the permeation side to consume the permeated oxygen. In this case, a high oxygen partial pressure gradient across the membrane was established, and a high hydrogen production rate of $6\,cm^3\,min^{-1}\,cm^{-2}$ at 900 °C was obtained. An even higher hydrogen production rate of $10\,cm^3\,min^{-1}\,cm^{-2}$ could be achieved by using Gd-doped CeO_2 as mixed-conducting membrane with an optimized microstructure [54]. However, hydrogen production by consuming the oxygen on the permeate side, using externally produced hydrogen, may represent a proof of principle, which is, of course, impractical. When methane is used to consume the

permeated oxygen by partial oxidation of methane (POM) according to $CH_4 + ½O_2 \rightarrow CO + 2H_2$, not only the oxygen permeation rate can be increased due to the higher oxygen partial pressure gradient across the membrane, but it is also possible to obtain synthesis gas (a mixture of carbon monoxide, CO, and hydrogen, H_2), which can be used to synthesize a wide variety of valuable hydrocarbons (diesel) or oxygenates (methanol), or which can be transformed at lower temperature as well into hydrogen by the water-gas shift reaction according to $CO + H_2O \rightarrow H_2 + CO_2$.

Figure 4 presents the concept of the simultaneous production of hydrogen and synthesis gas in a BCFZ perovskite hollow-fiber membrane reactor. At temperatures of 800–900 °C, water is sent to the steam/core side of the BCFZ hollow fiber and, at these temperatures, water starts to dissociate into hydrogen and oxygen. When the oxygen partial pressure on the core/steam side of the BCFZ hollow fiber is higher than that on the shell/methane side, oxygen permeates from the steam/core side to the methane/shell side, where oxygen is quickly consumed by the POM. Thus, oxygen and hydrogen become separated, and the water splitting can continue. Obviously, the hydrogen production rate directly depends on the rate of oxygen removal from the water dissociation system. As shown in **Figure 4**, a high hydrogen production rate of about 2.25 $cm^3\,min^{-1}\,cm^{-2}$ at 900 °C is obtained.

We can learn from **Figure 5** that the hydrogen production rate increases as the temperature rises from 800 to 950 °C and a hydrogen flux of 3.1 $cm^3\,min^{-1}\,cm^{-2}$ was obtained at 950 °C [52]. When the temperature is increased, the equilibrium constant of the endothermic water splitting will increase

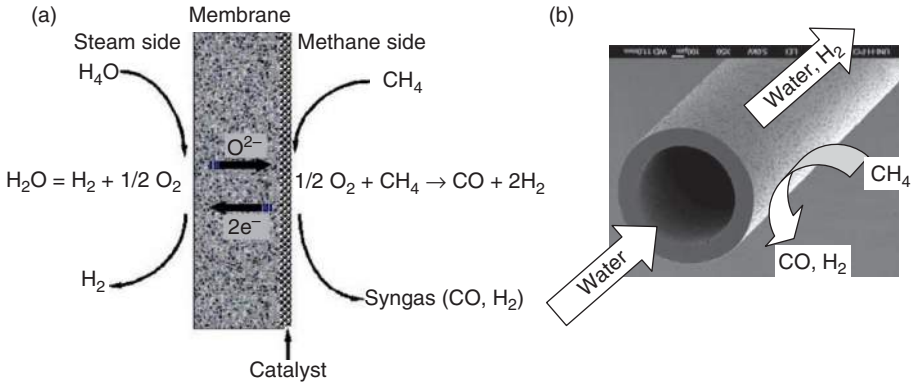

Figure 4 The concept of simultaneous production of hydrogen and synthesis gas by combining water splitting and partial oxidation of methane (POM): (a) reaction mechanism and (b) its realization in a perovskite oxygen-permeable hollow-fiber membrane.

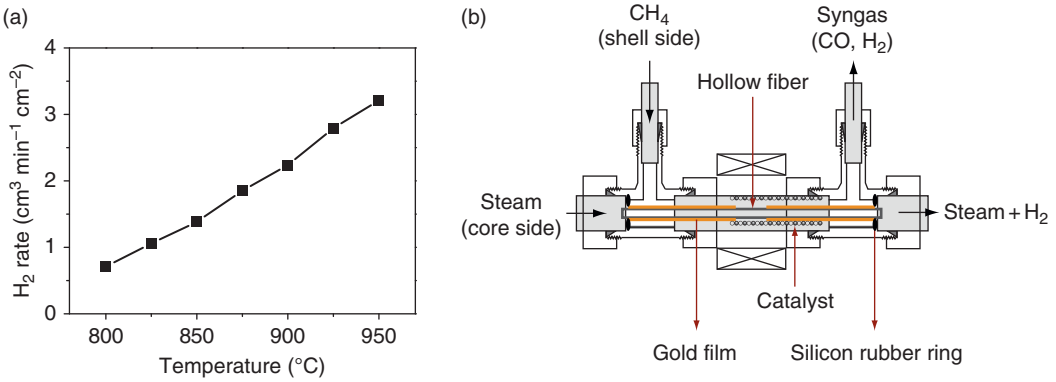

Figure 5 H_2 production by water splitting: (a) hydrogen generation on the core/steam side as a function of temperature [52]; and (b) the experimental setup. Core/steam side: $F_{H2O} = 30\ cm^3\,min^{-1}$ and $F_{He} = 10\ cm^3\,min^{-1}$. Shell/methane side: 50 $cm^3\,min^{-1}$ ($F_{He} = 45\ cm^3\,min^{-1}$, $F_{Ne} = 3\ cm^3\,min^{-1}$, and $F_{CH4} = 2\ cm^3\,min^{-1}$). Amount of packed Ni/Al_2O_3 catalyst: 0.8 g. Effective membrane area: 0.89 cm^2.

according to the van't Hoff equation. Therefore, the equilibrium is shifted toward the water dissociation and more hydrogen can be produced. Moreover, with increasing temperature, both the rate of the POM and the permeability of the BCFZ hollow-fiber membrane will increase. So, the hydrogen production rate becomes higher with rising temperature.

In fact, not only hydrogen is produced as retentate on the steam/core side of the BCFZ hollow-fiber membrane after water condensation, but also synthesis gas (CO and H_2) can be simultaneously produced on the methane/shell side. The exit gas of the methane/shell side mainly consists of H_2, CO, and small amounts of CO_2, H_2O, and unreacted methane. According to previous studies [79, 81], the so-called POM process using a Ni-based catalyst is first a total oxidation followed by steam and CO_2 reforming. However, the products of total oxidation (CO_2 and H_2O) can be transformed with a fine-tuned amount of unreacted methane by catalytic steam- and dry-reforming steps to synthesis gas.

3.01.3 Selectivity Enhancement in Distributor/Contactor-Type Membrane Reactors Operating under Reaction Kinetics Conditions

3.01.3.1 Partial Oxidation of Hydrocarbons by Nonselective Supply of Oxygen through a Porous Membrane as Reactor Wall

Pore membranes can be used for the nonselective feeding of air or oxygen through membranes, thus providing a low and uniform oxygen partial pressure along the axial dimension of a tube reactor [2, 9]. Because of the slight differences of the kinetic diameters of oxygen (0.344 nm) and nitrogen (0.364 nm), the air dosing is usually not combined with an oxygen enrichment. The concept is based on the different dependencies of the rates of partial and total oxidation (hydrogenation), respectively, on the concentration of oxygen (hydrogen). If the reaction rate is described by a power law, the exponent of the oxygen (hydrogen) concentration in the rate equation is higher for total oxidation (hydrogenation) than that for partial oxidation (hydrogenation). A low oxygen (hydrogen) partial pressure along the reactor should be beneficial, therefore, for a high oxygenate (hydrogenate) selectivity.

In the oxidative dehydrogenation of ethane (ODE), the selectivity and yield for ethylene were found to increase by ≈10% if air is dosed continuously along a porous tube reactor [16]. A similar improvement of the selectivity of 8–10% compared to a conventional packed bed reactor at equal conversions was found for the oxidative dehydrogenation of propane (ODP) [55].

In the case of the maleic acid (MA) anhydride synthesis by *n*-butane partial oxidation on vanadium phosphorous oxide (VPO), reactor simulations did forecast improved selectivities by oxygen distribution along the length axis of the tube reactor [56]; however, in the experiments, only a modest improvement of selectivity was found [57]. Due to a low oxygen/*n*-butane ratio at the reactor inlet, the vanadium catalyst was in a reduced state. With increasing conversion of *n*-butane, the oxygen/*n*-butane ratio increased and the V^{5+} species responsible for the MA selectivity were formed. However, by doping the VPO catalyst with Co or Mo, the active V^{5+} species could be stabilized even at the low oxygen/*n*-butane ratio of 0.6 [58].

As a last example for improved selectivities in partial oxidations when the oxygen is fed into the reactor through a porous wall, the direct oxidation of propane to acrolein is addressed. Acrolein selectivities which were two- to fourfold higher than those in the classical co-feed reactor were obtained at equal propane conversion (**Figure 6**) [59].

3.01.3.2 POM to Synthesis Gas in a Perovskite Hollow-Fiber Membrane Reactor

In Section 3.01.3.1, the nonselective dosing through the porous reactor wall was taken to control the partial pressure of a gaseous reactant over the reactor, whereas, here, the selective dosing of oxygen from air through a highly oxygen-selective perovskite membrane is discussed.

An attractive route for the utilization of natural gas is its conversion to synthesis gas ($CO + H_2$). Up to now, the strongly endothermic steam reforming (StR) is the dominant process for producing syngas from natural gas giving a H_2/CO ratio of 3, which is unsuitable for methanol or Fischer–Tropsch synthesis. Therefore, the slightly exothermic POM to syngas, which gives a H_2/CO ratio of 2, has drawn much attention. Although POM with air as the oxygen source is a potential alternative to StR, the downstream requirements cannot tolerate the presence of nitrogen. Therefore, pure oxygen is required, and a significant part of the investment costs associated with conventional POM to syngas

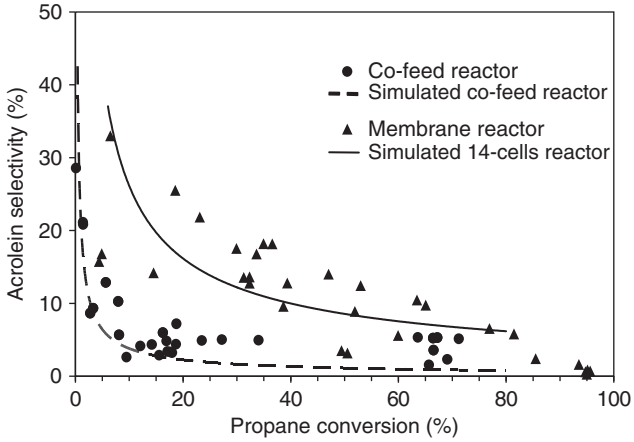

Figure 6 Direct partial oxidation of propane to acrolein in a conventional co-feed reactor and in a membrane reactor with oxygen dosage through a porous membrane [59]: experimental data and simulation of the acrolein selectivity as a function of the propane conversion. The bifunctional catalyst $Ag_{0.01}Bi_{0.85}V_{0.54}Mo_{0.45}O_4$ was deposited as layer direct on the porous wall of the reactor.

is those of the oxygen separation plant. In comparison with StR, the catalytic POM is estimated to offer cost reductions of about 30% [60]. Dense mixed oxygen-ion- and electron-conducting membranes are selectively permeable to oxygen at high temperatures between 800 and 900 °C. Thus, from air only the oxygen ions can be transported through the membrane to the reaction side, where it reacts with the methane to syngas. Local charge neutrality is maintained by the counter-current transport of electrons. No external electrodes and electricity are needed and cheap air can be used as oxygen source for POM; the pure oxygen separation and the POM reaction are combined in one reactor and hot spots, as in the conventional co-feed reactor, can be eliminated due to the gradual feeding of oxygen through the membrane.

So far, mainly relatively thick disk-shaped membranes with a limited membrane area were studied because disks can be easily fabricated by a conventional pressing method. Although a multiple planar stack can be adopted to enlarge the membrane area to an industry-relevant scale, many problems, such as the high-temperature sealing and the pressure resistance, have to be faced [61]. Tubular membranes with diameters in the centimeter range with thick walls were developed to reduce the engineering difficulties, especially the problems associated with the high-temperature sealing [62]. However, their small surface-area-to-volume ratio and their relatively thick walls lead to a low oxygen flux and make them unfavorable in practice. A membrane with a thin wall in a hollow-fiber geometry can solve the problems mentioned above. Compared to the disk and tubular membranes, hollow-fiber membranes possess much larger membrane area per unit volume for oxygen permeation [63, 64]. Furthermore, the resistance of the hollow-fiber membrane as a full material (i.e., nonsupported) to oxygen permeation is very much reduced due to the thin wall as it is the case for supported thin perovskite films. Other model solutions are multichannel monoliths, tube-and-plate assemblies, or single-hole tubes. Praxair has developed about 2-m-long single-hole tubes prepared by extrusion [65]. The so-called tube-and-plate concept of Air Products consists of 10 cm × 10 cm plates connected with a central support tube for the pure oxygen [66–68]. Hydro Oil and Energy developed a multichannel monolith for oxygen separation [69]. Whereas the industrial realization of a catalytic membrane reactor is still an aim that is difficult to realize, the implementation of a perovskite-based plant for the production of oxygen-enriched air or of air separation seems to be easier feasible. By Vente *et al.* [70] the membrane geometries of single-hole tubes, multichannel monoliths, and hollow fibers for air separation are evaluated.

Looking back, the breakthrough in the wide application of membranes in dialysis, natural gas and refinery gas treatment is closely linked to the development of organic hollow fibers spun from organic polymers. Therefore, there are increasing activities to prepare inorganic hollow fibers, including gas-tight perovskite hollow fibers for oxygen transport

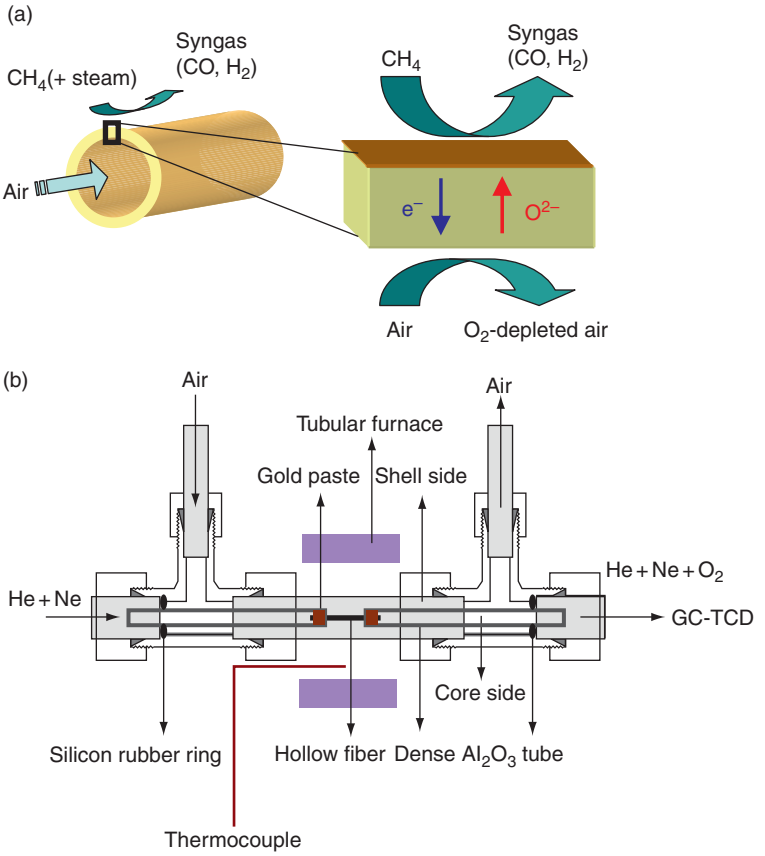

Figure 7 Partial oxidation of methane (POM) to synthesis gas: (a) scheme of the POM reaction with oxygen separated from air. Air is sent through the core side of the perovskite hollow-fiber membrane; oxygen is transported through the mixed ion and electron-conducting membrane to the shell side where the catalytic partial and total oxidations of methane followed by steam reforming and dry reforming take place [17]. (b) The one hollow-fiber catalytic membrane reactor using gold paste for the hot sealing of the fiber. Effective fiber length: 11.9 mm, outer diameter: 0.88 mm, inner diameter: 0.52 mm [17].

at elevated temperatures (e.g., References 71–74). Recently, from the modified perovskite composition BCFZ ($x+y+z=1.0$) [75], O_2-permeable hollow-fiber membranes, with high O_2 permeation flux and excellent thermal and mechanical properties, have been prepared [76–78]. **Figure 7**(**a**) schematically shows a hollow-fiber membrane reactor; **Figure 7**(**b**) demonstrates the experimental setup. Two ends of the hollow fiber were sealed by Au paste and placed in a gas-tight dense alumina tube. Therefore, such an Au-sealed short piece of a hollow-fiber membrane can be kept in the middle of the oven, thus ensuring real isothermal conditions.

In the POM to synthesis gas, the optimization of a laboratory-scale reactor as shown in **Figure 7** using BCFZ hollow-fiber membranes [76] gave CO selectivities of $S(CO)=96\%$ for methane conversions $X(CH_4)=95\%$ if the commercial Ni-based StR catalyst (Süd-Chemie) is placed around and behind the perovskite hollow fiber (seen from reactor inlet to the outlet direction) (**Figure 8**). The BCFZ hollow-fiber membrane reactor could be operated up to 300 h in the POM without failure [17]. Air, as the oxygen source, was passed through the tube side of the fiber; methane and the catalyst were outside. Knowing that the mechanism of the POM cannot be stopped at the intermediates CO and H_2, this reaction can be viewed as a total oxidation followed by the so-called dry and steam reforming of the total oxidation products CO_2 and H_2O by CH_4 [79]. Therefore, the above-mentioned StR catalyst was used. However, two problems had to be solved: (1) coke deposition occurs and results in a mechanical blocking of the reactor after about 50 h time on stream. By using methane/steam mixtures as the feed with $CH_4/H_2O \leq 1$, coke deposition could be completely avoided. (2) The BCFZ hollow fiber was destructed by $BaCO_3$ formation in the cold region of

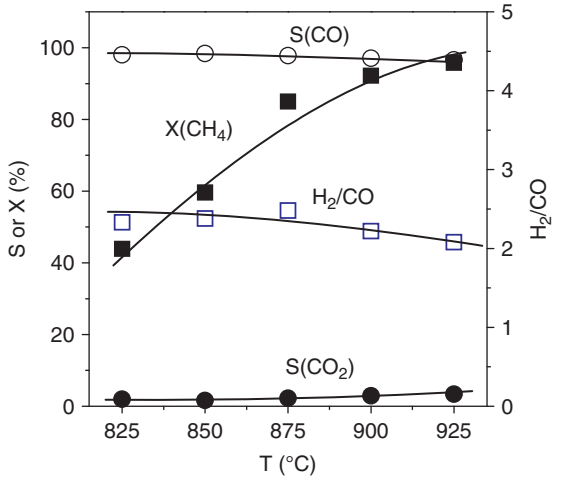

Figure 8 CH_4 conversion, CO and CO_2 selectivities, as well as H_2/CO ratio of the $BaCo_xFe_yZr_zO_{3-\delta}$ (BCFZ) perovskite hollow fiber used as membrane reactor in the partial oxidation of methane (POM) reaction as a function of temperature. To avoid coking, the feed contained 8.4 vol.% steam [17].

the reactor near to the reactor outlet at about 600 °C. Since CO_2 formation cannot be avoided completely, carbonate formation had to be stopped for thermodynamic reasons by having the whole perovskite fiber at 875 °C. This required a novel hot sealing technique for short pieces of a hollow fiber by using Au paste (**Figure 7**(**b**)). As a result, the laboratory-scale reactor could be operated several hundred hours in the POM (**Figure 9**).

Figure 10 represents the possible pathways in the POM showing an interplay of total and partial oxidations as well as reforming reactions as it was proposed by Kondratenko and Baerns [80]. We could obtain high methane conversions and high CO selectivities only, when some Ni-based StR catalyst was packed behind the oxygen permeation zone (zone 3 in **Figure 8**) where the reforming of the total oxidation products, CO_2 and H_2O, with unreacted CH_4 can take place. Consequently, the synthesis gas formation from methane in a mixed-conducting perovskite membrane reactor is called an oxidation-reforming process [79, 81].

Perovskite hollow-fiber membranes were successfully tested over several hundred hours in the POM to synthesis gas (typical product gas composition 65% H_2, 31% CO, 2.5% unreacted CH_4, and 1.5% CO_2) and the production of oxygen-enriched air (O_2 content between 30% and 45%). When arranged in bundles, hollow fibers can reach high membrane area per reactor/permeator volume. Economic goals, as membrane area per m^3 permeator volume of the order of $5000\,m^2\,m^{-3}$ at a price of about $1000\,€m^{-2}$ noninstalled area, are met by the perovskite hollow fibers. Based on our results, the amount of oxygen necessary for a methanol plant with a capacity of 2000 tons day^{-1} based on POM could be delivered by 4 600 000 hollow fibers. Assuming a fiber length of 1 m, this would lead – depending on the packing – to a cylindrical module of only 4-m diameter.

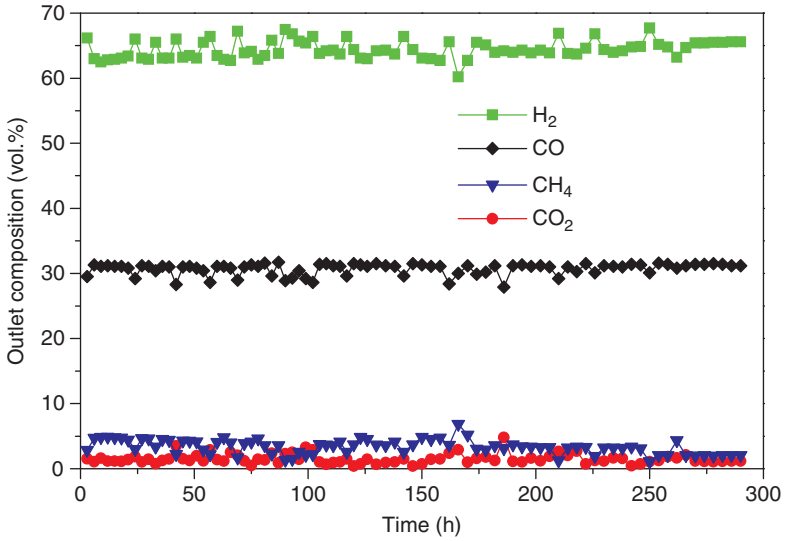

Figure 9 Off-gas composition in the partial oxidation of methane (POM) reaction. The gas composition 65% H_2, 31% CO, 2.5% CH_4, and 1.5% CO_2 corresponds to $X(CH_4) = 95\%$, $S(CO) = 96\%$, and $S(CO_2) = 4\%$, feed = CH_4 with 55 ml min^{-1} + H_2O with 5 ml min^{-1}, temperature = 875 °C; pressures on both sides of the $BaCo_xFe_yZr_zO_{3-\delta}$ (BCFZ) hollow-fiber membrane: 1 bar [17].

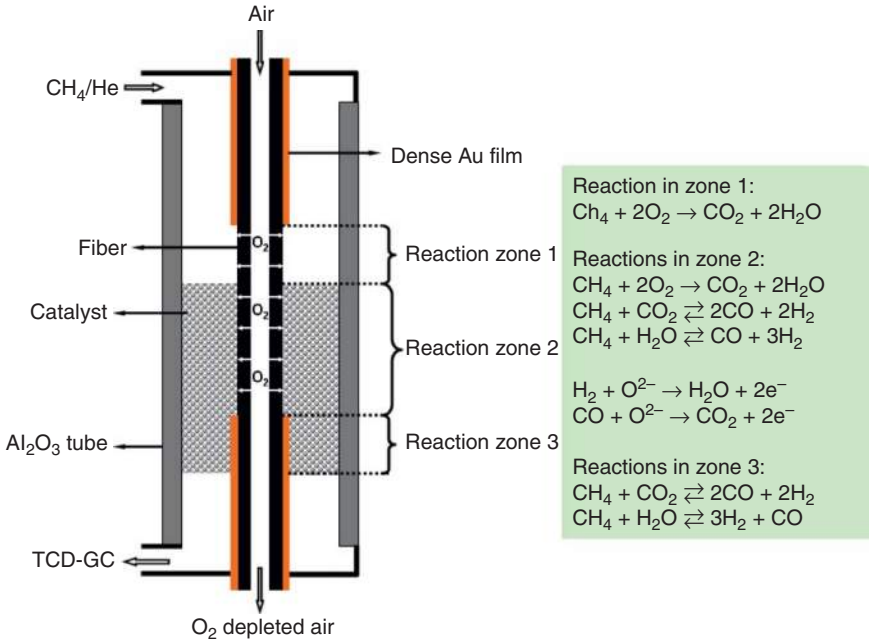

Figure 10 Reaction pathways in the catalytic perovskite hollow-fiber membrane reactor [81]. Note that the Ni catalyst can be in different redox states according to the surrounding gas phase: In zone 1, the catalyst is present mainly as $NiAl_2O_4$; in zone 2, as NiO/Al_2O_3; and in zone 3, as Ni/Al_2O_3.

It should be noted that mixed-oxygen-ion- and electron-conducting membranes in hollow-fiber geometry have been successfully tested not only for the syngas production but also for the preparation of oxygen-enriched air [82, 83], the oxi-dehydrogenation of hydrocarbons to the corresponding olefins [84], and the oxidative coupling of methane (OCM) to C_{2+} hydrocarbons. These processes are discussed in the following section.

3.01.3.3 Hydrocarbon Partial Oxidation with Selective Oxygen Supply

Oxidative ODE and ODP to the respective olefins is considered as a promising alternative to the (catalytic) thermal dehydrogenation, since there is no equilibrium constraint on the conversion. However, the yields attained so far in the oxidative dehydrogenations in conventional co-feed reactors are too low for an industrial application. However, during the past few years, remarkable progress could be observed in the classical co-feed ODE, especially by reaction engineering measures, leading to ethene yields up to 56% at 71% selectivity in autothermal oxidative dehydrogenation at short contact time of ~45 ms, using catalysts as igniters [85]. A high propene yield of 30% was obtained on K-Mo catalysts on SiO_2–TiO_2 supports using a diluted feed (92.5% inert, 5% propane, and 2.5% O_2) [86]. Propene yields of 22% are reported on intercalated Mo catalysts also for diluted feeds (73% inerts, 18% propane, and 9% O_2) [87]. A reasonable propene yield of 18% with an excellent space time yield of 12 kg propene $kg^{-1}\,h^{-1}$ was obtained for VO_x on MCM-48 [88].

First results on oxidative dehydrogenations using oxygen-transporting membranes showed superior yields compared to classical co-feed fixed-bed reactors. In ODE using planar and tubular oxygen-conducting membranes from $Ba_{0.5}Sr_{0.5}Co_{0.8}Fe_{0.2}O_{3-\delta}$ an ethene selectivity of 80% at 84% conversion was found at 800 °C [89, 90]. The same material reached 66% ethene yield at 807 °C, which could be further increased to 76% at 777 °C by incorporation of Pd clusters [91, 92]. An ethene yield of 56% per pass, together with an ethene selectivity of 80%, was achieved in a dense tubular ceramic membrane reactor made of $Bi_{1.5}Y_{0.3}SmO_3$ at 875 °C [93].

Compared to ODE, there are only a few papers on ODP in mixed ion–electron-conducting (MIEC) membrane reactors. Using a $Ba_{0.5}Sr_{0.5}Co_{0.8}Fe_{0.2}O_{3-\delta}$ perovskite and a diluted feed (90% inert and 10% propane), propene selectivities of 44.2% were found [94]; at low propane conversion (5%), the propene

selectivity was 52%. These results show that – in contrast to ODE – there is no improvement for ODP, as yet, in using oxygen-transporting membrane; the performances reported are still below those of classical co-feed fixed-bed reactors.

Because of the high temperatures in the perovskite membrane reactors for the ODE and ODP, an overlap of the desired oxidative dehydrogenation with the noncatalytic gas-phase dehydrogenation, including cracking, coking, and other high-temperature reactions, takes place [84]. The performance of MIEC membrane reactors depends on membrane geometry as well: for ODE using $Ba(Co,Fe,Zr)O_{3-\delta}$ membranes with a disk geometry almost 80% selectivity to ethene was observed, whereas hollow-fiber membranes reached only 40% (**Figure 11** and **Table 3**). This was explained by the different contact times in the two reactor configurations, that is, with hollow-fiber membrane, deep oxidation of ethene to CO and CO_2 could not be avoided. Once ethene is formed, it reacts again with lattice oxygen or gaseous oxygen to form CO_x and H_2O.

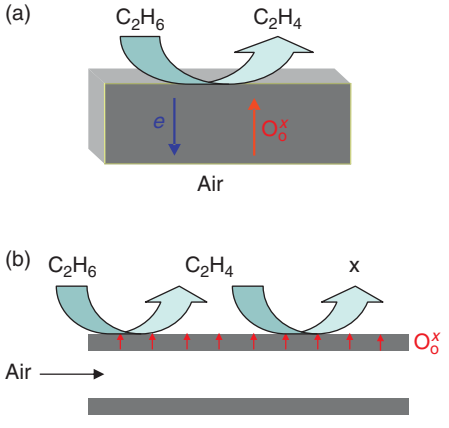

Figure 11 Comparison of the oxidative dehydrogenation of ethane (ODE) in the oxygen-transporting disk membrane reactor (a) and in the hollow-fiber membrane reactor (b) [84]. For the results see **Table 3**.

Similar to ODE and ODP, the OCM to C_2 hydrocarbons (ethane and ethene) is a widely studied topic in C_1 chemistry. Methane activation for OCM by lattice oxygen from an MIEC membrane looks promising as well (**Figure 12**). However, the high-temperature level where the oxygen-transporting membranes work implies that side reactions, such as thermal cracking and a variety of radical reactions, occur. Most probably, in oxygen-transporting membrane reactors (1) direct POM at the perovskite surface, (2) formation of radicals at the perovskite and/or catalyst surface, and (3) radical reactions both at the catalyst surface and in the gas phase occur simultaneously. Therefore, solid catalysts were proposed to support the OCM reaction. One of the highest C_2 yields, that is, 35% at a C_2 selectivity of 54%, was obtained in a tubular membrane reactor with a $Bi_{1.5}Y_{0.3}Sm_{0.2}O_{3-\delta}$ MIEC membrane [95]. However, the feed was strongly diluted (2% CH_4 in He): BaSrCoFe $O_{3-\delta}$ [96] and $BaCeGdO_{3-\delta}$ [97] of different chemical compositions. Typical results are C_2 selectivities of 70–90% for methane conversions below 10% and diluted feeds. If the CH_4 content in the feed is increased, the C_2 selectivity drops below 40%.

On the one hand, the direct supply of oxygen from air through an oxygen-transporting membrane for ODE, ODP, and OCM seems to be very promising. On the other hand, the high temperatures of 800–900 °C, usually applied to achieve sufficient high oxygen flux, spoil the selectivity of these reactions. There are recent attempts to develop oxygen-transporting materials with sufficient oxygen flux at low temperatures, such as 500–600 °C. As an example, **Figure 13** shows the oxygen fluxes through a BCFZ hollow-fiber perovskite membrane. **Figure 13(a)** shows the low-temperature oxygen fluxes through a BCFZ hollow-fiber membrane after 20 min time on stream. As **Figure 13(b)** shows, the oxygen fluxes decrease with permeation time but the initial oxygen-transport characteristics can be

Table 3 Oxidative dehydrogenation of ethane to ethylene according to $C_2H_6 + 1/2\ O_2 \rightarrow C_2H_4 + H_2O$ (see **Figure 11**)

			Product selectivity (%)			
Reactor types	*Membrane surface area (cm^2)*	*C_2H_6 conversion (%)*	*C_2H_4*	*CH_4*	*CO*	*CO_2*
Disk membrane	0.9	85.2	79.1	10.7	5.4	4.8
Hollow fiber	3.52	89.6	39.9	12.1	15.4	32.6

Comparison between a $Ba(Co,Fe,Zr)O_{3-\delta}$ perovskite disk and a hollow-fiber membrane reactors at 850 °C. Feed: 40 $ml_N\,min^{-1}$, ethane diluted with 90% He on the core side; air flow rate on the shell side: 300 $ml_N\,min^{-1}$) [84].

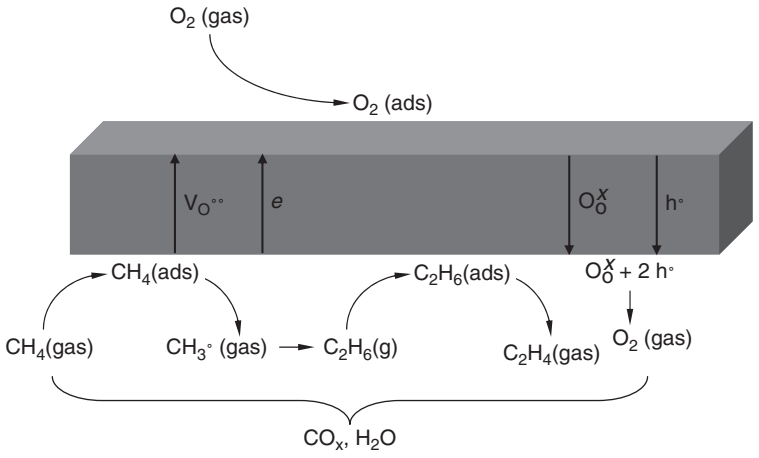

Figure 12 Possible mechanisms of the oxidative coupling of methane (OCM) in an oxygen-transporting membrane reactor [94].

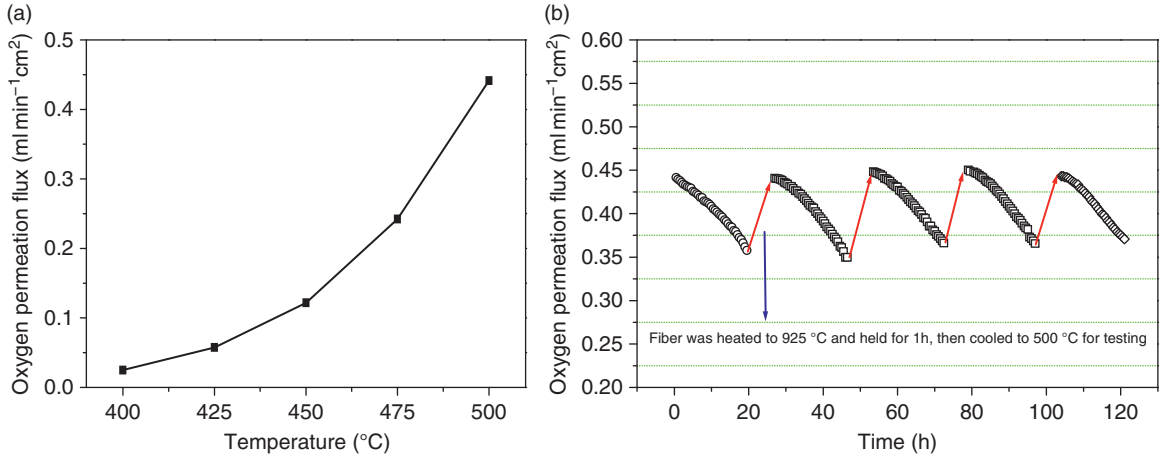

Figure 13 Low-temperature oxygen permeation (flow rate: 150 ml min^{-1} air on the shell side, 30 ml min^{-1} He on the core side; 0.43 cm^2 effective membrane area) [98]: (a) oxygen permeation flux through a $BaCo_xFe_yZr_zO_{3-\delta}$ (BCFZ) hollow-fiber membrane as a function of temperature, and (b) oxygen permeation fluxes through a BCFZ hollow-fiber membrane as a function of time at 500 °C (flow rate: 150 ml min^{-1} air on the shell side, 30 ml min^{-1} He on the core side; the effective area of hollow-fiber membrane: 0.43 cm^2).

restored after a 1-h treatment of the spent BCFZ hollow-fiber membranes at 925 °C in air [98].

3.01.3.4 *p*-Xylene Oxidation to Terephthalic Acid in a Reactor with a Bifunctional Membrane

There are ambitious attempts to combine membrane layers of different functionality. As a first example, for shape-selective oxidations, a thin Ti-doped silicalite-1 layer was crystallized on a BCFZ oxygen-transporting perovskite membrane in disk geometry [99, 100]. If a mixture of the xylene isomers would be in contact with this bilayer membrane facing the Ti-modified silicalite-1 layer, it can be expected that mainly the *p*-xylene isomer will enter the silicalite-1 layer and will become oxidized to the terephthalic acid with the oxygen released from the perovskite membrane. As **Figure 14** shows, this concept works indeed. From a technical C_8 stream, it is the *p*-xylene, indeed, that has been partially oxidized to terephthalic acid.

3.01.3.5 Partial Hydrogenation of Cyclooctadiene to Cyclooctene in a Pore-through-Flow Membrane Reactor

The partial hydrogenation of a di-olefine to the corresponding monoolefine represents a consecutive reaction of the type A → B → C. The pore-through-flow membrane reactor, as a special type of a

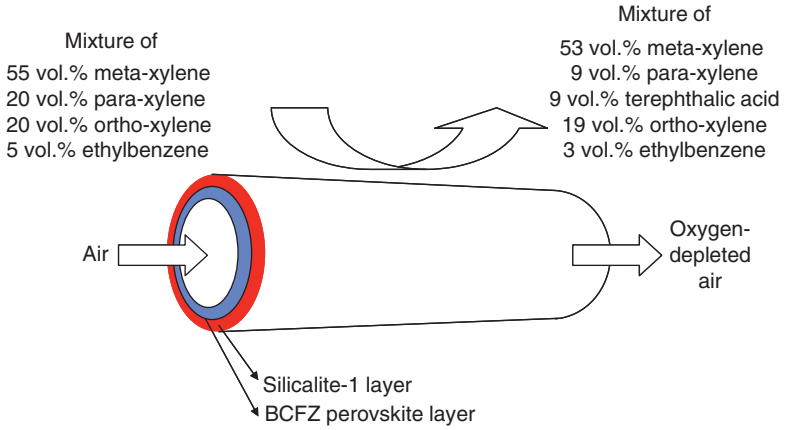

Figure 14 Partial oxidation of *p*-xylene from a technical C_8 mixture to terephthalic acid in a bilayer $BaCo_xFe_yZr_zO_{3-\delta}$ (BCFZ)/Ti-silicalite-1 membrane reactor at 850 °C [100].

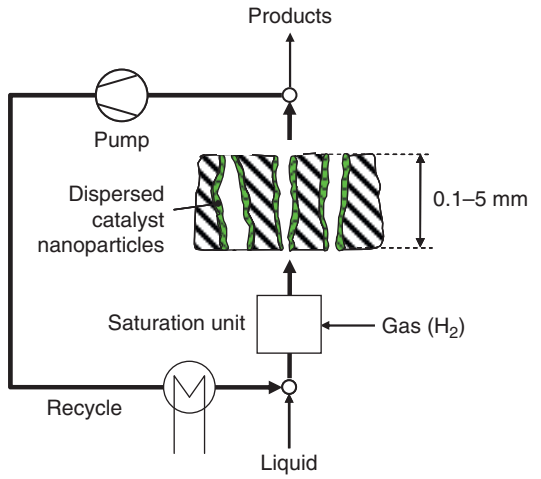

Figure 15 Schema of the pore-through-flow catalytic membrane reactor for hydrogenations of multi-unsaturated hydrocarbons as a special case of a catalytic membrane contactor reactor: the Pd catalyst is placed on the pore walls over the whole cross section of a symmetric membrane. In every loop, the feed becomes H_2-saturated again [2].

membrane contactor, was used for the partial hydrogenation of 1,5-cyclooctadiene (COD) to cyclooctene (COE) (**Figure 15**). A catalytic membrane contactor is a device in which a membrane containing a catalytically active phase is used to provide the reaction zone, thereby the membrane not necessarily has a separative function. In the selective hydrogenation of COD to COE, we have the case of a reaction network of the type $A \xrightarrow{+H_2} B \xrightarrow{+H_2} C$, where the consecutive reaction of the desired intermediate B to C should be avoided. In fixed-bed reactor with catalyst pellets, the selectivity of such reactions is limited by mass transport due to diffusion processes into and out of the pores of the catalyst. This pore diffusion increases the contact time of the intermediate B at the catalytically active sites, which promotes the formation of C. In the pore-through-flow membrane reactor, the selectivity limitation by diffusion can be avoided because the reactants pass the membrane in a fast convective flow. As a consequence, higher activity and increased selectivity to the intermediate product C can be expected. By applying a high flow rate, this operation mode allows one to eliminate the influence of the diffusional resistance present in conventional porous catalysts, thus offering the perspective to exploit the true kinetic properties of the solid active phase, that is, higher activity and improved selectivity in consecutive reactions. The catalytically functionalized pores of the membrane provide a medium with defined contact times for the co-feed of hydrogen and an unsaturated hydrocarbon. Applications of membranes with built-in catalysts for gas/liquid reactions have been reviewed by Dittmeyer *et al.* [101].

A number of authors have investigated membrane contactors to improve the performance of gas/liquid reactions, mainly of hydrogenations. Several groups studied the selective hydrogenation of nitrate and nitrite in water to nitrogen on bimetallic Pd/Cu- and Pd/Sn- or monometallic Pd catalysts, which were either directly deposited into porous ceramic membranes [102–104] or embedded as alumina-supported powder catalysts in porous polymer membranes. Others tested the pore-through-flow concept for the selective hydrogenation of edible oils [105] and of various unsaturated organic substrates,

such as 1-octyne to octene, phenylacetylene to styrene, COD to COE, and geraniol to citronellol [106].

The porous alumina membranes were deposited with Pd by wet impregnation with a Pd salt solution and subsequent activation by a reducing agent. Their catalytic activity and selectivity were investigated in a reactor system constructed as a loop of a saturation vessel and a membrane module for the partial hydrogenation of COD to COE (see **Figure 16**). Details about impregnation procedure and experimental setup are given by Schomäcker *et al.* [107]. The hydrogenation reactions were transferred from laboratory to the pilot scale at Bayer Technology Services GmbH. The volume of the saturation unit was increased from 0.2 to 5.2 l and the membrane area from 20 to 500 cm^2. The flow rate of the reaction mixture per membrane area was kept constant. The loop reactor is shown in **Figure 16**(**a**). The 27-tube membrane module used is shown in **Figure 16**(**b**). The functionalization of the ceramic tubes by Pd particles was done according to the same procedure that was used for single membrane tubes. The COD hydrogenation experiments were performed in a range of 30–60 °C, 0.1–1 MPa hydrogen pressure, and 0.5–2 $kg\,m^{-2}\,s^{-1}$ circulation flow rates and using membrane tubes with a pore diameter of 0.6–3.0 µm. Both in the laboratory and in the pilot scale, the same loop reactor, the scheme of which is shown in **Figure 15**, was used. The H_2-saturated liquid is pumped as feed at high flow rates through the membrane, thus eliminating the diffusive mass transfer resistance.

For the partial hydrogenation of COD, the selectivity for COE is higher in the pore-through-flow membrane reactor compared to a fixed-bed reactor or a slurry reactor with catalyst pellets (**Figure 17**). The highest COE selectivity (95% at complete conversion) is obtained in a slurry reactor with a suspended powder catalyst, because all mass transfer limitations are avoided here. The same result is obtained in the pore-through-flow membrane reactor, indicating that the hydrogenation reaction in the pore-through-flow membrane reactor is indeed only controlled by the microkinetics of the reaction and not by mass transfer effects, such as pore diffusion (**Table 4**).

The selective hydrogenation of COD to COE was successfully scaled up to the pilot scale by a factor of 27. This factor was applied to the system volume, membrane area, and circulation flow rate in order to ensure constant reaction conditions. As **Figure 18** shows, the COD conversion and the COE selectivity were comparable in the laboratory-scale apparatus, using a single-tube membrane and in the pilot-scale apparatus using a bundle of 27 membrane tubes. In the pilot plant reactor, the reaction is even somewhat faster than on laboratory scale, while the selectivities are the same within experimental error. The difference in the rates may be explained by a higher amount of palladium and better dispersion of palladium within the membrane capillary bundle. With these data, a space–time yield for COE of 1 $mol\,l^{-1}\,h^{-1}$ and a productivity of 30 $mol\,h^{-1}\,g_{palladium}^{-1}$ is obtained. The pore-through-flow membrane reactor

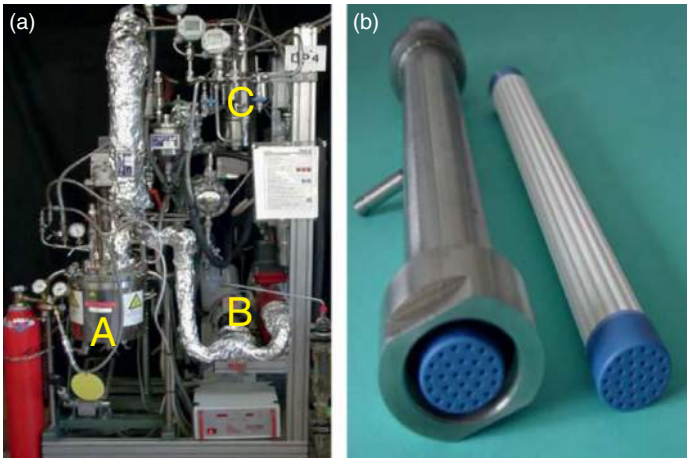

Figure 16 Pilot-scale loop membrane contactor reactor for the selective hydrogenation working due to the pore-through-flow principle (a) and the porous 27-tube ceramic module used in the scale-up (b). A: saturation unit, B: circulation pump, C: membrane module [17].

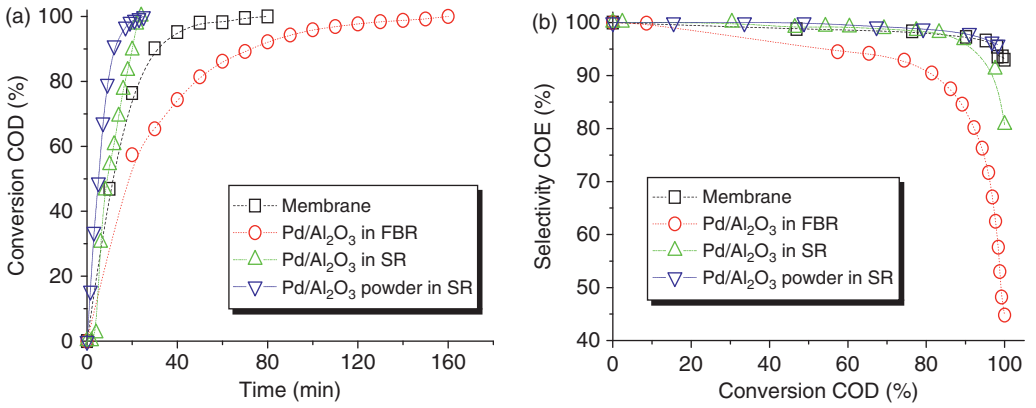

Figure 17 Selectivity improvement when conducting the partial hydrogenation of cyclooctadiene (COD) to cyclooctene (COE) at 50 °C and 1 MPa H_2 pressure as a model reaction for a consecutive reaction of the type A → B → C in a pore-through-flow reactor (porous α-alumina membrane; circulation flow rate 120 ml min^{-1} = 0.5 kg m^{-2} s^{-1}) in comparison with a conventional fixed-bed reactor (FBR) and a slurry reactor (SR). Equal amount of 1 mg Pd for all reactors: Pd/Al_2O_3 (egg-shell type) as 3-mm pellet catalyst with 0.5 wt.% Pd. COD concentration is 0.4 mol l^{-1}: (a) COD conversion vs. time, and (b) COE selectivity vs. COD conversion [17].

Table 4 Selectivities for cyclooctene (COE) in the selective hydrogenation of cyclooctadiene (COD) at complete conversion of COD [17]

Reactor type	*Selectivity for COE at X(COD) ≈ 100 %*
Pore-through-flow membrane	94%
Slurry (with powder catalyst)	95%
Fixed bed (with shell catalyst)	45%

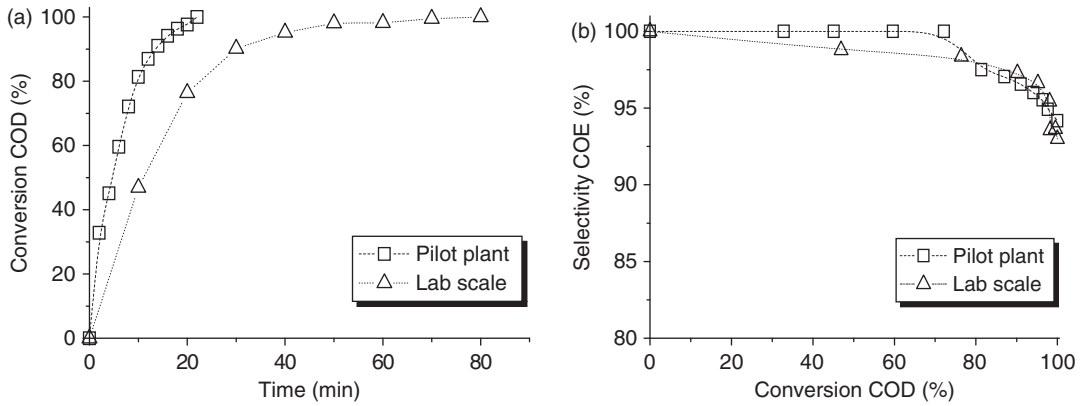

Figure 18 Scale-up of the partial hydrogenation of cyclooctadiene (COD) to cyclooctene (COE) in a pore-through-flow membrane reactor from the laboratory scale to a pilot plant [17, 106], overall volume of lab scale reactor 0.2 l, membrane area 20 cm^2, amount of Pd = 1 mg; overall volume of pilot reactor 5.2 l, membrane area 500 cm^2, amount of Pd = 30 mg. 50 °C, 1 MPa hydrogen pressure, $c_{COD,0}$ = 0.41 mol l^{-1}, pore diameter 1.9 μm, and circulation flow rate 0.5 kg m^{-2} s^{-1}: (a) COD conversion vs. time, and (b) COE selectivity vs. COD conversion.

used for the partial hydrogenation of a multiunsaturated hydrocarbon was successfully scaled up into the pilot scale. For a process to produce 1 ton h^{-1} of a product by a partial hydrogenation with a similar kinetics than COD hydrogenation, an overall volume of 2–10 m^3 would be required, depending on a

suitable reactant concentration. This solution would be circulated through a membrane module with 60 m^2 of porous alumina membrane containing 20 g of palladium. The volume of this membrane module would be below 1 m^3.

3.01.4 Removal of Oxygen as a Reaction Rate Inhibitor in the NO_x Decomposition in an Extractor-Type Membrane Reactor

Nitrous oxide (N_2O) has recently received much attention since it greatly contributes to the greenhouse effect and causes a severe destruction of the ozone layer in the stratosphere. N_2O is produced by both natural and anthropogenic sources. Compared to the natural sources, N_2O emissions, which can be reduced in the short term, are associated with chemical and energy industries. The major N_2O emission of chemical production comes from adipic acid and nitric acid plants. In the past few decades, significant efforts have been devoted to the development of technologies for N_2O reduction, mainly the selective catalytic reduction (SCR), and the catalytic decomposition of N_2O to O_2 and N_2. The major drawback of the SCR is the high cost associated with the consumption of reductants. Direct catalytic decomposition of N_2O without addition of reducing agents is an attractive and economical option to reduce N_2O emission. Catalysts, including supported noble metals, metal oxides, and perovskites, have been reported to be active in the direct catalytic N_2O decomposition. However, metal-oxide catalysts suffer from oxygen inhibition and a low reaction rate of the N_2O decomposition is observed.

The problem of product poisoning in the direct catalytic decomposition of N_2O could be solved by *in situ* removal of the inhibitor oxygen, using a perovskite membrane of the composition BCFZ in hollow-fiber geometry [108]. The BCFZ membrane fulfills two tasks: it acts as (1) a catalyst for the decomposition of N_2O and (2) a membrane for the removal of the rate-inhibiting surface oxygen. The basic concept is shown in **Figure 19**: N_2O catalytically decomposes on the perovskite membrane surface to N_2 and surface oxygen (O^*) according to $N_2O \rightarrow N_2 + O^*$. Subsequently, O^* is removed as oxygen ions (O^{2-}) through the membrane, while local charge neutrality is maintained by counter-diffusion of electrons (e^-). In order to ensure a sufficient driving force for the oxygen transport through the membrane,

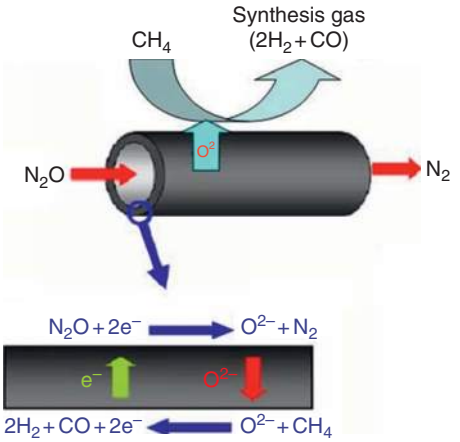

Figure 19 Mechanism of the direct decomposition of N_2O to N_2 with *in situ* removal of the rate-inhibiting surface oxygen by perovskite hollow-fiber membrane [108].

methane is fed to the permeate side of the membrane to consume the permeated oxygen via the POM to synthesis gas according to $CH_4 + O^{2-} \rightarrow CO + 2H_2 + 2e^-$. As a result, surface oxygen (O^*) can be quickly removed by the membrane once it is generated from N_2O decomposition. Therefore, the average amount of adsorbed oxygen (O^*) is reduced and a higher reaction rate of the N_2O decomposition is obtained.

In order to demonstrate this concept, we carried out experiments with and without oxygen removal using a BCFZ perovskite hollow-fiber membrane. N_2O was fed to the core side and no sweep gas was applied at the shell side, which means that none of the oxygen surface species produced by the decomposition of N_2O was removed by permeation through the membrane. The corresponding results are shown in **Figure 20**(**a**). The N_2O decomposition increases with increasing temperature; however, the conversion is relatively low (< 30% even at 900 °C). The catalytic decomposition of N_2O on the perovskite membrane surface mainly proceeds in two steps: (1) decomposition of N_2O into N_2 and adsorbed surface oxygen (O^*) according to Equation (1) and (2) desorption of surface oxygen as O_2 to the gas phase according to $O^* \rightleftarrows \frac{1}{2}O_2 + *$. This reaction, that is, the oxygen–oxygen recombination, is known to be the rate-limiting step in N_2O decomposition [109, 110]. Since the surface oxygen O^* generated by the N_2O decomposition occupies the surface active site for the decomposition of N_2O, only a low N_2O conversion is obtained. Contrary to this poor conversion, if methane as an oxygen-consuming sweep gas is fed

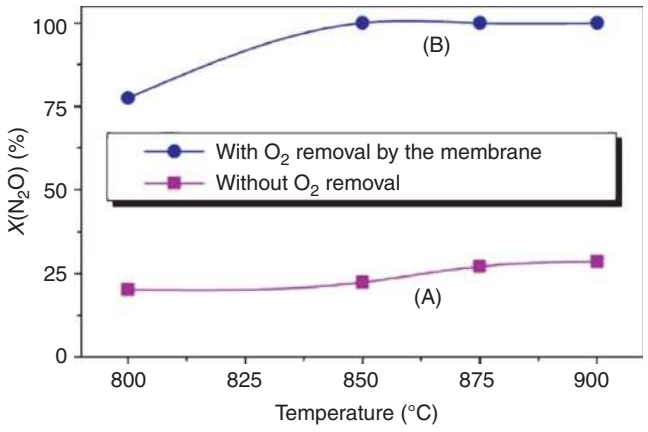

Figure 20 Conversion of N_2O at different temperatures with or without oxygen removal via a perovskite hollow-fiber membrane [108]. Experimental details – core side: 30 $cm^3\,min^{-1}$($F_{N2O} = 6\,cm^3\,min^{-1}$, $F_{He} = 24\,cm^3\,min^{-1}$); shell side: (A) no oxygen-consuming sweep gas applied, and (B) with methane as oxygen-consuming sweep gas, 40 $cm^3\,min^{-1}$ ($F_{CH4} = 8\,cm^3\,min^{-1}$, $F_{Ne} = 12\,cm^3\,min^{-1}$ and $F_{H2O} = 20\,cm^3\,min^{-1}$); membrane area: 0.86 cm^2. Amount of Ni-based catalyst on shell side: 1.2 g.

to the shell side, the N_2O decomposition is significantly improved as shown in **Figure 20**(**b**).

The membrane approach presented here has to use a reducing agent, so that it would be sustainable and economically attractive to combine the N_2O removal with the simultaneous production of valuable chemicals. Here, we used the permeated oxygen to produce the N_2-free synthesis gas. **Figure 21** shows the CO selectivity and CH_4 conversion on the shell side as well as the N_2O conversion on the core side as a function of time. N_2O in the core side was completely converted. Simultaneously, synthesis gas is obtained with a methane conversion of 90% and a CO selectivity of 90% for at least 60 h of operation. The technology is more feasible when the concentrations of nitrous oxide in the off-gas are sufficiently high, such as in adipic acid plants.

The same mechanism, similar to that of the N_2O decomposition, could be successfully applied for the NO splitting into the elements [111]. **Figure 22** shows the concept of NO decomposition in the BCFZ perovskite hollow-fiber membrane reactor. First, the adsorbed NO is catalytically decomposed on the surface of the BCFZ membrane into N_2 and surface oxygen (O^*), based on the reaction NO $\rightarrow 1/2N_2 + O^*$ [112, 113]. Then, the surface O^* is removed as oxygen ions (O^{2-}) via the perovskite oxygen-transporting membrane, and local charge neutrality is maintained by the counter-diffusion of electrons (e^-). Thus, the surface oxygen (O^*) can be continuously removed via the BCFZ membrane once it is generated from NO decomposition, which will result not only in a kinetic acceleration of NO

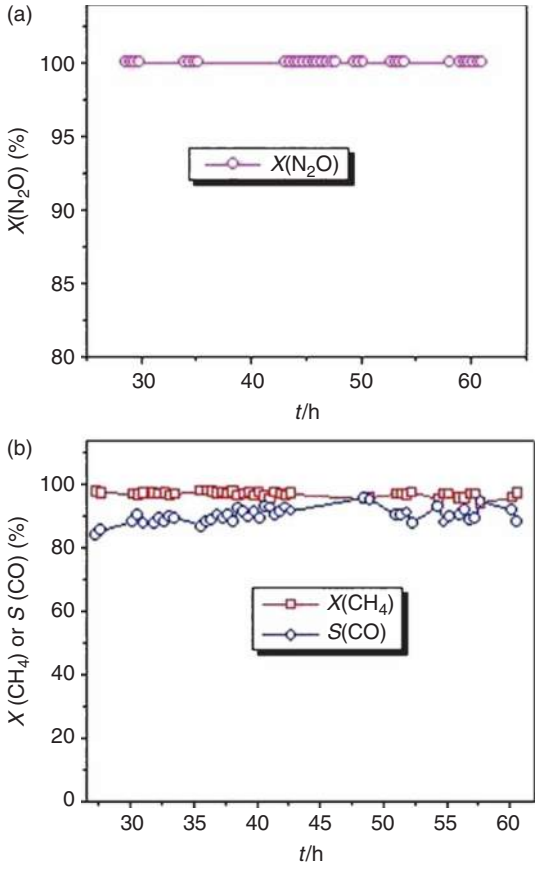

Figure 21 N_2O conversion (a), methane conversion and CO selectivity (b) as a function of time on stream at 875 °C [108]. Experimental details – core side: 30 $cm^3\,min^{-1}$ ($F_{N2O} = 6\,cm^3\,min^{-1}$, $F_{O2} = 1.5\,cm^3\,min^{-1}$, $F_{He} = 22.5\,cm^3\,min^{-1}$); shell side: 40 $cm^3\,min^{-1}$ ($F_{CH4} = 23\,cm^3\,min^{-1}$, $F_{H2O} = 17\,cm^3\,min^{-1}$); membrane area: 0.86 cm^2. Amount of Ni-based catalyst on shell side: 1.2 g.

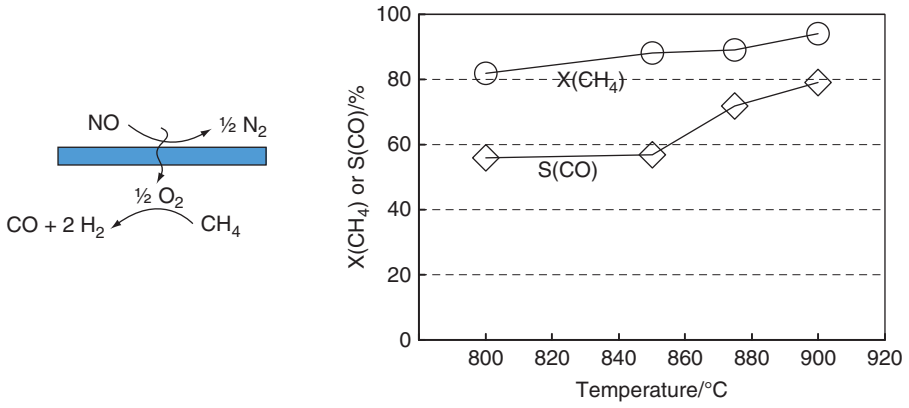

Figure 22 Scheme for the use of NO as oxygen source in synthesis gas production (left), and CH_4 conversion (○) and CO selectivity (◇) in the catalytic partial oxidation of methane in a BCFZ perovskite hollow fiber membrane reactor as a function of temperature (right) (after [111]).

Table 5 Conversion of NO at different temperatures without and with oxygen removal using methane as oxygen consuming sweep gas

Temperature (°C)	*(a): X(NO) (%) without O_2 removal*	*(b): X(NO) (%) with O_2 removal*
800	1	29
850	1	60
875	1	100
900	3	100
925	3	100

Experimental details–core side: 30 $cm^3\,min^{-1}$(F_{NO} = 3 $cm^3\,min^{-1}$, F_{Ne} = 1 $cm^3\,min^{-1}$, F_{He} = 26 $cm^3\,min^{-1}$); shell side: (a) no sweep gas applied, and (b) methane as oxygen consuming sweep gas, 50 $cm^3\,min^{-1}$ (F_{CH4} = 8 $cm^3\,min^{-1}$, F_{He} = 37 $cm^3\,min^{-1}$, and F_{H2O} = 5 $cm^3\,min^{-1}$); 0.5 g Ni-based catalyst packed on shell side [111].
Reproduced from Jiang, H., Xing, L., Czuprat, O., *et al. Chem. Commun.* **2009**, *44*, 6738–6740.

decomposition, but also in the prevention of NO_2 formation. Table 5 shows the NO conversion for different temperatures.

3.01.5 Conclusions

There are numerous examples for the application of membranes to enhance a chemical reaction, such as a dehydrogenation, partial oxidation, isomerization, or an esterification. The traditional concept for an application of membranes in reactors is focused on conversion enhancement. If under equilibrium-controlled reaction conditions product molecules like hydrogen or water can be removed from the reactor through a permselective membrane, conversion and yield of e.g. dehydrogenations or esterifications can be increased. The corresponding reactor is called membrane extractor reactor.

By dosing one of the educts selectively or nonselectively through the reactor wall, the partial pressure of this reactant can be fine-tuned along a reactor dimension. Thus, the selectivity of a kinetically controlled reaction can be influenced via the partial pressure of a component. As a general rule, low partial pressures of oxygen/hydrogen support a partial, instead of a total, oxidation/hydrogenation. The corresponding reactor is called membrane distributor/contactor reactor. The so-called pore-through-flow membrane reactor is a special type of membrane contactor.

In Section 3.01.4, the successful application of an extractor-type membrane reactor in the case of the reaction rate inhibition was dealt with. As an example, the rate inhibition of the NO_x decomposition by the product molecule oxygen was discussed. The new concept allows one to enhance the reaction rate of catalytic processes, where the recombination and/or desorption of one of the reaction products is the

rate-limiting step. Using a semipermeable membrane, which facilitates *in situ* removal of an inhibiting species on a catalyst or catalyst support, helps to effectively reduce the surface concentration of the inhibiting species and, therefore, increases the reaction rate.

Up to now, there are no chemical membrane reactors in high-temperature operation in the chemical industry; fuel cells and biochemical processes are exceptions. It is believed that the use of oxygen-transporting perovskite-type membranes in combination with a catalyst in partial oxidations, and the selective hydrogenation of unsaturated hydrocarbons in the pore-through-flow membrane reactor as a special case of a catalytic membrane contactor are promising candidates for incipient industrial applications of catalytic membrane reactors.

3.01.6 Acknowledgments

The author thanks the team of the German Lighthouse Project CaMeRa (Catalytic Membrane Reactor) for the stimulating cooperation: Drs. Werth, Langanke and Caspary from Uhde GmbH, Drs. Wolf and Warsitz from Bayer Technology Services GmbH, Dr. Hoting and Dipl.-Ing. Nassauer from Borsig GmbH, Prof. Wang from South China Technical University Guangzhou, Prof. Dittmeyer from DECHEMA e.V., Dr. Schiestel from Fraunhofer IGB, Prof. Schomäcker from Technical University Berlin, Dr. Schmidt from BASF AG, Profs. Seidel-Morgenstern and Tsotsis as well as Dr. Hamel from Max-Planck-Institute Magdeburg and Otto-von-Guericke-University Magdeburg, Drs. Kölsch and Noack from Leibniz Institute for Catalysis Berlin and last but not least Dr. Voigt from Hermsdorf Institute for Technical ceramics. The German Ministry of Education and Research (BMBF) is thanked for financing this project under the auspices of ConNeCat (Competence Network on Catalysis). Further, J.C. thanks the DFG for supporting the International Research Group on Diffusion in Zeolites (Ca 147-11/1 and 11/2).

References

[1] Koros, W. J., Ma, Y. H., Shimidzu, T. *Terminology for Membranes and Membrane Processes*; IUPAC Recommendations from 1996, http://www.che.utexas.edu/nams/IUPAC/iupac.html (accessed December 2009).
[2] Dittmeyer, R., Caro, J. Catalytic Membrane Reactors. In *Handbook of Heterogeneous Catalysis*, 2nd edn.; Ertl, G., Knözinger, H., Schüth, F., Weitkamp, J., Eds.; Wiley-VCH: Weinheim, 2008; pp 2198–2248.
[3] Sanchez-Marcano, J. G., Tsotsis, T. T. *Catalytic Membranes and Membrane Reactors*; Wiley-VCH: Weinheim, 2002.
[4] Paglieri, S. N., Way, J. D. *Sep. Purif. Methods* **2002**, *31*, 1.
[5] Kemmere, M. F., Keurentjes, J. T. F. Industrial Membrane Reactors. In *Membrane Technology in the Chemical Industry*; Nunes, S. P., Peinemann, K. V., Eds.; Wiley-VCH: Weinheim, 2001; Chapter 5, pp 229–258.
[6] Liu, S., Tan, X., Li, K., Hughes, R. *Catal. Rev. Sci. Eng.* **2001**, *43*, 147.
[7] Maschmeyer, T., Jansen, K., Thomas, J. M., Eds. *Top. Catal.* **2004**, *29*.
[8] Dittmeyer, R., Höllein, V., Daub, K. *J. Mol. Catal. A: Chem.* **2001**, *173*, 135.
[9] Emig, G., Liauw, M. A. *Top. Catal.* **2002**, *21*, 11.
[10] Dixon, A. G. *Int. J. Chem. React. Eng.* **2003**, *1*, R6.
[11] Coronas, J., Santamaria, J. *Top. Catal.* **2004**, *29*, 29.
[12] Drioli, E., Romano, M. *Ind. Eng. Chem. Res.* **2001**, *40*, 1277.
[13] Julbe, A., Farusseng, D., Guizard, C. *Catal. Today* **2005**, *104*, 102.
[14] Julbe, A., Farusseng, D., Guizard, C. *J. Membr. Sci.* **2001**, *181*, 3.
[15] Drioli, E., Criscuoli A., Curcio, E. *Membrane Contactors: Fundamentals, Applications and Potentialities*; Membrane Science and Technology Series 11; Elsevier: Amsterdam, 2006.
[16] Seidel-Morgenstern, A. Analysis and Experimental Investigation of Catalytic Membrane Reactors. In *Integrated Chemical Processes*; Sundmacher, K., Kienle, A., Seidel-Morgenstern, A., Eds.; Wiley-VCH: Weinheim, 2005; pp 359–392.
[17] Caro, J., Caspary, K. J., Hamel, C., *et al. Ind. Eng. Chem. Res.* **2007**, *46*, 2286.
[18] Drioli, E., Giorno, L. *Biocatalytic Membrane Reactors: Applications in Biotechnology and the Pharmaceutical Industry*; Taylor and Francis: London, 1999.
[19] Rios, G. M., Belleville, M. P., Paolucci, D., Sanchez, J. *J. Membr. Sci.* **2004**, *242*, 189.
[20] Coronas, J., Santamaria, J. *Top. Catal.* **2004**, *29*, 29.
[21] Illgen, U., Schäfer, R., Noack, M., Kölsch, P., Kühnle, A., Caro, J. *Catal. Commun.* **2001**, *2*, 339.
[22] Schäfer, R., Noack, M., Kölsch, P., Stöhr, M., Caro, J. *Catal. Today* **2003**, *82*, 15.
[23] Ciavarella, P., Casanave, D., Moueddeb, H., Miachon, S., Fiaty, K., Dalmon, J.-A. *Catal. Today* **2001**, *67*, 177.
[24] Alshebani, A., Landrivon, E., Schiestel, T., Miachon, S., Dalmon, J.-A. *Proceedings of the 4th International Zeolite Membrane Meeting*, Zaragoza, Spain, July 2007; p 67.
[25] Corma, A., Rey, F., Rius, J., Sabater, M., Valencia, S. *Nature* **2004**, *431*, 287.
[26] Tiscornia, I., Valencia, S., Corma, A., Téllez, C., Coronas, J., Santamaria, J. *Proceedings of the 4th International Zeolite Membrane Meeting*, Zaragoza, Spain, July 2007; p 78.
[27] Karanikolos, G. N., Stoeger, J., Wydra, J. W., Garcia, H., Corma, A., Tsapatsis, M. *Proceedings of the 4th International Zeolite Membrane Meeting*, Zaragoza, Spain, July 2007; p 61.
[28] Kiyozumi, Y., Nemoto, Y., Nishide, T., Nagase, T., Hasegawa, Y. *Proceedings of the 4th International Zeolite Membrane Meeting*, Zaragoza, Spain, July 2007; p 57.
[29] Kita, H., Li, X., Nagamatsu, T., Tanaka, K. *Proceedings of the 4th International Zeolite Membrane Meeting*, Zaragoza, Spain, July 2007; p 18.
[30] Yajima, K., Nakayama, K., Niino, M., Tomita, T., Yoshida, S. *Proceedings of the 9th International Conference on Inorganic Membranes (ICIM-9),* Lillehammer, Norway, SINTEF, 2006; p 401.

[31] Espinoza, R. L., Du Toit, E., Santamaria, J. M., Menendez, M. A., Coronas, J., Irusta, S. *Stud. Surf. Sci. Catal.* **2000**, *130*, 389.
[32] Rohde, M. P., Unruh, D., Schaub, G. *Ind. Eng. Chem. Res.* **2005**, *44*, 9653.
[33] Rohde, M. P., Schaub, G., Khajavi, S., Jansen, J. C., Kapteijn, F. *Proceedings of the 4th International Zeolite Membrane Meeting*, Zaragoza, Spain, July 2007; p 49.
[34] Zhu, W., Gora, L., van den Berg, A. W. C., Kapteijn, F., Jansen, J. C., Moulijn, J. A. *J. Membr. Sci.* **2005**, *253*, 57.
[35] Khajavi, S., Jansen, J. C., Kapteijn, F. *Stud. Surf. Sci. Catal.* **2007**, *170*, 1028.
[36] Caro, J., Noack, M., Kölsch, P. *Adsorption* **2005**, *11*, 215.
[37] Kwan, M. S. M., Leung, A. Y. L., Yeung, K. L. *Proceedings of the 4th International Zeolite Membrane Meeting,* Zaragoza, Spain, July 2007; p 15.
[38] Jensen, K. F. *Chem. Eng. Sci.* **2001**, *56*, 293.
[39] Wan, Y. S. S., Chau, J. L. H., Yeung, K. L., Gavriilidis, A. *Microporous Mesoporous Mater.* **2001**, *42*, 157.
[40] Chau, J. L. H., Wan, Y. S. S., Gavriilidis, A., Yeung, K. L. *Chem. Eng. J.* **2002**, *88*, 187.
[41] Chau, J. L. H., Yeung, K. L. *Chem. Commun.* **2002**, *9*, 960.
[42] Chau, J. L. H., Leung, A. Y. L., Yeung, K. L. *Lab-on-a-Chip* **2003**, *3*, 53.
[43] Leung, A. Y. L., Yeung, K. L. *Chem. Eng. Sci.* **2004**, *59*, 4809.
[44] Leung, A. Y. L., Yeung, K. L. *Stud. Surf. Sci. Catal.* **2004**, *154*, 671.
[45] Lai, S. M., Martin-Aranda, R., Yeung, K. L. *Chem. Commun.* **2003**, *2*, 218.
[46] Lai, S. M., Ng C. P., Martin-Aranda, R., Yeung, K. L. *Microporous Mesoporous Mater.* **2003**, *66*, 239.
[47] Zhang, X. F., Lai, S. M., Martin-Aranda, R., Yeung, K. L. *Appl. Catal. A* **2004**, *261*, 109.
[48] Yeung, K. L., Zhang, X. F., Lau, W. N., Martin-Aranda, R. *Catal. Today* **2005**, *110*, 26.
[49] Lau, W. N., Yeung, K. L., Zhang, X. F., Martin-Aranda, R. *Stud. Surf. Sci. Catal.* **2007**, *170*, 1460.
[50] Wan, Y. S. S., Yeung, K. L., Gavriilidis, A., van Steen, E., Callanan, L. H., Claeys M., *Eds. Stud. Surf. Sci. Catal.* **2004**, *154*, 285.
[51] Wan, Y. S. S., Yeung, K. L., Gavriilidis, A. *Appl. Catal. A* **2005**, *281*, 285.
[52] Jiang, H., Wang, H. H., Schiestel, T., Werth, S., Caro, J. *Angew. Chemie* **2008**, *120*, 9481.
[53] Balachandran, U., Lee, T. H., Wang, S., Dorris, S. E. *Int. J. Hydrogen Energy* **2004**, *29*, 291.
[54] Balachandran, U., Lee, T. H., Dorris, S. E. *Int. J. Hydrogen Energy* **2007**, *32*, 4451.
[55] Ramos, R., Menendez, M., Santamaria, J. *Catal. Today* **2000**, *56*, 239.
[56] Alonso, M., Lorences, M. J., Pina, M. P., Patience, G. S. *Catal. Today* **2001**, *67*, 151.
[57] Miachon, S., Dalmon, J.-A. *Top. Catal.* **2004**, *29*, 59.
[58] Mota, S., Volta, J.-C., Vorbeck, G., Dalmon, J.-A. *J. Catal.* **2000**, *193*, 319.
[59] Kölsch, P., Smejkal, Q., Noack, M., Schäfer, R., Caro, J. *Catal. Commun.* **2002**, *3*, 465.
[60] Koh, A., Chen, L., Johnson, B., Khimyak, T., Leong, W., Lin, J., *Presented at the 1st World Hydrogen Technologies Convention (WHTC-1)*, Singapore, 3–5 October 2005.
[61] Dyer, P. N., Richards, R. E., Russek, S. L., Taylor, D. M. *Solid State Ion.* **2000**, *134*, 21.
[62] Wang, H. H., Cong, Y., Yang, W. S. *J. Membr. Sci.* **2002**, *210*, 259.
[63] Tan, X. Y., Liu, Y. T., Li, K. *AIChE J.* **2005**, *51*, 1991.
[64] Liu, S. M., Gavalas, G. R. *J. Membr. Sci.* **2005**, *246*, 103.
[65] Van Hassel Prasad, R., Chen, J., Lane, J. Ion-Transport Membrane Assembly Incorporating Internal Support. US Pat. 6,565,632, 2001.
[66] Armstrong, P. A., Bennet, D. L., Foster, E. P. T., van Stein, E. E. Ceramic Membrane Development for Oxygen Supply to Gasification Applications. In *Proceedings of the Gasification Technology Conference*, San Francisco, CA, USA, 27–30 October 2002.
[67] Armstrong, P. A., Sorensen, J., Foster, E. P. T. ITM Oxygen: An Enabler for IGCC. In *Proceedings of the Gasification Technology Conference*, San Francisco, CA, 12–15 October 2003.
[68] Armstrong, P. A., Bennet, D. L., Foster, E. P. T., van Stein, E. E. ITM Oxygen for Gasification. In *Proceedings of the Gasification Technology Conference*, Washington, DC, USA, 3–6 October 2004.
[69] Bruun, T. *Design Issues for High Temperature Ceramic Membrane Reactors. In Proceedings of the 6th International Catalysis in Membrane Reactors,* Lahnstein, Germany, 2004.
[70] Vente, J. F., Haije, W. G., Ijpelaan, R., Rusting, F. T. *J. Membr. Sci.* **2006**, *278*, 66.
[71] Tan, X., Liu, Y., Li, K. *AIChE J.* **2005**, *51*, 1991.
[72] Tan, X., Liu, Y., Li, K. *Ind. Eng. Chem. Res.* **2005**, *44*, 61.
[73] Liu, S., Gavalas, G. R. *J. Membr. Sci.* **2005**, *246*, 103.
[74] Liu, S., Gavalas, G. R. *Ind. Eng. Chem. Res.* **2005**, *44*, 7633.
[75] Tong, J. H., Yang, W. S., Cai, R., Zhu, B. C., Lin, L. W. *Catal. Lett.* **2002**, *78*, 129.
[76] Schiestel, T., Kilgus, M., Peter, S., Caspary, K. J., Wang, H. H., Caro, J. *J. Membr. Sci.* **2005**, *258*, 1.
[77] Tablet, C., Grubert, G., Wang, H. H., *et al. Catal. Today* **2005**, *104*, 126.
[78] Caro, J., Wang, H. H., Tablet, C., *et al. Catal. Today* **2006**, *118*, 128.
[79] Chen, C. S., Feng, S. J., Ran, S., Zhu, D. C., Lin, W., Bouwmeester, H. J. M. *Angew. Chem. Int. Ed.* **2003**, *42*, 5196.
[80] Kondratenko, E. V., Baerns, M. Synthesis Gas Generation by Heterogeneous Catalysts. In *Encyclopedia of Catalysis*; Horvyth, I., Ed.; Wiley: New York, 2003; Vol. 6, pp 424–456.
[81] Wang, H. H., Tablet, C., Schiestel, T., Werth, S., Caro, J. *Catal. Commun.* **2006**, *7*, 907.
[82] Wang, H. H., Caro, J., Werth, S., Schiestel, T. *Angew. Chem. Int. Ed.* **2005**, *44*, 2.
[83] Hamel, C., Seidel-Morgenstern, A., Schiestel, T., *et al. AIChE J.* **2006**, *52*, 3118.
[84] Wang, H. H., Tablet, C., Schiestel, T., Caro, J. *Catal. Today* **2006**, *118*, 98.
[85] Mulla, S. A. R., Buyevskaya, O. V., Baerns, M. *J. Catal.* **2001**, *197*, 43.
[86] Watson, R. B., Ozkan, U. S. *J. Catal.* **2000**, *191*, 12.
[87] Mitchell, P. C. H., Wass, S. A. *Appl. Catal. A* **2002**, *225*, 153.
[88] Brückner, A., Rybarczyk, P., Kosslick, H., Wolf, G.-U., Baerns, M. *Stud. Surf. Sci. Catal.* **2002**, *142*, 1141.
[89] Wang, H. H., Cong, Y., Yang, W. *Chem. Commun.* **2002**, *14*, 1468.
[90] Wang, H. H., Cong, Y., Yang, W. *Catal. Lett.* **2002**, *84*, 101.
[91] Rebeilleau, M., van Veen, A. C., Farrusseng, D., *et al. Stud. Surf. Sci. Catal.* **2004**, *147*, 655.
[92] Rebeilleau, M., Rosini, S., van Veen, A. C., Farrusseng, D., Mirodatos, C. *Catal. Today* **2005**, *104*, 131.
[93] Akin, F. T., Lin, Y. S. *J. Membr. Sci.* **2002**, *209*, 457.
[94] Wang, H. H., Cong, Y., Zhu, X., Yang, W. *React. Kinet. Catal. Lett.* **2003**, *79*, 351.
[95] Akin, F. T., Lin, Y. S. *Catal. Lett.* **2002**, *78*, 239.
[96] Shao, Z., Dong, H., Xiong, G., Cong, Y., Yang, W. *J. Membr. Sci.* **2001**, *183*, 181.

[97] Lu, Y., Dixon, A. G., Moser, W. R., Ma, Y., Balachandran, U. *Catal. Today* **2000**, *56*, 297.
[98] Wang, H. H., Tablet, C., Caro, J. *J. Membr. Sci.* **2008**, *322*, 214.
[99] Caro, J., Wang, H. H., Noack, M., *et al.* Double Layer Membrane for Shape Selective Partial Oxidation of Hydrocarbons. EP 06 112 764.3, 18 April 2007.
[100] Caro, J., Wang, H. H., Noack, M., *et al.* Composite Membrane. WO 2007/118902 A2, 25 October 2007.
[101] Dittmeyer, R., Svajda, K., Reif, M. *Top. Catal.* **2004**, *29*, 3.
[102] Ilinich, O. M., Cuperus, F. P., Nosova, L. V., Gribov, E. N. *Catal. Today* **2000**, *56*, 137.
[103] Ilinich, O. M., Gribov, E. N., Simonov, P. A. *Catal. Today* **2003**, *82*, 49.
[104] Reif, M., Dittmeyer, R. *Catal. Today* **2003**, *82*, 3.
[105] Fritsch, D., Bengtson, G. *Catal. Today* **2006**, *118*, 121.
[106] Schmidt, A., Haidar, R., Schomäcker, R. *Catal. Today* **2005**, *104*, 305.
[107] Schomäcker, R., Schmidt, A., Frank, B., Haidar, R., Seidel-Morgenstern, A. *Chem. Ing. Tech.* **2005**, *77*, 549.
[108] Jiang, H., Wang, H. H., Liang, F., Werth, S., Schiestel, T., Caro, J. *Angew. Chem. Int. Ed.* **2009**, *48*, 2983.
[109] Bulushev, D. A., Kiwi-Minsker, L., Renken, A. *J. Catal.* **2004**, *222*, 389.
[110] Bennici, S., Gervasini, A. *Appl. Catal. B* **2006**, *62*, 336.
[111] Jiang, H., Xing, L., Czuprat, O., *et al*. *Chem. Commun.* **2009**, *44*, 6738–6740.
[112] Burch, R. *Top. Catal.* **2003**, *24*, 97.
[113] Burch, R., Millington, P. R., Walker, A. P. *Appl. Catal. B* **1994**, *4*, 65.

Biographical Sketch

J. Caro is currently a C4-Professor of physical chemistry at Leibniz University, Hannover, Germany, and the director of the Institute for Physical Chemistry and Electrochemistry. Between 1970 and 1973, he studied chemistry at Leipzig University; he received his PhD in 1977 from the Physics Department of Leipzig University on molecular diffusion of guest molecules in porous media by nuclear magnetic resonance (NMR) methods, supervised by Profs. Kärger and Pfeifer. Later, he worked at the Academy of Sciences in Berlin-Adlershof in adsorption, permeation, and catalysis. In 2001, he was appointed the chair of physical chemistry at Hannover University. During 2005–06, he was the president of the German Catalysis Society. During 2003–06, he was the speaker of the Lighthouse Project of the German Research Ministry 'Membranes for catalysis' (with 12 partners from industry and academia) under the auspices of Das Kompetenznetzwerk Katalyse (ConNeCat, competence network catalysis). J. Caro is the author of 200 papers, 37 patents, and the member of the editorial boards of five journals (e.g., *Advanced Materials*, *Microporous and Mesoporous Materials*, and *Catalysis Communications*).

3.02 Computer-Aided Model-Based Design and Analysis of Hybrid Membrane Reaction-Separation Systems

R Gani and P T Mitkowski, Technical University of Denmark, Lyngby, Denmark

V Soni, BASF SE, Ludwigshafen, Germany

3.02.1	**Introduction**	26
3.02.2	**Simultaneous Design of Membrane Process**	27
3.02.2.1	Design Problem Definition	28
3.02.2.2	Simultaneous Design Framework	29
3.02.2.2.1	Need for a systematic model-based design framework	30
3.02.2.2.2	Multilevel modeling	30
3.02.2.2.3	Solution approaches	31
3.02.3	**Synthesis Design of Hybrid Processes**	33
3.02.3.1	Problem Definition	34
3.02.3.2	Model-Based Framework	34
3.02.3.2.1	Hybrid process design and analysis (stage 1)	34
3.02.3.2.2	Implementation (stage 2)	39
3.02.3.2.3	Validation (stage 3)	39
3.02.3.3	Generic Model for a Hybrid Process	39
3.02.4	**Computer-Aided Methods and Tools**	42
3.02.4.1	Model Library	43
3.02.5	**Case Studies**	44
3.02.5.1	Simultaneous Design of Membrane and Separation Process – A Conceptual Study	44
3.02.5.1.1	Design problem definition	44
3.02.5.1.2	Model equations and characterizing variables	44
3.02.5.1.3	Solution approaches	45
3.02.5.2	R–S Hybrid Process – Propionic Acid Case Study	46
3.02.5.2.1	Stage 1: Hybrid process design and analysis	46
3.02.5.2.2	Implementation (stage 2)	49
3.02.5.2.3	Validation (stage 3)	50
3.02.6	**Conclusions**	51
References		54

Glossary

Computer-aided framework Architecture of the software tool.

Computer-aided methods and tools Mathematical model-based solution procedures that have been converted into software tools.

Group contribution method Method for property prediction of chemicals and their mixtures where molecular structure of the chemicals is represented by a set of functional groups (of atoms).

Hybrid process Process obtained by combining at least two unit operations, which may be same or different, to achieve improvements in terms of performance, flexibility, and/or better utilization of resources.

Incidence matrix Representation of equations (in rows) and variables occurring in columns. It helps to identify the structure of the model equations.

Modified UNIFAC A group-contribution model for the prediction of activities of chemicals in the liquid phase.

Revrese design approach First define design targets and then identify design alternatives that match these targets.

3.02.1 Introduction

The chemical process could either be a single unit operation or a combination of several operations involving, for example, reactions and separations. Often, one or more chemical reactions are involved, but other ways of changing chemical (or material) composition may be used, such as mixing or separation processes. In this chapter, the synthesis and design of hybrid processes are considered. Concerns on the sustainability of the modern society coupled with the economic and industrial activities of the chemical and related industries are leading to demands for improved process performance, more flexible process operation, and better utilization of resources. A hybrid process, which by definition combines two or more process operations (same or different) to achieve specified design targets, offers opportunities for process improvements and thereby more sustainable process designs [1].

A reaction process converts a set of raw materials (reacting chemicals) to a set of products (desired chemicals), satisfying a set of atomic balance constraints and different conditions of operation. A separation process may be used to transform a mixture of chemicals (e.g., the effluent from a reactor) into two or more compositionally distinct products. The classification of separation processes can be based on the means of separation: mechanical or chemical. Depending on the feed mixture, various processes can be employed to separate the chemicals.

Process design involves the design of a new process and/or the modification or expansion of an existing process. To obtain the desired physical and/or chemical transformation of species, the process must be designed accordingly. The process design essentially amounts to deciding which unit operations need to be performed on given feed streams in order to obtain optimal end-use product streams at minimal costs [2]. Model-based process design is a quantitative problem solving approach employing the use of heuristics, simulation, and optimization. An important first step is to develop or obtain the appropriate mathematical model representing the specific processing route and to identify the important design variables to which this processing route is sensitive to. When more than one processing option is considered, the availability of a model-based computer-aided framework becomes desirable. In many cases, the separation processes may be assisted by special chemicals (materials) and these are termed in this chapter as the formulated/structured chemical materials. Examples of these materials are catalysts for reaction systems, solvents for solvent-based separations/reactions, polymers for membrane-based separation processes, polymeric micro-capsules for controlled-delivery systems, and so on. Any process that requires these assisting structured materials depends very much on their properties, which, in turn, depend on their structure. Therefore, in order to design a process which is assisted by structured materials, it is important to design the membrane together with the process.

Hybrid processes offer opportunities for improving the reaction functionality by facilitating a greater conversion of reactants to desired products and for enhancing the separation efficiency by uniquely offering selective separation of components from a mixture. Whu *et al.* [3] explored the use of organic solvent-resistant nanofiltration membrane in the synthesis of pharmaceutical products where the valuable products were separated from the smaller-molecular-weight by-products and residual reactants present in the reaction mixture. They also examined the potential enhancement of reactant conversion, reduction of reaction time, and the elimination of subsequent downstream separation. In addition, the advantage of membrane techniques, especially vapor permeation and pervaporation combined with reactive distillation, has been employed in the synthesis of methyl *tert*-butyl ether by Matouq *et al.* [4] and in the production of *n*-propyl propionate by Buchaly *et al.* [5] giving very promising results.

Design of a hybrid process scheme needs to take into account the interdependency of the combined

operations in terms of process conditions (defined by temperature, pressure, and/or compositions) to determine the optimal configuration. The need for a hybrid process arises because a design target cannot be achieved by a single operation. Therefore, different combinations need to be tried until those that satisfy the process constraints as well as the design targets are identified. Obviously, while experiment-based trial and error approaches validate the design as it is being identified, there is no guarantee that the optimal design has been found and they are resource and time intensive. Another alternative solution approach defines an initial search space by employing a model-based technique. In this case, the models must be reliable and need to be integrated with process synthesis-design tools to solve a large range of hybrid process design problems efficiently. For efficient identification of feasible designs of hybrid process schemes, the models are used in qualitative and quantitative analyses (principal steps of the model-based technique) for each of the constituent processes (e.g., pervaporation, vapor permeation, nanofiltration, distillation, and reactor) at different modeling depths. For each feasible design alternative, the performance criteria are calculated and from this, an optimal subset is selected for final validation and analysis through rigorous modeling and/or experiments. In this way, the expensive experimental resources are used for verification rather than for search.

In this chapter, two model-based computer-aided frameworks for design of hybrid process schemes and for simultaneous design of membrane and membrane-based separation process are presented together with the main elements of the frameworks – the design technique, the modeling tool box, the knowledge-base and the corresponding methods, and tools. The types of membrane-based processes considered are, membrane-based liquid and gas separation processes using polymeric membranes, whose design/selection is also considered. A case study illustrating the use of the general model for membrane-based operations together with the reverse approach for simultaneous design of membrane as well as the membrane-based separation process is presented. A second case study highlighting the application of the framework for design of hybrid process schemes, including verification by experiments for the enhancement of the synthesis of *n*-propyl propionate from 1-propanol and propionic acid, is presented.

3.02.2 Simultaneous Design of Membrane Process

A membrane-based separation process separates an influent stream into two effluent streams known as the permeate and the retentate with the help of a membrane. The membrane can be defined essentially as a barrier, which separates two phases and restricts transport of specific chemicals in a selective manner. The stream that permeates through the membrane is the permeate stream and the one retained by the membrane is the retentate. Either of the two streams could be the end-use products in a membrane-based separation process. If the aim is to concentrate a product, the retentate will usually be the end-use product stream. However, in the case of purification, the retentate or the permeate may be the desired end-use product and depends on the impurities that have to be removed.

Polymeric membranes can be classified as porous membranes or nonporous membranes, which are very similar in structure and function to a conventional filter. They have rigid, highly voided structures with randomly distributed, interconnected pores (normally in the order of 0.01–10 μm in diameter). Nonporous membranes (also referred as dense membranes) consist of a dense film through which the permeant is transported by diffusion under the driving force of a pressure, concentration, or electric potential. The separation is mainly determined by the diffusivity and solubility of the permeant through the membrane material. Thus, nonporous membranes can separate permeant of similar sizes, given their solubility is significantly different.

Membrane-based separation is an important process that has been extensively used for many gas separations, such as separation of hydrogen from gaseous mixtures of nitrogen and/or methane, recovery of hydrogen from product streams in ammonia production process, separation of methane from biogas produced by oxidation of biomass, enrichment of oxygen from an air stream for medical or combustion purposes, removal of water vapor and/or carbon dioxide and/or hydrogen sulfide from natural gas, and removal of volatile organic chemicals (VOCs) from air or exhaust streams. Usually, nonporous polymeric membranes are employed for these membrane-based gas separation processes.

Membrane-based separation processes are also used for liquid separations. Typical examples are concentration and/or purification of the product as

well as in water and in wastewater treatment. They have a wide application range covering several industrial sectors, such as the chemical, food and beverage, and diary industries. They are also applied in fermentation (and biotechnology) and in wastewater treatment. Liquid separation using membranes can mainly be divided in two groups: one where there is a phase change and one where there is not. Pervaporation and membrane distillation are examples of liquid separation using membranes with phase change, while nano- and microfiltration are examples of liquid separation using membranes without phase change. In this work, however, we focus on liquid separation using membranes with phase change. The membranes used in these processes are classified according to the nature of the separation being performed. Hydrophilic membranes are used to remove water from organic solutions. These types of membranes are typically made of polymers with glass transition temperatures above room temperatures. Polyvinyl alcohol is an example of a hydrophilic membrane (i.e., as assisting structured material). Organophilic membranes are used to recover organic chemicals from solutions. These membranes are typically made up of elastomer materials (polymers with glass transition temperatures below room temperature). The flexible nature of these polymers makes them ideal for allowing organic compounds to pass through. Examples of this type of polymeric membranes are nitriles, butadiene rubber, and styrene butadiene rubber [6].

3.02.2.1 Design Problem Definition

Given the details of the feed mixture and the product (in terms of product purity or recovery), determine the required degree of separation (e.g., in terms of permeability in a membrane-based separation) and then identify polymeric membranes that match this design target. Schematic diagram of a process with the use of structured materials is shown in **Figure 1**.

The different variables shown in the figure are explained below:

- $\underline{I}$, Inlet variables: Vector $\underline{I}$ defines feed inlet variables such as the feed flow rate, temperature, pressure, and composition.
- $\underline{X}$, Outlet variables: End-use product parameters are given by vector $\underline{X}$, for example, product composition, and purity.
- $\underline{Y}$, State variables: Vector $\underline{Y}$ represents the state variables such as temperature and pressure (process parameters).
- $\underline{P}$, Performance criteria: Vector $\underline{P}$ defines the performance criteria of the process, for example, product recovery and concentration factor as compared to the feed, which is normally a function of the outlet variables $\underline{X}$.
- $\underline{\theta}$, Properties of the assisting structured materials: The properties of the assisting structured materials that effect the process are defined by vector $\underline{\theta}$. These properties depend on variables defined by vector $\underline{d}$, which could be either state variables $\underline{Y}$ or microscopic structural parameters of the

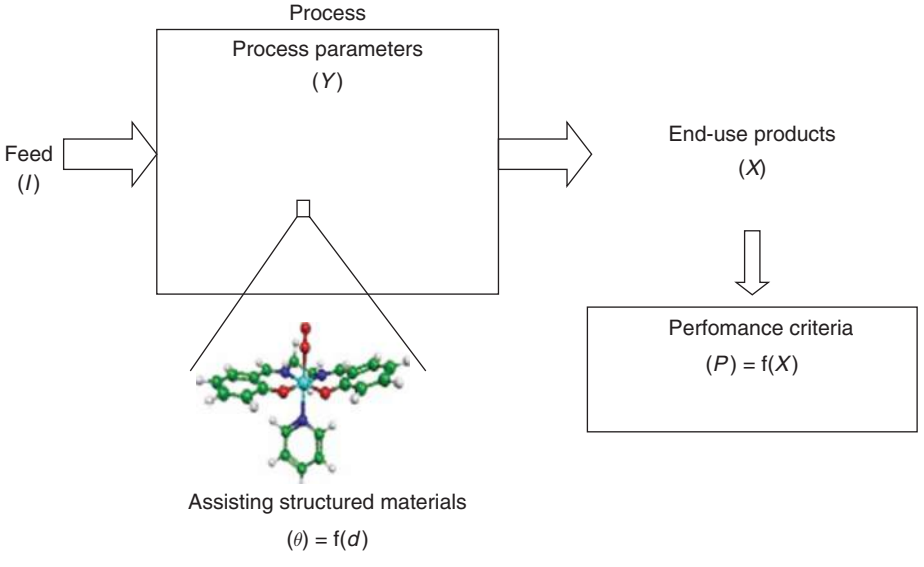

Figure 1 Schematic diagram of the process.

materials $\underline{S}$ (e.g., chemical structure, branch length/frequency if the material is made of polymer).

- $\underline{M}$, Geometry of the process unit: The performance of the process also depends on the geometry of the process module (defined by vector $\underline{M}$), for example, reactor geometry, membrane separator structure, like length or height of the module, thickness of the membrane or membrane area, co-current or counter-current flow, etc.

Based on the above definition of variables, the simultaneous design problem is defined as follows. For given feed conditions ($\underline{I}$), the objective is to design the process to match the desired performance criteria ($\underline{P}$) set by market or process demands for the end-use products. Therefore, for a known $\underline{I}$ and $\underline{P}$, the design variables could be related to the process conditions ($\underline{Y}$), the structural parameters of the assisting structured materials ($\underline{S}$), and/or the unit geometry ($\underline{M}$). For an already existing plant, due to economic reasons, it is sometimes not possible to alter the unit geometry or the structured materials. In such a case, the design variables would only be related to the process conditions, which will also have an impact on the properties of the structured materials in most cases.

In the case of a new process design, there is more freedom to choose the design variables. The design variables could be a combination of process and structured material parameters for simultaneous product-process design. In the case of the design of the structured material only (where design variables are only the parameters related to the structured material), the procedure requires to relate the end-use product targets to the properties of the structured material and then use the relation between the properties and the microscopic structural parameters to design the structured material.

3.02.2.2 Simultaneous Design Framework

The architecture of a general design framework for simultaneous process–product design is highlighted in **Figure 2**. The salient features of the design framework include model generation, model validation, and model application. Model generation involves development of all multilevel process and structured material property models. Once the models are developed, it is important to validate the models with experiments. The validated models can be employed for process and product design. In this work, this is done by using a reverse design

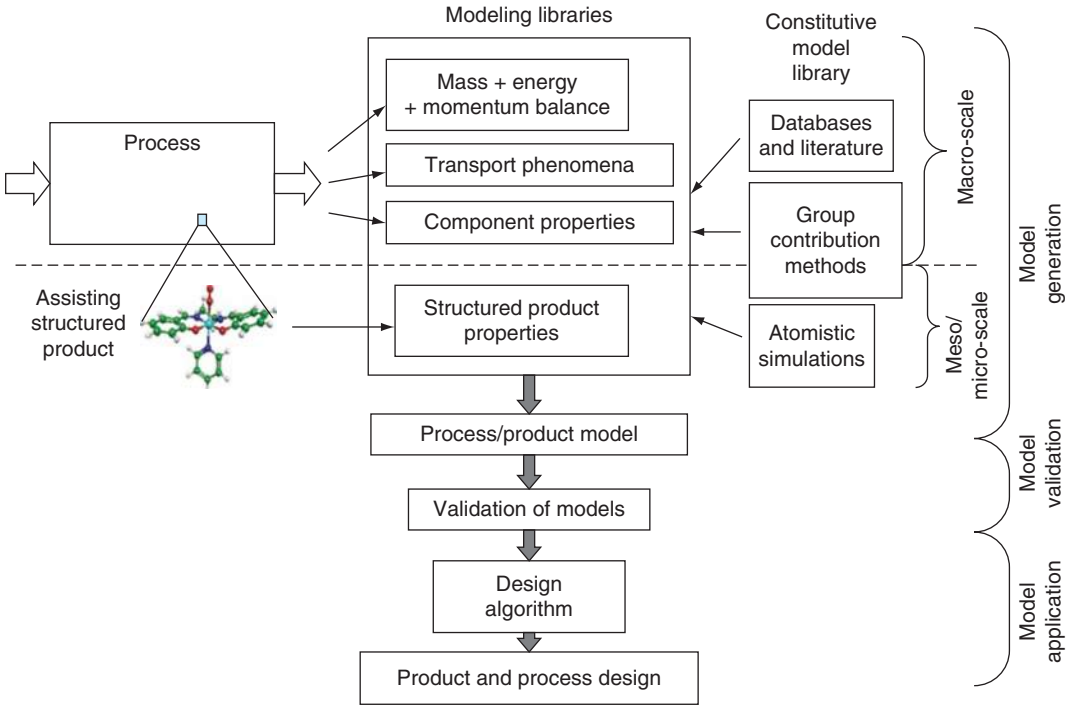

Figure 2 Architecture of a model-based design framework.

algorithm. All these features are explained in the subsequent sections.

3.02.2.2.1 Need for a systematic model-based design framework

Most process–product design problems are solved on an experiment-based trial and error procedure. While they provide validation of the process–product, they are time consuming, expensive, and do not guarantee an optimal product or use of a wide search space. Validated models coupled with easy generation of models and their flexible use for purposes of design can eliminate some of the time and expenses in process–product development. As highlighted in **Figure 2** of the model-based design framework, a systematic design for the simultaneous process–product design is shown. The process models and the product models could be of different scales that need to be solved simultaneously. It is thus important to have a framework that gives a stepwise procedure to solve different levels of interdependent models with relevant design algorithms together in a way that leads to a simultaneous process and product design with computational ease.

A design framework, including macro-scale process models and meso-/micro-scale models for properties of structured materials, has been developed (**Figure 2**). The model-based design framework divides the design technique into a subset of tasks corresponding to model generation, model validation, and model application step in a systematic way. Various components of this design framework are explained in the subsections below.

3.02.2.2.2 Multilevel modeling

For a model-based product–process design procedure, it is required to develop or obtain a rigorous process model that relates the raw material conditions, process conditions, component properties, flow behavior, transport phenomena, structured material properties, equipment geometry, etc. Process models may be considered to be composed of balance equations (mass, energy, and momentum), constitutive equations, and conditional equations [7] (equilibrium, controller, and defined relations). The constitutive models may include physical and chemical properties of the chemical species present in the system or phenomena models and their dependence on the process conditions. Another kind of constitutive models could be the property models for the structured materials giving the properties as a function of their structure.

As mentioned in the section above, there is a need to integrate different levels of process and product models in one framework in order to perform simultaneous process–product design. For a process shown in **Figure 1**, various equations, variables, constitutive models, etc., are enumerated below:

- Balance equations: For a given boundary for a process, balance equations can be derived based on mass, energy, and momentum conservation principles. For any given process (see **Figure 1**), if state variables such as temperature, pressure, and composition are defined by vector $\underline{Y}$, then the balance equations can in general be written as

$$\frac{\mathrm{d}\,Y}{\mathrm{d}z} = f\left(\underline{Y}, \underline{X}, \underline{\theta}, \underline{I}, \underline{M}, \underline{\xi}\right) \tag{1}$$

  which are subject to

$$\mathrm{IC}: \underline{Y}(z=0) = \underline{Y}_0 \tag{2}$$

$$\mathrm{BC}: \underline{Y}(z=z_{\mathrm{end}}) = \underline{Y}_z \tag{3}$$

  where z is the independent variable, that could be time or space, vector $\underline{X}$ is the outlet variables, vector $\underline{\theta}$ is structured material properties, vector $\underline{I}$ is inlet (feed stream) variables, vector $\underline{M}$ is variables related to geometry of the process unit, and vector $\underline{\xi}$ is the chemical and physical properties of the various chemical species in the system. For the evaluation of the balance equations, there is a need for evaluating different variables and integration of different scales of constitutive models. The balance equations give profiles of composition, temperature, pressure, etc., with respect to time and/or space.
- Control/definition equations: These are normally conditional equations, for example, equilibrium, control, or defined relations [7]. Another example of control/definition equations are the equations defining the performance criteria of the process, such as product recovery or concentration factor as compared to the feed, given in terms of the outlet variables. All these conditions must be satisfied in order to obtain a feasible design. The performance criteria $\underline{P}$ is usually a function of the outlet variables $\underline{X}$:

$$P = f(X) \tag{4}$$

- Constitutive equations 1: *Component properties* – From Equation (1) it can be noted that the process model needs the evaluation of some chemical and physical properties of the chemical species (defined by $\underline{\xi}$)

present in the system. These properties could be, for example, the density, viscosity, activity coefficients, specific heat, molecular weight, or vapor pressure. $\underline{\xi}$ are generally functions of state variables $\underline{Y}$ and chemical formula ($\underline{c_f}$), and since these states may change over time and/or space (see Equation (1)), the property models should also be functions of the rate of change of the state variables:

$$\xi = f\left(Y, c_f\right) = f(T, P, x, cf) \tag{5}$$

In this work, the pure component properties have been estimated using property models based on group contribution methods. In these models, the property of a compound is estimated as a summation of the contributions of the functional groups such as CH_3, CH_2, OH, etc., which can occur in the molecular structure [8]. The general form of this type of models is

$$f\left(\underline{\xi}\right) = \sum\nolimits_i (N_i C_i) + \sum\nolimits_j \left(M_j D_j\right) + \sum\nolimits_k (O_k E_k) \tag{6}$$

where $f(\underline{\xi})$ is a property function for the property $\underline{\xi}$ to be estimated, N_i, M_j, and O_k are numbers of time of first-, second-, and third-order groups i, j, and k appearing in the molecular structure representation, respectively. C_i, D_j, and E_k are the corresponding group contributions for the property function $f(\underline{\xi})$. A list of other forms of property prediction methods that can be used can be found in Soni *et al.* [9].

- Constitutive equations 2: *Structured material property models* – The process performance depends on some key properties of the structured materials defined by vector $\underline{\theta}$. These properties could be reaction rate constants or dissociation constants for reactive systems; driving forces for distillation or liquid–liquid extraction; thermodynamic or kinetic properties for solution diffusion-based separation; selectivity of solvents for solvent-based separation; and polymer structure-related properties (e.g., porosity and tortuosity) for membrane-based separation. The property parameters $\underline{\theta}$ in turn depend on variables $\underline{d}$, which could be either a function of the process variables Y or a function of microscopic structural parameters of the structured materials $\underline{S}$. This dependence of properties on structure or process variables is usually given in the following generic form:

$$\theta = f(\underline{d}) \tag{7}$$

Soni *et al.* [9] propose three different calculation approaches to obtain properties $\underline{\theta}$ as a function of process variables or variables related to the structured materials (Equation (7)):

1. Extensive literature survey where property values are readily available for specific structured materials that could be either experimentally measured or predicted from empirical models. These types of models can only be used for materials listed in the databases.
2. Group contribution models, where variables $\underline{d}$ are the values of the weights of the groups that form the chemical formula of the structured material. This approach provides more freedom to choose the product composition and the ability to design the structured material with more versatility compared to a simple database search.
3. The properties, as mentioned earlier, are intimately related to not only its chemical composition but also molecular conformation. For most structured materials, experimental techniques to measure the needed properties may not exist or could be very expensive and time consuming. Theoretical and simulation advances along with the developments in computational technologies are now making it possible to address the design challenges related to novel materials through advanced atomistic simulations [10].

Once property data have been obtained using atomistic simulations for different structures and process conditions, closed-form models relating the properties with structures and architectures of the materials could be obtained by regression [11].

3.02.2.2.3 Solution approaches

For the simultaneous process–product design, the widely used conventional design algorithm is designated in this chapter as the forward solution approach. Due to obvious limitations in the use of this solution approach such as being computationally expensive and iterative in nature, a new reverse design approach is proposed. The reverse solution approach (reverse algorithm) splits the design procedure into two stages, hence solving different scales of models separately and thereby making the design procedure computationally simpler and more efficient. The two algorithms are compared with each other below.

The model has N equations, where $N = N_N + N_P + N_{SM}$ (N_N being the process equations, N_P the performance equations, and N_{SM} the structural

material property equations), with M variables (out of which M_X are number of output variables, M_Y are number of process variables, M_I are number of input variables, M_θ are number of structural material property variables, M_M are number of process geometry variables, and M_ξ are number of chemical species property variables). The degrees of freedom is $DF = M - (N_N + N_{SM})$, which means that D_F variables out of M_X, M_Y, M_I, M_θ, M_M, and M_ξ must be specified to solve the $N_N + N_{SM}$ model equations.

In the forward approach, M_X, M_Y, M_θ, M_M, and M_ξ are calculated for given values of M_I and M_M. Using the calculated values of $\underline{X}$, the specified values of $\underline{P}$ are checked (through N_P equations). If they do not match, new sets of M_I and/or M_M are specified and the procedure is repeated.

In the reverse approach, from the specified values of $\underline{P}$, using N_P performance equations N_P number of outlet variables (e.g., $\underline{X}_{NP}$ out of total $\underline{X}$ outlet variables) are calculated. This means that M_{XNP} variables (calculated from N_P equations) are no longer unknown variables in the original $N_N + N_{SM}$ equation set. So, for the original model, the number of equations and variables has not changed but M_{XNP} variables that were originally unknown have now become known variables in the model. This means that since the number of unknown variables in the original model is the same, M_{XNP} number of variables from the solved N_P equations are now specified to calculate the structured material property variables (giving values of the target property variables $\underline{\theta}$).

The common requirements for both the algorithms are the availability of process models, identification of the design variables, setting the performance criteria for the end-use products, identification of the key properties of the structured material, and availability of the property models for the key properties. Once data (information) for all of these have been obtained, either of the design algorithms can be used.

Forward design algorithm: The forward design algorithm is described below in terms of the sequential calculation steps (work flow).

- Step I: For a given feed $\underline{I}$ and performance criteria $\underline{P}$, obtain the process model and identify the process design variables ($\underline{d}_1$) and the structured material design variable ($\underline{d}_2$).
- Step II: Choose the process conditions ($\underline{d}_1$) and the structured material ($\underline{d}_2$) that could be used for this process. This fixes the design variables ($\underline{d}_2$) as the structure of the structured material $\underline{S}$ is fixed through the selection of the material.
- Step III: Calculate the properties of structured material ($\underline{\theta}$) using the property models embedded in the process model, where properties are a function of $\underline{S}$ and/or process conditions.
- Step IV: Solve the process model to determine the values of the outlet variables $\underline{X}$.
- Step V: Compare the calculated ($\underline{X}$) against the performance criterion ($\underline{P}$). If the criteria are satisfied, stop. Otherwise, repeat from step II.

The new set could have different process conditions, different structure of the structured material or a completely different structured material. This procedure should be repeated until the desired performance criterion $\underline{P}$ is achieved.

Reverse design algorithm: In contrast to the forward approach, the reverse approach [11] employs two design stages and one validation stage. In the first stage only the process model is solved, whereas in the second stage the property models for the structured material are solved independently of the process models. The work flow for the reverse design approach is described below in terms of the sequential steps:

- Stage A: Setting the design targets.
- Step A-I: Similar to forward design algorithm, for a given feed $\underline{I}$ and performance criterion $\underline{P}$, the first step is to obtain the rigorous process model and identify the design variables.
  - Step A-II: Calculate the outlet variables ($\underline{X}$) using the values of the performance criteria ($\underline{P}$).
  - Step A-III: Calculate the target property values, defined by $\underline{\theta}_{target}$, with specified inlet and outlet variables.
- Stage B: Matching the design targets.
  - Step B-IV: Use different property models to identify the structured materials that match the design targets ($\underline{\theta}_{target}$) for the properties. In this stage, an extensive database search could also be made to identify the structured material with ($\underline{\theta}_{target}$) property values.
  - This procedure gives a set of options for the structured material and the best choice is made based on if the material is readily available or is a new material. At this point, it is also important to investigate if it is feasible

to manufacture the structured material economically.

- Stage C: Validating the design.
  - Step C-V: Validate the different selection from step B-IV, through rigorous simulations.

Comparison of algorithms: Forward design algorithm is essentially a trial and error procedure. For each proposed design in terms of process variables (process design) or variables related to the structured material (product design), the process model has to be solved iteratively. All the steps of the algorithm have to be repeated until one of the proposed designs matches the performance criteria. Depending on the choice of the structured material, there may or may not be any solution. In the case of reverse design algorithm, however, the structured material property variables are unknown variables when solving the process model. For a given feed and performance criteria, values of these variables are calculated from the process model. Therefore, there is no trial and error or iterations required to match the performance criteria.

With the forward design approach, since the properties of the structured material chosen need to be evaluated during the solution of the process model, the constitutive model for these properties is embedded in the process–product model. It should be noted that the constitutive model must be specified before the solution can be attempted. Therefore, the design depends on the choice of this model. In contrast, the reverse design algorithm is independent of the choice of the constitutive model. In the second stage of the algorithm, as many constitutive models as available, are used (including databases) to predict the structure of the material matching the target (design) properties ($\underline{\theta}_{target}$). From the calculated (matched) values of the structured material property variables, the inlet variables, and the known outlet variables, values of all other process variables are back-calculated.

Another disadvantage of having the property models embedded in the process model is that it may become computationally demanding to solve both models together. For instance, for pervaporation process the key property that affects the solution diffusion mechanism is permeability. Its calculation generally needs diffusivity and solubility data, which for a given component/polymer system can be predicted by using a group contribution method. The above-mentioned calculations depend on the composition, temperature, and pressure at each spatially discrete point of the membrane module. Consequently, incorporating them in the membrane model, when possible, is not simple. On the other hand, in the reverse design algorithm, many polymers may be designed (identified) without having to repeatedly solve the membrane process model coupled with the corresponding polymer property model.

3.02.3 Synthesis Design of Hybrid Processes

The design of hybrid process schemes where reaction (R) and separation (S) operations are combined into R–S and S–S hybrid process schemes is considered, as illustrated in **Figure 3**. The objective is to identify the best-possible hybrid process configuration for R–S and S–S systems with desired targets for improvements (or enhancements) in addition to the original process constraints. The process enhancements could be defined, for example, in terms of

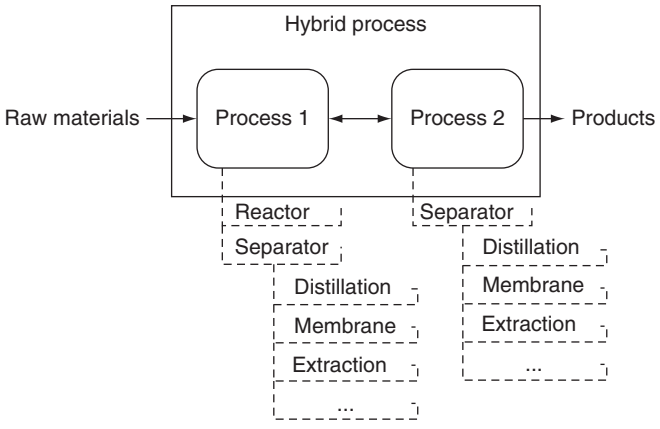

Figure 3 Schematic representation of the hybrid process with R–S or S–S options.

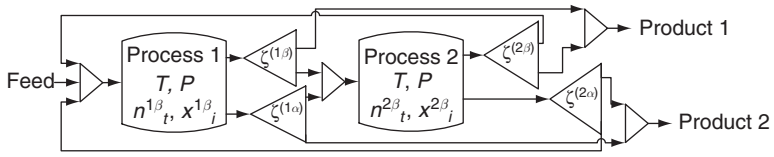

Figure 4 Superstructure for a hybrid process flowsheet.

higher product yield, faster reaction time, better selectivity in reaction operations, and/or higher product purity, lower energy consumption, and lower environmental impact for separation operations. Note that it is not possible to achieve the desired process enhancements (design targets) if the reaction or separation operations are performed individually. **Figure 4** illustrates a superstructure of hybrid schemes consisting of all possible combinations of reaction and separation operations.

3.02.3.1 Problem Definition

Given the details of the feed materials and the desired process objectives, determine the feasible set of hybrid process schemes that can satisfy all the process and operational constraints and then identify, from the feasible set, the hybrid scheme that best matches the desired design target of process performance enhancement. Also, consider the use of a membrane-based separation technique in different hybrid process schemes. The process enhancements may be established in terms of reaction operation parameters (such as product yield and reaction time) and/or separation operation parameters (such as product purity, separation efficiency, and energy consumption).

3.02.3.2 Model-Based Framework

As shown in **Figure 5**, the framework consists of three stages: (1) hybrid process design and analysis, (2) process implementation (including experimental setup), and (3) process-model validation.

3.02.3.2.1 Hybrid process design and analysis (stage 1)

For the first stage, a systematic model-based methodology for process design and analysis of hybrid reaction–separation (R–S) and separation–separation (S–S) systems has been developed. This methodology consists of four main steps as highlighted in **Figure 5**, which also shows the data flow and the computer-aided tools used. Only reactions in liquid phase are considered. The main steps of the methodology are described below.

Step 1a-S. Separation data analysis: The objective of this step is to gather available information about the given mixture which needs to be separated with or without the occurrence of reaction(s). The mixture is analyzed in order to identify the physical boundaries defined in terms of temperature, pressure, and/or composition, within which the separation operations may take place. The analysis consists of identification of mixture type, analysis of pure component properties for the chemicals present in the system, and an analysis of the mixture properties within the defined physical boundaries.

Based on the information of chemicals present in the mixture to be separated, it is classified as ideal or nonideal (for example of type: polar, aqueous, electrolyte, polymer, etc.) in order to select the appropriate thermodynamic property models and to establish the data needed for the pure component and mixture property analyses. The method used is the knowledge-based system developed by Gani and O'Connell [12] for the selection of appropriate thermodynamic property models.

An initial estimate of the system boundaries is quickly established through an analysis of the pure component properties of the chemicals present in the system. For example, knowledge of boiling points and melting points helps establish the liquid-phase region in terms of temperature at a specified pressure. A liquid phase is likely to exist at a temperature, which is higher than largest pure component melting point and lower than the lowest pure component boiling point. Information on mutual miscibility plays an important role in reactor and separation process design. Through the evaluation of the solubility parameters (Hansen and/or Hildebrandt), it is possible to establish existence of phase split. In this case, a database of pure component properties may be used together with pure component property prediction software to fill in the gaps in the properties database.

The mixture analysis is needed to establish the available driving forces that may be used for

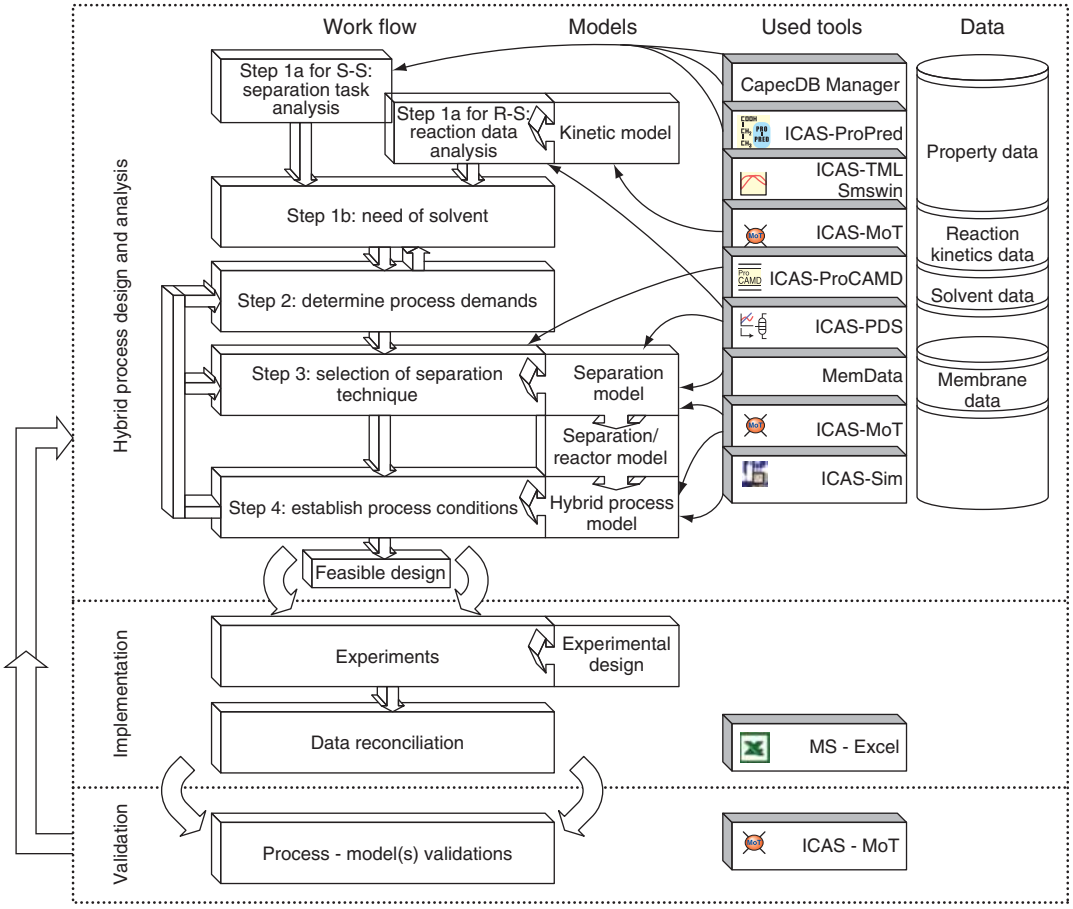

Figure 5 Framework with data flow and associated computer-aided tools.

different separation techniques, feasibility of the use of some separation techniques, and the data (and/or models) needed for separation process synthesis and design. First a list of all binary pairs of chemicals from the mixture to be separated is prepared. Then each binary pair is ordered according to the driving force (calculated with available data and/or model). Based on this list, a list of feasible separation techniques and/or binary pairs for which solvents or membranes may be used for achieving the desired separation is identified. In this case, if data for ternary systems are also collected, they will help evaluate the predictive power to the selected property model. If performance of the selected thermodynamic models is not acceptable, the model parameters are re-estimated or fine-tuned.

Step 1a-R: Reaction analysis: This step is necessary only when reactions occur within the process. Appropriate reaction data need to be collected and/or retrieved from a database. The reaction data need to establish the following: number of reactions and for each reaction, the reaction stoichiometry, the reaction form (kinetics or equilibrium; exothermic or endothermic), the reaction conditions (temperature, pressure, and phases involved) as well as known conversions or yield, and mode of operation (batch or continuous). Based on the reaction data, the design target for the hybrid process may be established – for example, the product yield must be higher than what a single reactor operation (i.e., without the R–S combination) may achieve. In the absence of experimental data, the reaction composition at chemical equilibrium for a given initial composition, temperature, and pressure can be computed by means of the reactive flash calculation procedure proposed by Pérez-Cisneros *et al.* [13]. If experimental data are available, the calculated values are compared with experimental data.

Step 1b. Establish need for solvent and/or membrane: In this step, the influence of solvents in the reaction is

considered in terms of whether a solvent is necessary or not. Generally, the use of an inert solvent might be considered if the reaction mass efficiency is smaller than 80% [14, 15]. The product yield is increased through the use of an appropriate solvent. For example, solvents are used to create a second phase with the product or precipitation of the product, or to dissolve the reactant(s). Also, when an undesired reaction occurs in the reaction system, a solvent creates another phase with the by-product. In nonreactive separation tasks, solvents might be needed for those binary pairs (from step 1a-S) which have been identified as infeasible with conventional techniques such as distillation. In these cases, solvent- or membrane-based separation techniques may be used. Typically, binary pairs that form azeotropes or close-boiling are good candidates for separation by solvents or membranes. Also, removal of a chemical from a liquid or gas mixture or removal of solids, membrane-based separation techniques may be used.

Step 2. Determine process demands: The objective of this step is to define the process demands based on the choice of the mode of operation – batch or continuous. This choice is made based on, among others, production rate and residence time. Also, process performance criteria (design targets) are defined in terms of desired product purity, reaction conversion, process yield, and processing time (in case of a batch process), which are used in the next steps to evaluate the generated process operation scenarios.

Step 3S. Selection of separation technique. In this step the separation techniques to be combined with either another separation task or a reaction task for the hybrid scheme are identified. The steps to follow are different for the S–S and R–S combinations. For hybrid S–S schemes, the following five-step procedure is used:

S3.1. Generate and/or collect data of phase compositions for the separation methods that are to be considered. Start the analysis by checking the feasibility of employing distillation for the specific separation task. List all components with their relative volatility, α_{ij}, values and rank the compounds in terms of their normal boiling point values. Retrieve vapor–liquid equilibrium data for each binary pair (already established in step 1a-S). If step 1a-S pointed to the need for solvents, the three-stage method for solvent selection as given by Harper and Gani [16] is employed, and for selected the solvent(s) and separation technique (such as liquid–liquid extraction or extractive distillation), the necessary (separation) equilibrium data are generated.

Also, for these separation tasks, data from the membrane database are retrieved; other sources of data are considered; or, the model-based design of membrane-based separation (see Section 3.02.2) is considered for each binary pair to determine if use of any membrane-based technique is feasible. If yes, data (such as compositions in the feed and the permeate or the retentate) related to the separation characteristics for the specific membrane-based operation are collected and/or generated.

S3.2. Calculate and plot all driving forces for each identified separation method and separation task (corresponding to the binary pair of compounds from step S3.1). The driving force, as defined by Bek-Pedersen and Gani [17], is the difference in compositions of compound i in two coexisting phases and is described by

$$\mathrm{FD}_i = \left|x_i^1 - x_i^2\right| \tag{8}$$

S3.3. Screen for feasible solutions. A feasible solution is characterized as having the driving force value more than zero in the entire separation operation region. In other words, it does not have any separation boundaries such as an azeotrope (where the driving force is zero). If at least one of the driving force curves is feasible in the entire separation region, combine it with other separation techniques which also have larger driving forces within the concentration range of interest. For example in the separation of binary mixture presented in **Figure 6**, neither of the separation methods (distillation and pervaporation) can alone achieve the desired high-purity product streams because both techniques have their own limitations. However, by combining distillation with pervaporation, it is possible to achieve the desired high-purity product streams (in this case, dehydrated ethanol).

S3.4. Feasible combinations obtained in the previous step are analyzed by the use of the derivative (FD_x) of driving force with respect to the key components. These derivatives identify the region where the individual separation technique becomes inefficient, indicated by the occurrence of a local minimum along the composition axis. However, since the objective is to design a process with

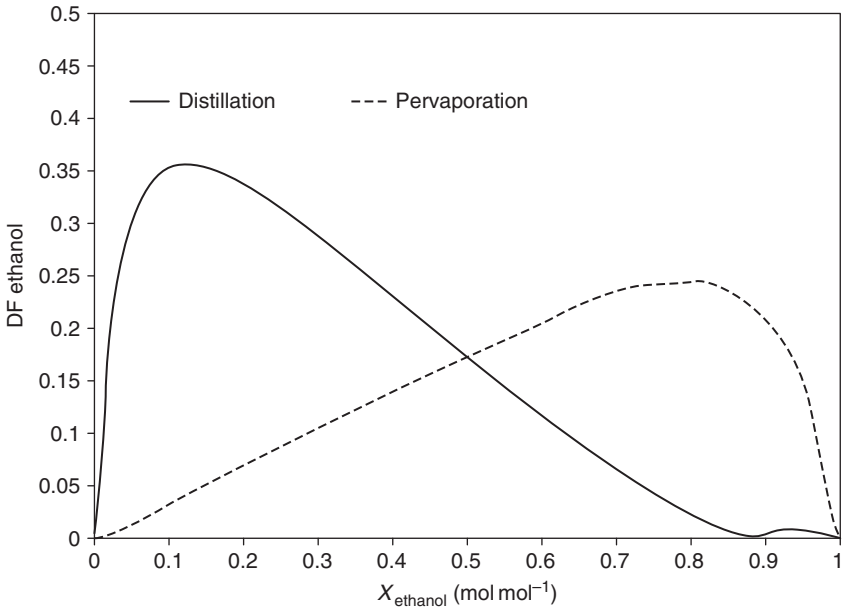

Figure 6 Driving force for feasible combination between distillation and pervaporation.

the largest driving force, a separation technique (e.g., *A*) may be considered with a separation technique (e.g., *B*) if at the same composition, separation technique *B* has a larger absolute value for FD_x than for separation technique A [18, 19]. For example, consider the separation of a binary mixture of water and acetic acid. The derivative FD_x (see **Figure 7**) for distillation (bold line) has a local minimum between $x_{H2O} = 0.80$ and 0.90. The FD_x value for pervaporation (dashed line in **Figure 7**) for the same composition range has a larger absolute value. Therefore, it is beneficial to combine distillation and pervaporation into a hybrid scheme in such a way that pervaporation is used to separate mixture from $x_{H2O} = 0.80$ to at least $x_{H2O} = 0.90$.

S3.5. Plot all feasible combinations (hybrid schemes) to identify those that are able to use the largest available driving force. Prepare a list in terms of descending driving forces used, for evaluate, selection in step 4.

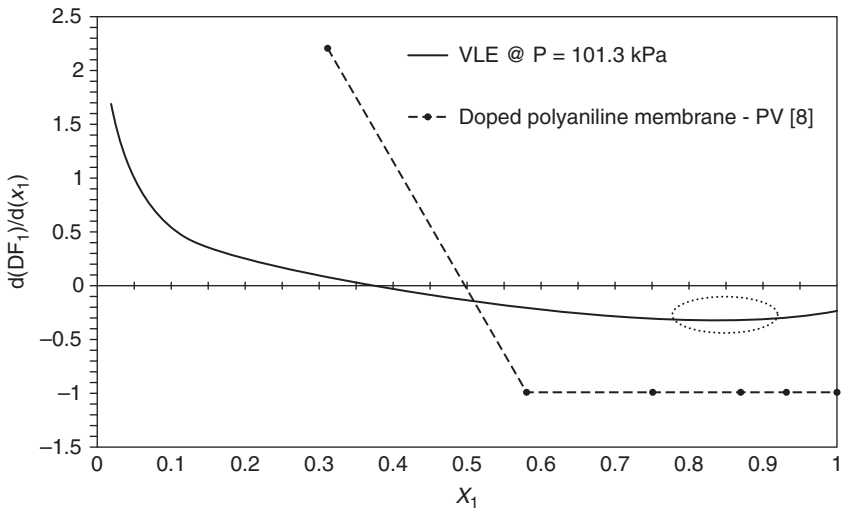

Figure 7 Derivative driving force for water–acetic acid mixture.

Step 3R. Selection of separation technique for R–S scheme: For hybrid reaction–separation schemes, the following five-step procedure is proposed. The objective here is to identify the compounds whose removal will enhance the reaction and, based on this, to select suitable separation techniques for the given reaction system.

R3.1. Based on reaction kinetics and identified mixture boundaries in step 1, identify reaction products whose selective removal will increase the conversion of reaction. In the case of multireaction systems, identify products whose removal will slow down and/or even eliminate unwanted reaction(s).

R3.2. Check for feasibility of distillation to remove the product(s) from reaction mixture. List all components with their relative volatility, α_{ij}, and rank the compounds by their normal boiling point values. If the identified reaction product from the previous step (R3.1) is in the top or bottom of the list and relative volatility is greater than 1.05, then use of distillation is recommended for separation of the product from the reacting mixture.

R3.3. Retrieve data from the membrane database or other appropriate literature sources if information on a membrane-based separation performing the same task for the same or similar mixture is available. Collect data related to separation characteristics and, for each membrane separation, list all the components according to decreasing component flux. Select the membrane for which the component that needs to be removed from the mixture (identified in step R3.1) is at the top of the list. If there is more than one membrane satisfying the required conditions, select all of them in this step for future screening in step R3.5.

R3.4. Analyze the possibility of adding a solvent to (a) create a second phase which would extract product(s) from reactants or (b) promote precipitation of a product. At this step the solvent selection methodology given by Gani *et al.* [14, 15] is applied. Note that in the case of activity driven reactions, the solvent may also decrease product activity and therefore move reaction equilibrium toward the product(s).

R3.5. Compare all separation techniques obtained in steps R3.2–R3.4, calculate the driving forces between products, plot and identify the separation technique, which offers the largest driving force for the corresponding separation task and leads to the desired reaction operation enhancement.

A list of feasible combinations that may lead to feasible hybrid process schemes for S–S and R–S is given in **Table 1** in terms of process barrier.

Step 4. Establish process conditions: In this step, for the separation techniques identified in step 3 and from a superstructure of hybrid schemes (see **Figure 4**), different process scenarios are generated and evaluated using performance criteria specified in step 2. The superstructure of hybrid process

Table 1 Candidate processes for hybrid S–S and R–S schemes

Process barrier	*Hybrid scheme*	*Other process scheme*
Homogeneous azeotrope	Distillation and membrane	Extractive separation Pressure swing distillation Pressure distillation
Heterogeneous azeotrope	Distillation and membrane	Azeotropic distillation Liquid–liquid extraction Distillation and decanter
Low relative volatility	Distillation and membrane	Extractive separation
Eutectic point	Crystallization and distillation/extraction (MSA required)	-
Removal of undesired compound(s)	Distillation/extraction and external agent[a] Membrane-based separation	-
Reaction equilibrium	Reactor and distillation (reactive distillation) Reactor and membrane (membrane reactor) Reactor and extraction Reactor and distillation with membrane	-

[a] External agent might be catalyst, adsorbent, or membrane.

schemes consists of two processes, process 1 and process 2, which are linked by four connectors, namely, $\xi^{1\alpha}$,$\xi^{1\beta}$,$\xi^{2\alpha}$, and $\xi^{2\beta}$. In this superstructure, each constituent process is allowed a maximum of two outlet and three inlet streams. Each constituent process corresponds to the single separation process where inlet streams are separated into two product streams. Each stream in **Figure 4** represents the chemicals present in the system and their corresponding molar flow rate.

3.02.3.2.2 Implementation (stage 2)

This stage is needed if the hybrid schemes from stage 1 need to be verified by experiment. In this case, an experimental setup needs to be built using the design data from stage 1. Note, however, that if and when experimental data are available, it is not necessary to perform experiments. Experiments need to be carefully planned in order to verify not only hybrid process schemes but also constitutive models such as reaction kinetics, component flux through the membrane, and phase equilibrium. The quality of the experimental data needs to be checked by formulating a proper data reconciliation problem.

3.02.3.2.3 Validation (stage 3)

In this stage a final validation is made by comparing model-based simulation results with experimental data if available (or collected in stage 2). Based on available experimental data, the model parameters may also be adjusted. The ultimate objective is to identify the hybrid scheme that best satisfies the process demands set in step 2.

3.02.3.3 Generic Model for a Hybrid Process

A simple generic model for any hybrid process represented by the superstructure (see **Figure 4**) has been developed. The model consists of mass and energy balance equations and connection equations. Depending on operation mode, batch, or continuous operations (selected in step 2), dynamic or steady-state models are generated for each process operation scenarios. Dynamic model is used when batch or semi-batch processes are considered, or when the effect of disturbances on the process variables needs to be investigated or when changes in any of the inlet or outlet streams change in time, namely

$$F_i^{1\text{in}} = f(t) \vee F_i^{2\text{in}} = f(t) \vee F_i^{1\alpha} = f(t) \vee F_i^{1\beta} = f(t) \vee F_i^{1\alpha} = f(t) \vee F_i^{2\beta} = f(t)$$

or for nonisothermal process operation, or if heat addition or heat removal is required. If steady-state analysis is needed, the corresponding process model is obtained by setting the left-hand side (LHS) of Equations (9) and (10) to zero.

Mass balance for compound i:

$$\left[\frac{\partial n_i}{\partial t}\right] = \left[\xi^1 \xi^{1\text{in}} F_i^{1\text{in}}\right] + \left[\xi^2 \xi^{2\text{in}} F_i^{2\text{in}}\right] - \left[\xi^1 \xi^{1\alpha} F_i^{1\alpha P}\right] - \left[\xi^1 \xi^{1\beta} F_i^{1\beta P}\right] - \left[\xi^2 \xi^{2\alpha} F_i^{2\alpha P}\right] - \left[\xi^2 \xi^{2\beta} F_i^{2\beta P}\right] - \left[\xi^R \left(\xi^{(\text{homog})} \sum_{k=1}^{NKR} \nu_{i,k}^{1\alpha} r_k^{1\alpha(\text{homog})} + \xi^{(\text{heterog})} \sum_{b=1}^{NKRb} \nu_{i,b}^{1\alpha} r_b^{1\alpha(\text{heterog})}\right)\right] \tag{9}$$

Energy balance:

$$\left[\frac{\partial H}{\partial t}\right] = \left[\xi^1 \xi^{1\text{in}} \sum_{i=1}^{NC} F_i^{1\text{in}} h_i^{1\text{in}}\right] + \left[\xi^2 \xi^{2\text{in}} \sum_{i=1}^{NC} F_i^{2\text{in}} h_i^{2\text{in}}\right] - \left[\xi^1 \xi^{1\alpha} \sum_{i=1}^{NC} F_i^{1\alpha P} h_i^{1\alpha P}\right] - \left[\xi^1 \xi^{1\beta} \sum_{i=1}^{NC} F_i^{1\beta P} h_i^{1\beta P}\right] - \left[\xi^2 \xi^{2\alpha} \sum_{i=1}^{NC} F_i^{2\alpha P} h_i^{2\alpha P}\right] - \left[\xi^2 \xi^{2\beta} a \sum_{i=1}^{NC} F_i^{2\beta P} h_i^{2\beta P}\right] + [Q_1] + [Q_2] \tag{10}$$

The existence of process 1 and/or process 2 is described by decision variable $\xi^1$and ξ^2. The outlet streams from process 1 are defined in terms of molar fraction $x_i^{1\alpha}$,$x_i^{1\beta}$ and outlet total molar flow rates $F_{\text{TOT}}^{1\alpha}$,$F_{\text{TOT}}^{1\beta}$ (defined by the designer):

$$F_i^{1\alpha} = a\xi^1 x_i^{1\alpha} F_{\text{TOT}}^{1\alpha}) \tag{11}$$

$$F_i^{1\beta} = a\xi^1 \xi^\beta x_i^{1\beta} F_{\text{TOT}}^{1\beta} \tag{12}$$

ξ^β defines existence of a second phase (β) in process 1. The component composition in process 1 depends on the separation factors $\sigma_i^{1\alpha}$ and $\sigma_i^{1\beta}$:

$$x_i^{1\alpha} = \frac{\sigma_i^{1\alpha} n_i}{\sum_{i=1}^{NC} \sigma_i^{1\alpha} n_i} \tag{13}$$

$$x_i^{1\beta} = \frac{\sigma_i^{1\beta} n_i}{\sum_{i=1}^{NC} \sigma_i^{1\beta} n_i} \tag{14}$$

From mass balance around process 2, the outlet streams are defined by the component separation factors $\sigma_i^{2\alpha}$ and $\sigma_i^{2\beta}$:

$$F_i^{2\alpha} = \sigma_i^{2\alpha}\xi^2\left(\xi^{2\text{in}}F_i^{2\text{in}} + F_i^{1\beta R} + F_i^{1\alpha R}\right) \tag{15}$$

$$F_i^{2\beta} = \sigma_i^{2\beta}\xi^2\left(\xi^{2\text{in}}F_i^{2\text{in}} + F_i^{1\beta R} + F_i^{1\alpha R}\right) \tag{16}$$

Existence of streams $F_i^{1\text{in}}$ and $F_i^{2\text{in}}$ is defined by binary decision variables $\xi^{1\text{in}}$ and $\xi^{2\text{in}}$, which can either be 0 or 1. Other streams are defined by decision variables $\xi^{1\alpha}$, $\xi^{1\beta}$, $\xi^{2\alpha}$, and $\xi^{2\beta}$ which can vary between 0 and 1, and expressed as follows:

$$F_i^{1\alpha P} = \xi^{1\alpha}F_i^{1\alpha} \tag{17}$$

$$F_i^{1\beta P} = \xi^{1\beta}F_i^{1\beta} \tag{18}$$

$$F_i^{1\alpha R} = \left(1-\xi^{1\alpha}\right)F_i^{1\alpha} \tag{19}$$

$$F_i^{1\beta R} = \left(1-\xi^{1\beta}\right)F_i^{1\beta} \tag{20}$$

$$F_i^{2\alpha P} = \xi^{2\alpha}F_i^{2\alpha} \tag{21}$$

$$F_i^{2\beta P} = \xi^{2\beta}F_i^{2\beta} \tag{22}$$

$$F_i^{2\alpha R} = \left(1-\xi^{2\alpha}\right)F_i^{2\alpha} \tag{23}$$

$$F_i^{2\beta R} = \left(1-\xi^{2\beta}\right)F_i^{2\beta} \tag{24}$$

In cases where minimum concentration of compound(s) in process 1 is necessary to start process 2, an additional binary variable a is defined (see Equation (25)) which depends on switching time (t_{switch}):

$$a = \text{if}\ \ (t \geq t_{\text{switch}})\ \ \text{than}\ \ (1)\ \ \text{else}\ \ (0) \tag{25}$$

The reaction rate of homogeneous reaction ($r_k^{1\alpha(\text{homog})}$) in general can be expressed by the following law of mass action:

$$r_k^{1\alpha(\text{homog})} = k_p^{(\text{homog})}V^{1\alpha}\prod_{i=1}^{NRK}\left(a_i^{1\alpha}\right)^{v_{i,k}^{1\alpha}} \tag{26}$$

When heterogeneous catalyst is used the reaction rate is expressed in many cases in the form of pseudo-homogeneous reaction kinetics:

$$r_h^{1\alpha(\text{heterog})} = k_p^{(\text{heterog})}m_{\text{cat}}L\prod_{i=1}^{NRK}\left(a_i^{1\alpha}\right)^{v_{i,h}^{1\alpha}} \tag{27}$$

The component activity $\alpha_i^{1\alpha}$ is defined by

$$\alpha_i^{1\alpha} = x_i^{1\alpha}\gamma_i^{1\alpha} \tag{28}$$

The enthalpies of each inlet and outlet stream from the hybrid process scheme can be calculated:

$$\begin{aligned} h_i^j &= \int_{T_0}^{T_j} C_{p_i}\mathrm{d}T + \zeta^j\Delta H_{\text{vap},i}^j \\ &= \left|A_i\cdot T + \frac{B_i\cdot T^2}{2} + \frac{C_i\cdot T^3}{3} + \frac{D_i\cdot T^4}{4} + \frac{E_i\cdot T^5}{5}\right|_{T_0}^{T_j} \\ &\quad + \zeta^j\Delta H_{\text{vap},i}^j \end{aligned} \tag{29}$$

This simple model consists of 23·NC +NRK+NRKh+2 equations summarized in **Table 2** with 36·NC +NRK·NC+2·NRK+NRKh·NC+2·

Table 2 List of equations in general hybrid process model

	Equations	*Number of equations*
Mass balance	9	NC
Energy balance	10	1
Outlet streams from process 1 and process 2	11–12, 15–16	4 NC
Molar composition	13–14	2 NC
Relations between streams	17–24	8 NC
t_{switch} condition	25	1
Reaction kinetics (homog.)	26	NRK
Reaction kinetics (heterog.)	27	NRKh
Components activity	28	2 NC
Components enthalpy	29	6 NC
Total number of ordinary differential equations (ODEs): NC +1		
Total number of algebraic equations (AEs): 22 NC +NRK+NRKh+1		
Total number of equations: 23 NC +NRK+NRKh+2		

NC, number of components; NRK, number of independent homogeneous reactions; NRKh, number of independent heterogeneous reactions.

NRKh+3 variables, which are reported in detail in **Table 3**, where NC is the number of components, NKR and NKRh are the number of independent homogeneous and heterogeneous reactions which occur only in phase (α). The degree of freedom is therefore equal to 13·NC +NRK·NC +NRK+NRKh·NC+NRKh+33 (see **Table 3** for a list of these variables).

The specific hybrid process model is obtained from the generic model by specifying all the decision variables (see **Table 3**), substituting them in the model equations (Equations (9)–(29)) which eliminates some of the terms in balance equations and Equations (11)–(29). Therefore, the specific hybrid process model contains fewer equations and variables

Table 3 List of variables in general hybrid process model

		Number
Differential variables		
Molar hold-up in hybrid process	n_i	*NC*
Enthalpy hold-up	H	1
Algebraic variables		
Outlet streams of process 1 and process 2	$F_i^{1\alpha}$, $F_i^{1\beta}$, $F_i^{2\alpha}$, $F_i^{2\beta}$	4 NC
Product streams	$F_i^{1\alpha P}$, $F_i^{1\beta P}$, $F_i^{2\alpha P}$, $F_i^{2\beta P}$	4 NC
Recycled streams	$F_i^{1\alpha R}$, $F_i^{1\beta R}$, $F_i^{2\alpha R}$, $F_i^{2\beta R}$	4 NC
Reaction rate (homogeneous)	$r_k^{1\alpha(\text{homog})}$	NRK
Reaction rate (heterogeneous)	$r_k^{1\alpha(\text{heterog})}$	NRK
Molar fraction	$x_i^{1\alpha}$,$x_i^{1\beta}$	2 NC
Component activity	$a_i^{1\alpha}$, $\gamma_i^{1\alpha}$	2 NC
Other variable	a	1
Enthalpies of inlet and outlet streams	$h_i^{1\text{in}}$, $h_i^{2\text{in}}$, $h_i^{1\alpha P}$, $h_i^{1\beta P}$, $h_i^{2\alpha P}$, $h_i^{2\beta P}$	6 NC
Decision variables (specify)		
Existence of process 1 and process 2	ξ^1, ξ^2	2
Existence of outlet streams from process 1 and process 2	$\xi^{1\alpha}$, $\xi^{1\beta}$, $\xi^{2\alpha}$, $\xi^{2\beta}$	4
Existence of inlet streams	$\xi^{1\text{in}}$, $\xi^{2\text{in}}$	2
Existence of reaction	ξ^R	1
Type of reaction	$\xi^{(\text{homog})}$, $\xi^{(\text{heterog})}$	2
Existence of second-phase when reaction occurs	$\xi^{R\beta}$	1
Switching time	t_{switch}	1
Phase of the stream (liquid or vapor)	ζ^j	6
Parameters (specify)		
Inlet streams of process 1 and process 2	$F_i^{1\text{in}}$,$F_i^{2\text{in}}$	2 NC
Total flow rates of outlet stream from process 1	$F_{\text{TOT}}^{1\alpha}$, $F_{\text{TOT}}^{1\beta}$	2
Reaction volume	$V^{1\alpha}$	1
Mass of catalyst	m_{CAT}	1
Concentration of active sides	L	1
Separation factors	$\sigma_i^{1\alpha}$, $\sigma_i^{1\beta}$, $\sigma_i^{2\alpha}$, $\sigma_i^{2\beta}$	4 NC
Temperature in hybrid process	T^j	6
Energy added	Q_1, Q_2	2
Known variables (specify)		
Stoichiometric coefficients (homogeneous)	$\upsilon_{i,k}^{1\alpha}$	NRK NC
Reaction rate constants (homogeneous)	$k_{p,k}^{(\text{homog})}$	NRK
Stoichiometric coefficients (heterogeneous)	$\upsilon_{i,h}^{1\alpha}$	NRKh NC
Reaction rate constants (heterogeneous)	$k_{p,k}^{(\text{heterog})}$	NRKh
Heat of vaporization	$\Delta H_{\text{vap},i}$	NC
Liquid heat capacity	A_i, B_i, C_i, D_i, E_i	5 NC
Reference temperature	T_0	1
Total unknown variables	22 NC+NRK + NRKh +1	
Total number of differential variables	NC +1	
Total number of specified variables	13 NC+NRK NC+NRK+NRKh NC+ NRKh+33	
Total number of variables in model equations (9–29)	36 NC+NRK NC+2 NRK+NRKh NC+ 2 NRKh+35	

NC, number of components; NRK, number of independent homogeneous reactions; NRKh, number of independent heterogeneous reactions.

(that need to be specified) when compared to the generic model. Note however that the generated specific model employs separation factors that need to be set or defined through additional model equations in a different scale. The detailed derivation of a specific hybrid process model is highlighted in Appendix A.

3.02.4 Computer-Aided Methods and Tools

Two model-based frameworks [11,19] presented above employ various computer-aided methods and tools, which are summarized in **Table 4**. Since the model-based design framework is also a computer-based approach, a number of computer aided tools are employed. Note that the choice of the computational tools is specific to the design problem being solved. For the simultaneous design of membrane-based separation processes and polymers that can be used as membranes as well as hybrid process schemes, a list of computational tools that may be used are given in **Table 4**.

ICAS-MoT [20]: It is an equation-based modeling tool capable of handling steady-state simulations (models based on algebraic equations), lumped and/or dynamic system simulations (models based on differential algebraic equations), distributed systems simulation (models based on partial differential equations), steady-state optimization, and dynamic parameter optimization [20]. This modeling tool performs translation, solution, analysis, and validation of mathematical models. The generated models in this work have been solved through ICAS-MoT.

Pro-Pred [21]: It is a pure component property estimation tool [8] that predicts pure component primary properties (dependent only on the molecular structures of the chemical): secondary properties (dependent on other properties) and functional properties (dependent on temperature and/or pressure). The molecular description is given in several ways: by drawing the molecular structure; by providing the SMILES string; or by providing the mol.file. Several methods for prediction of properties are available [8, 22, 23]. Pro-Pred [23] was used for the estimation of pure component properties for various components involved in the case studies.

TML [24]: This tool is a thermodynamic model library (TML) for predicting thermodynamic properties of mixtures and is part of the integrated computer-aided system called ICAS [21]. For predictions of activity coefficients of compounds in liquid solution, TML has been used. The thermodynamic models library contains a wide range of G^E-based activity coefficient models and equations of state.

LAMMPS: LAMMPS, which stands for Large-scale Atomic/Molecular Massively Parallel Simulator, is a molecular dynamics program (LAMMPS: Distributed by Sandia National Laboratories, a US Department of Energy (DOE) laboratory).

Table 4 Computer-aided tools used in the framework

Name of tool	*Purpose*	*Used in*	*Reference*
CAPEC DB Manager	Retrieval of pure component properties and mixture properties	Step 1a-S	Nielsen and Gani [24]
ICAS-ProPred	Prediction of pure component properties based on various group contribution methods	Step 1a-S	Marrero and Gani [8]
ICAS-TML	VLE, LLE calculations. Estimation of thermodynamic model parameters.	Step 1a-S	Sales-Cruz and Gani [20]
SMSWin	VLE, LLE and SLE calculations.	Step 1a-S	Gani [21]
ICAS-MoT	Solution and analysis of user defined model.	Step 1a-S, Step 1b, Steps 3-4 Stage 3	Sales-Cruz and Gani [20]
ICAS-ProCAMD	Computer-aided tool for molecular and mixture design; used for solvents design.	Step 3	Gani [21]
ICAS-PDS	Reactive flash calculation.	Step 1a	Gani [21]
	Design and synthesis of distillation-based separation schemes.	Step 3	
MemData	Search of membrane-based separation used for mixture separation.	Step 3	Mitkowski [19]
ICAS-Sim	Process simulation and optimization.	Step 4	Gani [21]

LAMMPS has potentials for soft materials (biomolecules and polymers) and solid-state materials (metals and semiconductors) and coarse-grained systems. It can be used to model atoms or, more generically, as a parallel particle simulator at the mesoscale or continuum levels. LAMMPS runs on single-processor machines or in parallel using message passing techniques and a spatial decomposition of the simulation domain. The code is designed to be easy to modify or extend with new functionality. LAMMPS is distributed by Sandia National Laboratories, a US Department of Energy (DOE) laboratory. Extensive equilibration of trajectories for molecular modeling to predict permeability of different structures of polymers was done with LAMMPS.

Materials Studio 4.0: Material Studio by Accelrys is a computational tool for molecular modeling of structured chemical products. In this work it was used to predict the solubility and diffusivity of small gas molecules through polymers at different temperatures.

The CAPEC Database Manager [25] contains data of pure component properties, solid solubility data, and binary phase equilibrium data. It has an easy-to-use interface for data retrieval and search.

SMSwin [21]: SMSWIN is a software package developed at Syngenta and currently maintained, further developed and integrated with ICAS. SMSWIN performs many useful calculations with respect to pure component and mixture properties and phase diagrams. Currently, ProPred [21] and the KT-UNIFAC [21] model have been integrated with SMSWIN.

ICAS-PDS [21]: This is a special tool box for design and analysis of separation processes involving vapor–liquid phases with or without reactions. For reactive and nonreactive systems, PDS calculates phase envelopes, distillation boundaries, residue curves, as well as columns design for specified product recoveries. For reactive flash calculations, the element-based approach [13] is available in ICAS-PDS.

ICAS-utility [21]: This is a tool-box to generate and analyze mixtures with respect to their phase diagrams and single unit separation. It also calculates the driving force plots needed for separation task selection and design of separation processes.

MemData [19]: The separation characteristics data for membrane-based operations are available in the MemData database. The data consist of the type of membrane-based process, operational conditions, and compositions of separated mixtures, membrane characteristics, component permeability, component flux, reference, and many more. The data stored in the MemData have been collected from the open literature and have been organized for efficient search/retrieval of the needed data.

ICAS-Sim provides process simulation options, such as process simulation and optimization with generic models and/or generated specific models

3.02.4.1 Model Library

A number of membrane-based models are available in the model library. **Figure 8** gives an overview of the membrane-based models available through the

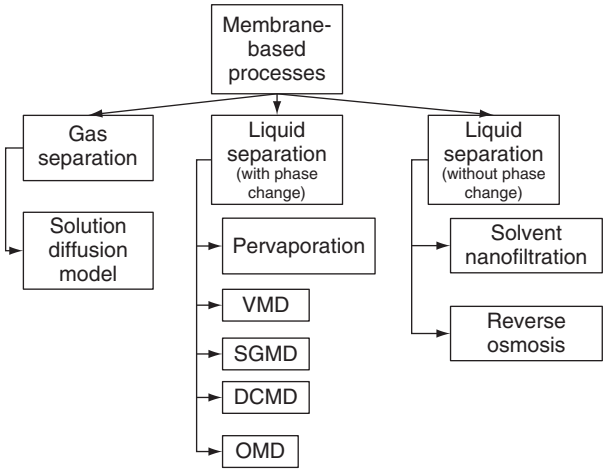

Figure 8 Models for membrane-based separation processes available in the model library of the framework (VMD: vacuum membrane distillation; SGMD: Sweeping gas membrane distillation; DCMD: direct contact membrane distillation; OMD: osmotic membrane distillation).

two frameworks [11, 19]. All the models listed in in the figure can be combined with other separation or reactor models through the generic model presented in Section 3.02.3.3.

3.02.5 Case Studies

Two case studies are presented here. The first involves the application of the simultaneous design of process and the structured material (polymeric membrane) highlighted through a conceptual case study (see Section 3.02.5.1). For additional details involving different membrane-based separation processes, the reader is directed to the paper of Soni *et al.* [9]. The synthesis design of an R–S hybrid process scheme is illustrated through a second case study (see Section 3.02.5.2) involving an esterificaton reaction combined with pervaporation to achieve a desired product yield. Here, the optimal hybrid process scheme has been verified by experiments. For more details, the reader is directed to the paper of Mitkowski *et al.* [26].

3.02.5.1 Simultaneous Design of Membrane and Separation Process – A Conceptual Study

A conceptual study to demonstrate the use of the design algorithms is presented in this section. In this case study, the model equations are solved using two different design algorithms and the differences in the solution steps are pointed out. The first step is to have the mathematical equations that constitute the process model. It is therefore important to define different types of equations (e.g., balance equations, constitutive equations, and constraint equations) and to identify different types of variables (e.g., differential variables, design variables, and known and unknown variables) associated to them. The model and variable analysis is an important step prior to model solution.

3.02.5.1.1 Design problem definition

For a given process, assisted by structured materials, the modeling goal is to determine the values of the design variables in the process that will satisfy the targeted performance criteria. The design variables are related to the process (process design) and/or the structured material (product design).

3.02.5.1.2 Model equations and characterizing variables

If $\underline{Y}$ represents the state variables that vary as a function of the dependent variable (time or space) within the process boundaries, then the balance equations can be derived from the laws of conservation of mass, momentum, and energy. For this conceptual study, the balance equations are given in the form:

$$0 = C_1(Y_1 \cdot A_1 + \theta_1 / X_2) \tag{30}$$

$$0 = C_2(Y_2 \cdot A_2 - \theta_2 \cdot X_1) \tag{31}$$

$$0 = C_1 \cdot X_2 + \theta_1 \cdot Y_3 - A_1 \tag{32}$$

Considering only the process at steady state, the LHS of Equations (30)–(32) is set to zero. $\underline{X}$ and $\underline{A}$ are vectors of intermediate variables that need to be evaluated for every evaluation of the right-hand side (RHS) of Equations (30)–(32) together with models or fixed data for $\underline{\theta}$ (the constitutive variables) and a vector of known parameters (vector $\underline{C}$). The model equations relating the intermediate variables $\underline{X}$ and $\underline{A}$ for this conceptual study are defined as

$$A_1 = b_1 \cdot X_1 + Y_1 \cdot (X_2)^2 \tag{33}$$

$$A_2 = \theta_2 / X_2 + Y_2 (X_1)^2 \tag{34}$$

$$X_1 = (A_1 \cdot Y_1 \cdot t)/(A_1 + A_2) \tag{35}$$

$$X_2 = (A_2 + Y_2)/t \tag{36}$$

where t is the residence time. A set of constitutive equations are now needed to complete the process model. Let us assume that the vector $\underline{\theta}$ is represented by θ_1 and θ_2 and are related to the variables Z_1 and Z_2 and the state variables Y_1 and Y_2 according to the following constitutive equations:

$$\theta_1 = Z_1 Z_2 Y_1 / (Z_1 + Z_2) \tag{37}$$

$$\theta_2 = [(Z_1)^2 + (Z_2)^2] / Y_2 \tag{38}$$

If θ_1 and θ_2 are the property values (such as permeability and flux), then the (structural) design variables Z_1 and Z_2 affecting the property values could be macroscopic (e.g., the molecular structural parameters), mesoscopic (e.g., atoms and connectivity), or microscopic (e.g., microscopic structural parameters such as orientation or alignment of the atoms or functional groups) in nature. Z_1 and Z_2 could also be related to the process design if they represent variables such as membrane area, temperature, or pressure of operation. In the process model (Equations (30)–(38)) listed above, Y_1 and Y_2 are the output variables, but

in process design, a desired value is usually specified for them (directly or indirectly). Indirectly, the optimal/desired values of Y_1 and Y_2 could be given in terms of process constraints (such as a desired product purity or recovery). Therefore, in a design problem, solution of process model must also satisfy some constraint equations (see Equations (39) and (40)):

$$P_1 - P_1(\underline{Y}, \underline{P}) = 0 \tag{39}$$

$$P_2 - P_2(\underline{Y}, \underline{P}) = 0 \tag{40}$$

Equations (30) and (40) represent a process model with process constraints and the solution of these equations gives a feasible design. The variables in this process model for design are listed in **Table 5(a)**.

Here, Y_1 and Y_2 are indirectly dependent on the design variables Z_1 and Z_2 and property variables θ_1 and θ_2. So, the idea is to find out the values of the design variables Z_1 and Z_2 that match the property (design) target values for θ_1 and θ_2 to find the design that satisfies the specified performance criteria (specified values of P_1 and P_2) given by Equations (39) and (40). Note also that we have nine equations (Equations (30)–(38)) plus two performance criteria equations (Equations (39) and (40)). Besides the design variables, Z_1 and Z_2, there are nine unknown variables (Y_1, Y_2, Y_3, A_1, A_2, θ_1, θ_2, X_1, and X_2) that need to be solved with the nine equations (Equations (30)–(38)).

Table 5(a) Variables definition

Variable	*Type*
Y_1 , Y_2 and Y_3	Dependent (differential or state) variables
Z_1 and Z_2	Design (decision) variables
θ_1 and θ_2	Property parameters (constitutive variables)
A_1, A_2, X_1, X_2	Intermediate variables (unknown)
P_1 and P_2	Performance criteria
C_1 and C_2	Known parameters

3.02.5.1.3 Solution approaches

Forward design algorithm: The step-by-step algorithm is given as follows (values of P_1 and P_2 are known):

- Step 1: Assume values of design variables Z_1 and Z_2.
- Step 2: Solve model equations (30)–(38) for Y_1, Y_2, Y_3, A_1, A_2, θ_1, θ_2, X_1, and X_2 with Z_1 and Z_2 as known variables (guessed) – the incidence matrix for this system of equations is given in **Table 5(b)** – it can be noted that given all input variables, output variables are calculated and then the design is checked.
- Step 3: Check if Equations (39) and (40) are satisfied. If yes, stop (solution found because the design variables and corresponding state variables match the desired process performance). Otherwise, assume new values for Z_1 and Z_2 and repeat from step 2.

Reverse design algorithm: The step-by-step algorithm is given below (values of P_1 and P_2 are known). The incidence matrix for this solution scheme is shown in **Table 5(c)**, which is divided into three partitions. The first partition solves Equations (39) and (40) for Y_1 and Y_2. The second partition solves Equations (30)–(36) for Y_3, A_1, A_2, θ_1, θ_2, X_1 and X_2. The third partition solves Equations (37) and (38) for Z_1 and Z_2 (where the target defined by θ_1, θ_2 is matched). It can be noted that no iterations are involved.

- Step 1: Use known values of P_1 and P_2 and Equations (39) and (40) to calculate for Y_1 and Y_2 (first partition).

Table 5(b) Incidence matrix for forward algorithm

Eqs.	X_1	X_2	Y_1	Y_2	Y_3	A_1	A_2	θ_1	θ_2	Z_1	Z_2
31	*			*			*		*		
30		*	*			*		*			
33	*	*	*			*					
34	*	*		*					*		
32		*			*	*		*			
35	*		*			*	*				
36	*			*			*				
37			*					*		*	*
38				*					*	*	*

* indicates the presence of the variable in the corresponding equation.

Table 5(c) Incidence matrix for reverse approach

Eqs.	Y_1	Y_2	X_1	X_2	Y_3	A_1	A_2	θ_1	θ_2	Z_1	Z_2
39	*	*									
40	*	*									
35	*		*			*	*				
36		*		*			*				
32				*	*	*		*			
33	*		*	*		*					
31		*	*				*		*		
30	*			*		*		*			
34		*	*	*			*		*		
37	*							*		*	*
38		*							*	*	*

* indicates the presence of the variable in the corresponding equation.

- Step 2: Solve Equations (30)–(36) (second partition) for X_1, X_2, Y_3, A_1, A_2, θ_1, and θ_2 for known values of Y_1 and Y_2 (reverse simulation to determine the design target) to define the target values of θ_1 and θ_2.
- Step 3: Use calculated θ_1 and θ_2 (and Y_1 and Y_2) to determine Z_1 and Z_2 from Equations (37) and (38) (match the design target). Note that there is no need to iterate if a consistent set of $\underline{P}$ was specified, that is, a match is found and that other forms of Equations (37) and (38) may also used as long as they give the correct behavior of the constitutive variables.

This conceptual case study illustrates that decomposing the model equations to solve the property (constitutive) model equations separately not only avoids the iterative trial and error approach but also makes the solution of equations computationally easier.

3.02.5.2 R–S Hybrid Process – Propionic Acid Case Study

The framework for hybrid process design/analysis has been tested by generating and verifying hybrid process schemes for synthesis of *n*-propyl-propionate from 1-propanol and propionic acid. *N*-propyl propionate is used as a paint thinner, a food additive, and as essence for perfumes by giving an apple-like, fruity taste. This ester is commercially available from the Dow Chemical Company with a minimum purity of 99.5 wt.%. The objective of the membrane-assisted hybrid separation scheme is to investigate the possibility of removing one of the products from the reacting mixture and thereby move the reaction equilibrium toward a higher product yield. A detailed solution of the problem can be found in Reference 27 and a summarized version is presented below.

3.02.5.2.1 Stage 1: Hybrid process design and analysis

Step 1a-S. Separation task analysis: The reaction effluent consists of water and three organic chemicals (1-propanol, propionic acid, and *n*-propyl propionate) and the mixture is classified as nonideal and of aqueous type and for phase equilibria calculations involving this mixture the Modified UNIFAC (Lyngby) [27] is selected for calculations of activities in the liquid phase. For the vapor phase, the SRK equation of state [28] is selected.

Since the largest melting temperature is 273.15 K and the lowest boiling temperature is 370.35 K, the mixture is assumed to be in the liquid state at 1 atm for temperature between 273.15 and 370.35 K. Since the solubility of water is almost 2 times higher than other components in the reacting mixture, formulation of a second liquid phase is likely (for more details, see Mitkowski *et al.* [19, 26]).

The total number of binary pairs of components that needs to be analyzed with respect to their boiling points is 6. The calculation and analysis of VLE-phase equilibrium data has identified three binary azeotropes and a ternary azeotrope (see **Table 6**).

Step1a-R reaction analysis: The esterification of 1-propanol with propionic acid to *n*-propyl propionate and water is represented by

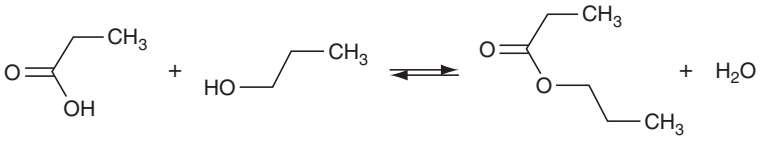

(41)

The reaction kinetics of this heterogeneous esterification reaction has been studied by Duarte *et al.* [29] at a pressure of 5 atm and temperatures ranging from 363.15 to 383.15 K. The reaction takes place only in the liquid phase in the presence of a heterogeneous catalyst Amberlyst 46, which is an acidic ion-exchange resin and can withstand a maximum temperature of 393.15 K. The use of this very selective catalyst eliminates other competing etherification reactions to form di-*n*-propyl ether and dehydration of propanol to propene. The chemical equilibrium of this reaction is expressed in terms of component activities [29]:

$$K_{eq} = \frac{a_{ProPro} \cdot a_{H2O}}{a_{PAc} \cdot a_{POH}} \tag{42}$$

To confirm that experimental data and equilibrium constant (K_{eq}) reported by Duarte *et al.* [29] do represent chemical equilibrium, reactive flash calculations were performed. The results confirmed that all experiments reached chemical equilibrium. Therefore, reaction parameters (K_{eq} and reaction rate parameter) given by Duarte *et al.* [29] describe this reaction system very well. Moreover, the assumption that only esterification reaction takes place, when Amberlyst 46 is used as catalyst, is also correct.

Based on reactive flash calculations performed at a wide range of temperatures (350–415 K) at atmospheric pressure, the corresponding phase diagrams are shown in **Figure 9**. The reactant ratio in all these

Table 6 List of azeotropes present in analyzed mixture

		Molar fraction (%)				
Composition	*Type of azeotrope*	*POH*	*H_2O*	*ProPro*	*ProAc*	*T (K) @ 1atm*
POH–H_2O–ProPro	Heterogeneous	24.50	57.82	17.68		359.46
ProPro–H_2O	Heterogeneous		68.63	31.37		363.14
H_2O–ProAc	Homogeneous		6.666		93.34	372.69
H_2O–POH	Heterogeneous	57.26	42.74			361.88

POH, 1-propanol; ProAc: propionic acid; ProPro: *n*-propyl propionate.

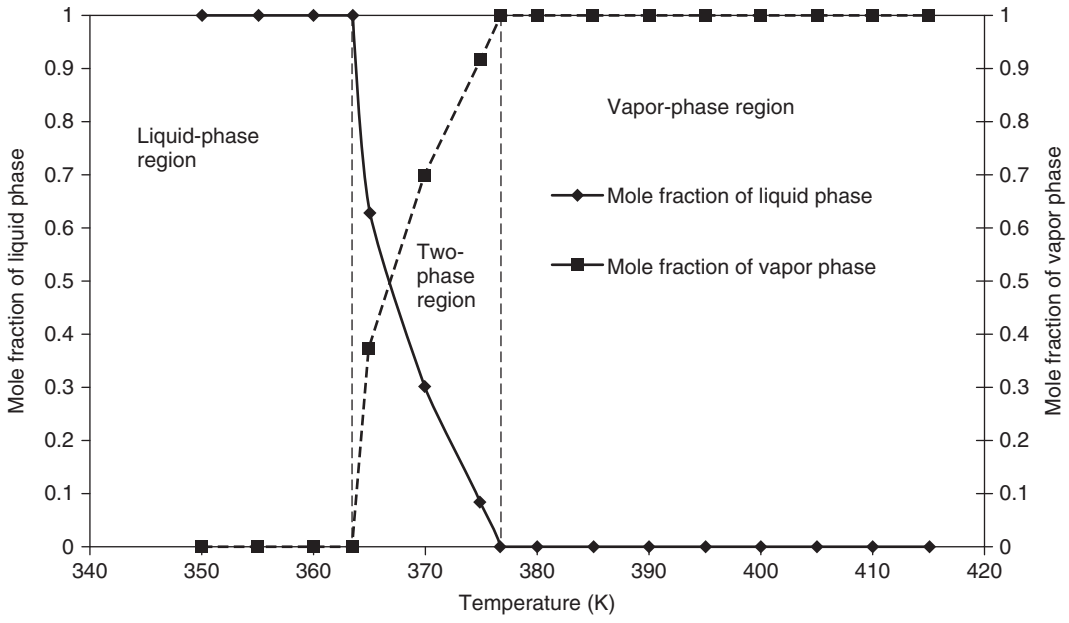

Figure 9 Phase fraction distribution at $P = 1$ atm.

calculations was 1:1 (1-propanol:propionic acid). The two-phase region was found to be between 363.4 and 376.7 K. The maximum temperature at which only liquid is present was found to be 363.4 K. Therefore, this temperature is defined as the maximum operating temperature.

Simulations of batch operations of the reactor were performed to determine the relationship between the product yield and feed ratios of 1-propanol to propionic acid. The results indicated that the process yield increased with increase of the molar ratio. However, the increase of molar ratio above 3 does not give significant increase in the yield; therefore, the range for this design variable was set between 2 and 3.

Step 1b. Need of solvent: In this study, the use of solvents was not investigated since all reactants were liquid and miscible within the operation window.

Step 2. Determine process demands: In this case study, the focus was on the batch operation of the process. The main objective was to obtain as high a conversion of acid to the ester product as possible. More precisely, a molar process yield >0.9 was the desired target. The time for the batch operation was limited to 12 h and the operating pressure was set to atmospheric pressure.

Step 3. Selection of separation technique: Since the continuous removal of product and/or products was likely to enhance the conversion of the reactants, therefore, in this step, techniques for downstream separation of the reactor effluents were identified through the procedure outlined in Section 3.02.3.2 (see step 3R of the methodology).

R3.1. Since the reaction is equilibrium controlled, the addition of the reactant in excess will increase the conversion of the limiting reactant, while removal of the product(s) will push the equilibrium toward the product(s) and simultaneously increase the overall conversion. Two options were considered: (1) remove the main ester product and (2) remove water. Since for the first option, the formation of heterogeneous azeotropes between alcohol, water, and ester had to be considered, the second option was found to be advantageous since water was present in all binary and ternary azeotropes (see **Table 6**). By removing water from the reactor effluent (quaternary mixture), the remaining ternary mixture of organic compounds would be free of separation boundaries.

R3.2. Analyzing the boiling points and relative volatilities, it was established that separation by simple distillation was not feasible. However, it was found that there was a significant difference in relative volatilities between products, water and ester, which pointed to the possibility of the use of reactive distillation to separate them. Also, the three components 1-propanol, water, and *n*-propyl propionate were likely to form a heterogeneous azeotrope at the top of the column.

R3.3. Based on data available in the MemDat database, it was found that many membrane-based separation processes offer selective removal of a specific chemical. For example, pervaporation and vapor permeation are widely used for dehydration of organic mixtures [30]. Comparison of driving force curves for different membrane processes for separation of binary mixtures of 1-propanol and water (see **Figure 10**) was made and the selectivity of these membranes was found to be close to 1. Since reaction proceeds in liquid phase, pervaporation was found to be favorable compared to vapor permeation because it does not need phase change of the feed.

R3.4. Addition of solvent was not investigated in this work.

R3.5. High selectivity toward water and a relatively large driving force available for pervaporation made it a favorable candidate for further investigation.

Step 4. Establish process conditions: In this step, hybrid process schemes together with corresponding specific models are developed. Simulations with the specific generated models were made at various conditions. From the superstructure (see **Figure 4**)for hybrid process schemes, the configuration as shown in **Figure 11**, where process 1 is a reactor and process 2 is a membrane-based separator for selective removal of water, was considered. Since Amberlyst 46 is a heterogeneous catalyst, a packed bad reactor with an additional tank to maintain a specific hold-up in the processing system was added.

From the general model (see Section 3.02.3.3) a dynamic process model was generated (for more details on the generated model, see Reference 26). Since a high conversion of acid was desirable, the introduction of excess of 1-propanol was

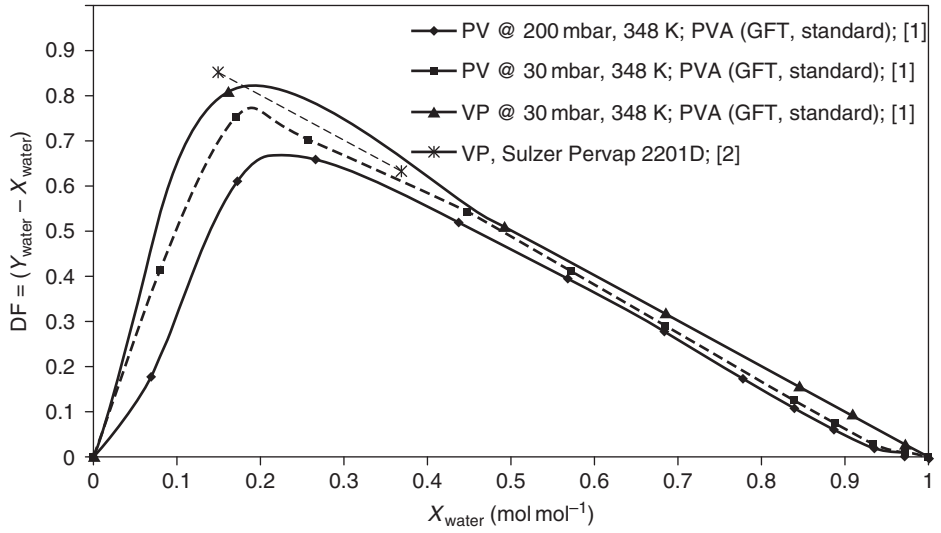

Figure 10 Driving force diagrams for membrane-based separation of binary mixture 1-propanol-water. VP – vapor permeation, PV – pervaporation, PVA – poly (vinyl alcohol) membrane. [1] – Will and Lichtenthaler [31], [2] – Mitkowski [19].

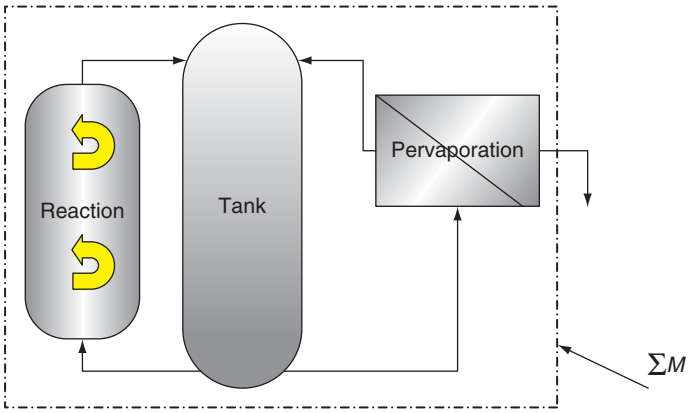

Figure 11 Hybrid reaction–separation scheme (with membrane assisted operation).

investigated to shift the reaction toward higher ester concentrations.

3.02.5.2.2 Implementation (stage 2)

The implementation stage involves the use of an experimental setup to verify the design obtained from stage 1. This was carried out in a systematic way by first establishing (through experiments) the constitutive models for reaction kinetic and the membrane-based separation as a function of temperature (between 343 and 353 K). Experiments were performed next to establish the membrane-based separation model. Membrane-assisted batch reaction experiments were designed next in order to verify the influence of identified operational variables on the overall process performance. The effect of the initial molar ratio of reactant (alcohol to acid), the mass ratio of catalyst to reaction mixture (m_{cat}/m_{mix}), and the switching time from batch reaction to the membrane-assisted batch reaction mode as well as the process temperature were investigated. Details of the experimental design for membrane-assisted batch reaction are given in Mitkowski *et al.* [26]. Finally, the multipurpose lab-scale hybrid process was designed and constructed in order to perform following process operations:

1. Heterogeneously catalyzed batch reaction (operation around packed bed reactor (PBR) and tank.

2. Membrane-based separation (operation around pervaporation unit and tank.
3. Membrane-assisted batch reaction (operation around pervaporation unit, tank, and PBR.

3.02.5.2.3 Validation (stage 3)

The process conditions, such as the ratio of the mass of catalyst to the mass of the reactants, the reactants ratio, the operating temperature, as well as the switching time have significant influence on the overall process performance, and therefore, these were further investigated. Validation results in terms of experimental observations as well as simulations corresponding to the experimental measurements are presented here. All simulation results have been obtained through the ICAS-MoT modeling tool [20] using the models developed in stage 2.

Heterogeneously catalyzed batch reaction: The reaction kinetic data have been verified with the aid of two experiments of heterogeneously catalyzed batch reaction. The simulation of the heterogeneously catalyzed batch reaction has been made with the developed specific model (see appendix of Mitkowski *et al.* [26] for more details). The transient concentrations profiles presented in **Figure 11** represent batch reaction experiment performed at an average temperature of 353.35 K. It can be noted from **Figure 11** that the concentration of substrates (1-propanol and propionic acid) is decreasing over time since concentration of products (*n*-propyl propionate and water) is increasing as reaction is taking place. The lines shown in **Figure 12** represent a simulation result which is in good agreement with experimental points (with accuracy of within 1%). The measured system was considered to be at chemical equilibrium when the concentrations of reactants and products did not change significantly after 150 min.

Membrane-based separation. Pervaporation: For better prediction and comparison of the membrane-assisted batch reaction simulation with experimental data, more detailed pervaporation model has been developed, based on the transmembrane component flux in pervaporation process [9, 11, 19, 26]. From results presented in **Tables 7** and **8**, it is clear that the membrane (PERVAP® 2201-D) is highly selective toward water because the permeate consists of more

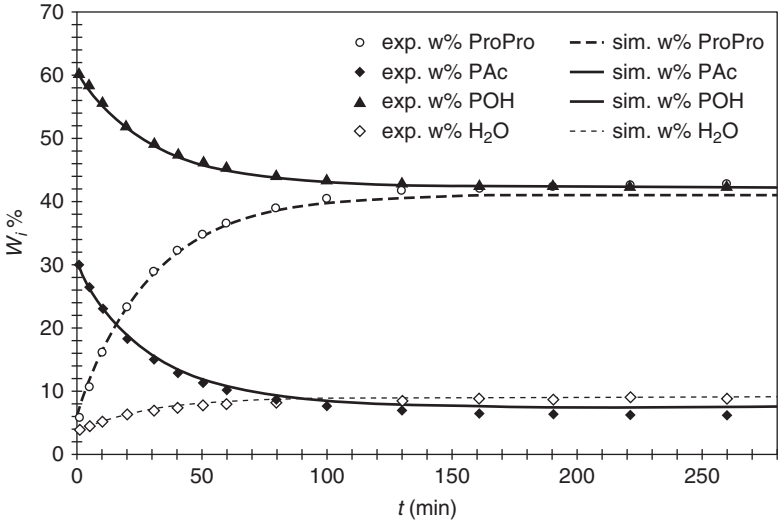

Figure 12 Batch reaction experiment, $T = 353.35$ K, $m_{cat}/m_{mix} = 0.22$, POH:ProAc = 2:1, $m_{mix} = 1328.9$ g (ProPro: *n*-propyl propionate; PAc: propionic acid; POH: 1-propanol).

Table 7 Pervaporation experiment at $T = 346.15$ K, $P_P = 10$ mbar

Components	$\bar{w}_i^{F,exp}$ ($g^{-1}g$)	$w_i^{P,exp}$ ($g^{-1}g$)	J_i^{exp} ($g^{-1}m^{-2.}$ min)	J_i^{calc} ($g^{-1}(m^{-2.}$ min)
Propionic acid	0.0890	0.0007	0.0399	0.0000
1-Propanol	0.7400	0.0054	0.0006	0.0000
N-propyl propionate	0.0931	0.0001	0.0011	0.0000
Water	0.0778	0.9939	7.4397	7.5080

Table 8 Pervaporation experiment at $T = 326.15$ K, $P_P = 8$ mbar

Components	$\bar{w}_i^{F,exp}$ *(gg^{-1})*	$w_i^{P,exp}$ *(gg^{-1})*	J_i^{exp} *(kgm^{-2} h^{-1})*	J_i^{calc} *(kgm^{-2} h^{-1})*
Propionic acid	0.0885	0.0005	0.0091	0.0000
1-Propanol	0.7305	0.0049	0.0014	0.0000
N-propyl propionate	0.0909	0.0001	0.0007	0.0000
Water	0.0901	0.9945	1.8436	1.8775

than 99% water. Only traces of organic compounds were found in the permeate. The flux of water was found to increase 4 times when temperature was increased by 25 K.

Membrane-assisted batch reaction: In this section the dynamic process model with semi-empirical Meyer–Blumenroth model for calculation of component flux was used. Six membrane-assisted batch reaction experiments were performed in order to verify the applicability of the process model for variations in process operational variables. The summary of all experiments is presented in **Table 9** where the product yield (measured) is calculated by

$$Y_{\mathrm{exp,ProPro}} = \frac{\left(\frac{m_{\mathrm{PAc}}^{in}}{M_{\mathrm{wPAc}}}\right) - \left(m_{\mathrm{total}}^{in} - m_{\mathrm{total,permeate}}^{t}\right)\left(\frac{w_{\mathrm{PAc}}^{in}}{M_{\mathrm{wPAc}}}\right)}{\left(\frac{m_{\mathrm{PAc}}^{in}}{M_{\mathrm{wPAc}}}\right)} \tag{43}$$

The heterogeneously catalyzed batch reaction was allowed to progress until a switching time, which is the time when the membrane-assisted batch reaction process starts, is reached. The results indicated that when the hybrid process was operated at temperatures above 345 K, the water fraction decreased immediately after switching time, pointing to a faster separation than reaction and thereby leading to a higher product yield. The same was observed for all membrane-assisted batch reaction operations, thereby confirming a higher conversion of reactants to the desired ester was feasible. The experiments also confirmed the model-based results from stage 2 – that the increase of process temperatures increased the product yield. The switching time, however, was found to have little influence on the yield. The experimentally measured data, in general, matched reasonably well with the corresponding simulation results, thereby confirming that the model validated earlier in separate experiments (e.g., heterogeneously catalyzed batch reaction and pervaporation) did not need further improvements, that is, the specific models generated and used for hybrid process design and analysis were acceptable.

The process yields obtained in the membrane-assisted batch reaction (hybrid process) are much higher than for heterogeneously catalyzed batch reaction obtained in the same process time of 720 min (see **Table 9**). The best result has been obtained for experiment 5 where the yield of propionic acid is 95.6%.

3.02.6 Conclusions

Two model-based computer-aided frameworks, one for simultaneous design of the membrane and the membrane-based operation and another for hybrid process design/analysis, have been presented together with computer-aided techniques for systematic investigation of processes involving membrane-assisted operations. Generic models for various types of membrane-based operations and R–S and S–S hybrid process schemes have been presented. The advantage of this framework is the ability to quickly set up model-based calculations for process design and analysis. The framework also includes work flows (based on the reverse approach)

Table 9 Comparison of process yield obtained in simulation for batch reaction and membrane-assisted batch reaction (process time = 720 min)

Experiment number	*6*	*5*	*4*	*3*	*2*	*1*
Yield P_{AC} (reaction) (mol mol^{-1})	83.9%	78.7%	73.2%	76.4%	75.0%	79.1%
Yield P_{AC} (membrane-assisted batch reaction) (mol mol^{-1})	87.4%	95.6%	85.0%	85.3%	90.2%	93.5%
Difference	3.5%	16.9%	11.8%	9.0%	15.2%	14.5%

for design of the membrane, the membrane-based separation process, as well as hybrid processes with or without membranes. The developed frameworks have been tested with several case studies – two of these have been discussed in this chapter.

From this work, it is clear that systematic model-based design techniques can help to quickly establish achievable design targets for process enhancements that otherwise would not be possible. For the second case study, the generated hybrid process scheme consisting of a reactor and a highly selective membrane separation unit showed advantages with respect to achieving increased product yield by overcoming limitations of equilibrium and kinetically controlled reaction. Current work is further extending the computer-aided framework in terms of membrane database, models, and case studies.

Appendix A: The specific hybrid process model is obtained from the generic model by specifying all decision variables (see **Table 3**), substituting them in the model equations (Equations (9)–(29)) which eliminates some of the terms in the balance equations and other corresponding Equations (12)–(29). Therefore, the specific hybrid model contains fewer equations and variables that need to be specified compared to the generic model. Note, however, that the generated specific hybrid model includes separation factors that need to be set or defined through additional model equations in a different scale. The derivation of a specific hybrid model is illustrated by the following example.

Let us define the decision variables as follows: $\xi^1 = 1$, $\xi^2 = 1$, $\xi^{1in} = 0$, $\xi^{2in} = 0$, $\xi^{1\alpha} = 1$, $\xi^{1\beta} = 1$, $\xi^{2\alpha} = 1$, $\xi^{2\beta} = 0$, $\xi^{R} = 1$, $\xi^{R\beta} = 0$, $\xi^{(homog)} = 1$, $\xi^{(heterog)} = 0$, $t_{switch} = 0$ and consider only dynamic mass balance. Substituting the decision variables to the model equations (Equations (9)–(29)) and simplifying them, the following mass balance is obtained:

$$\left[\frac{\partial n_i}{\partial t}\right] = -\left[\sigma_i^{2\alpha} x_i^{1\alpha} F_{TOT}^{1\alpha}\right] + \left[\sum_{k=1}^{NKR} \nu_{i,k}^{1\alpha} r_k^{1\alpha(homog)}\right] \quad (44)$$

All existing process streams are related by the following equations:

$$F_i^{1\alpha} = x_i^{1\alpha} F_{TOT}^{1\alpha} \quad (45)$$

$$F_i^{2\alpha} = \sigma_i^{2\alpha} x_i^{1\alpha} F_{TOT}^{1\alpha} \quad (46)$$

$$F_i^{2\beta} = \sigma_i^{2\beta} x_i^{1\alpha} F_{TOT}^{1\alpha} \quad (47)$$

$$x_i^{1\alpha} = \frac{n_i}{\sum_{i=1}^{NC} n_i} \quad (48)$$

$$F_i^{1\alpha R} = F_i^{1\alpha} \quad (49)$$

$$F_i^{1\beta R} = F_i^{1\beta} \quad (50)$$

$$F_i^{2\alpha P} = F_i^{2\alpha} \quad (51)$$

$$F_i^{2\beta R} = F_i^{2\beta} \quad (52)$$

$$r_k^{1\alpha(homog)} = k_p^{(homog)} V^{1\alpha} \prod_{i=1}^{NRK} \left(a_i^{1\alpha}\right)^{\nu_{i,k}^{1\alpha}} \quad (53)$$

where $r_k^{1\alpha(homog)}$ is given by Equation (26). In order to solve this model only $\sigma_i^{2\alpha}$, $\sigma_i^{2\beta}$, $\nu_{i,k}^{1\alpha(homog)}$, $F_{TOT}^{1\alpha}$, $k_{p,k}^{(homog)}$, and the initial conditions for n_i (for all i) need to be provided. Note that when $t_{switch} = 0$, α is equal to 1 since this is the beginning of the operation. The derived model represents the hybrid process scheme shown in **Figure 13**. Summarizing, by setting values for the decision variables, the general model equations has been transformed and a specific process model is easily generated without losing any of the important characteristics of the general model and is analyzed and solved (through a DAE solver).

Advantage of such a reformulated model is simplicity to investigate the performance of different hybrid process schemes rapidly and efficiently. Using the superstructure of hybrid process schemes together with the generic model and the specific details of the process design problem, the specific

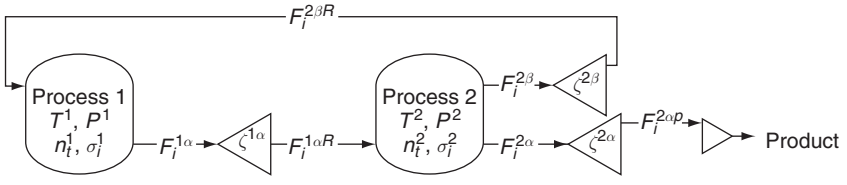

Figure 13 Example of generated hybrid scheme, separation (Process 2) assisting reaction (Process 1).

hybrid R–S or S–S process schemes are generated and tested. Note that by allowing the product from one operational scenario to serve as the feed to a subsequent operational scenario leads to the design of a network.

Note that in the generic model the component separation factors ($\sigma_i^{1\alpha}$, $\sigma_i^{1\beta}$, $\sigma_i^{2\alpha}$, $\sigma_i^{2\beta}$) are specified and are therefore constant. However in some cases, these separation factors depend on the feed composition and specific condition of the separation technique (like in pervaporation, where the transmembrane component fluxes depend on the difference between activities in the feed and permeate sides of the membrane). In this case, separation factors need to be computed using additional models. The component separation factor is defined as the ratio between inlet and outlet component flow rate from the process (Equation (54)):

$$\sigma_i = \frac{F_i^{\text{out}}}{F_i^{\text{in}}} \tag{54}$$

Knowing the process component inlet flow rate, the component outlet flow rate can be easily computed by using appropriate models for the separation factors (which are actually design targets). For example, when pervaporation is selected as process 2, the process inlet is

$$F_i^{in} = F_i^{2in} + F_i^{1\beta R} + F_i^{1\alpha R} \tag{55}$$

Therefore for given inlet flow rate the outlet component, flow rate can be calculated using various kinds of models. In such case the component flux ($\mathcal{J}_i$) is related to the component and membrane-specific permeance (Q_i) and the driving force between the feed and permeate (ΔDF) which is expressed by Equation (56). The driving force in general is expressed as the difference in chemical potential between the feed and the permeate side [32]:

$$\mathcal{J}_i = Q_i \cdot \Delta DF = Q_i \cdot \Delta\mu_i \tag{56}$$

Permeance can be expressed as the constant permeability (short-cut model) or by the one of the other permeance models summarized in **Table 10**.

When a two-phase flash operation is considered as the separation technique for process 2, the separation factors can be obtained by solving the model equations representing a two-phase flash separation scheme, which involves solving the following overall mass balance equations (Equation (57)), component compositions in phase-2α (Equation (58)), and the component compositions in phase-2β (Equation (59)):

$$F_{\text{TOT}}^{2\alpha} = F_{\text{TOT}}^{\text{in}} - F_{\text{TOT}}^{2\beta} \tag{57}$$

$$0 = x_i^{2\alpha} - \frac{z_i F_{\text{TOT}}^{\text{in}}}{\left(K_i F_{\text{TOT}}^{2\beta} - F_{\text{TOT}}^{2\alpha}\right)} \tag{58}$$

$$0 = x_i^{2\beta} - K_i x_i^{2\alpha} \tag{59}$$

In additional, the solution of Equations (57)–(59) must also satisfy the equilibrium condition, defined by

$$0 = \sum_{i=1}^{NC} x_i^{2\beta} - \sum_{i=1}^{NC} x_i^{2\alpha} \tag{60}$$

The K-values (see Equations (58) and (59)) are calculated through Equations (61) and appropriate models for calculating the component fugacity coefficients in the coexisting phases (e.g., the SRK-EOS [29] equation of state):

$$K_i = \frac{\phi_i^{2\beta}}{\phi_i^{2\alpha}} \tag{61}$$

The inlet composition z_i is defined by

$$z_i = \frac{F_i^{\text{in}}}{F_{\text{TOT}}^{in}} \tag{62}$$

Table 10 Experimental and semi-experimental models of permeance

Mass transport model	*Permeance (Q_i)*	*Notice*
Short-cut-model	Q_i^0	Constant permeability
Arrhenius	$Q_i^0 \cdot \exp\left(-\frac{E_i}{R}\left(\frac{1}{T^0} - \frac{1}{T}\right)\right)$	Temperature dependence of permeance
Empirical correlation	$Q_i^0 w_i^{\text{F}}$	Weight fraction dependency
Meyer–Blumenroth	$\frac{P_i}{\tilde{\gamma}_i}$	Dependence of activity in the membrane
Sorption/diffusion	$\frac{\dot{D}_{\text{M},i} C_{\text{M},i}}{a_{\text{M},i}} \frac{1}{l_{\text{M}}}$	Dependence of activity in the membrane

$$F_{\mathrm{TOT}}^{\mathrm{in}} = \sum_{i=1}^{NC} F_i^{\mathrm{in}} \tag{63}$$

Finally, the component molar outlet flow rates are calculated through Equations (64) and (65) and models (or fixed values) for the corresponding separation factors:

$$F_i^{2\alpha} = x_i^{2\alpha} F_{\mathrm{TOT}}^{2\alpha} \tag{64}$$

$$F_i^{2\beta} = x_i^{2\beta} F_{\mathrm{TOT}}^{2\beta} \tag{65}$$

This two-phase flash model consists of $6NC+3$ equations (Equations (57)–(65)), $NC+2$ specified variables ($F_{\mathrm{TOT}}^{\mathrm{in}}$, $F_{\mathrm{TOT}}^{2\alpha}$, F_i^{in}), and $5NC+1$ unknown variables ($F_{\mathrm{TOT}}^{2\alpha}$, $F_{\mathrm{TOT}}^{2\beta}$, z_i, K_i, $x_i^{2\beta}$,$x_i^{2\alpha}$,$F_{\mathrm{TOT}}^{2\beta}$), not counting the fugacity coefficients and their models.

In a similar manner, it is possible to generate specific models for various hybrid process schemes where according to the process description, it would be necessary to define the new separation factors. Different process models can be found in Mitkowski *et al.* [26].

References

[1] Lipnizki, F., Field, R. W., Ten, P.-K. *J. Membr. Sci.* **1999**, *153*, 183–210.
[2] Nishida, N., Stephanopoulos, G., Westerberg, A. W., Nishida, I. *AIChE J.* **1981**, *27*, 321–351.
[3] Whu, J. A., Baltzis, B. C., Sirkar, K. K. *J. Membr. Sci.* **1999**, *163*, 319–331.
[4] Matouq, M., Tagawa, T., Goto, S. *J. Chem. Eng. Jpn.* **1994**, *27*, 302–306.
[5] Buchaly, K., Kreis, P., Górak, A. *Chem. Eng. Process.* **2007**, *46*, 790–799.
[6] Mulder, M. *Basic Principles of Membrane Technology*; Kluwer: Dordrecht, 1996.
[7] Russel, B. M., Henriksen, J. P., Jorgensen, S. B., Gani, R. *Comput. Chem. Eng.* **2000**, *24*, 967–973.
[8] Marrero, J., Gani, R. *Fluid Phase Equilib.* **2001**, *183–184*, 183–208.
[9] Soni, V., Abildskov, J., Jonsson, G., Gani, R. *Comput. Chem. Eng.* **2009**, *33*, 644–659.
[10] Tsolou, G., Mavrantzas, V. G., Makrodimitri, Z. A., Economou, I. G., Gani, R. *Macromolecules* **2008**, *41*, 6228–6238.
[11] Soni, V. Simultaneous Model-Based Design of Process and Assisting Structured Materials. PhD Thesis, Technical University of Denmark, Lyngby, Denmark, 2008.
[12] Gani, R., O'Connell, J. P. *Comput. Chem. Eng.* **1989**, *13*, 397–404.
[13] Pérez-Cisneros, E., Gani, R., Michelsen, M. L. *Chem. Eng. Sci.* **1997**, *52*, 527–543.
[14] Gani, R., Jiménez-González, C., Constable, D. J. C. *Comput. Chem. Eng.* **2005**, *29*, 1661–1676.
[15] Gani, R., Gómez, P. A., Folić, M., Jiménez-González, C., Constable, D. J. C. *Comput. Chem. Eng.* **2008**, *32*, 2420–2444.
[16] Harper, P. M., Gani, R. *Comput. Chem. Eng.* **2000**, *24*, 677–683.
[17] Bek-Pedersen, E., Gani, R. *Chem. Eng. Process.* **2004**, *43*, 251–262.
[18] Mitkowski, P. T., Jonsson, G., Gani, R. *Inż. Chem. Procesowa* **2007**, *28*, 769–781.
[19 Mitkowski, P. T. Computer Aided Design and Analysis of Reaction–Separation and Separation–Separation Systems. PhD Thesis, Technical University of Denmark, Lyngby, Denmark, 2008.
[20] Sales-Cruz, M., Gani, R. A. Modelling Tool for Different Stages of the Process Life. In *Computer Aided Chemical Engineering*; Asprey, S. P., Macchietto, S., Eds.; Elsevier: Amsterdam, 2003; Vol. 16, pp 209–249.
[21] Gani, R. ICAS Documentations. *CAPEC Internal Report*; Technical University of Denmark: Lyngby, Denmark, 2001.
[22] Klincewicz, K. M., Reid, R. C. *AIChE J.* **1984**, *30*, 137–142.
[23] Constantinou, L., Gani, R. *AIChE J.* **2004**, *40*, 1697–1710.
[24] Nielsen, T. L., Gani, R. *Fluid Phase Equilib.* **2001**, *183–184*, 13–20.
[25] Nielsen, T. L., Abildskov, J., Harper, P. M., Papaeconomou, I., Gani, R. *J. Chem. Eng. Data* **2001**, *46*, 1041–1044.
[26] Mitkowski, P. T., Buchaly, C., Kries, P., Jonsson, G., Gorak, A., Gani, R. *Comput. Chem. Eng.* **2009**, *33*, 551–574.
[27] Larsen, B. L., Rasmussen, P., Fredenslund, A. *Ind. Eng. Chem. Res.* **1987**, *26*, 2274–2286.
[28] Soave, G. *Chem. Eng. Sci.* **1972**, *27*, 1197–1203.
[29] Duarte, C., Buchaly, C., Kreis, P., Loureiro, J. M. *Inż. Chem. Procesowa* **2006**, *27*, 273–286.
[30] Koszorz, Z., Nemestothy, N., Ziobrowski, Z., Belafi-Bako, K., Krupiczka, R. *Desalination* **2004**, *162*, 307–313.
[31] Will, B., Lichenthaler, R. N. *J. Membr. Sci.* **1992**, *68*, 119–125.
[32] Lipnizki, F., Trägårdh, G. *Sep. Purif. Methods* **2001**, *30*, 49–125.

Relevant Websites

http://lammps.sandia.gov/ – LAMMPS: Distributed by Sandia National Laboratories, a US Department of Energy (DOE) laboratory.

Biographical Sketches

Rafiqul Gani is a professor of systems design at the Department of Chemical and Biochemical Engineering, The Technical University of Denmark and the director of Computer Aided Process Engineering Center (CAPEC). His current research interests include the development of computer-aided methods and tools for modeling, property estimation, process–product synthesis and design, and process-tools integration. Professor Gani is editor-in-chief of the journal *Computers and Chemical Engineering* , the series editor for the Elsevier CACE book series, and serves in the editorial advisory board of several other journals. Professor Gani is a member of the executive board of the EFCE, a fellow of the AIChE, and also a fellow of IChemE.

Vipasha Soni was a PhD student at CAPEC, Department of Chemical Engineering, DTU, Lyngby, during the period 2005–08. Dr. Soni successfully defended her PhD thesis on 'Simultaneous model-based design of process and assisting structured material' in January 2008, under the supervision of Prof Rafiqul Gani.

Piotr T. Mitkowski was a PhD student at CAPEC, Department of Chemical Engineering, DTU, Lyngby, during the period 2005–08. Dr. Mitkowski successfully defended his PhD thesis on 'Computer aided design and analysis of reaction–separation and separation–separation system' in May 2008, under the supervision of Prof. Rafiqul Gani.

3.03 Modelling and Simulation of Catalytic Membrane Reactors

G Barbieri, F Scura, and A Brunetti, Institute on Membrane Technology, ITM-CNR, at University of Calabria Rende (CS), Italy

3.03.1	**Introduction**	58
3.03.2	**Mathematical Modeling of Catalytic MRs**	60
3.03.2.1	Tubular MR	61
3.03.2.2	Catalytic Membranes	62
3.03.2.3	A Two-Separate-Phase Enzyme-Loaded MR	63
3.03.2.4	Pore-through Flow Mode Enzyme-Loaded MR	64
3.03.2.5	Energy Balance	65
3.03.3	**Simulations**	66
3.03.3.1	Tubular Pd-Based MRs	66
3.03.3.2	A Two-separate-Phase Enzyme-Loaded MR	71
3.03.3.3	Pore-through Flow Mode: An Enzyme-Loaded MR	72
3.03.4	**Potentiality and Perspectives of MRs**	73
References		76

Nomenclature

A	surface area (m^2)
C	concentration ($mol\,m^{-3}$)
C_p	specific heat ($J\,mol^{-1}\,K^{-1}$)
D	diffusivity ($m^2\,s^{-1}$)
E	activation energy ($J\,mol^{-1}$)
F	molar flow rate ($mol\,s^{-1}$)
h	enthalpy ($J\,mol^{-1}$)
ID	inner diameter (m)
J	permeating flux ($mol\,m^{-2}\,s^{-1}$)
k	kinetic constant
$K_{equilibrium}$	equilibrium constant
K_p	equilibrium constant in terms of partial pressures
k	thermal conductivity ($W\,m^{-1}\,K^{-1}$)
L	length (m)
m	reactant feed molar ratio (–)
n	number of mole (–)
N	molar flux ($mol\,m^{-2}\,s^{-1}$)
OD	outer diameter (m)
P	pressure (Pa)
Permeability	self-explanatory ($mol\,m^{-1}\,s^{-1}$ Pa)
Permeability	self-explanatory ($mol\,m^{-1}\,s^{-1}$ $Pa^{-0.5}$) (Sieverts)
Permeance	self-explanatory ($mol\,m^{-2}\,s^{-1}$ Pa)
Permeance	self-explanatory ($mol\,m^{-2}\,s^{-1}Pa^{-0.5}$) (Sieverts)
Permeating flux	self-explanatory ($mol\,m^{-2}\,s^{-1}$)
Q	volumetric flow rate (m^3(STP)$\,s^{-1}$)
R	gas law constant ($8.314\,J\,K^{-1}\,mol^{-1}$)
RI	recovery index
r	radial coordinate (m)
r_{ij}	*j*th reaction rate referred to the *i*th species ($mol\,m^{-3}\,s^{-1}$)
S	solubility ($mol\,l^{-1}$)
T	temperature (°C or K)
t	time (s)
U	overall heat transfer coefficient ($W\,m^{-2}\,K^{-1}$)
V	volume (m^3)
X	conversion (–)
z	axial coordinate (m)
δ	membrane thickness shell thickness for interfacial reaction (m)
ε	porosity (–)
ρ	density ($g\,m^{-3}$)

τ	space time (s)	$\dot{\Psi}$	heat generated by chemical reactions ($W\,m^{-2}$)
τ	tortuosity		
$\nu_{I,\varphi}$	stoichiometric coefficient with respect to the reference component of *i*th species in *j*th reaction	φ	enthalpy flux associated to hydrogen permeation ($W\,m^{-2}$)

3.03.1 Introduction

In the last decade, membrane science and technology has greatly improved, particularly in relation to the possibility of its application to substituting conventional technologies, integrating various membrane operations in the industrial cycles, with overall important benefits to product quality, plant compactness, environmental impact, energetic aspects, etc. The boost to redesigning the traditional operations was introduced by the process intensification strategy [1, 2], an innovative methodology for process and plant design that proposes a new design philosophy for achieving significant reductions (by factors of 10–100 or more) in plant volume and at the same production capacity or improving overall efficiency, etc.

Membrane reactors (MRs) represent an interesting alternative to traditional reactors (TRs) for their peculiarity. They are defined, in fact, as the most important class of the multifunctional reactor, being able to carry out simultaneously reaction and selective separation in the same vessel. A permselective membrane, dividing the reactor into two reaction volumes, reaction and permeate sides, allows the selective removal of products from the reaction volume to the permeation one, under the effect of a permeation driving force. The driving force is a function of the species chemical potential on the reaction and permeate sides (e.g., species partial pressures in gas-phase systems). The simultaneous reaction-separation process implies several advantages, reduces the load of the downstream separation, because both (permeate and retentate) the outlet streams leaving the MR are concentrated in the more and less permeable species, respectively. In addition, the separation/purification is not required in the special case of pure permeate.

In general, the advantages of MRs operation with respect to traditional ones are as follows:

- yield enhancement of equilibrium-limited reactions, owing to the possibility of a continuous removal of one or more reaction products;
- selectivity enhancement;
- coupling of two or more reactions, for example, dehydrogenation (endothermic) with an hydrogenation (exothermic) on the two membrane sides;
- modification of reaction mechanisms by the removal of main or secondary products by means of appropriate configurations of the catalytic membranes;
- higher residence time owing to the product removal;
- lower operating conditions (e.g., temperature) having analogous conversion, etc.; and
- controlled addition of a reactant through the membrane in particular for reactions such as partial oxidations where the same oxygen amount can be fed in a distributed way along with the whole membrane length.

The overall effect is an improving of the global efficiency of the process both in terms of better performance (conversion, selectivity, yield, etc.) and reduction of the reaction volume [3, 4] and catalyst amount in the case of catalytic reactions.

The membrane present in the reactor can be inert or catalytic. In the first case, it acts only as a separator and is coupled with a catalytic bed in which the reaction takes place. In the other case, the catalyst is distributed in the membrane and the reaction takes place inside it or on the membrane surface.

Gas-phase reactions and in particular hydrogenation/dehydrogenations (e.g., hydrogen production, upgrade and cleanup, partial oxidation) carried out using Pd-based, zeolite, perovskite membranes are considered in this chapter as examples of reactions carried out in MRs with an inert membrane (**Table 1**).

These reactions were widely studied [5–33] and some investigations are still in progress both experimentally and by modeling. A scheme of a catalytic MR as shown in **Figure 1** presents a tube-in-tube configuration, where the inner tube is the selective membrane.

Table 1 Examples of reactions investigated in catalytic MRs and catalytic membranes

Reaction	*Membrane*	
Dehydrogenation of:		
iso-butene	Dense	Silica
Ethylbenzene to styrene	Dense	Pd–Ag
Ethane to ethylene	Dense; porous	Pd–Ag; Al_2O_3
1-butene to butadiene	Dense	Pd
n-butane	Porous	γ-Al_2O_3
Methanol	Porous	γ-Al_2O_3
Hydrogenation of:		
Butenes	Dense	Pd–Sb
Butadiene	Dense	Pd
Ethylene to ethane	Dense; porous	Pd; Al_2O_3
Other		
Methane steam reforming (MSR)	Dense	Pd–alloy
Methane dry reforming	Dense	Pd–alloy
Partial oxidation of methane (POM)	Dense	Pd-based, perovskite
Water gas shift (WGS)	Dense	Pd–alloy
CO cleanup	Porous	Zeolite
Decomposition of H_2S	Porous	γ-Al_2O_3
Oxidation of secondary amine (liquid phase)	Porous; dense	Polymeric
Photooxidation of *n*-pentanol (liquid phase)	Porous; dense	Polymeric

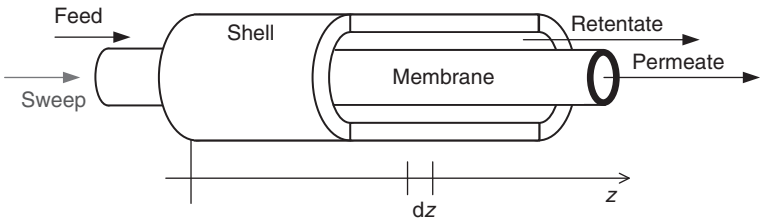

Figure 1 Scheme of a tubular membrane reactor.

The function of porous or dense, ceramic, or metallic membranes is only to remove selectively one or more species from the reaction volume; however, these membranes do not participate actively in the reaction (inert membrane). The permeating species are collected inside the core of the inner tube, which is the permeate side. The driving force promoting the permeation is given by the partial pressure difference of the *i*-species on both the membrane sides. This can be created reducing the partial pressure on the permeate side by means of a sweep gas (inert such as N_2, Ar, and He), or increasing the pressure on the retentate/reaction side. The increase of the feed pressure allows a permeate stream concentrated in the permeating species to be obtained, not requiring further separation steps, which would be necessary if a sweep gas were used. The choice on which volume (annular space or tube core) can be used for the reaction depends also on the energy transport [34]. If the reactions such as methane steam reforming (MSR) are energy intensive, the annular space gives a better heat exchange than that shown by same MR geometry with the catalyst packed inside the membrane.

As stated previously, the membranes can also have catalytic properties. In this case, since the reaction takes place inside the membrane, the concentration of reactants and products arises inside the membrane itself. In particular, the fact that the reactants flow through the membrane pores, passing at a short distance from the catalytic sites, leads to a higher reactant–catalyst interaction with improved possibility in terms of conversion and selectivity (**Figure 2**).

A very high conversion can be achieved, for example, in a purification process [35] operated by reaction when the component to be removed has a concentration lower than the other desired species.

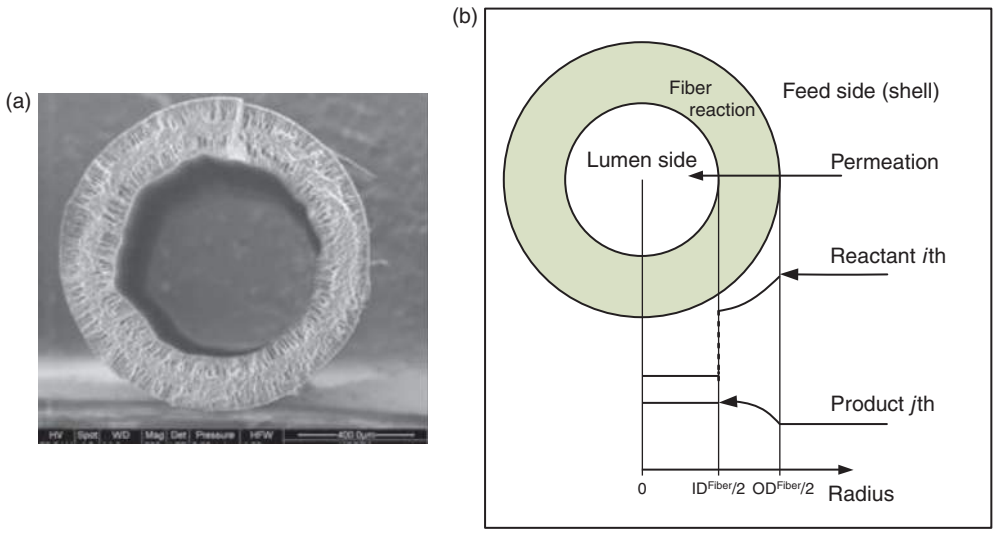

Figure 2 (a) Cross section (scanning electron micrograph (SEM)) of a polyvinylidene fluoride (PVDF) hollow fiber membrane loaded with Pd for in water dissolved oxygen removal [36]. (b) Scheme of a catalytic membrane with a cylindrical geometry (tubular, capillary, or hollow fiber).

3.03.2 Mathematical Modeling of Catalytic MRs

A mathematical model of an MR is a set of equations (partial or ordinary differential equations, algebraic equations), which are able to simulate all the possible evolutions of the variables describing the modeled system in accordance with operating conditions: the local variables (temperature, pressure, composition, etc.) and the overall ones (e.g., flow rates, conversion, and recovery). The general structure of these equations is the same as that of TRs. Generally, these equations are the momentum, mass, and energy balances written for the reaction and permeate volumes (**Figure 3**) and for the membrane (only for the catalytic membranes). The local velocity field can be considered known/assigned in most cases. Moreover, for the liquid-phase reactions in which no significant heat development is expected (e.g., membrane bioreactors for wastewater treatment) and for isothermal reactions, the energy balance can also be neglected.

In general, a mass balance accounts for the net mass flow through an MR ('in' − 'out' + 'production' = 'accumulation'). The total mass entering into a system (in) must react (production) or leave the system (out) or accumulate in it (accumulation). If steady-state condition is considered, the accumulation on the reaction and permeate sides is zero. The expressed mass balance, on the reaction side, contains the term related to the *i*th permeating species through the membrane. In the mass balance for the permeate side, the same permeation term has to be considered with the opposite sign with respect to the reaction side.

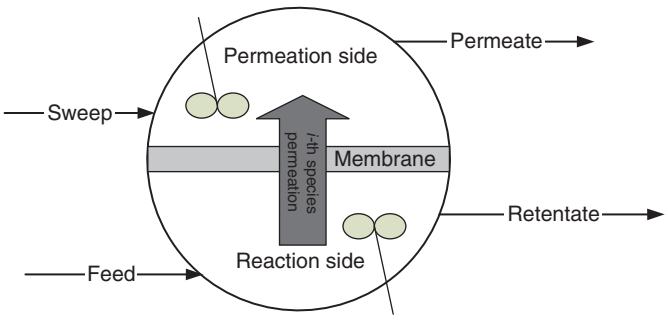

Figure 3 Scheme of a catalytic membrane reactor (MR).

Usually, no reaction occurs in the permeate side, even if some examples of coupled reactions in MRs [37, 38] are present in the literature. In such a case, the species produced on one membrane side permeates through the membrane and reacts on the other membrane side [39].

The above-reported considerations are general and independent of the membrane type. The permeating flux law depends on the permeation mechanism (solution-diffusion in dense or metallic membranes, viscous, or Knudsen flux in porous membranes, etc.).

In the case of solution-diffusion mechanism (for instance, dense polymeric membranes) the ith species permeating flux through the membrane can be expressed as

$$\mathcal{J}_i^{\text{Permeating}} = \frac{S_i D_i}{\text{Thickness}} \left(P_i^{\text{Feed side}} - P_i^{\text{Permeation side}} \right) \quad (1)$$

where D is the diffusion and P the pressure.

For Pd-based membranes, the only permeating species is the hydrogen (infinite membrane selectivity) and the permeating flux has to be expressed with Sieverts' law:

$$\mathcal{J}_{H_2}^{\text{Sievert}} = \frac{\text{Permeability}_{H_2}}{\text{Thickness}} \left(\sqrt{P_{H_2}^{\text{Feed side}}} - \sqrt{P_{H_2}^{\text{Reaction side}}} \right) \quad (2)$$

In the case of porous membrane, when the pore size is comparable or smaller than the mean free path of molecules (e.g., microporous or zeolite membranes), the permeation of species controlled by the Knudsen diffusion and the permeating flux is expressed by

$$\mathcal{J}_i^{\text{Permeating}} = d_{\text{pore}} \frac{\varepsilon}{\tau} \sqrt{\frac{1}{3\,R\,T\,M_i}} \frac{\Delta P_i}{\text{Thickness}} \quad (3)$$

where ε is the porosity, τ the space time, and P the pressure.

The MRs might be distinguished as:

- distributed parameter systems, such as tubular MRs, in which the state variables for both reaction and permeate sides depend on axial and/or radial position and
- lumped parameter systems such as completely stirred MRs, in which both reaction and permeate sides are described by global variables.

3.03.2.1 Tubular MR

A tubular MR is a tube-in-tube device in which the inner tube is a permselective membrane promoting the selective mass transfer of reactants/products between the reaction and permeation sides. On both sides, species compositions, temperature, and pressures change along the reactor length and radial direction; in addition, the permeation rate through the membrane changes along the reactor length. Therefore, in general, these systems must be described by partial differential equations (PDEs).

A one-dimensional (1D) mathematical model provides satisfactory description of systems in which radial gradients can be neglected. In this section, a 1D mathematical model for gas-phase reactions in tubular MRs operating in steady state is presented. The hypotheses are listed below:

1. Absence of radial species concentration profiles.
2. Assigned velocity field (plug flow on both membrane sides).
3. Isobaric conditions on both membrane sides (negligible pressure drops in the catalytic bed of laboratory-scale reactors. However, Ergun's equation can be used for large-scale MRs).
4. Ideal gas behavior on both membrane sides.
5. Pseudo-homogeneous description of heterogeneous catalytic reactions: the void fraction and specific catalytic surface are included into the reaction rate expressions.

The mass balances on both membrane sides for a tubular MR must be written for a differential reference volume, of dz length (see **Figure 1**). The MR configuration (reaction in the lumen or in the annulus) does not affect the mass balance equations for both the reaction and permeation side.

The equations and the corresponding boundary conditions (all defined at the inlet of the system, initial value problem for the co-current configuration) for the plug flow MR are reported in Equations (4) and (5) for the reaction and permeate sides, respectively. This equation set can be used indifferently for the reaction in the annulus or in the lumen. All the constitutive equation terms are reported in **Table 2** for the reaction side.

The peculiarity in Equation (4) is given by the term

$$-\frac{A^{\text{Membrane}}}{V^{\text{Reaction}}} \mathcal{J}_i^{\text{Permeating}}$$

expressing the permeation of the species through the membrane, with $\mathcal{J}_i^{\text{Permeating}}$ being the permeating flux, which can be expressed, for instance, by one of the equations (1)–(3), depending on the membrane type considered. The selective removal of one or more species involved in the reaction (reaction

Table 2 Mass balance of a tubular MR with cylindrical symmetry plug-flow MR (1D-first order model) – co-current flow configuration – steady state

Reaction side	$-\frac{dN_i^{Reaction}}{dz}+\sum_{j=1}^{N_{Reactions}} v_{i,j}r_j-\frac{A^{Membrane}}{V^{Reaction}}J_i^{Permeating}=0$	(4)
	B.C. $N_i^{Reaction}\|_{z=0}=N_i^{Feed}$	
Permeate side	$-\frac{dN_i^{Permeation}}{dz}+\frac{A^{Membrane}}{V^{Permeation}}J_i^{Permeating}=0$	(5)
	B.C. $N_i^{Permeation}\|_{z=0}=N_i^{Sweep}$	

product) enhances the conversion as a direct consequence of the Le Chatelier principle (i.e., improving the kinetics by means of reduction of the reverse reaction rate, increase of residence time owing to the reduction of reaction side flow rate).

The equations of the permeate side are constituted of the same terms as at the reaction side, except the one relative to the chemical reaction. The term of the permeating flux through the membrane has a positive sign because in this case H_2 enters the permeation volume (see **Figure 1**). In case MR operates as a reactant distributor, the signs of the permeation terms for both the reaction and permeation sides have to be reversed.

In the case of nonnegligible axial dispersion, a term related to diffusive transport for the species along the MR axis must be added in the equations. A 1D second-order model has to be considered and an additional boundary conditions (B.C.s) (e.g., Danckwerts' condition expressing the absence of the concentration gradient at the reactor exit) is required for both the reaction and permeation volumes.

When radial profiles cannot be neglected, the composition, temperature, and pressure depend on the radial coordinate and a different differential (axial and radial) reference volume must be assumed. In this case also, a term related to radial diffusion appears in the balance equations and the mathematical model is second-order 2D . In the meantime, the term related to the permeation disappears from the equation; in fact, the membrane permeation is taken into account by means of the B.C. at the membrane surface. This B.C., expressing the permeating flux between the two membrane phases, is the same for both the reaction and permeate sides. Further, a second B.C. for the radial coordinate is required (e.g., the absence of radial flux on the symmetry axis and shell internal surface for tube and annulus, respectively) (**Table 3**).

3.03.2.2 Catalytic Membranes

In the case of noninert membrane, the mass, energy, and momentum balances have to be considered also for the membrane itself as well as the feed/retentate and sweep/permeate volumes. In particular, the catalytic conversion of species that selectively permeate through the membrane produces species concentration and also temperature profiles along the membrane thickness. These profiles depend not only on membrane catalytic activity and/or on catalyst distribution inside the membrane, but also on the permeating flux of reactants through the membrane. In general, the operating conditions (temperature, pressure, and stream composition) and the membrane permselectivity affect the species-selective permeation and, therefore, the reactants conversion and reactions selectivity. For this reason, usually, mass balance equations in the membrane phase have to be coupled to the mass balance of the external phases.

Table 3 Constitutive terms of mass balance equation

$-\frac{\partial N_i^{Reaction}}{\partial z}$	Convective flux variation of *i*th species along the reaction side
$+\sum_{j=1}^{N_{Reactions}} v_{i,j}r_j$	Reaction term involving *i*th species in all the reactions
$-\frac{A^{Membrane}}{V^{Reaction}}J_i^{Permeating}$	Permeation term of the *i*th species through the membrane

The enzyme-loaded MRs are an important category of reactors that are increasingly becoming a valuable alternative to traditional processes, for example, in pharmaceutical application, water treatment, and food processes. The enzyme interacts in the membrane pores with species transported via convection or diffusion; the reactants are progressively converted and the products continuously removed.

A typical enzyme-loaded MR has a tube (hollow fiber)-and-shell configuration in which the big enzyme molecules are immobilized in the pores of asymmetric microfiltration membranes [40].

Depending on the process application (e.g., resolution of racemic mixtures in pharmaceutical industry or wastewater treatment), a different main transport mechanism can arise in the enzyme-loaded membrane.

In particular, two different examples of enzyme-loaded MRs are discussed:

- A two-separate-phase MR for kinetic resolution of racemic mixtures
- A pore-through flow for liquid-phase-dissolved species conversion.

3.03.2.3 A Two-Separate-Phase Enzyme-Loaded MR

The S-naproxen methyl ester hydrolysis via lipase is considered as an important reaction widely used in nonsteroidal anti-inflammatory drug production.

The reaction takes place at the interface between two immiscible phases, the organic phase containing only the reactant (S-naproxen methyl ester) and an aqueous buffer solution in which only the product (S-naproxen acid) is dissolved. The interface between the organic and aqueous immiscible phases is located inside the membrane pores.

The two separate phases, contained in two different tanks, are continuously recycled into the hollow fiber membrane module. The S-naproxen diffuses from the bulk organic phase toward the interface inside the membrane. From a modeling point of view, the interface of phases where the reaction takes place is assumed to be a slight shell located in the membrane at a given radial position, depending on operating conditions, namely the transmembrane pressure difference. The thickness of this reactive layer has to be assumed comparable to the dimension of enzyme molecules.

Looking at the whole system, the high stream recycling rate and the low reaction kinetics allow the external mass transfer resistances to be neglected since no radial concentration profiles in the feed/retentate and sweep/permeate sides or along (axial) the hollow fiber membranes arise. Thus, both membrane sides can be considered as lumped parameter systems. In such a case, the two different membrane sides can be considered as two time-evolving batch systems, the concentration of reactant and product being described by taking into account the instantaneous fluxes between the bulk phases and membrane.

Therefore, only the radial transport (diffusion and reaction of reactants and diffusion of products) occurring in the hollow fiber membranes characterizes this system and is considered in the modeling. A conceptual scheme is shown in **Figure 4**.

Considering an interfacial layer located on the external membrane surface and a shell side feed configuration (i.e., the products are recovered in the hollow-fiber core), Equation (6) gives the transient, 1D, second-order mass balances and the initial and boundary conditions (I.C. and B.C.s) in dimensionless form for a Michaelis–Menten kinetics. The signs '+' or '−' have to be referred to the product (S-naproxen acid) and reactant (S-naproxen methyl ester), respectively:

$$\frac{\partial C_i}{\partial t} + \left[\frac{1}{r}\frac{\partial}{\partial r}\left(-r\frac{\partial C_i}{\partial r}\right)\right] = \pm G^2\Phi^2\,\frac{D_{\text{Ester}}}{D_i}\left(\frac{C_{\text{Ester}}}{1+C_{\text{Ester}}}\right),$$

$$i = \text{ester or acid}$$

$$t = 0 \Rightarrow C_i = 0 \ \text{(I.C.)}$$

$$r = 1 \Rightarrow C_{\text{Ester}} = C_{\text{Ester}}(t) \ \text{ and } \ \frac{\partial C_{\text{Acid}}}{\partial r} = 0 \ \text{(B.C. 1)}$$

$$r = \frac{\text{OD}^{\text{Membrane}} - 2\delta}{\text{OD}^{\text{Membrane}}} \Rightarrow \frac{\partial C_{\text{Ester}}}{\partial r} = 0 \ \text{ and } \ C_{\text{Acid}} = C_{\text{Acid}}(t) \ \text{(B.C. 2)} \tag{6}$$

$$\text{Thiele modulus, } \Phi^2 = \frac{V_{\text{MAX}}\cdot\delta^2}{D_{\text{Ester}}K_{\text{M}}} \tag{7}$$

where V is the volume, C the concentration, D the diffusivity, and K the kinetic constant.

$$\text{Geometric factor, } G^2 = \frac{\left(\text{OD}^{\text{Membrane}}\right)^2}{4(\text{layer thickness})^2} \tag{8}$$

where OD is the outer diameter.

The Thiele modulus is the ratio of the intrinsic chemical reaction rate in the absence of mass transfer limitation to the rate of diffusion through the membrane pores and G^2 is a geometric factor, depending on the length reference value used for the dimensionless variables and δ is the layer thickness.

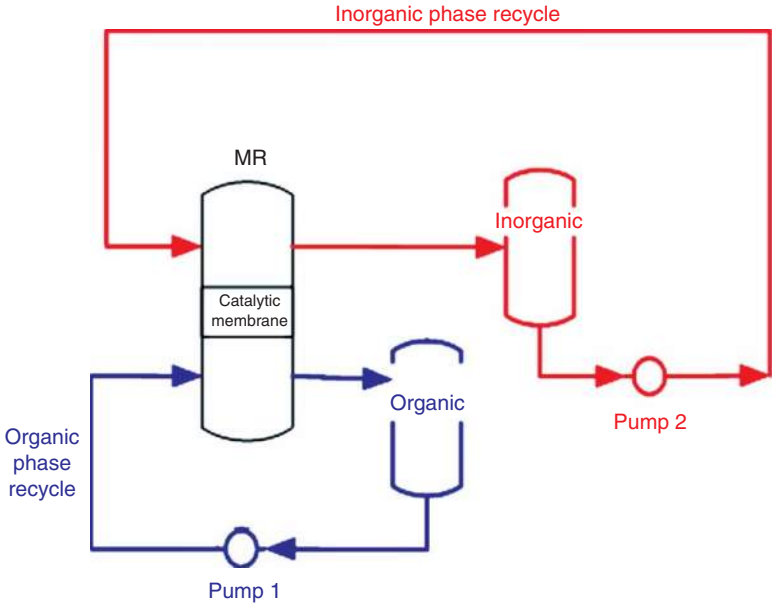

Figure 4 Two separate phase enzyme-loaded membrane reactor (MR).

Equation (9) expresses the time evolution of reactant (S-naproxen methyl ester) taking into account its permeating flux ($\mathcal{J}_{\text{Ester}}(t)$). A similar equation can be obtained for the evolution of S-naproxen acid in the buffer solution (Equation (10)):

$$C^{\text{bulk}}_{\text{Ester}}(t) = C^{0}_{\text{Ester}} - \frac{A^{\text{Membrane}}}{V^{\text{Organic}}} \int_0^t \mathcal{J}_{\text{Ester}}|_{r=1}\,\mathrm{d}t \qquad (9)$$

$$C^{\text{bulk}}_{\text{Acid}}(t) = C^{0}_{\text{Acid}} + \frac{A^{\text{Membrane}}}{V^{\text{Inorganic}}} \int_0^t \mathcal{J}_{\text{Acid}}|_{r=1}\,\mathrm{d}t \qquad (10)$$

3.03.2.4 Pore-through Flow Mode Enzyme-Loaded MR

The second proposed example deals with the modeling of wastewater-contained phenol degradation in enzyme-loaded MR. In some applications, the porous membrane acts as support, with the double advantage of both improving the contact/interaction between the immobilized enzyme and reactant molecules contained in the feed stream flowing through the membrane and reducing the separation cost of enzyme from reactant mixtures at the end of homogeneous phase batch operations. In the second case, each single membrane pore can be considered as a plug flow reactor in which the reactant stream, flowing from the feed/retentate to the sweep/permeate side, is progressively converted. With respect, for instance, to the case of the two-separate-phase enzyme-loaded MR, the mass balance equations contain also the term related to the convective flux, besides the diffusive and, obviously, the reactive ones (**Table 4**).

In the case of lumped parameter systems (no species profiles in the bulk phases), the steady-state, 1D, second-order, dimensionless species mass balance equations in membrane and related B.C.s for a reactant species are

$$\text{Pè}_{\text{Phenol}}\, G \frac{\partial C_{\text{Phenol}}}{\partial r} = \left(\frac{1}{r}\frac{\partial C_{\text{Phenol}}}{\partial r} + \frac{\partial^2 C_{\text{Phenol}}}{\partial r^2}\right) - \Phi^2 G^2 \frac{C_{\text{Phenol}}}{1+\xi C_{\text{Phenol}}} \qquad (11)$$

$$r = \text{OR} \Rightarrow C = C^{\text{Feed}}_{\text{Phenol}} \text{ (B.C. 1)}$$

$$r = \text{IR} \Rightarrow \frac{\partial C_{\text{Phenol}}}{\partial r} = 0 \text{ (B.C. 2)}$$

$$\text{Peclet number, } \text{Pè}_{\text{Phenol}} = \frac{v_r \cdot \delta}{D_{\text{Phenol}}} \qquad (12)$$

The Peclet number, $\text{Pè}_{\text{Phenol}}$, relates the advection of a flow to its diffusion, while Φ^2 and G^2 are the same dimensionless groups already defined in Equations (7) and (8); $\tau = \delta/v_{\text{r}}$ is the residence time, $\xi = C^{\text{Feed}}_{\text{Phenol}}/K_{\text{M}}$ is dimensionless Michaelis–Menten constant. Finally, the velocity field in the porous membrane, v_{r}, can be predicted by Darcy's law or Brinkman's equation. An equation similar to Equation (11) must be considered for the reaction product.

Table 4 Energy balance equations of a tubular MR plug-flow MR (1D-first order model) – steady-state

$$-\sum_{i=1}^{N\ \text{species}} \mathrm{N_i Cp_i}\,\frac{\partial T^{\text{Annulus}}}{\partial z}+\frac{U^{\text{Shell}}A^{\text{Shell}}}{V^{\text{Annulus}}}\left(T^{\text{Furnace}}-T^{\text{Annulus}}\right)+$$

$$-\frac{U^{\text{Membrane}}A^{\text{Membrane}}}{V^{\text{Annulus}}}\left(T^{\text{Annulus}}-T^{\text{Lumen}}\right)+\Psi+\varphi\,\frac{A^{\text{Membrane}}}{V^{\text{Annulus}}}=0 \tag{13}$$

Annulus

I.C. $T^{\text{Annulus}}|_{t=0}=T^{\text{Annulus, Initial}}$

B.C. $T^{\text{Annulus}}|_{z=0}=T^{\text{Feed}}$ or T^{Sweep}

$$-\sum_{i=1}^{N\ \text{species}} N_i Cp_i\,\frac{\partial T^{\text{Lumen}}}{\partial z}+\frac{U^{\text{Membrane}}A^{\text{Membrane}}}{V^{\text{Lumen}}}\left(T^{\text{Annulus}}-T^{\text{Lumen}}\right)+$$

$$+\Psi+\varphi\frac{A^{\text{Membrane}}}{V^{\text{Lumen}}}=0 \tag{14}$$

Lumen

I.C. $T^{\text{Lumen}}|_{t=0}=T^{\text{Lumen, Initial}}$

B.C. $T|_{z=0}=T^{\text{Feed}}$ or T^{Sweep}

3.03.2.5 Energy Balance

Usually, heat developed during chemical reactions promotes a temperature profile. Any temperature variation means variations of kinetics (reaction rate) and, specifically for MRs, species permeance and permeating flux. When the heat involved in the reaction produces a sensible temperature change (e.g., the MSR in a highly endothermic reaction), the energy balances for both the membrane sides have to be considered as part of the equation set in addition to the mass balances. In the cases in which a low concentration dissolved species reacts in a liquid phase (e.g., the S-naproxen methyl ester hydrolysis), negligible thermal effects can be assumed. In any case, the knowledge of the temperature profiles and the effect that these profiles produce on the membrane properties allow the MRs to be performed in the best operating conditions.

Equations (13) and (14) are the energy balances and the corresponding initial and boundary conditions written down for the 1D tube-in-tube systems. These equations have to be coupled to the mass balance equations (4) and (5). The energy balance contains the heat exchange between the two membrane sides and that transported by the permeated species. The annulus exchanges heat with the furnace and lumen side, whereas the stream in the lumen exchanges heat only with the annular volume.

The heat generated by the reaction, (see Table 5), is present in the equation of the annulus

Table 5 Characteristic terms of energy balance in MRs

$$\varphi=\begin{cases}0 & \text{on reaction side}\\ J_i^{\text{Permeating}}\left(h_i^{T^{\text{Reaction}}}-h_i^{T^{\text{Permeation}}}\right) & \text{on permeation side}\end{cases}$$

Temperature variation owing to enthalpy flux associated with *i*th species permeation (15)

$$\Psi=\begin{cases}\sum_{j=1}^{N^{\text{Reaction}}} r_j\left(-\Delta H_j\right) & \text{on reaction side}\\ 0 & \text{on permeation side}\end{cases}$$

Heat produced by chemical reactions (16)

or lumen side, depending on the configuration used. The contribute transported by permeated species, φ, is different from zero on the permeate side (it contributes to increase the temperature), but is null on the other side, because it leaves the reaction side at the same temperature. The system behaves as a splitting point of a stream, where only the extensive variables (flow rate, stream enthalpy, etc.) but not the intensive one (e.g., temperature) undergo variations.

3.03.3 Simulations

In this section, the analysis of some simulations of catalytic MRs and catalytic membranes is provided, with the aim to highlight the role of selective permeation through the membrane of some of the involved species on conversion and selectivity of reaction.

In particular, as in the previous section, some examples of tubular MRs (1D models for Pd-based MRs) and enzyme-loaded MRs are discussed.

The main parameters affecting the MR performance are:

- reaction and permeation pressures;
- temperature on both membrane sides;
- space velocity, space–time residence;
- feed molar ratio;
- reactor length;
- sweep factor; and
- amount of immobilized catalyst (enzyme).

The main variables expressing the MR performance are:

- conversion;
- species recovery;
- volume index; and
- conversion index.

The temperature strongly affects the performance of an MR both in terms of conversion and recovery of the permeating species. Although from a thermodynamic point of view the temperature promotes endothermic (e.g., MSR) or depletes exothermic (e.g., water gas shift, WGS) reactions, it always acts positively on the kinetics and, in an MR, on permeation too.

3.03.3.1 Tubular Pd-Based MRs

Figures 5 and **6** show the CO conversion and H_2 recovery calculated with a 1D nonisothermal model [41], simulating the WGS reaction in a Pd–Ag MR. The simulations were carried out for two equimolecular feed mixtures, the first one containing only CO and H_2O, the other having a typical syngas composition and, thus, containing H_2 and CO_2 also.

CO conversion in both MR and TR shows an increasing trend following the kinetics at a low reactor temperature, then decreases for a reactor temperature higher than 250 °C, owing to the limitations imposed by the thermodynamics of the WGS exothermic reaction. For both the feed mixtures, CO conversion of an MR is always higher than that of a TR and exceeds also the traditional reactor equilibrium conversion (TREC). However, TREC is significantly exceeded when a H_2-containing mixture is fed to the MR.

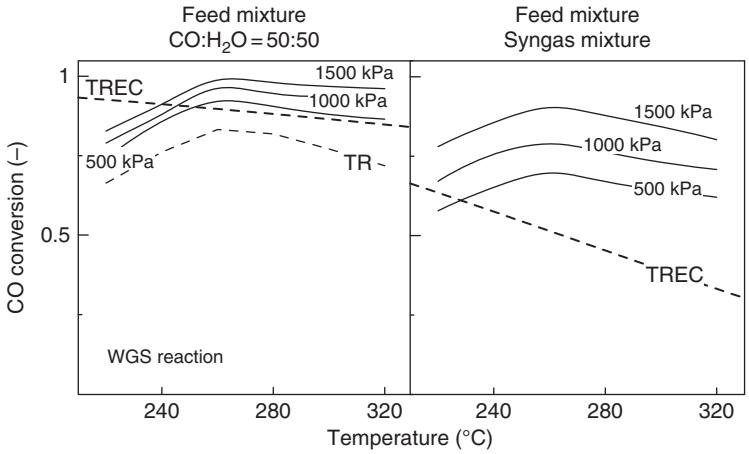

Figure 5 CO conversion as a function of the furnace temperature at different feed pressure, for two CO–H_2O equimolecular feed [41].

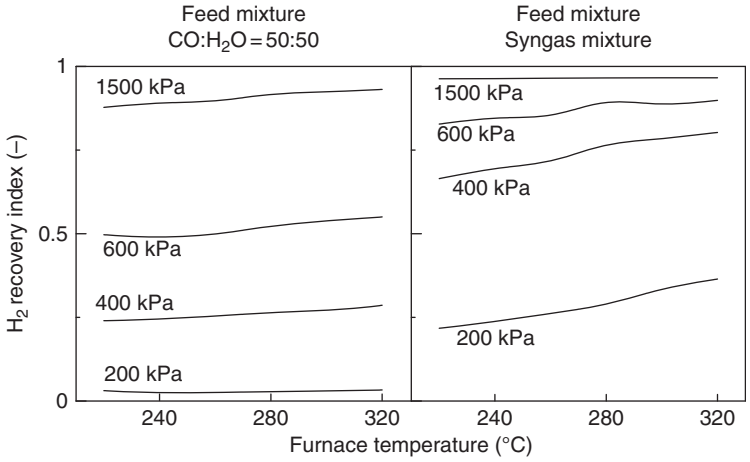

Figure 6 Recovery index as a function of the furnace temperature at different feed pressures [41].

H_2 recovery increases with the temperature, since H_2 permeation is favored and it is much higher as the feed pressure is much higher, owing to the increase in driving force. Higher recoveries were obtained with the H_2-containing mixture, confirming the greater advantages in the use of an MR with respect to the conventional applications.

Figure 7 shows CO conversion and H_2 recovery of a tubular Pd–Ag MR in which the WGS reaction is performed. The simulations carried out with a 1D model analyze the effect of the Damköhler's number (the ratio between reaction rate and convective mass transport rate) on the MR performances:

$$Da = kC_o^{n-1}\tau \tag{17}$$

Both CO conversion and H_2 recovery increase along the MR up to a plateau, which is reached faster for a higher *Da*. In particular, a high *Da* (higher space time) favors CO conversion and thus the H_2 produced, allowing higher H_2 recovery to be obtained. On the contrary, a low *Da* (reaction time much higher than space time) indicates that less H_2 is produced by the reaction with consequent low recoveries.

By means of the model it was possible to analyze the temperature profiles corresponding to CO conversion and compare them with TR results, at given *Da*, temperature, and different feed pressures. **Figure 8** shows that the CO conversion profile increases along the reactor length. As the feed pressure increases, higher CO conversions are obtained at a shorter MR length, owing to the positive effect of the pressure on H_2 permeation. Temperature profiles increase on the first part of the MR and then decrease because the heat exchange is higher than the heat

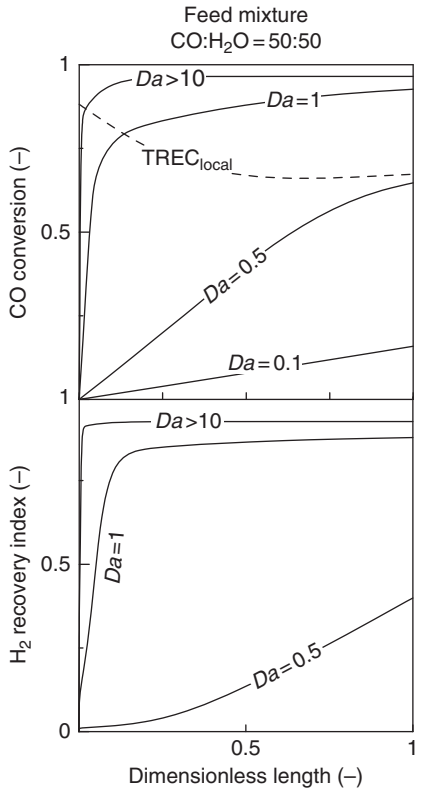

Figure 7 CO conversion and H_2 recovery profiles as a function of reactor length at different *Da*. Furnace temperature = 280 °C; feed pressure = 1000 kPa; and permeate pressure = 100 kPa [41].

generated by the reaction. Therefore, the maximum temperature and, thus, the slope of the temperature profile after the maximum depend on CO conversion establishing the heat production. The temperature reduces when CO conversion tends to a plateau,

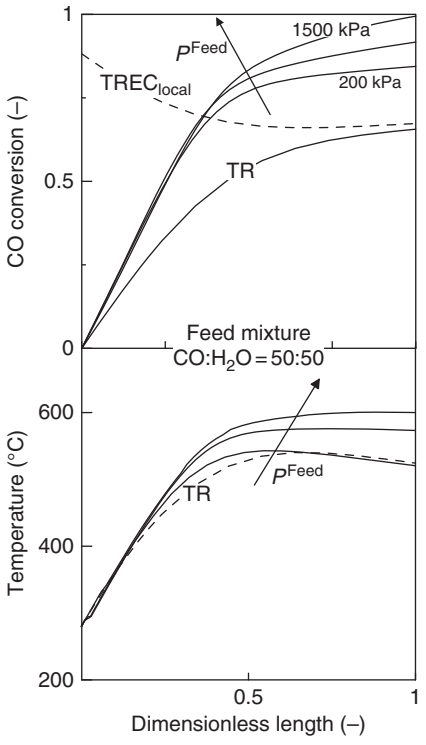

Figure 8 CO conversion and temperature profiles as a function of reactor at different feed pressures. Furnace temperature = 280 °C and $Da = 1$ [41].

since when CO is almost completely converted the net heat flux leaves the system by conductive exchange with the external environment.

An analogous model, taking into account also the energy transfer associated with the hydrogen permeation through a Pd-based membrane during MSR reaction, was used for analyzing the energy transport for different (annular and tubular) configurations of the MR. In particular, the simulations at different furnace temperatures showed that in all the cases the annular MR has higher efficiency with respect to the tubular MR (**Figure 9**). In fact, an annular MR reaches the equilibrium conversion in a shorter reactor length, since the endothermic reaction energy requirement can be more easily supplied from the furnace to the annulus with respect to the tube side (lower overall energy transfer resistance). The energy required by reaction increases with the temperature due to an increase in the equilibrium conversion. Further, the difference in the conversion between annular and tubular configurations increases with the temperature due to an increasing difference in the overall heat transfer coefficient between the furnace and reaction side.

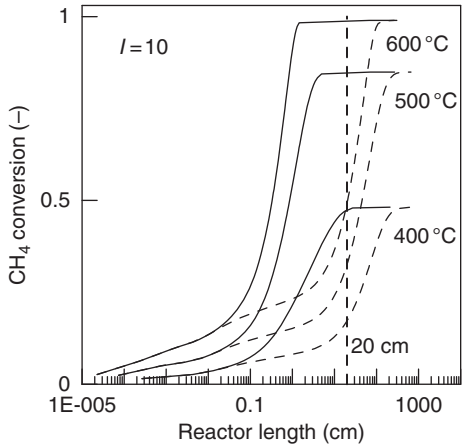

Figure 9 Methane conversion for annular (solid lines) and tubular (dashed lines) membrane reactors (MRs) at several furnace temperatures. Operating conditions: reaction side pressure = 100 kPa; permeate side pressure = 100 kPa; sweep factor = 10; feed molar ratio = 3; CH_4 feed flow rate = 200 cm^3 (1 bar, 25 °C) min^{-1} [42].

The analysis of the species profiles along the reactor axis gives interesting indications also for foreseeing the MR behavior as a function of some operative parameters. In the simulation of WGS reaction in Pd–Ag MR, Brunetti *et al.* [3, 41] proposed the analysis of the species distribution and partial pressure profiles along the MR axis at different feed pressure and Damköhler's numbers. In the case of only reactants containing mixture (**Figure 10**), all the species, except H_2, present monotonic profiles. H_2 profile increases in the first part of the reactor, reaches a maximum, and then decreases. In fact, in the first part its concentration increases, owing to both its production due to the reaction and, until an opposite driving-force exists, the back-permeation through the membrane (in $z = 0$, there is no H_2 in the reaction side and 100% of H_2 in the permeation side). On the second part of the MR, the H_2 concentration decreases since the H_2 permeation flux is higher than its production by the reaction.

When the second mixture is fed to the MR, H_2 begins to permeate also at $z = 0$ (**Figure 11**), the H_2 partial pressure on the reaction side being higher than that of the permeation side. The retentate H_2 partial pressure decreases until it reaches a plateau (no more significant permeation).

The MR length at which the partial pressure profile achieves a plateau depends on the feed condition (*Da* and feed pressure). A low *Da* (the catalyst is not enough to give higher conversions and as a consequence higher hydrogen production, **Figure 12**) means a space time lower than the

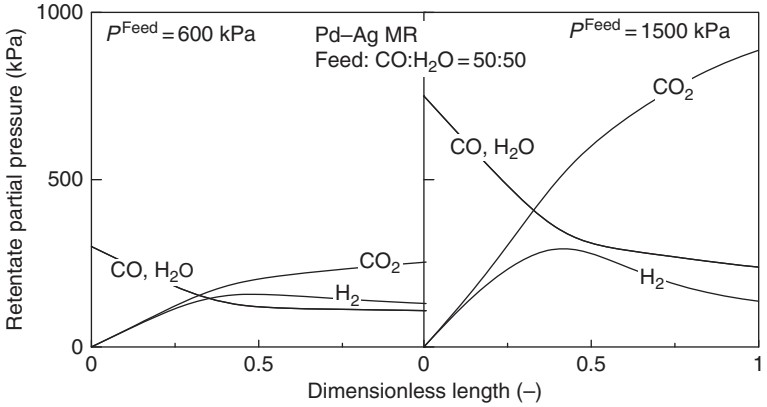

Figure 10 Partial pressure profiles on the retentate side of a Pd–Ag membrane reactor (MR). Furnace temperature = 280 °C and feed: CO:H_2O = 50:50 [41].

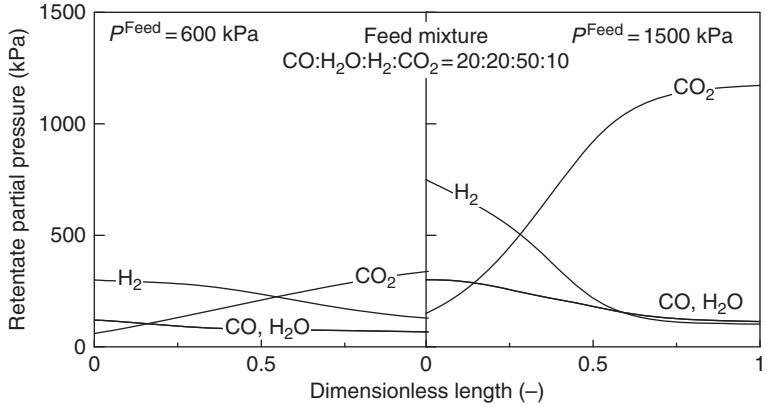

Figure 11 Partial pressure profiles on the retentate side of a Pd–Ag membrane reactor (MR). Furnace temperature = 280 °C and feed: H_2 containing mixture [41].

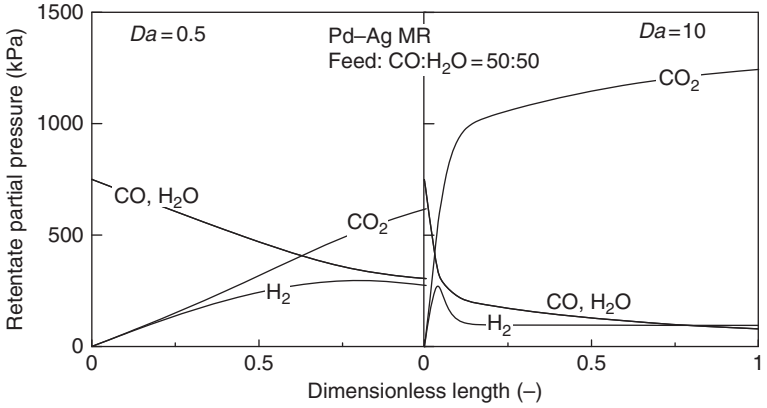

Figure 12 Partial pressure profiles on the retentate side of a Pd–Ag membrane reactor (MR). Furnace temperature = 280 °C and feed: CO:H_2O = 50:50 [41].

characteristic reaction time, and thus the reactor volume is not sufficient to complete the reaction, this being the rate-determining step. Furthermore, only a part of H_2 produced by the reaction is recovered on the permeate side, and a significant residual permeation driving force is observed at the MR outlet. On the contrary, for a high *Da*, the residence time between the reactants and the catalyst is enough to achieve higher conversions and, as a consequence, higher hydrogen production.

Caravella *et al.* [43] presented an interesting analysis about the advantages in using a permeative-stage MR instead of a conventional MR. In this study, a unit consisting in intermediate Pd-based membrane stages for H_2 permeation alternated to reactive stages was considered with the aim to maximize some important performance indexes for the reaction considered (namely, CH_4 conversion and H_2 recovery in the case of MSR reaction). In particular, using a 1D model and assuming the total length for all the reactive stages equal to one of the permeative stages, two optimal distributions of these lengths were found (providing the highest CH_4 conversion or the highest H_2 recovery). The performances obtained from the optimization were compared to the ones of a conventional MR with the same total amount of catalyst and installed membrane area. The authors showed (**Figure 13**) that the permeative-stage MR allows, alternatively, the CH_4 conversion or H_2 recovery of a conventional MR (dashed line in the plots) to be exceeded, depending on the considered optimization criterion (objective function). While CH_4 conversion remains constant along the permeative stages, H_2 recovery reduces along the reactive stages, but this reduction has to be considered apparent owing to the fact that the total already permeated H_2 is now compared with an increasing amount of produced H_2 (the reaction is continuous).

The modeling and simulation analysis is not only important for the prediction of the system performance, but it can also provide useful tools to foresee some important phenomena occurring in a membrane system that must be taken into account in the MR design. One of these is the concentration polarization that affects the permeation capability of a membrane reducing the permeation driving force of the faster species. In particular, Caravella *et al.* [44] quantified this phenomenon in the so-called polarization maps for the hydrogen separation membrane system with a Pd–Ag membrane. These maps provide an opportune factor, the concentration polarization coefficient (CPC), corresponding to a driving force reduction term that must be considered in Sieverts' law. The CPC depends on operating conditions and must be included in the permeating flux expression. The CPC is obtained as the ratio of the flux calculated considering the resistance of all the elementary steps involved in the H_2 permeation (**Figure 14**) and the one obtained by Sieverts' law utilizing the bulk driving force and hydrogen permeance.

The analysis showed that the polarization effect (**Figure 15**) can be relevant (CPC higher than 20%) not only when using very thin membranes (1–5 μm), but also when thicker membranes (e.g., 50 μm) are operated in specific conditions (CPC = 0.05–0.10).

When radial functions (e.g., polarization concentration) unfavorably affecting the MR performance begin to be important, 2D mathematical models are needed in order to provide exhaustive prediction of MRs. For instance, in Pd-based membrane applications a fast H_2 permeation, a slow radial species

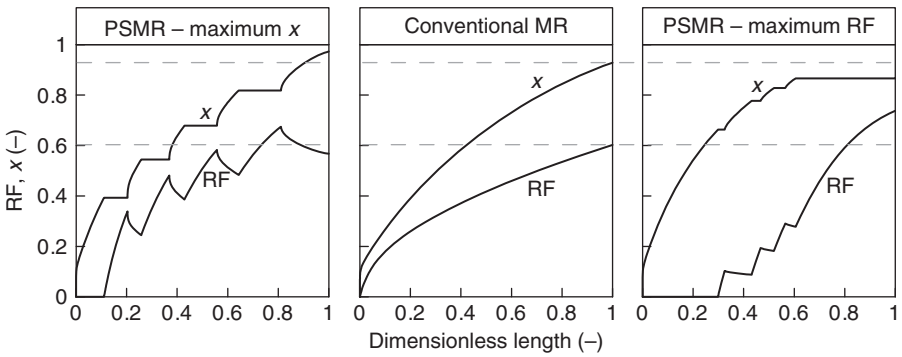

Figure 13 Comparison between the performances (CH_4 conversion, *x*, and H_2 recovery index, RF) of the permeative stages membrane reactor (MR) (in the two considered optimization criteria) and MR. $T = 600\,^{\circ}C$. Dashed lines MR values.
Reproduced from Caravella, A., Di Maio, F. P., Di Renzo, A. *J. Membr. Sci.* **2008**, *321*, 209–221, with permission from Elsevier.

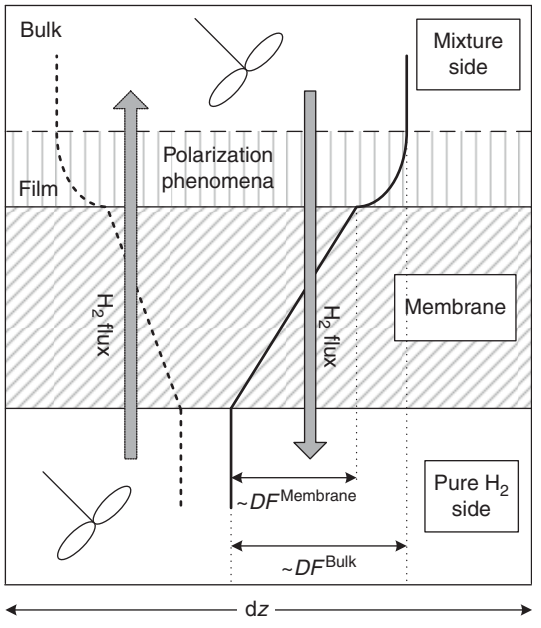

Figure 14 Schematic representation of hydrogen permeation in a generic point of a tube-in-tube permeator. The solid and dashed lines indicate the forward and backward permeation case, respectively. The profiles are intended to be those of the hydrogen partial pressure, even in the membrane, where the concentration of the atomic hydrogen is expressed in terms of equivalent pressure [44].

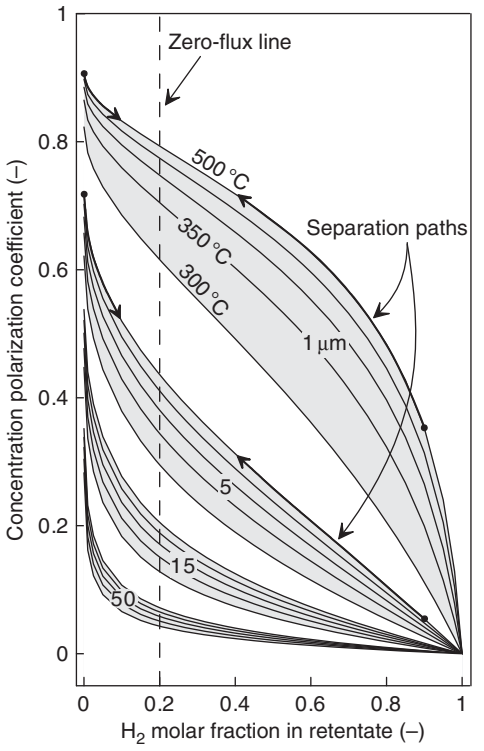

Figure 15 Polarization maps as a function of the H_2 molar fraction in the retentate for different temperatures and membrane thicknesses. The temperatures for the higher thicknesses are the same as for the 1 μm case in the same order. The thicker arrows at 1 and 5 μm indicate the separation paths. $P^{Retentate} = 1000$ kPa and $P^{Permeate} = 200$ kPa, $Re \approx 5200$ [44].

diffusion, and an enhanced velocity gradient in the feed/retentate side are all factors promoting the permeating species radial profiles.

Tiemersma *et al.* [45] elaborated a radial diffusion model that provides better prediction than the ideal plug flow mode, mostly when a high sweep factor promotes a high H_2 recovery (high H_2 flux). In particular, a 2D pseudo-homogeneous model was developed for simulating autothermal reforming of methane in a packed-bed MR. Even if radial concentration profiles are not very pronounced with the currently available membrane fluxes, the model shows how an increased membrane permeability (by a factor of 2 and 4 with respect to the reference case with a 4.5-μm thick membrane) enhances transport of hydrogen also producing significant concentration polarization (**Figure 16**). At a higher permeability, the relative difference in H_2 weight fraction between the center and the membrane wall (at 10% of the reactor length) increases from 8% to approximately 30% at quadrupled permeability, indicating that at higher membrane permeabilities indeed mass transport limitations to the membrane wall will negatively affect the reactor performance resulting in a decrease of H_2 permeation driving force.

3.03.3.2 A Two-separate-Phase Enzyme-Loaded MR

In the case of the S-naproxen methyl ester hydrolysis, solving the PDE system reported in Equation (9) is possible to evaluate the species concentration profiles in the respective phases inside the membrane pores at the two interface sides [46]. In particular, using the overall mass balance equations (Equation (9)), the organic bulk phase S-naproxen methyl ester conversion as a function of time for values of three Thiele moduli was evaluated and is shown in **Figure 17**. The same figure also indicates some experimental data carried on a laboratory scale setup (full circles, [47]). According to the fact that the higher the Φ^2 (Equation (7)) the higher the catalytic activity, increasing this parameter a higher

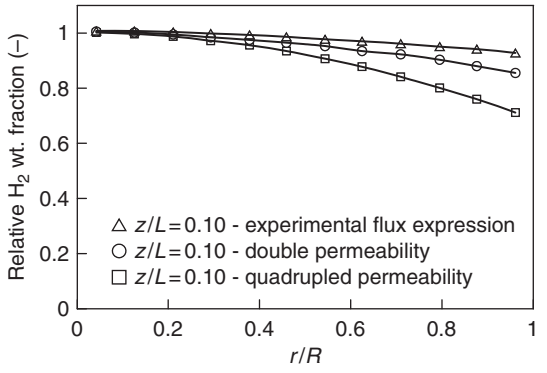

Figure 16 Relative H_2 weight fraction profiles at different membrane permeability in $z/L = 0.1$. Reproduced from Tiemersma, T. P., Patil, C. S., van Sint Annaland, M., Kuipers, J. A. M. *Chem. Eng. Sci*. **2006**, *61*, 1602–1616, with permission from Elsevier.

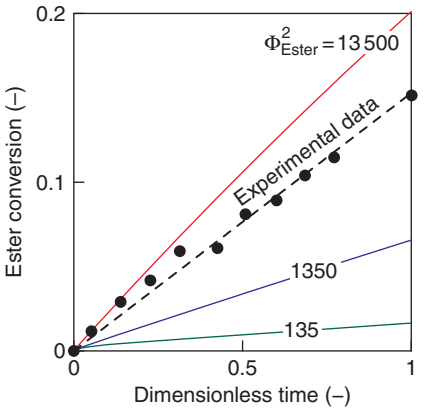

Figure 17 S-naproxen methyl ester conversion as a function of dimensionless operation time for different value of the Thiele modulus [49].

S-naproxen methyl ester conversion is achieved in the enzyme-loaded MR.

In particular, since the right V_{MAX} and K_M values for the immobilized lipase in porous asymmetric membranes are unknown and the effective S-naproxen methyl ester diffusivity was experimentally evaluated [48], the modeling allows the Michaelis–Menten kinetic parameters to be estimated, providing a conversion trend matching the experimental data:

$$\Phi^2 = \frac{V_{MAX} \cdot \delta^2}{D_{Ester} K_M}$$

where V is volume, D is diffusivity, and K is kinetic constant.

3.03.3.3 Pore-through Flow Mode: An Enzyme-Loaded MR

Regarding the biodegradation of wastewater-contained phenol by means of tirosinase in a hollow fiber MR, **Figure 18** [50] shows the predicted phenol concentration profile along the radial coordinate inside the porous enzyme-loaded membrane, at different Thiele modulus (Φ^2). A large value of Φ^2 indicates that the process is diffusion limited while its small value means limitation by reaction kinetics. In this case, the phenol concentration reduces monotonically from its maximum value (the feed concentration) at the outer membrane surface. A large value of this parameter (Φ^2) indicates a fast kinetics. The higher the Thiele modulus, the higher the phenol conversion (i.e., the lower the phenol concentration at the inner membrane surface). Based on these results, much more enzyme should be loaded in unitary membrane area to accelerate the biotransformation of the phenol.

Figure 19 shows the effect of feed composition on the enzyme-loaded MR performance. In particular, the conversion was evaluated as a function of phenol feed concentration for three Thiele modulus values (1, 5, and 10) at a Peclet of 3.04. Any change in the reactant feed concentration means a variation of the dimensionless Michaelis–Menten parameter (ξ). As expected, the higher the feed concentration, the lower the phenol conversion, owing to the fixed

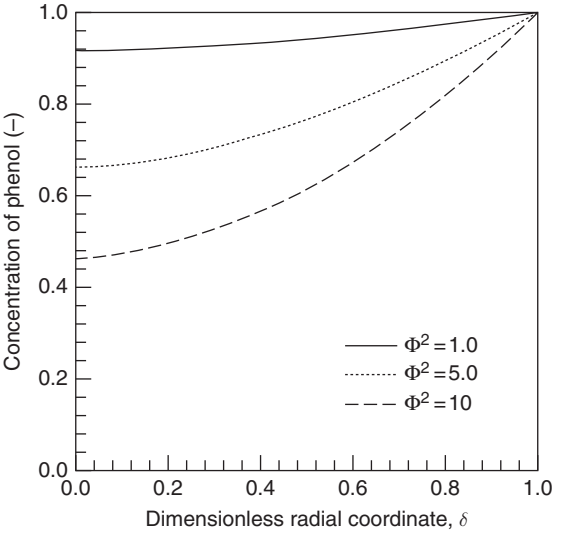

Figure 18 Effect of Thiele modulus on concentration profile of phenol ($\xi = 0.014$ and Pé = 3.04). From Choi, S.-H., Scura, F., Barbieri, G., *et al*. *Korean Membr. J.* **2009**, *19*(1), 72–82.

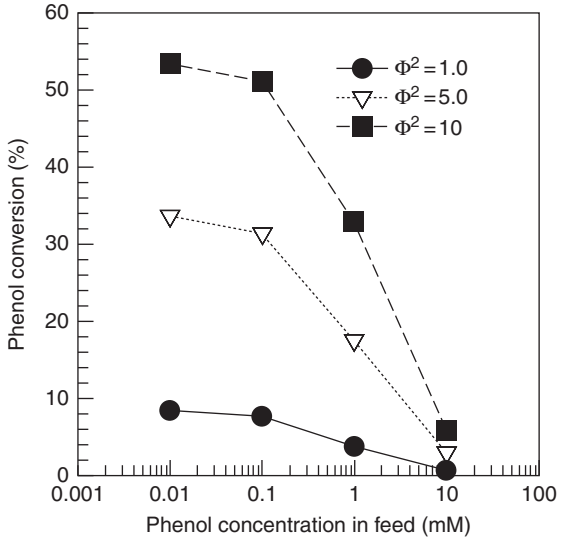

Figure 19 Phenol conversion for different feed concentration at different Thiele modulus. From Choi, S.-H., Scura, F., Barbieri, G., *et al*. *Korean Membr. J.* **2009**, *19*(1), 72–82.

biocatalyst loading, at a fixed Thiele modulus. At a higher Φ^2, the phenol conversion is shifted toward higher values. The MR is able to process a higher amount of phenol for a concentrated feed with respect to a diluted one, in a given operation time. Considering, for instance, the case of $\Phi^2 = 10$, passing phenol feed concentration from 0.1 to 1 mM, the conversion reduces from 51% to 33%. However, in the second case (1 mM) the overall amount of converted reactant is about six times the one converted when the feed composition is 10-fold lower.

3.03.4 Potentiality and Perspectives of MRs

Today, membrane technologies are becoming a valuable alternative to the traditional process, not only in the field of separations [51], but also in the field of chemical transformations [52]. In fact, MRs are today well studied, developed, and applied to an increasing number of processes in all the fields of chemical industry.

For instance, in H_2 production for fuel-cells-powered vehicles or turbines, by means of natural gas steam reforming, apart from the enhanced exploitation of the fossil fuels (higher conversion and H_2 recovery at a given operating condition), the use of MRs allows in the meantime to concentrate the produced CO_2 (in the retentate stream).

Currently, MRT (Membrane Reactor Technology) has developed a proven, proprietary technology to generate low-cost, high-purity hydrogen [53, 54] more efficiently than conventional methods of steam-methane reforming natural gas. Based on patented fluidized-bed Pd-alloy MR technology, the process combines hydrocarbon reforming, shift conversion and hydrogen purification in a single step.

One unit was supplied to Tokyo Gas, giving improved performance in comparison with fixed-bed membrane reformers (**Figure 20**). Another unit was also provided to BOC (BOC Gases – a company of The Linde Group [55]) in a project sponsored by the US Department of Energy. Actually, the units are initially geared to capacities in the 15–50 $N\,m^3\,h^{-1}$ range; the technology can be readily scaled to higher and/lower capacities as required by the applications.

MTR is also working to combine sorbent-enhanced reforming, with calcined-limestone capture of CO_2, with membrane-enhanced reforming. This combination can improve reforming efficiency, greenhouse gas capture, and better energy integration.

Recently, new metrics for comparing membrane operation performances with those of conventional units have been introduced [56, 57, 58]. With respect to the existing indicators, these new metrics take into account the size, the flexibility, and the yield of the plants. They are useful for having an immediate indication of the eventual gain that a membrane operation offers with respect to a traditional one. In this sense, they are useful also for indicating whether the membrane or the traditional operation is more suitable for a specific process. In particular, referring to the evaluation of the MRs performances, the following indexes were defined [41]:

- volume index (VI), defined as the ratio of the catalytic volume of an MR and a TR, for reaching a set CO conversion:

$$\text{Volume index} = \left.\frac{\text{Volume}^{\text{MR}}}{\text{Volume}^{\text{TR}}}\right|_{\text{Conversion}} \tag{18}$$

- conversion index (CI), the ratio between the conversion of an MR and a TR, for a set reaction volume:

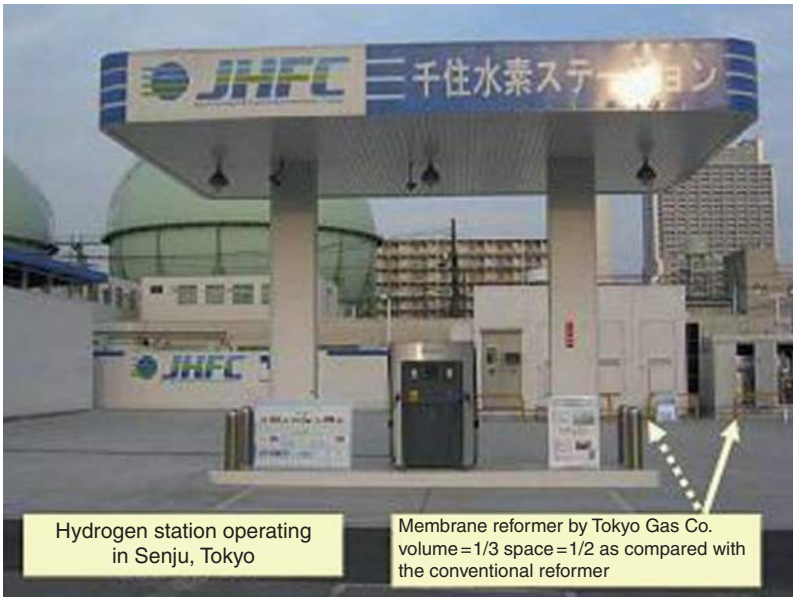

Figure 20 Photograph of the Tokyo gas hydrogen fuel station [53].

$$\text{Conversion index} = \left.\frac{\text{Conversion}^{MR}}{\text{Conversion}^{TR}}\right|_{\text{Catalyst}} \qquad (19)$$

The volume index is an important parameter in installing new plants which must be characterized by low size and high productivities. VI is an indicator of the productivity of MR and it compares the MR reaction volume with that of a TR, necessary to achieve a set conversion.

VI ranges from 0 to 1. A low VI means that the reaction volume required by an MR to reach a set CO conversion is much lower than that necessary for a TR. As a consequence, the catalyst weight necessary in MR is significantly reduced.

Considering the WGS reaction as a case study, it can be seen that VI is a decreasing function of the feed pressure, owing to the positive effect that the latter has in an MR on CO conversion. MR reaction volume is 75% of the TR one at 600 kPa and reduces down to 25% at 1500 kPa, when an equimolecular mixture is fed and a final conversion of ~80% (corresponding to 90% of the TREC) is considered. This means a reduction in plant size and related costs (**Figure 21**). Feeding a

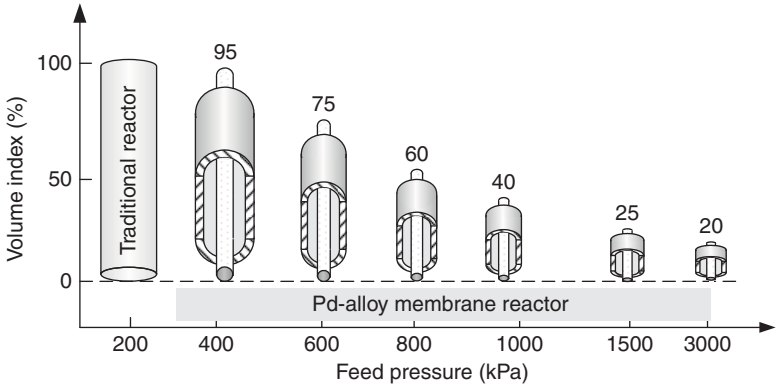

Figure 21 Volume index as a function of feed pressure feeding an equimolecular mixture. Furnace temperature = 280 °C. Set CO conversion 90% of the traditional reactor equilibrium conversion (TREC). Reproduced from Brunetti A., Caravella A., Barbieri G., Drioli E., *J. Membr. Sci.* **2007**, 306, 329–340, with permission from Elsevier.

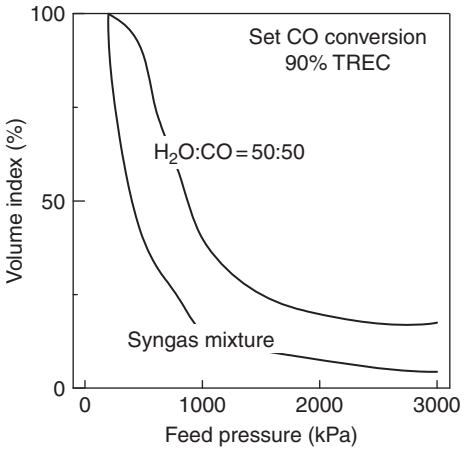

Figure 22 Volume index as a function of feed pressure with two feeds. Furnace temperature = 280 °C. Set CO conversion 90% of the traditional reactor equilibrium conversion (TREC).

typical syngas stream containing also hydrogen (20:20:50:10 = $CO:H_2O:H_2O:CO_2$) into the Pd–Ag MR, the VI is further lower owing to the low value of the equilibrium conversion (**Figure 22**). Therefore, the catalyst amount necessary to reach a suitable conversion is drastically reduced with clear gain also in terms of plant size reduction.

Figure 23 shows the dependence of the VI on the reactor temperature. Feeding an equimolecular mixture or a syngas stream VI decreases at the higher temperature, owing to the positive effect that the temperature has on the hydrogen permeation,

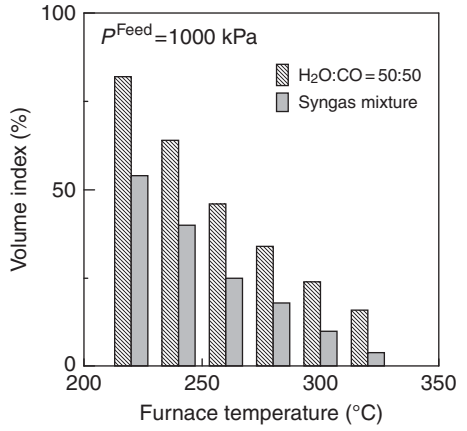

Figure 23 Volume index as a function of feed pressure with two different feeds. Feed pressure = 1000 kPa. Set CO conversion 90% of the traditional reactor equilibrium conversion (TREC).

which implies higher CO conversion and that, in other terms, less catalyst volume is required at higher temperature for reaching a set CO conversion. This effect is much more evident for the reformate feed stream containing also hydrogen.

Another improvement in the MR configuration that leads to a further reduction of the VI was proposed by Barbieri *et al.* [59]. Referring to the feed mixtures at high CO content, the authors proposed to allocate the membrane only in the second part of the catalytic bed, in order to assure a good exploitation of the whole membrane area for the permeation. Considering an equimolecular feed mixture, at 600 kPa the innovative MR showed a VI of 40%, lower than that shown by the simple MR (65%) at the same operating conditions (**Figure 24**).

This suggests the clear gain in the use of the innovative solution that, allowing the problems related to the good exploitation of the membrane area to be overcome, shows further reaction volume reduction with respect to that achieved with the traditional MR. From the evaluation of VI, also considering membranes other than Pd–Ag, such as silica, it was observed that globally the MR offers better performance than TR. At high feed pressure, the reaction volume of the MR with the silica membrane was calculated to be one-half of the TR volume at the same operating conditions, but higher than that of a Pd–Ag MR (**Figure 25**).

This effect is mainly due to the fact that Pd–Ag shows infinite hydrogen, whereas a microporous membrane is permeable also by the other gases; hence, more catalyst volume is required for reaching the same CO conversion.

The capability of reaching a conversion higher than a TR, exceeding the TR equilibrium limits, is a typical

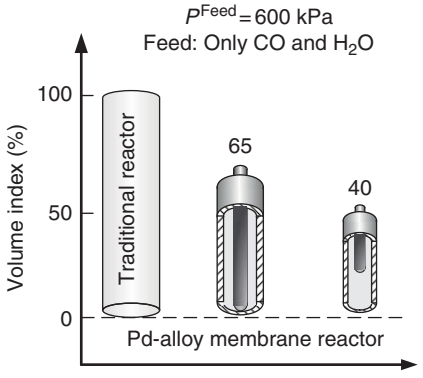

Figure 24 Comparison of the volume index of typical and innovative membrane reactor (MR) configuration.

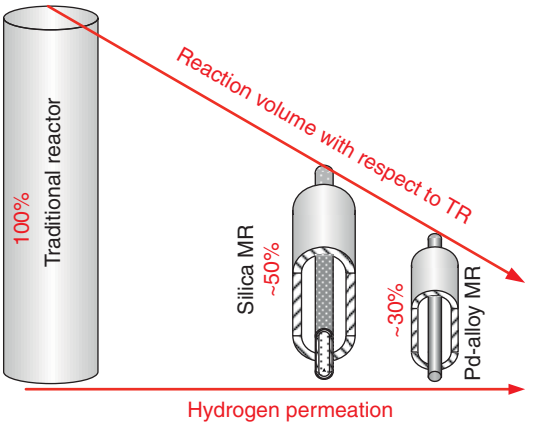

Figure 25 Reaction volume reduction for different membrane types. Furnace temperature = 280 °C and feed pressure = 1200 kPa.

property of an MR. The conversion index, defined as the ratio between the conversion achieved in an MR and that of a TR, for a set reaction volume, gives an evaluation of the gain in terms of conversion and its use is particularly indicated when the feed mixture also contains reaction products. A high CI implies a relevant gain in terms of conversion achieved in an MR with respect to the conventional reactor one, with the same reaction volume, meaning better raw material exploitation and lower waste. The MR are pressure-driven systems. Therefore, CI is an increasing function of the feed pressure as shown in **Figure 26**.

In particular, a CI of ~2 was achieved at 200 kPa, whereas a CI of ~6 was reached at 1500 kPa feeding the reformate stream (20:20:50:10=CO:H_2O:H_2O:CO_2). However, already at 500 kPa, a CI is equal to 4. When an equimolecular feed containing only reactants is fed to MR, CI ranges from 1.5 to 1 because the TR conversion is already high. However, a CI equal to 1.5 indicates ~95% of CO conversion, implying not only a pure H_2 stream in the permeate side but also a CO_2 concentrated retentate stream easy to recover.

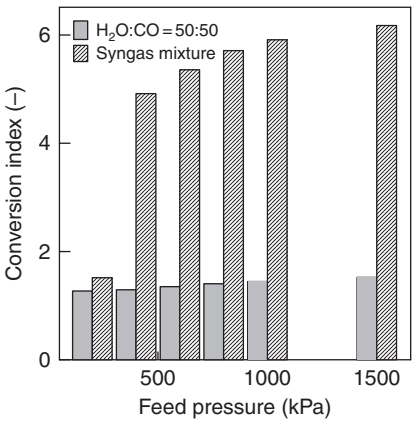

Figure 26 Conversion index as a function of the feed pressure for different feeds. Furnace temperature = 280 °C.

Acknowledgment

The Italian Ministry of Education, University and Research, Progetto "FIRB–CAMERE RBNE03JCR5 – Nuove membrane catalitiche e reattori catalitici a membrana per reazioni selettive come sistemi avanzati per uno sviluppo sostenibile" is gratefully acknowledged for cofunding this work.

References

[1] Stankiewicz, A., Moulijn, J. A. *Ind. Eng. Chem. Res.* **2002**, *41*, 1920–1926.
[2] Drioli, E., Romano, M. *Ind. Eng. Chem. Res.* **2001**, *40*, 1277–1300.
[3] Brunetti, A., Caravella, A., Barbieri, G., Drioli, E. *J. Membr. Sci.* **2007**, *306*, 329–340.
[4] Barbieri, G., Brunetti, A., Tricoli, G., Drioli, E. *J. Power Sources* **2008**, *182*, 160–167.
[5] Brunetti, A., Barbieri, G., Drioli, E. *Chem. Eng. Proc.: Process Intensification* **2008**, *477*, 1081–1089.
[6] Kikuchi, E., Uemiya, S., Sato, N., Inoue, H., Ando, H., Matsuda, T. *Chem. Lett.* **1989**, *3*, 489–492.
[7] Uemiya, S., Sato, N., Inoue, H., Ando, H., Kikuchi, E. *Ind. Eng. Chem. Res.* **1991**, *30*, 585–592.
[8] Criscuoli, A., Basile, A., Drioli, E. *Catal. Today* **2000**, *56*, 53–64.
[9] Barbieri, G., Bernardo, P. Experimental Evaluation of Hydrogen Production by Membrane Reaction. In *Carbon Dioxide Capture for Storage in Deep Geologic Formations – Results from the CO_2 Capture Project*; Thomas, D., Benson, S., Eds.; Elsevier: New York, 2004; Vol. 1, Chapter 22, pp 385–408.
[10] Onstot, W. J., Minet, R. G., Tsotsis, T. T. *Ind. Eng. Chem. Res.* **2001**, *40*, 242–251.
[11] Sjardin, M., Damen, K. J., Faaij, A. P. C. *Energy* **2006**, *31*(14), 2187–2219.
[12] Bracht, M., Alderliesten, P. T., Kloster, R., *et al. Energy Convers. Manage.* **1997**, *38*, S159–S164.
[13] Yeung, K. L., Zhang, X., Lau, W. N., Martin-Aranda, R. *Catal. Today* **2005**, *110*(1–2), 26–37.
[14] Dudukovic, M. P. *Catal. Today* **1999**, *48*(1–4), 5–15.
[15] Sun, J., Desjardins, J., Buglass, J., Liu, K. *Int. J. Hydrogen Energy* **2005**, *30*(11), 1259–1264.
[16] Majumder, D., Broadbelt, L. J. *AIChE J.* **2006**, *52*(12), 4214–4228.
[17] Collins, J. P., Way, J. D., Kraisuwansarn, N. *J. Membr. Sci.* **1993**, *77*(2–3), 265–282.
[18] Chmielewski, D., Ziaka, Z., Manousiouthakis, V. *Chem. Eng. Sci.* **1999**, *54*, 2979–2984.
[19] Belgued, M., Pareja, P., Amariglio, A., Amariglio, H. *Nature* **1991**, *352*, 789–790.
[20] Koerst, T., Deelen, M. J. G., Van Santen, R. A. *J. Catal.* **1992**, *138*, 101–110.

[21] Gryaznov, V. *Catal. Today* **1999**, *51*, 391–395.
[22] Armor, J. N. *J. Membr. Sci.* **1998**, *147*, 217–233.
[23] Coronas, J., Santamaria, J. *Catal. Today* **1999**, *51*, 377–389.
[24] Sirkar, K. K., Shanbhag, P. V., Kovvali, A. S. *Ind. Eng. Chem. Res.* **1999**, *38*, 3715–3727.
[25] Drioli, E., Basile, A., Criscuoli, A. *Clean Prod. Process.* **2000**, *2*, 179–186.
[26] Julbe, A., Farrusseng, D., Guizard, C. *J. Membr. Sci.* **2001**, *181*, 3–20.
[27] Tosti, S., Bettinali, L., Violante, V. *Int. J. Hydrogen Energy* **2000**, *25*, 319–325.
[28] Belgued, M., Amariglio, A., Pareja, P., Amariglio, H. *J. Catal.* **1996**, *161*, 282–291.
[29] She, Y., Dardas, Z., Gummalla, M., Vanderspurt, T., Emerson, S. *ACS Div. Fuel Chem., Preprints* **2005**, *50*(2), 561–566.
[30] Xu, Z.-Q., Chen, Q.-L., Lu, G.-Z. *Petrochem. Technol.* **1999**, *28*(6), 362–370.
[31] Assaf, E. M., Jesus, C. D. F., Assaf, J. M. *Braz. J. Chem. Eng.* **1998**, *15*(2), 160–166.
[32] Lin, Y.-M., Liu, S.-L., Chuang, C.-H., Chu, Y.-T. *Catal. Today* **2003**, *82*(1–4), 127–139.
[33] Capobianco, L., Del Prete, Z., Schiavetti, P., Violante, V. *Int. J. Hydrogen Energy* **2006**, *31*, 1079–1090.
[34] Marigliano, G., Barbieri, G., Drioli, E. *Catal. Today* **2001**, *67*(1–3), 85–99.
[35] Bernardo, P., Algieri, C., Barbieri, G., Drioli, E. *Sep. Purif. Technol.* **2008**, *62*, 631–637.
[36] Barbieri, G., Brunetti, A., Scura, F., *et al. Korean Membr. J.* **2006**, *8*(1), 1–12.
[37] Abo-Ghander, N. S., Grace, J. R., Elnashaie, S. S. E. H., Lima, C. J. *Chem. Eng. Sci.* **2008**, *63*(7), 1817–1826.
[38] Gobina, E., Hou, K., Hughes, R. *Chem. Eng. Sci.* **1995**, *50*, 2311–2319.
[39] Barbieri, G., Scura, F., Brunetti, A. Mathematical Modelling of Pd-Alloy Membrane Reactors. In *Inorganic Membranes: Synthesis, Characterization and Applications*; Mallada, R., Menendez, M., Eds.; Membrane Science and Technology Series; Elsevier: Amsterdam, 2008; Vol. 13, Chapter 9, pp 325–400 (ISBN 978 0 444 53070 7; ISSN 0927-5193, doi:10.1016/S0927-5193(07)13009-6).
[40] Nagy, E. Mathematical Modelling of Biochemical Membrane Reactors. In *Membrane Operations Innovative Separations and Transformations*; Drioli, E., Giorno, L., Eds.; Wiley-VCH: Weinheim, 2009; Chapter 14, pp 309–324 (ISBN-10:3-527-32038-5; ISBN-13:978-3-527-32038-7).
[41] Brunetti, A., Caravella, A., Barbieri, G., Drioli, E. *J. Membr. Sci.* **2007**, *306*(1–2), 329–340.
[42] Marigliano, G., Barbieri, G., Drioli, E. *Catal. Today* **2001**, *67*, 85–99.
[43] Caravella, A., Di Maio, F. P., Di Renzo, A. *J. Membr. Sci.* **2008**, *321*, 209–221.
[44] Caravella, A., Barbieri, G., Drioli, E. *Sep. Purif. Technol.* **2009**, *66*, 613–624.
[45] Tiemersma, T. P., Patil, C. S., van Sint Annaland, M., Kuipers, J. A. M. *Chem. Eng. Sci.* **2006**, *61*, 1602–1616.
[46] Zhang, J., Barbieri, G., Scura, F., Giorno, L., Drioli, E. *Desalination* **2006**, *200*, 514–515.
[47] Giorno, L., D'Amore, E., Mazzei, R., *et al. J. Membr. Sci.* **2007**, *295*, 95–101.
[48] Giorno, L., Zhang, J., Drioli, E. *J. Membr. Sci.* **2006**, *276*, 59–67.
[49] Scura, F., Barbieri, G., Giorno, L., Zhang, J., Drioli, E. Mathematical Modelling of Two Separate Phases Enzymatic Membrane Reactor. In *6th European Congress of Chemical Engineering (ECCE-6)*, Copenhagen, Denmark, 16–20 September 2007; Book of Abstracts; Gani, R., Dam-Johansen K. Eds.; Vol. 2, pp 143–144.
[50] Choi, S.-H., Scura, F., Barbieri, G., *et al. Korean Membr. J.* **2009**, *19*(1), 72–82.
[51] Baker, R. W. Membrane Gas-Separation: Application. In *Membrane Operations Innovative Separations and Transformations*; Drioli, E., Giorno, L., Eds.; Wiley-VCH: Weinheim, 2009; Chapter 8, pp 37–74 (ISBN-10:3-527-32038-5; ISBN-13:978-3-527-32038-7).
[52] Specchia, S., Fino, D., Saracco, G., Specchia, V. Inorganic Membrane Reactors. In *Structured Catalysts and Reactors*, 2nd edn.; Cybulski, A., Moulijn, J. A., Eds.; CRC: Boca Raton, FL, 2006; Chapter 18, pp 615–662.
[53] http://membranereactor.com/images/2003-05-16-0007.pdf.
[54] http://membranereactor.com/technology_body_right.html.
[55] BOC, http://www.boc.com (accessed November 2009).
[56] Brunetti, A., Barbieri, G., Drioli, E. *Chem. Eng. Sci.* **2009**, *64*(15), 3448–3454.
[57] Criscuoli, A., Drioli, E. *Ind. Chem. Eng. Res.* **2007**, *46*, 2268–2271.
[58] Sikdar, S. K. *AIChE J.* **2003**, *49*, 1928–1932.
[59] Barbieri, G., Brunetti, A., Tricoli, G., Drioli, E. *J. Power Sources* **2008**, *182*, 160–167.

Biographical Sketches

Dr. Giuseppe Barbieri is currently a researcher, and a member of, the Scientific Committee of the Institute on Membrane Technology of National Research Council, Rende CS – Italy. His expertise is in the field of membrane science and engineering from modeling to experimental investigations of membrane gas separation, catalytic membrane reactors for high- and low-temperature reactions, etc. He was/is responsible for some co-funded projects from the EU (Hydrofueler, GRACE), and the Ministry of Foreign Affairs of Italy in the field of hydrogen production, separation, and its purification, also for feeding proton exchange membrane (PEM) fuel cells and in carbon dioxide separation by means of polymeric membranes. He has authored numerous publications in international journals and congress proceedings in the field of membrane science and engineering. He served on the scientific Committee of International Conferences and as reviewer for some scientific journals.

Dr. Francesco Scura has been involved, as a nonpermanent staff member (postdoctoral position), with the Institute on Membrane Technology, National Research Council of Italy, ITM-CNR, since 2003. In 2008, he gained his PhD in chemical and materials engineering from the University of Calabria (Italy), upon defending his thesis titled "Engineering of Membrane Gas Separation". His main research fields are membrane gas separation and membrane reactors.

Dr. Adele Brunetti, has been involved, as a nonpermanent staff member, with the Institute on Membrane Technology, National Research Council of Italy, ITM-CNR, since 2004. In 2008, she gained her PhD in chemical and materials engineering from the University of Calabria (Italy), upon defending her thesis titled "Integrated Membrane Plant for Pure Hydrogen Production". Currently, she is holding a postdoctoral position at the ITM-CNR in the field of membrane gas separation. Her research activities are mainly in the fields of catalytic membrane reactors, fuel processing, and membrane gas separation.

3.04 Multiphase Membrane Reactors

R Di Felice, G Capannelli, and A Comite, University of Genoa, Genoa, Italy

3.04.1	**Introduction**	82
3.04.1.1	Some General Considerations on Membrane Reactors	82
3.04.1.2	Materials for Membrane Reactors	83
3.04.1.3	Catalytic Membrane Preparation	84
3.04.2	**Overview of Multiphase Membrane Reactors**	86
3.04.2.1	The Reaction Takes Place in One of the Two Fluid Phases	86
3.04.2.1.1	The reaction takes place outside the membrane	87
3.04.2.1.2	The reaction takes place inside the membrane	88
3.04.2.1.3	The reaction takes place inside the membrane structure	89
3.04.2.2	The Reaction Takes Place on a Catalyst	90
3.04.2.2.1	The catalysts are placed in the membrane lumen	90
3.04.2.2.2	The catalysts are placed on the membrane surface	91
3.04.2.2.3	The catalysts are dispersed on the membrane structure	92
3.04.3	**The Mathematical Modeling of Multiphase Membrane Reactors**	93
3.04.3.1	Membrane Contactors	93
3.04.3.1.1	Membrane contactors working in wetted mode with negligible homogeneous reaction	94
3.04.3.1.2	Membrane contactor reaction working in nonwetted mode with negligible homogeneous reaction	96
3.04.3.2	Evaluation of Local Mass Transfer Coefficients in the Boundary Layers Located on Both Sides of the Membrane Surface	97
3.04.3.2.1	Membrane contactors in the presence of a homogeneous reaction in the liquid phase	98
3.04.3.3	Catalytic Three-Phase Membrane Reactors	99
3.04.3.3.1	Internal diffusion in a TPCMR	101
3.04.3.3.2	Influence of external mass transfer	102
3.04.3.4	Some Considerations on the Mass Balance in Membrane Contactors and Three-Phase Membrane Reactors	103
3.04.4	**Conclusions**	105
References		105

Nomenclature

A_M	membrane area (m^2)
C_A	molar concentration of specie A ($mol\ m^{-3}$)
D	diffusivity ($m^2\,s^{-1}$)
Da	Damköler number (–)
D_{eff}	effective diffusivity ($m^2\,s^{-1}$)
D_K	Knudsen diffusivity ($m^2\,s^{-1}$)
D_{eff}^K	effective Knudsen diffusivity ($m^2\,s^{-1}$)
D_{eff}^m	effective molecular diffusivity ($m^2\,s^{-1}$)
E_{app}	apparent activation energy ($J\,mol^{-1}$)
E_{diff}	activation energy describing the temperature dependence of the specie A diffusivity ($J\,mol^{-1}$)
E_{in}	intrinsic activation energy ($J\,mol^{-1}$)
E_{sat}	activation energy describing the temperature dependence of the specie A solubility ($J\,mol^{-1}$)
Gz	Graetz number (–)
H	Henry constant (–)
k	kinetic constant ($m\,s^{-1}$)
k_c	local mass transfer coefficient ($m\,s^{-1}$)
k_g	mass transfer coefficient in the gas-phase boundary layer ($m\,s^{-1}$)
k_l	mass transfer coefficient in the liquid-phase boundary layer ($m\,s^{-1}$)
K_G	overall mass transfer coefficient defined against the gas-phase molar concentration ($m\,s^{-1}$)

K_L	overall mass transfer coefficient defined against the liquid-phase molar concentration ($m\,s^{-1}$)
L	membrane length (m)
M	molecular mass ($mol\,kg^{-1}$)
N_A	molar flux ($mol\,s^{-1}\,m^{-2}$)
P	pressure (Pa)
r_A	reaction rate per volume of catalyst ($mol\,s^{-1}\,m^{3}$)
r'_A	reaction rate per mass of catalyst ($mol\,s^{-1}\,kg$)
Re	Reynolds number (–)
r_p	pore radius (m)
Sc	Schmidt number (–)
Sh	Sherwood number (–)
t_M	membrane thickness (m)
u	fluid velocity ($m\,s^{-1}$)
V_M	membrane volume (m^3)
δ	dimensionless coordinate (–)
Δ_p	breakthrough pressure (Pa)
ε	porosity (–)
η_{int}	internal effectiveness factor (–)
$\eta_{overall}$	overall effectiveness factor (–)
θ	contact angle (–)
μ	viscosity ($kg\,m^{-1}\,s^{-1}$)
ρ	membrane density ($kg\,m^{-3}$)
σ	surface tension ($N\,m^{-1}$)
τ	tortuosity (–)
ϕ	Thiele modulus (–)

Subscripts

G, g	gas phase
i	interface
L, l	liquid phase
r	radial coordinate in channel geometry
x, z	axial coordinate

3.04.1 Introduction

There is very little doubt that membranes were certainly conceptualized and introduced for their ability to separate different components by exploiting their different physical characteristics. Nevertheless, their use as a process plant unit, where a chemical reaction also takes place, has been proved to be of enormous potential, and a very large number of studies have been carried out in universities and research center laboratories. At the same time, membrane chemical reactors have started to become a reality in modern process plants. Process intensification is one of the many reasons for such a vast interest: the possibility, for example, to merge the reaction and the separation step in a single unit is far too appealing to leave it uninvestigated [1].

To provide a thorough review of all the scientific works published in the past few decades on the subject of membrane reactors is not an aim of the present work, and, in any case, it would be an impossible task given the sheer size of the information currently available. For this purpose, the reader can refer to excellent works which have been published in recent years for a summary of scientific advancements, starting, for example, from the work of Krishna and Sie [2] who addressed the individuation of the best reactor configuration compatible with process requirements for multiphase reactor systems, to the contributions by Coronas and Santamaria [3] and by Dixon [4] devoted to the development and opportunities in the use of inorganic membrane reactors, to finally the recent presentation of Rios *et al.* [5] who reported the huge potential applications in the not-so-distant future of membranes in biotechnology.

As any other chemical reactor unit, membrane reactors can be first classified depending on the presence or absence of a catalytic material to enhance reaction rate. Moreover, the reaction can take place on the inner side of the membrane, or the outer side, or inside the membrane structure itself, so that six possible arrangements can be identified overall. Each arrangement is briefly described, and typical results from the literature are presented in the next section.

3.04.1.1 Some General Considerations on Membrane Reactors

In general, membranes are used to separate selectively at least one of the components present in a gas or liquid phase. An interesting and less-known use of membranes is their use as an interface, which segregates two different fluid phases, with a chemical reaction also taking place. The two fluid phases can be two immiscible liquids, or a gas phase and a liquid phase. The role of the membrane is to offer a well-defined and constant contact area between the two fluid phases. When no chemical reaction is taking place on a catalyst, as in a membrane contactor, the

membrane is simply used to interface the two phases; the use of the proper membrane configuration and geometry allows the achievement of a very high interphase contact area in very small volumes and, in turn, in very compact systems. The mass transfer between the two phases interfaced by the membrane is obviously improved or enhanced in the presence of a homogeneous reaction in one of the two phases.

In a three-phase catalytic membrane reactor, the membrane has catalytic properties such that a reaction takes place in the membrane structure. The mass transfer phenomena, typical of a membrane contactor, can also be encountered in a three-phase catalytic membrane reactor; in this case, the overall efficiency concerning the effective catalytic layer utilization will depend, as discussed subsequently, both on the influence of the mass transfer rate in the two phases and on the combined mass transfer and reaction rate in the catalytic membrane structure.

The interface area per unit of system volume is related to the geometry and configuration of the membrane module [6]. Different membranes and membrane modules are now commercially available, and each of them can be characterized in terms of packing density. Packing density is usually defined as the ratio between the membrane surface area and the volume of the membrane module. **Table 1** shows some typical membrane packing density values. Membranes can have different geometries, for example, as

1. flat sheets which can be assembled either in a plate and frame or in a spiral-wound module; or
2. tubes (single or multichannel) or hollow fibers (diameter between 50 μm and 3 mm).

Hollow-fiber membranes offer the highest interfacial area and are therefore thoroughly investigated for applications in membrane contactors [7].

Table 1 Packing density of some membrane modules

Membrane geometry and module	*Packing density ($m^2\,m^{-3}$)*
Single plate	30–40
Plate and frame	200–400
Spiral wound	300–900
Single tube	30–300
Multichannel	300–600
Hollow fiber	9000–30 000

Adapted from Hsieh, H.P. *Inorganic Membranes for Separation and Reaction*. Elsevier: Amsterdam, 1996.

3.04.1.2 Materials for Membrane Reactors

Membrane reactors material can be inorganic or polymeric. The commercially available hollow fibers are polymeric, but there is a great effort in exploring methods to manufacture mechanically resistant inorganic hollow fibers. Polymeric porous membranes are usually employed as membrane contactors; however, recently, there is a growing interest in the use of zeolite membranes [8]. Both polymeric and inorganic porous catalytic membranes are used for catalytic membrane reactors, and there are also some examples of dense polymeric catalytic membrane reactors. The catalyst is introduced in the membrane porosity using various methods, such as impregnation techniques (using catalyst precursors which may or may not interact with the membrane material) or homogeneous controlled precipitation [9].

In three-phase catalytic membrane reactors, the membrane usually acts as an interface between two phases. The membrane then imposes the modality of meeting between the reactants contained in the different fluid phases and, eventually, with the catalytic specie contained in the membrane structure. It is then clear that the proper membrane material selection and a suitable design of the catalytic membrane are crucial for the success and effectiveness of a three-phase membrane reactor.

The selection of the membrane material and structure is clearly related to the characteristic the reaction environment (solvent properties of the fluid phases, pH) and to the operating conditions (e.g., temperature and pressure). Membranes are typically made from polymers or inorganic materials (e.g., ceramics and metals) or from polymer-inorganic composites. Since the application of membrane reactors for gas- or vapor-phase reactions requires a good thermal stability of materials, a greater interest has been typically devoted to inorganic materials. With specific reference to three-phase membrane reactors, the possibility of using milder operating conditions opens new and interesting opportunities for polymeric membranes as well. The choice of a suitable material for a membrane reactor is related to its stability in the reaction environment during the reaction and on the operation time. Moreover, the presence of a hydrophobic or hydrophilic character can have an influence on the reactor performance, since the membrane is filled by one fluid rather than the other one. Considering a three-phase membrane reactor working between a gas phase and an aqueous phase, most of the nonhydrosoluble polymeric

membranes could find an application. When one of the reacting phases is (1) an aqueous phase containing aggressive components (e.g., chlorine) or (2) an organic solvent, the compatibility or the stability of the polymeric membrane in the solvent at the operating conditions should be verified.

Polymeric membranes are widely available in the market in several configurations and with different structures. For the applications as membrane contactors and, in turn, as membrane reactors, the flat, tubular, and hollow-fiber configurations are the most investigated. Polymeric membranes to be applied in three-phase membrane reactors can be dense or porous. For example, a dense membrane can be applied to a fluid phase containing a reactant, which, because of its solubility in the membrane polymer, can diffuse on the other side of the membrane to meet the gas-phase reactant. Concerning porous membranes, the pore distribution along the membrane thickness can be uniform (symmetric membranes) or can vary with/without the presence of cavities. The membrane synthesis methods now available allow one to obtain several distribution models of pore and cavities, especially for hollow-fiber membranes.

Common inorganic materials for membranes are single oxides (alumina, titania, and zirconia) or mixed oxides (e.g., alumina–titania and alumina–zirconia), aluminosilicates and zeolites, and porous stainless steel, glass, or carbon. Inorganic composite membranes can be obtained by the combination of the previous inorganic materials. **Table 2** summarizes the stability characteristics of some ceramic materials. Inorganic membranes studied for the application in multiphase membrane reactor usually have a tubular geometry, either single channel (**Figure 1(a)**) or multichannel (**Figures 1(b)**–**1(f)**). Recently, inorganic hollow-fiber membranes are under development and, in principle, they can offer a higher packing density, although they are in many cases still too brittle; therefore, they will probably find interesting applications as three-phase membrane reactors in the near future.

3.04.1.3 Catalytic Membrane Preparation

The deposition of the catalyst in the membrane structure can be carried out using different methods, which in turn results in different catalytic activity and catalytic site distribution. A review about the preparation methods of polymeric catalytic membranes was given by Ozdemir *et al.* [10], which is not reiterated here. Most of the deposition methods on inorganic supports have been adapted from the traditional ways of deposition of a catalyst on pellets; a general overview is presented in the following paragraphs with the aim to introduce the reader to a topic that still requires further investigations.

When a catalytic membrane reactor is considered, it can be interesting to tune the catalyst distribution inside the membrane structure. **Figure 2** shows some possible catalyst distributions. **Figure 2(a)** refers to a membrane made up of a single support material on which the catalysts have been deposited homogeneously all over the membrane structure (case 1) or preferentially in a specific position in the membrane itself (cases 2 and 3). Conversely, **Figure 2(b)** represents a membrane made up of two different materials, with the catalysts deposited only in one of the materials. Needless to say, since in three-phase membrane reactors the membrane acts as an interface between the two reacting phases, a catalyst deposition which results in a distribution of the active specie leading to a reduction of the diffusion path of reactants would be desirable.

Table 2 Chemical and thermal stability of some inorganic materials for membrane preparation

Composition	*Stability in acid and alkali*	*Notes*
Alumina	Stable in HCl, HNO_3 Unstable in HF, H_3PO_4, hot H_2SO_4, hot NaOH	pH stability: 0–14 α-Alumina shows a wider pH stability range than γ-alumina
Titania	Stable in HCl, HNO_3, NaOH Unstable in HF, hot H_2SO_4	pH stability: 0–14
Zirconia	Stable in HCl, HNO_3, NaOH Unstable in HF, H_3PO_4, hot H_2SO_4	Unstable under hydrothermal conditions pH stability: 0–14
Silica	Stable in HCl, HNO_3, H_2SO_4, H_3PO_4 Unstable in HF, NaOH	pH stability: 0–10

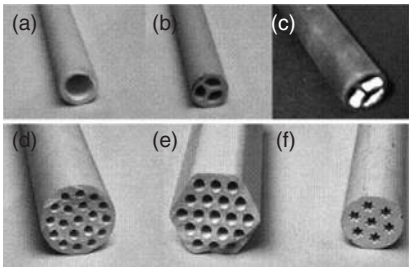

Figure 1 Some commercial ceramic membrane modules: (a) single-channel module; (b, c) three-channel ceramic (b) and composite carbon–ceramic (c) modules; (d–f) multichannel modules.

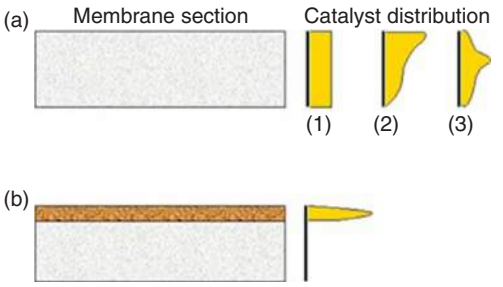

Figure 2 Catalyst distribution in catalytic membranes. (a) The membrane is constituted of a top layer containing the catalyst. (b) The catalyst distribution (1, 2, or 3) can be coupled with different pore-size distributions along the membrane cross section (1, 2, or 3).

Basically, the catalyst deposition techniques from solutions of the catalyst or of a catalyst precursor can be roughly grouped into two functional categories:

1. *Deposition techniques without interactions with the membrane material.* The deposition process of the catalyst is practically independent of the nature of the membrane material. The membrane is impregnated or dipped into solution of the catalyst precursor for a certain time. The starting membrane can be dry or wet with the same solvent used for the preparation of the catalyst precursor solution. The impregnation operation can be repeated many times in order to increase the catalyst loading on the membrane. Depending on the pore size of the membrane, different impregnation times can result in differing penetrations of the precursor solution in the membrane structure and, in turn, on different catalyst distributions. The membrane, after contact with the precursor solution, is dried, then stabilized (e.g., by calcination), and activated prior to use in the reactor. An example of membranes prepared by impregnation with a catalyst precursor solution (H_2PtCl_6 aqueous solution) followed by a drying step can be found in the work by Vospernik *et al.* [11] for the preparation of Pt/ceramic membranes and Bottino *et al.* [12] for the preparation of noble-metal catalysts on ceramic membrane supports. Espro *et al.* [13], in order to carry out the selective oxidation of light alkanes by Fe^{2+}–H_2O_2 Fenton system, prepared Nafion-based porous catalytic membranes from a paste of carbon and Teflon supported on a carbon paper followed by incipient wet impregnation with a Nafion isopropanol solution.

The precipitation methods can be included in this category as well. The porous membrane is impregnated with a solution of the catalyst precursor (e.g., a nitrate of the metal) and the precipitation in an insoluble specie of the catalyst is induced, for example, by addition of a base (in order to precipitate the hydroxide of the metal). Since the precipitating agent could be consumed by the precursor in the solution surrounding the membrane rather than by the precursor solution filling the pores, a slow precipitation rate would be preferable. An effective method to obtain a uniform precipitation is to use urea, which decomposes very slowly at 90 °C giving a homogeneous OH^- concentration both in the bulk and in the pores [14].

2. *Deposition techniques involving interaction with the membrane material.* Many membrane materials offer the presence of functional groups on the pore wall surface, which can interact with a proper catalyst precursor. The ion-exchange method is one such type of well-known technique. Some functional groups (e.g., hydroxyl group) can have a different charge value (positive or negative) at different pH. The pH value where the number of positive charges on the surface equals the number of negative charges and the overall charge is neutral is called point of zero charge (PZC). When pH > PZC, the membrane surface is negatively charged, while at pH < PZC, the membrane surface is positively charged. A positively charged surface can easily interact with an anion of the catalyst precursor (e.g., $PtCl_6^{2-}$) in solution and, on the other hand, a negatively charged surface can interact with a cation specie of the catalyst in solution. Examples of application of the ion-exchange technique to catalytic membrane preparation can be found in Reference [15] for the preparation of catalytic ceramic membranes. In some cases, it can be convenient to introduce suitable functional groups or compounds in the membrane structure in order to exploit the interaction with the catalyst precursor. Bottino *et al.* [16] prepared polyvinylidene fluoride

membranes functionalized with polyvinylpyrrolidone in order to favor the interaction of the membrane surface with the platinum precursor. Usually, a deposition technique based on the interaction or a reaction with functional groups present on the surface of membrane pore walls results in a better dispersion of the catalytic specie. Moreover, when the membrane is constituted of different materials geometrically arranged (e.g., a high surface top layer of a hydroxyl-group-rich oxide on a macroporous support with low density of surface functional groups), the deposition of the catalyst will occur only in the interacting material of the membrane (e.g., in the top layer).

Among the methods which cannot be classified in the previous two categories, vapor deposition methods (e.g., chemical vapor deposition (CVD)) were used for catalytic membrane preparation in some specific cases. Reif and Dittmeyer [17] prepared catalytic membranes by metal-organic CVD process with palladium(II)-hexafluoroacetylacetonate as palladium precursor. Palladium was obtained in the form of highly dispersed metal clusters on the ceramic membrane top layer.

Finally, an interesting preparation of composite polymeric–ceramic catalytic membranes was reported by Choi *et al.* [18] where heteropolyacid–polymer composite catalytic membranes were obtained for the vapor-phase decomposition of methyl *tert*-butyl ether (MTBE). A porous ceramic tube was coated with a polyphenylene oxide/heteropolyacid layer.

Figure 3 shows examples of different catalyst distributions, which can be obtained on catalytic membranes prepared in our laboratories. The membrane depicted in **Figure 3(a)** was obtained by the urea-precipitation method of iron oxide (in the stabilized form) on an asymmetric macroporous alumina support. The precipitation of the catalyst occurred in all the pores of the tubular support (the red color is uniform on all the membranes).

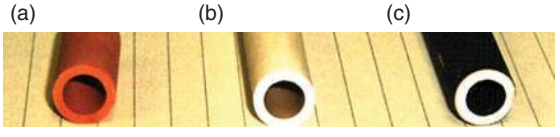

Figure 3 (a) Alumina membrane with a distribution of iron oxide along all the cross section; (b) asymmetric alumina membrane with platinum in the 5-nm top layer inside the tube; and (c) alumina membrane with two Pt/zeolite layers.

The membrane in **Figure 3(b)** was prepared by the ion-exchange technique using a H_2PtCl_6 solution at pH 3 and a membrane comprising a γ-alumina top layer (PZC $\approx$ 8) on an α-alumina macroporous support (low density of hydroxyl groups). It can be easily noted that the catalyst was preferentially deposited on the internal γ-alumina top layer. Finally, the membrane in **Figure 3(c)** was obtained by deposition of a zeolite layer (ZSM-5) on both the external and the internal side of a macroporous ceramic tube and by subsequent Pt deposition by ion exchange.

3.04.2 Overview of Multiphase Membrane Reactors

This section gives a short overview of the main types of multiphase membrane reactors. As mentioned earlier, the membrane reactors are classified depending on the presence or absence of a catalysis, and on whether the reaction takes place in the membrane lumen, in the membrane structure, or outside the membrane itself. For each case, a typical result taken from the vast literature available is presented.

3.04.2.1 The Reaction Takes Place in One of the Two Fluid Phases

The case considered here is that of a two-phase noncatalytic reaction, with one of the reactants being present in one of the phases and the reaction taking place in the other phase. In general, we can describe this as a reaction where reactant A is present in phase 1, reactant B is present in phase 2, and the reaction takes place either in phase 1 or in phase 2. Gas–liquid and liquid–liquid systems are the classical cases for this phenomenon, cases that have been extensively reported in literature. For the gas–liquid case, reactive adsorption of a component from a gas stream, such as carbon dioxide removal with an ammine solution, is probably the most commonly used case to illustrate a system of this type in practical terms [19–21], whereas the reaction of an aqueous phase with an organic phase for nanoparticle production [22– 25] is often used as an example to illustrate the characteristic behavior of a liquid–liquid system. Being the most common, we very often refer to the case where the reaction of a component from the gas phase takes place in the liquid phase with a component already present there,

although we should keep in mind that the reaction could take place in the gas phase as well (or the first component could be from a different liquid phase).

Similar to any other multiphase reaction system, it is obvious that the use of a membrane reactor is not essential for the conduction of the reaction, and conventional devices, such as bubble column, spray tower, and packed tower, are normally used in industry. However, as pointed out by Li and Chen [26], membrane systems have various ascertained and potential advantages in the area of

- operational flexibility,
- cost,
- scale-up, and
- behavior prediction.

Clearly, the presence of the membrane reduces mass transfer rate. This rate could be even further reduced if laminar flow is established in one or both phases; however, overall advantages seem to outdo disadvantages [27].

The way the whole process is arranged is rather straightforward: one phase will flow inside the membrane hollow fibers, with the other phase flowing outside in a longitudinal mode (either countercurrently or concurrently) or in cross-flow mode. The choice of longitudinal or cross-flow module will depend on various variables whose influence goes beyond the limit of the present report; in any case, however, it is of paramount importance to establish precisely the position of the interface that separates physically the two phases. Two limiting situations can arise: (1) the interface is situated practically on the outside surface of the membrane fiber and (2) the interface is situated on the inner surface of the membrane fiber. Nevertheless, these two situations are easier to describe mathematically, whereas the intermediate case, with the interface inside the membrane structure, is most likely the one generally encountered in practice and, at the same time, the least susceptible to precise mathematical modeling.

Finally, we should consider that, regardless of the interface position, the chemical reaction can then take place inside, outside, or in the solid structure of the membrane, and these cases are now discussed separately.

3.04.2.1.1 The reaction takes place outside the membrane

The situation arises when one of the reacting components flow inside the membrane fibers, whereas the reaction takes place in the other phase which is situated completely outside the membrane fiber.

There are many examples which belong to this category. The most commonly studied and reported in the literature are probably carbon dioxide absorption by a reactive liquid solution [28, 29] or water or wastewater treatment by oxidation with the use of air, pure oxygen, or ozone [30].

The first problem that must be considered in order to satisfy the present assumption of reaction taking place outside the membrane fibers, however, is the assurance that the liquid does not penetrate into the membrane.

This problem is known in the scientific community as membrane wettability. For a given liquid, the minimum pressure to be applied on the liquid phase so that it would enter the membrane pore is given by the well-known Laplace equation (to be presented and discussed later), which indicates the maximum threshold pressure required by the liquid phase in order to avoid entering the membrane pores. Obviously, this pressure depends on the physical characteristics of the membrane, such as the membrane material (which has a direct influence on the contact angle) and the membrane pore size. Detailed advices on the membrane wettability conditions have been given in many papers and are not repeated here, but they address the following areas:

- use of hydrophobic membrane;
- membrane surface modification;
- composite membrane;
- denser fiber membranes;
- liquid with suitable surface tension; and
- operating conditions.

In order to give an idea of the qualitative behavior of the membrane reactor working with the present arrangement, some results, which are reported here, are taken from a specific work that had investigated CO_2 removal from a gaseous stream by a reactive solution [31]. In that work, capillary membranes Accurel S6/2 (Membrana, Germany) were used. Four modules were prepared using different numbers of capillary membranes (1, 3, 10, and 18) with the same length of 17 cm, in order to obtain different contact areas. Tests were performed using the laboratory-scale plant. A gas mixture containing 15% (v/v) of CO_2 and 85% of N_2, which is the typical composition of a flue gas from a coal combustion plant, of was fed to the membrane lumen. Monoethanolamine (MEA) and NaOH aqueous solutions were used as CO_2 absorbents. The liquid phase was fed on the shell side of the membrane module with a recirculation pump at a flow rate of about $100\,l\,h^{-1}$. Its

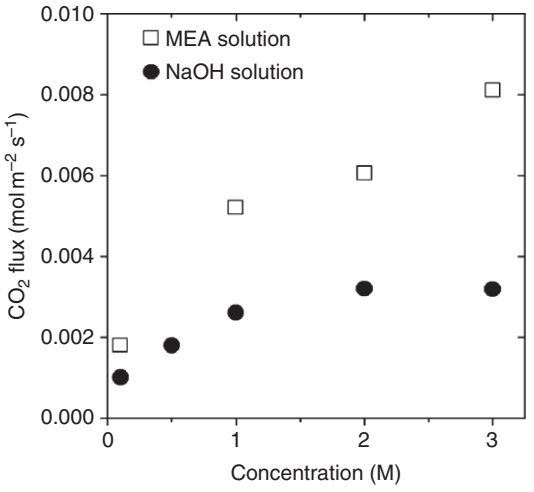

Figure 4 Membrane gas–liquid reactor: the effect of the absorbent solution composition on the carbon dioxide flux from a gas stream.

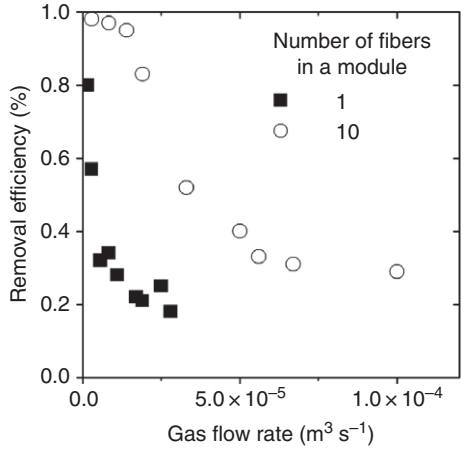

Figure 5 Membrane gas–liquid reactor: the effect of gas flow rate and interfacial area on carbon dioxide removal efficiency.

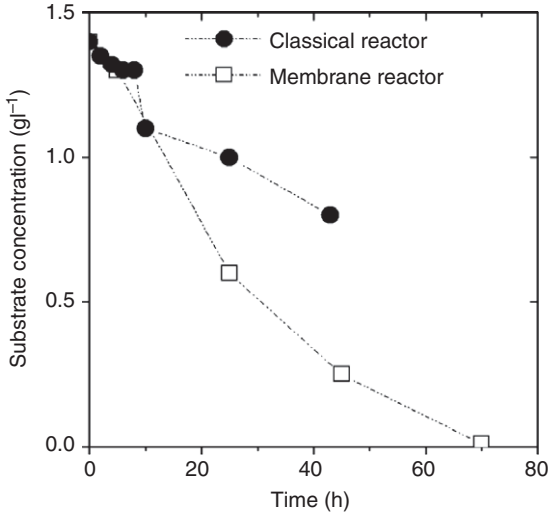

Figure 6 Comparison of substrate concentration with time for a classical and a membrane reactor system.

pressure was kept at a proper value, in order to avoid any possible penetration of the solution into the membrane pores as well as any gas bubble formation in the absorbent solution. Temperature was varied between 20 and 60 °C. The influence of the various operating parameters was investigated experimentally with the results supporting expected behavior.

Figure 4, for example, illustrates the influence of the type of reacting liquid, quantified by carbon dioxide transferred through the membrane. MEA has a definite better performance when compared with NaOH solution, indicating therefore that in this process the reaction, together with diffusion, affects the overall rate. The effect of overall contact area and gas flow rate is depicted in Figure 5. As expected, CO_2 removal increases by increasing contact area and decreases by increasing gas flow rate in the membrane module.

The second example considered here concerns water (or wastewater) biological treatment apparatus. In the classical arrangement, one of the reactants (oxygen) is supplied to the aqueous solution to be treated through a gas sparger positioned at the bottom of the reacting tank. In the alternative membrane-using solution, air (or oxygen) is supplied with the help of a fiber-membrane module. This solution has been tested by few authors [32, 33], with very good results, as Figure 6 shows, which compare substrate consumption when air is fed through the membrane as well as through the sparger.

Moreover, it should be stressed that this solution is particularly appealing if the same membrane is then used as solid/liquid separator, as investigated by Parameshwaran *et al.* [33]. They reported that the same submerged membrane was very effective in alternatively aerating the liquor and filtrating clear water, which resulted in the treated water having very good characteristics as far as chemical (chemical oxygen demand (COD), nitrates content, etc.) and physical (turbidity and color) parameters were concerned.

3.04.2.1.2 The reaction takes place inside the membrane

Since the publication of the first seminal works (Qi and Cussler [34, 35], Kreulen *et al.* [36, 37]), the

arrangement with the gas phase flowing outside and the liquid phase flowing inside the membrane channel has also been taken into consideration. There is no general consideration that would make one arrangement preferable to the other, the choice depending on the specific system and the operational constraint to be respected. With the liquid moving inside the fiber in laminar flow regime, the volume available for the chemical reaction is generally much more restricted. Examples reported in literature are nearly entirely devoted to the case of absorption of a gas component, such as CO_2, H_2S, SO_2, and NH_3, by a liquid reacting aqueous phase. The component to be removed from the gas stream has to diffuse through the membrane and then has to react with the liquid. As in the case seen earlier when the reaction takes place outside the membrane, diffusion and reaction are the important steps controlling the overall process rate, and this was clearly put forward in one of the earliest works to deal with this subject [35]. The experimental findings by Qi and Cussler, summarized in **Figure 7**, for the adsorption of different gas species by a NaOH 1 M solution, show different overall removal efficiencies, depending on the component adsorbed, for the same apparatus and identical conditions. From the result obtained, the authors concluded that the absorption of H_2S, SO_2, and NH_3 was controlled by the resistance in the membrane, but the absorption of CO_2 was probably controlled by both diffusion and reaction in the liquid.

The effect of the liquid velocity in the fiber on the amount of CO_2 transferred from the gas to the liquid solution was reported by Kreulen *et al.* [37] and reproduced here in **Figure 8**, indicating, as expected, the positive influence of the liquid velocity. Needless to say, the increase in efficiency function of the liquid velocity in the fiber must, however, take into consideration the negative effect on the pressure drop on the liquid side, and, as usual, a compromise must be sought. The results of Kreulen *et al.* [37] also indicate that there is a different overall behavior, depending on a possible transition from laminar to turbulent flow regime when the velocity is increased.

In agreement with previous works, Kim and Yang [38] reported the effect on CO_2 removal efficiency by varying different operational parameters together with three adsorbent solutions and concluded that the choice of the optimum working point will depend on temperature, module size, flow rate of gas and liquid, and overall mass transfer.

3.04.2.1.3 The reaction takes place inside the membrane structure

For the example reported in the previous section, hydrophobic membranes are generally employed so that the membrane pores are occupied completely by the gas phase. If the membrane is hydrophilic, the pores are filled with stagnant liquid, with negative effect on mass transfer. As pointed out earlier, liquid-phase pressure should not exceed breakthrough pressure of the membrane to prevent membrane wetting.

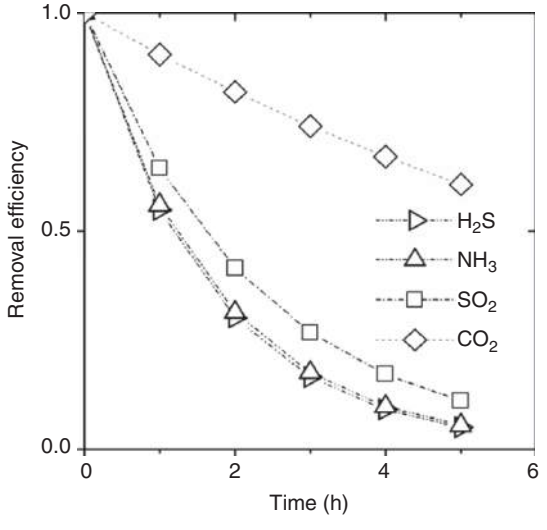

Figure 7 Removal efficiency in a gas–liquid membrane reactor for various absorbed gases.

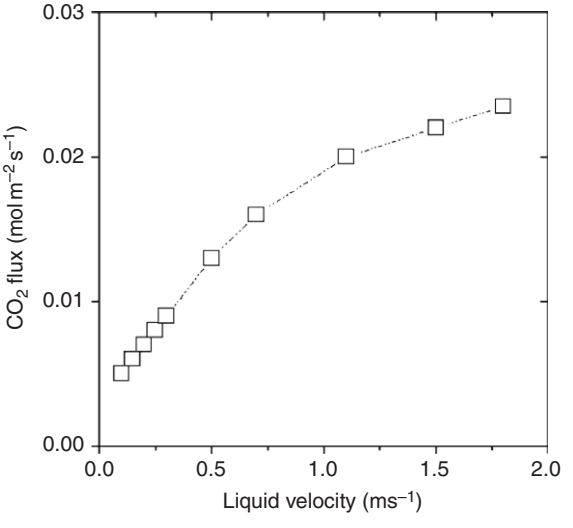

Figure 8 The effect of liquid velocity in a gas–liquid membrane reactor on carbon dioxide flux.

However, the control of the process conditions is generally quite difficult and some membrane wetting is to be expected in many practical applications – wetting which is facilitated by the occurrence of phenomenon, such as capillary condensation or the presence of polluting component, which can decrease liquid surface tension.

The occurrence of membrane wetting leads to a degradation of the membrane performance, given the increased influence of mass transfer on the overall rate, as the reaction in this case takes place completely, or at least in part, inside the membrane structure, and the reactant must diffuse there in order to react and, at the same time, products must diffuse back [39].

Although it is difficult in principle to estimate if wetting phenomenon is taking place, a comparison between observed membrane performance with the ones expected from theory is a valid indication of establishing the occurrence of wetting. This is well illustrated in the following example reported by Mavroudi *et al.* [21] who found the membrane performance, expressed in terms of CO_2 outlet concentration to be different from the values calculated using the assumption of nonwetted system (**Figure 9**).

The same conclusion can be drawn from the work of Bao and Trachtenberg [19] who presented their data in terms of CO_2 permeance and found that experimental permeance was much lower than expected and attribute the disagreement to partial wetting. A good fit with experimental observation was then searched by using the wetting fraction as adjustable parameter (**Figure 10**). Needless to say, this approach requires a good description of the membrane behavior, which is dealt with subsequently.

3.04.2.2 The Reaction Takes Place on a Catalyst

In this section, multiphase membrane reactors, where the reaction rate is facilitated by the use of catalysts, are considered. The presence of the catalysts will obviously simplify the analysis as the reaction will take place exclusively where the catalysts have been physically deposited, although all the problems indicated in the previous sections will still exist, as the reactant will have to reach the catalysts in order to react and the product will have to leave the catalysts and join the exit stream for the process to be completed.

This specific process has also been studied and presented in a very comprehensive manner in previous works of the highest quality, such as those of Dittmeyer *et al.* [40, 41] and, as before, only a very brief summary is given here.

3.04.2.2.1 The catalysts are placed in the membrane lumen

The first situation we consider here concerns a multiphase reaction system where the membrane controls the addition of reactants or the preferential removal of products from the main stream. The

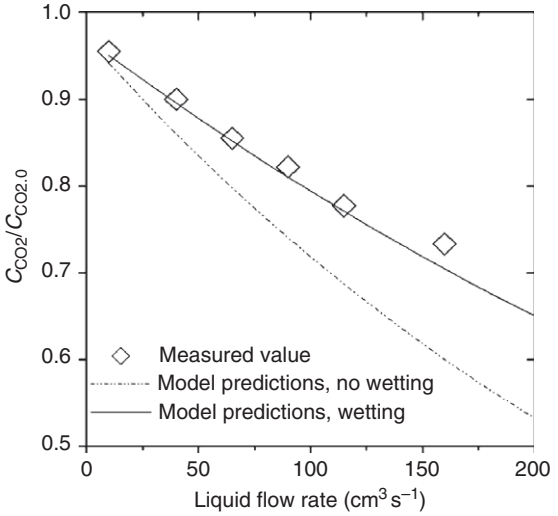

Figure 9 Measured and predicted carbon dioxide removal efficiency for a partially wetted gas–liquid membrane reactor function of liquid flow rate.

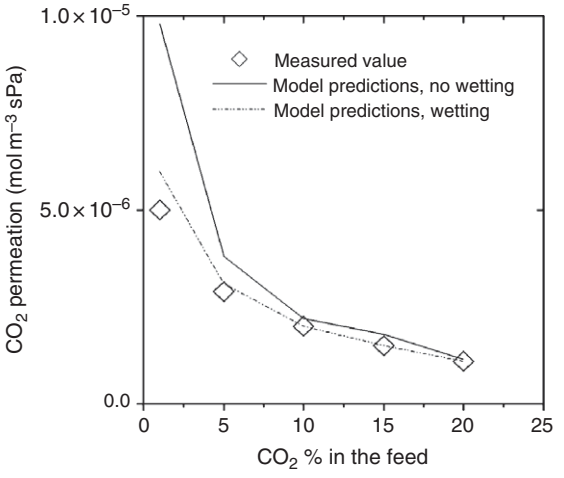

Figure 10 Measured and predicted carbon dioxide permeation rates for a partially wetted gas–liquid membrane reactor function of carbon dioxide concentration in the feed.

catalysts are placed away from the membrane structure, most generally in the form of a fixed bed inside the membrane lumen, although some suggestions of using the catalysts in a fluidized bed state have also been put forward. Given the passive role played by the membrane in this case, the system is generally referred to as inert membrane reactor.

Selective or preferential product removal is the most common process studied, and given the relatively easy way to separate hydrogen from other compounds, it is not surprising that dehydrogenation reactions are greatly favored in the inert membrane configuration. Other popular areas of study are equilibrium reactions: the potential advantages here are obvious, given that the removal of one of the products will keep the system away from the equilibrium composition, with a resulting increase in overall conversion.

Reactant distribution through the membrane to a fixed bed of catalysts is indicated for series–parallel reactions, with the aim of increasing the selectivity of one product compared to the others. It is considered that the increase in selectivity can be achieved by controlling the relative concentration of the reactants, such as the local oxygen concentration in various oxidations. Moreover, the use of a membrane can also result in an overall safer operation, given the possibility to control hot spot formation and runaway reactions.

One typical example of the cases discussed above is reported in **Figure 11**, referring to the investigation of the classical gas–water shift reaction [42], which depicts how hydrogen production can be increased when an inert membrane reactor, selectively separating the hydrogen from the gas stream, is employed.

The cases discussed above all refer to the reactions carried out in the gas phase. One exception found in the literature is the work by Piera *et al.* [43]. They studied oligomerization of *i*-butene by carrying out the reaction in the liquid phase over a catalytic bed. The bed was placed inside a zeolite inert membrane which allowed to remove *i*-octane, the intermediate product, representing the desired product compared to other larger hydrocarbon (C_{12+}). *i*-Octane was removed via the membrane in the gas phase through a pervaporation process. Experimental results quite clearly showed how the selectivity to *i*-octane could be increased, by a more or less large amount depending, for example, on the space velocity, with the use of an inert membrane compared to a traditional fixed-bed reactor (see **Figure 12**).

3.04.2.2.2 The catalysts are placed on the membrane surface

In the situation considered here, the reactant from the gas phase meets the other reactant from the liquid phase inside the structure of the catalytic layer deposited on the membrane where the reaction occurs. Hydrogenations and oxidations are examples of reactions which can be carried out in three-phase systems [13, 44–48]. Various modes of system feed can be used, as schematically represented in

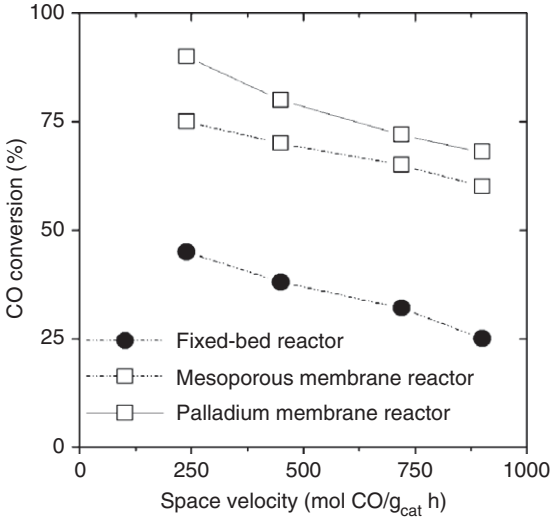

Figure 11 Comparison of carbon monoxide conversion in different water–gas shift reactors function of space velocity.

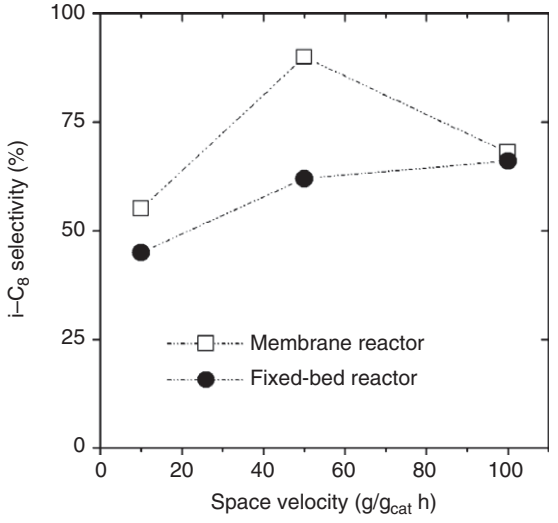

Figure 12 Measured selectivity for two different liquid–liquid reactors: classical fixed-bed and membrane reactor.

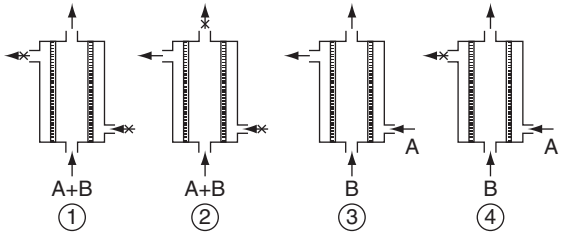

Figure 13 Different feed and product arrangement for a gas–liquid catalytic membrane reactor.

Figure 13, where A and B represent the gas and the liquid reactants [17].

Without going into a very detailed description, the analysis of Figure 13 reveals that at least four different feeding configurations are possible. In case 1, the membrane is exploited only as a catalyst support, the two reactants are fed from the same point, and the system resembles very much a monolith chemical reactor. In case 2 also the reactants are fed together to the membrane reactor, but there they are forced through the membrane where the catalysts are deposited so that an improved contact between fluid and solid phases is achieved. In cases 3 and 4, the feed arrangement is different from the previous example considered, in the sense that gas and liquid are fed to the two different sides on the membrane. The difference between the two cases concerns the way the product streams are collected, separately in case 3 and mixed together in case 4, so that a phase is forced to pass though the membrane.

Experimental evidence of the advantages resulting in the use of a gas–liquid catalytic membrane reactor has been presented, among others, by Bottino *et al.* [12] who investigated competitive hydrogenation isomerization of methylenecyclohexane and compared the results with tests carried out on a conventional slurry reactor (SR). As evidenced in Figure 14, the novel membrane reactor configuration utilized does not seem to be mass transfer limited, with the reaction rate steadily increasing with temperature as expected in kinetic controlled processes.

Another example reported in literature concerns oxidation of liquid effluent with air (or pure oxygen), which was comprehensively investigated and reported in a series of papers [15, 49–58] where the results of a joint project involving both universities and industries, financially supported by the European Union, were disseminated. The project aimed at the comparison between a novel gas–liquid catalytic membrane reactor and traditional technologies used in the industry for the treatment of liquid effluents. Different inert

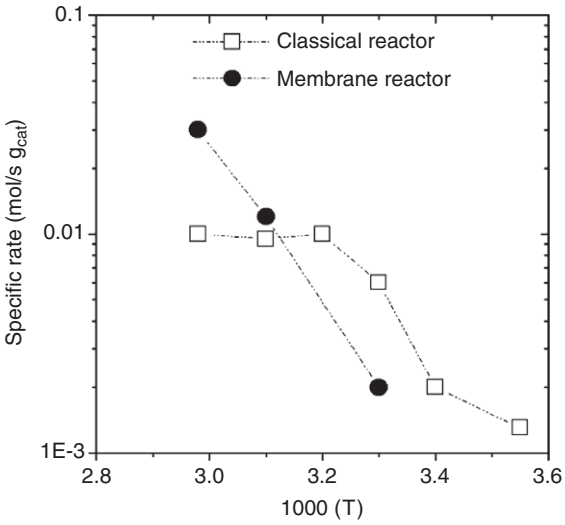

Figure 14 Measured specific reaction rate for a fixed-bed and a membrane reactor.

material membrane types were utilized, either single channel or multiple channel with a thin layer of Pt catalysts (6.2–7 $g_{Pt}\,m^{-2}$) being deposited with an impregnation technique. Details of the investigation are reported in the original papers, to which readers are referred to for specific points. However, overall, the conclusions clearly pointed out that the novel catalytic membrane reactor could be successfully used for the process, and thanks to milder temperature and pressure operating conditions and a better catalyst utilization, it compared favorably from an economic viewpoint when weighed against traditional processes. If we limit our attention here to the working regime of the systems as resulting from the laboratory and pilot-scale rigs, it could be that the membrane reactor was not limited by mass transfer but operated in kinetic regime (Figures 15 and 16).

3.04.2.2.3 The catalysts are dispersed on the membrane structure

Contrary to the case reported in the previous section, there are situations where the catalysts are distributed all over the membrane structure. This solution has been studied and reported extensively, especially for enzyme-catalyzed reaction, and multiphase membrane reactors offer some very peculiar advantages in tackling this situation.

Many examples have been reported in literature [59–66] and the hydrolysis of a poorly water soluble ester to the corresponding carboxylic acids, a highly water-soluble product, is reported here as an example [63].

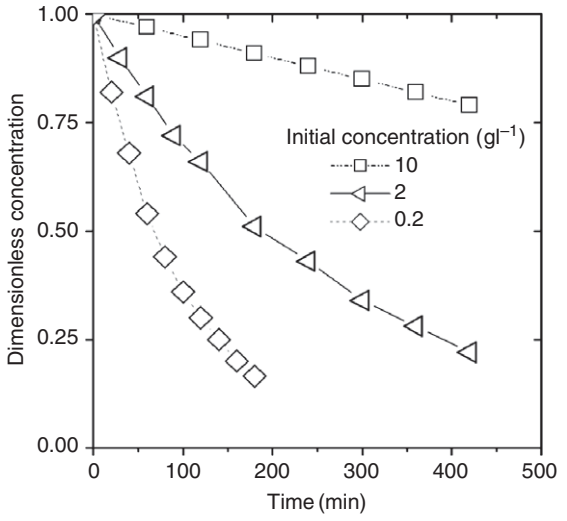

Figure 15 Outlet concentrations in gas–liquid catalytic membrane reactor function of time for different initial concentrations.

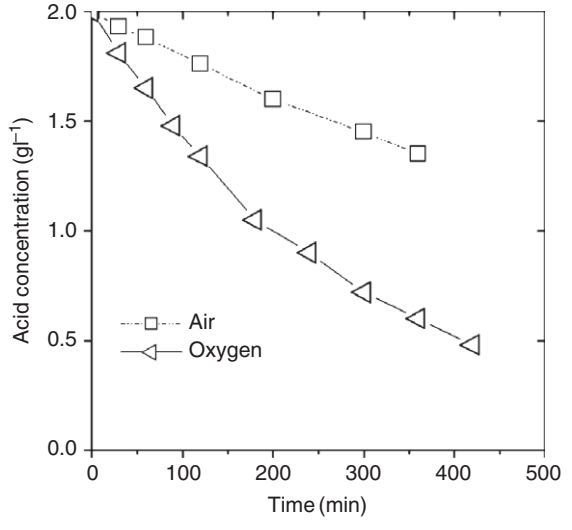

Figure 16 Outlet concentrations in gas–liquid catalytic membrane reactor function of time for different feed concentration.

The process arrangement is made up of a hydrophilic membrane loaded with the active enzyme, the membrane separating the immiscible organic and aqueous process stream. In this manner, the interface of the phases is placed on the side of the membrane in contact with the organic phase. Reactants diffuse into the membrane from the organic phase, react inside the membrane structure, and the products are removed from the aqueous side. The membrane, therefore, acts both as enzyme support and as phase contactor, avoiding all the problems connected with the dispersion of one liquid phase into another.

Experimental tests have demonstrated a small effect on yield and selectivity for different enzyme loading, indicating in this way that the enzyme is efficiently utilized in the range investigated [59].

3.04.3 The Mathematical Modeling of Multiphase Membrane Reactors

In this section, the rate at which process takes place in a membrane reactor is considered. It is obvious, by definition, that as we are considering a chemical reaction, the overall rate must take into account the reaction kinetic; therefore, no general conclusions can be reached because the kinetic rate law is a specific characteristic of the given process. It is well known that the overall rate, in a multiphase reactor, must consider both mass transfer and reaction rate [67–69], with one of the two being the limiting step when the other is much faster. Therefore, the considerations are generally valid for the mass transfer step, the reaction step depending obviously on the specific reaction. First, the limiting case of negligible reaction rate in a membrane contactor is presented, then the effect of a noncatalyzed reaction is discussed, and, finally, the overall effect of a catalytic reaction in a membrane reactor is presented.

3.04.3.1 Membrane Contactors

Membrane contactors allow to avoid some disadvantages of the traditional fluid–fluid contactors as well as packed or bubble columns [7, 70, 71]. In most of the traditional contacting devices, the two fluid phases (e.g., the gas and the liquid phases) are interdependent, and if the operating conditions and materials are not properly selected, emulsion formation, foaming, unloading, or flooding can occur. In many traditional contacting devices (except for packed towers), the contact between the two phases takes place in a dispersive way [72]. For example, in a spray tower the liquid is introduced in a continuous gas phase in small droplets, while in a bubble column the gas phase is in bubbles immersed in the liquid continuous phase. In general, the interfacial area is not always easy to assess for such systems, and can strongly change with the operating conditions.

The use of a membrane makes the contact nondispersive and the fluid–fluid interface is located at the mouth of membrane pores. Therefore, the two

fluid flows are independent, and the interfacial area is known and constant for each condition, since it corresponds to the membrane area. The advantages with respect to many traditional contactor devices are that the emulsion formation can be avoided, no density difference between the two fluids is required, and a low solvent holdup can be used. Since a very large membrane surface can be used in membrane contactors, the achieved efficiency is high and the scale-up from a small up to a larger unit is easy, thanks to the modular nature of commercial membranes.

On the other hand, the presence of a membrane between the two phases introduces an additional mass transfer resistance, which, however, can be minimized by a proper choice of the membrane.

If we consider a porous membrane keeping in contact a gas and a liquid phase, two extreme situations can be found:

1. Membrane pores can be completely filled by the liquid phase, and then the membrane contactor operates in the wetted mode (**Figure 17(a)**). This situation occurs when the membrane material has affinity for the liquid phase (e.g., both the membrane and liquid phase are either hydrophilic or hydrophobic).
2. Membrane pores are occupied only by the gas phase, so the membrane contactor operates in the nonwetted mode (**Figure 17(b)**). The nonwetting fluid (liquid phase) can displace the wetting fluid (gas phase) only when its pressure overcomes the breakthrough pressure defined by

$$\Delta p = \frac{2\sigma\cos\theta}{r_p} \tag{1}$$

where r_p is the pore radius, σ is the surface tension (or the interfacial tension when a liquid–liquid system is considered), and θ is the contact angle between the wetting fluid and the membrane pore.

In general, since the membrane is not symmetric in structure and is characterized by a pore-size distribution, the real situation could easily correspond to a partially wetted membrane. In this work, the effect of pore-size distribution is ignored throughout.

In the following subsections, overall mass transfer coefficient for both the cases is evaluated in the absence or presence of a homogeneous reaction in the liquid phase.

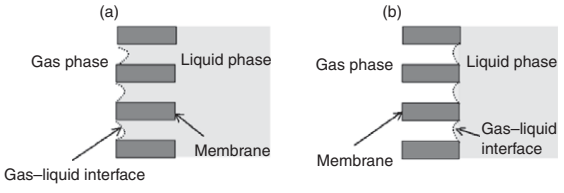

Figure 17 Two operating modes of membrane contactors: (a) wetted mode; (b) nonwetted mode.

3.04.3.1.1 Membrane contactors working in wetted mode with negligible homogeneous reaction

The concentration profile of the A specie absorbed from the gas phase into the liquid phase, *B*, through a membrane contactor working in wetted mode, can be depicted as in **Figure 18**.

Since the liquid phase wets the membrane, the interface between the gas and the liquid phases corresponds to the gas side surface of the membrane. In general, the following mass transfer resistances can be met by *A* diffusing from the gas side to the liquid side:

- mass transfer from the bulk of the gas phase to the gas–liquid interface at the pore mouth;
- dissolution of A into the liquid phase;
- mass transfer of A through the liquid phase wetting the membrane; and
- mass transfer of the specie A from the membrane to the bulk of the liquid phase.

Similarly, the specie constituting or being present in the liquid phase could also follow an opposite path from the liquid phase to the gas phase. We will assume that the liquid phase is nonvolatile and does not transfer toward the gas phase.

Starting from the concentration profile drawn in **Figure 18**, material balances can be written in terms

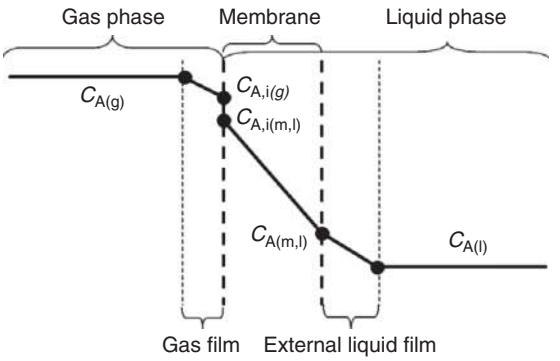

Figure 18 Concentration profile without reaction for a membrane contactor operating in wetted mode, in accordance with the film model.

of molar fluxes through the membrane surface of area A_M and the local mass transfer coefficients.
Mass transfer resistance in the gas film interfacing the membrane:

$$N_A = k_g(C_{A(g)} - C_{Ai(g)}) \tag{2}$$

Mass transfer through the wetted membrane:

$$N_A = k_M(C_{Ai(m,l)} - C_{A(m,l)}) \tag{3}$$

Mass transfer through the external liquid film:

$$N_A = k_l(C_{A(m,l)} - C_{A(l)}) \tag{4}$$

The dissolution of A in the liquid phase is considered to be at the equilibrium and the Henry's law is assumed as

$$C_{Ai(m,l)} = HC_{Ai(m,g)} \tag{5}$$

The molar flux can be also written in terms of overall mass transfer coefficients referred to the gas phase concentrations

$$N_A = K_G(C_{A(g)} - C^*_{Ai(g)}) = K_G\left(C_{A(g)} - \frac{C_{A(l)}}{H}\right) \tag{6}$$

or to the liquid phase concentrations

$$N_A = K_L(C^*_{Ai(l)} - C_{A(l)}) = K_L(HC_{A(g)} - C_{A(l)}) \tag{7}$$

where

$$C^*_{Ai(l)} = HC_{A(g)} \tag{8}$$

and

$$C^*_{Ai(g)} = \frac{C_{A(l)}}{H} \tag{9}$$

obviously will be

$$\frac{K_L}{K_G} = H \tag{10}$$

From Equations (2)–(4), using the Henry's law and by comparison with Equation (6) or (7), the overall mass transfer coefficients, K_L and K_G, can be expressed in terms of the local mass transfer coefficients corresponding to each resistance met by the specie A during the absorption process through the membrane contactor:

$$K_L = \frac{1}{\left(\frac{H}{k_g} + \frac{1}{k_M} + \frac{1}{k_l}\right)} \tag{11}$$

or

$$K_G = \frac{1/H}{\left(\frac{H}{k_g} + \frac{1}{k_M} + \frac{1}{k_l}\right)} \tag{12}$$

In other words, the total mass transfer resistance (e.g., $1/K_L$) is due to the contribution of the gas phase resistance (e.g., H/k_g), the wetted membrane resistance ($1/k_M$), and the mass transfer resistance in the liquid phase ($1/k_l$). The evaluation of the mass transfer resistances in the liquid and gas phases adjacent to the membrane depends on the flow conditions on both sides of the membrane, which is discussed later.

For the moment, we focus on the evaluation of the mass transfer coefficient expressing the resistance offered by the membrane. In the wetted membrane, the mass transfer resistance is offered by the liquid incorporated in the membrane pores. The membrane volume is defined as

$$V_M = A_M t_M \tag{13}$$

where t_M is membrane thickness.

However, not all the membrane geometric volume V_M is available for diffusion of the dissolved A. The volume fraction filled by the liquid corresponds to the porosity, ε, of the membrane:

$$\varepsilon = \frac{V_{pores}}{V_M} \tag{14}$$

Using the stagnant film model [73, 74], the membrane mass transfer coefficient can be defined as

$$k_M = \frac{D_{eff}}{t_M} \tag{15}$$

where D_{eff} is the effective diffusivity.

For membranes constituted of macropores or mesopores, it may be sufficient to consider the solute diffusion coefficient in the liquid phase multiplied for a factor taking into account the presence of the membrane:

$$D_{eff} = \frac{\varepsilon}{\tau} D_{AB} \tag{16}$$

D_{AB} is the binary diffusivity of A in the B liquid. The effective diffusivity corrects the binary diffusivity, since the liquid is only filling the membrane porosity, ε, and that the A specie traveling from one side of the membrane to the other side has to follow a more or less tortuous path defined by the tortuosity, τ.

The binary diffusion of the solute can be evaluated using well-known correlations [75]. The Wilke–Chang diffusivity is often used to evaluate the binary diffusivity:

$$D_{AB} = \frac{7.4 \times 10^{-12}(\varphi M_B)^{1/2} T}{\mu_B V_A^{0.6}} \tag{17}$$

where D_{AB} is the mutual diffusion coefficient of solute A at very low concentration in solvent B ($m^2\,s^{-1}$), M_B the molecular weight of solvent B (g mol^{-1}), T the temperature (K), μ_B the viscosity of solvent B (cP), φ the association factor of solvent B (dimensionless), and V_A the molar volume of solute A at its normal boiling temperature ($cm^3\,mol^{-1}$).

V_A can be evaluated from the critical volume V_c using the Tyn and Claus method:

$$V_A = 0.285 V_c^{1.048} \tag{18}$$

For microporous membranes and, in particular, zeolite membranes, the estimation of the diffusivity can be more difficult and has to be carried out considering the specific characteristic of membrane and the permeating species.

3.04.3.1.2 Membrane contactor reaction working in nonwetted mode with negligible homogeneous reaction

For a membrane contactor operating in the nonwetted mode, the film model allows one to depict the situation represented in **Figure 19**. The gas–liquid interface is now located on the liquid side of the membrane. The molar flux can be written in terms of local mass transfer coefficients for each resistance step, or in terms of overall mass transfer coefficients. Using the same approach applied for the wetted membrane, the overall mass transfer coefficients can be written in terms of the local mass transfer coefficients corresponding to the single resistance encountered by the diffusing A specie from gas to liquid phase.

In addition, we can express the molar fluxes in terms of overall mass transfer coefficients:

$$N_A = K_G\left(C_{A(g)} - C^*_{Ai(g)}\right) \tag{19}$$

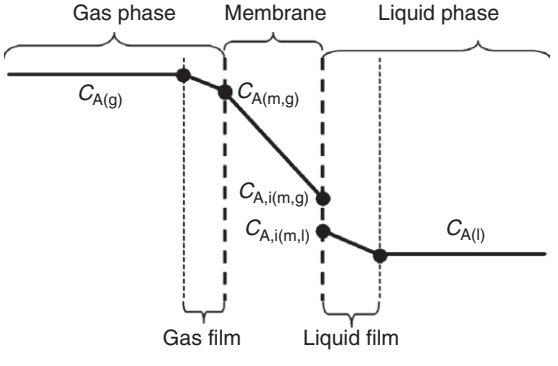

Figure 19 Concentration profiles in a membrane contactor operating in the nonwetted mode without any reaction.

and

$$N_A = K_L\left(C^*_{Ai(l)} - C_{A(l)}\right) \tag{20}$$

where

$$C^*_{Ai(g)} = \frac{C_{A(l)}}{H} \tag{21}$$

$$C^*_{Ai(l)} = HC_{A(g)} \tag{22}$$

Then it will result that

$$K_G = \frac{1/H}{\frac{H}{k_g} + \frac{H}{k_M} + \frac{1}{k_l}} \tag{23}$$

$$K_L = \frac{1}{\frac{H}{k_g} + \frac{H}{k_M} + \frac{1}{k_l}} \tag{24}$$

As we have seen above, the mass transfer coefficient, k_M, depends on the structure of the porous membrane and it can be evaluated again using Equations (13) and (14).

When the membrane is macroporous, molecular diffusion is the main mechanism driving mass transfer. Gas molecular diffusion can be evaluated using well-known correlations [75]. For example, the Fuller–Schettler–Giddings correlation for binary diffusivity D_{AB} ($m^2\,s^{-1}$) is

$$D_{AB} = \frac{1 \times 10^{-7} T^{1.75} M_{AB}^{1/2}}{P\left[\left(\sum v\right)_A^{1/3} + \left(\sum v\right)_B^{1/3}\right]^2} \tag{25}$$

where the atomic diffusion volumes $\left(\sum v\right)_i$ for single molecules are tabulated or calculated from the atomic composition using the atomic structural diffusion-volume increments v_i; T is the temperature in K and P the pressure in bar; M_{AB} is defined from the molecular masses M_A, M_B of the diffusing species (g mol^{-1}) by

$$M_{AB} = \frac{2}{\left(\frac{1}{M_A} + \frac{1}{M_B}\right)} \tag{26}$$

If the membrane pore size is comparable to the mean free path, a Knudsen mechanism can be dominant and a Knudsen effective diffusivity can be expressed as [76]

$$D_{eff}^K = D_K \frac{\varepsilon}{\tau} \tag{27}$$

where

$$D_K = 48.5 d \sqrt{\frac{T}{M}} \tag{28}$$

When a combined bulk-Knudsen diffusion mechanism is controlling the mass transport, then

the Bonsaquet equation can approximate the effective diffusivity:

$$\frac{1}{D_{\text{eff}}} = \left(\frac{1}{D_{\text{eff}}^{\text{m}}} + \frac{1}{D_{\text{eff}}^{\text{K}}}\right) \tag{29}$$

3.04.3.2 Evaluation of Local Mass Transfer Coefficients in the Boundary Layers Located on Both Sides of the Membrane Surface

The estimation of the mass transfer coefficients in the boundary layers depends on the fluid dynamic regime occurring on each side of the membrane. Mass transfer rate, in theory, can be evaluated by utilizing physical models (film model, penetration model, etc.) [73, 74], which have been proposed in the past decades in chemical engineering. However, here, a more practical and simple approach is reported which relies on experimental observations and dimensionless data elaboration.

Mass transfer coefficients in the boundary layers can be estimated using correlations expressed in terms of dimensionless groups:

$$Sh \propto Re^{\alpha} Sc^{\beta} f(\text{geometry}) \tag{30}$$

where Sh is the Sherwood number, which compares the mass transfer rate in the interface with the diffusion rate in the bulk fluid phase:

$$Sh = \frac{k_c \ell}{D} \tag{31}$$

When Sh is known, the mass transfer coefficient, k_c, in the boundary layer can be estimated. Therefore, Sh is often correlated with the Reynolds number, Re:

$$Re = \frac{\ell u \rho}{\mu} \tag{32}$$

and the Schmidt number, Sc:

$$Sc = \frac{\mu}{\rho D} \tag{33}$$

As for membrane contactors, the Graetz number has proven to be useful. The Graetz number characterizes the laminar flow in a duct:

$$Gz = \frac{ul^2}{DL} \tag{34}$$

The parameters and the form of correlations depend on the system geometry and on the fluid dynamic near the membrane surface. The fluid can be in a turbulent regime or in a laminar flow regime. If the fluid is in a laminar flow regime ($Re < 2100$), an entry region will be followed by a fully developed flow region and the correlations will be different in both situations. Therefore, in the case of a laminar flow regime, it is convenient to use a correlation which averages Sh over the entire length of the duct. **Table 3** summarizes some correlations which can be used to estimate the mass transfer coefficients in different fluid dynamic situations, in ducts with cylindrical or flat geometry.

Table 4 shows similar correlations for the external side of the membrane when the geometry is cylindrical, like in hollow-fiber membranes. In that case, a dependence on the packing fraction of the fibers in the module can be present in the correlation.

Finally, also a Sherwood number (namely, wall Sherwood number) can be defined for a hollow fiber membrane:

$$Sh_{\text{w}} = \frac{k_{\text{M}} d_{\text{M}}}{D} \tag{35}$$

where d_{M} is the diameter of the channel in the fiber.

Table 3 Mass transfer correlations for ducts of various geometries

Duct geometry	*Correlation*	*Application*
Cylinder	$Sh = 3.67$	Laminar region; fully developed flow or $Gz < 10$
Cylinder	$Sh = \left(3.67^3 + 1.62^3 Gz\right)^{1/3}$	Laminar region: $10 < Gz < 20$
Cylinder	$Sh = 1.62\left(\frac{ud^2}{DL}\right)^{1/3}$	Laminar region: $Gz > 20$
Cylinder	$\text{Sh} = 0.026\, Re^{0.8} Sc^{0.33}$	Turbulent region $Re > 20\,000$
Parallel plate	$Sh = 7.54$	Laminar region; fully developed flow
Parallel plate	$\text{Sh} = 0.036\, Re^{-0.2} Sc^{-0.67}$	Turbulent region $Re > 10^6$

Adapted from Gabelman, A., Hwang, S.-T. *J. Membr. Sci.* **1999**, *159*, 61–106; and Basmadjian, D. *Mass Transfer: Principles and Applications*; CRC Press: Boca Raton, FL, 2004.

Table 4 Mass transfer correlations for shell side of hollow-fiber modules

Correlation	*Application*
$Sh = 1.25\left(\frac{Re\, d_e}{L}\right)^{0.93} Sc^{0.33}$	$0.5 < Re < 500$ and packing fraction of the fibers =0.03; flow parallel to the fibers
$Sh = 0.019\, Gz$	$Gz < 60$; closed packed fibers; flow parallel to the fibers
$Sh = 0.61\, Re^{0.32} Sc^{0.33}$	$0.6 < Re < 49$; pd=0.003 flow across the fibers

Adapted from Basmadjian, D. *Mass Transfer: Principles and Applications;* CRC Press; Boca Raton, FL, 2004.

3.04.3.2.1 Membrane contactors in the presence of a homogeneous reaction in the liquid phase

The physical mass transfer between the two phases interfaced by the membrane has been described in terms of an overall mass transfer coefficient which lumped all the single mass transfer resistances met by the component diffusing from one phase (e.g., gas phase) to the other (e.g., liquid phase).

In the chemical absorption, the component from the gas phase reacts in the liquid phase. The effect of the reaction on mass transfer can be again lumped in an overall mass transfer coefficient. The modeling treatment of the membrane contactor in presence of a chemical reaction is similar to the one reported in traditional chemical engineering textbooks [77, 78], with the introduction of the term relative to mass transfer through the membrane. In the following discussion, only some commonly used concepts and definitions are discussed, without giving a detailed explanation of all possible cases. It will be useful to introduce this matter to the reader to refer to more detailed textbooks on multiphase mass transfer with homogeneous chemical reactions. **Figure 20** shows as example of the interface concentration profiles for a membrane contactor in nonwetted mode, in the presence of a homogeneous reaction in the liquid phase. The membrane acts as an additional resistance in the gas-phase side.

For instantaneous reactions, the reactants meet and react in a reaction plane (**Figure 20**(**a**)) and the position of this reaction plane in the film depends on the relative diffusivity of the two reactants. When the reaction rate is comparable to the mass transfer rate, the reaction takes place again in the liquid film but in a reaction zone (**Figures 20**(**b**) and **20**(**c**)). When the reaction rate is extremely slow, the reaction occurs in the bulk of the liquid phase (**Figure 20**(**d**)). The reader can try to draw similar profiles for the case of a wetted membrane.

Based on such considerations, it seems reasonable to define a parameter that can give an idea of the relative importance of chemical reaction rate and physical mass transfer rate. In the specific literature Hatta number, *Ha*, is often introduced, which is a dimensionless number defined as

$$H_a = \frac{\text{maximum conversion rate of A in the film for unit of interface area}}{\text{maximum diffusional transport through the film without reaction}} \qquad (36)$$

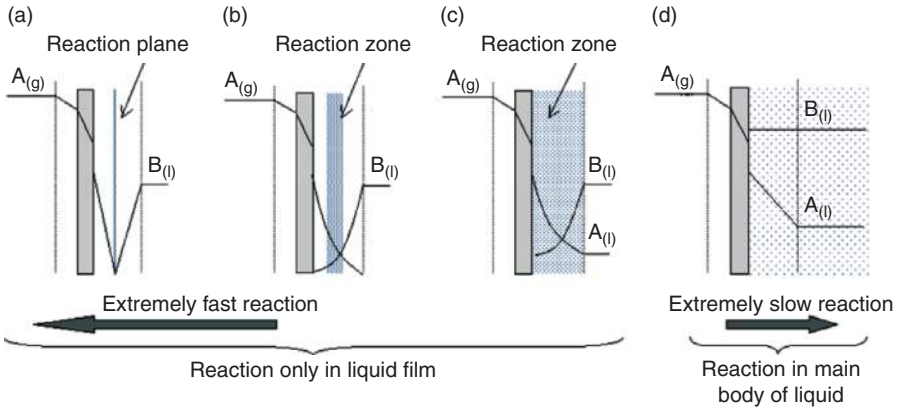

Figure 20 Profile concentration for different kinetic regimes for mass transfer in a nonwetted membrane contactor with reaction $A_{(g)} + bB_{(l)} \rightarrow Products_{(l)}$.

For example, for a first-order reaction $A_{(g)} + bB_{(l)} \rightarrow Products_{(l)}$ having the following reaction rate equation:

$$(-r_A) = kC_A \tag{37}$$

the Hatta number is

$$Ha = \delta\sqrt{\frac{k}{D_A}} = \frac{\sqrt{kD_A}}{k_{l0}} \tag{38}$$

where δ is the film thickness, D_A is the component A diffusivity in the liquid phase, and k_{l0} is liquid-phase mass transfer coefficient in absence of reaction, defined as

$$k_{l0} = \frac{D_A}{\delta} \tag{39}$$

Considering the case of a nonwetted membrane as an example, the molar flux through the interface for the liquid phase can be

$$N_A = k_l E_{A0}\left(C_{Ai(m,l)} - C_{A(l)}\right) \tag{40}$$

Equation (35) takes into account the presence of a reaction in the liquid phase through the enhancement factor, E_{A0}, which compares the absorption rate with and without chemical reaction:

$$E_{A0} = \frac{\begin{array}{c}\text{absorption rate of a gas in the liquid}\\ \text{in the presence of a chemical reaction}\end{array}}{\begin{array}{c}\text{absorption rate in the absence of}\\ \text{chemical reaction}\end{array}} = \frac{k_l}{k_{l0}} \tag{41}$$

The enhancement factor is a function of (1) the maximum possible enhancement factor, (2) the Hatta number, and (3) component A liquid bulk concentration:

$$E_{A0} = f(E_\infty, Ha, C_{A(l)}) \tag{42}$$

The maximum enhancement factor, E_∞, is obtained when an extremely fast reaction takes place; it can be obtained by

$$E_\infty = 1 + \frac{D_B C_{B(l)}}{\nu_B D_A C_{Ai(m,l)}}\left(\frac{D_B}{D_A}\right)^{n-1} \tag{43}$$

where $n = 1$ and $n = 0.5$, depending if the film model or penetration model is assumed, respectively.

The general expressions of E_{A0} are quite complex and we suggest the reader to refer to specialized textbooks [77]. In the presence of a reaction, the enhancement factor can assume value (up to 1000) that can greatly enhance the mass transfer in the contacting system. When a chemical reaction is extremely slow, then $E_{A0} \rightarrow 1$.

Considering the example of the membrane contactor, the molar flux of A can be still expressed with an in-series resistance model:

$$N_A = \left(\frac{1}{\frac{H}{k_g} + \frac{H}{k_M} + \frac{1}{k_l E_{A0}}}\right)\left(C^*_{A(l)} - C_{A(l)}\right) \tag{44}$$

As expected, in all the cases, the presence of the membrane as interphase contactor introduces an additional mass transfer resistance. However, by properly choosing the membrane, this resistance can be low, and the very high interfacial area offered by some membrane configurations can allow a successful application of the membrane contactor.

3.04.3.3 Catalytic Three-Phase Membrane Reactors

In a three-phase catalytic membrane reactor (TPCMR), a gas and a liquid stream are brought in close contact using a catalytic membrane. The reactant from the gas phase meets the other reactant from the liquid phase inside the structure of the catalytic membrane where the reaction occurs. In the TPCMR, the catalytic membrane offers the interface between the two phases, being at the same time in the place where the reaction can take place. When the system is compared to classical arrangements, such as slurry or three-phase fluidized bed reactors (where the catalyst is suspended into the fluid), various advantages and features can be pointed out. Catalytic reactions in gas–liquid–solid (GLS) systems are usually carried out using an SR or a trickle bed reactor (TBR) [79, 80]. In the SR, the gas phase (dispersed phase) is bubbled into the liquid phase (continuous phase), containing particles of the catalyst. The catalyst is moving with the other two phases. The TBR is a vertical fixed bed of catalyst. Usually, the liquid phase is introduced from the top of the fixed bed, while the gas phase is introduced from the bottom. The reactant in the gas phase has to dissolve in the liquid phase where the other reactant is and both reactants have to reach the catalytic site to give the product of reaction.

In an SR, the catalyst particle, with a size generally ranging from 1 to 50 μm, is dispersed into the liquid phase by stirring. The gas is dispersed into the liquid phase in bubbles with a size ranging from 0.5 to

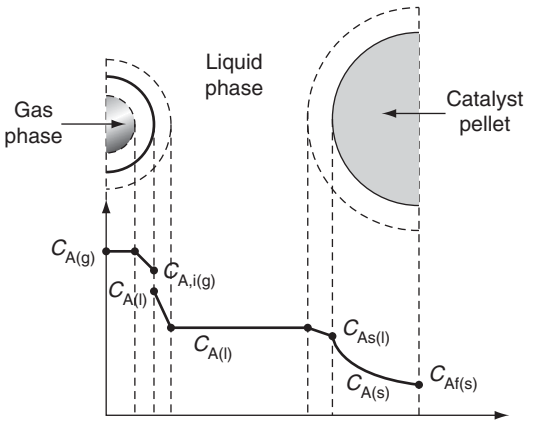

Figure 21 Interface concentration profile of the reactant A in a gas–liquid–solid reaction in a slurry reactor.

5 mm (depending on the gas dispersion system and on its power). The reaction takes place when both the reactants, which are respectively in the liquid phase and in the gas phase, meet on the catalyst particle. The reactive process in a conventional SR system can be generally described as composed of the following steps (**Figure 21**). Considering the gas-phase reactant and assuming that the reactant in the liquid phase and the reaction product are not volatile (they are not stripped by the gas phase) we have:

1. mass transfer of the gaseous reactant from the gas phase through the gas film, in turn, through the gas–liquid interface (if the gas phase is composed only by the reactant, this resistance is not considered);
2. dissolution of the reactant in the liquid phase;
3. mass transfer through the liquid film on surrounding the gas phase;
4. mass transfer through the liquid film on the particle of the catalyst; and
5. diffusion and reaction inside the porous structure of the catalyst.

Obviously, the product of reaction has to diffuse back from the catalyst particle to the liquid phase.

The influence of mass transfer on the overall reaction rate of a TPCMR is completely different and is due to the modality of contact between the two fluid phases and the solid catalytic phase (the membrane). **Figure 22** schematically shows the situation occurring in a catalytic membrane constituted of a catalytic layer supported by a macroporous structure which does not participate in the reaction.

In a TPMR, the catalyst is a thin layer (in the order of a few microns) and is generally wetted by the liquid phase. The gas phase is directly available both on the liquid phase and on the catalyst surface.

The main difference between the membrane reactor and the traditional reactor in three-phase systems is in the different paths that the reactants have to use to reach the catalytic site. In the SR, the mass transfer path is usually longer than in the membrane reactor. As a consequence, the overall resistance to mass transfer can be smaller than in traditional three-phase reactors. Another advantage is related to catalyst deposition on the membrane active layer, which eliminates any catalyst loss due to elutriation from the fluid flow in the reactor.

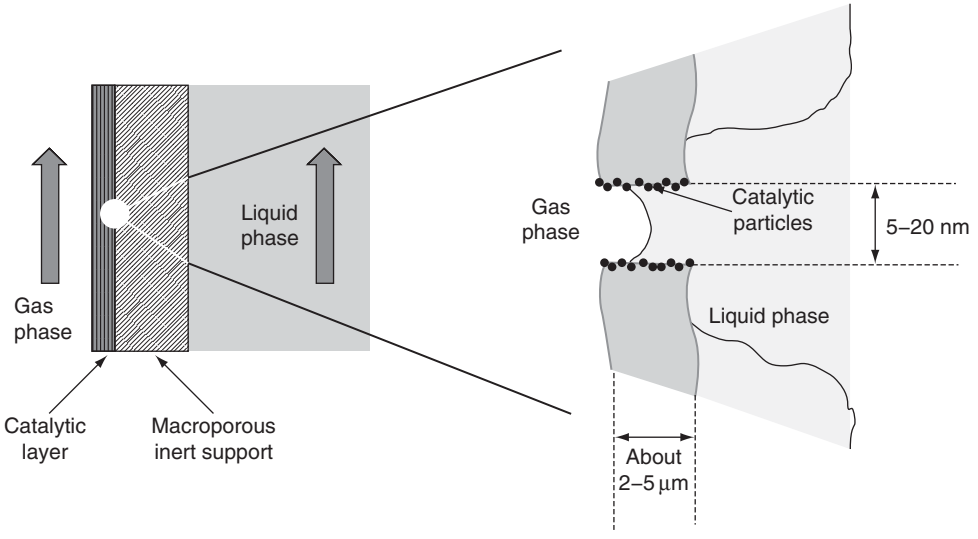

Figure 22 Contact between the two phases on the catalytic layer of a membrane reactor.

3.04.3.3.1 Internal diffusion in a TPCMR

The particular case where the liquid phase wets a catalytic porous symmetric membrane is considered and, for the sake of simplicity, no inert support is present in the membrane. For the time being, the presence of eventual mass transfer resistances in both the liquid and the gas phases will not be considered and a first-order reaction $A_{(g)}+bB_{(l)}\rightarrow C_{(l)}$ is assumed to occur on the catalytic membrane. The expected concentration profiles of the reactants and products in the catalytic membrane are depicted in Figure 23.

For our purpose, the thin catalytic membrane can be considered as a slab. It is useful to write the differential mass balance of the reactants in a differential volume of the catalytic membrane, dV, defined as

$$dV = A_M dz \tag{45}$$

where z is the coordinate perpendicular to the membrane surface of area A_M.

Considering the reactant A, the material balance

$$\{\text{rate of accumulation of A}\} = \{\text{rate of flow of A into the system}\} - \{\text{rate of flow of A out of the system}\} + \{\text{rate of generation of A by chemical reaction within the system}\} \tag{46}$$

we can write

$$0 = N_A|_z A_M - N_A|_{z+dz} A_M + R_A dV \tag{47}$$

where the first-order reaction rate is expressed by

$$R_A = -kC_A \tag{48}$$

and eliminating the membrane area in all the terms, we obtain

$$0 = N_A|_z - N_A|_{z+dz} - kC_A dz \tag{49}$$

Based on the Taylor approximation, for the infinitesimal dz length

$$N_A|_{z+dz} = N_A|_z + \left.\frac{dN_A}{dz}\right|_z dz \tag{50}$$

and using the Fick's law

$$N_A = -D_{eff}\frac{dC_A}{dz} \tag{51}$$

the following differential equation is obtained

$$\frac{d^2C_A}{dz^2} - \frac{k}{D_{eff}}C_A = 0 \tag{52}$$

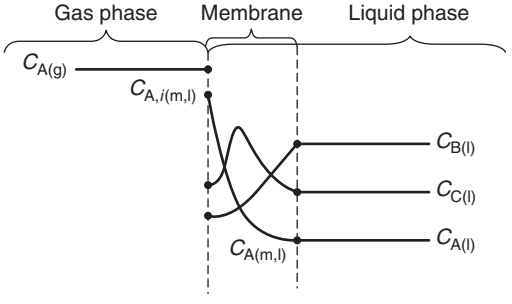

Figure 23 Profile concentration for a three-phase catalytic membrane reactor with the reaction $A_{(g)}+bB_{(l)}\rightarrow C_{(l)}$ and without mass transfer limitation in the gas and liquid phases.

The second-order differential equation (47) solved for the boundary conditions, which are common in the considered system, will give the profile concentration of the reactant A along the catalytic membrane of thickness t_M:

$$C_A|_{z=0} = C_{AS} \tag{53}$$

$$\left.\frac{dC_A}{dz}\right|_{z=t_M} = 0 \tag{54}$$

Introducing dimensionless parameters, the fractional coordinate in z direction is:

$$\delta = \frac{z}{t_M} \tag{55}$$

The dimensionless concentration is:

$$C^* = \frac{C_A}{C_{AS}} \tag{56}$$

The square of the Thiele modulus [78]:

$$\phi^2 = L\frac{k}{D_{eff}} \tag{57}$$

Equation (47) written in a dimensionless form becomes

$$\frac{d^2C^*}{d\delta^2} - \phi^2 C^* = 0 \tag{58}$$

The obtained differential equation is a homogeneous linear second-order differential equation of the type

$$y'' + ay = 0 \tag{59}$$

and its characteristic equation is

$$\lambda^2 + a = 0 \tag{60}$$

where

$$\lambda = \pm\sqrt{-a} = \pm\phi \tag{61}$$

The general solution of the differential equation (52) is

$$C^* = M_1 e^{-\phi\delta} + M_2 e^{\phi\delta} \tag{62}$$

where M_1 and M_2 are constants, which can be obtained by imposing the boundary conditions (stated by Equations (48) and (49)) in a dimensionless form:

$$C^*|_{\delta=0} = 1 \tag{63}$$

$$\left.\frac{dC^*}{d\delta}\right|_{\delta=1} = 0 \tag{64}$$

by deriving Equation (57)

$$\frac{dC^*}{d\delta} = M_1\phi e^{-\phi\delta} + M_2\phi e^{\phi\delta} \tag{65}$$

M_1 and M_2 can be evaluated as

$$M_1 = \frac{e^{\phi}}{e^{\phi} + e^{-\phi}} \tag{66}$$

$$M_2 = \frac{e^{-\phi}}{e^{\phi} + e^{-\phi}} \tag{67}$$

Therefore, concentration profile in the catalytic membrane is described by

$$C^* = \frac{e^{\phi(1-\delta)} + e^{-\phi(1-\delta)}}{e^{\phi} + e^{-\phi}} \tag{68}$$

which can be rewritten in terms of hyperbolic functions:

$$C^* = \frac{\cosh[\phi(1-\delta)]}{\cosh\phi} \tag{69}$$

A similar expression can be obviously obtained for the reactant B.

At this point, the concept of effectiveness factor can be introduced [81, 82]. The effectiveness factors η_{int} is defined as

$$\eta_{int} = \frac{\text{Observed reaction rate}}{\text{Reaction rate at external surface conditions}} = \frac{N_A|_{z=0}\cdot A_M}{r(C_{AS})\cdot V_M} = \frac{-D_{eff}\frac{dC}{dz}|_{z=0}\cdot A_M}{r(C_S)\cdot V_M} \tag{70}$$

The effectiveness factor compares the reaction rate in the presence of diffusion in the membrane structure and the reaction rate not limited by the internal diffusion. This is also known as internal effectiveness factor because it refers to the catalyst utilization efficiency influenced only by the diffusion in the porous catalytic layer.

Since

$$\frac{A_M}{V_M} = \frac{1}{t_M} \tag{71}$$

and

$$-D_{eff}\frac{dC_A}{dz} = -\frac{D_{eff}A_M}{L}C_{AS}\frac{dC^*}{d\delta} \tag{72}$$

where

$$\frac{dC^*}{d\delta} = -\frac{\phi\sinh[\phi(1-\delta)]}{\cosh\phi} \tag{73}$$

with

$$\left.\frac{dC^*}{d\delta}\right|_{\delta=0} = -\phi\tanh\phi \tag{74}$$

the effectiveness factor for the catalytic membrane referred to the reactant A is obtained:

$$\eta_{int} = \frac{\tanh\phi}{\phi} \tag{75}$$

When η_{int} tends to 1, the catalyst in the membrane layer is effectively used.

For a reaction rate of nth order

$$(-r_A) = \eta k C^n_{i(m,l)} \tag{76}$$

and the Thiele modulus becomes

$$\phi = t_M\left(\frac{kC_S^{n-1}}{D_{eff}}\right)^{1/2} \tag{77}$$

3.04.3.3.2 *Influence of external mass transfer*

We have seen how the internal diffusion can influence the reaction rate in the catalytic membrane reactor. The presence of mass transfer resistance in the gas phase is now considered. **Figure 24** shows a qualitative view of the concentration profiles in such situation.

In this case, it is convenient to write the mass transfer rate in terms of rate of diffusion per catalytic membrane mass:

$$-r'_A = N_A\frac{A_M}{V_M\rho_M} = k_g\frac{A_M}{V_M\rho_M}\left[C_{A(g)} - C_{Ai(g)}\right] \tag{78}$$

At the gas–liquid interface, the concentration of A in both phases is in equilibrium according to Henry's law:

$$C_{Ai(m,l)} = HC_{Ai(g)} \tag{79}$$

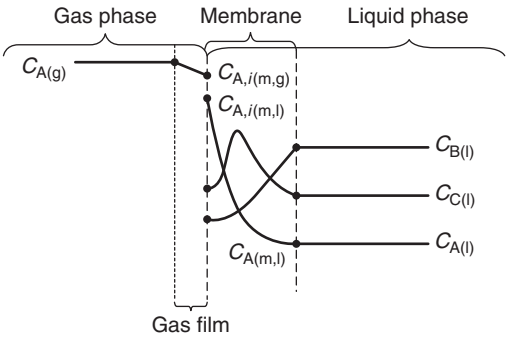

Figure 24 Profile concentration for a three-phase catalytic membrane reactor with the reaction $A_{(g)}+bB_{(l)}\rightarrow C_{(l)}$ and with mass transfer limitation in the gas phase.

Diffusion and reaction in the catalytic membrane is described by

$$-r'_A = \eta(-r'_{AS}) = \eta k' C_{Ai(m,l)} \tag{80}$$

and equating the Equations (82) and (84), the overall rate equation for A can be obtained:

$$-r'_A = \frac{1}{\frac{HV_M\rho_M}{k_g A_M} + \frac{1}{\eta_{int}k}} C_{A(g)} \tag{81}$$

The overall effectiveness can be defined as

$$\eta_{overall} = \frac{\eta_{int}}{1+\eta_{int}\frac{HkV_M\rho_M}{k_g A_M}} = \frac{\eta_{int}}{1+\eta_{int}Da} \tag{82}$$

where Damköler number, *Da*, expresses the relative rates of the intraphase reaction to external mass transport.

Cini and Harold [82] carried out pioneering studies on TPCMR and classified different situations considering the influence of different mass transport resistances. For each considered situation, they obtained some expressions for the apparent activation energy.

When the reaction is limited neither by internal nor by external mass transfer ($\eta_{overall} = 1$, $\eta_{int} = 1$), by plotting the logarithm of the observed reaction rate against the inverse of the temperature (Arrhenius type diagram)

$$E_{app} = -R\frac{d(\ln \text{ rate})}{d\left(\frac{1}{T}\right)} \tag{83}$$

the apparent activation energy will correspond to the intrinsic activation energy of the reaction:

$$E_{app} = E_{in} \tag{84}$$

For the gas-phase mass transfer limitation

$$E_{app} = E_{sat} + \frac{E_{in}+E_{diff}}{2} \tag{85}$$

3.04.3.4 Some Considerations on the Mass Balance in Membrane Contactors and Three-Phase Membrane Reactors

In the previous sections, the local mass balances at the interfaces were presented for some typical conditions that can be encountered with membrane contactors and three-phase membrane reactors. We have also seen that, when an external mass transfer is present in the gas and the liquid phases, the estimation of local mass transfer coefficients depends on the type of fluid dynamic regime governing on the fluid phase interfacing the membrane.

Figure 25 shows a system where the two phases are separated by the membrane, and each of them is well mixed. With this assumption, the concentration profile in the reactor volume will be constant on both sides of the membrane. On the other hand, **Figure 26** shows the case where both the fluids on the two sides of the membrane are moving along the axial direction; then, a profile of both velocity and concentration can take place along the reactor length in the two sides of the membrane. **Figure 27** shows a membrane separating a fluid in well-mixed condition from the other with concentration and fluid velocity dependent on the reactor length.

Consequently, it then seems clear that material balances in the phase contacting the membrane should be written keeping into account the fact that, because of the membrane presence, a concentration profile of the components can be both in the axial direction and in the direction perpendicular to the membrane surface (in cylindrical geometries as well as in hollow fibers, along the radial direction). This fact can lead to partial differential equations, which often need to be solved numerically. Therefore, when possible, some simplifying assumptions can

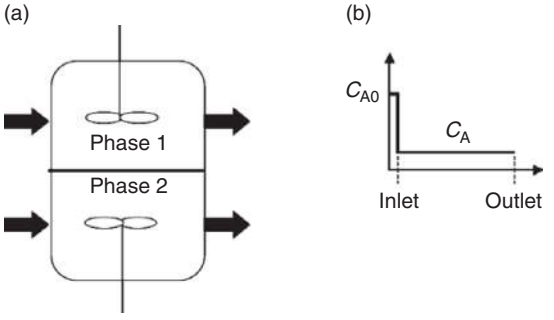

Figure 25 The membrane separates two fluids in well-mixed conditions.

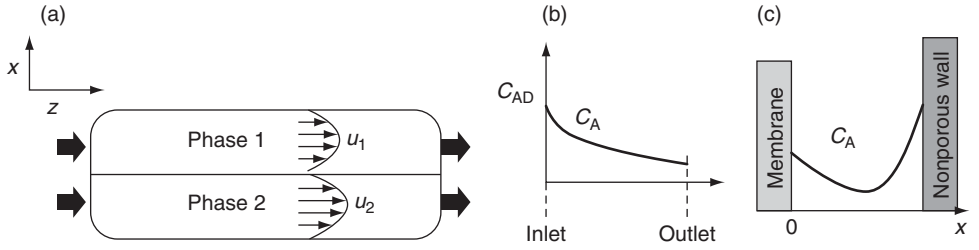

Figure 26 The membrane separates two fluids in laminar flow conditions.

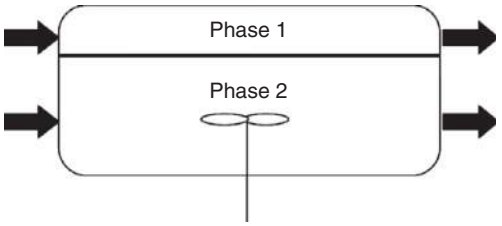

Figure 27 The membrane separates a fluid in laminar flow condition from a fluid in well-mixed conditions.

help reduce the two-dimensional problems to a one-dimensional problem.

For example, hollow fibers and tubular membranes are commonly used as membrane contactors and three-phase membrane reactors. Typically, the flow regime in the lumen of such tubular membranes is laminar and the consequence for both fluid velocity and component concentration profiles is that they depend not only on the axial coordinate but also on the radial position.

When the gas phase (there is no reaction term) flows into the inner side of the hollow fiber, the mass balance of the component A in the gas phase in cylindrical coordinates takes the following form (where the dispersion effects along the axial direction are neglected) (**Figure 28**):

$$u_r \frac{\partial C_{A,g}}{\partial z} = D_{A,g}\left[\frac{1}{r}\frac{\partial}{\partial r}\left(r\frac{\partial C_A}{\partial r}\right)\right] = D_{A,g}\left[\frac{\partial^2 C_A}{\partial r^2} + \frac{1}{r}\frac{\partial C_A}{\partial r}\right] \tag{86}$$

If a developed laminar regime is assumed, the radial velocity profile is parabolic and can be described by

$$u_r = 2u_m\left[1-\left(\frac{r}{R}\right)^2\right] \tag{87}$$

The boundary conditions for a wetted membrane are

$$D_{A,g}\left(\frac{\partial C_{A(g)}}{\partial r}\right)_{r=R} = -k_M\left(C_{A(g)}|_{r=R} - C_{A,i(g)}\right) \tag{88}$$

$$\left(\frac{\partial C_{A(g)}}{\partial r}\right)_{r=0} = 0 \tag{89}$$

$$C_{A(g)}|_{z=0} = C_{A0(g)} \tag{90}$$

On the contrary, when the liquid phase (in presence of a homogeneous reaction) flows inside the membrane lumen, then the material balances are

$$u_r \frac{\partial C_{A(l)}}{\partial z} = D_{A(l)}\left[\frac{\partial^2 C_A}{\partial r^2} + \frac{1}{r}\frac{\partial C_A}{\partial r}\right] - kf(C_A, C_B) \tag{91}$$

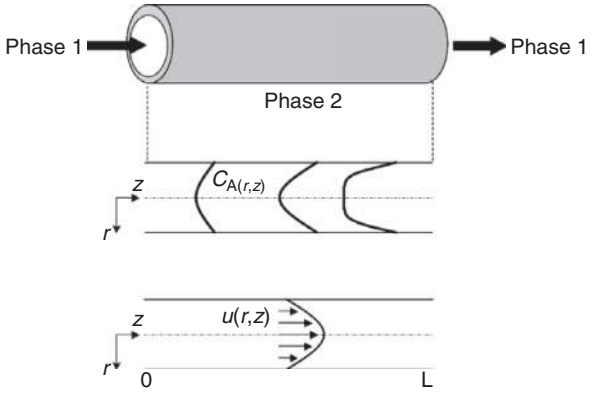

Figure 28 Expected concentration profile in the radial direction for a tubular membrane geometry.

and the boundary conditions for a nonwetted membrane are

$$D_{A,g}\left(\frac{\partial C_{A(g)}}{\partial r}\right)_{r=R} = \left(\frac{1}{\frac{1}{k_g}+\frac{1}{k_M}}\right)\left(C_{A(g)} - C_{A,i(g)}\right) \quad (92)$$

$$D_{A,g}\left(\frac{\partial C_{B(l)}}{\partial r}\right)_{r=R} = 0 \quad (93)$$

since B is assumed nonvolatile at the centerline of the tube

$$\left(\frac{\partial C_{A(l)}}{\partial r}\right)_{r=0} = \left(\frac{\partial C_{B(l)}}{\partial r}\right)_{r=0} = 0 \quad (94)$$

and the initial conditions are

$$C_{A(l)}\big|_{z=0} = 0 \quad (95)$$

$$C_{B(l)}\big|_{z=0} = C_{B0} \quad (96)$$

These are partially differential equations that must be solved numerically or by applying some simplifying assumptions, allowing the reduction to a one-dimensional problem after defining, for example, an average concentration in the flowing fluid as

$$C_{A,av} = \frac{\int_0^R C_{A(r,z)}\,dS}{dS} \quad (97)$$

3.04.4 Conclusions

A membrane used as an interface between different fluid phases offers a novel contact modality between the phases, which can be used to improve the mass transfer of components between them (concept of membrane) or to carry multiphase heterogeneous reactions (TPCMR) with less mass transfer limitations than in traditional reactors. The approach to the matter given in this chapter would be a starting point for further studies on the topic.

References

[1] Lim, S. Y., Park, B., Hung, F., Sahimi, M., Tsotsis, T. T. *Chem. Eng. Sci.* **2002**, *57*, 4933–4946.
[2] Krishna, R., Sie, S. T. *Chem. Eng. Sci.* **1994**, *49*, 4029–4065.
[3] Coronas, J., Santamaria, J. *Catal. Today* **1999**, *51*, 377–389.
[4] Dixon, A. G. *Int. J. Chem. Reactor Eng.* **2003**, *1*, R6.
[5] Rios, G. M., Belleville, M.-P., Paolucci-Jeanjean, D. *Trends Biotechnol.* **2007**, *25*, 242–246.
[6] Hsieh, H. P. *Inorganic Membranes for Separation and Reaction.* Elsevier: Amsterdam, 1996.
[7] Gabelman, A., Hwang, S.-T. *J. Membr. Sci.* **1999**, *159*, 61–106.
[8] Wu, S., Gallot, J.-E., Bousmina, M., Bouchard, C., Kaliaguine, S. *Catal. Today* **2000**, *56*, 113–129.
[9] Regalbuto, J. *Handbook of Catalyst Preparation*; CRC Press: Singapore, 2006.
[10] Ozdemir, S. S., Buonomenna, G., Drioli, E. *Appl. Catal. A: Gen.* **2006**, *307*, 167–183.
[11] Vospernik, M., Pintar, A., Bercic, G., *et al*. *Chem. Eng. Sci.* **2004**, *59*, 5363–5372.
[12] Bottino, A., Capannelli, G., Comite, A., Del Borghi, A., Di Felice, R. *Sep. Purif. Technol.* **2004**, *34*, 239–245.
[13] Espro, C., Arena, F., Frusteri, F., Parmaliana, A. *Catal. Today* **2001**, *67*, 247–256.
[14] Hermans, L. A. M., Geus, J. W. *Preparation of Catalysts II*; Elsevier: Amsterdam, 1979; p 113.
[15] Uzio, D., Peureux, J., Giroir-Fendler, A., Torres, M., Ramsay, J., Dal mon, J.-A. *Appl. Catal. A: Gen.* **1993**, *96*, 83–97.
[16] Bottino, A., Capannelli, G., Comite, A., Di Felice, R. *Desalination* **2002**, *144*, 411–416.
[17] Reif, M., Dittmeyer, R. *Catal. Today* **2003**, *82*, 3–14.
[18] Choi, J. S., Song, I. K., Lee, W. Y. *Catal. Today* **2001**, *67*, 237–245.
[19] Bao, L., Trachtenberg, M. C. *Chem. Eng. Sci.* **2005**, *60*, 6868–6875.
[20] Bottino, A., Capannelli, G., Comite, A., Firpo, R., Di Felice, R., Minacci, P. *Desalination* **2006**, *200*, 609–611.
[21] Mavroudi, M., Kaldis, S. P., Sakellaropoulos, G. P. *Fuel* **2003**, *82*, 2153–2159.
[22] Charcosset, C., Fessi, H. *J. Membr. Sci.* **2005**, *266*, 115–120.
[23] He, F., Wang, P., Jia, Z., Liu, Z. *J. Membr. Sci.* **2003**, *227*, 15–21.
[24] Zarkadas, D. M., Sirkar, K. K. *Chem. Eng. Sci.* **2006**, *61*, 5030–5048.
[25] Chen, G. G., Luo, G. S., Xu, J. H., Wang, J. D. *Powder Technol.* **2004**, *139*, 180–185.
[26] Li, J.-L., Chen, B.-H. *Sep. Purif. Technol.* **2005**, *41*, 109–122.
[27] Gabelman, A., Hwang, S.-T. *J. Membr. Sci.* **1999**, *159*, 61–106.
[28] Kumar, P. S., Hogendoorn, J. A., Feron, P. H. M., Versteeg, G. F. *Chem. Eng. Sci.* **2002**, *57*, 1639–1651.
[29] Wang, R., Li, D. F., Liang, D. T. *Chem. Eng. Process.* **2004**, *43*, 849–856.
[30] Heng, S., Yeung, K. L., Djafer, M., Schrotter, J.-C. *J. Membr. Sci.* **2007**, *289*, 67–75.
[31] Bottino, A., Capannelli, G., Comite, A., Di Felice, R., Firpo, R. *Sep. Purif. Technol.* **2008**, *59*, 85–90.
[32] Gonzalez-Brambila, M., Monroy, O., Lopez-Isunza, F. *Chem. Eng. Sci.* **2006**, *61*, 5268–5281.
[33] Parameshwaran, K., Visvanathan, C., Ben Aim, R. *J. Environ. Eng.* **1999**, *125*, 825–834.
[34] Qi, Z., Cussler, E. L. *J. Membr. Sci.* **1985**, *23*, 333–345.
[35] Qi, Z., Cussler, E. L. *J. Membr. Sci.* **1985**, *23*, 321–332.
[36] Kreulen, H., Smolders, C. A., Versteeg, G. F., van Swaaij, W. P. M. *J. Membr. Sci.* **1993**, *78*, 197–216.
[37] Kreulen, H., Smolders, C. A., Versteeg, G. F., van Swaaij, W. P. M. *J. Membr. Sci.* **1993**, *78*, 217–238.
[38] Kim, Y.-S., Yang, S.-M. *Sep. Purif. Technol.* **2000**, *21*, 101–109.
[39] Keshavarz, P., Fathikalajahi, J., Ayatollahi, S. *J. Hazard. Mater.* **2008**, *152*, 1237–1247.
[40] Dittmeyer, R., Hollein, V., Daub, K. *J. Mol. Catal. A: Chem.* **2001**, *173*, 135–184.
[41] Dittmeyer, R., Svajda, K., Reif, M. *Top. Catal.* **2004**, *29*, 3–27.
[42] Criscuoli, A., Basile, A., Drioli, E. *Catal. Today* **2000**, *56*, 53–64.
[43] Piera, E., Tellez, C., Coronas, J., Menendez, M., Santamaria, J. *Catal. Today* **2001**, *67*, 127–138.
[44] Peureux, J., Torres, M., Mozzanega, H., Giroir-Fendler, A., Dalmon, J.-A. *Catal. Today* **1995**, *25*, 409–415.

[45] Torres, M., Sanchez, J., Dalmon, J.-A., Bernauer, B., Lieto, J. *Ind. Eng. Chem. Res.* **1994**, *33*, 2421–2425.
[46] Diakov, V., Varma, A. *AIChE J.* **2003**, *49*, 2933–2936.
[47] Schmidt, A., Wolf, A., Warsitz, R., *et al*. *AIChE J.* **2008**, *54*, 258–268.
[48] Bottino, A., Capannelli, G., Comite, A., Di Felice, R. *Catal. Today* **2005**, *99*, 171–177.
[49] Vospernik, M., Pintar, A., Levec, J. *Chem. Eng. Process.* **2006**, *45*, 404–414.
[50] Vospernik, M., Pintar, A., Bercic, G., Levec, J. *J. Membr. Sci.* **2003**, *223*, 157–169.
[51] Vospernik, M., Pintar, A., Bercic, G., Levec, J. *Catal. Today* **2003**, *79–80*, 169–179.
[52] Bercic, G., Pintar, A., Levec, J. *Catal. Today* **2005**, *105*, 589–597.
[53] Iojoiu, E. E., Landrivon, E., Reader, H., Torp, E. G., Miachon, S., Dalmon, J.-A. *Catal. Today* **2006**, *118*, 246–252.
[54] Iojoiu, E. E., Miachon, S., Landrivon, E., Walmsley, J., Reader, H., Dalmon, J.-A. *Appl. Catal. B: Environ.* **2006**, *69*, 196–206.
[55] Iojoiu, E. E., Walmsley, J., Reader, H., Miachon, S., Dalmon, J.-A. *Catal. Today* **2005**, *104*, 329–335.
[56] Miachon, S., Perez, V., Crehan, G., *et al*. *Catal. Today* **2003**, *82*, 75–81.
[57] Reader, H., Bredesen, R., Crehan, G., *et al*. *Sep. Purif. Technol.* **2003**, *32*, 349–355.
[58] Iojoiu, E. E., Miachon, S., Dalmon, J.-A. *Top. Catal.* **2005**, *33*, 135–139.
[59] Lopez, J. L., Matson, S. L. *J. Membr. Sci.* **1997**, *125*, 189–211.
[60] Giorno, L., Zhang, J., Drioli, E. *J. Membr. Sci.* **2006**, *276*, 59–67.
[61] Findrik, Z., Presecki, A. V., Vasic-Racki, D. *J. Biosci. Bioeng.* **2007**, *104*, 275–280.
[62] Liu, J., Cui, Z. *J. Membr. Sci.* **2007**, *302*, 180–187.
[63] Giorno, L., D'Amore, E., Mazzei, R., *et al*. *J. Membr. Sci.* **2007**, *295*, 95–101.
[64] Gonzo, E. E., Gottifredi, J. C. *Biochem. Eng. J.* **2007**, *37*, 80–85.
[65] Yawalkar, A. A., Pangarkar, V. G., Baron, G. V. *J. Membr. Sci.* **2001**, *182*, 129–137.
[66] Bessarabov, D. G., Theron, J. P., Sanderson, R. D. *Desalination* **1998**, *115*, 279–284.
[67] Park, B., Ravi-Kumar, V. S., Tsootsis, T. T. *Ind. Eng. Chem. Res.* **1998**, *37*, 1276–1289.
[68] Kieffer, R., Charcosset, C., Puel, F., Mangin, D. *Comput. Chem. Eng.* **2008**, *32*, 1325–1333.
[69] Pedernera, M., Mallada, R., Menendez, M., Santamaria, J. *AIChE J.* **2000**, *46*, 2489–2498.
[70] Dindore, V. Y., Brilman, D. W. F., Versteeg, G. F. *Chem. Eng. Sci.* **2005**, *60*, 467–479.
[71] Bathia, S., Long, S. W., Kamaruddin, A. H. *Chem. Eng. Sci.* **2004**, *59*, 5061–5068.
[72] Treybal, R. E. *Mass-Transfer Operations*; McGraw-Hill: Singapore, 1981.
[73] Basmadjian, D. *Mass Transfer: Principles and Applications*; CRC Press: Boca Raton, FL, 2004.
[74] Bird, R. B., Stewart, W. E., Lightfoot, E. N. *Transport Phenomena*; Wiley-VCH: New York, 2007.
[75] Reid, R. C., Prausnitz, J. M., Poling, B. E. *The Properties of Gases and Liquids*; McGraw-Hill: Singapore, 1988.
[76] Cunningham, R. E., Williams, R. J. J. *Diffusion in Gases and Porous Media*; Plenum: New York, 1980.
[77] Westerterp, K. R., Van Swaaij, W. P. M., Beenackers, A. A. C. M. *Chemical Reactor Design and Operation*; Wiley: New York, 1988.
[78] Carberry, J. J. *Chemical and Catalytic Reaction Engineering*; McGraw-Hill: New York, 1976.
[79] Fogler, H. S. *Elements of Chemical Reaction Engineering*; Prentice Hall: Upper Saddle River, NJ, 1999.
[80] Biardi, G., Baldi, G. *Catal. Today* **1999**, *52*, 223–234.
[81] Torres, M., Sanchez, J., Dalmon, J. A., Bernauer, B., Lieto, J. *Ind. Eng. Chem. Res.* **1994**, *33*, 2421–2425.
[82] Cini, P., Harold, M. *AIChE J.* **1991**, *37*, 997–1008.

Biographical Sketches

Gustavo Capannelli has been an associate professor of industrial chemistry at the University of Genoa since 1990. He obtained his degree in industrial chemistry at the University of Genoa in 1974. He held a position as researcher at the University of Genoa until 1987. From 1987 to 1990, he was associate professor of industrial chemistry and of petrochemistry and technology of oil products at the University of Messina (Italy). His research activity is principally dedicated to the preparation and characterization of membranes and their application, not only to conventional membrane processes (microfiltration, ultrafiltration, nanofiltration, reverse osmosis, etc.), but also to innovative fields (catalytic membranes, catalytic membrane reactors, membrane contactors, etc.). He is a coordinator of the Laboratory of Electronic Microscopy and of the Membrane and Membrane Processes Research Group, both based at the Department of Chemistry and Industrial Chemistry, University of Genoa. Gustavo Capannelli has been the head and proponent of numerous research activities and collaborations with several industries, research centers, and public and private organizations. Gustavo Capannelli has coauthored more than 120 publications (mainly published in international journals) and 13 patents.

Antonio Comite obtained his degree in industrial chemistry at the University of Genoa in 1998 with a thesis titled 'Volatile organic compounds removal by a catalytic membrane combustor.' In 2005, he discussed a PhD thesis titled 'Development of inorganic membrane reactors.' His research activity mainly focuses on heterogeneous catalysis and the application and development of membrane reactors in catalysis, covering different topics such as catalyst preparation, characterization (morphological, structural, etc.), testing (activity, kinetic parameter estimation, etc.), catalytic inorganic membranes and supports characterization (gas permeability, structural properties, etc.), and catalytic membrane reactors (applied to both gas-phase reactions and three-phase reactions). Recently, his interest has also been focused on innovative membrane and electrodes for fuel cells. He has coauthored many publications and congress communications.

Renzo Di Felice is currently a professor of chemical reactor engineering at the University of Genoa (Italy). He obtained his bachelor's degree in chemical engineering from the University of L'Aquila (Italy) in 1981, and his PhD and DSc (Eng) from the University of London (UK) in 1988 and 1997, respectively. Before moving to Genoa, Renzo Di Felice was an assistant professor at the University of L'Aquila from 1983 to 1992. During this period, he spent 2 years at the Department of Chemical and Biochemical Engineering, University College London. He was also involved in teaching and research at the University of Addis Ababa (Ethiopia) and at the National University of Singapore (Singapore).

His research is focused on the fluid dynamic behavior of two-phase suspensions, with particular relevance on liquid–solid systems – a field for which he has obtained international recognition. Recently, his attention has also been focused on multiphase membrane reactors. Renzo Di Felice has authored more than 100 papers in international scientific journals. He is a member of the American Institute of Chemical Engineers (AIChE), the Institution of Chemical Engineers (IChemE), and the Italian Association of Chemical Engineering (AIDIC).

3.05 Catalytic Membranes and Membrane Reactors

E Fontananova and E Drioli, Institute of Membrane Technology, ITM-CNR, University of Calabria, Rende (CS), Italy

3.05.1	Introduction	110
3.05.2	Classification of MRs	111
3.05.3	Membrane Functions in a MR	111
3.05.4	Organic MRs	121
3.05.5	Immobilization of Catalysts in Membranes	122
3.05.6	Industrial Applications of MRs and the As-Yet Existing Limitations	128
References		130

Glossary

Convective flow The movement of particles forced by the action of a fluid.

Electrochemical potential The sum of the chemical and electrical potentials for a component which, in the presence of a gradient of the electrochemical potential, will tend to move from areas with higher electrochemical potential to areas with lower electrochemical potential; it is expressed in units of energy (usually J mol^{-1}).

Hydrophobic recovery A phenomenon that can occur when polar groups are grafted by plasma technique on hydrophobic polymeric surfaces. This comprises the orientation with the time of the untreated polymeric chains outward the modified interface, and that of the grafted polar groups inward, leading to the recovery of the surface properties of the original polymer and to the reduction of the polar groups available on the surface.

Membrane contactor Membrane operation in which a membrane facilitates the diffusive mass transfer between two contacting phases (liquid–liquid, gas–liquid, gas–gas, etc.) without dispersion of one phase within another.

Membrane fouling The deposition of retained particles, colloids, emulsions, suspensions, macromolecules, salts, etc. on or in the membrane during a membrane separation process.

Membrane module A unit in which one or more membranes (in flat or tubular configuration) are packed.

Molecular imprinted polymer Polymer prepared in the presence of a template molecule successively extracted, thus leaving complementary cavities able to work as molecular recognition site for the original molecule.

Molecular weight cutoff (MWCO) The minimum molecular weight of a solute to obtain a rejection of 90% in a membrane separation process. The MWCO is expressed in daltons and determined by measuring the rejection of materials with various molecular weights that usually consist of biological molecules (e.g., albumin) or organic polymers (e.g., dextran).

Plasma State of matter electrically conducting produced when the atoms in a gas become ionized.

Polymer electrolyte membrane or proton exchange membrane (PEM) Membrane made from ionomers (polymer with fixed ionic groups) that is able to conduct protons.

Polymers of intrinsic microporosity (PIMs) Polymers with behavior like molecular sieves in the solid state; because of their rigid and contorted molecular structures, they are unable to pack efficiently.

Polyoxometalalte or polyoxoanions (POM) Polyanionic metal oxide cluster of early transition metals (V, Nb, Ta, Mo, W, etc.).

Turnover number (TON) The number of moles of product produced for each mole of catalyst (products (mol)/catalyst (mol)).

3.05.1 Introduction

Membrane reactors (MRs) are multifunctional reactors combining a chemical reaction (generally catalytically promoted) with a membrane-based separation. MRs have been investigated since the 1970s, primarily employing polymeric membranes in enzymatic reactions or metal membranes for high-temperature reactions.

MRs are today accepted as proven technology for many biotechnological applications; however, there is a huge potential for these integrated systems in various industrial sectors.

The necessity to realize a sustainable growth, also by the so-called process intensification (PI) strategy [1], is the driving force of the increasing worldwide interest in MRs in different fields, including not only biochemical and petrochemical, but also chemical production, environmental remediation, and energy sector.

The PI strategy consists of innovative equipment design and process development methods that are expected to bring substantial improvements in manufacturing and processing, decreasing production costs, equipment size, energy consumption, and waste generation, as well as improving remote control, information fluxes, and process flexibility [1].

Reactive separations respond well to the requirements of this strategy, not only combining a reaction with a separation process, at the equipment level (multifunctional reactors), but also introducing functional interrelations between the operations involved, resulting in an improved process [2].

MRs are examples of reactive separations which, in comparison with other reactive separations (reactive distillation, reactive adsorption, and reactive crystallization/precipitation), present the advantages to use intrinsically more clean and energy-efficient separation routes for high-quality products.

In numerous cases, membrane separation processes operate at much lower temperature, especially when compared with thermal processes such as reactive distillation. As a consequence, they might provide a solution in the case of limited thermal stability of catalyst and products. Furthermore, by membrane separation processes, it is also possible to separate nonvolatile components.

Various membrane unit operations are available today for a wide spectrum of industrial applications, such as microfiltration (MF), ultrafiltration (UF), nanofiltration (NF), reverse osmosis (RO), gas separation (GS) and vapor separation (VS), pervaporation (PV), dialysis (D), electrodialysis (ED), and membrane contactors (MCs).

The possibility to integrate various membrane operations in the same process, or in combination with conventional separation units, allows, in many cases, one to obtain better performance in terms of product quality, plant compactness, environmental impact, and energy use [3–6].

A special case of integrated membrane system, with much interest in the logic of the PI strategy, is represented by the MRs.

The combination of advanced separation and chemical conversion realized in an MR allows one to achieve many advantages in comparison to traditional reactors, depending on the specific functions performed by the membrane [7].

However, in order to have a synergic combination of the separation and reaction process that allows one to obtain optimal performances, a multidisciplinary approach in the MR design is necessary.

In this approach, different disciplines, such as chemistry, chemical engineering, membrane engineering, and process engineering, give their specific contribution to the general objective to obtain improved performance in terms of productivity and sustainability (**Figure 1**).

In the following sections, the advantages and the as-yet existing limitations of MRs technology are presented. It is shown that the selective membrane-based separation and transport of the products and/or the reagents from or toward the reactor can increase the yield and/or the selectivity of some processes.

The downstream processing of the products can be substantially facilitated by an appropriate process design when they are removed from the reaction mixture by means of a membrane [8].

Moreover, when the membrane is used to immobilize a homogeneous catalyst, the catalyst recovery,

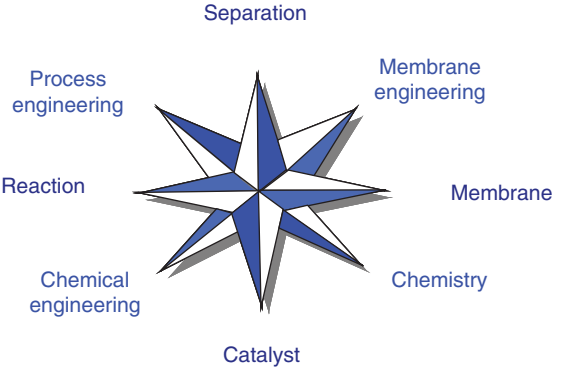

Figure 1 Multidisciplinary approach in the membrane reactor design.

regeneration, and reuse in successive catalytic runs, are generally easier in comparison with other heterogeneous catalytic systems.

The membrane can also define the reaction volume (e.g., by providing a contacting zone for two immiscible phases, as in phase-transfer catalysis), excluding polluting solvents and reducing the environmental impact of the process membrane [8].

In the past few years, significant progress has also been made in the modeling and simulation for investigating the overall performance of the MRs in terms of mass transport of substrates/products, by determining the concentration and velocity profiles. The ultimate goal is to improve the reactor performance by optimizing the reactor design and operative conditions, as well as providing important inputs for the realization of membranes and catalysts through the understanding and optimization of structural/functional relationships at the molecular level in the systems investigated.

New metrics such as the volume index and conversion index have also been recently proposed as simple and valuable tools analyzing the volume reduction or improved conversion shown by MRs in the logic of the PI strategy [9].

The scientific literature on MRs is significant today; however, practically only few large-scale industrial applications have been reported, principally in the biotechnology field.

MRs are today successfully applied in small-scale operations; however, for their use on a large industrial scale, additional efforts, mainly related to the optimization of membrane manufacturing and reactor design, are required.

3.05.2 Classification of MRs

As there are different ways to combine a catalyst with a membrane in a MR, there are numerous possible categorizations of these systems (**Figure 2**) [10].

The most general is based on transport function of the membrane, and it is possible to have extractor, distributor, and contactor type MRs [11].

The nature of the membrane material (organic or inorganic) is another criterion used to distinguish between the MRs [8, 12].

Another possible classification is based on the role of the membrane in the catalytic process. If the membrane is itself catalytically active, the MR is indicated as a catalytic membrane reactor (CMR); alternatively, if the membrane provides only a separation function and the catalyst is in solution, in the packed-bed or fluidized-bed configuration, the system is indicated as inert or membrane-assisted reactor [13].

The nature of the catalyst, biological or artificial, is also used as a classification tool [14].

3.05.3 Membrane Functions in a MR

The variety in the MR classification reflects the diversity of the functions that the membrane can serve in the reactor (**Figure 3**). Typical examples are the separation of products from the reaction

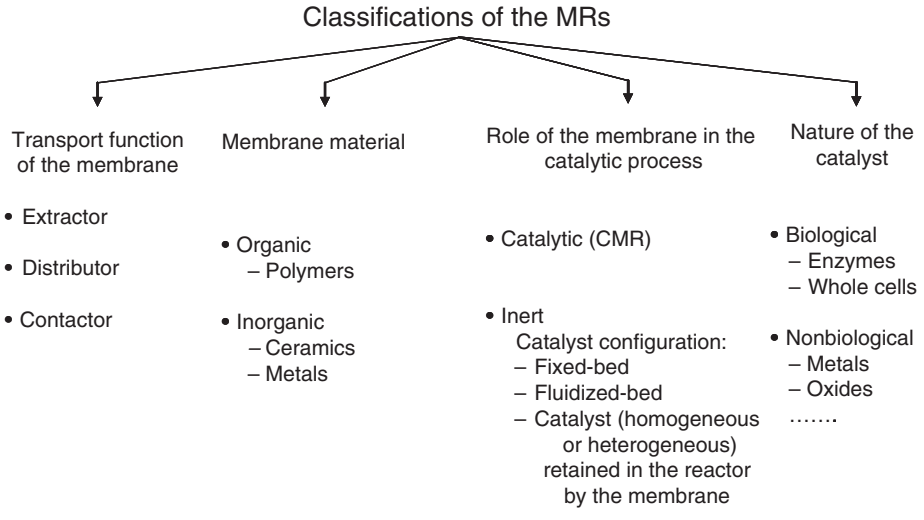

Figure 2 Some possible classifications of the membrane reactors.

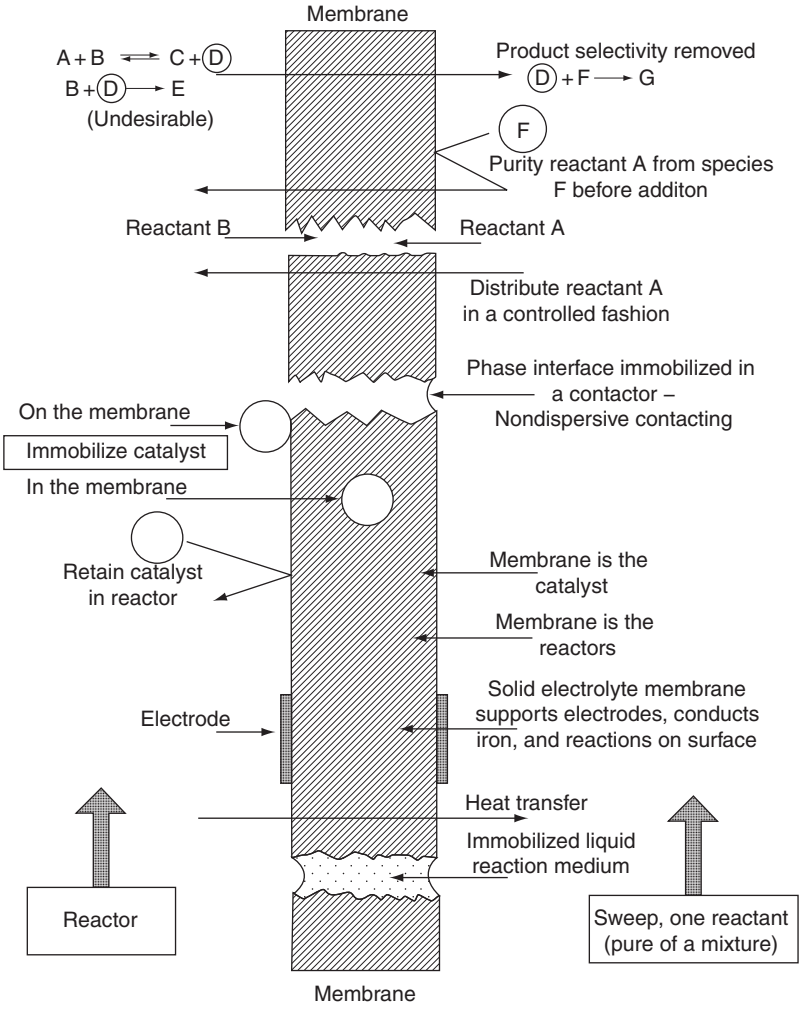

Figure 3 Schematization of the different functions of a membrane in a membrane reactor. Reproduced with permission from Sirkar, K. K., Shanbhag, P. V., Kovvali, A. S. *Ind. Eng. Chem. Res.* **1999**, *38,* 3715–3737.

mixture, the separation of a reactant from a mixed stream for introduction into the reactor, and the controlled addition of reactants.

In a membrane extractor the removal of one or more products allows the enhancement of the conversion of thermodynamically controlled reactions (**Figure 4**, i), as in esterification and dehydrogenation reactions in which the removal respectively of water or hydrogen increases the reaction yield.

In a membrane extractor it is also possible to have an improvement of the selectivity toward an instable intermediate product by its selective extraction from the reaction zone (**Figure 4**, ii). In addition, the downstream processing is substantially facilitated.

Numerous examples of extractor-type MRs have been applied in H_2-producing reactions such as methane steam reforming (MSR; Equation (1)) and water gas shift (WGS; Equation (2)) [15]:

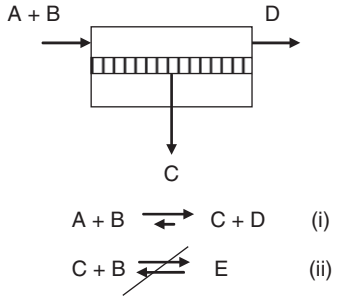

Figure 4 Selective removal of a product in a membrane extractor for a thermodynamically controlled reactions with consequent conversion (i) and/or selectivity increase (ii).

$$CH_4 + H_2O \Leftrightarrow CO + 3\,H_2 (\Delta H_{298K} = 206\ \text{kJ mol}^{-1}) \quad (1)$$

$$CO + H_2O \Leftrightarrow CO_2 + H_2 (\Delta H_{298K} = -41\ \text{kJ mol}^{-1}) \quad (2)$$

$$CH_4 + 2\,H_2O \Leftrightarrow CO_2 + 4\,H_2 (\Delta H_{298K} = 165\ \text{kJ mol}^{-1}) \quad (3)$$

According to Le Chatelier's principle, the H_2 removal by a Pd-based membrane (having a theoretically infinite selectivity for H_2) allows the shifting of these equilibrium-limited reactions and the consequent yield increase. The reforming operating temperatures can be reduced from the conventional 700–800 °C down to 500–550 °C, thanks to this equilibrium shift.

Tokyo Gas Co., Ltd. and Mitsubishi Heavy Industries have recently developed a membrane reformer system with nominal high-purity hydrogen (99.999% level) production capacity of 40 N m^3 h^{-1} from natural gas (typical composition used: 88.5% CH_4, 4.6% C_2H_6, 5.4% C_3H_8, and 1.5% C_4H_{10}) [16].

The reformer has 112 reactor tubes, each of which has two planar-type membrane modules composed of stainless steel support and palladium–rare earth metal-based alloy films of less than 20-μm thickness (**Figure 5**).

A Ni-based catalyst supported on alumina (Ni/Al_2O_3) is used in two forms: pellet form of 2–3-mm diameter in the primary catalyst bed, and a specially designed monolithic corrugated form placed close to the membrane modules to prevent mechanical damages to membrane surface as a result of friction between the catalyst and membrane.

The CO produced in an MSR reaction and separated from H_2 can be burned to CO_2 in the WGS reaction (Equation (2)). The role of the WGS is to increase H_2 yield (Equation (3)) and decrease the CO concentration, which is a poison for some catalysts used in downstream processing, as in ammonia synthesis or oil dehydrogenation. Moreover, the heat released in the exothermic WGS can be used in the endothermic MSR.

Many interesting advantages have been demonstrated in PV-assisted catalysis in which the membrane works as extractor. In PV reactor, both inorganic or organic and catalytic or inert membranes have been used.

PV is today considered as an advantageous alternative for the separation of liquid mixtures, which are difficult or impossible to separate by conventional distillation methods.

In PV-assisted catalysis, contrary to the reactive distillation, the separation efficiency is not limited by relative volatility of the species to be separated; moreover, in PV only a fraction of feed is forced to permeate through the membrane and undergoes the liquid-to vapor-phase change and, as a consequence, energy consumption is generally lower compared to distillation.

In the PV-assisted catalysis, the continuous extraction of one of the formed products is used to improve conversion of the reactants or to increase reaction selectivity.

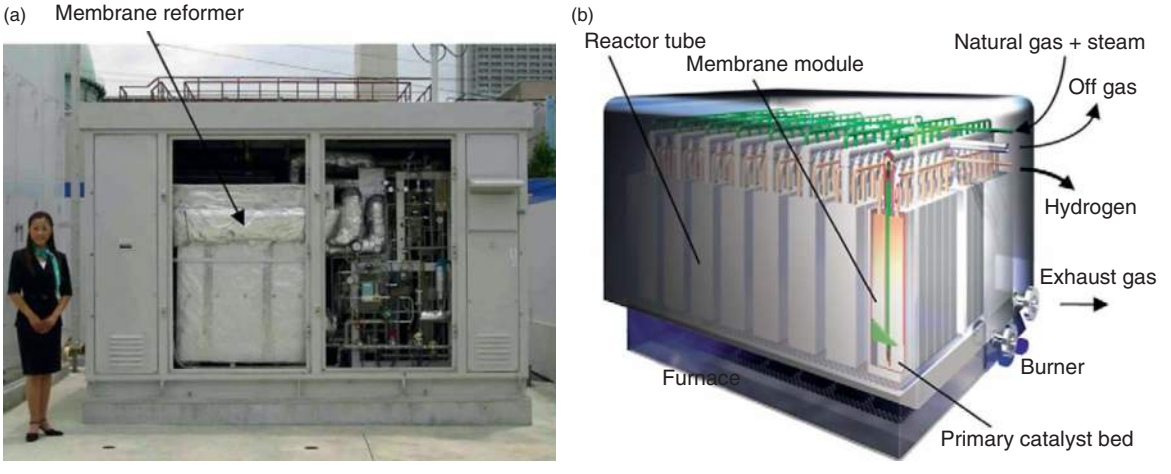

Figure 5 External view (a) and scheme of the membrane reformer (b) developed by Tokyo Gas Co., Ltd. and Mitsubishi Heavy Industries. Reproduced with permission from Shirasaki, Y., Tsuneki, T., Ota, Y., Yasuda, I., Tachibana, S., Nakajima, H. *Int. J. Hydrogen Energy* **2009**, *34*, 4482–4487.

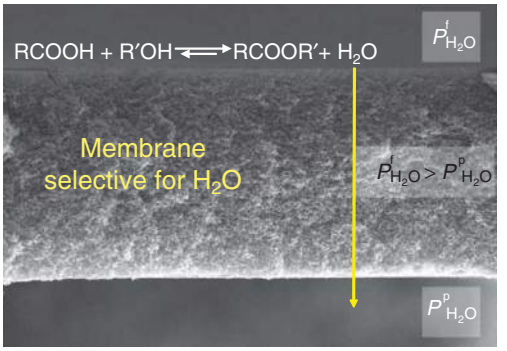

Figure 6 Schematization of water removal under the driving force of a partial pressure gradient in a pervaporation (PV)-assisted esterification process. $P^f_{H_2O}$ and $P^p_{H_2O}$ are respectively the water partial pressure in the feed and permeate side and $P^f_{H_2O} > P^p_{H_2O}$.

By far the most-studied reaction combined with PV, is the esterification, an equilibrium-limited reaction with a great deal of industrial relevance.

The conversion can exceed the equilibrium limit, by the selective removal through the membrane of water (**Figure 6**).

The esterification of acetic acid with ethanol (Equation (4)) has been investigated using zeolite membranes grown hydrothermally on the surface of a porous cylindrical alumina support (the membrane has not catalytic activity but only separation function; the catalyst used for the reaction is Amberlyst 15 cation-exchange resin dispersed in solution under stirring at 343 K) [17]:

$$CH_3CO_2H + CH_3CH_2OH <=> CH_3CO_2CH_2CH_3 + H_2O \quad (4)$$

The conversion exceeded the equilibrium limit by the selective removal through the membrane of water and reached to almost 100% within 8 h [17].

The same reaction has also been successfully carried out using a polymeric (inert) hydrophilic poly(vinyl alcohol) (PVA) membrane (Pervap 1000, Sulzer) and Amberlyst resins [18].

A catalytic membrane has been instead developed by coating the Pervap membrane with a thin superficial layer of catalyst particles in PVA solution [18].

In the first configuration (inert membrane), reaction and separation were conducted in two separate steps; in the second one (catalytic membrane), the two processes have been carried out in a single step, demonstrating an increase up to 60% in ethyl acetate conversion [18].

In addition to PVA, Nafion [19], and chitosan [20] membranes are also frequently used for the selective water extraction in PV-assisted, equilibrium-limited reactions.

The extraction of an instable intermediate product by a membrane represents a possible method to increase the selectivity of reactions in which the desired product is more reactive than the reagents and can give a secondary product. An interesting example is the direct synthesis of phenol by benzene oxidation. The oxidation reaction has low selectivity because phenol is more reactive toward oxidation than benzene, and a relevant formation of over-oxidized by-products is typically found (benzoquinone, hydroquinone, etc.).

An increase of the reaction selectivity has been obtained in a photocatalytic MR employing a microporous hydrophobic polypropylene membrane to remove phenol from the aqueous to the organic phase. The phenol, formed in water during the photocatalytic process by using TiO_2 as suspended catalyst, is selectively extracted to the organic phase constituted by the benzene, working as both reactant and extraction solvent [21].

The membrane can also work as a distributor in the MR by dosing of the reactants and increasing the selectivity of kinetically controlled reactions such as hydrogenation and selective oxidation, preventing hot spots and side reactions (**Figure 7**).

The controlled addition of the reactants by the membrane can reduce possible dangerous interactions (e.g., with flammable or explosive mixtures) by controlling the composition of the local reactants.

The membrane can be also used as upstream separation unit, selectively dosing (and distributing) one component from a mixture (**Figure 8**).

In numerous examples of distributor MRs, inorganic membranes are employed for reagents

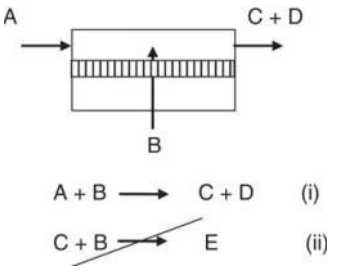

Figure 7 Dosing of a reactant in a membrane distributor for a kinetically controlled reaction (i) and avoiding of an undesired reaction (ii).

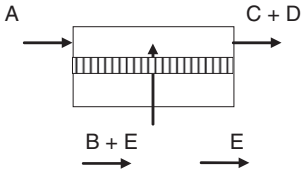

Figure 8 Integration of separation and distribution functions in a membrane distributor reactor.

dosing/separation, such perovskite membranes for O_2 [22] and Pd/α-Al_2O_3 [23], or zeolite membranes [24, 25] for H_2. These systems are used in high-temperature hydrogenation or oxidation reactions.

However, selective hydrogenation or selective oxidation reactions at mild conditions can also be carried out by means of solid electrolyte MRs working as distributors, and employing low-temperature proton conductors coated by catalytic layers on their surfaces or hot-pressed between two catalytic gas diffusion layers [26].

The most established low-temperature proton conductors are polymer electrolyte membranes (PEMs) made of ion-exchange perfluoropolymers such as Nafion (Du Pont), Aciplex (Asahi Chemical), Flemion (Asahi Glass), and Gore-Select (Gore and Associates), used both in polymer electrolyte membrane fuel cells (PEMFCs) for energy conversion and in MRs [27].

The polymers discussed above are also called long-side-chain (LSC) perfluoro-ionomers in order to distinguish them from the so-called short-side-chain (SSC) perfluoro-ionomers initially proposed in the 1980s by the Dow Chemical Company (under the trade name Dow Ionomer) and more recently by the Solvay Solexis (under the trade name Hyflon Ion) [28]. These SSC ionomers are characterized by shorter pendant groups carrying the ionic functionality, higher crystallinity, and higher glass transition (T_g) than LSC ionomers at given equivalent weight [29].

Considering the high cost of the perfluoropolymers and the partial decay of their proton conductivity at temperatures higher than 90–100 °C [30], a huge number of nonfluorinated polymer ionomers, such as the sulfonated poly(butadiene styrene) block copolymer, polystyrene, polyimides, poly(arylether sulfones), poly(arylether ketones), polyphosphazenes, and polybenzimidazole, have been investigated as starting material to prepare PEMs [31–33].

Moreover, organic–inorganic (hybrid) proton exchange membranes have also been realized in order to improve the membrane performance by dispersion/linking of inorganic additives, such as SiO_2, TiO_2, ZrO_2, zirconium phosphate, and heteropolyacids, in the polymeric matrix [34].

To understand the proton mechanism in PEMs, it is necessary to keep in mind that protons cannot exist in the bare state (except in particular situation such as plasmas and synchrotron rings) [35], but they strongly interact with electronic density of the surrounding environment. The proton localization within the valence electron density of electronegative species (e.g., nitrogen and oxygen) and self-organization due to solvent interactions, play a key role in the proton diffusivity.

In hydrated solid proton conductors, the transport can occur by a vehicle or by a Grotthus-type mechanism [36, 37].

In the first one the protons are linked to a vehicle, in the specific case, water (e.g., as H_3O^+ and $H_5O_2^+$ ions), and they diffuse together under a gradient of electrochemical potential.

In the Grotthus mechanism, the vehicle molecules are stationary and the transport involves the structural intermolecular reorganization of hydrogen bonds with the concomitant reorientation of the vehicle molecules (protons hopping) as illustrated schematically in **Figure 9**.

At low water content, the rate of bond breaking and forming is significantly reduced. Moreover, the interaction of the water molecules with the acid functional groups of the polymer polarizes the protons near the anionic sites. This distribution and, as a consequence, the inhomogeneous electrostatic potential distribution depend on the chemical interaction of the protons with the anions (effect of the pK_a), the local dielectric constant of the water and the spatial separation of the acid groups. The decreasing of both the acidity and the dielectric constant as well as the increasing of the separation distance between the polar groups favor the restriction of proton transport through

$$H_2OH^+\text{---}OH_2\text{---}OH_2 \Leftrightarrow H_2O\text{---}H^+OH_2\text{---}OH_2 \Leftrightarrow H_2O\text{---}H_2O\text{---}H^+OH_2$$

Figure 9 Schematization of the proton transport by Grotthus mechanism.

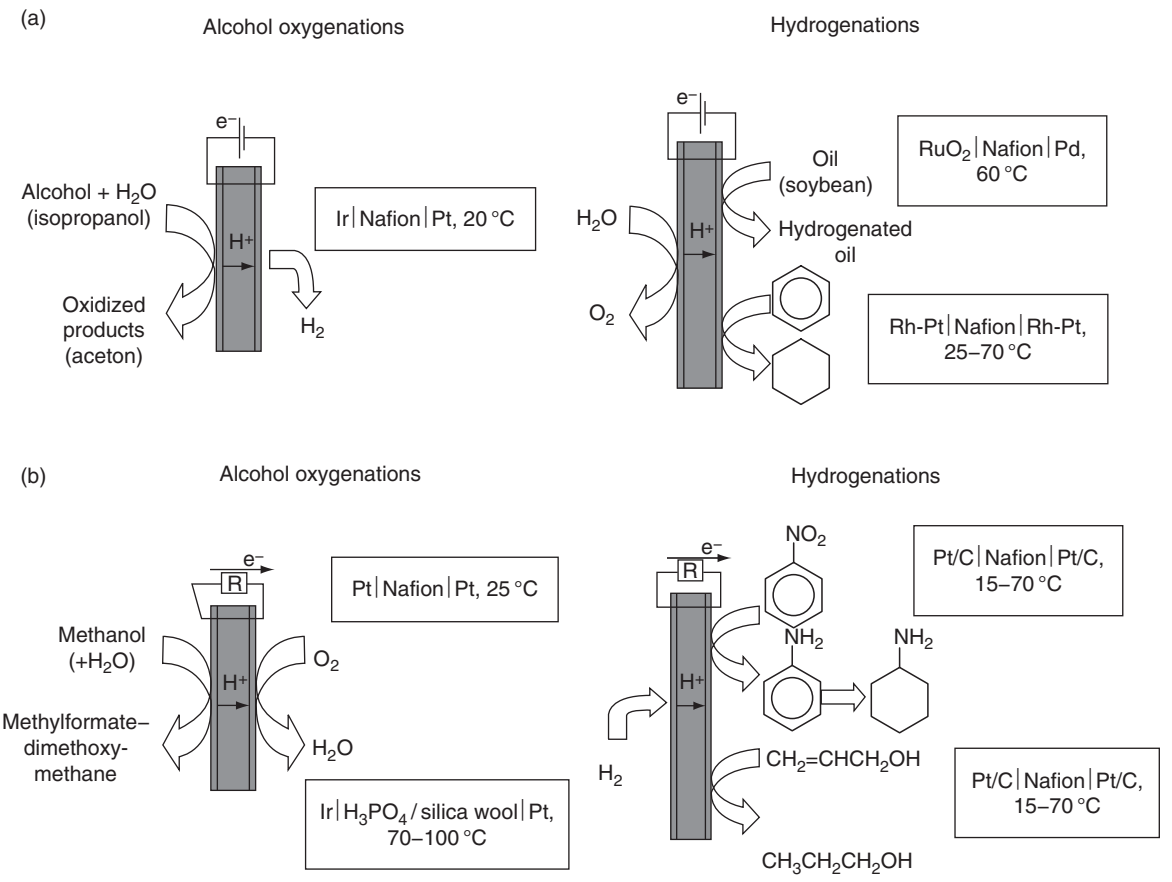

Figure 10 Proton exchange membrane (PEM) reactors operating in electrolysis (a) and electrochemical modus (b). Reproduced with permission from Sundmacher, K., Rihko-Struckmann, L. K., Galvita, V. *Catal. Today* **2005**, *104*, 185–199.

the hydrophilic domains and reduce the transport coefficient [37].

PEM reactors operating in electrolysis configurations (**Figure 10(a)**; external electric energy input is used as driving force to transport charged species through the solid electrolyte) have been used for the oxidation of various aliphatic alcohols with oxygen produced by *in situ* water electrolysis [38].

The electrolysis of water has also been used in hydrogenation reactions [39, 40].

PEM reactor can also work in the electrochemical configuration (**Figure 10(b)**; electric power output from the electrochemical process) [26].

In both configurations, a PEM is used to separate the anode compartment, where the oxidation reaction occurs, from the cathode compartments, where the reduction reaction takes place. The PEM selectively transports the protons from the anode to the cathode, avoiding the direct contact of the anodic with the cathodic reagents.

The membrane can also define the reaction volume facilitating the contact between the reactants. An interfacial membrane contactor can provide a contacting zone for two immiscible phases excluding polluting solvents and reducing the environmental impact of the process (**Figure 11**).

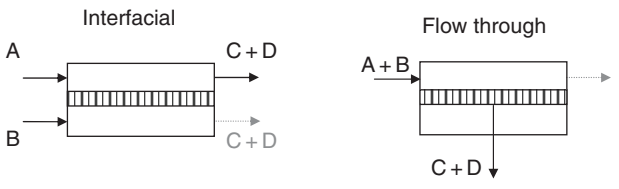

Figure 11 Membrane reactors in which the membrane works as an interfacial or a flow-through contactor.

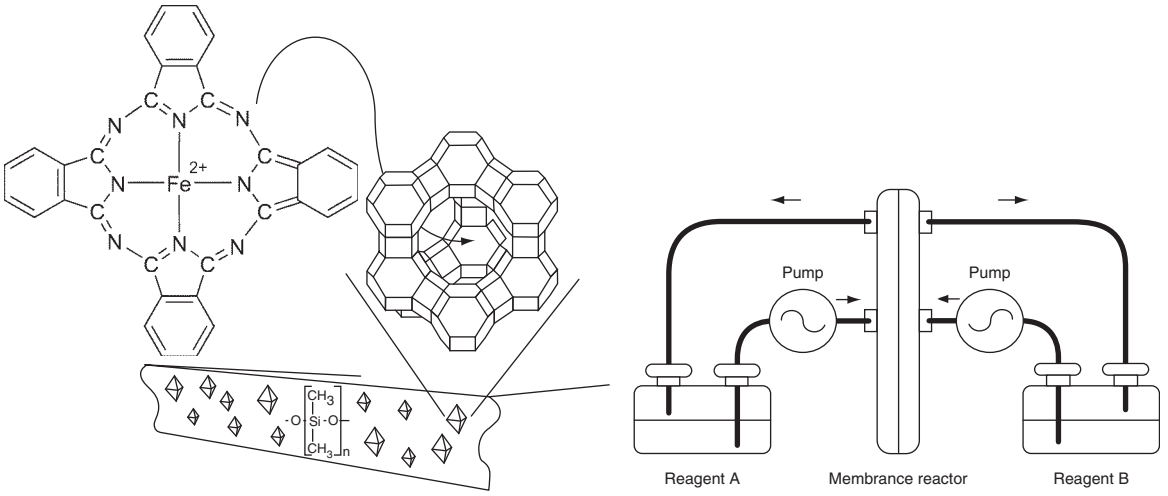

Figure 12 Representation of the polydimethylsiloxane (PDMS) membrane occluding the iron phthalocyanine included in the supercages of a zeoliteY and scheme of the catalytic membrane contactor. Reproduced with permission from Vankelecom, I. F. J., Parton, R. F., Casselman, M. J. A., Uytterhoeven, J. B., Jacobset, P. A. *J. Catal.* **1996**, *163*, 457–464.

Iron phthalocyanine encaged in zeolite Y (FePcY, this type of catalyst is also indicated as zeozyme) has been occluded in a polydimethylsiloxane (PDMS) membrane and successfully used in a catalytic membrane contactor for cyclohexane oxidation by tertiary-butyl hydroperoxide at room temperature (**Figure 12**) [41].

By separating the two immiscible reactant phases, the membrane eliminates the need for a common solvent and actively controls the concentration of the reactants near the catalytic sites.

An efficient process using a catalytic membrane contactor for oxidation of dissolved compounds in water has been developed in order to reduce the chemical oxygen demand and the total organic carbon in industrial wastewaters [42a–d].

Oxygen has been employed as a green oxidant in the CMR using porous ceramic membranes containing Pt nanoparticles in the top layer operating in an interfacial gas–liquid contactor configuration [42b].

Wastewater is pumped along the catalytic layer side, while air or oxygen flows along the other side of the contactor. The gas–liquid interface is then located within the membrane wall by means of a transmembrane differential pressure used to compensate the gas–liquid capillary pressure (**Figure 13**).

It has been demonstrated that this configuration favors a better accessibility of the reactants to the

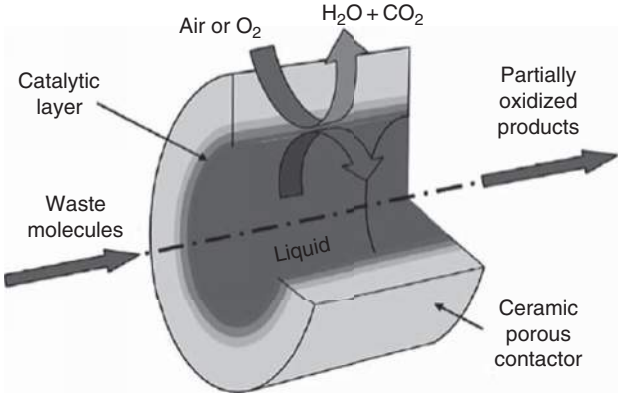

Figure 13 Operative principle of the interfacial membrane contactor used for the oxidation of dissolved compounds in wastewater. Reproduced with permission from Iojoiu, E. E., Landrivon, E., Raeder, H., Torp, E. G., Miachon, S., Dalmon, J.-A. *Catal. Today* **2006**, *118*, 246–252.

catalyst, which improves the conversion rates [42b]. The catalytic activity of the catalyst was up to 4 times higher than in the conventional perfectly mixed stirred tank reactor [42c–d].

This process can operate at much lower temperatures and pressures than the conventional wet air oxidation or incineration and it offers much smaller volume requirements than biological treatment plants. This catalytic membrane contactor has been successfully upscaled from lab scale to pilot unit [42].

A three-phase catalytic MR (3PCMR) has been used in the selective oxidation of propane to oxygenates (*n*-propanol, isopropanol, propionic aldehyde, and acetone), taken as reaction model for the conversion of light alkanes into higher value-added products under mild conditions [43].

Polymeric membranes, both in flat and tubular configuration, made of an amorphous polyarylenetherketone indicated as PEEK-WC [44], have been functionalized by deposition of Nafion (used as co-catalyst) from a isopropanol solution (Nafion loading 1 mg cm^{-2}).

The catalytic membranes have been tested in the 3PCMR using an aqueous liquid phase containing the Fe^{2+}–H_2O_2 Fenton system, and a gas phase constituted of a propane/helium mixture, operating in the temperature range 70–120 °C and with a pressure difference between the gas and the liquid phase of 3 kPa. The catalytic test has been performed in batch mode with separate recirculation of the two phases; the oxygenated product formed was trapped in the gas phase (**Figure 14**).

Nafion/PEEK-WC catalytic membranes denoted a good performance in the selective oxidation of propane (from 0.2 to 0.50 μmol g^{-1}_{Nafion}), with a higher selectivity to the primary products (*n*-propanol and isopropanol) operating with the catalytic hollow-fiber membranes. This configuration allows one to achieve a higher productivity value per unit of reactor volume than those obtained with a flat one (0.36–2.91 $\mu mol_{oxyg}\, cm^{-3}\, s^{-1}$) [43].

PVA functionalized with sulfosuccinic acid and Nafion membranes has been used as a solid acid catalyst in the transesterification of soybean oil, carried out in a contactor-type CMR [45]. The concentration profiles obtained with the catalysts in the form of pellets exhibited an initial induction period, which disappears when the reaction is performed in the MR keeping in contact the methanol with the soybean oil without accumulation of the glycerol product in the membrane, also reducing the inhibition effect of the product.

When the membrane is catalytically active, as it is made of a catalytic material (many metal membranes have catalytic activity) or the catalyst is immobilized in the membrane, the control of the contact-time

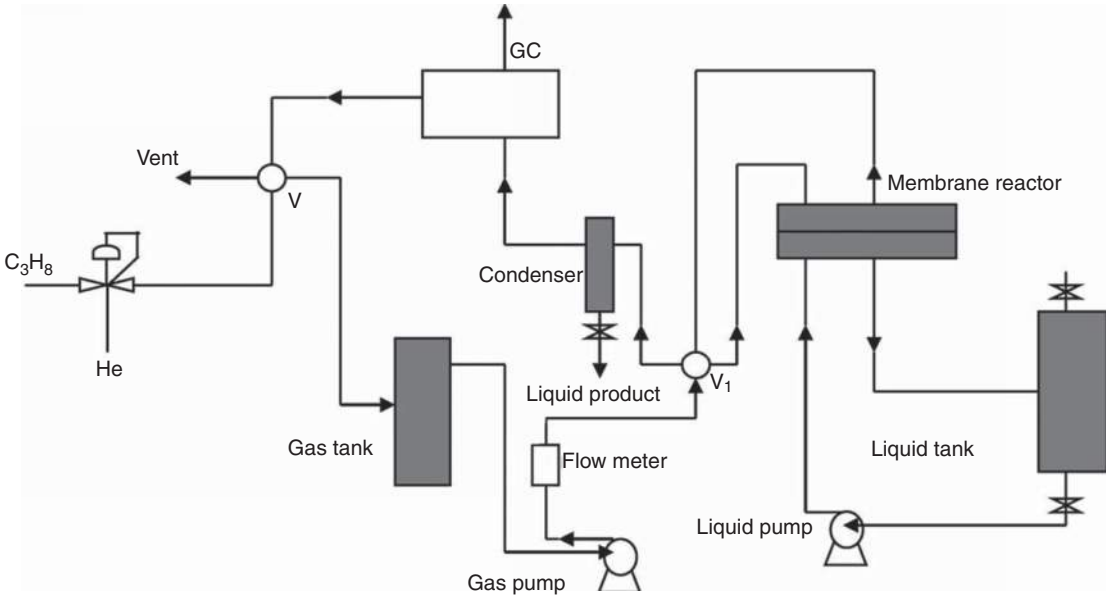

Figure 14 The three-phase catalytic membrane reactor used for the selective oxidation of propane to oxygenates. GC, gas chromatography. Reproduced with permission from Espro, C., Arena, F., Tasselli, F., Regina, A., Drioli, E., Parmaliana, A. *Catal. Today* **2006**, *118*, 253–258.

reactant-catalyst, by the control of the convective flux in the flow-through CMR, can improve the reaction selectivity [46]. This represents a fundamental advantage of MRs in comparison with traditional heterogeneous reactors.

In classical heterogeneous catalysis (catalyst absorbed or linked in porous polymeric or inorganic solids), the conversion and selectivity of the catalytic process are in fact often limited by the diffusion of the reagents to the catalytic sites and the product from them.

On the contrary, the convective flux in a catalytic MR is easier to control and to adjust to the reaction kinetic, by the control of the driving force and/or the membrane structure and properties.

In a membrane separation process, the transport rate of a component can be activated by various driving forces such as gradients in concentration, pressure, temperature, or electrical potential. In numerous membrane processes, more than one driving force is involved (pressure and concentration in gas separation, concentration and electrical potential in electrodialysis, etc.); however, all these parameters can be included in one thermodynamic function, the electrochemical potential η (**Figure 15(a)**). For a single component i transported, the flux $\mathcal{J}_i$ can be described by a semi-empirical equation:

$$\mathcal{J}_i = -L \cdot \frac{\mathrm{d}\eta_i}{\mathrm{d}x} \tag{5}$$

where $\frac{\mathrm{d}\eta_i}{\mathrm{d}x}$ is the gradient in electrochemical potential of the component i and L is a phenomenological coefficient.

In multi-component systems, driving forces and fluxes are interdependent, giving rise to more complex interactions [47].

Of course, the transport depends on the membrane structure and, for a dense membrane in which the transport occurs by a solution–diffusion mechanism, on the membrane material as well.

The contact time (τ) between the catalytic membrane and the reactant can be estimated by

$$\tau = \frac{\delta}{\mathcal{J}_i} \tag{6}$$

where δ is the membrane thickness.

Moreover, in a catalytic membrane, especially if polymeric, the catalyst entrapment in the functional microstructured environment constituted by the membrane can have a positive influence on the transition states and reaction kinetics by electronic and weak interactions, as well as by spatial restriction and transport dynamics (**Figure 15(b)**).

Porous polymer membranes based on polyacrylic acid (PAA) have been functionalized with Pd nanoparticles prepared from $Pd(OAc)_2$ with reducing agents such as $NaBH_4$ or $LiAlH_4$ [48]. The effect of the membrane porosity, catalyst loading, and flow rate of the reactant mixture, on the catalytic behavior of these membranes, has been investigated in the gas-phase partial hydrogenation of propyne to propylene (Equation (7)) carried out at 298 K:

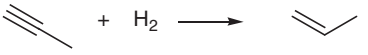

(7)

The range of flow rate investigated was varied from 20 to 80 ml min^{-1} corresponding from about 4 to 1 second of residence time of the reactants in the catalytic membrane. Increasing the flow rate (decreasing the residence time) resulted in a decreased conversion and an increased selectivity (**Figure 16**).

In addition, the membrane porosity influenced the catalytic performance: the conversion decreased with increasing porosity because, with equal amount of catalytic particles but larger pore diameters, the catalyst is more widely distributed. On the contrary, a

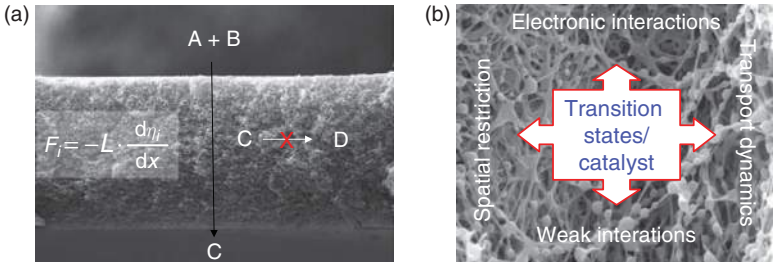

Figure 15 Examples of specific effects of the catalyst entrapment in the functional microstructured environment offered by the membrane: (a) increase of the reaction selectivity by control of the convective flux in a flow-through catalytic membrane reactor; (b) influence on the transition states and reaction kinetics by electronic and weak interactions, as well as by spatial restriction and transport dynamics.

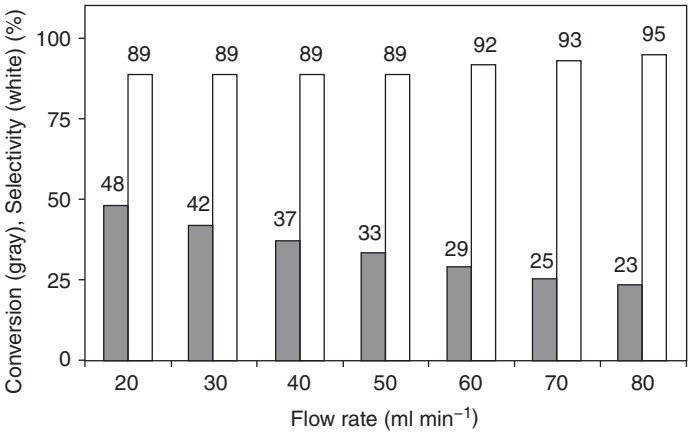

Figure 16 Conversion of propyne and selectivity to propene vs. flow rate of the gas phase (membrane porosity: 58%; Pd loading: 2 mg; $T = 298$ K; H_2 pressure 1 bar). Reproduced with permission from Groschel, L., Haidar, R., Beyer, A., Colfen, H., Frank, B., Schomacker, R. *Ind. Eng. Chem. Res.* **2005**, *44*, 9064–9070.

better distribution of the catalyst is expected in a membrane with lower porosity and a faster conversion occurred operating at the same flow rate (20 ml min^{-1}) and catalyst loading (2.0 mg) [48].

The selectivity to propene decreases with the increasing of the conversion because of the competitive conversion of propene to propane (Equation (8)):

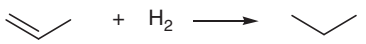

(8)

However, the plot of the selectivity versus conversion for different Pd loadings (from 2.0 to 5.5 mg) and porosities (10% or 20%) falls on the same trajectory (within the experimental error), indicating that there is no change in the kinetics of the reactions due to mass-transfer effects caused by the different membrane structures or catalyst contents. The conversion/selectivity depends on the residence time in the catalytic membrane; this parameter can be more easily modulated than in a fixed-bed reactor (FBR) employing an egg-shell catalyst specially developed for partial hydrogenation reactions [48].

PAA membranes loaded with Pd nanoparticles have also been used for the selective hydrogenation in liquid phase of various unsaturated substrates in a flow-through catalytic MR operating at 323 K and 40-bar hydrogen pressure [49].

Compared to experiments carried out with supported catalysts (Pd/C and Pd/Al_2O_3) in an FBR or a slurry reactor (SR), the selectivity for the desired products can be increased up to 50% in the MR for the geraniol conversion to citronellol (**Figure 17**), versus 20% and 40%, respectively, in the FBR and SR (100% conversion for all reactors), avoiding mass-transfer limitations on reaction kinetics. However, the reaction in the SR proceeds much faster than in the MR and FBR [49].

In some specific cases, the mass transport can be coupled, at least in principle, with the heat transport through a metal membrane for reactions occurring at the two opposite sides of the membrane. For example, the heat dissipated in an exothermic reaction (like hydrogenation) can be used in an endothermic reaction (dehydrogenation reactions), taking place at the opposite side of a membrane (palladium membrane selective for hydrogen) [50, 51].

The membrane can also be used for the retention of the catalyst in the reactor by using a membrane with appropriate molecular weight cutoff (MWCO). However, in the selection of the membrane, it is necessary to consider that the MWCO depends on the solvent and the solution composition (and polarity) can greatly vary during the reaction [8].

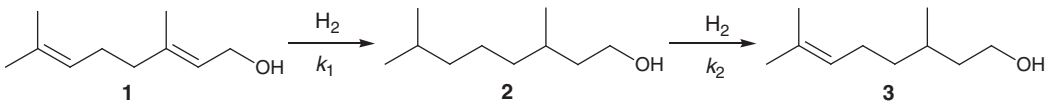

Figure 17 Reaction scheme of hydrogenation of geraniol (**1**), to citronellol (**2**) and tetrahydrogeraniol (**3**). $k_1 \approx k_2$.

In some cases, the catalyst retention can be optimized by enlargement of the catalyst in the form of dendrimers, hyperbranched polymers, and catalyst bound to a soluble polymer [52].

Recently, the coupling of solvent-resistant nanofiltration (SRNF) with homogeneous reactions has opened up new possibilities [53].

SRNF, compared to traditional separation techniques (distillation, chromatography, and extraction), allows one to reduce energy cost and waste production in the recovery of homogeneous catalysts.

The process is carried out in continuous or in batchwise filtration–reaction cycles. The second operative mode is usually employed if the operative conditions (solvent, temperature, pressure, etc.) are not adequate for the membrane.

The catalyst can be also immobilized inside or on the membrane surface, generally allowing an easy catalyst recovery, reuse, and regenerations in successive catalytic runs. Moreover, when a catalyst is heterogenized within or on the surface of a membrane, the membrane composition (characteristics of the membrane material: hydrophobic or hydrophilic, presence of chemical groups with acid or basic properties, etc.) and the membrane structure (dense or porous, symmetric or asymmetric) can positively influence the catalyst performance, not only by the selective sorption and diffusion of reagents and/or products, but also by influencing the catalyst activity through electronic (electron-donating and electron-withdrawing groups) and conformational effects (stabilization of the transition states). These effects are similar to those occurring in biological membranes.

3.05.4 Organic MRs

In the previous section, numerous examples of MRs operating with catalytic or inert membranes, made of inorganic (ceramics or metals) or organic materials (polymers), have been reported.

Inorganic membranes are widely used in the field of high-temperature reactions because of their high chemical and thermal stability.

Organic membranes are usually employed when the reaction temperatures are lower, such as in the field of fine chemicals or when biocatalysts are present.

The use of organic membranes in MRs elicits much interest because a much wider choice of polymeric materials is available as compared with inorganic membranes; the cost of the polymer membranes is generally lower and the preparation protocols allow a better reproducibility (**Table 1**). The relatively low operating temperatures, typical of the polymeric membranes, are also associated with less stringent demands for materials used in the reactor construction [8].

Despite polymeric membranes being generally less resistant to high temperatures and aggressive chemicals compared to inorganic ones, polymeric materials that could resist under rather harsh conditions are currently available, such as PDMS, polyvinylidene fluoride (PVDF), Hyflon, Nafion, and polyimides [54].

However, the development of polymer membranes having advanced or novel functions is a key issue to be addressed in order to better exploit the potentialities of polymer membranes in MRs. Important approaches addressing this aim have been presented by Ulbricht in a recent review [55] (**Figure 18**):

1. development of polymer membranes in the form of composite or mixed-matrix membranes in which an organic and an inorganic phase coexist in order to have synergistic effect on transport properties, mechanic and thermal stability, as well as to introduce new functionalities;
2. advanced functionalization by coating of functional layer or grafting of functional groups on the membrane surface or inside the pores;

Table 1 Organic vs. inorganic membranes

Advantages	*Limitations*
Lower capital costs	Lower thermal stability
Wider choice of materials for different applications	Lower resistance to harsh environments
Higher permeability at lower temperatures	Lower inertness to microbial degradation
Higher packing density (membrane surface per unit volume) in modules	Lower selectivity
Better developed technology to manufacture polymer membranes and modules	More difficult cleaning after fouling
Easier membrane to module sealing	Lower resistance to high pressure drops

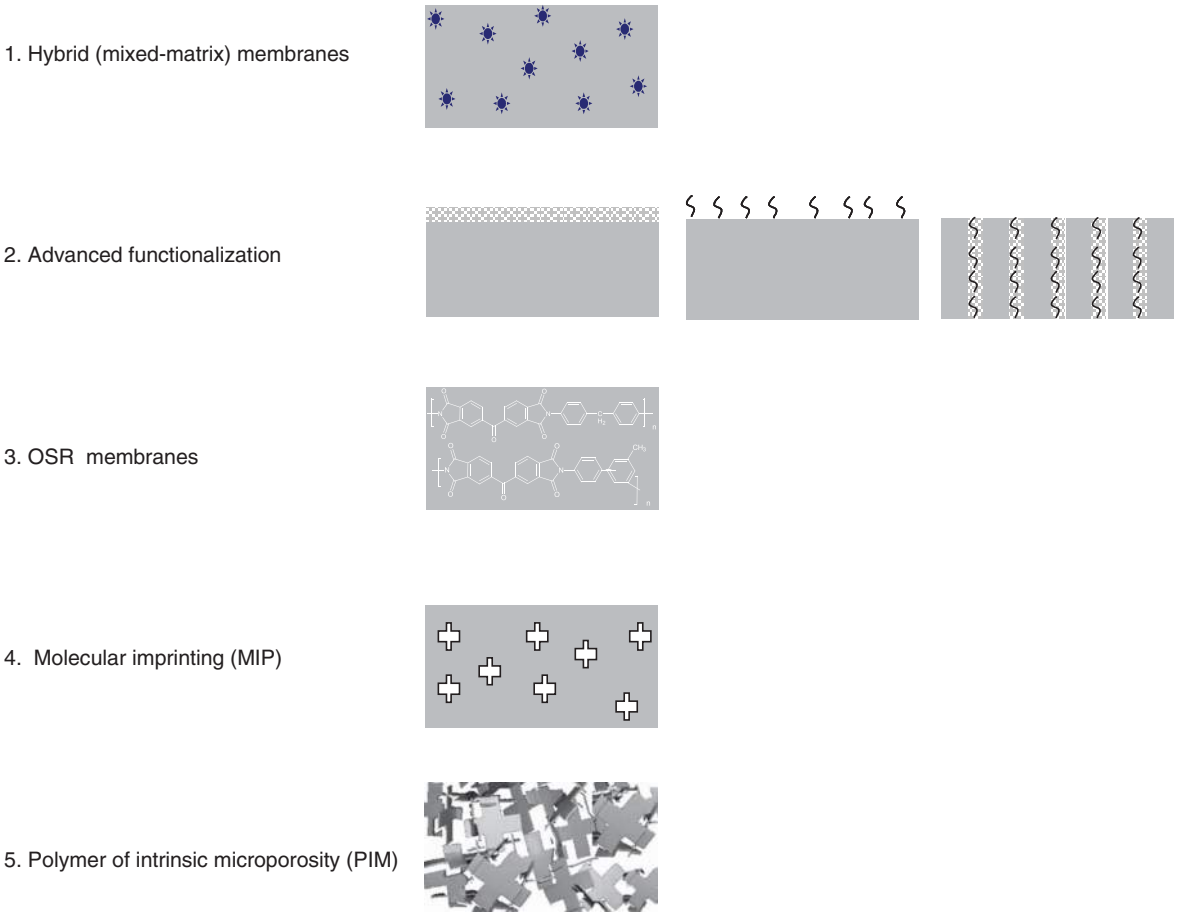

Figure 18 Some relevant breakthroughs in polymer membranes.

3. development of organic solvent-resistant (OSR) membranes (in particular, NF membranes – SRNF);
4. use of templates for realizing molecular imprinted (MIP) membranes; and
5. synthesis of novel polymers with controlled architecture such as polymers of intrinsic microporosity (PIMs) [56].

Of course, the strategies devoted to obtain advanced membrane materials have to be combined with novel processing technologies of polymers in order to obtain tailored structures controlling the density, size, size distribution, shape, and alignment of membrane pores, on a nanometric scale.

The basic objective is to obtain ordered structures similar to track-etched polymer and anodically oxidized alumina membranes, and tailored surface properties, such as biological membranes, but prepared by simple, reliable, reproducible, and economical methods.

Micro-fabrication, self-assembling, and phase separation micro-molding are tending toward this direction; however, more work is necessary to obtain systems commercially competitive and available on a large scale [57–60].

3.05.5 Immobilization of Catalysts in Membranes

The main requirements that must be considered to produce an ideal catalyst are: low costs, high selectivity, high stability under reaction conditions, nontoxicity and the possibility to recover and reuse it reducing the cost and environmental impact of the catalytic process [61, 62].

In this perspective, the heterogenization of catalysts has interesting implications because it allows the reuse of the same catalyst several times. Among the

different heterogenization methods, the entrapping of a catalyst in/on a membrane offers new possibilities for the design of new catalytic processes.

In addition to the membrane selection criteria ((1) stability (mechanical, thermal, and chemical); (2) rejection; (3) permeability and selectivity; (4) fouling tendency; and (5) cost (capital and operating)) that have to be considered in a membrane-assisted reactor, additional technical complexities, such as catalyst stability during the immobilization procedure; influence of the catalyst particles on the membrane properties (mechanical, transport, etc.); effect of the catalyst loading, dimensions and distribution, on the catalytic efficiency; and leaching of the catalyst in liquid phase, are present in the design and realization of catalytic membranes by the immobilization of catalyst in/on the membrane.

However, catalytic membranes deserve special advantages that in many cases justify these additional efforts.

In the design of a catalytic membrane, major issues in the polymer selection are the mechanical, thermal, and chemical stability under reaction conditions (**Figure 19**).

It is fundamental to realize a stable catalyst immobilization in order to avoid its leaching out from the membrane. Different immobilization strategies can be used in order to achieve this goal: covalent bindings, electrostatic interactions, and weak interactions (van der Waals or hydrogen bonds) of the catalyst with the membrane or catalyst encapsulation.

A good affinity for the catalyst is desirable in order to avoid catalyst leaching and to have a good adhesion between the polymer and the catalyst, with an optimal dispersion of the latter.

The affinity between a compound and the membrane polymer can be often anticipated by the calculation of the affinity parameters [54, 63]. These parameters reflect the ability to form hydrogen bond, polar and van der Waals interactions in condensed phase.

The polymer/catalyst affinity can be also improved by an appropriate chemical functionalization of one or both components.

Ideally, the solvent used for the reaction needs to be a nonsolvent for the catalyst, and the membrane should be free from excessive swelling.

It is also possible in some cases to improve the catalyst retention in the membrane by the catalyst enlargement as dendrimers, hyperbranched polymers, and catalyst bound to a soluble polymer [52].

Mass transfer of the reagents to the catalytic sites, and of the product away from them, should be fast enough in order to not limit the reaction but, at the same time, the contact-time catalyst/reagent should also be appropriate.

For a porous membrane, the choice of the polymer material is of less importance for transport properties in comparison with a dense membrane,

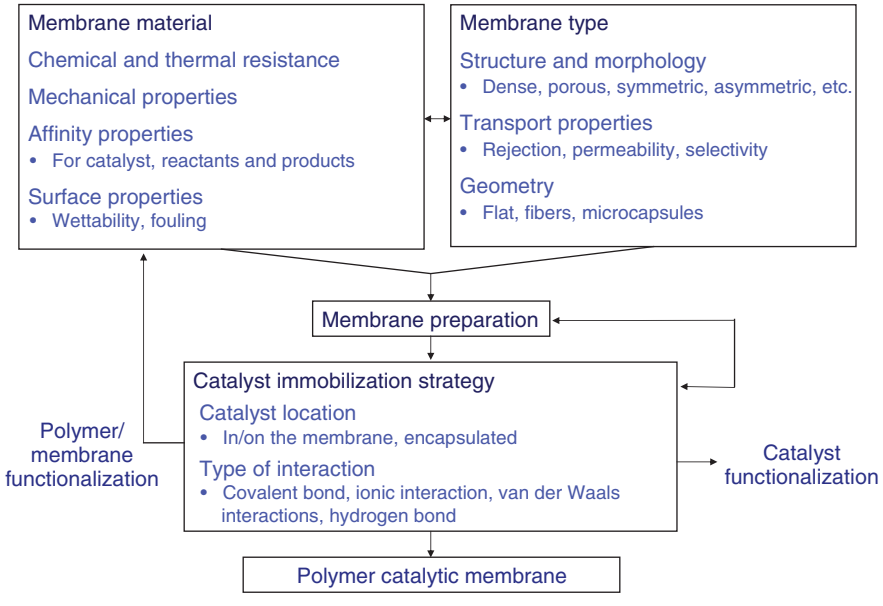

Figure 19 Basic flow sheet of polymer catalytic membranes design.

because permeation does not take place through the polymer matrix, but through the membrane pores [8]. However, the membrane material is relevant for the membrane stability and surface properties, such as wettability and fouling tendency.

The membrane preparation conditions depend on the membrane material and desired structure and morphology. In the case of a polymer catalytic membrane, the incorporation of the catalyst complicates the process because the catalyst should be firmly entrapped in the membrane and the catalyst structure and activity have to be preserved during the membrane preparation procedure.

Moreover, the properties (including transport properties) of a catalytic membrane are usually different from those of a pure polymer membrane prepared in the same conditions.

Different techniques for polymeric membrane preparation are currently available and can also be opportunely employed to prepare catalytic membranes; for example, phase inversion, coating, sintering, stretching and track etching [64].

The most versatile is the phase-inversion technique, in which a polymer is transformed, in a controlled mode, from a liquid to a solid state (the membrane).

In some cases, the catalyst is entrapped in/on the membrane already formed, by covalent bonds, electrostatic interaction, and absorption by weak interactions or physical entrapment. Alternatively, the catalyst immobilization can be carried out at the same time of the membrane formation, for example, by dispersing the catalyst in the polymer casting solution and successive phase inversion.

An interesting example of catalyst immobilization is the heterogenization of the decatungstate ($W_{10}O_{32}^{4-}$), a polyoxometalalte (POM, polyanionic metal oxide cluster of early transition metals) [65], having interesting properties for application in oxidation catalysis for fine chemistry and wastewater treatments (**Figure 20**).

Decatungstate exhibits particularly interesting properties for the photocatalytic detoxification of wastewater since its absorption spectrum ($\lambda_{max} = 324$ nm) partially overlaps the ultraviolet (UV) solar emission spectrum opening the potential route for an environmentally benign solar-photo-assisted application [66].

However, decatungstate has some relevant limitations: it is characterized by low quantum yields, small surface area, poor selectivity, and limited stability at pH higher than 2.5 [67].

Membrane technology can offer interesting possibilities in order to overcome these limitations by the multi-turnover recycling associated to heterogeneous supports, the selectivity tuning as a function of the substrate affinity toward the membrane phase, and the effect of the polymeric micro-environment on catalyst stability and activity.

In this respect, the design of alternative heterogeneous photo-oxygenation systems able to employ visible light, oxygen, mild temperatures, and solvent

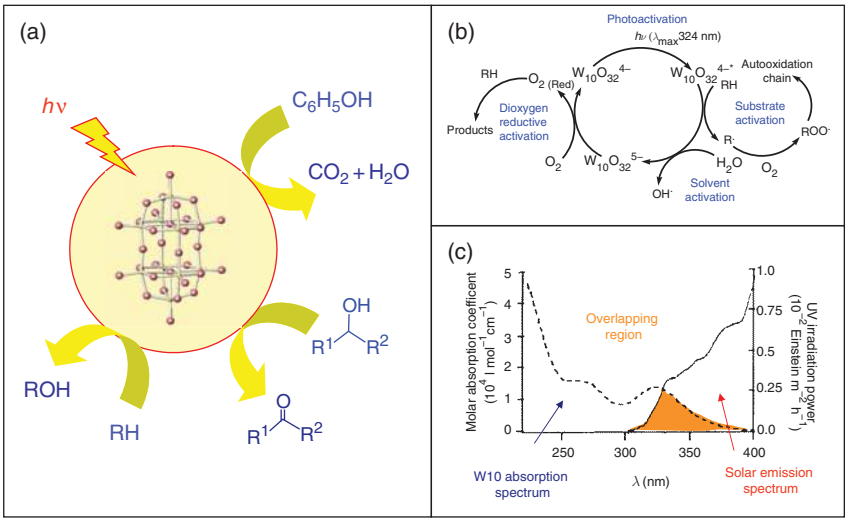

Figure 20 Fundamentals aspects of decatungstate catalytic activity: applications in selective oxidations in photo-assisted synthetic procedures as well as in environmental remediation (a); composite activation mechanism in the photocatalytic oxidation cycle (b); partial overlapping of decatungstate (W_{10}) absorption spectrum and solar emission spectrum (c).

with a low environmental impact (water or neat reaction) has been investigated by the immobilization of the decatungstate in polymer membranes [68, 69].

The successful heterogenization has been guaranteed by a proper choice of both, the catalyst and the polymer material.

Considering the interest toward the photo-oxidation reactions of organic substrates, principally in aqueous phase, two hydrophobic polymer materials have been selected for membrane preparations: the partially fluorinated PVDF and the perfluorinated polymer Hyflon AD60X. Both polymers are transparent in the region of interest of the catalyst, characterized by a high chemical, thermal, and UV stability. Moreover, the use of a fluorinated media to carry out aerobic oxidation reactions is particularly useful because of the well-known high solubility of oxygen in fluorinated environment.

In order to improve the catalyst/polymer interactions, and to avoid catalyst leaching out from the membrane, liphophilic (insoluble in water) derivatives of the decatungstate have been employed: the tetrabutilammonium salt ($(n\text{-}C_4H_9N)_4W_{10}O_{32}$ indicated as $TBAW_{10}$) and a fluorous-tagged decatungstate ($([CF_3(CF_2)_7(CH_2)_3]_3CH_3N)_4W_{10}O_{32}$ indicated as $R_fN_4W_{10}$) (**Figures 21(a)** and **21(b)**).

The first one has been heterogenized in PVDF membranes (**Figure 21(c)**) and used for the aerobic photo-oxidation of phenol in water [70]. This reaction has been chosen because phenol and its derivatives constituted one of the main organic pollutants to be removed from wastewater, and the development of new effective and environmental benign methods for phenol degradation is an important research area [71].

The second one has been heterogenized in perfluorinated Hyflon membranes (**Figure 21(d)**) and used in the solvent-free oxygenation of benzylic hydrocarbons [72].

PVDF polymeric matrix can interact with liphophilic salt of decatungstate by van der Waals interactions. The insaturation of electron donor–electron acceptor

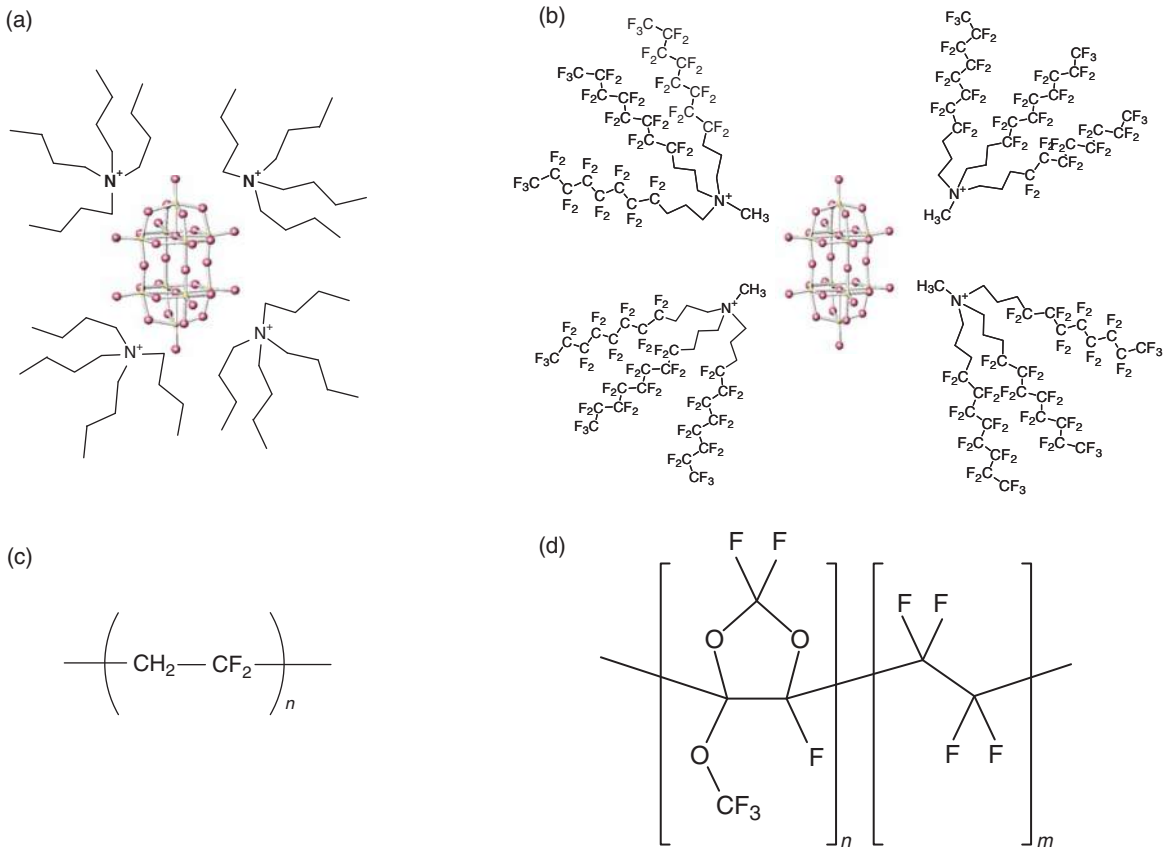

Figure 21 Decatungstate in the form of the tetrabutilammonium salt ($(n\text{-}C_4H_9N)_4W_{10}O_{32}$) (a) and fluorous-tagged decatungstate, ($([CF_3(CF_2)_7(CH_2)_3]_3CH_3N)_4W_{10}O_{32}$) (b); the PVDF (c) and the Hyflon (d; $n = 0.85\, m = 0.15$ in Hyflon AD60X) polymers used as membrane materials.

interactions between the catalyst and fluorinated polymer is also possible [73].

The $TBAW_{10}$ heterogenization can be carried out by solubilization of the catalyst into the polymer solution using a common solvent (dimethylacetamide) to prepare nano-hybrid membrane (PVDF-W_{10}) using the phase-inversion technique. The catalytic membranes obtained are characterized by a homogeneous distribution of the catalyst in membrane, as evident from scanning electron micrographs (SEMs) in backscattered electron (BSE) mode (**Figure 22(a)**) and linear X-ray (RX) maps on the cross sections.

Solid-state characterization techniques (Fourier transform infrared (FT-IR) analysis; UV–Vis spectroscopy in diffuse reflectance) confirmed that the catalyst structure and spectroscopic properties have been preserved within the membranes.

The dependence of the phenol degradation rate by the catalyst loading in membrane and the transmembrane pressure has been investigated, allowing one to identify the catalytic membrane with catalyst loading 25.0 wt.% and operating at 1 bar (contact time 22 s), as the more efficient system [70].

The rates of phenol degradation catalyzed by homogeneous $Na_4W_{10}O_{32}$ and heterogeneous PVDF-W_{10} (25.0 wt.%) have been compared in similar operative conditions. The amount of phenol degraded in the homogeneous and heterogeneous reaction was similar. In both cases, after 5 h of reaction, about 50% of the phenol is converted (starting from 150 ml of a 0.002-M phenol solution). However, in the case of the homogeneous reaction, several persistent intermediates were observed, and only the 34.0% of mineralization to CO_2 and water has been obtained. On the contrary, during photodegradation performed by PVDF catalytic membrane, the phenol converted is also mineralized to CO_2 and H_2O, as confirmed by a similar (49%) percentage of total organic carbon loss.

The high catalytic activity of the PVDF-W_{10} membranes, in comparison to the homogeneous catalyst, can be ascribed to the selective absorption of the organic substrate from water on the hydrophobic PVDF polymer membrane that increases the effective phenol concentration around the catalytic sites, allowing an intensive contact in the flow-through CMR.

Moreover, the polymeric hydrophobic environment protects the decatungstate from the conversion to an isomer absorbing only light under 280 nm,

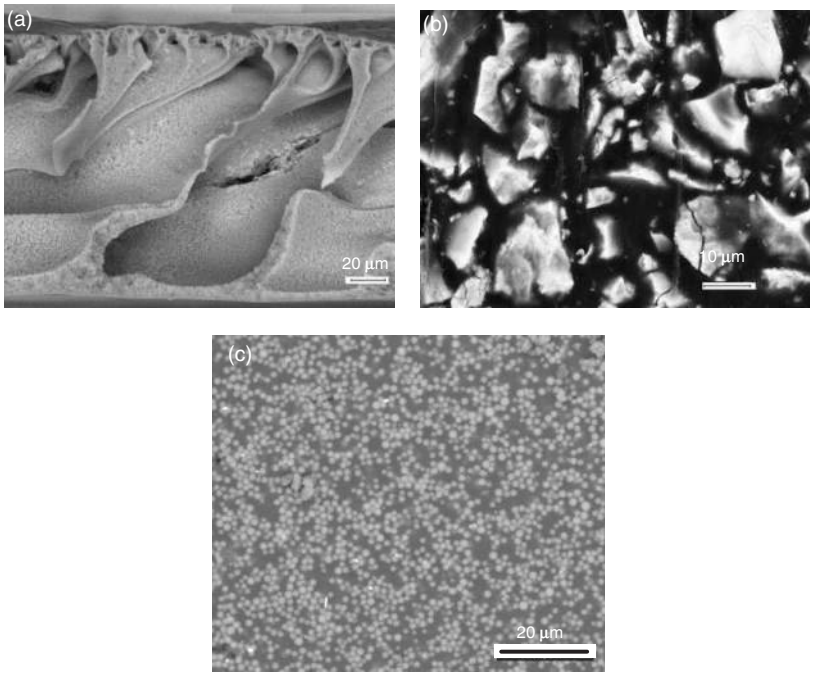

Figure 22 Scanning electron microscope (SEM) images in backscattered electron (BSE) of membranes containing decatungstate: cross section of a porous polyvinylidene fluoride (PVDF) membrane containing $TBAW_{10}$ (a); down surface of an Hyflon membrane immobilizing the $TBAW_{10}$ catalyst (b); down surface of an Hyflon membrane immobilizing the $R_fN_4W_{10}$ catalyst (c).

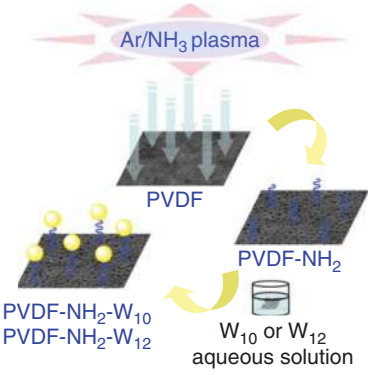

Figure 23 Heterogenization of catalysts on the surface of plasma-functionalized PVDF membranes.

which instead occurs in homogeneous solution at pH > 2.5 [70].

Polymeric catalytic membranes have also been prepared by immobilizing photocatalytic POMs, sodium deacatungstate ($Na_4W_{10}O_{32}$; W_{10}) [74, 75] and phosphotungstic acid ($H_3PW_{12}O_{40}$; W_{12}) [76], on the surface of PVDF membranes modified by Ar/NH_3 plasma discharges (PVDF-NH_2) (**Figure 23**).

Polar chemical groups (principally NH_2, together with OH, CN, NH, and CO) have been grafted by a NH_3 plasma discharge on the upper surface of PVDF membranes, pretreated with Ar in order to control hydrophobic recovery [77].

The groups grafted on the surface are able to bind the W_{10} or W_{12} catalysts dissolved in aqueous solution, forming charge transfer complexes.

Surface-diagnostic techniques, such as X-ray photoelectron spectroscopy (XPS; **Table 2**), contact angle (CA) measurements, and RX maps, have been used to attest the surface modification.

The XPS N% value can be taken as a measure of the efficiency of the grafting of N-groups after the NH_3 plasma treatments.

The N content is lowered from 9.4 for PVDF-NH_2, to 6.2 for the PVDF-NH_2-W_{10} and 5.1 for PVDF-NH_2-W_{12} surfaces, since W_{10} or W_{12} is added to the surface, and W%, O% (and P% for the second one) XPS value increase.

The catalytic membranes obtained (PVDF-NH_2-W_{10} and PVDF-NH_2-W_{10}) showed superior performances (higher reaction rates) compared to the corresponding homogeneous catalysts in the aerobic phenol degradation reaction carried out in an un-buffered solution [74–76].

Table 2 XPS analysis carried out on the up surface of the PVDF pure membrane, of the membrane treated with Ar/NH_3 plasma (PVDF-NH_2) and the catalytic membranes containing W_{10} or W_{12} catalysts (respectively PVDF-NH_2-W_{10} and PVDF-NH_2-W_{12})

Membrane	*C%*	*O%*	*W4f%*	*P2p%*	*F%*	*N%*
PVDF	54.2	1.9	-	-	43.8	/
PVDF-NH_2	57.6	4.7	-	-	28.0	9.4
PVDF-NH_2-W_{10}	58.9	19.1	3.3	-	12.1	6.2
PVDF-NH_2-W_{12}	53.1	18.3	3.5	0.4	19.3	5.1

Data from Lopez, L. C., Buonomenna, M. G., Fontananova, E., *et al*. *Adv. Funct. Mater.* **2006**, *16*, 1417–1424.
Lopez, L. C., Buonomenna, M. G., Fontananova, E., Drioli, E., Favia, P., d' Agostino, R. *Plasma Process. Polym.* **2007**, *4*, 326–333.
Fontananova, E., Donato, L., Drioli, E., Lopez, L., Favia, P., d'Agostino, R. *Chem. Mater.* **2006**, *18*, 1561–1568

The $TBAW_{10}$ has also been heteorogenized in the Hyflon matrix; however, the low affinity between the catalyst and the polymeric matrix (no common solvents between the two systems) induced the formation of irregular catalyst aggregates, not well dispersed in the polymeric matrix, which tend to precipitate toward the down surface (**Figure 22(b)**).

On the contrary, in the case of the fluorous-tagged decatungstate, SEM images of the membrane surface (**Figure 22(b)**) and cross section highlight a homogeneous distribution of the catalyst domains which appear as spherical particles with uniform size (**Figure 22(c)**).

The cationic amphiphiles R_fN^+ groups induce the self-assembly of the surfactant-encapsulated clusters [78, 79] (R_fN^+ groups capped on $W_{10}O_{32}^{4-}$) which, during membrane formation process, gives supramolecular assemblies of the catalyst, stabilized by the polymeric matrix.

The dimensions of these clusters and, as a consequence, the surface area and catalytic activity of the decatungstate, can be modulated acting on the membrane preparation conditions. Increasing the membrane formation time by an increase of the membrane thickness (increase of the casting solution initial thickness) the mean dimensions of the $R_fN_4W_{10}$ clusters became larger because they have more time for aggregate before the solidification of the membrane (**Figure 24**).

In addition, the increase of the catalyst loading contributes to increase in the mean dimension of the clusters.

The catalytic Hyflon-based membranes have been tested in batch solvent-free oxygenation of benzylic C–H bonds of the ethylbenzene (**Figure 25**) at 25 °C

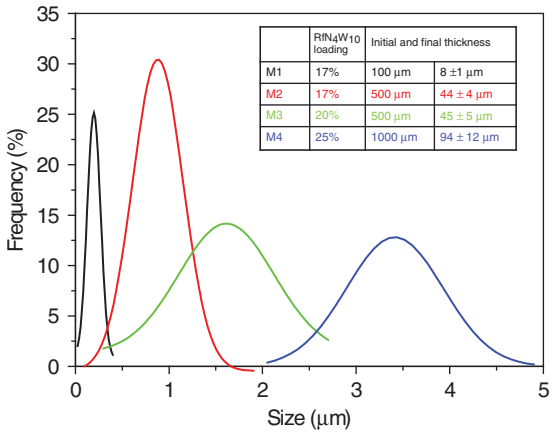

Figure 24 $R_fN_4W_{10}$ cluster dimension distribution in the Hyflon membranes for different catalyst loading and membrane thickness.

under O_2 atmosphere (membrane cut in small pieces and immersed in ethylbenzene).

The key observation was provided by an increase of the selectivity toward the alcohol (product of interest) and turnover number (TON) when the catalyst is heterogenized in Hyflon membrane (**Table 3**, entries 4–7) in comparison with homogeneous catalysts (entries 1 and 2) or the catalyst heterogenized in PVDF (entry 3). Moreover, the use of the fluorous-tagged decatungstate well dispersed in Hyflon membrane (entries 5 and 6) improves the TON in comparison with the $TBAW_{10}$ only physically entrapped in Hyflon (entry 4).

Only with the thicker Hyflon membrane (entry 7) the TON was lower because in the operative condition used the reagent can only diffuse inside the membrane and mass transfer limitations reduce the process efficiency.

The catalytic membranes with smaller catalyst cluster are characterized by a higher activity in the photo-oxygenation of ethylbenzene (entries 5–7).

Better performance is expected using these membranes in a CMR operating with flow through.

3.05.6 Industrial Applications of MRs and the As-Yet Existing Limitations

Despite the clear advantages of the MRs and the numerous lab-scale studies, only few large-scale plants are running yet, principally in biotechnological applications, employing polymeric membranes.

Membrane bioreactors (MBRs) are already recognized as the best available technology for wastewater

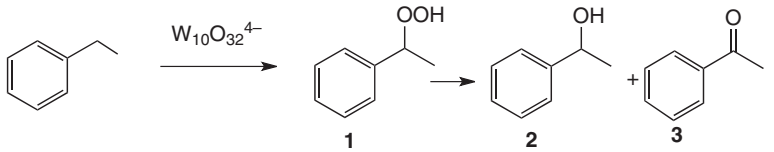

Figure 25 Photo-oxygenation of ethylbenzene. The products are hydroperoxide (**1**), alcohol (**2**), and acetophenone (**3**).

Table 3 Photocatalytic oxygenation of ethylbenzene by homogeneous decatungstate or heterogeneous catalytic membranes made of PVDF or Hyflon

	Catalyst	*Solvent*	*Cat. (μmol)*	*Products (mM) (% 1:2:3)*	*TON*
1	[a]TBA W_{10}	CH_3CN	0.20	64 (36:32:32)	351
2	[a]R_fN_4 W_{10}	HFP	0.18	95 (56:23:21)	581
3	PVDF-TBA W_{10}	Neat	0.32	23 (45:23:32)	78
4	Hy- TBA W_{10}	Neat	0.20	81 (14:66:20)	443
5	Hy- R_fN_4 W_{10} (thickness 7 μm)	Neat	0.03	94 (16:46:38)	3447
6	Hy- R_fN_4 W_{10} (thickness 50 μm)	Neat	0.18	196 (25:41:34)	1198
7	Hy- R_fN_4 W_{10} (thickness 94 μm)	Neat	0.70	270 (15:48:37)	424

[a] Pseudo-neat conditions by addition of 20 ml of solvent (HFP = hesafluoroisopropanol).
1: peroxide, 2: alcohol, 3: keton. Reaction conditions: ethylbenzene, 1.1 ml; pO_2, 1 atm; $\lambda < 345$ nm; T = 25 °C; 4 h irradiation time. Turnover number calculated as: products (mol)/catalyst (mol).
Data from Carraro, M., Gardan, M., Scorrano, G., Drioli, E., Fontananova, E., Bonchio, M. *Chem. Commun.* **2006**, *43*, 4533–4535.

treatments and the capacity of installed plants is increasing continuously, even if fouling problems still limit their performance and their costs need to be reduced [80].

A MBR (i.e. membrane reactor employing biological catalysts) is composed of two parts: the biological reactor in which the reaction occurs (active sludge containing purifying bacteria) and the membrane module for the physical separation of the different compounds.

MBRs can be classified into two main groups according to their configurations. The first group, commonly known as the recirculated or external MBRs, involves the recirculation of the solution through a membrane module that is outside the bioreactor. Both inner-skin and outer-skin membranes can be used in this application.

The second configuration is the integrated or submerged MBRs, involving outer-skin membranes that are internal to the bioreactor.

Over 1000 MBRs are currently in operation around the world with approximately 66% in Japan, and the remaining part largely in Europe and North America. Of these installations, about 55% use submerged membranes, while the rest have external membrane modules [81].

One of the largest MBR units in the world was recently built in Porto Marghera (Venice, Italy) in order to extract remaining pollutants in tertiary water prior to disposal into the Venetian Lagoon [82].

The UF unit, containing submerged PVDF hollow-fiber membranes (ZeeWeed® by Zenon), is designed to treat 1600 $m^3 h^{-1}$ of wastewater with a chemical oxygen demand (COD) per hour of 445 kg and the suspended matter of the treated water is <1 mg l^{-1} [82].

There are two interconnected UF lines, each line contains 4 units composed by 9 ZeeWeed® modules and the total membrane area is 100 000 m^2.

Large-scale applications can also be found with enzymatic membrane reactors (EMRs) in which enzymes are immobilized in/on the membrane, or retained by a membrane in the reactor.

The recent trend toward environmentally friendly technologies makes these biocatalytic MRs particularly attractive because of their ability to operate at moderate temperature and pressure, and to reduce the formation of by-products [83].

Enzymes, compared to artificial catalysts, generally permit greater stereospecificity and higher reaction rates under milder reaction conditions.

Degussa has installed several EMRs (hydrophilic UF hollow fibers used for enzyme retention) for pilot, small, and large-scale acylase process, used for the enzymatic resolution of *N*-acetyl-D,L-amino acids (**Figure 26**) [84].

The nominal capacity of the Degussa large-scale plant, dedicated to producing enantiomerically pure L-amino acids via EMR technology using the acylase process, is several hundreds of tons per year.

Another EMR (Sepracor reactor) has been used at industrial level for the production of (−)MPGM (3-(4-methoxyphenyl)glycidic acid methyl ester), an important intermediate for the production of diltiazem hydrochloride, a coronary vasodilator [85].

The reactor utilizes lipase from *Serratia marcescens* immobilized in hollow-fiber UF hydrophilic membranes for the enantioselective hydrolysis of (+)MPGM to (2S,3R)-(+)-3-(4-methoxyphenyl)-glycidic acid and methanol, starting from a (+/−)MPGM racemic mixture [86]. The pilot

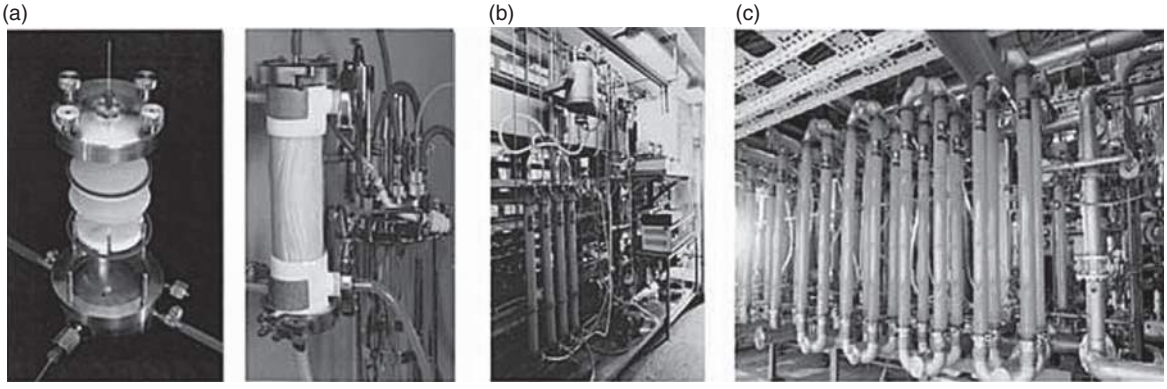

Figure 26 Enzyme membrane reactors at different scales: (a) lab scale, (b) pilot scale, and (c) production scale. Reproduced from Wöltinger, J., Karau, A., Leuchtenberger, W., Drauz, K. *Adv. Biochem. Eng./Biotechnol.* **2005**, *92*, 289–316.

plant Sepracor reactor annually produces about 40 kg (–)MPGM per square meter of membrane.

From a general analyses of the MR technology, it is evident that the limitations of these technology are principally related to the manufacturing costs of the membranes and membrane modules, and their limited durability over long times.

In order to better exploiting the potentialities of this technology, it is important to develop advanced (catalytic) membranes and modules with acceptable costs, stable in a wide range of solvents and conditions, and showing high and reproducible performance in the long term.

The design of an efficient MR needs to be derived from an application-based multidisciplinary approach, and high-throughput screening methods and mathematical modeling are fundamental tools for the analyses and better understanding and optimization of these promising multifunctional reactors.

References

[1] Charpentier, J.-C. *Ind. Eng. Chem. Res.* **2007**, *46*, 3465.
[2] Stankiewicz, A. *Chem Eng. Process* **2003**, *42*, 137–144.
[3] Raluy, G., Serra, L., Uche, J. *Energy* **2006**, *31*, 2025–2036.
[4] Frenkel, V. *Int. Desalin. Water Reuse Q* **2008**, *17*, 47–50.
[5] Jiao, A., Cassano, E., Drioli, J. *Food Eng.* **2004**, *63*, 303–324.
[6] Drioli, E., Criscuoli, A., Curcio, E. *Membrane Contactors: Fundamentals, Applications and Potentialities, Membrane Science and Technology Series, 11*; Elsevier: Amsterdam, 2006.
[7] Sirkar, K. K., Shanbhag, P. V., Kovvali, A. S. *Ind. Eng. Chem. Res.* **1999**, *38*, 3715–3737.
[8] Vankelecom, I. F. J. *Chem. Rev.* **2002**, *102*, 3779.
[9] Brunetti, A., Caravella, A., Barbieri, G., Drioli, E. *Chem. Eng. Sci.* **2009**, *64*, 3448–3454.
[10] Drioli, E., Fontananova, E. Membrane Reactors. In *Ullmann's Encyclopedia of Industrial Chemistry*; Wiley-VCH Verlag GmbH & Co.: KGaA, 2010.
[11] Caro, J. *Chin. J. Catal.* **2008**, *29*(11), 1169.
[12] Drioli, E., Fontananova, E. Membrane Reactors. In *Advanced Membrane Technology and Applications;* Li, N. N., Fane, A. G., Ho, W. S. W., Matsuura, T., Eds.; Wiley: Hoboken, NJ, 2008; Chapter 27, pp 703–718.
[13] Sanchez-Marcano, J. G., Tsotsis, T. T. Membrane Reactors. In *Ullmann's Encyclopedia of Industrial Chemistry*; Wiley-VCH, Ed.; Wiley-VCH: Weinheim, 2005; pp 223–242.
[14] Drioli, E., Giorno, L. *Biocatalytic Membrane Reactors: Application in Biotechnology and the Pharmaceutical Industry*; Taylor and Francis: Padstow, 1999.
[15] Heinzel, A., Vogel, B., Hubner, P. *J. Power Sources* **2002**, *105*, 202–207.
[16] Shirasaki, Y., Tsuneki, T., Ota, Y., Yasuda, I., Tachibana, S., Nakajima, H. *Int. J. Hydrogen Energy* **2009**, *34*, 4482–4487.
[17] Tanaka, K., Yoshikawa, R., Ying, C., Kita, H., Okamoto, K. *Catal. Today* **2001**, *67*, 121.
[18] Rivas, M. E., Fierro, J. L. G., Guil-López, R., Peña, M. A., La Parola, V., Goldwasser, M. R. *Catal. Today* **2008**, *133–135*, 809–814.
[19] Parulekar, S. J. *Ind. Eng. Chem. Res.* **2007**, *46*, 8490.
[20] de Souza, K. C. *Catal. Today* **2008**, *133*, 809.
[21] Molinari, R., Caruso, A., Poerio, T. *Catal. Today* **2009**, *144*, 81–86.
[22] Wang, H. H., Cong, Y., Yang, W. *Catal. Lett.* **2002**, *84*, 101.
[23] Yonghua, Z., Hongqi, Y., Schomäcker, R. *Chin. J. Catal.* **2007**, *28*(8), 715–719.
[24] Chommeloux, B., Cimaomo, S., Jolimaitre, E., Uzio, D., Magnoux, P. Sanchez, J. *Microporous Mesoporous Mater.* **2008**, *109*, 28–37.
[25] Cruz-Lopez, A., Guilhaume, N., Miachon, S., Dalmon, J.-A. *Catal. Today* **2005**, *107–108*, 949–956.
[26] Sundmacher, K., Rihko-Struckmann, L. K., Galvita, V. *Catal. Today* **2005**, *104*, 185–199.
[27] Kreuer, K. D. *J. Membr. Sci.* **2001**, *185*, 29–39.
[28] Arcella, V., Troglia, C., Ghielmi, A. *Ind. Eng. Chem. Res.* **2005**, *44*, 7645–7651.
[29] Ghielmi, A., Vaccarono, P., Troglia, C., Arcella, V. *J. Power Sources* **2005**, *145*, 108–115.
[30] Fontananova, E., Trotta, F., Jansen, J. C., Drioli, E. *J. Membr. Sci.* **2010**, *348*, 326–336.
[31] Souzy, R., Ameduri, B. *Prog. Polym. Sci.* **2005**, *30*, 644–687.
[32] Kerres, J. A. *J. Membr. Sci.* **2001**, *185*, 3.
[33] Hickner, M. A., Ghassemi, H., Kim, Y. S., Einsla, B. R., McGrath, J. E. *Chem. Rev.* **2004**, *104*, 4587–4612.
[34] Alberti, G., Casciola, M., Capitani, D., *et al. Electrochim. Acta* **2007**, *52*, 8125–8132.
[35] Colomban, P., Ed. *Chemistry of Solid State Materials. 2. Proton Conductors: Solids, Membranes and Gels – Materials and Devices*; Cambridge University Press: Cambridge, 1992.
[36] Kreuer, K.-D. *Chem. Mater.* **1996**, *8*, 610–641.
[37] Kreuer, K.-D. *Solid State Ionics* **2000**, *136–137*, 149–160.
[38] Simond, O., Comninellis, C. *Electrochem. Acta* **1997**, *42*, 2013.
[39] Itoh, N., Xu, W. C., Hara, S., Sakaki, K. *Catal. Today* **2000**, *56*, 307.
[40] An, W., Hong, J., Pintauro, P., Warner, K., Neff, W. *J. Am. Oil Chem. Soc.* **1999**, *76*, 215.
[41] Vankelecom, I. F. J., Parton, R. F., Casselman, M. J. A., Uytterhoeven, J. B., Jacobset, P. A. *J. Catal.* **1996**, *163*, 457–464.
[42a] Iojoiu, E. E., Landrivon, E., Raeder, H., Torp, E. G., Miachon, S., Dalmon, J.-A. *Catal. Today* **2006**, *118*, 246–252.
[42b] Iojoiu, E. E., Miachon, S., Landrivon, E., Walmsley, J. C., Ræder, H., Dalmon, J.-A. *Appl. Catal. B* **2007**, *69*, 196.
[42c] Miachon, S., Perez, V., Crehan, G. *et al. Catal. Today* **2003**, *82*, 75.
[42d] Iojoiu, E. E., Walmsley, J. C., Ræder, H., Miachon, S., Dalmon, J.-A. *Catal. Today* **2005**, *104*, 329.
[43] Espro, C., Arena, F., Tasselli, F., Regina, A., Drioli, E., Parmaliana, A. *Catal. Today* **2006**, *118*, 253–258.
[44] Fontananova, E., Basile, A., Cassano, A., Drioli, E. *J. Inclus. Phenom. Macrocycl. Chem.* **2003**, *47*, 33–37.
[45] Guerreiro, L., Castanheiro, J. E., Fonseca, I. M., Martin-Aranda, R. M., Ramos, A., Vital, J. *Catal. Today* **2006**, *118*, 166–171.
[46] Westermann, T., Melin, T. *Chem. Eng. Process.* **2009**, *48*, 17–28.
[47] Drioli, E., Curcio, E., Fontananova, E. Mass Transfer Operation – Membrane Separations. In *Chemical Engineering. Encyclopedia of Life Support Systems (EOLSS), Developed under the Auspices of the UNESCO*;

Bridgwater, J., Molzahn, M., Pohorecki, R., Eds.; Eolss Publishers: Oxford (http://www.eolss.net).
[48] Groschel, L., Haidar, R., Beyer, A., Colfen, H., Frank, B., Schomacker, R. *Ind. Eng. Chem. Res.* **2005**, *44*, 9064–9070.
[49] Schmidt, A., Haidar, R., Schomacker, R. *Catal. Today* **2005**, *104*, 305–312.
[50] Gryaznov, V. *Catal. Today* **1999**, *51*, 391.
[51] Itoh, N., Godvind, R. *Ind. Eng. Chem. Res.* **1989**, *28*, 1554.
[52] Dioos, B. M. L., Vankelecom, I. F. J., Jacobs, P. A. *Adv. Synth. Catal.* **2006**, *348*, 1413–1446.
[53] De Smet, K., Aerts, S., Ceulemans, E., Vankelecom, I. F. J., Jacobs, P. A. *Chem. Commun.* **2001**, *7*, 597–598.
[54] Van Krevelen, D. W. *Properties of Polymers*, 3rd edn.; Elsevier: Amsterdam, 1990.
[55] Ulbricht, M. *Polymer* **2006**, *47*, 2217–2262.
[56] Park, H. B., Jung, C. H., Lee, Y. M., *et al. Science* **2007**, *318*, 254–258.
[57] Hashemi, M., Achenbach, S., Klymyshyn, D., Moazed, B., Lee, J. *Microsyst. Technol.* 2009, doi: 10.1007/s00542-009-1002-3 (online first; published online 31 December).
[58] Ma, M., Hill, R. M. *Curr. Opin. Colloid Interface Sci.* **2006**, *11*, 193–202.
[59] Vogelaar, L., Lammertink, R. G. H., Wessling, M. *Langmuir* **2006**, *22*, 3125–3130.
[60] Clapper, J. D., Sievens-Figueroa, L., Guymon, C. A. *Chem. Mater.* **2008**, *20*, 768–781.
[61] Gladysz, J. A. *Pure Appl. Chem.* **2001**, *73*, 1319–1324.
[62] Hill, C. L. *Nature* **1999**, *401*, 436–437.
[63] Barton, A. F. M. *Handbook of Polymer–Liquid Interaction Parameters and Solubility Parameters*; CRC Press: Boca Raton, FL, 1990.
[64] Strathmann, H., Giorno, L., Drioli, E. *An Introduction to Membrane Science and Technology*; CNR: Roma, 2006 (ISBN 88-8080-063-9).
[65] Kozhevnikov, I. V. *Chem. Rev.* **1998**, *98*, 171.
[66] Texier, I., Giannotti, C., Malato, S., Richter, C., Delaire, J. *Catal. Today* **1999**, *54*, 297.
[67] Mylonas, A., Papaconstantinou, E. *Polyhedron* **1996**, *15*, 3211–3217.
[68] Bonchio, M., Carraro, M., Scorrano, G., Fontananova, E., Drioli, E. *Adv. Synth. Catal.* **2003**, *345*, 1119–1126.
[69] Bonchio, M., Carraro, M., Gardan, M., Scorrano, G., Drioli, E., Fontananova, E. *Top. Catal.* **2006**, *40*, 133–140.
[70] Drioli, E., Fontananova, E., Bonchio, M., Carraro, M., Gardan, M., Scorrano, G. *Chin. J. Catal.* **2008**, *29*(11), 1152.
[71] Kormali, P., Dimoticali, D., Tsipi, D., Hiskia, A., Papaconstantinou, E. *Appl. Catal. B – Environ.* **2004**, *48*, 175.
[72] Carraro, M., Gardan, M., Scorrano, G., Drioli, E., Fontananova, E., Bonchio, M. *Chem. Commun.* **2006**, *43*, 4533–4535.
[73] Burdeniuc, J., Sanford, M., Crabtree, R. H. *J. Fluorine Chem.* **1998**, *91*, 49.
[74] Lopez, L. C., Buonomenna, M. G., Fontananova, E., *et al. Adv. Funct. Mater.* **2006**, *16*, 1417–1424.
[75] Lopez, L. C., Buonomenna, M. G., Fontananova, E., Drioli, E., Favia, P., d' Agostino, R. *Plasma Process. Polym.* **2007**, *4*, 326–333.
[76] Fontananova, E., Donato, L., Drioli, E., Lopez, L., Favia, P., d'Agostino, R. *Chem. Mater.* **2006**, *18*, 1561–1568.
[77] Favia, P., Sardella, P., Gristina, E., d'Agostino, R. *Surf. Coat. Technol.* **2003**, *169–170*, 707.
[78] Bu, W., Li, H., Sun, H., Yin, S., Wu, L. *J. Am. Chem. Soc.* **2005**, *127*, 8016.
[79] Li, H., Sun, H., Qi, W., Xu, M., Wu, L. *Angew. Chem. Int. Ed.* **2007**, *46*, 1300.
[80] Le-Clech, P., Chen, V., Fane, A. G. *J. Membr. Sci.* **2006**, *284*, 17–53.
[81] Van de Roest, H. F., Lawrence, D. P., Van Bentem, A. G. N. *Membrane Bioreactors for Municipal Wastewater Treatment. STOWA Report*. IWA Publishing: London, 2002.
[82] Vigiano, C. *Chim. Ind.* **2007**, *5*, 90–94.
[83] Giorno, L., Drioli, E. *Trends Biotechnol.* **2000**, *18*, 339.
[84] Wöltinger, J., Karau, A., Leuchtenberger, W., Drauz, K. *Adv. Biochem. Eng./Biotechnol.* **2005**, *92*, 289–316.
[85] Kemmere, M. F., Keurentjes, J. T. F. In *Industrial Membrane Reactors, in Membrane Technology in the Chemical Industry;* Nunes, S. P., Peinemann, K. V., Eds.; Wiley-VCH: Weinhim, 2001.
[86] Shibatani, T., Omori, K., Akatsuka, H., Kawai, E., Matsumae, H. *J. Mol. Catal. B: Enzym.* **2000**, *10*, 141.

Biographical Sketches

Graduated cum laude in chemistry at the University of Calabria (Italy) in 2001, Enrica Fontananova received a PhD in chemical engineering and materials in 2007.

Since 2001 she has been a tutor in chemistry at the Engineering Faculty of the University of Calabria and a contract researcher at the Institute on Membrane Technology (ITM-CNR).

Her research activity includes polymer and mixed-matrix membrane preparation; chemical–physical and electrochemical characterization of membranes; transport phenomena in membranes; membrane reactors; fuel cells; and membrane contactors.

She was awarded the 1st Prize for "New ideas for industrial applications" (NanoMemPro Awards) at the Euromembrane conference 2006.

In 2009 she held an invited keynote on "Membrane Reactors" at the Euromembrane conference in 2009.

She has coauthored more than 20 scientific papers on membrane science and technology, published on international journals, five chapters of scientific books, two chapter of electronic encyclopedia, and more than 70 publications on congress proceedings.

Enrico Drioli is full professor at the School of Engineering of the University of Calabria. He has been professor of chemistry and electrochemistry at the School of Engineering of the University of Naples, dean of the School of Engineering of the University of Calabria, director of the Institute on Membranes and Chemical Reactors of the National Research Council, and director of the Institute on Membrane Technology of Consiglio Nazionale delle Ricerche (CNR).

His main research activities focus on membrane science and engineering; membranes in artificial organs; integrated membrane processes; membrane preparation and transport phenomena in membranes; membrane distillation and membrane contactors; and catalytic membrane and catalytic membrane reactors.

He received the following awards and honors: Doctorate Honoris Causa from the University of Paul Sabatier of Toulouse; International Cooperation Honor Award given by the Membrane Industry Association of China for his special dedication to the International Cooperation between China and Europe in the field of membrane and science technology; guest professor in the Environment and Safety Engineering Department at the Jiangsu Polytechnic University, China; honorary member of the A. V. Topchiev Institute of Petrochemical Synthesis at

the Russian Academy of Sciences, Moscow; Doctorate Honoris Causa in Chemistry and Chemical Technology from the Russian Academy of Science; and honorary professor at the China Northwest University in Xi'an, Shaanxi, People's Republic of China.

He is involved in many international societies and scientific committees. Currently, he is member of various editorial boards and international advisory boards as well as chairman of the Working Party on Membranes of the European Federation of Chemical Engineering.

He is author of more than 530 scientific papers and 18 patents in the field of membrane science and technology.

3.06 Pervaporation Membrane Reactors

B Van der Bruggen, Katholieke Universiteit Leuven, Leuven, Belgium

3.06.1	Introduction	135
3.06.2	Definition of a Pervaporation Membrane Reactor	137
3.06.3	Conventional Approach Using Reactive Distillation	138
3.06.4	R1-Type Pervaporation Membrane Reactors	140
3.06.5	R2-Type Pervaporation Membrane Reactors: Esterification Reactions	142
3.06.5.1	Pervaporation-Aided Esterification	142
3.06.5.2	Esterification of Acetic Acid and Ethanol	143
3.06.5.3	Esterification of Acetic Acid with Other Alcohols	148
3.06.5.4	Esterification Reactions with Other Acids	150
3.06.6	R2-Type Pervaporation Membrane Reactors: Reactions Other than Esterification Reactions	151
3.06.7	Conclusions	158
References		159

3.06.1 Introduction

Pervaporation is a well-known membrane separation technique for liquids. The term pervaporation itself reflects the process principle: it is a contraction of permeation and evaporation. **Figure 1** shows schematically a pervaporation setup in which a (heated) liquid feed circulates over the membrane surface [1]. A vacuum is applied to the permeate side to create a driving force. One (or several) of the feed components sorbs into the membrane, diffuses through the membrane, and desorbes into the vapor phase at the permeate side, where usually condensation takes place. In this manner, a separation is achieved between components in the feed mixture that are easily sorbed and have a fast diffusion through the membrane, and components that have less affinity with the membrane. Vaporization may occur near the downstream face of the membrane, such that the membrane can be considered to operate with two zones, a liquid-phase zone and a vapor-phase zone. The exact point in the membrane where the liquid becomes vapor is not determined and, in fact, cannot be determined. During transport through the membrane, all species are present as individual molecules within a solid membrane structure, so that a phase cannot be defined. Nevertheless, the conditions are very different at both sides of the membrane, which may lead to problems due to different swelling behavior at the feed side of the membrane compared to the permeate side of the membrane.

Thus, the membrane characteristics largely determine the separation potential between components in the feed mixture. It should be understood that pervaporation is best applied for feed solutions having a relatively low concentration in the permeant, because sensible heat of the feed mixture provides the enthalpy of vaporization of the permeant. On the other hand, the concentration should not be too low since the driving force in pervaporation is the difference in concentration between the feed and the permeate. The hydrophilic or hydrophobic nature of the membrane are the main determinants of separation, although solute size may also play a role [2]. In this sense, three types of membranes are distinguished: hydrophilic membranes, hydrophobic membranes, and organophilic membranes (the latter sometimes corresponding to hydrophobic). Hydrophilic membranes preferentially transport water from a (nonaqueous) mixture. Hydrophobic membranes do the opposite: they have the least affinity with water and preferentially transport nonpolar, organic compounds. Organophilic membranes may have more specific affinities for organic solvents, not necessarily at the end of the polarity scale [3].

Polymeric (organic) membranes are most often used in industrial applications, for example, for dehydration of organic solvents (hydrophilic membranes), for recovery of organic components from water (hydrophobic membranes), and for the separation of organic mixtures (organophilic membranes).

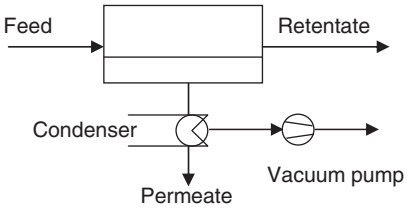

Figure 1 Schematic diagram of the pervaporation process.

Research was initially focused on the application of pervaporation in wastewater treatment, using hydrophobic (typically poly(dimethyl siloxane) (PDMS)) membranes [4–13]. This has not led to a breakthrough on industrial scale, due to two fundamental reasons. The first is related to the process cost, which is high in comparison with conventional wastewater treatment techniques. During this time, before the awareness of the cradle-to-cradle principle, waste and wastewater were considered end-of-pipe fractions not having any added value to production; the target was usually to discharge at the lowest possible cost. This, of course, did not catalyze the use of pervaporation.

A second reason was more fundamental: the driving force used within the process is a difference in partial pressure, that is, concentration. Typical applications in wastewater treatment where pervaporation can be applied are in the low concentration range, yielding a low to very low driving force. Although this may be technically possible, it is not the target concentration range for applying pervaporation.

In industrial applications, pervaporation has to compete with conventional separation processes, such as distillation, liquid–liquid extraction, adsorption, and stripping. Pervaporation is a promising alternative to conventional energy-intensive technologies for being more economical, safe, and ecofriendly, and for having interesting energetic aspects [14–16]. In the chemical industry, pervaporation is explored for separations that are difficult to achieve by distillation, for example, separations giving azeotropic mixtures and separations of components with a small difference in volatility. Hydrophilic pervaporation for solvent dehydration was more successful as a stand-alone process. Already in the 1980s, this application was suggested as an attractive solution for alcohol–water separations [17–20]. In the 1990s, pervaporation became well established in this application, using, for example, polyvinylalcohol (PVA) membranes, but also with a broad range of newly developed polymeric membranes, and even ceramic membranes [21–30]. Pilot-scale plants were set up [31, 32], and solvent dehydration slowly became an accepted application for pervaporation. Nowadays, numerous publications can be found regarding advanced applications of solvent dehydration using pervaporation, shifting the challenge from well-established alcohol applications to other solvents such as benzene [33], tetrahydrofuran (THF) [34, 35], caprolactam [36], and 2,2,2-trifluoroethylamine (TFEA) [37]. Dehydration of acetic acid–water mixtures is a special challenge, which has been studied since the 1990s [38–44], but remains an unsolved question, mainly due to insufficient membrane stability [45]. However, the search for the ideal membrane is ongoing [46–48].

However, in general, pervaporation as a stand-alone technique will rarely offer the optimal solution, but as part of a hybrid process, combined with, for example, distillation, it is very promising for difficult separations and may yield considerable energy savings. Until now, penetration of hybrid processes including pervaporation in the (petro)chemical industry has not gone very far for two reasons: (1) the methodology for design and optimization of pervaporation-based hybrid processes is still insufficiently developed; and (2) commercially available polymeric membranes are not generally applicable to organic solutions, due to insufficient chemical and temperature stability. However, the principle of applying pervaporation as a hybrid process, making advantage of the optimal working range for each individual process, is widely understood. Lipnizki *et al.* [49] have discussed hybrid separation processes based on pervaporation, and have given several examples of possible processes, such as benzene–cyclohexane separation, dimethyl carbonate–methanol, water–ethanol, fusel oil–water, water–isopropanol, and water–methyl isobutyl ketone (MIBK). Applications of hybrid separation processes can even be found in wastewater treatment [50].

Challenges in developing hybrid processes, in addition to insufficient membrane stability that can be encountered in specific applications, are related to process simulation and the optimal design of hybrid processes. As pointed out by Stephan *et al.* [51], a distillation column and a pervaporation membrane module can be combined in different ways:

1. the membrane module is placed in the column feed stream;
2. the membrane feed stream is taken as a side stream from the column and the permeate and retentate streams are fed back to the column; and

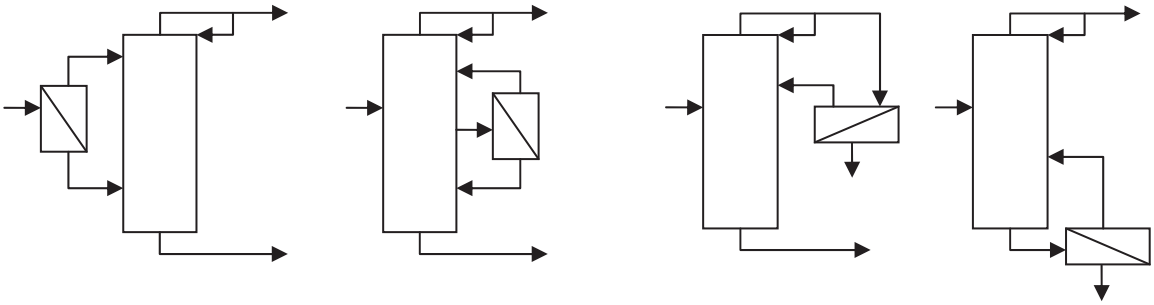

Figure 2 Schematic representation of a distillation–pervaporation hybrid process in different configurations.

3. the membrane is located on the head or bottom of the column performing the final product purification.

This is schematically depicted in **Figure 2**.

The determination of the optimal configuration remains a nontrivial matter due to the introduction of many extra degrees of freedom in the hybrid system. The optimal configuration will, for instance, be determined by the product-purity requirements, specified operating conditions, and the separation characteristics of the installed membrane components. Moreover, the economic optimization desired or required in an industrial context should also take into consideration the operating cost of (thermal and mechanical) energy consumption, together with information about the investment cost of the hybrid configuration (total number of separation stages of conventional separation process, size of chemical reactor, required membrane area, and so on).

A further integration of pervaporation can be achieved when not only separation processes are considered, but also when pervaporation is integrated with a chemical reactor. Again, this may involve hydrophilic, hydrophobic, or organophilic membranes, although hydrophilic membranes for removal of water from a reaction medium are by far the most used membranes. The sections in the following describe the possible applications of pervaporation in combination with reactors that have been described in the literature.

3.06.2 Definition of a Pervaporation Membrane Reactor

Lipnizki *et al.* [49] distinguished various possible hybrid processes involving pervaporation, including both separation-type and reaction-type hybrid processes. The latter are an offspring of two different processes (a separation and a reaction) and are denoted as R-type hybrid processes. Two configurations are distinguished (**Figure 3**). In the first one, denoted as type R1, the pervaporation unit removes the product from within the reactor (or from a recycle loop around the reactor). In this case, the product removal improves the productivity of the reactor, so that the overall process can be considered to be integrated and optimized. Therefore, the combination of both is a hybrid process. Type R2 is similar, but in this case not the final product from the reactor is removed, but a side product, which is often water. By using a hydrophilic pervaporation membrane, the equilibrium in a reaction can shift to a higher product yield in this case. Again, the removal of the by-product influences the reaction (in a positive way) so that the combination of reaction and separation can be considered to be a hybrid process.

Lipnizki *et al.* [49] pointed out that applications of pervaporation-based hybrid processes generally cover the separation of all kinds of liquid mixtures in all concentration ranges. An overview of applications already running or in development given by

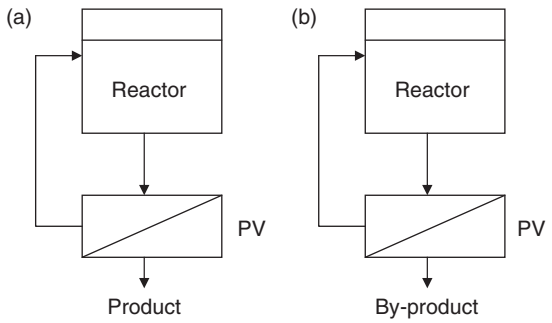

Figure 3 R-type (reaction) hybrid processes: (a) type R1 (removal of reactor product) and (b) type R2 (removal of by-product) [49].

Table 1 Potential hybrid processes of type S1

Process	*Application*	*Hybrid?*	*Membrane*
Ethanol–water	Azeotrope ethanol–water	PV-distillation	Hydrophilic
Benzene–cyclohexane	Azeotrope benzene–cyclohexane	Extractive distillation-PV	Organophilic (Bz)
Acetic acid dewatering	Small fractions of water from acetic acid	PV–RO	Hydrophilic
Carboxylic acid ester production	Azeotrope with methanol	PV-distillation	Organophilic (MeOH)
Isopropanol production	Azeotrope with water	PV-distillation	Hydrophilic
Dimethylcarbonate production	Azeotrope with methanol	PV-distillation	Organophilic
Dimethyl acetal production	Azeotrope with water	PV-distillation	Hydrophilic
Ethyl *t*-butyl ether production	Azeotrope with C4	PV-distillation	Organophilic

Modified from Lipnizki, F., Field, R. W., Ten, P. K. *J. Membr. Sci.* **1999**, *153*, 183–210.

Lipnizki *et al.* [49] involves only hybrid processes of type R2. These include butyl acetate production, *n*-butyl oleate production, diethyltartrate production, dimethyl urea (DMU) production, ethyl acetate production, ethyl carboxylate production, ethyl oleate production, ethyl valerate production, isopropyl propionate production, MIBK production, hexadecyl eruciate production, and propyl propionate production. All these processes were already described in the literature in the 1990s, which proves that many applications can be defined and, moreover, have industrial relevance. Hybrid processes of type R1 are to be found in wastewater and biotechnology applications and were not included in **Table 1**. Hybrid processes of type R2 were found to make use of hydrophilic membranes, due to the fact that the vast majority of these applications are based on the removal of water. The reaction equilibrium shifts in these reactions when water is removed, so that the reactor is operated in a more efficient way, at enhanced yield. The membranes used in these applications may be made of PVA, PVA/polyacrylonitrile (PAN), polyetherimide (PEI), or 4,4′-oxydiphenylene pyromellitimide (POPMI).

For the realization of the process, two process designs can be applied [49]. The pervaporation unit can be an external process, with a loop from the reactor to the membrane unit and back to the reactor. Alternatively, the pervaporation unit can be directly integrated in the reactor; this layout is often referred to as a membrane reactor in the literature, although in both cases the pervaporation unit and the reactor influence each other mutually, and optimization of the design must take this interdependency into account. Both layouts are schematically represented in **Figure 4**, with the external pervaporation unit on the left-hand side and the internal pervaporation unit on the right-hand side. Important parameters for such an optimization are the selectivity of the membranes, process temperature, and pervaporation feed stream composition [49].

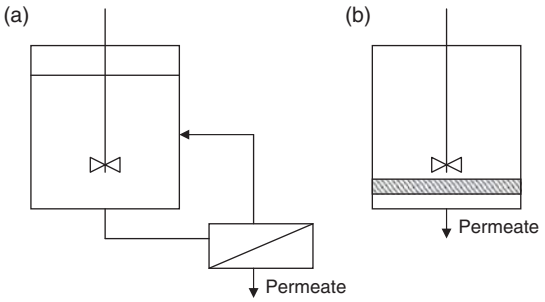

Figure 4 Schematic representation of two possible layouts for reactor-pervaporation unit, with (a) external pervaporation unit and (b) internal pervaporation unit.

Type-R2-pervaporation-based hybrid processes can be used in esterification reactions, or can be used in other reactions such as the production of DMU, MIBK, and methyl *t*-butyl ether (MTBE), among others. The classification proposed by Lipnizki *et al.* [49] is further used in this chapter.

3.06.3 Conventional Approach Using Reactive Distillation

Kulprathipanja [52] described possible reaction–separation possibilities, including reactive distillation, combined extraction–reaction units, combination of absorption with reaction, combination of adsorption with reaction, reactive membrane separation (including pervaporation membrane separation, but also

other applications such as membrane bioreactors), and reactive crystallization. The most conventional approach to enhance the yield of a chemical or biochemical conversion in a reactor is by using reactive distillation. Similar to a pervaporation membrane reactor, a reactive distillation may also integrate a reaction and a separation. However, the separation is carried out in a traditional way using a distillation column.

The chemical reaction in a reactive distillation usually takes place in the liquid phase, often in the presence of or at the surface of a solid catalyst in contact with the liquid phase [53]. Terrill *et al.* [54] described the fundamentals of the process in a general way. Typically, two components A and B are involved. In the classical approach, it is assumed that these are a close boiling or azeotropic mixture, since distillation is taken as a reference. However, it is obvious that when a comparison is made to pervaporation membrane reactors, this assumption is irrelevant, since the separation unit (distillation in this case) is only used to remove one of the reaction products in the conversion. A reactive entrained E is introduced into the distillation column; if A is the lower boiling component, it is preferable that E be higher boiling component than B and that it reacts selectively and reversibly with B to produce reaction product C, which also has a higher boiling point than component A and does not form an azeotrope with A, B, or C. Component A is removed from the distillation column as distillate, and components B and C, together with any excess E, are removed as bottoms. Components B and E are recovered from C in a separate distillation step, where the reaction is reversed to completely react C back to B and E; B is taken off as distillate, and E is taken off as bottoms and recycled to the first column [53].

However, A and B may also be two reagents in a reaction, yielding C and D where C is the desired product and D is a by-product. This concept dates back from 1921 when Backhaus [55] obtained a patent for esterification reactions in a distillation column. Early experimental observations were reported by Leyes and Othmer [56], for the esterification of acetic acid with an excess of *n*-butanol in the presence of sulfuric acid as a catalyst to produce butyl acetate and water. This is thought feasible when the reaction takes place in the liquid phase, with temperatures and pressures similar for reaction and separation. The reaction should be limited by the equilibrium such that if one or more of the products can be removed, the reaction can be driven to completion, avoiding a large excess of reactants to achieve a high conversion. For reactions that are irreversible, it is thought more economical to carry out reaction and separation in different units. In general, reactive distillation is not attractive for supercritical conditions, for gas-phase reactions, and for reactions that take place at high temperatures and pressures or that involve solid reactants or products [53].

It is not surprising that the esterification of acetic acid and ethanol to yield ethyl acetate and water is the most-studied application of reactive distillation [57]. When distillation is considered, the boiling points of the reagents and reaction products should be taken into account: at atmospheric pressure, the boiling points of ethyl acetate, ethanol, water, and acetic acid are 77.1, 78.4, 100, and 118.1 °C, respectively. This means that water has an intermediate boiling point between ethyl acetate and ethanol on the one hand, and acetic acid on the other. Moreover, minimum boiling binary azeotropes are formed by ethanol and water at 78.2 °C with 10.57 mol.% ethanol, and by ethanol and ethyl acetate at 71.8 °C with 46 mol.% ethanol. A minimum boiling binary heterogeneous azeotrope is formed by ethyl acetate and water at 70.4 °C with 24 mol.% water, and a ternary, minimum boiling azeotrope is formed by ethanol–ethyl acetate–water at 70.3 °C with 12.4 mol ethanol and 60.1 mol.% water. Thus, this system is extremely complex and nonideal. Therefore, reactive distillation is not the most straightforward solution. In addition, even when the intrinsic challenges related to the mixtures involved can be solved, reactive distillation still has the fundamental disadvantages that (1) pure water cannot be selectively removed at the top or bottom of the column and (2) energy requirements related to the distillative separation are high.

In spite of these disadvantages, several studies of reactive distillation were published for esterification reactions and other reactions. Some of the esterification reactions include the reaction of acetic acid and butanol to *n*-butyl acetate [58], esterification of succinic acid with ethanol [59], esterification of 1-propanol and propionic acid to propyl propionate [60], synthesis of triethyl citrate from citric acid and ethanol [61], esterification of acrylic acid with 1,4-butanediol to produce 4-hydroxybutyl acrylate [62], the reaction of acetic acid with methanol to methyl acetate and water [63–65], esterification of lactic acid with *n*-butanol [66], and esterification of citric acid with ethanol [67]. Many more studies can be found on these and other esterification reactions.

An interesting suggestion in that context is given by Buchaly *et al.* [68], who described the combination of reactive distillation with membrane separation, for the heterogeneously catalyzed *n*-propyl propionate synthesis from 1-propanol and propionic acid. The membrane module is located in the distillate stream of the reactive distillation column in order to selectively remove the produced water without use of entrainers. Although this is not an example of a pervaporation membrane reactor, it recognizes the need for more innovative separation processes in esterification reactions.

Reactions other than esterification for which reactive distillation has been suggested, less reported, include the reaction of formaldehyde and methanol to produce methylal and water, using a solid catalyst [69], the production of ethyl *t*-butyl ether (ETBE) [70], and the production of MTBE [71–74].

3.06.4 R1-Type Pervaporation Membrane Reactors

The potential of membrane reactors has already been understood in the 1990s, although some membrane processes still had to come of age [75]. Drioli *et al.* [76] pointed out that traditional membrane separation operations, which are already largely utilized in many different areas, are today completed with new membrane systems, including (catalytic) membrane reactors. The possibility to redesign important industrial production cycles by combining various membrane operations available in the separation and conversion units, so realizing highly integrated membrane processes, is an attractive opportunity because of the synergetic effects that can be reached. Additionally, the design of the integrated membrane production cycle satisfies the requirements for an advanced process intensification strategy.

R1-type pervaporation membrane reactors can be mainly found in biotechnology, where the pervaporation unit removes the product that is obtained from a fermentation broth. It is clear that biotechnological processes have evolved significantly during the last 15 years, so that this type of membrane reactors is still in a growth phase. Nevertheless, its prospects are remarkably good, and a continuous growth can be expected. A general prospect on the use of membranes in biotechnology can be found in a review paper by Lutz *et al.* [77].

The production of bioethanol is a logical application. Vane [78] suggests a pervaporation-bioreactor hybrid process for ethanol fermentation and dehydration, making use of a hydrophobic membrane for ethanol extraction, and a hydrophilic membrane for further purification by dehydration (**Figure 5**).

In the fermentation broth, the yield of ethanol is limited by its concentration, so that production essentially is operated at a very low efficiency. By removing the ethanol continuously using a pervaporation membrane, the yield can be drastically increased. A plant design comprising fermentation, pervaporation followed by distillation and dehydration was suggested by O'Brien *et al.* [79]. It was found that fermentation coupled to pervaporation is cost effective on condition that a satisfactory flux can be achieved in the pervaporation unit, together with a separation factor above 10. Later on, Wasewar and Pangarkar [80] carried out a more advanced economical evaluation for a hybrid fermentation–pervaporation–distillation continuous process for the production of 30 000 l day^{-1} of ethanol with a concentration of 95%. Composite hollow fiber polydimethyl siloxane membranes were used for pervaporation. It was found that the minimum direct

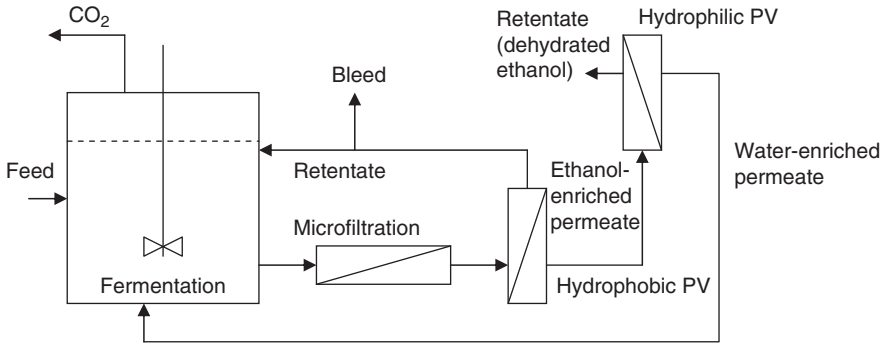

Figure 5 Fermentation reactor coupled to hydrophobic pervaporation for ethanol extraction, with microfiltration pretreatment, and dehydration with hydrophilic pervaporation [78].

production cost of ethanol was about 0.2 $\$ l^{-1}$, at a concentration of ethanol in the fermenter of 55 $kg\,m^{-3}$. These results were further refined by Arifeen *et al.* [81], who proposed a novel design for a wheat-based biorefinery for bioethanol production integrated with a pervaporation membrane for ethanol concentration, and fuel-grade ethanol purification by pressure-swing distillation. The production cost was found to be within the range of 0.13–0.25 $\$ l^{-1}$, for a production capacity of the plant of 37.85–126.8 $ml\,yr^{-1}$. This was a confirmation of the earlier findings.

Ikegami *et al.* [82] used a silicone rubber coated silicalite membrane to extract ethanol from a fermentation process using pervaporation. The membrane was thought to be highly ethanol selective; in this manner, the recovered ethanol concentration in the permeate was 67% (w/w), which was a significant improvement. It was also noted that succinic acid and glycerol, by-products created during fermentation, may interfere with the membrane performance. In a further study [83], they observed that a stabilized production of bioethanol from *Zymomonas mobilis* was influenced by the nutrients used for the preparation of the fermentation broths. In the separation of a broth prepared with yeast extract, pervaporation performance was greatly compromised by accumulation of substances having a ultraviolet (UV) absorption maximum at approximately 260 nm. When a broth was prepared with corn steep liquor without the accumulation of these substances, the permeate ethanol concentration did not decrease. Treating the prepared broth with activated carbon was effective in restraining the decrease in total flux. It was also found that lactic acid, present in corn steep liquor, adsorbed on the silicalite crystals. Therefore, it was concluded that it is important to prepare ethanol fermentation broths by *Z. mobilis* in which the lactic acid concentration is as low as possible.

The role of succinic acid was also understood by Nakayama *et al.* [84], who tried finding fermentative yeasts secreting no organic acids, in order to avoid the inhibition of ethanol permeation by succinic acid. *Pichia* and *Candida* yeasts were tested, and *Candida krusei* IA-1 showed the highest ethanol productivity, comparable to strains of *Saccharomyces cerevisiae*, but with much less production of acid. The reduction was about three times under semi-aerobic conditions, but under aerobic conditions, the strain IA-1 showed no acid production at all. It was concluded that *C. krusei* IA-1 efficiently takes up succinic acid and metabolizes it in the Krebs cycle, producing an extremely low level of by-products in the culture medium.

Hydrophobic membranes that can be used for ethanol removal are discussed in a review by Huang *et al.* [85]. These include membranes made of poly(1-trimethylsilyl-1-propyne) (PTMSP) [86, 87], PDMS [88–90], zeolite membranes [91–93], and composite membranes of silicalite-1 particles dispersed in PDMS [94–96]. Separation factors reported for ethanol–water separation in the literature are in the order PDMS (4.4–10.8) < PTMSP (9–26) < composite membranes (7–59) < zeolite membranes (12–106).

In addition to ethanol, butanol also may be considered for removal by a pervaporation membrane. Qureshi and Blaschek [97] present an economic assessment to produce butanol from corn using the hyper-butanol producing strain of *Clostridium beijerinckii* BA101. Butanol is recovered by distillation, but may be more economically produced by pervaporation. In a further study [98], pervaporation is successfully applied (with high productivity obtained). It is remarked that the application of pervaporation on an industrial scale is expected to decrease the overall cost of production significantly.

Another possible extract from fermentation reactors are aroma components [99]. This has not been explored in detail yet, presumably because of the complex nature of the aroma compounds involved. Aroma recovery using pervaporation is well known in the food industry [100, 101]; it may also be another interesting new application for R1-type pervaporation membrane reactors, when specific aromas are produced.

Application of R1-type pervaporation membrane reactors in wastewater treatment is less often applied. It should be reminded that in this type of reactors, the product is to be removed by pervaporation. Wastewater treatment involves the production of purified water, which is not considered a valuable product. Furthermore, the matrix is composed of water, so that it is not feasible to remove all of the product. In some cases, however, it may be possible to recover a specific component by using a hybrid process. Lipnizki and Field [102], for example, describe a combination of adsorption and pervaporation to recover phenol from wastewater. The study was successful, but cannot be classified as a R1-type reactor since the adsorption unit is essentially a separation unit, not a reactor. In another application, pervaporation was combined with ozonation. The purpose was to treat phthalate-contaminated water by ozonation, which was evaluated by measuring total organic carbon (TOC) values. A membrane contactor was used

to increase the TOC reduction; pervaporation was used for simultaneous removal of water, which yielded a 40% TOC reduction [103]. Again, the product from this operation is purified water, whereas the components that were present in the water had to be destroyed.

3.06.5 R2-Type Pervaporation Membrane Reactors: Esterification Reactions

3.06.5.1 Pervaporation-Aided Esterification

Lipnizki *et al.* [49] gave an overview of the state of the art in using R2-type pervaporation membrane reactors at the end of the 1990s. The integration of pervaporation into the conventional esterification process offers the opportunity to shift the chemical equilibrium by removing water. In esterification, water is a by-product, which is continuously removed from the chemical reactor by the pervaporation membrane. The idea of removing water as a by-product in chemical reactions was fast understood, which led to an early patent [104].

Esters are one of the most useful classes of organic compounds, which can be converted to a variety of other compounds. They can be used for synthetic polymer; volatile esters lend pleasant aromas to many fruits and perfumes. This leads to their extensive use in the fragrance and flavor industry. Natural fruit flavors are complex blends of many esters with other organic compounds. Synthetic fruit flavors are usually simple blends of just a few esters with a few other substances [105].

The general structure of an ester is written as RCOOR. Thus, they contain a carboxylic group and two chains, which can be short or long. When both groups are methyl groups, methyl acetate is obtained, a volatile ester with a pleasant odor. Ethyl acetate has an ethyl group linked to the oxygen atom in the carboxylic group and also has a pleasant odor. An endless variety of esters can be derived and can be further used in aromas or in other applications.

Esterifications are among the simplest and most often performed organic transformations. The preparation of esters is usually carried out starting from a carboxylic acid and an alcohol:

$$\mathrm{RCOOH} + \mathrm{R'OH} \leftrightarrow \mathrm{RCOOR'} + \mathrm{H_2O}$$

Alternative pathways to prepare esters exist, but are less applicable. Possibilities are preparation from acid halides and alcohols, from an anhydride and an alcohol or phenol, and from a carboxylate and a reactive alkyl halide. All these reactions do not have water as by-product but may be less applicable, and not considered further here.

Lactones are cyclic esters, which are fairly common in natural sources, for example, vitamin C and nepetalactone, the cat attractant in catnip, are both lactones. These esters are also important compounds and are formed from molecules that contain a carboxyl group and a hydroxyl group. These molecules undergo an intramolecular esterification, with again water as the by-product.

However, esterification is a reversible reaction. Hydrolysis, involving the addition of water and a catalyst (e.g., NaOH), yields the sodium salt of the original carboxylic acid and the alcohol. As a result of this reversibility, esterification reactions are typically equilibrium reactions and therefore need to be driven to completion according to the Le Chatelier–Braun principle, stating that "any change in status quo prompts an opposing reaction in the responding system." For esterification reactions, this means that the equilibrium shifts to the right when water is removed; thus, to a higher conversion into the ester.

The idea of using a pervaporation module to remove water from an esterification reaction was already suggested by Kita *et al.* [106], for esterification of carboxylic acid with ethanol. Remarkably, they used an asymmetric PEI membrane, and not a PVA membrane as did many other researchers. Later, David *et al.* [107, 108] described the esterification reactions of 1-propanol and 2-propanol by propionic acid, and established a model describing the kinetics of the system, with reaction rates determined experimentally.

Parulekar [109] presented an analysis of pervaporation-aided esterification of organic acids. The efficacy of pervaporation in driving esterification of lactic and succinic acids with ethanol (both reversible reactions) in particular, was shown to be very high, leading to near completion by stripping water from the reaction medium. Parulekar generalized this approach to reversible condensation reactions, where one of the products (always water) is removed by a membrane, in several reactor–separator configurations. The esterification of lactic acid and alcohol was already described in an earlier work [110], where a comparison was made of the reaction with and without pervaporation. A catalyst

(Amberlyst XN-1010) was used. It was observed that the fractional conversions of the two reactants and the yield of ethyl lactate exceeded the corresponding maximum values in a reaction-only operation by stripping of the by-product water. Furthermore, they argue that in order to achieve a high ester yield, it is typical to use a large/excess volume of alcohol, or follow the reaction by distillation to remove *in situ* products to drive the equilibrium to the ester side [111]. Employing a large excess of one reactant leads to higher cost of subsequent separations to recover the unused reactant, and operations involving reaction followed by distillation have several pitfalls. Coupling the reaction with water removal by pervaporation, however, allows one to attain near near-total utilization of the stoichiometrically limiting reactant within a reasonable time. Challenges were mainly found in the limited solubility of succinic acid, with the risk of precipitation of succinic acid on the membrane surface. The suspended succinic acid crystals can be abrasive and plug the narrow channels in a compact membrane module. This problem was solved by applying simultaneous esterification of lactic and succinic acid, which may be a commercially viable solution since both acids are derived from fermentation and agriprocessors may be interested in producing both ethyl lactate and diethyl succinate. It was concluded that the benefits of increased production of the esters in the separation-aided reaction process will outweigh the costs associated with additional equipment required (pervaporation module and vacuum pump). Conventional multistage distillation could be used to separate and recover ethyl lactate and diethyl succinate from the pervaporation retentate, since the alcohol–ester mixtures are not prone to azeotrope formation.

3.06.5.2 Esterification of Acetic Acid and Ethanol

The most reported esterification reaction by far is the reaction of ethanol with acetic acid to yield ethyl acetate (and water). Although experimental work was booming after 2000, pervaporation-assisted esterification of ethanol and acetic acid was previously known (and patented) [112]. This patent from the University of Chicago comprised the esterification of lactic acid, propionic acid, butyric acid, acetic acid, and succinic acid (and combinations thereof) with an alcohol, including the reaction of acetic acid and ethanol, aided by the use of a pervaporation membrane. The first reported observations in the literature were obtained from a continuous tube membrane reactor equipped with PVA pervaporation membranes [113]. These are classical membranes that can be used in any application where water has to be removed in nonexcessive conditions. The membranes were inert, which means that the catalyst in this application was separated from the membrane. The process was compared to distillation, and it was found that a decrease of the energy input of over 75% could be achieved, and a 50% reduction in investment and operating costs. Similarly, Krupiczka and Koszorz [114] used a GFT Pervap 1005 membrane, which is also made of PVA, and derived a three-parameter model to describe the concentration profiles in the process. They used a kinetic approach for both the conversion reaction and the pervaporative removal of water, which led to fairly simple equations that could describe the concentration profiles quite well. The model was limited to only three differential equations, which could be easily solved by the Runge–Kutta procedure. It was, however, necessary to take activities into account instead of concentrations, which is not surprising in this system. Tanna and Mayadevi [115] used a somewhat different method to analyze a membrane reactor. The performance of the pervaporation membrane reactor was represented by a two-step series model. A distinction was made between the kinetic regime of the reactor, where the performance of the pervaporation membrane reactor was similar to that of a batch reactor; in the intermediate and equilibrium regime, the performance of the pervaporation membrane reactor was superior. The membrane flux was the most important factor in the intermediate region, whereas the selectivity was more important in the equilibrium region. It was suggested to select a low flux membrane for the reactor, with sufficient surface area.

A detailed model of a pervaporation membrane reactor based on available experimental data for the esterification of acetic acid with ethanol was presented by Lim *et al.* [116]. They state that reactive distillation, which favorably shifts the equilibrium through product removal, is becoming more common in plant-scale production. Nevertheless, this operation is energy intensive and pervaporation membrane reactors may be a competitive alternative to reactive distillation. A simulation model was developed and used to describe a number of alternative reactor configurations, and to analyze the factors that affect and optimize the performance. The model was

developed in terms of activities for both the reactor and transport through the pervaporation membrane, in order to consider nonideal effects into account. The authors make a detailed analysis of a plug flow pervaporation membrane reactor (PFPMR), a continuous stirred pervaporation membrane reactor (CSPMR), a batch pervaporation membrane reactor (BPMR), a recycle plug flow pervaporation membrane reactor (RPFPMR), a recycle continuous stirred pervaporation membrane reactor (RCSPMR), and a recycle batch pervaporation membrane reactor (RBPMR). These configurations are schematically represented in **Figure 6**.

Zhu *et al.* [117] used a hydrophilic composite polymeric-ceramic membrane for the same application and obtained good results. However, this membrane was also inert (noncatalytic).

In terms of reactor design, Dams and Krug [118] analyzed three different layouts for the connection of the pervaporation unit (using inert, noncatalytic membranes) with the reactor. This is illustrated in **Figure 7**.

The first layout was a combination of pervaporation with a distillation column. The latter was used to recover unreacted ethanol from the reactor, to a top product from the distillation column containing *c.* 87 wt.% ethanol and 13 wt.% water, which was then further treated by pervaporation. In this layout, pervaporation is rather used in a hybrid separation process, not as a pervaporation membrane reactor. The concentration of ethanol after pervaporation was 98 wt.%. The second layout is the classical approach of a pervaporation membrane reactor where the liquid mixture is fed to a pervaporation unit with a hydrophilic membrane. This was technically more difficult than the first layout, because of additional requirements for membrane stability and integrity, but history has proved that this is feasible. In the third layout of **Figure 7**, the pervaporation unit was used to dehydrate a circulated stream evaporated from the reaction mixture. This was advantageous because the vapors did not contain any acids or esters, and were composed of ethanol and water. This would shield the membrane from interaction with these compounds. Energy costs of the three layouts were compared: the reduction of energy consumption with the conventional distillative approach as a reference was 58%, 93%, and 78%. The same results were observed by comparing the investment costs.

Brüschke *et al.* [119] proposed an alternative process layout, as shown in **Figure 8**. The starting point for this configuration was the observation that both a batch process and a continuous cascade operation with recycling would lead to high investment costs. The chemical reactor in **Figure 8** is operated in batch mode; the reaction product was recycled by the first pervaporation unit to reduce water contents without significant concentration changes [49]. A bleed stream was taken from the recycle stream, and was completely dehydrated in a second pervaporation unit. Subsequently, the retentate stream from the second pervaporation unit was further processed in a second reactor with a layout similar to the first reactor (including two-step pervaporation treatment, as shown in **Figure 8**). A conversion rate of 97% was obtained with a final water concentration of less than 0.5 wt.% [119].

Recent work on pervaporation-aided esterification of acetic acid and ethanol focuses on the development of new membrane structures and catalysts integrated with the membranes. The fixation of the catalyst to a membrane was proposed by Shah and Ritchie [120]. However, in this work, a microfiltration was proposed instead of a pervaporation membrane. This membrane does not have any molecular-separation properties, and should therefore only be considered in view of catalyst fixation. The microfiltration membrane may play a role as a pretreatment prior to pervaporation (as shown in **Figure 5**), in combination with the catalytic activity. A polyethersulfone microfiltration was taken as the starting point. The catalytic sites were located on each repeat unit of sulfonated polystyrene chains grafted in the flow pathways of the membrane. The catalytic membranes proved to possess good site accessibility with no separation and corrosion problems. A moderate loss (~25%) of grafted polystyrene in the reaction permeate was observed in the experiments. An increase in the molar mass of the sulfonated polystyrene grafts decreased the loss by 60%, and when the membrane catalyst was prepared by free-radical polymerization, graft loss was negligible. Nevertheless, the (catalytic) microfiltration step requires an additional pervaporative removal of water if a pervaporation membrane reactor is envisaged.

Bernal *et al.* [121] used a catalytically active inorganic pervaporation membrane, which acts both as catalyst and separator. An acid zeolite, H-ZSM-5, was used in what was called an active zeolite membrane reactor (AZMR). Zeolite membranes have pores in the range of molecular sizes, which implies that they are capable of very specific interactions (e.g., selective adsorption and molecular sieving)

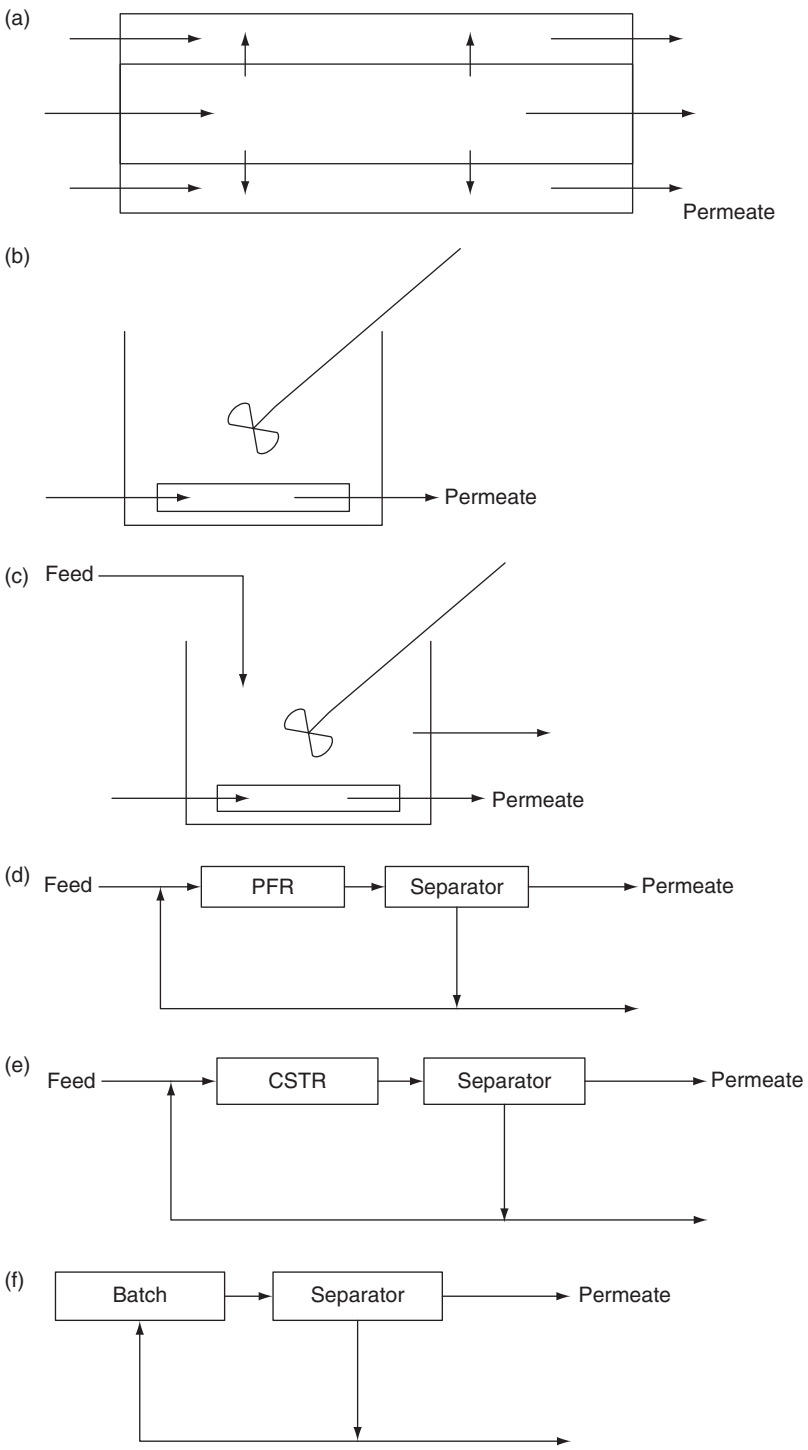

Figure 6 Schematic representation of membrane reactor configurations considered by Lim *et al*. [116]: (a) PFPMR, (b) CSPMR, (c) BPMR, (d) RPFPMR, (e) RCSPMR, and (f) RBPMR.

with the target molecules, and their characteristics make them ideal candidates to integrate reaction and separation [122]. In spite of this, the number of publications regarding the use of zeolite membrane reactors in esterification is rather limited; most studies use a discontinuous configuration similar to that

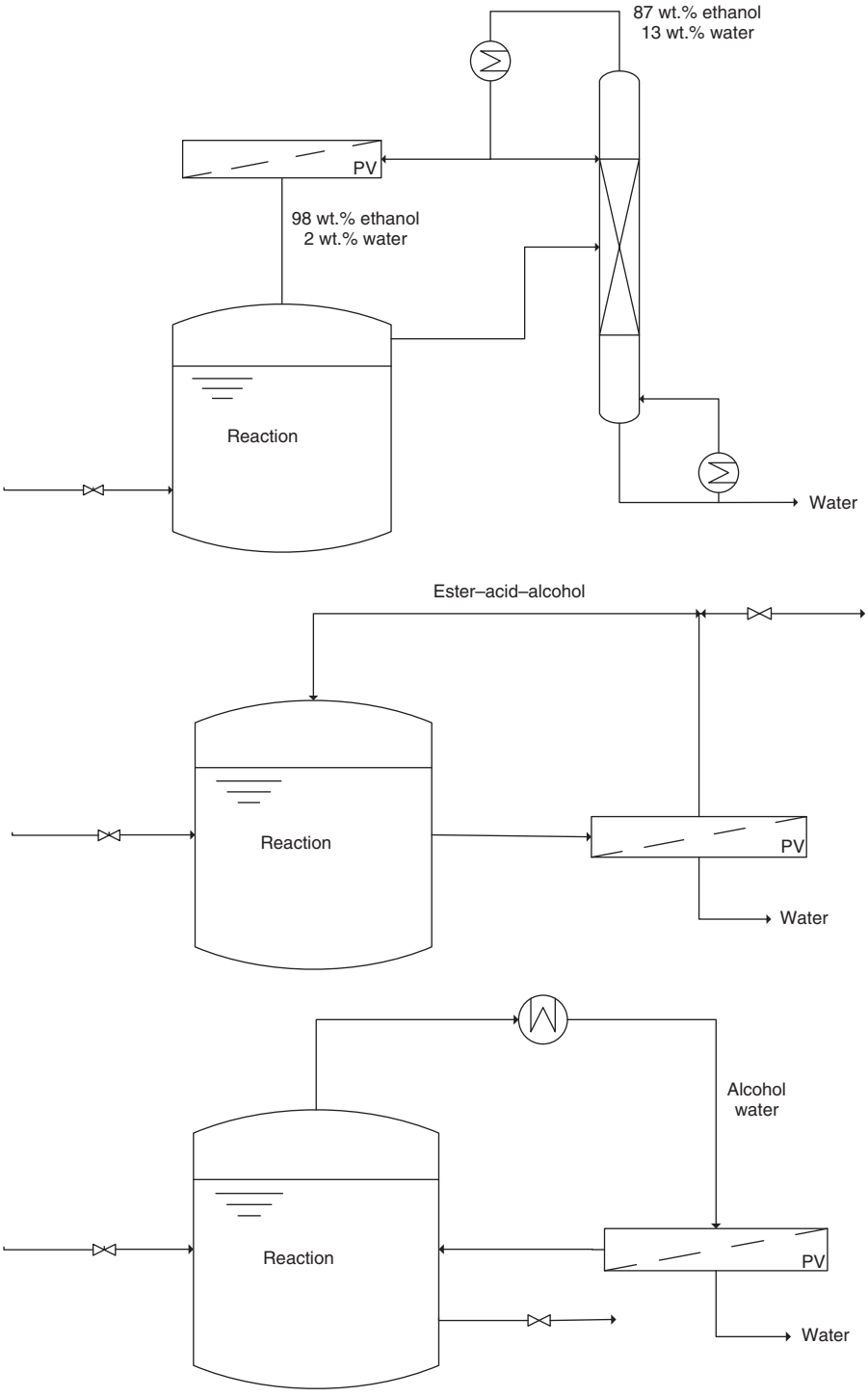

Figure 7 Alternative process layouts for pervaporation-assisted esterification based on inert (noncatalytic) membranes. Modified from Lipnizki, F., Field, R. W., Ten, P. K. *J. Membr. Sci*. **1999**, *153*, 183–210 and Dams, A., Krug, J. Pervaporation Aided Esterification – Alternatives in Plant Extension for an Existing Chemical Process. In *Proceedings of the Fifth International Conference on Pervaporation Processes in the Chemical Industry*; Bakish, R., Ed.; Bakish Material Corporation: Eaglewood, NJ, 1991; pp 338–348.

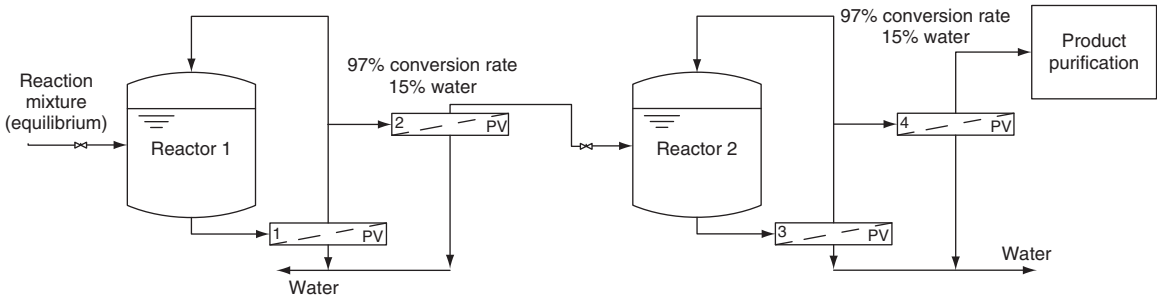

Figure 8 Alternative process layout as proposed by Brüschke *et al*. [119], in a hybrid process configuration combining batch and cascade operation.

described for polymeric membranes. Gao *et al.* [123] and Tanaka *et al.* [124] studied the esterification of acetic acid and alcohol, catalyzed by an exchange resin, using a zeolite A-PVA composite membrane, and a zeolite T membrane, respectively. Membranes were prepared according to a procedure described by Tuan *et al.* [125]. The membranes were tested at 423 K for 14 h, or at 348 K for 70.5 h, at a pH 3.5 after reaction. The zeolite was found stable under these (reaction) conditions. The differences in the performance of the reactor, compared to a classical approach with a polymeric, noncatalytic membrane are mainly to be found in the elevated reaction conditions (which is favorable), and, in fact, that water and ethyl acetate are now formed on the membrane itself, which influences significantly the transport through the membrane. The AZMR configuration yielded higher conversions than other reactor configurations, where the H-ZSM-5 catalyst was either packed as a powder inside an impervious tube, or inside a tubular Na-ZSM-5 membrane.

A similar approach was followed by de la Iglesia *et al.* [126], who described the preparation of two-layered mordenite-ZSM-5 membranes for the same reaction. The two-layered approach is interesting, since it combines the catalytic activity and the required hydrophilicity in a smart way. The principle is schematically shown in **Figure 9**. Mordenite was preferred to zeolite A in the hydrophilic layer, due to its lower content in aluminum and hence higher stability under acidic conditions. This was shown in another publication [127], where mordenite and zeolite A have been tested in the esterification of acetic acid with ethanol in a continuous membrane reactor packed with the catalyst Amberlyst^{TM} 15. Both membranes were capable of shifting the equilibrium very fast. Mordenite membranes, however, showed a great resistance to the acidic reaction medium, with

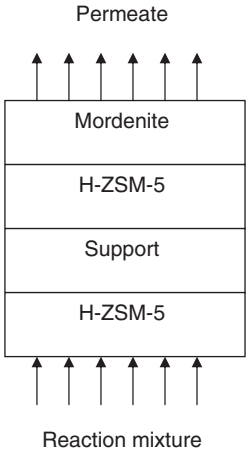

Figure 9 Two-layered membrane concept as proposed by de la Iglesia *et al*. [126].

conversions of about 90% maintained for 5 days of experiment, with very high separation factors (H_2O/EtOH and H_2O/Hac). In the case of zeolite A, membrane conversion dropped dramatically because of the instability of this zeolite to the reaction acidic conditions. This instability problem could be solved with the two-layered concept [126]. A specific challenge in this concept was to maintain the stability of the membrane after synthesis of the first layer, during synthesis of the second layer. Detailed synthesis procedures can be found in this publication [126].

The membrane was then tested with the esterification of acetic acid with ethanol as a typical application. It was found that the combination of the catalytic activity and the hydrophilicity was successful; when calcination was carried out under an atmosphere of air saturated with water vapor, the hydrophilic character persisted by acting positively upon the distribution of OH groups in the mordenite framework. Further optimizations that were

suggested are the adjustment of zeolite composition, and the membrane thickness.

Catalytic membranes were also developed based on classical polymeric membranes. Figueiredo *et al.* [128] carried out pervaporation-assisted esterifications using Amberlyst 15 and 35 as catalysts and the hydrophilic Sulzer membrane Pervap 1000 (PVA) in the pervaporation unit. They compared this conventional configuration with the performance of a catalytic membrane that was developed by coating the Pervap 1000 membrane with a thin superficial layer of tiny catalyst particles in PVA solution. In the aqueous casting solution, PVA and Amberlyst 35 had a concentration of 3%; maleic acid, used as a cross-linker, was added in the molar ratio of maleic acid/PVA 1:10. An increase up to 60% in ethyl acetate conversion was observed for the catalytic membrane operated at a temperature of 60 °C. It was also mentioned that the concentration of catalyst used in catalytic membranes is much lower than usually applied in conventional catalytic reactors.

A further integrated process was considered by Park and Tsotsis [129]. They integrated the pervaporation step in a hybrid pervaporation membrane reactor with adsorption on the permeate side. It is suggested that coupling pervaporation with adsorption could provide synergies in overcoming the equilibrium limitations in reversible reactions such as the esterification of acetic acid by ethanol catalyzed by sulfuric acid. This assumption would particularly hold for dilute reacting systems, slow reactions, nonvolatile products, or imperfect membranes. The main reason for using an additional adsorption reaction is to enhance product evacuation at the permeate side of the membrane, which can be critical especially in the cases mentioned above. Adsorption is a very effective solution to this problem. A PEI-ceramic composite pervaporation membrane was used (synthesis described in detail in Reference 129), and $CaSO_4$ as the water adsorbent. It was found that the PVMR-adsorbent system shows significantly improved performance over the PVMR in the absence of the sorbent. At 343 K, for example, the conversion of the PVMR-adsorbent system is about 10% higher than that of the conventional tubular reactor, 8% higher than the equilibrium conversion, and 5% higher than the PVMR conversion in the absence of a water-removal adsorbent. However, it was understood that the purchase of adsorbent and additional equipment are extra costs for the hybrid process, making it less attractive for general applications of condensation reactions coupled with a pervaporation unit. The hybrid adsorption membrane reactor (HAMR) was further used in a hybrid-packed bed catalytic membrane reactor (CMR) coupling the methane steam reforming reaction through a porous ceramic membrane with a CO_2 adsorption system [130].

3.06.5.3 Esterification of Acetic Acid with Other Alcohols

Esterification reactions with acetic acids and other alcohols follow roughly the same approach and evolution. A discontinuous esterification reactor using a commercial PVA membrane (GFT Pervap 1005) for benzyl alcohol acetylation (reaction of benzyl alcohol with acetic acid) was studied by Domingues *et al.* [131]. In this study, kinetic parameters of the esterification reaction combined with pervaporation were derived from time-dependent mass balances in the reactor, in a similar but somewhat differently elaborated approach than Krupiczka and Koszorz [114] used for the reaction of acetic acid with ethanol. Rönnback *et al.* [132] studied the esterification kinetics of acetic acid with methanol in the presence of hydrogen iodide as a homogeneous acid catalyst. They observed that the catalyst appeared in a side reaction: hydrogen iodide was esterified by methanol to methyl iodide. The kinetic model in this case required unraveling the precise reaction mechanism, which was supposed to be the nucleophilic attack of methanol to the carbenium ion formed through proton donation to acetic acid. Rate equations (concentration based as well as activity based) were derived, and the kinetic and equilibrium parameters included in the rate equations were estimated from experimental data with regression analysis. In this manner, the esterification reaction could be reasonably well modeled.

Methyl acetate synthesis from methanol and acetic acid was also studied by Assabumrungrat *et al.* [133]. They distinguished three modes of operation, namely semi-batch (SB-PVMR), plug flow (PF-PVMR), and continuous stirred tank (CS-PVMR). A classical approach was followed with Amberlyst-15 catalyst and a PVA membrane. It was observed that the membrane's selectivity for water was compromised by significant permeation of methanol. It was remarked that a membrane with high selectivity is essential for PVMR to achieve a high reactor performance. Considering the modes of operation, it was concluded that PF-PVMR is favorable although there are some ranges of operating conditions where

CS-PVMR is superior to PF-PVMR. The flow characteristics in the reactor, arising from different modes of operation, affect the reactor performance through the influence on the reaction and permeation rates along the reactor.

Esterification of butanol and acetic acid to produce butyl acetate was studied by Bitterlich *et al.* [134]. The conventional process for this reaction also makes use of a homogeneous catalyst, that is, sulfuric acid, which has to be neutralized by adding sodium hydroxide after the reaction. The by-product water had to be removed by distillation afterward. Bitterlich *et al.* used a fixed bed of immobilized acid in an ion exchange resin to replace the sulfuric acid, and replaced the distillation column by a pervaporation unit making use of a conventional PVA membrane [49]. Wasewar *et al.* [135] made a similar study on esterification of acetic acid with *n*-butanol. They investigated the effects of various parameters such as process temperature, initial mole ratio of acetic acid over *n*-butanol, and the ratio of the effective membrane area over the volume of reacting mixture and catalyst content, from which optimal values were derived. Li and Wang [136] proposed a kinetic model for esterification based on the reaction of acetic acid with *n*-butanol, using *p*-toluene sulfonic acid and super solid acid ($SO_4^{2-}/ZrO_2 - SiO_2$ type) as a catalyst. In this model, they took the reaction temperature into account by implementing an Arrhenius equation for the flux in pervaporation; the water concentration in the feed was also taken into account.

Peters *et al.* [137] considered the esterification reaction between acetic acid and butanol as a model reaction to examine the viability of composite catalytic hollow fiber pervaporation membranes for condensation reactions. Critical process parameters and aids in an optimal design of a catalytic membrane were identified through a parametric study, studying the influence of catalyst position, catalytic layer thickness, reaction kinetics, and the membrane permeability on the performance of the CMR. Ceramic hollow fiber membranes were considered with the reacting liquid at the shell side of the membrane. The composite catalytic membranes consisted of a support coated with a water-selective layer and on top of that a porous catalytic layer. It was assumed that the membrane reactor behaved as an ideal isothermal plug flow reactor (axial diffusion in the catalytic layer and in the liquid is not taken into account); external transport limitations on the permeate side are negligible under the pressure conditions at the permeate side, although concentration polarization effects in the shell side are taken into account; the membrane is completely water selective (no other species than water will permeate through the membrane), and the catalyst particles are assumed to be nonporous, and the catalytic activity is uniformly distributed along the catalyst coating layer. A one-dimensional catalyst model was used with mass transfer to and from the catalytic layer and diffusion and reaction occurring in the catalytic layer, solved in Matlab using a Runge–Kutta procedure in the axial direction coupled with a differential element method for the mass transfer and reaction in the radial direction. The ratio of water removal to water production, which was found to be the key factor for the performance of a pervaporation-coupled esterification process, was studied through the ratio of feed flow rate to membrane surface area and the amount of catalyst present in the reactor. When the catalytic layer thickness was increased, it was found that the conversion becomes no longer limited by the amount of catalyst present in the reactor but by diffusion in the catalytic layer. The optimal catalyst layer thickness for the case studied under the assumptions made was about 100 μm. The exact value of this optimum, however, is a function of the reaction kinetics and the membrane permeability.

Attempts to use a catalytically active membrane for this application were also reported by Zhu and Chen [138]. A crosslinked PVA dense active layer was coated on a porous ceramic plate support. Several practical problems were to overcome in this study, but eventually a 95% conversion could be reached. Temperature and initial molar ratio of acid to alcohol or catalyst concentration were suggested as optimization parameters.

Liu *et al.* [139] improved the performance of crosslinked PVA membranes in an esterification reactor for esterification of acetic acid with *n*-butanol catalyzed by $Zr(SO_4).4H_2O$, in a temperature range of 60–90 °C. To this purpose, the separation of water from acetic acid was compared to the performance of the membrane in the quaternary system water/acetic acid/*n*-butanol/butyl acetate, with a kinetic model for the esterification. The model was based on simple Fickian diffusion through the pervaporation membrane, which corresponds to the model proposed by Lee [140]. Coupling effects between water permeation and the permeation of other compounds were observed. In a further publication, Liu and Chen [141] modeled the esterification reaction of acetic acid and *n*-butanol in more detail, using a rigorous kinetic approach including expressions for the rate

constants of the esterification reactions. The applicability of the model equation was proven by a comparison with experimental data.

Zeolite membranes for pervaporation-aided esterification of acetic acid and *n*-butanol are to date less studied. Zhou *et al.* [142] prepared high performance a&b-oriented zeolite T membranes by a microwave-assisted thermal method, and applied them to a pervaporation membrane reactor for this conversion operated at 383 K. A conversion of acetic acid of 100% was reported without any loss of reactants or products, compared to a conversion of only 68% in the absence of the zeolite T membrane.

Another esterification reaction with acetic acid is the conversion of acetic acid and isoamylic alcohol [143]. To this purpose, PVA membranes were crosslinked with sulfosuccinic acid (SSA) and compared to PVA membranes in which the sulfonic groups were introduced by anchoring 5-sulfosalisilic acid (SA) on the PVA chains. It was observed that the crosslinking had a positive effect when the crosslinking degree increased from 5% to 20%; however, a further increase up to 40% did not have a great influence on the conversion. A similar trend was observed for the membranes treated with 5-SA. The stability of the membranes was also evaluated, by using them in consecutive batch experiments; about 80% of the initial activity could be maintained.

3.06.5.4 Esterification Reactions with Other Acids

Similar to the reaction with acetic acid, other acids can also be esterified, yielding a wide range of esters that can be used in various applications. For example, David *et al.* [107, 108] studied the esterification of 1-propanol and 2-propanol with propionic acid to produce propyl propionate and isopropyl propionate, and the use of a hybrid process based on pervaporation to assist the esterification reaction. In this (early) application, a PVA membrane was used external to the reactor.

Esterification of oleic acid with ethanol in the presence of *p*-toluene sulfonic acid to yield ethyl oleate was studied by Okamoto *et al.* [144]. They used an asymmetric hydrophilic PEI membrane and a 4,4′-oxydiphenylene pyrromellitimide (POPMI) membrane in a configuration in which the pervaporation membrane is integrated within the reactor (cf. **Figure 4(b)**). The reaction, operated at temperatures up to 383 K and at atmospheric and elevated pressures, was modeled by combining the kinetics of the reaction with the permeate flux equation for pervaporation. In this manner, the influence of various parameters on the conversion could be predicted so that the reaction conditions could be selected in view of an envisaged conversion of 98%.

Reaction kinetics were also considered by Keurentjes *et al.* [145] for esterification of tartaric acid with ethanol. The reaction of tartaric acid with ethanol is catalyzed by methanesulfonic acid and is a two-step esterification, as shown in **Figure 10**.

The reactions can be represented schematically [145] as

$$A + B \leftrightarrow C + H_2O$$

$$C + B \leftrightarrow D + H_2O$$

where A = tartaric acid, B = ethanol, C = ethyl tartrate, and D = diethyl tartrate. Thus, in this reaction the final product is not ethyl tartrate, but diethyl tartrate, which influences the kinetic model. In addition, activity coefficients have to be taken into account, which can be done by using, for example, UNIFAC group contribution methods. However, the

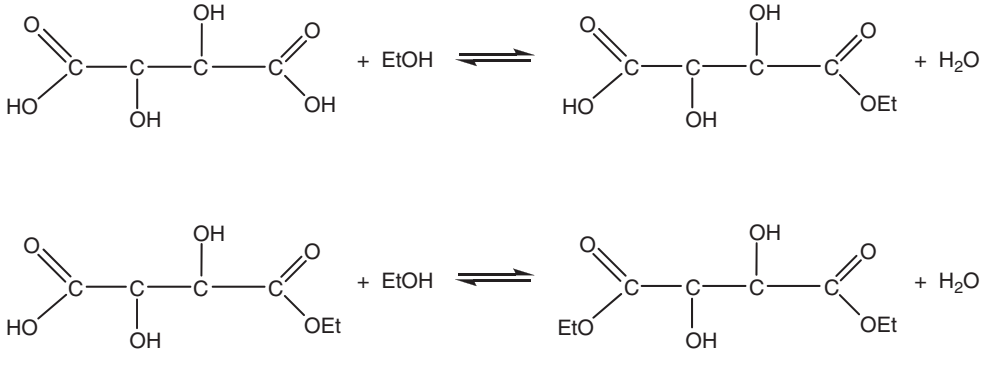

Figure 10 Two-step esterification of tartaric acid with ethanol [145].

authors indicate that although activity coefficients are significantly different from unity, a concentration-based description leads to the same result because the effects of individual activity coefficients are mutually compensated. The conversion to diethyl tartrate can be well predicted in this manner. The authors further remark that the ratio of membrane surface area to reactor volume (A/V) should be optimized since a too high value would lead to a loss of ethanol, whereas a too low value would compromise the removal of water through the pervaporation membrane.

Further modeling was carried out by Holtmann and Gorak [146], who used a dynamic model to simulate the synthesis of esters in membrane reactors in general, and by Wasewar [147]. Wasewar modified and improved a model for pervaporation-aided esterification of benzyl alcohol acetylation, using concentrated sulfuric acid as a catalyst, in view of a sensitivity analysis of the various parameters used in the reactor. The modified model allowed to predict the reaction time necessary to achieve a given conversion as a function of various parameters, and determine the membrane surface area required for this conversion.

Another application, the esterification of erucic acid and cetyl alcohol (hexadecyl) to form hexadecyl eruciate was studied by Nijhuis *et al.* [148]. In this case, the reactor was not a chemical reactor but a biochemical reactor, and the reaction was a biocatalytic reaction. The hybrid process comprised an external pervaporation unit with hydrophilic hollow fiber membranes; the reactor was an enzymatic packed bed reactor. The conversion in the conventional process was limited to 53%, which was increased to over 90% in the pervaporation-aided process. Reduced energy consumption and investment costs were indicated.

Similarly, Kwon *et al.* [149] described the esterification of oleic acid with *n*-butanol in a lipase-catalyzed reaction at room temperature in isooctane, in the formation of *n*-butyl oleate. A nonporous cellulose acetate membrane was used in the pervaporation unit. It was suggested that pervaporation is potentially applicable to remove the water produced from various other enzymatic processes as well, such as in the synthesis of several other esters, peptides, and glycosides in a solvent system as well as in a solvent-free system.

Ni *et al.* [150] described the esterification reaction of valeric acid and ethanol applying *p*-toluene sulfonic acid as a catalyst, for the formation of ethyl valerate. In this case, hydrophilic-modified aromatic polyimide membranes were used. The conversion rate of valeric acid obtained in this way was 95.2%.

Heterogeneous catalysis was not frequently reported for esterification reactions other than that of acetic acid and ethanol. Nemec and Van Gemert [151] considered esterifications in a batch process using heterogeneous catalysis and a pervaporation unit for water removal and shifting the reaction toward product formation, based on the reaction between tartaric acid and ethanol as a model system. This reaction is relatively slow. The study was based on available experimental data on currently commercially available catalysts and ceramic pervaporation membranes, using three different process configurations that differ in the degree of coupling and reaction (cf. **Figure 7**). It was suggested that a completely integrated multifunctional reactor was not a viable concept for this case study, since the optimal requirements for both processes differ. For configurations where the catalytic reaction and the separation are performed in separate units, the end design is thought to depend on practical issues (e.g., membrane stability and ease of operation) [151]. Other esterification reactions (with acids other than acetic acid) in heterogeneous catalysis are less studied and reported.

3.06.6 R2-Type Pervaporation Membrane Reactors: Reactions Other than Esterification Reactions

Although esterification reactions are by far the most studied reactions that can be enhanced by integrating a pervaporation unit to the reactor, it is evident that many other chemical or biochemical reactions might also benefit from selective product evacuation by a pervaporation membrane, in order to shift the equilibrium to a higher product yield. This approach can be followed for all reactions, on condition that:

1. it concerns an equilibrium reaction and
2. the by-product formed in the reaction can be selectively removed by a pervaporation membrane.

In most cases, the by-product is water, which can be easily separated from the reaction products by using a hydrophilic pervaporation membrane. The only exception is methanol, for which the separation (methanol–water) is often insufficient due to the fact that methanol is a relatively small and polar

molecule. Most other separation factors are sufficient for application in a pervaporation membrane reactor.

This type of application usually requires catalytic membranes that can ensure a good separation together with the catalytic activity needed in the envisaged reaction. A review of these membranes is given by Ozdemir *et al.* [152]. They remark that most studies combining membranes and catalysts concern gas-phase reactions at relatively high temperature, in which inorganic membranes made from ceramics or metals are applied. When the reaction temperatures are lower, dense or porous polymeric membranes are used. However, many important reactions involve the gas phase, so that gas-phase membrane reactors are more developed than pervaporation membrane reactors. This also appears from a review of applications of membrane separation processes in the petrochemical industry [153]. Typical examples for membrane reactors given are dehydrogenation, oxidative coupling of methane, steam reforming of methane, and the water–gas shift reaction. However, it is acknowledged that an improvement of productivity can be obtained by using membrane reactors, by shifting the chemical equilibrium and using the membrane for removal of a (by-)product. Specifications that are referred to are separation factors above 5, high fluxes (not quantified), and a membrane lifetime of several months at least. Inorganic membranes are described, in view of their application in gas-phase membrane reactors. Pervaporation is mentioned for hybrid separations, and for the separation of VOCs (volatile organic compounds) from water.

Ozdemir *et al.* focus also on pervaporation membrane reactors for esterification and other reactors, and also point out some important advantages of this concept: the separation efficiency is not limited by relative volatility as in distillation, only a fraction of the feed that is permeated through the membrane undergoes a liquid-to-vapor phase change, resulting in a lower energy consumption compared to distillation, and pervaporation can be operated at a temperature that matches the optimal temperature for reaction. Catalytically active pervaporation membranes (also called bifunctional membranes, i.e., catalytic and separative) can be prepared either by blending (typically a blend of a hydrophilic polymer such as PVA with a polymer possessing specific properties for catalysis such as poly(styrenesulfonic) acid) or by catalyst entrapment in a polymeric matrix. In the latter method, a solid catalyst is immobilized into the polymeric structure. Zeolites are often reported as materials for high-performance membranes in pervaporation membrane reactors, since they allow the combination of separation and catalytic activity as bifunctional membranes [154].

A possible application of (nonesterification) pervaporation membrane reactors is the dehydration reaction of butanediol to form THF, catalyzed by $H_3PW_{12}O_{40}$. Liu and Li [155] studied this reaction by immobilizing the catalyst in a membrane structure and used this membrane in pervaporation. $H_3PW_{12}O_{40}$ was supported on ceramic plates by dipping to form catalytic plates. These ceramic supports were bilayer composite ultrafiltration (UF) membranes of a γ-alumina matrix. A crosslinked PVA layer was formed onto the catalytic plates by spin coating; the resulting hydrophilic top layer had a reported thickness of 10–20 μm. This is a somewhat particular approach since the catalyst is now entrapped in the support layer and not in the top layer. The authors provided two reasons for this: one is that the permeance of the support is large, so that the major flow resistance is at the PVA layer rather than at the support and the second reason is that a thicker matrix can support more catalyst than a thin PVA layer and may thus yield a higher catalytic activity. This was also previously reported [156]. This means that water permeation precedes the catalytic activity in normal operation. In this case, the membrane direction had to be reversed: the skin layer of the membrane faced the permeate and the catalytic matrix faced the liquid mixture. The reactants are transported to the active layer as a liquid flow through the capillaries of the support; during the reaction, THF and water are formed on catalytically active sites. Water is then selectively permeated across the active layer to the permeate. A good performance and a good catalytic stability of the membrane was observed within the experimental range.

Another application that can be considered is the synthesis of ETBE from *tert*-butyl alcohol and ethanol [157]. The synthesis of a *tert*- ether is another typical example of equilibrium-limited reactions, with catalytic activity strongly inhibited by the presence of water and generally low conversions due to limits imposed by thermodynamics. For synthesis of ETBE, the common pathway is the reaction between ethanol and isobutene. However, isobutene is obtained from refinery cracking operations, and the supply is limited. A possible alternative to isobutene is *tert*-butyl alcohol, which is a major by-product of propylene oxide production from isobutene and propylene in the ARCO process [158]. ETBE can be

produced from *tert*-butyl alcohol by either a direct or an indirect method [157]. In the direct method, ETBE is produced from *tert*-butyl alcohol and ethanol in one reactor. In the indirect method, *tert*-butyl alcohol is dehydrated to isobutene in a first reactor, and isobutene further reacts with ethanol to produce ETBE in a second reactor. The direct method was described before [159] and is interesting in view of application in a pervaporation membrane reactor, as an alternative to reactive distillation [160, 161]. Assabumrungrat *et al.* [157] compared three modes of reactor operation: a SBR, a CSTR, and a PFR. It was found that the CSTR mode had a superior performance only in a limited range of operating conditions (at low yields). Furthermore, it was advised to operate the pervaporation membrane reactor at low temperature with a high ratio of membrane area to catalyst weight, and with the feed ratio of ethanol and *tert*-butyl alcohol at the stoichiometric value or lower, in view of enhancing ETBE yields.

MTBE production can be carried out based on a similar reaction with *tert*-butyl alcohol, replacing ethanol by methanol. MTBE production in a hybrid process combining a pervaporation membrane reactor with reactive distillation was proposed by Matouq *et al.* [162]. This principle is schematically shown in **Figure 11**. Two types of catalysts, ion exchange resin and heteropoly acid (HPA), were examined, with HPA showing the largest selectivity. On the top of the distillation column, an azeotropic mixture of MTBE and methanol was obtained as the final product (further separation was not considered). In this case, a loss of methanol in the pervaporation unit can be assumed, so that it would be necessary to select a very selective membrane, possibly with a relative low flux. The experiments were carried out with PVA membranes, but it can be assumed that this can be optimized in terms of membrane performance.

The production of DMU and MIBK follows roughly the same pattern. Production of DMU was considered by Heroin *et al.* [163]. In the production of DMU, a mixture of water, CO_2, and methyl amine is obtained. In the conventional approach, this solution was separated by distillation, which required the addition of NaOH to form Na_2CO_3 with CO_2, in order to avoid deposition of carbamate at the top of the distillation column and in the condenser [49]. Using a pervaporation membrane reactor, the water

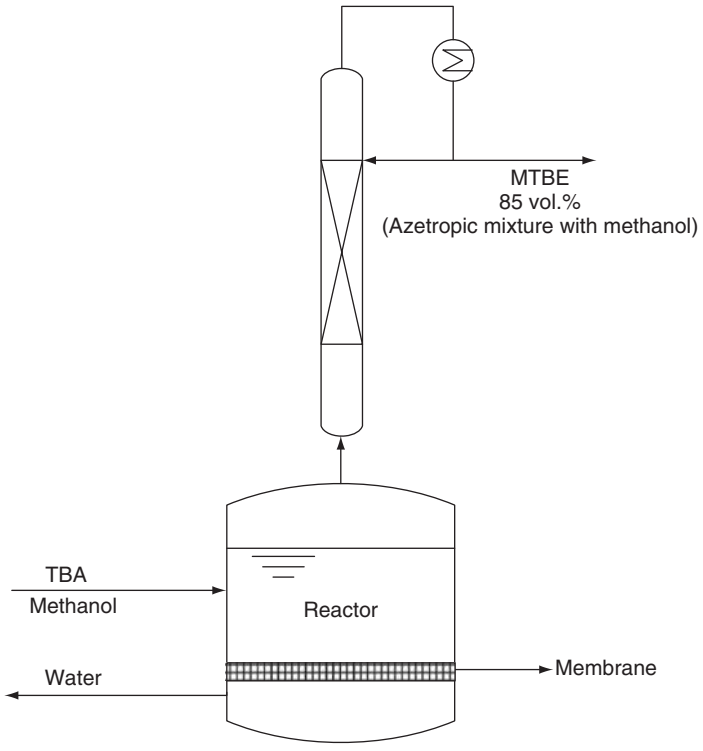

Figure 11 Pervaporation membrane reactor combined with reactive distillation for the production of MTBE in a hybrid process. Modified from Matouq, M., Tagawa, T., Goto, S. *J. Chem. Eng. Jpn*. **1994**, *27*, 302–306.

could be selectively removed so that CO_2 and methyl amine could be recycled to the reactor. The membranes used in this application were somewhat special, based on PVA but with a porous polysulfone substructure and a polyphenylene sulfide fleece. An 86% reduction in the amine to be separated was achieved, encompassing a 91% reduction in CO_2 production and the same reduction in NaOH consumption.

The purification of MIBK can be carried out with a pervaporation-based hybrid process [49], but pervaporation can also play a role in the reactor itself. This was studied by Staudt-Bickel and Lichtenthaler [164, 165]. MIBK is a solvent for paints and protective coatings, and can be produced in two ways. The conventional method is a three-step procedure (for reactions, see **Figure 12**) in which the first step is a base-catalyzed aldol condensation of acetone, followed by an acid-catalyzed dehydration, and finally hydrogenation of the resulting unsaturated ketone using a metal catalyst. The first step is limited by the equilibrium of the condensation reaction, and yields in the last two steps are rather low. However, the reaction can also be carried out in one step using a bifunctional catalyst of the type palladium/acid organic ion exchanger [166]. Due to the high polarity of the sulfonated organic ion exchanger catalyst, water formed in the reaction accumulates in the pores of the ion exchanger and hinders the accessibility of the active sites at the palladium surface to the less polar organic reactant mesityloxide. This compromises the reactor yield drastically. Removal of water would both solve the problems with the catalyst and enhance the conversion of acetone.

Staudt-Bickel and Lichtenthaler [164, 165] used hydrophilic crosslinked PVA membranes (PVA-1001) between two reactors for removal of water in this concept. Two configurations were considered. In a first configuration (**Figure 13**), the feed mixture of the pervaporation unit contains only MIBK, water, and the heavy by-products, because acetone and the low volatile by-products have already been removed

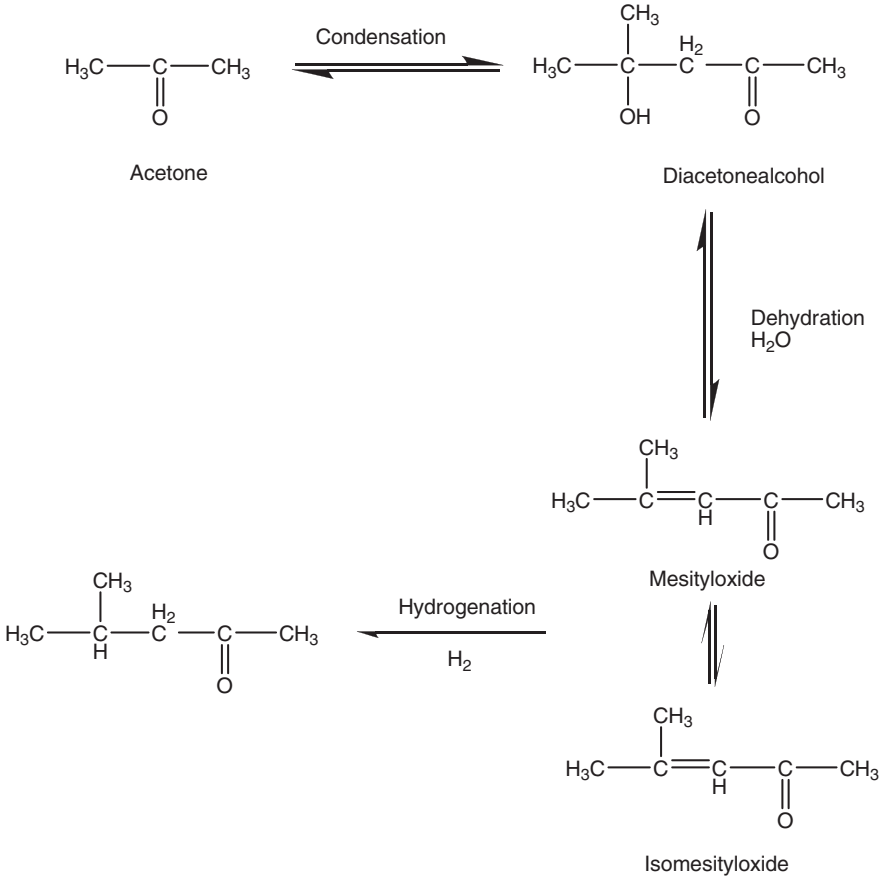

Figure 12 Synthesis of MIBK using a three-step procedure [164].

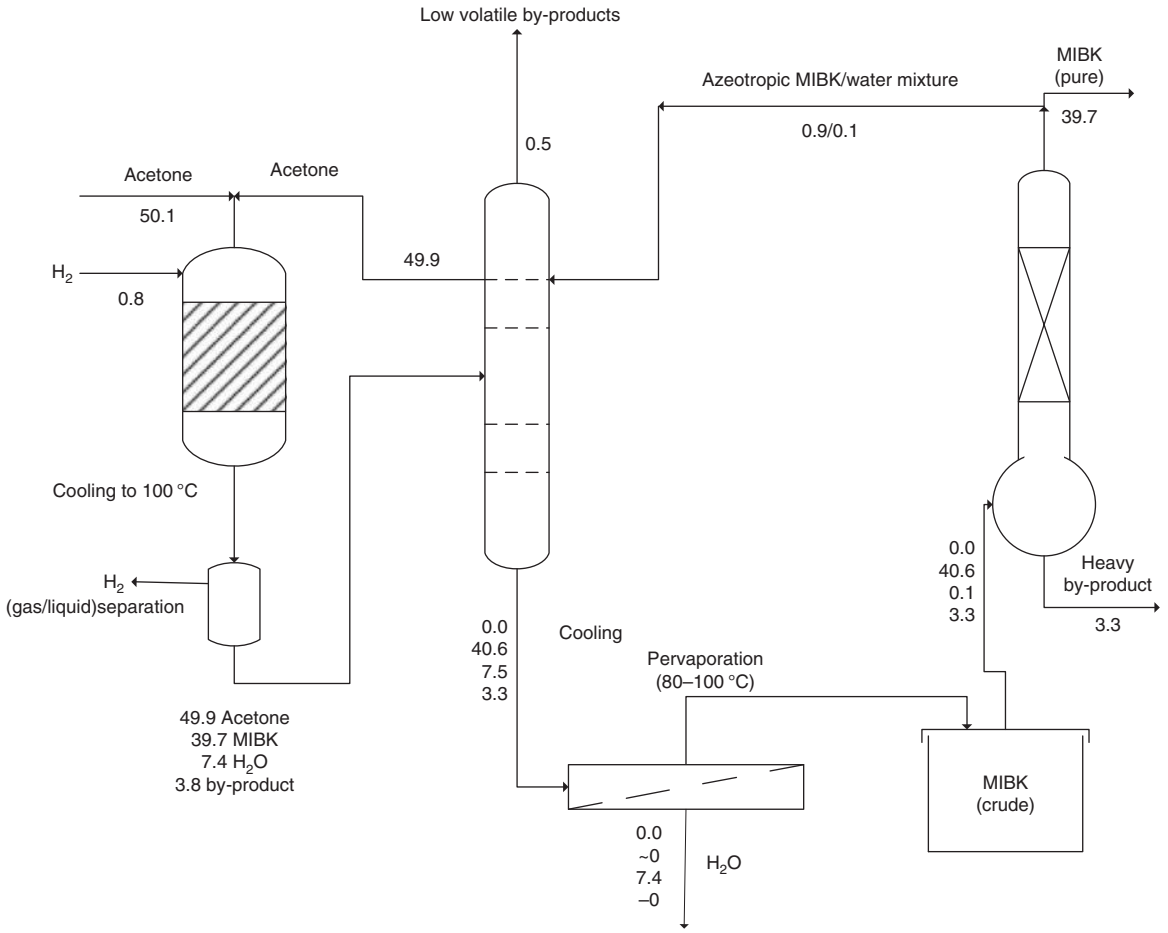

Figure 13 Hybrid process integrating pervaporation in the purification step for MIBK production [164] – alternative with distillation prior to pervaporation.

in the first distillation column. The permeate has a low concentration of organic components and can be sent to a wastewater treatment plant. The retentate is mainly MIBK (with only 0.1% water compared to 1.5% in the conventional process) and can be distilled directly in the product distillation column. **Figure 14** is a second alternative. After hydrogen separation, the pervaporation unit is placed. In this case, the permeate also contains some acetone. The retentate has a high concentration of unreacted acetone and is fed to a second reactor for further conversion of acetone. The product mixture from the second reactor contains much more MIBK but has to be treated as before, in a conventional purification process or by using another pervaporation unit. The process layout shown in **Figure 14** would double acetone conversion by the introduction of a pervaporation unit and a second reactor.

The production of acetaldehyde diethylacetal from the reaction between ethanol and acetaldehyde catalyzed by the acid resin Amberlist® 15 using a simulated moving bed reactor (SMBR) was studied by Silva and Rodrigues [167]. Acetaldehyde diethylacetal is an important raw material for fragrances and pharmaceuticals and is used in the flavoring of spirit drinks. It is also used for the design of synthetic perfumes to increase the resistance to oxidation, and as oxygenated additives to diesel fuel because they drastically reduce the emission of particles and NO_x. Diethylacetal production involves a reversible reaction of acetaldehyde and ethanol in acid medium to yield acetal and water [168, 169]. The reaction is catalyzed by mineral or carboxylic acids, which have to be neutralized after the reaction and removed. Heterogeneous catalysts such as acid ion exchange resins or zeolites can also be used; these can

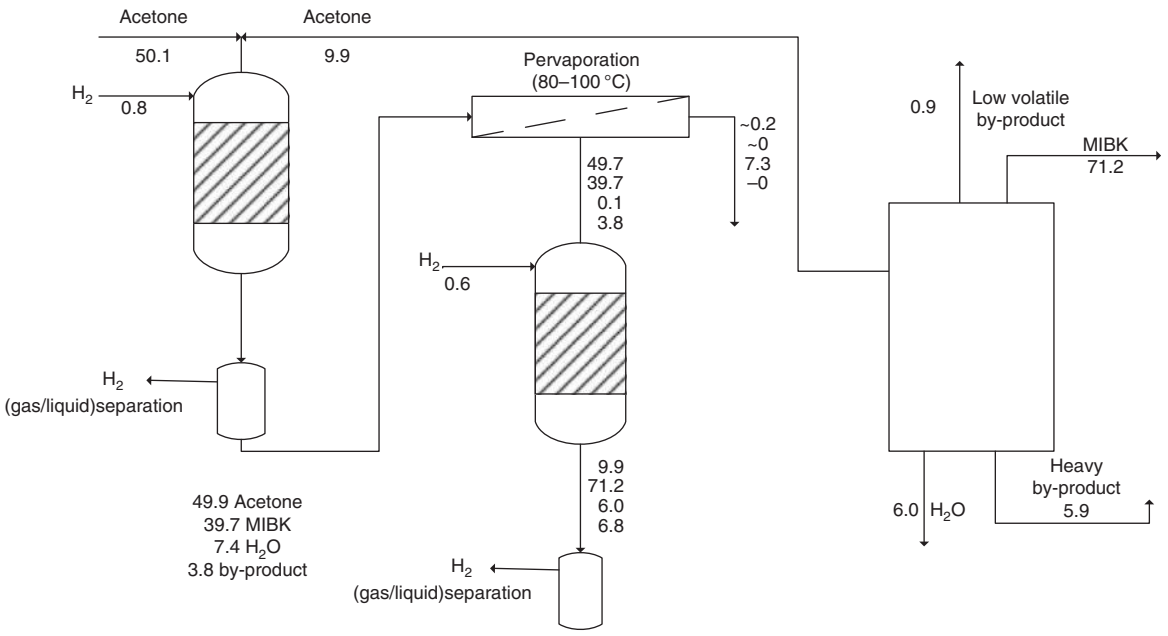

Figure 14 Hybrid process integrating pervaporation in the purification step for MIBK production [164] – alternative with pervaporation directly after hydrogen separation.

be separated from the reaction product more easily. Common catalysts that can be used (generally for esterification and etherification reactions) include Dowex 50 (Dow Chemical, Midland, MI), Amberlite® IR120, Amberlite® A15 and 36 (Rohm and Haas, Philadelphia, PA), and Lewatit® (Bayer AG, Leverkusen, Germany). Azeotropic and reactive distillation have been suggested [167], but the complexity of the vapor–liquid and liquid–liquid equilibrium (the acetal–ethanol–water system exhibits three binary azeotropes and one ternary azeotrope) make this very difficult. Therefore, an SMBR was proposed to enhance the reaction; this is based upon a set of interconnected columns packed with a solid, which acts as both adsorbent and catalyst. However, a pervaporation membrane reactor may also be applied for this purpose. The reaction is a typical application in which water is obtained as a by-product; the conversion could be increased by using an inert or catalytically active membrane.

For general application of pervaporation membrane reactors to different kinds of condensation reactions, the concept of counter-current reactive separation processes may be interesting. The principles and mass transfer are explained by Qi and Sundmacher [170]. Counter-current separative reactors may improve the reactor performance by, for example, shifting the chemical equilibrium, as is the case in pervaporation membrane reactors. The additional feature that is added in this concept is the possibility of recycling one of the products, either at the top of the unit or at the bottom of the unit. This is schematically shown in **Figure 15**.

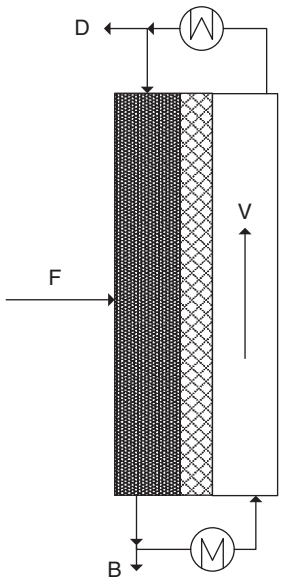

Figure 15 Reactive pervaporation in a counter-current process design with recycle [170].

When some assumptions are made (chemical reactions only take place in the liquid phase, the whole column is reactive and catalyst percentage in the column is constant, a nonreactive total reboiler and total condenser are used, the separative reactor is described as a packed-bed tower, the molar overflow of vapor is constant, and overall mass transfer coefficients related to the vapor phase can be used), a general model can be derived for any counter-current separative reactor for any applicable reaction. This was applied to the synthesis of MTBE from methanol and isobutene in a pervaporation membrane reactor [170]. From the results, it is possible to derive the requirements for the membrane as a function of the conversion needed. In the case studied, it is remarked that a less selective membrane with a low material price is sufficient.

Another concept that may be of use for pervaporation membrane reactors is the membrane microreactor [171]. These are, in fact, miniaturizations of a packed-bed membrane reactor (PBMR) and a CMR. This is driven by the quest for clean and efficient on-site, on demand, and on time, distributed production of chemicals. Miniaturization can improve heat and mass transfer by two combined effects: (1) the diffusion distance within the reactor is much lower and (2) the interfacial area per unit reactor volume is larger [172]. This leads to a rapid mass and heat transfer, even in laminar regime. For membrane reactors in particular, a very large membrane area in a small and compact unit is obtained by assembling small membrane pieces. This is especially advantageous for inorganic membranes, since these are brittle and therefore difficult to produce on a larger scale. Enhanced mass transfer and improved membrane separation were reported by Leung and Yeung [173]. In addition, supra-equilibrium conversion, improved selectivity, and product purity are reported [174], along with the prevention of catalyst poisoning and deactivation in the production of MTBE [175]. The Knoevenagel condensation reaction of benzaldehyde and ethyl cyanoacetate to form ethyl 2-cyano-3-phenylacrylate was carried out in a CMR by Yeung *et al.* [171]. Zeolite membranes were used (preparation method described in detail in Reference 171) with catalysts deposited onto the microchannels of the reactor. The microreactor was also modeled by a simple three-dimensional reactor model to be applied on the Knoevenagel condensation reaction, assuming an isothermal, steady-state operation. The influence of the reactor geometry (channel width and membrane location), the membrane separation, and catalyst properties were evaluated and the results were compared with experimental data. The authors concluded that CMRs often perform better than PBMRs, but they are more difficult to prepare since the membrane must exhibit both good catalytic and separation properties. A composite NaA–Faujasite micromembrane was found to combine successfully the good catalytic properties of Cs–Faujasite for the Knoevenagel condensation reaction and the excellent separation properties of a NaA membrane for water separation. By using a computational model, an optimum membrane microreactor was described as having narrow channels coated with a thin, uniform layer of catalyst with the membrane layer located immediately next to the catalyst. A selective separation membrane with a water permeation rate equivalent to the water production rate in the reactor is sufficient to achieve supra-equilibrium conversion in the membrane microreactor. Practical limitations to the membrane microreactor design and operation were imposed primarily by the thermodynamics and fluid properties of the reaction mixture [171].

Interesting applications of pervaporation membrane reactors can be found in the petrochemical industry, answering the challenge faced by refiners to produce environmentally friendly gasoline with sufficiently high research octane number (RON). Paraffins larger than C_6, such as heptane, are usually converted into aromatic compounds. Since regulation aims to reduce aromatic compounds in gasoline, an alternative for the use of the higher alkanes is hydroisomerization. Besides the isomerization reaction, the separation of high octane value isomers from lower ones is also of great importance in the hydroisomerization process. Maloncy *et al.* [176] made a technical and economical evaluation of a zeolite-membrane-based heptane hydroisomerization process on an industrial scale, aiming at the production of high octane number heptane isomers. They proposed a concept comprising two reactors (each with a different catalyst), and a separation with a zeolite membrane. In the first reactor, *n*-heptane is converted to mono- and dibranched isomers. The second reactor is used to convert preferably 2,4-dimethylpentane into 2,2,3-trimethylbutane, the isomer with the highest RON (109.0). The separation unit is used to separate the final product of the process composed of the dibranched 2,2-DMP, 3,3-DMP, and tribranched 2,2,3-TMB from smaller components, especially 2,4-DMP that is sent to the second reactor. A zeolite membrane with a channel aperture of 0.52×0.58 nm in the orthorhombic phase was used.

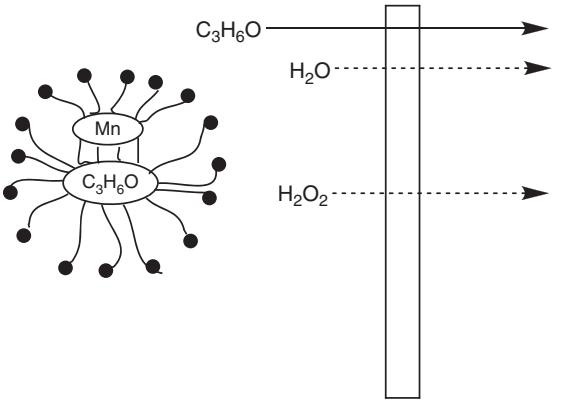

Figure 16 Schematic representation of pervaporation coupled to micellar catalysis. Modified from Ozdemir, S. S., Buonomenna, M. G., Drioli, E. *Appl. Catal. A: Gen.* **2006**, *307*, 167–183. and Heijnen, J. H. M., de Bruijn, V. G., van den Broeke, L. J. P., Keurentjes, J. T. F. *Chem. Eng. Proc*. **2003**, *42*(3), 223–230.

Heijnen *et al.* [177] proposed the use of relatively nonpolar pervaporation membranes for the epoxidation of propene to propene oxide based on micellar catalysis. This is schematically represented in **Figure 16**. The homogeneous catalyst has, in this case, been incorporated in micelles, whereas the membrane is only separative. Two goals can be achieved in the pervaporation membrane reactor [152]: the more hydrophobic propene oxide preferably dissolves in the membrane and diffuses through the membrane matrix, while the water and the oxidant are retained to a larger extent; the micelle-incorporated catalyst can be reused. This application is one of the few cases where the membrane is hydrophobic and not water, but a nonpolar component is preferentially transported.

Tijsen *et al.* [178] produced highly substituted granular carboxymethyl starch from potato starch in a batch reactor. Isopropanol appeared to be the optimal medium to prevent the substituted starch from swelling and to keep it in a granular form. The degree of substitution was increased by using consecutive batch reactions where a lower water concentration is used. A hybrid configuration was used in which the pervaporation unit was used to selectively remove water, in order to maintain the correct water/isopropanol (IPA) ratio for the reactor. Good results were obtained in terms of IPA recovery: nearly 100% of the IPA remained in the system. It must be emphasized that the pervaporation unit is here proposed rather as a hybrid separation tool (integrated with a distillation unit) than as part of a pervaporation membrane reactor. This approach is a conventional azeotropic separation between IPA and water, as an alternative to azeotropic distillation. The use of a distillation–pervaporation tandem avoids the use of the typical entrainer, cyclohexane. It was argued that the zeolite 4A membrane (described in Reference 179) and a ceramic membrane (described in Reference 25) yield the best results for IPA/water separation. Nevertheless, the concept could be significantly improved by considering a further integration of reaction and separation.

3.06.7 Conclusions

Pervaporation membrane reactors show great promise for both biochemical reactors and chemical reactors. In biochemical reactors, a product is obtained from a microbial conversion, which is typically limited by the concentration of the desired product. These are usually R1-type pervaporation membrane reactors, in which the desired product is removed by the membrane. In this case, a hydrophobic pervaporation membrane is needed since the reaction product is typically an organic compound (ethanol in the case of bioethanol production, but butanol also often is produced; aroma compounds and even specific organics in wastewater are also possible). A pervaporation-bioreactor hybrid process for ethanol fermentation and dehydration would make use of a hydrophobic membrane for ethanol extraction, followed by a hydrophilic membrane for further purification of the bioethanol. Membranes used for R1-type pervaporation membrane reactors are often polymeric, such as PDMS (filled and unfilled).

Application of pervaporation membrane reactors in chemical conversions has a strong focus on esterification reactions. In principle, all esterifications can be enhanced by using a pervaporation membrane to remove water from the reaction medium. Esterification reactions involve an acid and an alcohol as reagents, and yield an ester and water as by-products. These reactions are reversible equilibrium reactions, which compromise their yield in normal circumstances. By removing water, the equilibrium of the reaction shifts to the right-hand side of the conversion, due to the of Le Chatelier–Braun principle. Hydrophilic pervaporation membranes, even classical PVA membranes, typically have a good selectivity for water. Therefore, the combination of a pervaporation membrane with an esterification

reactor is a logical combination. Pervaporation membrane reactors are an alternative for reactive distillation, which uses the same principles of hybridization but using distillation as the separation technique. It is obvious that distillation is more complex and consumes more energy than pervaporation.

Reactions that have been studied are often those with acetic acid. Esterification with ethanol has been described extensively for nonoptimized PVA membranes. Later on, catalytic membrane structures that allow combining the reaction and separation, both at or by the membrane, were also described. This was extended to other esterification reactions with acetic acid and also with other acids.

Surprisingly, the use of pervaporation membrane reactors for other condensation reactions are sparsely described to date. This is partially due to the scale of production, but may still be optimized in the future. Etherification reactors are among the most logical applications, since they also produce water as a by-product, which is identical to esterification reactors. Some examples have already been described, the most known being the production of MTBE and ETBE. Other reactions for which a pervaporation membrane reactor can be useful include the dehydration reaction of butanediol to THF, the production of DMU and of MIBK, and the production of acetaldehyde diethyl acetal from ethanol and acetaldehyde.

Modeling of pervaporation membrane reactors is very important both for simulation and for selecting the optimal reaction conditions. For example, membrane selection can be critical since separation and flux of pervaporation membranes have a typical tradeoff: good selectivities often correspond to low fluxes and vice versa. Modeling can be done by using a kinetic approach, describing the conversion in the reactor as a function of time and concentration, and the flux through the membrane (coupled to the kinetic reaction equations) as a function of concentration and membrane properties. This approach can be a basis for a more elaborated concept of countercurrent membrane separations in membrane cascades with internal recycle, or the concept of membrane microreactors, in which mass transfer is optimized by increasing drastically the interfacial area per unit reactor volume, and by decreasing the diffusion distance within the reactor.

In general, it should be concluded that pervaporation membrane reactors can be expected to become standard solutions for all equilibrium-limited reactions, in particular when water is one of the products. Further evolutions are to be expected in improving the efficiency of the pervaporation membranes, especially in terms of catalytic activity. Reactor designs from classical bulk reactors to highly efficient, intensified reactor concepts are also thought to become a trend.

For biochemical conversions, where typically a hydrophobic membrane is needed, it can be expected that more development work is to be done on membrane structures, including new selective polymers, hybrid membrane structures, and multilayer membranes. Because biochemical reactors are also more complex in terms of process control and fluctuations, more emphasis is needed on improving the reactor efficiency, including interactions between the reaction mixture and the membrane, especially when these concerns components that may compromise the performance of the membrane by effects of fouling and membrane deterioration.

Acknowledgments

The Research Council of the K.U. Leuven is gratefully acknowledged for financial support to this work (OT/2006/37). The author also wishes to thank Siavash Darvishmanesh for valuable contributions to the drawing of the figures used in this chapter.

References

[1] Mulder, M. *Basic Principles of Membrane Technology*, 2nd edn.; Kluwer: Dordrecht, 1996.
[2] Baig, F. U. Pervaporation. In *Advanced Membrane Technology and Applications*; Li, N. N., Fane, A. G., Ho, W. S., Matsuura. T., Eds.; Wiley: New York, 2008; pp 469–488.
[3] Lipnizki, F., Haussmans, S., Ten, P. K., Field, R. W., Laufenberg, G. *Chem. Eng. J.* **1999**, *73*(2), 113–129.
[4] Dotremont, C., Goethaert, S., Vandecasteele, C. *Desalination* **1993**, *91*, 177–186.
[5] Dotremont, C., Vandenende, S., Vandommele, H., Vandecasteele, C. *Desalination* **1994**, *95*, 91–113.
[6] Dotremont, C., Brabants, B., Geeroms, K., Mewis, J., Vandecasteele, C. *J. Membr. Sci.* **1995**, *104*, 109–117.
[7] Srinivas, B. K., Elhalwagi, M. M. *Comput. Chem. Eng.* **1993**, *17*(10), 957–970.
[8] Athayde, A. L., Baker, R. W., Daniels, R., Le, M. H., Ly, J. H. *Chem. Techol.* **1997**, *27*(1), 34–39.
[9] Kondo, M., Sato, H. *Desalination* **1994**, *98*(1–3), 147–154.
[10] Ji, W. C., Hilaly, A., Sikdar, S. K., Hwang, S. T. *J. Membr. Sci.* **1994**, *97*, 109–125.
[11] Yang, D. L., Majumdar, S., Kovenklioglu, S., Sirkar, K.,K. *J. Membr. Sci.* **1995**, *103*(3), 195–210.
[12] Liu, M. G., Dickson, J. M., Cote, P. *J. Membr. Sci.* **1996**, *111*(2), 227–241.
[13] Visvanathan, C., Basu, B., Mora, J. C. *Ind. Eng. Chem. Res.* **1994**, *34*(11), 3956–3962.

[14] Jonquières, A., Clément, R., Lochon, P., Néel, J., Dresch, M., Chrétien, B. *J. Membr. Sci.* **2002**, *206*(1–2), 87–117.
[15] Smitha, B., Suhanya, D., Sridhar, S., Ramakrishna, M. *J. Membr. Sci.* **2004**, *241*(1), 1–21.
[16] Van Hoof, V., Van den Abeele, L., Buekenhoudt, A., Dotremont, C., Leysen, R. *Sep. Purif. Technol.* **2004**, *37*(1), 33–49.
[17] Taketani, Y., Minematsu, H. Dehydration of Alcohols Water Mixtures through Composite Membranes by Pervaporation. In *Abstracts of Papers of the American Chemical Society*; 1984, 188, 133-INDE.
[18] Reineke, C. E., Jagodzinski, J. A., Denslow, K. R. *J. Membr. Sci.* **1987**, *32*(2–3), 207–221.
[19] Sander, U., Soukup, P. *J. Membr. Sci.* **1988**, *36*, 463–475.
[20] Kraetz, L. *Desalination* **1988**, *70*(1–3), 481–485.
[21] Jin, S., Mora, J. C. *Desalination* **1991**, *80*(1), 71–84.
[22] Ohya, H., Choi, H. S., Hino, T., *et al. Makromol. Chem. Macromol. Symp.* **1993**, *70*(1), 341–349.
[23] Lai, J. Y., Chu, Y. H., Huang, S. L., Yin, Y. L. *J. Appl. Polym. Sci.* **1994**, *53*(8), 999–1009.
[24] Huang, R. Y. M., Feng, X. S. *Sep. Sci. Technol.* **1993**, *28*(11–12), 2035–2048.
[25] Van Gemert, R. W., Cuperus, F. P. *J. Membr. Sci.* **1995**, *105*(3), 287–291.
[26] Feng, X. S., Huang, R. Y. M. *J. Membr. Sci.* **1996**, *109*(2), 165–172.
[27] Wang, X. P., Shen, Z. Q., Zhang, F. Y., Zhang, Y. F. *J. Membr. Sci.* **1996**, *119*(2), 191–198.
[28] Burshe, M. C., Netke, S. A., Sawant, S. B., Joshi, J. B., Pangarkar, V. G. *Sep. Sci. Technol.* **1997**, *32*(8), 1335–1349.
[29] Rahal, A., Mas, A., Elharfi, A., Dobreva-Schue, R., Schue, F. *Eur. Polym. J.* **1998**, *34*(1), 17–22.
[30] Atra, R., Vatai, G., Bekassy-Molnar, E. *Chem. Eng. Proc.* **1999**, *38*(2), 149–155.
[31] Tsuyumoto, M., Teramoto, A., Meares, P. *J. Membr. Sci.* **1997**, *133*(1), 83–94.
[32] Chang, J. H., Yoo, J. K., Ahn, S. H., Lee, K. H., Ko, S. M. *Korean J. Chem. Eng.* **1998**, *15*(1), 28–36.
[33] Gutch, P. K., Pandey, L. K., Saxena, C. *J. Appl. Polym. Sci.* **2008**, *110*(1), 203–209.
[34] Ray, S., Ray, S. K. *Chem. Eng. Proc.* **2008**, *47*(9–10), 1620–1630.
[35] Chapman, P., Loh, X. X., Livingston, A. G., Li, K., Oliveira, T. A. C. *J. Membr. Sci.* **2008**, *309*(1–2), 102–111.
[36] Zhang, L., Yu, P., Luo, Y. B. *J. Membr. Sci.* **2007**, *306*(1–2), 93–102.
[37] Ahn, H., Lee, H., Lee, S. B., Lee, Y. *J. Membr. Sci.* **2007**, *291*(1–2), 46–52.
[38] Maeda, Y., Tsuyumoto, M., Karakane, H., Tsugaya, H. Separation of Water–Acetic Acid Mixture by Pervaporation through Aromatic Polymer Membranes. In *Proceedings of Fifth International Conference on Pervaporation Processes in the Chemical Industry*, Heidelberg, Germany, 11–15 March; Bakish, R., Ed.; Bakish Material Corporation: Eaglewood, NJ, 1991; pp 31–44.
[39] Ruckenstein, E., Chen, H. H. *J. Membr. Sci.* **1992**, *66*(2–3), 205–210.
[40] Koops, G. H., Nolten, J. A. M., Mulder, M. H. V., Smolders, C. A. The Development of Thin-Film Composites and Asymmetric Integrally Skinned Membranes for the Dehydration of Acetic-Acid by Pervaporation. In *Proceedings of Sixth International Conference on Pervaporation Processes in the Chemical Industry*, Ottawa, ON, Canada, 27–30 September; Bakish, R., Ed.; Bakish Material Corporation: Eaglewood, NJ, 1992; pp 335–351.
[41] Yoshikawa, M., Shimidzu, T., Maeda, Y., Magara, K., Tsugaya, H. *J. Membr. Sci.* **1993**, *83*(1–2), 157–162.
[42] Sano, T., Ejiri, S., Hasegawa, M., *et al. Chem. Lett.* **1995**, *2*, 153–154.
[43] Ray, S. K., Sawant, S. B., Joshi, J. B., Pangarkar, V. G. *J. Membr. Sci.* **1998**, *138*(1), 1–17.
[44] Kusumocahyo, S. P., Sudoh, M. *J. Membr. Sci.* **1999**, *161*(1–2), 77–83.
[45] Vane, L. M., Bowen, T. C., Meier, R. G. *J. Membr. Sci.* **2007**, *298*(1–2), 117–125.
[46] Chen, J. H., Liu, Q. L., Zhu, A. M., Zhang, Q. G. *J. Membr. Sci.* **2008**, *320*(1–2), 416–422.
[47] Nagase, T., Kiyozumi, Y., Hasegawa, Y., Inoue, T., Ikeda, T., Mizukami, F. *Chem. Lett.* **2007**, *36*(5), 594–595.
[48] Kittur, A. A., Choudhari, S. K., Kariduraganavar, M. Y. *Compos. Interfaces* **2006**, *13*(4–6), 523–534.
[49] Lipnizki, F., Field, R. W., Ten, P. K. *J. Membr. Sci.* **1999**, *153*, 183–210.
[50] Lipnizki, F., Field, R. W. *Sep. Sci. Technol.* **2001**, *3*(15), 3311–3335.
[51] Stephan, W., Noble, R. D., Noval, C. A. *J. Membr. Sci.* **1995**, *99*, 259–272.
[52] Kulprathipanja, S. *Reactive Separation Processes*; Taylor and Francis: New York, 2002.
[53] Seader, J. D., Henley, E. J. Enhanced Distillation and Supercritical Extraction,*Separation Process Principles,* 2nd edn.; Wiley: Hoboken, NJ, 2006; pp 401–448.
[54] Terrill, D. L., Sylvestre, L. F., Doherty, M. F. *Ind. Eng. Chem. Proc. Des. Develop.* **1985**, *24*, 1062–1071.
[55] Backhaus, A. A. Continuous Process for the Manufacture of Esters. US Pat. 1,400,849, 20 December 1921.
[56] Leyes, C., Othmer D. *Trans. AIChE* **1945**, *41*, 157–196.
[57] Chang, Y. A., Seader, J. D. *Comp. Chem. Eng.* **1988**, *12*(12), 1243–1255.
[58] Arpornwichanop, A., Koomsup, K., Assabumrungrat, S. *J. Ind. Eng. Chem.* **2008**, *14*(6), 796–803.
[59] Kolah, A. K., Asthana, N. S., Vu, D. T., Lira, C. T., Miller, D. J. *Ind. Eng. Chem. Res.* **2008**, *47*(15), 5313–5317.
[60] Kotora, M., Buchaly, C., Kreis, P., Gorak, A., Markos, J. *Chem. Papers* **2008**, *62*(1), 65–69.
[61] Kolah, A. K., Asthana, N. S., Vu, D. T., Lira, C. T. Miller, D. J. *Ind. Eng. Chem. Res.* **2008**, *47*(4), 1017–1025.
[62] Yang, J. I., Choi, S. H., Park, J., Lee, K. Y. *Canad. J. Chem. Eng.* **2007**, *85*(6), 883–888.
[63] Chandrakar, A. K., Agarwal, V. K., Chand, S., Wasewar, K. L. *Int. J. Chem. Reaction Eng.* **2007**, *5*, A81.
[64] Agreda, V. H., Partin, L. R. Reactive Distillation Process for the Production of Methyl Acetate. US Pat. 4,435,595, 6 March 1984.
[65] Agreda, V. H., Partin, L. R., Heise, W. H. *Chem. Eng. Prog.* **1990**, *86*(2), 40–46.
[66] Kumar, R., Mahajani, S. M. *Ind. Eng. Chem. Res.* **2007**, *46*(21), 6873–6882.
[67] Kolah, A. K., Asthana, N. S., Vu, D. T., Lira, C. T., Miller, D. J. *Ind. Eng. Chem. Res.* **2007**, *46*(10), 3180–3187.
[68] Buchaly, C., Kreis, P., Gorak, A. *Chem. Eng. Proc.* **2007**, *46*(9), 790–799.
[69] Masamoto, J., Matsuzaki, K. *J. Chem. Eng. Jpn.* **1994**, *27*, 1–5.
[70] Bisowarno, B. H., Tian, Y. C., Tade, M. O. *Chem. Eng. J.* **2004**, *99*(1), 35–43.
[71] Smith, L. A. Catalytic Distillation Process. US Pat. 4,307,254, 22 December 1981.
[72] Smith, L. A. Catalytic Distillation Structure. US Pat. 4,443,559, 17 April 1984.
[73] Smith, L. A. Method for the Preparation of Methyl Tertiary Butyl Ether. US Pat. 4,978,807, 1990.
[74] DeGarmo, J. L., Parulekar, V. N., Pinjala, V. *Chem. Eng. Prog.* **1992**, *88*(3), 43–50.
[75] Sirkar, K. K. *Chem. Eng. Commun.* **1997**, *157*, 145–184.

[76] Drioli, E., Criscuoli, A., Curcio, E. *Chem. Eng. Technol.* **2003**, *26*(9), 975–981.
[77] Lutz, S., Rao, N. N., Wandrey, C. *Chem. Eng. Technol.* **2006**, *29*(12), 1404–1415.
[78] Vane, L. *J. Chem. Technol. Biotechnol.* **2005**, *80*, 603–629.
[79] O'Brien, D. J., Roth, L. H., McAloon, A. J. *J. Membr. Sci.* **2000**, *166*(1), 105–111.
[80] Wasewar, K. L., Pangarkar, V. G. *Chem. Biochem. Eng. Quarterly* **2006**, *20*(2), 135–145.
[81] Arifeen, N., Wang, R., Kookos, I. K., Webb, C., Koutinas, A. A. *Biotechnol. Prog.* **2007**, *23*(6), 1394–1403.
[82] Ikegami, T., Kitamoto, D., Negishi, H., *et al. J. Chem. Technol. Biotechnol.* **2003**, *78*(9), 1006–1010.
[83] Ikegami, T., Negishi, H., Yanase, H., *et al. J. Chem. Technol. Biotechnol.* **2007**, *82*(8), 745–751.
[84] Nakayama, S., Morita, T., Negishi, H., Ikegami, T., Sakaki, K., Kitamoto, D. *FEMS Yeast Res.* **2008**, *8*, 706–714.
[85] Huang, H. J., Ramaswamy, S., Tschirner, U. W., Ramarao, B. V. *Sep. Purif. Technol.* **2008**, *62*, 1–21.
[86] Nagase, Y., Takamura, Y., Matsui, K. *J. Appl. Polym. Sci.* **1991**, *42*, 185–190.
[87] Gonzalez-Velasco, J. R., Gonzalez-Marcos, J. A., Lopez-Dehesa, C. *Desalination* **2002**, *149*, 61–65.
[88] Slater, C. S., Hickey, P. J., Juricic, F. P. *Sep. Sci. Technol.* **1990**, *25*, 1063–1077.
[89] Takegami, S., Yamada, H., Tsujii, S. *J. Membr. Sci.* **1992**, *75*, 93–105.
[90] Chen, X., Ping, Z. H., Long, Y. C. *J. Appl. Polym. Sci.* **1998**, *67*, 629–636.
[91] Sano, T., Yanagishita, H., Kiyozumi, Y., Mizukami, F., Haraya, K. *J. Membr. Sci.* **1994**, *95*, 221–228.
[92] Ikegami, T., Yanagishita, H., Kitamoto, D., *et al. Biotechnol. Technol.* **1997**, *11*, 921–924.
[93] Ikegami, T., Yanagishita, H., Kitamoto, D., *et al. Biotechnol. Lett.* **1999**, *21*, 1037–1041.
[94] Vankelecom, I. F. J., Depre, D., De Beukelaer, S., Uytterhoeven, J. B. *J. Phys. Chem.* **1995**, *99*(13), 193–197.
[95] Vankelecom, I. F. J., De Beukelaer, S., Uytterhoeven, J. B. *J. Phys. Chem. B* **1997**, *101*, 5186–5190.
[96] Moermans, B., De Beukelaer, S., Vankelecom, I. F. J., Ravishankar, R., Martens, J. A., Jacobs, P. A. *Chem. Commun.* **2000,** 2467–2468.
[97] Qureshi, N., Blaschek, H. P. *Food Bioprod. Process.* **2000**, *78*(C3), 139–144.
[98] Qureshi, N., Blaschek, H. P. *J. Ind. Microbiol. Biotechnol.* **2001**, *27*(5), 287–291.
[99] Schafer, T., Crespo, J. G. Extraction of Aromas from Active Fermentation Reactors by Pervaporation. In *Integration of Membrane Processes into Bioconversions*, Veszprem, Hungary, 22–27 August; BelafiBako, K., Gubicza, L., Mulder, M., Eds.; XVIth European Membrane Society Annual Summer School on Integration of Membrane Processes into Bioconversions; 1999.
[100] Raisi, A., Aroujalian, A., Kaghazchi, T. *J. Membr. Sci.* **2008**, *322*(2), 339–348.
[101] Garcia, V., Diban, N., Gorri, D., Keiski, R., Urtiaga, A., Ortiz, I. *J. Chem. Technol. Biotechnol.* **2008**, *83*(7), 973–982.
[102] Lipnizki, F., Field, R. W. *Sep. Sci. Technol.* **2001**, *36*(15), 3311–3335.
[103] Heng, S., Yeung, K. L., Julbe, A., Ayral, A., Schrotter, J. C. *Microporous Mesoporous Mater.* **2008**, *115*(1–2), 137–146.
[104] Jennings, J. F., Binning, R. C. Removal of Water Generated in Organic Chemical Reactions. US Pat. 2,8556.070, 1960.
[105] Fessenden, R. J., Fessenden, J. S. *Organic Chemistry*; Brooks/Cole: Pacific Grove, CA, 1990.
[106] Kita, H., Sasaki, S., Tanaka, K., Okamoto, K., Yamamoto, M. *Chem. Lett.* **1988**, *12*, 2025–2028.
[107] David, M. O., Gref, R., Nguyen, T. Q., Neel, J. *Chem. Eng. Res. Des.* **1991**, *69*(4), 335–340.
[108] David, M. O., Gref, R., Nguyen, T. Q., Neel, J. *Trans. Inst. Chem. Eng.* **1991**, *69*, 341–346.
[109] Parulekar, S. J. *Ind. Eng. Chem. Res.* **2007**, *46*(25), 8490–8504.
[110] Benedict, D. J., Parulekar, S. J., Tsai, S. P. *Ind. Eng. Chem. Res.* **2003**, *42*(11), 2282–2291.
[111] Benedict, D. J., Parulekar, S. J., Tsai, S. P. *J. Membr. Sci.* **2006**, *281*, 435–445.
[112] Datta, R., Tsai, S. Esterification of Fermentation-Derived Acids via Pervaporation. US Pat. 5723639, 16 October 1995.
[113] Waldburger, R. M., Widmer, F. *Chem. Eng. Technol.* **1996**, *19*(2), 117–126.
[114] Krupiczka, R., Koszorz, Z. *Sep. Purif. Technol.* **1999**, *16*, 55–59.
[115] Tanna, N. P., Mayadevi, S. *Int. J. Chem. Reactor Eng.* **2007**, *5*, A5.
[116] Lim, S. Y., Park, B., Hung, F., Sahimi, M., Tsotsis, T. T. *Chem. Eng. Sci.* **2002**, *57*, 4933–4946.
[117] Zhu, Y., Minet, G., Tsotsis, T. T. *Chem. Eng. Sci.* **1996**, *51*, 4103–4113.
[118] Dams, A., Krug, J. Pervaporation Aided Esterification – Alternatives in Plant Extension for an Existing Chemical Process. In *Proceedings of the Fifth International Conference on Pervaporation Processes in the Chemical Industry*; Bakish, R., Ed.; Bakish Material Corporation: Eaglewood, NJ, 1991; pp 338–348.
[119] Brüschke, H. E. A., Ellinghorst, G., Schneider, W. H. Optimization of a Coupled Reaction – Pervaporation Process. In *Proceedings of the Seventh International Conference on Pervaporation Processes in the Chemical Industry*; Bakish, R., Ed.; Bakish Material Corporation: Eaglewood, NJ, 1995; pp 310–320.
[120] Shah, T. N., Ritchie, S. M. C. *Appl. Catal. A: Gen.* **2005**, *296*, 12–20.
[121] Bernal, M. P., Coronas, J., Menendez, M., Santamaria, J. *Chem. Eng. Sci.* **2002**, *57*, 1557–1562.
[122] Coronas, J., Santamaria, J. *Sep. Purif. Methods* **1999**, *28*(2), 127–177.
[123] Gao, Z., Yue, Y., Li, W. *Zeolites* **1996**, *16*(1), 70–74.
[124] Tanaka, K., Yoshikawa, R., Ying, C., Kita, H., Okamoto, K. *Catal. Today* **2001**, *67*(1–3), 121–125.
[125] Tuan, V. A., Falconer, J. L., Noble, R. D. *Ind. Eng. Chem. Res.* **1999**, *38*, 3635–3645.
[126] de la Iglesia, O., Irusta, S., Mallada, R., Menendez, M., Coronas, J., Santamaria, J. *Microporous Mesoporous Mater.* **2006**, *93*, 318–324.
[127] de la Iglesia, O., Mallada, R., Menendez, M., Coronas, J. *Chem. Eng. J.* **2007**, *131*, 35–39.
[128] Figueiredo, K. C. D., Salim, V. M. M., Borges, C. P. *Catal. Today* **2008**, *133–135*, 809–814.
[129] Park, B. G., Tsotsis, T. T. *Chem. Eng. Proc.* **2004**, *43*, 1171–1180.
[130] Fayyaz, B., Harale, A., Park, B. G., Liu, P. K. T., Sahimi, M., Tsotsis, T. T. *Ind. Ng. Chem. Res.* **2005**, *44*(25), 9398–9408.
[131] Domingues, L., Recasens, F., Larrayoz, M. A. *Chem. Eng. Sci.* **1999**, *54*, 1461–1465.
[132] Rönnback, R., Salmi, T., Vuori, A., *et al. Chem. Eng. Sci.* **1997**, *52*(19), 3369–3381.
[133] Assabumrungrat, S., Phongpatthanapanich, J., Praserthdam, P., Tagawa, T., Goto, S. *Chem. Eng. J.* **2003**, *95*, 57–65.
[134] Bitterlich, S., Meissner, H., Hefner, W. Enhancement of the Conversion of Esterification Reactions by Non-Porous

Membranes. In *Proceedings of the Fifth International Conference on Pervaporation Processes in the Chemical Industry*; Bakish, R., Ed.; Bakish Material Corporation: Englewood, NJ, 1991; pp 273–281.
[135] Wasewar, K. L., Patidar, S., Agarwal, V. K. *Int. J. Chem. Reactor Eng.* **2008**, *6*, A93.
[136] Li, X., Wang, L. *J. Membr. Sci.* **2001**, *186*, 19–24.
[137] Peters, T. A., Fontalvo, J., Vorstman, M. A. G., Keurentjes, J. T. F. *Chem. Eng. Res. Des.* **2004**, *82*(A2), 220–228.
[138] Zhu, Y., Chen, H. *J. Membr. Sci.* **1998**, *138*, 123–134.
[139] Liu, Q., Zhang, Z., Chen, H. *J. Membr. Sci.* **2001**, *182*, 173–181.
[140] Lee, C. *J. Appl. Polym. Sci.* **1975**, *19*(1), 83–95.
[141] Liu, Q. L., Chen, H. L. *J. Membr. Sci.* **2002**, *196*, 171–178.
[142] Zhou, H., Li, Y., Zhu, G., Liu, J., Lin, L., Yang, W. *Chin. J. Catal.* **2008**, *29*(7), 592–594.
[143] Castanheiro, J. E., Ramos, A. M., Fonseca, I. M., Vital, J. *Appl. Catal. A: Gen.* **2006**, *311*, 17–23.
[144] Okamoto, K., Yamamoto, M., Otoshi, Y., *et al. J. Cem. Eng. Jpn.* **1993**, *26*(5), 475–481.
[145] Keurentjes, J. T. F., Janssen, G. H. R., Gorissen, J. J. *Chem. Eng. Sci.* **1994**, *49*(24), 4681–4689.
[146] Holtmann, T., Gorak, A. *Chem. Ing. Technol.* **2000**, *72*(8), 867–871.
[147] Wasewar, K. L. *Int. J. Chem. Reactor Eng.* **2007**, *5*, A6.
[148] Nijhuis, H. H., Kemperman, A., Derksen, J. T. P., Cuperus, F. P. Pervaporation Controlled Biocatalytic Reactions. In *Proceedings of the Sixth International Conference on Pervaporation Processes in the Chemical Industry*; Bakish, R., Ed.; Bakish Material Corporation: Englewood, NJ, 1992; pp 368–379.
[149] Kwon, S. J., Song, K. M., Hong, W. H., Rhee, J. S. *Biotechnol. Bioeng.* **1995**, *46*(4), 393–395.
[150] Ni, X., Xu, Z., Shi, Y., Hu, Y. *Water Treat.* **1995**, *10*, 115–120.
[151] Nemec, D., Van Gemert, R. *Ind. Eng. Chem. Res.* **2005**, *44*(25), 9718–9726.
[152] Ozdemir, S. S., Buonomenna, M. G., Drioli, E. *Appl. Catal. A: Gen.* **2006**, *307*, 167–183.
[153] Tahkt Ravanchi, M., Kaghazzchi, T., Kargari, A. *Desalination* **2009**, *235*, 199–244.
[154] Caro, J., Noack, M., Kolsch, P. *Adsorpt. – J. Int. Adsorpt. Soc.* **2005**, *11*(3–4), 215–227.
[155] Liu, Q. L., Li, Q. B. *J. Membr. Sci.* **2002**, *202*, 89–95.
[156] Liu, Q. L., Jia, P. S., Chen, H. F. *J. Membr. Sci.* **1999**, *159*(1–2), 233–241.
[157] Assabumrungrat, S., Kiatkittipong, W., Praserthdam, P., Goto, S. *Catal. Today* **2003**, *79–80*, 249–257.
[158] Yang, B. L., Goto, S. *Sep. Sci. Technol.* **1997**, *32*(5), 971–981.
[159] Yin, X. D., Yang, B. L., Goto, S. *Int. J. Chem. Kinetics* **1995**, *27*(11), 1065–1074.
[160] Quitain, A., Itoh, H., Goto, S. *J. Chem. Eng. Jpn.* **1999**, *32*(3), 280–287.
[161] Quitain, A., Itoh, H., Goto, S. *J. Chem. Eng. Jpn.* **1999**, *32*(4), 539–543.
[162] Matouq, M., Tagawa, T., Goto, S. *J. Chem. Eng. Jpn.* **1994**, *27*, 302–306.
[163] Heroin, C., Spiske, L., Hefner, W. Dehydration in the Synthesis of Dimethylurea by Pervaporation. In *Proceedings of the Fifth International Conference on Pervaporation Processes in the Chemical Industry*; Bakish, R., Ed.; Bakish Material Corporation: Englewood, NJ, 1991; pp 349–361.
[164] Staudt-Bickel, C., Lichtenthaler, R. N. *J. Membr. Sci.* **1996**, *111*, 135–141.
[165] Staudt-Bickel, C., Lichtenthaler, R. N. Integration of Pervaporation for the Removal of Water in the Production Process of Methylisobutylketone (MIBK). In *Proceedings of the International Congress on Membranes and Membrane Processes (ICOM)*, Yokohama, Japan, 18–23 August 1996; pp 394–395.
[166] Wöllner, J., Engelhardt, F. Process for the Single Stage Manufacture of Methyl Isobutyl Ketone. US Pat. 3,405,178, October 1968.
[167] Silva, V. M. T. M., Rodrigues, A. E. *AIChE J.* **2005**, *51*(10), 2752–2768.
[168] Bramwiche, P. L., Mudgan, M., Stanley, H. M. Manufacture of Diethyl Acetal. US Pat. 2,519,540, 1950.
[169] Petersen, M. L. Process for the Production of Liquid Acetals. US Pat. 4,024,159, 1977.
[170] Qi, Z., Sundmacher, K. *Sep. Purif. Technol.* **2004**, *34*, 201–211.
[171] Yeung, K. L., Zhang, X., Ngar Lau, W., Martin-Aranda, R. *Catal. Today* **2005**, *110*, 26–37.
[172] Jensen, K. F. *Chem. Eng. Sci.* **2001**, *56*(2), 293–303.
[173] Leung, A. Y. L., Yeung, K. L. *Chem. Eng. Sci.* **2004**, *59*(22–23), 4809–4817.
[174] Lai, S. M., Martin-Aranda, R., Yeung, K. L. *Chem. Commun.* **2003**, *2*, 218–219.
[175] Salomon, M. A., Coronas, J., Menéndez, M., Santamaria, J. *Appl. Catal. A: Gen.* **2003**, *200*(1–2), 201–210.
[176] Maloncy, M. L., Maschmeyer, Th., Jansen, J. C. *Chem. Eng. J.* **2005**, *106*, 187–195.
[177] Heijnen, J. H. M., de Bruijn, V. G., van den Broeke, L. J. P., Keurentjes, J. T. F. *Chem. Eng. Proc.* **2003**, *42*(3), 223–230.
[178] Tijsen, C. J., Voncken, R. M., Beenackers, A. A. C. M. *Chem. Eng. Sci.* **2001**, *5*, 411–418.
[179] Jafar, J. J., Budd, P. M. *Sep. Sci. Technol.* **1997**, *28*, 305–311.

Biographical Sketch

Bart Van der Bruggen is a chemical engineer by education. After obtaining his PhD from K.U. Leuven, Belgium, he worked as a visiting scientist at the University of North Carolina in Chapel Hill, the Institute for Membrane Technology in Calabria, Italy, and Lappeenranta University of Technology in Finland. In 2004, he obtained a permanent position at K.U. Leuven in Belgium (professor since 2009). He leads the research division Applied Physical Chemistry and Environmental Technology within the department of chemical engineering, and is internationally known as a reference in membrane research. He has authored over 100 publications in international journals and received several national and international prizes as recognition for his work. In addition to his activities at K.U. Leuven, he has also been serving as a vice-president in the Council of the European Membrane Society (EMS) since 2009, as an associate editor for the *Journal of Chemical Technology and Biotechnology*, and as an editor for *Separation and Purification Technology*.

3.07 Photocatalytic Processes in Membrane Reactors

R Molinari and A Caruso, University of Calabria, Arcavacata di Rende (CS), Italy

L Palmisano, University of Palermo, Palermo, Italy

3.07.1	**Introduction**	166
3.07.2	**Photocatalysis as a Green Process**	166
3.07.2.1	Basics of Heterogeneous Photocatalysis	167
3.07.2.1.1	Mechanism	167
3.07.2.1.2	Photocatalytic reaction parameters	168
3.07.3	**Photocatalytic Activity of Semiconductor Materials**	170
3.07.3.1	Photocatalysts	170
3.07.3.2	Titanium Dioxide	170
3.07.3.3	New Generation of Photocatalysts	170
3.07.4	**Applications of the Photocatalytic Technologies**	172
3.07.4.1	Purification Processes	172
3.07.4.1.1	Total oxidation of environmental pollutants	172
3.07.4.1.2	Removal of toxic metal ions	173
3.07.4.1.3	Conversion of inorganic contaminants	173
3.07.4.1.4	Antimicrobial and antitumor activity	173
3.07.4.2	Synthetic Pathways	173
3.07.4.2.1	Selective oxidations and reductions	173
3.07.4.2.2	Functionalization	174
3.07.4.2.3	Hydrogen evolution	174
3.07.4.3	Photocatalysis Coupled with Other Technologies	174
3.07.5	**Potentials and Limits of the Photocatalytic Processes**	175
3.07.6	**PMRs with Suspended Catalyst**	176
3.07.6.1	Introduction	176
3.07.6.2	Variables Influencing the Performance of PMRs	176
3.07.6.3	Types of PMRs	177
3.07.6.3.1	Pressurized membrane photoreactors	177
3.07.6.3.2	Submerged (depressurized) membrane photoreactors	178
3.07.6.3.3	Photocatalytic membrane contactors	179
3.07.6.4	Future Perspectives: Solar Energy	180
3.07.7	**Outline on Kinetic Models in Heterogeneous Photocatalytic Reactions and Modeling of Membrane Photoreactors**	181
3.07.7.1	Introduction	181
3.07.7.2	Adsorption Kinetics	181
3.07.7.3	Photocatalytic Kinetics	182
3.07.7.4	Quantum Yield and Relative Photonic Efficiency	183
3.07.7.5	Modeling of PMR	184
3.07.8	**Case Study: Partial and Total Oxidation Reactions in PMRS**	185
3.07.8.1	One-Step Synthesis and Separation of Phenol in a PMC	185
3.07.8.2	Photodegradation of Pharmaceutical in PPMR and SPMR	186
3.07.9	**Conclusions**	188
References		189

Glossary

Dye sensitization A system catalyst/dye illuminated with visible light.
Photocatalytic process A process requiring a semiconductor as photocatalyst and a light of appropriate wavelength.
Photolysis A process requiring only light of appropriate wavelength.
Synergistic effect The resulting effect is more than the sum of the two separate effects.

3.07.1 Introduction

Photocatalytic membrane reactors (PMRs) represent an interesting alternative technology useful both in the field of water and air purification and as a synthetic pathway. The necessity to develop chemical products and industrial processes that reduce or eliminate the use and the generation of toxic substances along with the risk for human health and for environment constitutes the aim of the research efforts based on the principles of green chemistry.

Heterogeneous photocatalysis is a technology extensively studied for about three decades, since Fujishima and Honda [1] discovered the photocatalytic splitting of water on TiO_2 electrodes in 1972, which includes a large range of reactions.

When a separation membrane method is coupled with a photocatalytic process, it is possible to obtain a synergistic effect minimizing environmental and economical impacts. In this hybrid system, in fact, the radicals produced by irradiation of the catalyst were exploited to perform partial or total redox reactions leading to selective products or clarified solutions which can be separated by the membrane.

Several characteristics make a PMR a green technology, as the safety of the photocatalyst used, the mild operative conditions, the possibility to operate in continuous mode, in which the recovery of the catalyst, the reactions, and the products separation occur in one step, with a remarkable time and cost saving.

The choice of an appropriate membrane and the knowledge of the parameters influencing the photocatalytic process represent, therefore, an important step in the design of a PMR. Besides, the possibility to perform the photocatalytic reactions using the solar light makes this process very interesting for future industrial applications.

3.07.2 Photocatalysis as a Green Process

Traditional processes for making chemical products are unsustainable in terms of resources and environmental impact. In particular, although in the last decades the chemical industries have made great improvements in the efficiency of their processes, the need to identify renewable feedstocks, the use of toxic or scarce catalysts, and the generation of hazardous waste effluents remain some of the unsolved problems which attract the scientific community [2]. The application of innovative scientific solutions to solve these problems is the main aim of the green chemistry, also known as sustainable chemistry. This new approach, based on the *12 Principles of Green Chemistry* originally published by Anastas and Warner [3], promotes innovative and sustainable chemical technologies which allow one to reduce or eliminate the use or generation of hazardous substances in the environmentally conscious design, manufacture, and use of chemical products and engineering processes . Several organizations in the world are involved in the development and promotion of these green concepts.

In this context, the PMRs, used both as purification methods and synthetic pathway, represent a promising green technology. As reported by several authors [4–7], green characteristics make photocatalysis an attractive process:

- the use of greener safer photocatalyst, as TiO_2 which is a component of pharmaceuticals and toothpastes;
- the use of mild oxidants, such as molecular oxygen;

- the possibility to work with mild reaction conditions running closer to room temperature and pressure;
- the requirement of very few auxiliary additives; and
- no production of harmful chemicals.

These potentialities are further improved when a membrane-separation technique is coupled to a photocatalytic route. PMRs, in fact, allow one to realize a continuous one-step process in which the reduction of the catalyst and solvent amounts, the minimization of the purification steps, and a better control of the equilibrium reactions can be achieved, avoiding the large amounts of waste products generally formed during a multistep process. Besides, a continuous reactor can be much smaller than the corresponding batch reactor and the use of an appropriate membrane can allow one to remove continuously higher purity products.

3.07.2.1 Basics of Heterogeneous Photocatalysis

Photocatalysis is an important technology widely studied in the last few decades. In particular, the scientific research has been addressed to the understanding of mechanisms, variables, and kinetic parameters which influence the whole process.

Heterogeneous photocatalysis is a term which describes a process in which the photocatalyst is in a different phase with respect to the substrate. In this condition, the reaction scheme implies the previous formation of an interface between the (solid) photocatalyst and a liquid or a gas phase containing the reactants. The comprehension of these phenomena is important in order to enhance the performance of photocatalytic systems.

3.07.2.1.1 Mechanism

A semiconductor presents an electronic structure characterized by a conduction band (CB) and a valence band (VB) separated by a bandgap of energy (E_G). The irradiation of the catalyst, with photons whose energy ($h\nu$) is equal to or greater than its bandgap, promotes an electron from the VB to the CB with the creation of electron–hole pair $\left(e_{cb}^- - h_{vb}^+\right)$ (Figure 1).

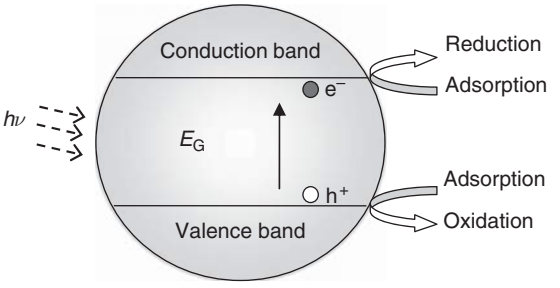

Figure 1 Energy bandgap of a semiconductor.

The lowest energy level of the CB defines the reduction potential of the photoelectrons while the highest one of the VB determines the oxidizing power of the photoholes, respectively. In the absence of suitable electron and hole scavengers, the input energy is dissipated as heat within a few nanoseconds by recombination. The initial step of the activation of the photocatalytic process is the photonic excitation of the catalyst and the main steps, representing the photocatalytic mechanisms, are proposed by several authors [8, 9]:

1. Excitation of the catalyst

$$TiO_2 + h\nu \rightarrow e^- + h^+$$

2. Adsorption on the catalyst surface

$$Ti^{IV} + H_2O \rightarrow Ti^{IV} - H_2O$$
$$Ti^{IV} + OH^- \rightarrow Ti^{IV} - OH^-$$
$$\text{catalyst site} + S_1 \rightarrow S_{1ads}$$

3. Electron and hole trapping

$$Ti^{IV} + e^- \rightarrow Ti^{III}$$
$$Ti^{IV} - H_2O + h^+ \rightarrow Ti^{IV} - OH^{\bullet} + H^+$$
$$Ti^{IV} - OH^- + h^+ \rightarrow Ti^{IV} - OH^{\bullet}$$
$$S_{1ads} + h^+ \rightarrow S_{1ads}{}^+$$
$$Ti^{III} + O_2 \rightarrow Ti^{IV} - O_2^{\bullet -}$$

4. Recombination of electron–hole pairs

$$e^- + h^+ \rightarrow \text{heat}$$

As widely accepted, the primary oxidants in these systems are the hydroxyl radicals generated by the oxidation of electron donor molecules (water or hydroxyl ions) in the VB. The attack of hydroxyl radicals to the substrate (S) can occur under different conditions:

$$Ti^{IV}-OH^{\bullet}+S_{1ads}\rightarrow Ti^{IV}+S_{2ads}$$
$$OH^{\bullet}+S_{1ads}\rightarrow S_{2ads}$$
$$Ti^{IV}-OH^{\bullet}+S_{1}\rightarrow Ti^{IV}+S_{2}$$
$$OH^{\bullet}+S_{1}\rightarrow S_{2}$$

In the CB acceptor molecules can be reduced if their reduction potential is higher than that of the photoelectrons, such as O_2 to yield superoxide ions or metal ions reduced to their lower valence states:

$$O_2+e^-\rightarrow O_2^{\bullet -}$$
$$M^n+e^-\rightarrow M^{(n-1)}$$

3.07.2.1.2 Photocatalytic reaction parameters

In this section, the main factors influencing a photocatalytic process are summarized.

Catalyst amount. A catalyst works accelerating the rate of a reaction without being consumed. Nevertheless, the ultraviolet (UV) light only (reported as photolysis) can induce the degradation of some organic substrates, but it is unable to mineralize the organic intermediates as reported in a study on the photodegradation of pharmaceuticals in water [10].

In a true heterogeneous catalytic regime, in which the photonic excitation of the catalyst surface represents the initial step of the process activation, the initial rate of the reaction is proportional to the amount of photocatalyst [11]. However, above a certain level of mass catalyst (m), the rate of reaction reaches a plateau condition that corresponds to the maximum amount of catalyst in which all the surface-active sites are illuminated and occupied by the substrate.

Besides, it was observed that agglomeration of catalyst particles occurs for high catalyst amount and consequently light penetration into suspension decreases, which leads to a decrease of photocatalyst activity [8, 12]. To avoid excess of catalyst and to ensure a satisfactory reaction efficiency, the optimum amount of catalyst must be used as function of substrate concentration.

Substrate concentration. The dependence of photocatalytic rate on substrate concentration is an aspect broadly studied in the literature. As reported by Konstantinou and Albanis [12] in a review on the photocatalytic degradation of azodyes, it is generally accepted that the degradation rate increases the substrate concentration to certain values, over which the rate decreases. This aspect can be explained by considering the mechanisms of photocatalytic reactions which involve the creation of OH radicals and substrate adsorption on catalyst surface.

Initially, the enhanced substrate concentration increases the probability of reaction between molecules and oxidizing species. A further increase, nevertheless, leads to a reduction in OH radical generation due to light scattering and to a decrease in the active catalyst sites available for OH radicals production.

pH of the aqueous solutions. The photocatalytic process is strongly affected by the pH of the reactive environment. In particular, pH changes can influence the acid–base properties of the catalyst surface and, therefore, the adsorption phenomena.

Several studies [12, 13] reported that under acidic condition the TiO_2 surface is positively charged, whereas in alkaline media it is negatively charged according to the following equilibrium:

$$TiOH+H^+\leftrightarrows TiOH_2^+$$
$$TiOH+OH^-\leftrightarrows TiO^-+H_2O$$

On this basis, although at alkaline pH the hydroxyl radicals are easier to be generated because of the higher number of hydroxide ions available on the catalyst surface, a decrease of the photocatalytic activity was observed probably due to repulsion phenomena between the negative-charged surface of TiO_2 and the hydroxyl anions.

Coulomb interaction can be hypothesized also between the catalyst and the substrate molecules. This aspect explains the different reaction products observed [8, 14] changing the pH value. Depending on the substrates, in fact, an increase of pH can determine a positive or negative effect on reaction rate. Anionic species are lesser or more adsorbed at alkaline or acidic pH, respectively, due to a different ionization state of the catalyst surface, as reported by Bekkouche *et al.* [13] in a study of adsorption of phenol on titanium oxide.

An increase of the reduction rate of BrO_3^- lowering the pH from 7 to 5 was observed also by Noguchi *et al.* [15], due to an enhancement of the electrical interaction between the anionic substrates and the positively charged surfaces of the TiO_2 photocatalyst which increases the amount of adsorbed BrO_3^-.

Moreover, at acidic condition, an aggregation of catalyst particles is observed which reduces the available catalytic active sites for photon absorption and

substrates adsorption leading to a decrease of the catalytic activity.

Presence of oxygen. Oxygen plays an important role in the photocatalytic oxidation of many substrates both as electron scavenger and as strong oxidant. Its reaction with the photoelectron in the VB allows one to prevent the electron–hole recombination prolonging the lifetime of the holes. Moreover, the superoxide ions formed ($O_2^{\bullet -}$ also initiate a chain of reactions leading to the creation of additional hydroxyl radicals through the formation of hydrogen peroxide:

$$O_2 + e^- \rightarrow O_2^{\bullet -}$$
$$O_2^{\bullet -} + H^+ \rightarrow HO_2^{\bullet}$$
$$HO_2^{\bullet} + e^- \rightarrow HO_2^-$$
$$HO_2^- + H^+ \rightarrow H_2O_2$$
$$H_2O_2 + e^- \rightarrow OH^{\bullet} + OH^-$$

Therefore, the reactive radical species formed enhance the photocatalytic efficiency of the whole process.

Presence of other species. Presence of other species in the reaction environment can give positive or negative effects on the rate of the photocatalytic process depending on the reaction mechanism.

In particular, the addition of oxyanion oxidants, such as $S_2O_8^{2-}$, BrO_3^-, IO_4^-, ClO_2^-, and ClO_3^-, increases the photoreactivity by scavenging the CB electrons and reducing charge-carrier recombination [8, 12]:

$$S_2O_8^{2-} + e^- \rightarrow SO_4^{2-} + SO_4^{\bullet -}$$
$$SO_4^{\bullet -} + H_2O \rightarrow SO_4^{2-} + {}^{\bullet}OH + H^+$$

Another oxidant species which influences positively the photocatalytic reaction is H_2O_2 due to the formation of hydroxyl radicals. However, as reported by Augugliaro *et al.* [16], an excess of H_2O_2 can have a detrimental effect because it acts as scavenger of VB holes and $^{\bullet}OH$, producing hydroperoxyl radicals which have a less oxidizing power than $^{\bullet}OH$:

$$H_2O_2 + 2h^+ \rightarrow O_2 + 2H^+$$
$$H_2O_2 + {}^{\bullet}OH \rightarrow H_2O + HO_2^{\bullet}$$

Other studies [17, 18] reported the influence of dissolved metal ions on the photocatalytic reactions. Metal cations, used in the highest oxidation state, act as photoelectron acceptors preventing the charge-carrier recombination:

$$M^{n+} + e^- \rightarrow M^{(n-1)+}$$

Moreover, the reduced species can react with H_2O_2 to give additional $^{\bullet}OH$ by photo-Fenton reaction according to the following general expression:

$$M^{(n-1)+} + H_2O_2 \rightarrow M^{n+} + {}^{\bullet}OH + OH^-$$

This aspect was broadly investigated by Brezová *et al.* [18] in a study on the photodegradation of phenol in titanium dioxide suspensions in the presence of dissolved metals. They observed the increase of the photodegradation rate by adding ferric ions but the presence of dissolved Mn^{2+}, Co^{2+}, Cr^{3+}, and Cu^{2+} ions was detrimental. In particular, the reduction of cupric ions into the unreactive form Cu^0 and its deposition on the catalyst surface and a competitive adsorption of Cr^{3+} ions on the TiO_2 surface, which probably causes the decrease of photocatalytic phenol degradation, were demonstrated. Instead, no effects were observed in the presence of Ca^{2+}, Mg^{2+}, Zn^{2+}, and Ni^{2+}.

As a different role of these metal ions on the photocatalytic efficiency was reported in other studies [8, 12, 17], it can be considered a controversial behavior depending on the physico-chemical properties of the substrates.

On the other hand, it was reported that codissolved anions, such as Cl^-, NO_3^-, and PO_4^{3-}, can affect the rate of reaction because of their possible adsorption onto TiO_2 surface, competing with the substrate and hampering the formation of $OH^{\bullet}$ radicals [12, 14].

Finally, negative effects can be expected in the presence of other organic molecules which can compete for the active sites of the catalyst surface, deactivate the photocatalyst, or act as light screens.

Wavelength and light intensity. As previously described, the first step in a photocatalytic process is irradiation of the catalyst surface. Several studies [11, 19, 20] reported that the rate of reaction depends on wavelength and intensity of the light source and on the absorption spectrum of the catalyst used. In particular, effective activation of the photocatalyst takes place only with photons which have a λ smaller than or equal to the absorbtion edge of the catalyst and this phenomenon is predominant at low light intensity [12], whereas a recombination of electron–hole pairs was supposed to occur at higher light intensity (these aspects will broadly be discussed in the following sections).

3.07.3 Photocatalytic Activity of Semiconductor Materials

3.07.3.1 Photocatalysts

A photocatalyst is a semiconductor material that must be able to convert the light energy of the irradiation in the chemical energy of the electron–hole pairs. Therefore, a suitable bandgap energy together with chemical and physical stability, nontoxic nature, availability, and low cost are important requirements to be taken into account to choose a solid photocatalyst.

Several semiconductor materials are used in the literature as photocatalysts, the most common ones are oxides (TiO_2, Fe_2O_3, SnO_2, ZnO, ZrO_2, CeO_2, WO_3, V_2O_5, etc.) or sulfides (CdS, ZnS, WS_2, etc.). Their redox potentials range between +4.0 and −1.5 V versus normal hydrogen electrode (NHE) for the valence and the CBs, respectively, allowing, therefore, their use to convert a wide range of molecules via photocatalytic reactions.

The most common semiconductor materials used in the literature with their bandgap energy and wavelength required for the activation are reported in **Table 1**.

3.07.3.2 Titanium Dioxide

The most widely used photocatalyst is the polycrystalline titanium dioxide, TiO_2, due to its strong catalytic activity, long lifetime of electron hole–pairs, high (photo)chemical stability in aqueous media and in a large range of pH (0–14), low cost (due to the abundance of Ti in the earth's crust), and harmlessness. It exists in nature in three different polymorphs: rutile, anatase (tetragonal minerals), and brookite (a rare orthorhombic mineral). All the three crystalline structures consist of deformed TiO_6 octahedra connected differently by corners and edges. The most stable form is rutile, whereas anatase and brookite are metastable and are readily transformed into rutile when heated [25]. These three types exhibit different photoactivity due to a difference in their energy structure. In particular, the position of the VB is deep and the photoproduced positive holes show sufficient oxidative power both in anatase and rutile forms. Nevertheless, the CB in the anatase polymorph is negative and it is lower than that of rutile; therefore, the reducing power of anatase type is higher. Moreover, the recombination rate of the photoproduced electron–hole pairs is usually higher for rutile.

It is worth noting, however, that not only the intrinsic electronic factors but also the surface physicochemical and morphological/textural properties of the photocatalysts can influence the photoactivity. Nanosized TiO_2 has been described to possess special characteristics and high photoactivity, due to quantum size effect and to high surface area.

Thanks to its high photocatalytic activity, TiO_2 is employed in a wide range of industrial applications: as a thickener in cosmetic and skin care products; to prevent white tiles, aluminum panels, glass, tents, paints, and coating materials; to protect tunnel lightings, mirrors, window blinds; as antibacterial in textile fibers, medical instruments, and supplies [5].

Table 1 Bandgaps energy and wavelengths of the classic photocatalysts [8, 21–24]

Semiconductor	*Bandgap (eV)*	*Bandgap wavelength (nm)*
TiO_2 anatase	3.2	387
TiO_2 rutile	3.0	380
Fe_2O_3	2.2	560
SnO_2	3.8	318
ZnS	3.7	335–336
ZnO	3.2	387–390
ZrO_2	5.0	460
WO_3	2.8	443
CdS	2.5	496–497
GaP	2.3	539–540
V_2O_5	2.0	600
CdSe	1.7	729–730
GaAs	1.4	886–887

3.07.3.3 New Generation of Photocatalysts

The efficiency of the classical photocatalysts is often reduced by some drawbacks, such as:

- quick recombination of the photogenerated electron–hole pairs (within 10–100 ns) which releases thermal energy or unproductive photons;
- high reactivity that leads to fast backward or secondary reactions with the formation of undesirable by-products; and
- a low absorption in the visible region which determines their inability to use solar light (less than 5% is used in the case of TiO_2 anatase).

In the previous years, therefore, the development of new efficient photocatalysts able to overcome these problems represents one of the main topics in the photocatalytic research.

Photocatalysts with a more stable charge separation, able to absorb visible light and more selective in the reactions pathway, are reported in the literature

both as modified common catalyst and newly synthesized semiconductor materials.

As reported by Ni *et al.* [26], the photocatalytic efficiency of the semiconductor materials can be improved by different techniques divided into two broad groups: photocatalyst modification (including noble metal loading, ion doping, and catalyst sensitization) and addition of chemical additives (such as electron acceptors or donors). Some of the most recent photocatalysts and their applications are reported in **Table 2**.

Transitional metal ion doping and noble metal loading have been extensively studied in order to enhance the photocatalytic activity of various photocatalysts [27–33]. The metal acts as electrons traps, while the photogenerated VB holes remain on the catalyst, provoking a decrease in the electron–hole recombination and increasing, therefore, the catalyst efficiency. Moreover, the metal could reduce the bandgap energy of the photocatalyst, thus shifting the photoresponse to the visible region [34–36]. This last effect was also obtained when the catalyst was doped with anions, such as N, F, C, and S [37–41].

To increase the efficiency of solar photocatalytic process, another approach is reported in the literature [42–48] consisting of composite systems in which a large bandgap semiconductor was coupled with a small bandgap semiconductor having a more negative CB level. In these systems, after irradiation with visible light, the electrons formed in the CB level of the small bandgap photocatalyst can be injected in that of the large bandgap semiconductor achieving also a wide electron–hole separation.

A similar result can be obtained with another modification technique reported as dye sensitization [49–51]. When the system catalyst/dye is illuminated with visible light, the dye acts as photosensitizer transferring the electrons to the CB of the catalyst.

In order to solve the photocatalytic drawbacks, several studies investigated on the addition of dissolved electron donors (such as BiO_3^-, CN^- [52], NO_3^-, and SO_4^{2-} [12]) or electron acceptors (such as Fe^{3+} [53], K^+, Mg^{2+}, Ca^{2+}, Zn^{2+}, and Co^{2+} [54]). Besides, several preparation techniques have been recently proposed to synthesize more efficient

Table 2 Some recent photocatalysts and their applications

Photocatalyst	*Reaction*	*Author*	*Year*
Arg-TiO_2	Selective reduction	[69]	2007
Acridine yellow G (AYG)	Total oxidation	[67]	2007
Cu-doped TiO_2	Total oxidation	[30]	2008
Membrane-W10	Oxidation	[70]	2006
V_2O_5/MgF_2 composite systems	Total oxidation	[43]	2008
Doped-TiO_2	Selective oxidation	[27]	2006
Pt-loaded $BiVO_4$	Total oxidation	[36]	2008
$ZnWO_4$	Photodegradation	[71]	2007
TiO_2 nanowires	Hydrogen evolution	[72]	2008
Fe-ZSM-5	Reduction	[73]	2007
Bi_2S_3/CdS	Partial reduction	[42]	2002
Ni-doped ZnS	Hydrogen production	[34]	2000
Dye sensitizer/photocatalyst systems	Solar photocatalysis	[51]	2008
Ag_2ZnGeO_4	Photodegradation	[64]	2008
Bi_3SbO_7	Total oxidation	[65]	2008
Fe(III)-OH complexes	Redox	[74]	2007
POM	Functionalization	[75]	2003
Zn phthalocyanine complexes	Photodegradation	[68]	2007
Pt, Au, Pd-doped TiO_2	Hydrogen production	[28]	2007
Hydrous alumina-doped TiO_2	Reduction	[15]	2003
Bi^{3+}-doped TiO_2	Reduction	[76]	2007
Activated carbon-ZnO	Photodegradation	[58]	2008
N-doped TiO_2	Photodegradation	[38]	2008
La-, Cu-, Pt-doped WO_3	Selective oxidation	[31]	2005
POM	Reduction	[77]	2004
F-doped TiO_2 film	Photodegradation	[41]	2008
Au/Fe_2O_3	Degradation (ox)	[29]	2007

photocatalysts immobilized on mesoporous support [55, 56], inert support [57], activated carbon (AC) [58, 59], ceramic membranes [60], building materials [61], and ceramic monolith channel [62]. Moreover, newly synthesized photocatalysts which allow a better control of the whole photocatalytic process, thanks to a delay in charge recombination and an enhanced activity under visible light irradiation, are reported in the recent photocatalytic works [63–68].

3.07.4 Applications of the Photocatalytic Technologies

Photocatalytic processes can be performed in various media. They include a great variety of reactions, such as partial or total oxidation, degradation of organic compounds, reduction reactions, fuel synthesis (e.g., H_2 production through water splitting), metal corrosion prevention, disinfection, etc.

The application fields of this technology can be divided in two main groups (**Figure 2**), purification processes and synthetic pathways, although combined reactions are often exploited to increase the efficiency of the system.

3.07.4.1 Purification Processes

3.07.4.1.1 Total oxidation of environmental pollutants

The main use of the photocatalytic techniques was the removal of organic pollutants in water and air. This application, which in the previous years has found an important relevance in commercial materials, has been widely studied in the literature. The growing resistance of various classes of organic compounds to common chemical and biological degradation treatments has focused the attention of the international scientific community on the development of alternative methods. In this context, photocatalysis represents a useful alternative green purification technique, because, as result of a chain of oxidation reactions, a wide range of organic molecules also containing in their structure heteroatoms can be mineralized to inorganic species: carbon to CO_2, hydrogen to H_2O, nitrogen to nitrate, sulfur to sulfates, and phosphorus to phosphate.

Contamination of wastewater is a very important environmental problem and many studies have been carried out with the aim to remove the most common pollutants by photocatalytic reactions: dyes [36, 48, 52, 64, 78, 79], pesticides and herbicides [51, 80, 81], pharmaceutical compounds [10, 82–84], hormones [85], and various toxic organic molecules [86–89].

In order to resolve the problem of the environmental effects of gaseous emissions from industries and other human activities, photocatalytic air treatments were also reported as a promising field of application of these processes. Several VOCs, such as MTBE [30], toluene [61, 90–92], bromomethane [56], benzene [47, 93], and formaldehyde [71], were successfully degraded by photocatalytic processes.

In the previous years, the purification property of the TiO_2 was exploited in building materials not only at laboratory levels but also in concrete structures for maintaining their esthetic characteristics, such as the church Dives in Misericordia in Rome (Italy), l'Ecole de Musique' in Chambéry (France), and the Marunouchi Building in Tokyo (Japan).

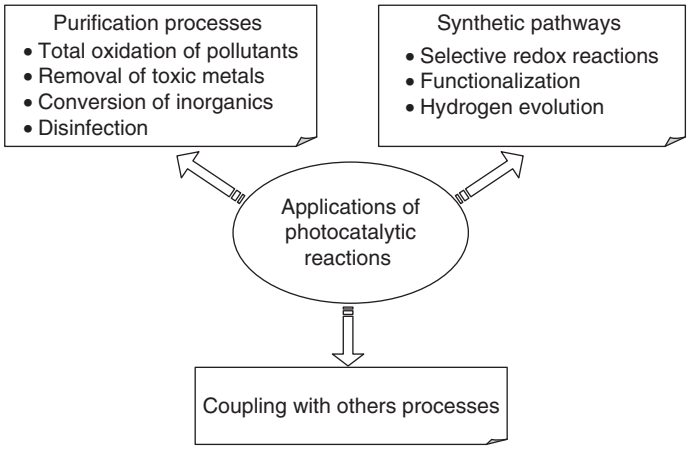

Figure 2 Main photocatalytic applications reported in the literature.

3.07.4.1.2 Removal of toxic metal ions

Metal ions are generally nondegradable and toxic in specific valence states. The reduction by semiconductor photocatalytic processes is a relatively new technique that can be used to change the hazardous ionic states of dissolved metal ions in wastewater [94].

The application of the photocatalytic reduction is reported to be effective to remove various toxic metal ions, such as Cr(VI) [73, 95–97], Hg(II) [98], and Pd(II) [77]. The reduction of such metals results not only in pollution prevention but also in recovery and reuse of valuable metal products with environmental and economic concerns, respectively.

Further investigations combined the reduction of metallic ions with the simultaneous degradation of organic contaminants achieving a synergic effect. Redox reactions were used in the literature for the purification of aqueous systems containing contaminants such as Cr(VI) and bisphenol A [74], Fe(VI) and ammonia [99], Cr(VI) and azodyes [100], and Ag(I) and dyes [40].

3.07.4.1.3 Conversion of inorganic contaminants

Photocatalytic processes have been exploited also for the conversion of other potentially toxic inorganic ions and molecules in the corresponding harmless forms.

In this context, photocatalytic reactions are reported in the literature to reduce bromate ions to Br^- [15], nitrite and nitrate to ammonia and nitrogen [76, 101], or to oxidize sulfite, thiosulfate and sulfide ions into innocuous SO_4^{2-} ions, PO_3^{3-} into PO_4^{3-}, or CN^- into NO_3^- [7, 102].

3.07.4.1.4 Antimicrobial and antitumor activity

Interesting recent researches investigated the possibility to use the photogeneration of active oxygenated radicals to attack the cell membrane of microorganisms and to cause their inactivation. The antimicrobial activity of UV-irradiated photocatalyst has been tested against several types of bacteria, yeasts, algae, and viruses [103–106].

Besides, the cytotoxicity of photocatalysis was also tested in the previous years for cancer treatment. Cai *et al.* [107], in a study on the effects of photoexcited TiO_2 particles on HeLa cells cultured *in vitro*, observed a complete cell death in the presence of TiO_2 (50 μg ml^{-1}) with 10-min UV irradiation. The antineoplastic photocatalytic effect was widely investigated by Fujishima *et al.* [108] by *in vitro* experiments which confirmed the inhibition of the tumor growth. They developed a device, built by modifying an endoscope, in order to access various parts of the human body. These studies extended, therefore, the application of photocatalytic processes to the medical field.

3.07.4.2 Synthetic Pathways

3.07.4.2.1 Selective oxidations and reductions

Due to the highly unselective reactions involved in the photocatalytic processes, the application of this technology was addressed mainly to the treatment of hazardous compounds in liquid and gas phases. However, it was widely demonstrated that selecting or modifying some photocatalytic parameters, such as the semiconductor surface or the wavelength, it is possible to control the reaction obtaining a better selectivity toward some products. On this basis, photocatalysis could represent an alternative synthetic route able to satisfy several of the principles of green chemistry. Several studies reported the selective oxidation of hydrocarbons in aqueous and organic phase [31, 109–113].

In a study on the partial photocatalytic oxidation of different benzene derivates, Palmisano *et al.* [112] demonstrated how the substituent groups can affect the selectivity to hydroxylated compounds. In particular, they observed that organic molecules containing an electron-withdrawing group (cyanobenzene, nitrobenzene, benzoic acid, etc.) were unselectively converted in a mixture of monohydroxy derivates, while in the presence of an electron donor group (phenol, phenylamine, *N*-phenylacetamide) the attack of OH radicals was selective in the *ortho* and *para* positions.

Park and Choi [114], studying the photocatalytic conversion of benzene to phenol, showed the possibility to enhance the phenol production yield and selectivity adding Fe^{3+} or/and H_2O_2 to the TiO_2 suspension or modifying the catalyst surface by deposition of Pt nanoparticles (Pt/TiO_2).

Gondal *et al.* [115] studied the photocatalytic activity of different semiconductor catalysts for the conversion of methane into methanol at room temperature in the aqueous solution. They observed a percentage conversion of 29%, 21%, and 20% using WO_3, TiO_2, and NiO, respectively. This selective oxidation reaction was also investigated by Taylor [31] using a lanthanum-doped tungsten oxide. They observed an increase in the methanol production

when an electron transfer reagent (hydrogen peroxide) was added to the solution. Moreover, selective photooxidation reactions were also reported to convert alcohols to carbonyls [116–118].

Palmisano *et al.* [118] studied the selective oxidation of 4-methoxybenzyl alcohol to *p*-anisaldehyde in organic-free aqueous TiO_2 suspensions, obtaining a considerable yield of 41.5% mol. The homemade photocatalysts were obtained under mild conditions and showed to be more selective than two common commercial samples, that is, TiO_2 Degussa P25 and Merck. Nevertheless, although the reported findings are very intriguing in the light of the possibility to potentially synthesize fine chemicals in green conditions, it should be highlighted that the initial alcohol concentration used in this work (~1.1 mM) is quite low in comparison with that used for typical organic syntheses.

Colmenares *et al.* [27] reported the use of different metal-doped TiO_2 systems for the gas-phase selective photooxidation of 2-propanol to acetone. They observed that doping the catalyst with Pd, Pt, or Ag caused an increase in molar conversion as compared to bare-TiO_2, whereas the presence of Fe and Zr had a detrimental effect.

Although the reduction ability of the CB is lower than the oxidizing power of the VB hole, several studies on the photocatalytic reduction of chemicals are reported in the literature to convert nitrobenzene compounds to the corresponding amino-derivates [69, 119–121], carbonate to methane and methanol [122–125].

3.07.4.2.2 Functionalization

In the previous years, many efforts have been made on the use of photocatalytic synthesis for the functionalization of organic compounds in various solvents, and several interesting results are reported in the literature. Photocatalyzed reactions were used to obtain dihydropyrazine by cyclization of propylene glycol with ethylenediamine [126], carbamate by carbonylation of *p*-nitrotoluene with EtOH [127], the monooxygenation and/or chlorination of cycloalkenes [75], monobrominated derivates from phenol and anisole [128], the addition of tertiary amines to alkenes [129], unsaturated amines adding cyclopentene and cyclohexene to imines [130], heterocyclic aldehydes by the reaction between heterocyclic bases and ethers [131], and propan-1-thiol by addition of H_2S on propene.

Moreover, the wide potentiality of photocatalysis was also applied for the transformation of functional groups such as selective cyclization of amino acids in aqueous suspensions [132, 133] or for the production of a coumarin compound from phenanthrene in an acetonitrile solution containing 8 wt.% water [134].

3.07.4.2.3 Hydrogen evolution

Hydrogen is considered as an attractive alternative energy source because it is a clean, storable, and renewable fuel that does not produce pollutants or greenhouse gases upon combustion. About 95% of the commercial hydrogen is produced from fossil fuels, such as natural gas, petroleum, and coal, although it may also be extracted from water via biological production or using electricity or heat. Therefore, the development of less expensive methods of bulk production of hydrogen represents an interesting field of scientific research.

Photocatalytic systems can offer a cleanest way to produce hydrogen; starting from 1972 when Fujishima and Honda [1] reported the photoelectrochemical hydrogen production using TiO_2 as catalyst, many studies have been performed in order to improve this reaction. Photocatalytic water splitting is a reaction in which water molecules are reduced by the electrons to form H_2 and oxidized by the holes to form O_2, using semiconductor materials. TiO_2 represents the main photocatalyst used in the literature for hydrogen evolution [26], although Kudo [135] demonstrated that other semiconductor materials, such as $Pt/SrTiO_3$, codoped with Cr and Sb or Ta, $Pt/NaInS_2$, $Pt/AgInZn_7S_9$ and Cu- or Ni-doped ZnS photocatalysts, showed high activities for the H_2 production from aqueous solutions under visible light irradiation.

Besides, other photocatalytic approaches were reported to produce hydrogen by reduction of ethanol aqueous solutions [28] or methanol solutions [72].

Moreover, Tan *et al.* [136, 137] reported an interesting work on the conversion of carbon dioxide with water into hydrogen and methane. This system could contribute to the control of CO_2 emission from industrial processes allowing, contemporarily, one to obtain interesting industrial products.

3.07.4.3 Photocatalysis Coupled with Other Technologies

An interesting application of photocatalysis, especially in the field of wastewater treatment, results from its coupling with other technologies, which exploited the synergistic effects to reduce the reaction time and to increase the efficiency of the overall process.

In the literature, several hybrid systems were obtained combining photocatalysis with chemical or physical operations [16]. A positive influence on the photocatalytic mechanism was achieved coupling photocatalysis with chemical operations such as ozonation [138–140], photo-Fenton reaction, ultrasonic irradiation [141], or electrochemical treatment.

When coupling is with methods such as biological treatment [142, 143], physical adsorption, or membrane systems [10, 89, 144, 145], the combination does not affect the mechanisms but increases the efficiency of the whole process.

These hybrid processes offer a good strategy to achieve a better wastewater treatment, particularly when photocatalysis is exploited to transform recalcitrant pollutants in nonrecalcitrant molecules which subsequently can be easily degraded by the conventional methods.

3.07.5 Potentials and Limits of the Photocatalytic Processes

Based on the considerations reported in the previous sections, heterogeneous photocatalysis can be considered as an attractive green process because it is effective to abate noxious species present in gaseous and aqueous effluents. More recently, this process was also shown to be useful to synthesize various types of industrially relevant chemicals, although in this case suitable selective photocatalysts should be chosen and few works have been carried out using only water as the solvent.

Several advantages related to the use of the photocatalytic processes for degradation purposes can be listed as follows:

1. possibility to be applied to a wide range of compounds in aqueous, gaseous, and solid phase;
2. short reaction times and mild experimental conditions, usually ambient temperature and pressure;
3. generally only oxygen from air without any additional additive is necessary;
4. effectiveness also with low concentration of pollutant(s);
5. possibility to destroy a variety of hazardous molecules with the formation of innocuous products, solving the disposal pollutant problem associated to the conventional wastewater treatment methods;
6. possibility to convert toxic metal ions in their nontoxic forms which can be recovered and reused;
7. synergistic effect(s) when coupled with other technologies; and
8. possibility to use sunlight.

Nevertheless, the application of photocatalytic process at industrial level is limited by different drawbacks related to the involved reactions and reactor configuration.

The development of photocatalytic systems requires the knowledge of kinetic models which include all the parameters influencing the process and allow one to plan a reactor useful for industrial applications.

As previously described, the radical reactions which occur in a photocatalytic process are highly unselective and very fast. When the purpose is to employ photocatalysis as synthetic pathway, it is important to control reaction kinetics in order to avoid secondary reactions which lead to undesirable products and reduce the yields of the process. In this respect, in the previous years, many efforts have been made with the aim to obtain more selective reactions modifying the classical semiconductor materials or synthesizing new photocatalysts.

On the contrary, regarding the reactor configuration, as observed by Choi [21], few studies have been performed for the design of efficient photoreactors for commercial exploitation. In particular, one of the main drawbacks takes into account the recovery of the catalyst and/or the separation of the products from the reactive environment.

For what concerns the catalyst, two operative configurations can be identified: catalyst suspended or catalyst immobilized on a support.

In the immobilized system, the catalyst can be coated on the walls of the reactor, supported on a solid substrate or deposited around the case of the light source, using supported materials such as alumina, zeolite [113, 146], AC [58, 59], silica support [11, 103, 147], glass beads [55, 56], and polymeric membranes [60, 70, 104, 148].

Several advantages are reported in the literature on the use of immobilized systems. For example, in a study on the photodegradation of 4-acetylphenol, Sobana *et al.* [58] observed that AC-zinc oxide catalysts showed a much more higher adsorption and photodegradation rate than bare ZnO due to a higher adsorption of the substrate on the AC. Besides, Xu *et al.* [41], studying the performance of several F-doped TiO_2 films, demonstrated that the photocatalytic activity of the prepared photocatalyst film almost remains the same after 3 times reusing, with a little decline after six cycles.

Another immobilized system was proposed by Tsuru *et al.* [149] for the gas-phase photocatalytic degradation of volatile organic pollutants using methanol as target molecule. In this study the TiO_2 catalyst was immobilized in a porous membrane and the permeate stream was oxidized with OH radicals after one-pass permeation through the TiO_2 membranes. Comparing the reaction rate using the PMR with that without the membrane permeation at various reaction conditions (residence time and feed concentration), an enhanced performance of photocatalytic reaction for the first system was observed.

Thus, the possibility to exploit the synergistic effects obtained with particular support, to recover the catalyst without additional separation steps and to design continuous flow photoreactors, makes the immobilized systems interesting for industrial application.

Nevertheless, as widely demonstrated in the literature [57, 81, 150–152], the suspended systems seem to be more efficient than those based on immobilized catalysts.

This evidence can be explained considering that heterogeneous catalysis is a surface phenomenon; therefore, the overall kinetic parameters depend on the real exposed catalyst surface area. In the supported systems, only a part of the photocatalyst is accessible to light and substrate. Besides, the immobilized catalyst suffers from the surface deactivation since the support could enhance the recombination of photogenerated electron/hole pairs and a limitation of oxygen diffusion in the deeper layers is observed.

Another important aspect which reduces practical application of photocatalytic process is the selective separation of the products or/and intermediates from the reactive environment. Separation systems such as distillation or precipitation can be useful to separate the final mixture; however, these techniques, involving further treatment steps, do not allow one to operate in continuous mode.

On this basis, more efforts in photocatalytic engineering and reactor development are required to realize an efficient photocatalytic reactor.

3.07.6 PMRs with Suspended Catalyst

3.07.6.1 Introduction

In a photocatalytic slurry reactor the recovery of the unsupported catalyst from the treated solution is one of the key challenges for large-scale application.

A very promising approach to overcome this and the other photocatalytic drawbacks (mentioned earlier) is the use of hybrid systems in which photocatalysis is coupled with a membrane module [144, 153–155].

In a PMR a synergistic effect can be obtained combining the advantages of classical photoreactors (catalyst in suspension) and those of membrane techniques (one-step separation).

A membrane process is a physical separation technique which does not involve a phase change and allows one to operate in continuous mode. When a suitable membrane is coupled to the photocatalytic process, it is possible not only the recovery and the reuse of the catalyst, but also the separation of the treated solution and/or of the reaction products.

Therefore, the choice of the membrane module configuration is mainly determined by the type of photocatalytic reaction and the membrane can assume many roles in the system, as catalyst recovery, separation of the products, rejection of the substrate, etc.

Moreover, membrane photoreactors allow operation in continuous systems [83] in which the reaction of interest and the selective separation of the product(s) simultaneously occur, avoiding in some cases the formation of by-products, resulting competitive with other separation technologies for what concerns material recovery, energy costs, reduction of the environmental impact, and selective or total removal of the components [156].

Interesting solutions involving the use of a membrane to enhance the performance of the photocatalytic processes have been proposed by several authors, although the few works in the literature demonstrate that the research on the PMRs is not sufficiently developed yet.

3.07.6.2 Variables Influencing the Performance of PMRs

From a practical point of view, the selection of the appropriate operative conditions is of critical importance to obtain a good performance of the PMR.

In the development of a PMR, it is important to take into account some parameters that influence the performance of the system and its applicability at industrial level.

The main purpose in the combination of a membrane process with a photocatalytic reaction is the necessity to recover and to reuse the catalyst. Moreover, when the process is used for the degradation of organic pollutants, the membrane must be able to reject the compounds and their intermediate

products, while if photocatalysis is applied to a synthesis, often the role of the membrane is the separation of the product(s) from the reaction environment.

In the former case, a useful parameter which expresses the ability of the membrane to maintain the substrate and its intermediates in the reactive environment is the rejection (R) or retention coefficient, defined as

$$R = \frac{C_f - C_p}{C_f} = 1 - \frac{C_p}{C_f}$$

where C_f and C_p are the solute concentrations in the feed and permeate, respectively.

High rejection values can be achieved when membranes with pore size smaller than the size of the molecules to be retained are used. Moreover, it is possible to increase the retention of the substrates by controlling other factors that can influence the separation properties of a membrane, such as the pH, the residence time of the substrates, and the concentration polarization phenomena.

In particular, some membranes can become electrically charged changing the pH and this property can be exploited to retain in the reactive environment molecules that otherwise can pass freely in the permeate. Thanks to Donnan effects, in fact, repulsive or attractive interactions between the substrate molecules and the membrane surface may occur if the charges are of the same or of different sign, respectively. In this condition, repulsive interactions increase rejection values, whereas attractive ones decrease them.

The residence time of substrate in the photocatalytic system is another important factor which influences the efficiency of photodegradation. Longer retention times, obtained reducing the permeate flux, resulted in a better organic removal [155]. This aspect can be explained considering that a longer residence time allows a greater contact between the molecules to be degraded and the catalyst.

However, since the PMR must be able to offer an high water permeate flux, it is important to find a good compromise among the permeate flux and the residence time in order to achieve a system for application purpose.

In a pressure-driven membrane process, the rejection phenomenon allows one to obtain a permeate in which the concentration of the substrate results lower than that in the retentate. Nevertheless, when an accumulation of excess particles takes place at the membrane surface, with the formation of a boundary layer, the concentration polarization occurs which causes a different membrane performance. Solutes with low molecular weight, deposited on the membrane, pass in the permeate leading to negative rejection values. Moreover, the layer deposited on the membrane surface increases the resistance to solvent flow and, therefore, reduces the permeate flux. This problem can be reduced generating a turbulent flow on the membrane surface which avoids or minimizes catalyst and drug deposition.

When the membrane is used to separate one or more products, it is more convenient to express the performance of the system in terms of a selectivity factor (α). For a mixture consisting of two components A and B, with concentrations in the retentate x_A and x_B and in the permeate y_A and y_B, respectively, $\alpha_{A/B}$ is given by

$$\alpha_{A/B} = \frac{y_A/y_B}{x_A/x_B}$$

In this case, the selectivity of the membrane toward the products becomes an important aspect of the separation process. The membrane must be able not only to selectively and quickly separate the product of interest, avoiding secondary reactions that would cause the formation of undesirable by-products, but also to maintain in the reactive ambient the catalyst and the other photocatalytic products.

3.07.6.3 Types of PMRs

Various types of membrane photoreactors were realized with the purpose of having an easy separation of the catalyst from the reaction environment and an efficient removal of pollutants from water and air.

In this section, some of the most recent studies on PMRs reported in the literature, divided on the base of the membrane module configuration used for the separation, are presented.

3.07.6.3.1 Pressurized membrane photoreactors

In the literature, the most studied configurations of membrane photoreactors were pressurized systems in which pressure membrane techniques, such as nanofiltration (NF), ultrafiltration (UF), and microfiltration (MF), were combined with a photocatalytic process. In these systems the catalyst, used both in the suspended configuration and immobilized on the membrane, is confined in the pressurized side of the permeation cell.

The first works reported in the literature [153, 156, 157] were performed with the aim to choose a

useful membrane material, stable in the reactive environment, and to identify the variables influencing the performance of the membrane photoreactor.

Molinari *et al.* [150] studied the performance of various photocatalytic membrane systems in the degradation of 4-nitrophenol using TiO_2 as catalyst. In particular, two configurations were investigated in which the irradiation source was placed on the recirculation tank or on the cell containing the membrane. Moreover, in the last configuration the efficiency of the process was investigated with the catalyst suspended, coated, or included in the membrane. Although the system in which the membrane was used only as a support for the catalyst showed a good synergy between the photocatalytic and the separation process, the configuration with the suspended catalyst and the irradiation of the recirculation tank turned out to be more interesting in terms of irradiation efficiency and membrane permeability, allowing also to select the membrane type depending on the photocatalytic process under study.

Further studies [158] demonstrated that the rate of pollutant photodegradation was strongly affected by the UV irradiation mode. By comparing the results obtained in two types of photoreactors, with external lamp and with immersed lamp, it was observed that the rate of photodegradation with the immersed lamp resulted 3 times higher than that of suspended one, although the power of the last was 4 times greater.

To solve the limitations of membrane technology in water treatments, due to membrane fouling caused by solute content in wastewater, Shon *et al.* [89] proposed an integrated photocatalysis – MF hybrid system in which photocatalytic reactions were exploited with the aim to photooxidize partially or completely the organic species that gave rise to the membrane fouling.

However, one of the major problems observed with pressurized flat sheet membrane systems is the membrane flux decline due to catalyst deposition and membrane fouling [10, 83, 159, 160].

Choo *et al.* [161], using an integrated photocatalysis/hollow fiber MF system for the degradation of trichloroethylene in water, observed that the membrane permeability was strongly affected by hydraulic conditions. In particular, they reported a reduction of permeability decreasing the cross-flow velocity due to deposition of TiO_2 particles on the membrane surface, leading to membrane fouling.

Therefore, this drawback, which makes the pressurized systems unsuitable for industrial applications, addressed the research toward the use of other configurations of membrane photoreactors.

3.07.6.3.2 Submerged (depressurized) membrane photoreactors

In the previous years, several studies were performed using submerged membrane modules coupled to photocatalytic systems for the removal of organic pollutants such as fulvic acid [162], bisphenol-A [155].

In the submerged membrane photocatalytic reactor (SMPR), the catalyst is suspended in an open-air reaction environment, the membrane is immersed in the batch and the permeate is sucked by means of a pump.

Fu *et al.* [162] studied the degradation of fulvic acid by using synthesized nanostructured TiO_2/silica gel catalyst particles in a submerged membrane photoreactor. They investigated the effects of some operative conditions, such as catalyst concentration, pH, and airflow on the performance of the overall process and demonstrated that a reduction of membrane fouling, and therefore, an improvement of the permeate flux rate, can be obtained using nanostructured TiO_2. This synthesized catalyst has an average particle size of 50 μm, which resulted small enough for the suspension, but big enough to avoid membrane fouling and to allow its easy separation.

Moreover, it is possible to prevent catalyst deposition and to reduce the membrane fouling which causes the membrane flux decline by controlling the hydrodynamic conditions near membrane surface. A useful strategy in this context is gas sparging at the bottom of the membrane [163, 164].

The efficiency of a hybrid system, combining a low-pressure submerged module in direct contact with the photocatalytic environment, was studied by Chin *et al.* [155] for the removal of bisphenol-A in water. In particular, studying the factor affecting the performance of the SMPR, they observed that the aeration, allowing a mechanical agitation, reduces the fouling of the membrane and keeps the TiO_2 well suspended in the solution, acting also on the size of catalyst aggregates. However, beyond an aeration of 0.5 l min^{-1} no enhancement of photodegradation rate was achieved, probably due to the presence of bubble clouds that could attenuate UV light transmission in the photoreactor.

Besides, in this study the effect of another strategy was investigated; an intermittent permeation method was applied in order to reduce membrane fouling, thus maintaining high flux at low aeration rate.

When suction is stopped, the aeration can shear the membrane surface facilitating the detachment of

catalyst particles and, therefore, avoiding their accumulation on the membrane.

The advantages of this approach were also investigated by Huang *et al.* [165] in a study on the operational conditions of SMPR, in which it was demonstrated that the sedimentation of the suspended catalyst can be controlled by applying fine-bubble aeration and an intermittent membrane filtration.

An intermittent operative procedure was also employed by Choi [21] in a work on the performance of submerged membrane photoreactors for 4-chlorophenol (4-CP) degradation. A pilot-scale photocatalysis-membrane hybrid reactor was constructed and characterized in terms of degradation efficiency and degree of membrane fouling. A complete degradation of the pollutant was achieved in 2 h and, in continuous runs, no fouling of the membrane was observed when an intermittent operation was used.

A common drawback reported when ultrafiltration or MF membrane in the described SMPR is used is the low rejection of compounds with small molecular weight, although high fluxes and good removal efficiency of organic molecules were obtained.

To overcome this problem, Choi *et al.* [166] proposed the use of NF submerged membranes in a bioreactor for domestic wastewater treatment. The NF cellulose acetate membrane used in this work allowed one to achieve a very good-quality permeate for a long-term operation, with a DOC concentration in the permeates which remained in the range 0.5–2.0 mg l^{-1} for the first 130 days.

Nevertheless, after 80 days, the relative flux of the NF membrane increased gradually and the transmembrane pressure decreased, probably due to the hydrolysis of the cellulose acetate in wastewater which, increasing the pore size and porosity, caused a deterioration of permeate quality.

3.07.6.3.3 Photocatalytic membrane contactors

Other types of membrane separation processes that can be useful when they are coupled with a photocatalytic system are the membrane contactors.

In a membrane contactor, the separation performance is determined by the distribution coefficient of a component in two phases and the membrane acts only as an interface. They can be divided in gas–liquid (G–L) and liquid–liquid (L–L) membrane contactors. In the first configuration, one phase is a gas or a vapor and the other phase is a liquid, while in the second one both phases are liquids. Depending on the type of membrane, the membrane phase may contribute to the overall mass transfer resistance.

Several photocatalytic hybrid systems in which the permeation module consists of a membrane contactor are reported in the literature for photodegradation processes, and their potentialities are greater than those of the systems previously described. In fact, they can be a useful solution to separate the product(s) of interest during a photosynthetic process and in particular, if a suitable membrane and a proper strip phase are chosen, it is possible to obtain a selective separation of the product(s) before the secondary reactions occur. Despite the advantages of these integrated systems, to our knowledge, in the literature few studies report the use of a membrane contactor module coupled to photocatalytic synthetic pathways [144, 145, 167].

Photocatalysis and direct contact membrane distillation. To solve the problems observed with pressure-driven membrane reactor, a useful alternative PMR was proposed by Mozia *et al.* [167] studying the photodegradation of azo dyes in aqueous solutions using a membrane distillation module to separate distilled water and TiO_2 Aeroxide® P25 as photocatalyst.

The separation in a membrane distillation process is based on the principle of vapor–liquid equilibrium; therefore ions, macromolecules, cells, and other nonvolatile components are retained on the feed side, whereas the volatile components are separated by means of a porous hydrophobic membrane and then condensed in cold distillate (distilled water).

The results reported in these studies showed a complete rejection of the dye and other nonvolatile compounds (organic molecules and inorganic ions); thus, the permeate was practically pure water. Some volatile compounds passed through the membrane, as indicated by TOC measurements in the distillate, although their concentration remained in the range of 0.4–1.0 mg l^{-1}. Moreover, it was found that the addition of TiO_2 (concentrations 0.1, 0.3, and 0.5 mg dm^{-3}) to the feed solution did not affect the permeate flux at least in the range investigated, which was about 0.34 $m^3\,m^{-2}\,d^{-1}$, similarly to those obtained during the process in which ultrapure water was applied. This last aspect is very interesting because it avoids the significant fouling observed with pressure-driven membrane processes, although the

higher energy consuming constitutes a disadvantage in terms of process costs.

Photocatalysis and pervaporation system. To reduce the heating cost of the solution needed to perform a separation with a membrane distillation module, an approach could be to combine photocatalysis with pervaporation. In pervaporation, the separation is not only based on the relative volatility of the components in the mixture, but only depends on the relative affinity of the components for the membrane. Keeping a vacuum on the permeate side of the membrane and maintaining the feed side at atmospheric pressure, a pressure difference is created which results in the driving force of the process. In this case, therefore, the choice of the membrane material is important to obtain a selective separation of the molecules.

Camera-Roda and Santarelli [145] proposed an integrated system in which photocatalysis is coupled with pervaporation as process intensification for the photocatalytic degradation of 4-CP in aqueous solutions. The aim of this work was to remove the intermediate organics formed in the first steps of the photodegradation of 4-CP which negatively affect the reaction rate, hindering the mineralization of the pollutant. To serve this purpose, organophilic pervaporation membranes were used so that most of the organic oxidation by-products permeated preferentially with respect to water.

Dialysis – photocatalysis. Another interesting separation approach was described by Azrague *et al.* [144] that proposed a particular type of membrane contactor photoreactor in which a dialysis membrane (used as a contactor) was combined with a photocatalytic system for the depollution of turbid waters. This study was addressed to solve the problem of light scattering observed when solid particles are present in the solution which decrease the rate of photocatalytic degradation of pollutant in water. On this basis, the membrane dialysis module was used to keep the solid particles in their initial compartment and, contemporarily, to concentrate the pollutant, thanks to a different concentration, on the other side of the membrane where the photocatalytic reaction took place until total mineralization. Since the separation occurs thanks to a diffusion of the pollutant through the membrane, no transmembrane pressure is needed, avoiding the fouling of membrane which is an expensive problem in case of pressure-driven membrane processes.

3.07.6.4 Future Perspectives: Solar Energy

As previously described, many studies have been performed with the purpose to develop photocatalyst and photocatalytic systems able to exploit the sun as a source of light [168, 169]. Solar energy is important for achieving sustainable processes because it constitutes a renewable, cheap, and clean energy source.

Although the use of sunlight makes the PMRs promising in industrial and environmental fields, very few studies were documented in the literature in this regard.

A hybrid system consisting of a solar photoreactor with the catalyst suspended coupled with a membrane reactor was reported by Augugliaro *et al.* [82] in a study on the photodegradation of lincomycin. The photooxidation experiments were carried out using compound parabolic collectors (CPCs), installed at the Plataforma Solar of Almerìa (PSA, Spain).

By means of some preliminary tests performed without the membrane, it was determined that photooxidation rate of lincomycin followed a pseudo-first-order kinetics with respect to the substrate concentration under the experimental conditions used. The high membrane rejection values measured for lincomycin and its degradation products demonstrated that the hybrid system allowed the separation of these species and also of the photocatalyst particles, although in the experiments carried out in continuous mode, an accumulation of organic molecules was observed in the system. This finding, which was dependent on solar irradiance and initial lincomycin concentration, can be explained by considering that the amount of photons entering the system was not sufficient to mineralize the organic carbon fed in the photoreactor.

Moreover, the experimental results obtained in the continuous mode showed that the presence of the membrane allowed reducing both the substrate and intermediates down to very low concentration levels, proving that the hybrid system could be very interesting from an economic point of view.

The photodegradation of pesticides in a solar pilot-scale photocatalytic system coupled to a separation process was also reported by Malato *et al.* [170]. In this work, performed also at the Plataforma Solar de Almerìa, the TiO_2 recycling was realized by an accelerated sedimentation process, while the treated clean water was discharged through a MF membrane to remove any small remaining catalyst residue.

3.07.7 Outline on Kinetic Models in Heterogeneous Photocatalytic Reactions and Modeling of Membrane Photoreactors

3.07.7.1 Introduction

The development of fundamental kinetic models represents an important topic in the field of photocatalytic processes because, as emphasized by Ollis [171], the discovered credible rate equations can allow the scale-up or reconfiguration of photocatalyst systems. In fact, one of the problems that hinders the use of this technology at the industrial level is the lack of validated kinetic models that allow the design of appropriate reactors reducing expensive and time-consuming steps required by the traditional empirical methodology for scaling up.

On these bases, Imoberdorf *et al.* [172] reported a kinetic study which predicts with good accuracy the performance of a pilot-scale photoreactor starting directly from laboratory experiments.

The development of a full scale-up procedure employing laboratory kinetic information was presented also by Satuf *et al.* [173] in a study on the photodegradation of 4-CP in a small slurry photoreactor. The kinetic model obtained describes the evolution of 4-CP as well as the formation and degradation of the main intermediate products. The intrinsic kinetic parameters estimated were used to model a bench scale reactor in which the experimental data obtained were in good agreement with the simulation results.

Therefore, knowledge of the reaction mechanism and of the effects of different variables on the reaction rate permits one to obtain a kinetic model which can describe the process independently of the shape and configuration of the reactor allowing the development of a photocatalytic technology for industrial application.

As previously described, the photocatalytic process can proceed through the adsorption of the substrate (S) on the catalyst surface (Cat), although this phenomenon is not a requirement for the reaction since the oxidizing species can diffuse into the bulk and react with the molecules.

When the reaction takes place on the catalyst surface, two consecutive reactions can be written:

$$\mathrm{S} + \mathrm{Cat} \underset{k_{-1}}{\overset{k_1}{\rightleftharpoons}} \mathrm{S-Cat} \tag{1}$$

$$\mathrm{S-Cat} \xrightarrow{k_S} \mathrm{P} \tag{2}$$

In this condition, the rate of the photocatalytic process (r_S) depends on the amount of substrate S adsorbed on the catalyst surface.

3.07.7.2 Adsorption Kinetics

The catalyst fractional site covered by S is expressed by the parameter θ reported as

$$\theta_S = \frac{Q_{\mathrm{ads}}}{Q_{\max}} \tag{3}$$

where Q_{ads} is the amount of substrate adsorbed onto the catalyst ($\mathrm{mol\,g^{-1}}$) and $Q_{\max}$ is the maximum number of molecules that can be adsorbed onto a gram of catalyst (e.g., TiO_2):

$$\theta_{\mathrm{ads}} = \frac{C_{\mathrm{in}} - C_{\mathrm{eq}}}{C_{\mathrm{cat}}} \quad Q_{\max} = \frac{C_{\mathrm{in}}}{C_{\mathrm{cat}}} \tag{4}$$

where C_{in} and C_{eq} are the initial and equilibrium concentrations of substrate ($\mathrm{mol\,l^{-1}}$) and C_{cat} is the amount of catalyst per unit amount of solution ($\mathrm{g\,l^{-1}}$).

θ_S depends on the substrate concentration in the reactive environment and it can be defined (at constant temperature) by the Langmuir adsorption isotherm, when the following assumptions are considered [174]: (1) the number of adsorption sites on the catalyst surface is limited and homogeneously distributed, (2) only one molecule can be adsorbed on a site, (3) the coverage of catalyst in a monolayer, and (4) no interactions occur between the adsorbed molecules. The Langmuir adsorption equation can be derived considering that:

1. the rate of the adsorption step (r_1) is proportional to substrate concentration and to fractional free catalyst sites:

$$r_1 = k_1 C_{\mathrm{eq}}(1-\theta_S) \tag{5}$$

2. the rate of desorption (r_{-1}) depends on the coverage catalyst surface:

$$r_{-1} = k_{-1}\theta_S \tag{6}$$

When Equation (1) reaches the equilibrium condition ($k_S \lll k_1$), r_1 and r_{-1} are equal; therefore,

$$k_1 C_{\mathrm{eq}}(1-\theta_S) = k_{-1}\theta_S \tag{7}$$

thus

$$\theta_S = \frac{k_1 C_{\mathrm{eq}}}{k_{-1} + k_1 C_{\mathrm{eq}}} = \frac{K_{\mathrm{ads}} C_{\mathrm{eq}}}{1 + K_{\mathrm{ads}} C_{\mathrm{eq}}} \tag{8}$$

in which $K_{\mathrm{ads}} = k_1/k_{-1}$ is the Langmuir adsorption constant.

By substituting Equation (3) into Equation (8) the following expression is obtained:

$$Q_{ads} = \frac{Q_{max} K_{ads} C_{eq}}{1 + K_{ads} C_{eq}} \tag{9}$$

The linear transformation of Equation (9) can be expressed as the function $C_{eq}/Q_{ads} = f(C_{eq})$ [174, 175]:

$$\frac{C_{eq}}{Q_{ads}} = \frac{1}{Q_{max} K_{ads}} + \frac{C_{eq}}{Q_{max}} \tag{10}$$

The ordinate at the origin of the straight line obtained is equal to $1/(Q_{max}\ K_{ads})$, whereas Q_{max} can be calculated from the reciprocal of the slope $a = 1/Q_{max}$.

3.07.7.3 Photocatalytic Kinetics

The widely accepted equation used to describe the photocatalytic kinetics is the Langmuir–Hinshelwood (L–H) kinetic model, in which the rate of oxidation is the limiting reaction rate at maximum coverage of catalyst. It is related to the substrate concentration by the parameter θ_S:

$$r_S = -\frac{dC}{dt} = k_S \theta_S = k_S \frac{K_{LH} C}{1 + K_{LH} C} \tag{11}$$

As demonstrated in many studies [11, 151, 174, 176, 177], for diluted solutions in which the substrate concentration is $<10^{-3}$ M, the values of $KLHC \ll 1$ and the L–H equation are simplified to a pseudo-first-order kinetic law with respect to C (Equation (12)). At higher initial substrate concentrations ($C > 5 \times 10^{-3}$ M), $K_{LH}C \gg 1$ and the reaction rate is of apparent zero order (Equation (13)):

$$r_S = k_S K_{LH} C = k_{app} C \tag{12}$$

$$r_S = k_S \tag{13}$$

The dependence of the initial photocatalytic rate on the respective initial concentration (C_0) of substrate can be obtained by the linear form of the L–H model:

$$\frac{1}{r_S} = \frac{1}{k_S} + \frac{1}{k_S K_{LH}} \frac{1}{C_0} \tag{14}$$

By plotting the inverse of the initial rate against the inverse of the initial concentration, a straight line is obtained in which the intercept gives the k_S value and the slope the K_{LH} value.

As reported in several studies [171, 174] a discrepancy between K_{ads} obtained in the adsorption isotherm and K_{LH} obtained from photocatalytic reaction can be observed. This aspect can be explained considering that the photocatalytic process is influenced by various parameters, such as oxygen, formation of by-products, light intensity, number of adsorption sites, reaction mechanism, and changes of electronic properties of catalyst surface under irradiation.

For these reasons, when the kinetic of the photocatalytic process is expressed by the L–H kinetic model, some assumptions must be taken into account.

Since the surface of TiO_2 catalyst is covered with hydroxyl groups and water molecules, they can compete with the substrate for the same active sites [174], Equation (11) should be expressed as

$$r_S = k_S \frac{K_{LH} C}{1 + K_{LH} C + K_w C_w} \tag{15}$$

where K_w is the solvent adsorption constant and C_w its concentration.

However, since the C_w is constant and it is $\gg C$, the part of the catalyst covered by water is unchanged over the whole range of concentration. Therefore, if the other experimental conditions (such as pH, catalyst dosage, photointensity, etc.) are held constant, C is only variable in the initial steps of reactions and the rate can be calculated by Equation (11).

The rate-determining step of the photocatalytic oxidation is the reaction between the OH radicals and the substrate. Augugliaro *et al.* [82] hypothesized that two different types of active sites exist over the catalyst surface. The first ones are able to adsorb the substrate while the others are able to adsorb oxygen molecules that act as electron trap generating OH radicals.

The reaction rate may be written in terms of modified L–H kinetic as

$$r_S = k'' \theta_S \theta_{O_2} \tag{16}$$

in which k'' is the surface second-order rate constant and θ_{O_2} the fractional sites coverages by oxygen:

$$\theta_{O_2} = \frac{K_{O_2} C_{O_2}}{1 + K_{O_2} C_{O_2}} \tag{17}$$

If the oxygen is regularly supplied, it can be assumed that the fractional site coverage by hydroxyl radicals is constant and it can be integrated in the apparent rate constant [11, 176]:

$$r_S = k'' \theta_S \theta_{O_2} = k_{app} \theta_S \tag{18}$$

Another important aspect, which must be taken into account studying the kinetic mechanisms of a photocatalytic process, is the presence in the reactive

environment of other species, mixture, or intermediate by-products, which may interfere in the adsorption and oxidation mechanism of the main substrate.

When n intermediate products are formed during a photocatalytic reaction, the L–H models assume the form [175, 178]:

$$r_S = k_S \frac{K_S C_S}{1 + K_S C_S + \sum_{i=1}^{n} K_i C_i} \tag{19}$$

where K_i is the binding constant of the intermediate products adsorbed onto catalyst surface and C_i their concentration. Assuming that C_i adsorbed can be neglected with respect to C_S and that the binding constants of the intermediates are the same to that of S, $K_{i=1} = K_{i=2} \ldots = K_S$, Equation (19) can be approximated to the L–H model.

The kinetic model of a multicomponent system can be obtained by similar considerations.

Biard *et al.* [147] in a study on the photodegradation rates of a binary mixture of propionic and butyric acids demonstrated that the degradation is inhibited when the two compounds are mixed in comparison to the pure acids due to a competitive adsorption on the catalyst active sites.

When the molecules or their by-products react together (chemical interaction), the proposed L–H kinetic equation is [136, 179, 180]

$$r_{S1} = k_{S1}\theta_{S1}\theta_{S2} = k_{S1} \frac{K_{S1} C_{S1} K_{S2} C_{S2}}{(1 + K_{S1} C_{S1} + K_{S2} C_{S2})^2} \tag{20}$$

If between two (or more) substrates no molecular interactions occur, Equation (20) can be simplified as [147, 181, 182]

$$r_{S1} = k_S\theta_{S1} = k_{S1} \frac{K_{S1} C_{S1}}{1 + K_{S1} C_{S1} + K_{S2} C_{S2}} \tag{21}$$

3.07.7.4 Quantum Yield and Relative Photonic Efficiency

As observed by Xu and Langford [183], modifications in the characteristics and adsorption capacity of the catalyst sites can occur when the surface is irradiated with UV photons, giving rise to different values of adsorption constants in the dark and in the photocatalytic reaction.

As reported in the literature [19, 20], the reaction rate is related to the photon flux ρ by

$$\frac{dC}{dt} = r \propto \rho^n \tag{22}$$

At low light intensities, a linear reaction rate is observed with the photon flux ($n = 1$); nevertheless, by increasing the light intensity a plateau is reached and the rate becomes proportional to the square root of ρ ($n = 1/2$). At very high values of photon flux, the reaction rate obeys zero-order kinetics with respect to light intensity ($n = 0$).

The relation between the rate of reaction and the photon flux can be expressed as quantum yield Φ, equal to the ratio of reaction rate to the theoretical maximum rate of photon absorption [9, 151, 184]:

$$\Phi_S = \frac{dN_S/dt}{d[h\nu]_{inc}/dt} \tag{23}$$

where N_S is the number of molecules converted and $[h\nu]_{inc}$ the incident photon flux.

Its theoretical maximum value is equal to 1 and it can vary with the nature of the catalyst, the experimental conditions, and the reaction considered [11].

As observed by Serpone [184], the measurement of Φ requires the knowledge of the action spectrum in the spectral region of interest for the reaction under investigation. When the action spectrum is unknown, it is preferable to use the quantum efficiency η, defined as the ratio of number of molecules which undergo a given event to the total number of photons absorbed in the spectral region used. This difference takes into account that only the photons actually absorbed induce the photocatalytic process, although in the literature these two parameters are often reported with the same meaning.

Since the rate of photon absorption is very difficult to be assessed due, in particular, to the light scattered by the molecules in the dispersion, we propose another parameter, the photonic efficiency (ζ), defined as the number of reactant molecules transformed or produced divided by the number of photons, at a given wavelength, incident onto the front window of the cell [184]:

$$\zeta = \frac{N_{molecules}(\text{mol s}^{-1})\ \text{transformed/produced}}{N_{photons}(\text{einstein s}^{-1})\ \text{incident inside reactor cell}} \tag{24}$$

To avoid unnecessary errors and to propose a method that could be used to cross-reference experiments independent from the reactor used, several authors [184, 185] used a relative photonic efficiency (ζ_r) which is related to an acceptable standard process.

Moreover, the ζ_r values can be converted into the quantum yield Φ, once a standard quantum yield

$\Phi_{standard}$ (for the given photocatalyst and the given substrate) has been determined by the relation

$$\Phi = \zeta_r \Phi_{standard} \quad (25)$$

Zhang *et al.* [186], in a study on the photocatalyzed N-demethylation and degradation of methylene blue (MB) in TiO_2 dispersions exposed to concentrated sunlight, used the relative photonic efficiency to demonstrate that MB photodecomposition under concentrated sunlight irradiation, measured against phenol, is identical to the efficiency measured under UV radiation, independent of photoreactor geometry, light sources, and operating mode used.

The understanding of these relations is fundamental to compare the activity of different catalysts for the same reaction and to estimate the energetic yield and the cost of the photocatalytic process.

3.07.7.5 Modeling of PMR

Although the membrane photoreactors have great potentialities, very few studies have been performed with the aim to understand the kinetic models influencing the performance of the separation process in these systems.

Model predictions can be used to optimize the performance of the reactor, to design the reactor, and to evaluate the performance of different membranes.

Depending on the photocatalytic reaction involved and on the type of membrane module used, the kinetic model changes its form, and consequently modeling a membrane photoreactor requires knowledge of the kinetic equations of the catalyst, the membrane, and the reactor configuration.

Azrague *et al.* [144] proposed a mathematical model (**Scheme 1**) for a system in which a photocatalytic reactor was combined with a dialysis membrane, used to concentrate organic pollutants from the feed tank in the photocatalytic reactor where they were degraded. By a preliminary study they demonstrated that, starting from the L–H kinetic model, the rate of the photocatalytic degradation followed a pseudo-zero-order kinetics (Equation (a)). Moreover, performing dialysis experiments (without irradiation), they assumed that mass transport of solutes was due to diffusion only and no exchange between the two compartments occurred. The authors described also the variation of concentration in the feed tank and in the reactor by differential equations (Equation (b)).

On these bases, a model based on diffusion through the membrane and zero-order reaction in the reactor was proposed (Equation (c)) for the described PMR. A good agreement with the experimental data, in a wide range of operating conditions, was demonstrated.

Chin *et al.* [155] used pseudo-first-order reaction kinetics combined with the ideal continuous stirrer tank reactor (CSTR) model to evaluate the effect of initial concentration of pollutant on the performance of a SMPR for the degradation of bisphenol-A in water (**Scheme 2**). This CSTR model, which takes

Photocatalytic kinetics

$$C_s = C_s^0 - k_{app}\, t \quad (a)$$

Separation kinetics

$$\frac{dC_s}{dt} = -\psi(C_s - C_a) \qquad \frac{dC_a}{dt} = \omega(C_s - C_a) \quad (b)$$

Modeling of PMR

$$\frac{dC_s}{dt} = -\psi(C_s - C_a) \qquad \frac{dC_a}{dt} = \omega(C_s - C_a) - k_{app} \quad (c)$$

where C_s and C_a are the pollutant concentration in the feed tank and in the photoreactor, respectively; C_s^0 is the initial substrate concentration in the feed tank; k_{app} the apparent zero-order rate constant; t is the irradiated time; $\psi = kA/V_s$ and $\omega = kA/V_a$ are abbreviations without name used to simplify the mathematical expressions; V_s and V_a are the volumes of the solutions in the feed tank and in the photoreactor, respectively; A the membrane area; k the average overall mass-transfer coefficient.

Scheme 1 Modeling of a dialysis membrane photoreactor proposed by Azrague *et al.* [144]

Equation in an isothermal stirred tank reactor

$$C_A - C_{Af} = -kC_A\vartheta$$

Differentiation

$$\frac{dC_A}{dt} = \frac{1}{\vartheta}(C_{Af} - C_A) - kC_A$$

Analytical solution

$$C_A(t) = C_A^0 e^{-(1/\vartheta + k)t} + \frac{C_{Af}}{1 + k\vartheta}\left[1 - e^{-(1/\vartheta + k)t}\right]$$

where C_A is the substrate concentration at time t; C_{Af} the feed concentration; θ is the residence time of substrate.

Scheme 2 Modeling of a submerged membrane photoreactor proposed by Chin *et al*. [155]

into account the importance of the residence time of the organic substrate in the system (assuming the membrane has zero retention of substrate), however, had only limited success. The discrepancies observed among the experimental data were attributed both to the effect of adsorption/desorption of organics on the membrane and to the variation of their rate constants.

3.07.8 Case Study: Partial and Total Oxidation Reactions in PMRS

In this section, some results obtained in our laboratories on the use of PMRs for partial or total photocatalytic reactions are reported and discussed. In particular, the performance of two PMRs for the one-step synthesis of phenol and for the degradation of pharmaceuticals in water are described.

3.07.8.1 One-Step Synthesis and Separation of Phenol in a PMC

Although the great potentiality of photocatalytic processes, especially when they are coupled with a membrane separation system, as above has been discussed, the research in the field of photocatalytic synthesis in a PMR still remains insufficient.

In this context, the aim of this study was to demonstrate the possibility to use a membrane photoreactor for organic synthesis, developing a hybrid system in which the photocatalytic reaction and the separation of the product of interest occurs in one step.

In particular, in this section the preliminary results obtained in a PMC for the one-step synthesis of phenol and its simultaneous separation are reported. TiO_2 has been used as catalyst, benzene as both reactant and extraction solvent, and a polypropylene membrane to separate the organic phase from the aqueous reactive environment.

Phenol is an important chemical intermediate of industrial interest, used as substrate to produce phenolic resins, pharmaceuticals, plastics, and agrochemicals. Its market demand exceeds 7 million tons a year and, actually, more than 90% of its global manufacture is realized by the three-step Cumene process, called also the Kellogg, Brown & Root (KBR) phenol process.

However, the one-step hydroxylation of benzene via green process represents an attractive alternative pathway for the direct synthesis of phenol and many studies have been performed with the aim to develop more efficient and environmentally benign processes.

A direct synthesis of phenol from benzene has been tried by several synthetic pathways [187–190] using also photocatalytic reactions [113, 114]. Nevertheless, the separation of phenol from the reactive environment and the recovery of the catalyst remain the main unsolved drawbacks. Besides, the low selectivity of the process and the higher reactivity of phenol toward the oxidation with respect to benzene lead to formation of oxidation by-products. To avoid these secondary products and to obtain an efficient phenol production, the use of a membrane system, with high phenol permeability and complete rejection to the catalyst, coupled with the photocatalytic process seems a useful solution.

The membrane photoreactor realized in this study consists of an external lamp placed on a batch reactor containing the aqueous solution with the catalyst in suspension; by means of a peristaltic pump the solution is withdrawn from the photocatalytic reactor to a

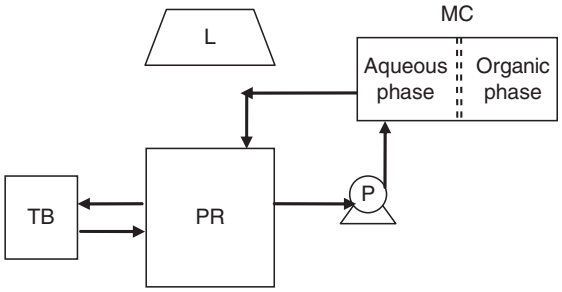

Figure 3 Scheme of the photocatalytic membrane contactor (PMC): PR, photoreactor system; MC, membrane contactor; L, ultraviolet (UV) lamp; TB, thermostatic bath; and P, peristaltic pump.

membrane contactor module in which a benzene solution is present as strip phase (**Figure 3**).

A set of preliminary experiments were performed in order to select the operative conditions to be employed in the batch and membrane systems. Due to the low solubility of benzene in water and to its high volatility, it was observed that there is the necessity to work with an excess of substrate in solution. It is worth noting that tests of photolysis and dark reactions carried out in the absence of the catalyst and UV light, respectively, showed that the oxidation reaction occurs in a true photocatalytic regime.

Batch experiments in the absence of the membrane were performed for determining the influence of some parameters (pH, catalyst concentration, light intensity, etc.) on the efficiency of the photocatalytic reaction.

The results showed that oxidation kinetics did not depend on the undissolved substrate but on its concentration in solution. Reaction rate increased at alkaline pH, due to a lower phenol adsorption onto the catalyst surface which reduced further oxidation reactions. Additional tests showed that oxygen from the surface contacting air did not represent the limiting reagent in our system. Negligible variations of the rate of phenol production were obtained (values ranging between 0.13 and 0.18 mg l^{-1} min^{-1} in the first 100 min) by changing the catalyst amount from 0.1 to 1 g l^{-1}.

A first set of experiments were carried out in the PMC varying the pH of the aqueous phase and investigating the effects of this parameter on the efficiency of the process.

By comparing the data obtained at pH values equal to 5.5 and 3.1, it was observed that the most acidic pH condition allows one to obtain a slightly increase in the phenol production in the aqueous phase (**Figure 4**) and a constant flux in the organic phase after 2 h (1.27 m mol h^{-1} m^{-2}).

Moreover the area of the three main HPLC peaks detected at retention times of 3.0, 3.6, and 3.9 min indicated that the acidic pH enabled to obtain a lower formation and extraction of these intermediates.

Further studies are in progress to enhance the system productivity and its separation efficiency.

3.07.8.2 Photodegradation of Pharmaceutical in PPMR and SPMR

Pharmaceutically active compounds (PhACs) are an important group of toxic organic contaminants that recently has attracted much attention to the international scientific community because of their presence in the aquatic environment. These compounds that reach the aquatic environment as refusals of the hospital structures, pharmaceutical industries, and municipal

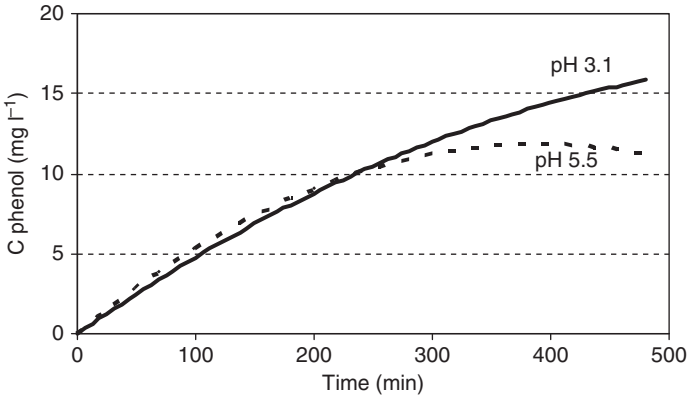

Figure 4 Phenol concentration in the aqueous phase vs. time in the photocatalytic oxidation tests performed in the photocatalytic membrane contactor (PMC) at pH 3.1 and 5.5 (Molinari R. *et al*., unpublished data).

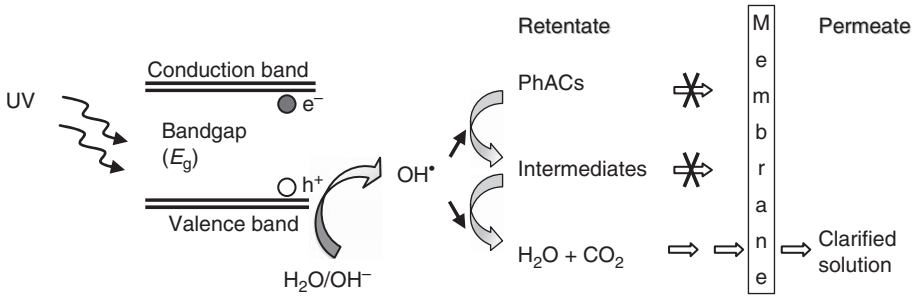

Figure 5 Degradation process in a photocatalytic membrane reactor.

sewage treatment plants are not completely removed during conventional wastewater treatments and are not biodegraded; therefore, they are detectable in the environment with concentration levels up to the $\mu g\,l^{-1}$ [191, 192]. Despite such values are lower than the maximum concentrations found in other industrial contaminants, PhACs are considered among the pollutants which cause greater health risks for humans and members of terrestrial and aquatic ecosystems [193].

Because of the drawbacks of the common purification methods, hybrid systems based on coupling membranes and photocatalysis could represent an useful solution to these problems.

In a PMR, the photocatalytic process allows the complete degradation (mineralization) of the organic molecules in harmless products and, contemporarily, the use of a suitable membrane allows to retain the pollutant and its degradation products in the reaction environment, to recovery and to reuse the photocatalyst and to separate the clarified solution (**Figure 5**).

The aim of this work was to study the use of PMRs for the degradation of the pharmaceuticals Gemfibrozil (GEM) and Tamoxifen (TAM) in water, using TiO_2 as suspended catalyst, investigating the performance of two system configurations of membrane photoreactors (pressurized and depressurized PMRs) [10].

The experimental plant used was an annular photoreactor with an immersed UV lamp connected with the permeation cell where a pressurized flat sheet membrane or a submerged (depressurized) membrane module were located.

Preliminary tests, performed in order to determine the influence of pH and concentration of aqueous suspensions of TiO_2 on particle aggregation and adsorption of organics, suggested a preferable operative pH range of 7 ± 3 and a catalyst concentration of $0.1\,g\,l^{-1}$ (which is an useful condition both from an economic and reaction efficiency point of view) to perform the experiments.

The efficiency of the photocatalytic process for the degradation of the drugs was investigated by photodegradation tests in the batch reactor without the membrane. It was observed that the kinetic trend of Gemfibrozil oxidation did not change by varying the pH in the $1-0.1\,g\,l^{-1}$ range of catalyst concentration, and a complete degradation of the drug was observed after about 20 min.

Another set of experiments was performed in order to characterize the membrane in the pressurized permeation cell in terms of rejection and flux with Gemfibrozil and catalyst solutions. Due to the deposition of the catalyst onto the membrane surface, an increase and a decrease of rejection and flux values was observed, respectively, when the same membrane was used for several runs. This problem was reduced by increasing the tangential flow in the permeation cell and by immersing the membrane, at the end of each run, in an aqueous solution containing an enzymatic detergent (Ultrasil 50) that allowed to reestablish the initial characteristics.

Two different operative procedures were used to investigate the behavior of the pressurized membrane photoreactors: closed and continuous membrane system. In the first one, the permeate was continuously recycled for determining the ability of the membrane to retain the drug and the oxidation products in the reaction ambient. In the second one, the removed permeate was replaced by an equal volume of initial feed drug solution in order to simulate the continuous photodegradation process that could be applied at the industrial level.

The results obtained in the tests performed in the closed membrane system showed that a quick and complete photodegradation of the two selected drugs resulted with a drug abatement of 99% after 20 min and a mineralization higher than 90% after about 120 min. Nevertheless, a small or no rejection to degradation products of both the drugs was evidenced.

The data achieved in the photodegradation tests with GEM solutions performed in the pressurized continuous system, underlined a good system operating stability, reaching steady-state conditions after ~120 min with a complete abatement of the drug and values of mineralization (60%) and permeate flux ($38.6\,l\,h^{-1}\,m^{-2}$) that remained constant until the end of the run. A TOC rejection of about 62% at steady-state conditions suggested to identify a membrane with higher rejection to the intermediate products, in order to maintain almost all of them in the reaction environment for sufficient time to achieve their complete degradation.

In order to solve the problem of membrane flux decline due to catalyst deposition and membrane fouling, observed in the NF membrane photoreactor with the suspended catalyst, the research has been addressed toward the use of a different configuration of membrane module located separately from the photoreactor, the depressurized (submerged) membrane system.

The obtained results showed a drug abatement of 100% after about 20 min and a mineralization of 44.5% after ~150 min in the retentate, but a complete passage of the Gemfibrozil and intermediate products was observed in the permeate.

The comparison of the data obtained in the two configurations of continuous membrane photoreactor (flat sheet and submerged membrane systems) confirmed that the presence of the suspended catalyst allowed a complete degradation of GEM in about 15–20 min and a partial mineralization of the organic intermediates with a TOC value at steady-state conditions in the retentate of about $4.2 \pm 0.7\,mg\,l^{-1}$.

The UF membranes used in the submerged system were not able to reject the drug and its degradation products compared to the NF membranes of the pressurized system that allowed a TOC rejection of (62 ± 5) % (**Figure 6**).

The submerged membrane photoreactor, however, proved more advantageous in terms of permeate flux, with values almost two times greater ($65.1\,l\,h^{-1}\,m^{-2}$) than those measured with the pressurized membranes.

This new configuration of membrane photoreactor in which the submerged membrane module was located separately from the photoreactor and the oxygen was bubbled on the membrane surface could be of interest to separate the photocatalytic zone from the separation zone with a reduction of the plant optimization problems.

Nevertheless, further studies are required to find other types of membranes, as for instance higher rejection NF-type or low rejection reverse osmosis-type membranes, more selective to substrates and intermediate products.

3.07.9 Conclusions

PMRs represent a very promising technology of great research and industrial interest.

The combination of heterogeneous photocatalysis with membrane processes allows one to obtain many advantages in terms of output and costs, thanks to their synergy.

It is well known that heterogeneous photocatalysis can be successfully used to photodegrade or to transform a wide range of molecules in liquid–solid and in gas–solid systems. Nevertheless, the knowledge of fundamentals of photocatalysis is essential to understand the mechanistic aspects and to find the parameters which influence the process under investigation. Moreover, the development of new photocatalysts and their application in the various research fields is a mandatory task.

Some drawbacks due to the use of a single technology can be minimized by coupling them.

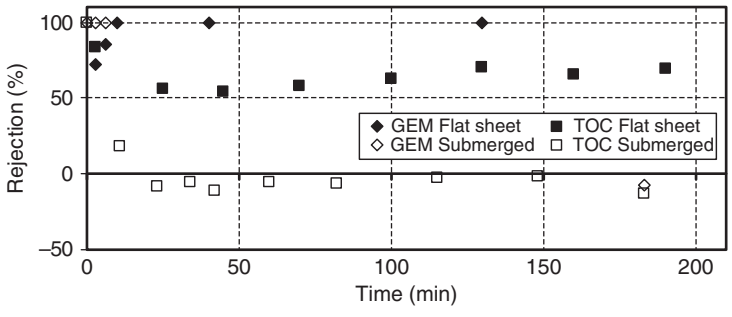

Figure 6 Comparison between flat sheet and submerged continuous photocatalytic membrane reactors (PMRs) for the degradation of Gemfibrozil (GEM).

Membrane processes, indeed, thanks to their selective properties, allow not only to recovery and to reuse the photocatalyst but also to enhance the residence time of the substrates to be degraded or to obtain a selective separation of the products.

The various described configurations of membrane photoreactors can be chosen to influence the performance of the photocatalytic systems and possible solutions can be found to solve some problems such as control of catalyst activity and fouling, selectivity, and rejection of the membrane.

A sustainable process can be obtained when a PMR is used to exploit the sun as a cheap and clean source of light.

Work carried out in our laboratories using PMRs showed the possibility to apply them in processes for total or partial oxidation of organic compounds in water.

PMRs can be considered a useful green system for water purification as well as for organic synthesis, although additional studies are still needed before taking advantage of their potentiality at industrial level.

References

[1] Fujishima, A., Honda, K. *Nature* **1972**, *238*, 37–38.
[2] Poliakoff, M., Licence, P. *Nature* **2007**, *450*, 810–812.
[3] Anastas, P., Warner, J. *Green Chemistry: Theory and Practice*; Oxford University Press: New York, 1998.
[4] Ollis, D. F. C. R. *Acad. Sci. Paris, Serie IIc, Chimie: Chemistry* **2000**, *3*, 405–411.
[5] Anpo, M. *Pure Appl. Chem.* **2000**, *72*, 1265–1270.
[6] Palmisano, G., Augugliaro, V., Pagliaro, M., Palmisano, L. *Chem. Commun.* **2007**, *33*, 3425–3437.
[7] Herrmann, J.-M., Duchamp, C., Karkmaz, M., *et al. J. Hazard. Mater.* **2007**, *146*, 624–629.
[8] Kavita, K., Rubina, C., Rameshwar, L. S. *Ind. Eng. Chem. Res.* **2004**, *43*, 7683–7696.
[9] Hoffmann, M. R., Martin, S. T., Choi, W., Bahnemannt, D. W. *Chem. Rev.* **1995**, *95*, 69–96.
[10] Molinari, R., Caruso, A., Argurio, P., Poerio, T. *J. Membr. Sci.* **2008**, *319*, 54–63.
[11] Herrmann, J.-M. *Top. Catal.* **2005**, *34*, 49–65.
[12] Konstantinou, I. K., Albanis, T. A. *Appl. Catal. B* **2004**, *49*, 1–14.
[13] Bekkouche, S., Bouhelassa, M., Hadj Salah, N., Meghlaoui, F. Z. *Desalination* **2004**, *166*, 355–362.
[14] Robert, D., Malato, S. *Sci. Total Environ.* **2002**, *291*, 85–97.
[15] Noguchi, H., Nakajima, A., Watanabe, T., Hashimoto, K. *Environ. Sci. Technol.* **2003**, *37*, 153–157.
[16] Augugliaro, V., Litter, M., Palmisano, L., Soria, J. *J. Photochem. Photobiol. C* **2006**, *7*, 127–144.
[17] Sýkora, J., Pado, M., Tatarko, M., Izakovič, M. *J. Photochem. Photobiol. A* **1997**, *110*, 167–175.
[18] Brezová, V., Blažková, A., Borošová, E., Čeppan, M., Fiala, R. *J. Mol. Catal. A: Chem.* **1995**, *98*, 109–116.
[19] Emeline, A. V., Ryabchuk, V., Serpone, N. *J. Photochem. Photobiol. A* **2000**, *133*, 89–97.
[20] Brosillon, S., Lhomme, L., Vallet, C., Bouzaza, A., Wolbert, D. *Appl. Catal. B* **2008**, *78*, 232–241.
[21] Choi, W. *Catal. Surv. Asia* **2006**, *10*, 16–28.
[22] Robertson, P. K. J. J. *Cleaner Prod.* **1996**, *4*, 203–212.
[23] Robert, D. *Catal. Today* **2007**, *122*, 20–26.
[24] Liu, X., Li, Y., Wang, X. *Mater. Lett.* **2006**, *60*, 1943–1946.
[25] Di Paola, A., Cufalo, G., Addamo, M., *et al. Colloids Surf. A* **2008**, *317*, 366–376.
[26] Ni, M., Leung, M. K. H., Leung, D. Y. C., Sumathy, K. *Renew. Sust. Energ. Rev.* **2007**, *11*, 401–425.
[27] Colmenares, J. C., Aramendía, M. A., Marinas, A., Marinas, J. M., Urbano, F. J. *Appl. Catal. A* **2006**, *306*, 120–127.
[28] Mizukoshi, Y., Makise, Y., Shuto, T., *et al. Ultrason. Sonochem.* **2007**, *14*, 387–392.
[29] Wang, C.-T. *J. Non-Cryst. Solids* **2007**, *353*, 1126–1133.
[30] Araña, J., Peña Alonso, A., Doña Rodríguez, J. M., Herrera Melián, J. A., Gonzáles Díaz, O., Pérez Peña, J. *Appl. Catal. B* **2008**, *78*, 355–363.
[31] Taylor, C. E. *Top. Catal.* **2005**, *32*, 179–184.
[32] Chen, C., Wang, Z., Ruan, S., Zou, B., Zhao, M., Wu, F. *Dyes Pigm.* **2008**, *77*, 204–209.
[33] Wu, G., Chen, T., Su, W., *et al. Int. J. Hydrogen Energy* **2008**, *33*, 1243–1251.
[34] Kudo, A., Sekizawa, M. *Chem. Commun.* **2000,** 1371–1372.
[35] Egerton, T. A., Mattinson, J. A. *J. Photochem. Photobiol. A* **2008**, *194*, 283–289.
[36] Ge, L. *J. Mol. Catal. A: Chem.* **2008**, *282*, 62–66.
[37] Ling, Q., Sun, J., Zhou, Q. *Appl. Surf. Sci.* **2008**, *254*, 3236–3241.
[38] Sun, H., Bai, Y., Jin, W., Xu, N. *Sol. Energy Mater. Sol. Cells* **2008**, *92*, 76–83.
[39] Peng, F., Cai, L., Yu, H., Wang, H., Yang, J. *J. Solid State Chem.* **2008**, *181*, 130–136.
[40] Wong, M.-S., Hsu, S.-W., Rao, K. K., Kumar, C. P. *J. Mol. Catal. A: Chem.* **2008**, *279*, 20–26.
[41] Xu, J., Ao, Y., Fu, D., Yuan, C. *Appl. Surf. Sci.* **2008**, *254*, 3033–3038.
[42] Kobasa, I. M., Tarasenko, G. P. *Theor. Chem. Acc.* **2002**, *38*, 255–258.
[43] Chen, F., Hua Wua, T., Ping Zhou, X. *Catal. Commun.* **2008**, *9*, 1698–1703.
[44] Li, S., Ma, Z., Zhang, J., Liu, J. *Catal. Commun.* **2008**, *9*, 1482–1486.
[45] Su, W., Chen, J., Wu, L., Wang, X., Wang, X., Fu, X. *Appl. Catal. B* **2008**, *77*, 264–271.
[46] Xia, H., Zhuang, H., Zhang, T., Xiao, D. *Mater. Lett.* **2008**, *62*, 1126–1128.
[47] Xiao, G., Wang, X., Li, D., Fu, X. *J. Photochem. Photobiol. A* **2008**, *193*, 213–221.
[48] Zang, Y., Farnood, R. *Appl. Catal. B* **2008**, *79*, 334–340.
[49] Jana, A. K. *J. Photochem. Photobiol. A* **2000**, *132*, 1–17.
[50] Gurunathan, K. *J. Mol. Catal. A: Chem.* **2000**, *156*, 59–67.
[51] Kuo, W. S., Chiang, Y. H., Lai, L. S. *Dyes Pigm.* **2008**, *76*, 82–87.
[52] Sohrabi, M. R., Ghavami, M. *J. Hazard. Mater.* **2008**, *153*, 1235–1239.
[53] Ortiz-Gómez, A., Serrano-Rosales, B., De Lasa, H. *Chem. Eng. Sci.* **2008**, *63*, 520–557.
[54] Qourzal, S., Barka, N., Tamimi, M., Assabbane, A., Ait-Ichou, Y. *Appl. Catal. A* **2008**, *334*, 386–393.
[55] Chen, Y., Stathatos, E., Dionysiou, D. D. *Surf. Coat. Technol.* **2008**, *202*, 1944–1950.
[56] Huang, J., Wang, X., Hou, Y., *et al. Microporous Mesoporous Mater.* **2008**, *110*, 543–552.
[57] Kansal, S. K., Singh, M., Sud, D. *J. Hazard. Mater.* **2008**, *153*, 412–417.
[58] Sobana, N., Muruganandam, M., Swaminathan, M. *Catal. Commun.* **2008**, *9*, 262–268.
[59] Zhang, X., Lei, L. *J. Hazard. Mater.* **2008**, *153*, 827–833.
[60] Wang, Y. H., Liu, X. Q., Meng, G. Y. *Mater. Res. Bull.* **2008**, *43*, 1480–1491.

[61] Demeestere, K., Dewulf, J., De Witte, B., Beeldens, A., Van Langenhove, H. *Build. Environ.* **2008**, *43*, 406–414.
[62] Du, P., Carneiro, J. T., Moulijn, J. A., Mul, G. *Appl. Catal. A* **2008**, *334*, 119–128.
[63] Bi, J., Wu, L., Li, Z., Wang, X., Fu, X. *Mater. Lett.* **2008**, *62*, 155–158.
[64] Li, X., Ouyang, S., Kikugawa, N., Ye, J. *Appl. Catal. A* **2008**, *334*, 51–58.
[65] Lin, X., Huang, F., Wang, W., Shan, Z., Shi, J. *Dyes Pigm.* **2008**, *78*, 39–47.
[66] Wu, L., Bi, J., Li, Z., Wang, X., Fu, X. *Catal. Today* **2008**, *131*, 15–20.
[67] Amat, A. M., Arques, A., Galindo, F., *et al. Appl. Catal. B* **2007**, *73*, 220–226.
[68] Marais, E., Klein, R., Antunes, E., Nyokong, T. *J. Mol. Catal. A: Chem.* **2007**, *261*, 36–42.
[69] Ahn, W.-Y., Sheeley, S. A., Rajh, T., Cropek, D. M. *Appl. Catal. B* **2007**, *74*, 103–110.
[70] Bonchio, M., Carraro, M., Gardan, M., Scorrano, G., Drioli, E., Fontananova, E. *Top. Catal.* **2006**, *40*, 133–140.
[71] Huang, G., Zhu, Y. *Mat. Sci. Eng. B* **2007**, *139*, 201–208.
[72] Jitputti, J., Suzuki, Y., Yoshikawa, S. *Catal. Commun.* **2008**, *9*, 1265–1271.
[73] Kanthasamy, R., Larsen, S. C. *Microporous Mesoporous Mater.* **2007**, *100*, 340–349.
[74] Liu, Y., Deng, L., Chen, Y., Wu, F., Deng, N. *J. Hazard. Mater.* **2007**, *139*, 399–402.
[75] Maldotti, A., Amadelli, R., Vitali, I., Borgatti, L., Molinari, A. *J. Mol. Catal. A: Chem.* **2003**, *204*, 703–711.
[76] Rengaraj, S., Li, X. Z. *Chemosphere* **2007**, *66*, 930–938.
[77] Troupis, A., Hiskia, A., Papaconstantinou, E. *Appl. Catal. B* **2004**, *52*, 41–48.
[78] Baran, W., Makowski, A., Wardas, W. *Dyes Pigm.* **2008**, *76*, 226–230.
[79] Yang, X., Xu, L., Yu, X., Guo, Y. *Catal. Commun.* **2008**, *9*, 1224–1229.
[80] Lhomme, L., Brosillon, S., Wolbert, D. *J. Photochem. Photobiol. A* **2007**, *188*, 34–42.
[81] Sakkas, V. A., Arabatzis, I. M., Konstantinou, I. K., Dimou, A. D., Albanis, T. A., Falaras, P. *Appl. Catal. B* **2004**, *49*, 195–205.
[82] Augugliaro, V., García-López, E., Loddo, V., *et al. Sol. Energy* **2005**, *79*, 402–408.
[83] Molinari, R., Pirillo, F., Loddo, V., Palmisano, L. *Catal. Today* **2006**, *118*, 205–213.
[84] Yurdakal, S., Loddo, V., Augugliaro, V., Berber, H., Palmisano, G., Palmisano, L. *Catal. Today* **2007**, *129*, 9–15.
[85] Zhang, Y., Zhou, J. L., Ning, B. *Water Res.* **2007**, *41*, 19–26.
[86] Huang, X., Leal, M., Li, Q. *Water Res.* **2008**, *42*, 1142–1150.
[87] Lair, A., Ferronato, C., Chovelon, J.-M., Herrmann, J.-M. *J. Photochem. Photobiol. A* **2008**, *193*, 193–203.
[88] Karunakaran, C., Dhanalakshmi, R. *Sol. Energy Mater. Sol. Cells* **2008**, *92*, 588–593.
[89] Shon, H. K., Phuntsho, S., Vigneswaran, S. *Desalination* **2008**, *225*, 235–248.
[90] Augugliaro, V., Coluccia, S., Loddo, V., *et al.* VOC's Abatement: Photocatalytic Oxidation of Toluene in Vapor Phase on Anatase TiO_2 Catalyst. In *Studies in Surface Science and Catalysis: 3rd World Congress on Oxidation Catalysis*; Grasselli, R. K., Oyama, S. T., Gaffney, A. M., Lyons, J. E. Eds. Elsevier: Amsterdam, 1997, pp 663–672.
[91] Augugliaro, V., Coluccia, S., Loddo, V., *et al. Appl. Cat. B: Environ.* **1999**, *20*, 15–27.
[92] Marcì, G., Addamo, M., Augugliaro, V., *et al. J. Photochem. Photobiol. A* **2003**, *160*, 105–114.
[93] Yan, T., Long, J., Chen, Y., Wang, X., Li, D., Fu, X. *C. R. Chimie* **2008**, *11*, 101–106.
[94] Chen, D., Ray, A. K. *Chem. Eng. Sci.* **2001**, *56*, 1561–1570.
[95] Aarthi, T., Madras, G. *Catal. Commun.* **2008**, *9*, 630–634.
[96] Cappelletti, G., Bianchi, C. L., Ardizzone, S. *Appl. Catal. B* **2008**, *78*, 193–201.
[97] Wang, L., Wang, N., Zhu, L., Yu, H., Tang, H. *J. Hazard. Mater.* **2008**, *152*, 93–99.
[98] Wang, X., Pehkonen, S. O., Ray, A. K. *Electrochim. Acta* **2004**, *49*, 1435–1444.
[99] Sharma, V. K., Chenay, B. V. N. *J. Appl. Electrochem.* **2005**, *35*, 775–781.
[100] Papadam, T., Xekoukoulotakis, N. P., Poulios, I., Mantzavinos, D. *J. Photochem. Photobiol. A* **2007**, *186*, 308–315.
[101] Ranjit, K. T., Krishnamoorthy, R., Varadarajan, T. K., Viswanathan, B. *J. Photochem. Photobiol. A* **1995**, *86*, 185–189.
[102] Augugliaro, V., Loddo, V., Marcì, G., Palmisano, L., López-Muñoz, M. J. *J. Catal.* **1997**, *166*, 272–283.
[103] Coronado, J. M., Soria, J., Conesa, J. C., *et al. Top. Catal.* **2005**, *35*, 279–286.
[104] Rincón, A. G., Pulgarin, C. *Appl. Catal. B* **2003**, *44*, 263–284.
[105] Guillard, C., Bui, T.-H., Felix, C., Moules, V., Lina, B., Lejeune, P. *C. R. Chimie* **2008**, *11*, 107–113.
[106] Kim, B., Kim, D., Cho, D., Cho, S. *Chemosphere* **2003**, *52*, 277–281.
[107] Cai, R., Kubota, Y., Shuin, T., Sakai, H., Hashimoto, K., Fujishima, A. *Cancer Res.* **1992**, *52*, 2346–2348.
[108] Fujishima, A., Rao, T. N., Tryk, D. A. *J. Photochem. Photobiol., C* **2000**, *1*, 1–21.
[109] Gonzales, M. A., Howell, S. G., Sikdar, S. K. *J. Catal.* **1999**, *183*, 159–162.
[110] Almquist, C. B., Biswas, P. *Appl. Catal. A* **2001**, *214*, 259–271.
[111] Du, P., Moulijn, J. A., Mul, G. *J. Catal.* **2006**, *238*, 342–352.
[112] Palmisano, G., Addamo, M., Augugliaro, V., *et al. Catal. Today* **2007**, *122*, 118–127.
[113] Shimizu, K., Akahane, H., Kodama, T., Kitayama, Y. *Appl. Catal. A* **2004**, *269*, 75–80.
[114] Park, H., Choi, W. *Catal. Today* **2005**, *101*, 291–297.
[115] Gondal, M. A., Hameed, A., Yamani, Z. H., Arfaj, A. *Chem. Phys. Lett.* **2004**, *392*, 372–377.
[116] Pillai, U. R., Sahle-Demessie, E. *J. Catal.* **2002**, *211*, 434–444.
[117] Mohamed, O. S. El-Aal, A., Gaber, M., Abdel-Wahab, A. A. *J. Photochem. Photobiol. A* **2002**, *148*, 205–210.
[118] Palmisano, G., Yurdakal, S., Augugliaro, V., Loddo, V., Palmisano, L. *Adv. Synth. Catal.* **2007**, *349*, 964–970.
[119] Zhang, T., You, L., Zhang, Y. *Dyes Pigm.* **2006**, *68*, 95–100.
[120] Maldotti, A., Andreotti, L., Molinari, A., Tollari, S., Penoni, A., Cenini, S. *J. Photochem. Photobiol. A* **2000**, *133*, 129–133.
[121] Brezová, V., Blažková, A., Šurina, I., Havlinová, B. J. *J. Photochem. Photobiol. A* **1997**, *107*, 233–237.
[122] Ku, Y., Lee, W. H., Wang, W. Y. *J. Mol. Catal. A: Chem.* **2004**, *212*, 191–196.
[123] Dey, G. R., Belapurkar, A. D., Kishore K., *J. Photochem. Photobiol. A* **2004**, *163*, 503–508.
[124] Yahaya, A. H., Gondal, M. A., Hameed, A. *Chem. Phys. Lett.* **2004**, *400*, 206–212.
[125] Sasirekha, N., Sardhar Basha, S. J., Shanthi, K. *Appl. Catal. B* **2006**, *62*, 169–180.
[126] Subba Rao, K. V., Srinivas, B., Prasad, A. R., Subrahmanyam, M. *Chem. Commun.* **2000,** 1533–1534.
[127] Maldotti, A., Amadelli, R., Samiolo, L., *et al. Chem. Commun.* **2005,** 1749–1751.
[128] Molinari, A., Varani, G., Polo, E., Vaccari, S., Maldotti, A. *J. Mol. Catal. A: Chem.* **2007**, *262*, 156–163.
[129] Marinković, S., Hoffmann, N. *Chem. Commun.* **2001,** 1576–1578.
[130] Schindler, W., Kisch, H. *J. Photochem. Photobiol. A* **1997**, *103*, 257–264.

[131] Caronna, T., Gambarotti, C., Palmisano, L., Punta, C., Recupero, F. *J. Photochem. Photobiol. A* **2005**, *171*, 237–242.
[132] Ohtani, B., Pal, B., Ikeda, S. *Catal. Surv. Asia* **2003**, *7*, 165–176.
[133] Takei, G., Kitamori, T., Kim, H.-B. *Catal. Commun.* **2005**, *6*, 357–360.
[134] Higashida, S., Harada, A., Kawakatsu, R., Fujiwara, N., Matsumura, M. *Chem. Commun.* **2006,** 2804–2806.
[135] Kudo, A. *Catal. Surv. Asia* **2003**, *7*(1), 31–38.
[136] Tan, S. S., Zou, L., Hu, E. *Catal. Today* **2008**, *131*, 125–129.
[137] Tan, S. S., Zou, L., Hu, E. *Sci. Technol. Adv. Mat.* **2007**, *8*, 89–92.
[138] Addamo, M., Augugliaro, V., García-López, E., Loddo, V., Marcì, G., Palmisano, L. *Catal. Today* **2005**, *107–108*, 612–618.
[139] Hernández-Alonso, M. D., Coronado, J. M., Maira, A. J., Soria, J., Loddo, V., Augugliaro, V. *Appl. Catal. B* **2002**, *39*, 257–267.
[140] Sun, L., Lu, H., Zhou, J. *Dyes Pigm.* **2008**, *76*, 604–609.
[141] Torres, R. A., Nieto, J. I., Combet, E., Pétrier, C., Pulgarin, C. *Appl. Catal. B* **2008**, *80*, 168–175.
[142] Parra, S., Sarria, V., Malato, S., Péringer, P., Pulgarin, C. *Appl. Catal. B* **2000**, *27*, 153–168.
[143] Brosillon, S., Djelal, H., Merienne, N., Amrane, A. *Desalination* **2008**, *222*, 331–339.
[144] Azrague, K., Aimar, P., Benoit-Marquié, F., Maurette, M. T. *Appl. Catal. B* **2007**, *72*, 197–204.
[145] Camera-Roda, G., Santarelli, F. *J. Sol. Energy Eng.* **2007**, *129*, 68–73.
[146] Zama, K., Fukuoka, A., Sasaki, Y., Inagaki, S., Fukushimac, Y., Ichikawa, M. *Catal. Lett.* **2000**, *66*, 251–253.
[147] Biard, P.-F., Bouzaza, A., Wolbert, D. *Appl. Catal. B* **2007**, *74*, 187–196.
[148] Rivas, L., Bellobono, I. R., Ascari, F. *Chemosphere* **1998**, *37*(6), 1033–1044.
[149] Tsuru, T., Kan-no, T., Yoshioka, T., Asaeda, M. *Catal. Today* **2003**, *82*, 41–48.
[150] Molinari, R., Palmisano, L., Drioli, E., Schiavello, M. *J. Membr. Sci.* **2002**, *206*, 399–415.
[151] Dijkstra, M. F. J., Buwalda, H., De Jong, A. F., Michorius, A., Wilkelman, J. G. M., Beenackers, A. A. C. M. *Chem. Eng. Sci.* **2001**, *56*, 547–555.
[152] Mascolo, G., Comparelli, R., Curri, M. L., Lovecchio, G., Lopez, A., Agostiano, A. *J. Hazard. Mater.* **2007**, *142*, 130–137.
[153] Molinari, R., Mungari, M., Drioli, E., *et al. Catal. Today* **2000**, *55*, 71–78.
[154] Tang, C., Chen, V. *Water Res.* **2004**, *38*, 2775–2781.
[155] Chin, S. S., Lim, T. M., Chiang, K., Fane, A. G. *Chem. Eng. J.* **2007**, *130*, 53–63.
[156] Molinari, R., Grande, C., Drioli, E., Palmisano, L., Schiavello, M. *Catal. Today* **2001**, *67*, 273–279.
[157] Sopajaree, K., Qasim, S. A., Basak, S., Rajeshwar, K. *J. Appl. Electrochem.* **1999**, *29*, 1111–1118.
[158] Molinari, R., Pirillo, F., Falco, M., Loddo, V., Palmisano, L. *Chem. Eng. Process.* **2004**, *43*, 1103–1114.
[159] Lee, S.-A., Choo, K.-H., Lee, C.-H., *et al. Ind. Eng. Chem. Res.* **2001**, *40*, 1712–1719.
[160] Le-Clech, P., Lee, E.-K., Chen, V. *Water Res.* **2006**, *40*, 323–330.
[161] Choo, K.-H., Chang, D.-I., Park, K.-W., Kim, M.-H. *J. Hazard. Mater.* **2008**, *152*, 183–190.
[162] Fu, J., Ji, M., Wang, Z., Jin, L., An, D. *J. Hazard. Mater.* **2006**, *131*, 238–242.
[163] Ghosh, R. *J. Membr. Sci.* **2006**, *274*, 73–82.
[164] Chan, C. C. V., Bérubé, P. R., Hall, E. R. *J. Membr. Sci.* **2007**, *297*, 104–120.
[165] Huang, X., Meng, Y., Liang, P., Qian, Y. *Sep. Purif. Technol.* **2007**, *55*, 165–172.
[166] Choi, J.-H., Fukushi, K., Yamamoto, K. *Sep. Purif. Technol.* **2007**, *52*, 470–477.
[167] Mozia, S., Tomaszewska, M., Morawski, A. W. *Catal. Today* **2007**, *129*, 3–8.
[168] Fernández, P., Blanco, J., Sichel, C., Malato, S. *Catal. Today* **2005**, *101*, 345–352.
[169] Sarria, V., Péringer, P., Cáceres, J., Blanco, J., Malato, S., Pulgarin, C. *Energy* **2004**, *29*, 853–860.
[170] Malato, S., Blanco, J., Vidal, A., *et al. Sol. Energy* **2003**, *75*, 329–336.
[171] Ollis, D. F. *Top. Catal.* **2005**, *35*, 217–223.
[172] Imoberdorf, G. E., Irazoqui, H. A., Alfano, O. M., Cassano, A. E. *Chem. Eng. Sci.* **2007**, *62*, 793–804.
[173] Satuf, M. L., Brandi, R. J., Cassano, A. E., Alfano, O. M. *Catal. Today* **2007**, *129*, 110–117.
[174] Guettaï, N., Amar, H. A. *Desalination* **2005**, *185*, 439–448.
[175] Gora, A., Toepfer, B., Puddu, V., Li Puma, G. *Appl. Catal. B* **2006**, *65*, 1–10.
[176] Bhatkhande, D. S., Kamble, S. P., Sawant, S. B., Pangarkar, V. G. *Chem. Eng. J.* **2004**, *102*, 283–290.
[177] Doll, T. E., Frimmel, F. H. *Water Res.* **2004**, *38*, 955–964.
[178] De Heredia, J. B., Torregrosa, J., Dominguez, J. R., Peres, J. A. *J. Hazard. Mater.* **2001**, *83*, 255–264.
[179] Wang, K.-H., Tsai, H.-H., Hsieh, Y.-H. *Appl. Catal. B* **1998**, *17*, 313–320.
[180] Rideh, L., Wehrer, A., Ronze, D., Zoulalian, A. *Catal. Today* **1999**, *48*, 357–362.
[181] Li Puma, G., Toepfer, B., Gora, A. *Catal. Today* **2007**, *124*, 124–132.
[182] Zmudziński, W., Sobczyńska, A., Sobczyński, A. *React. Kinet. Catal. Lett.* **2007**, *90*, 293–300.
[183] Xu, Y., Langford, C. H. *J. Photochem. Photobiol. A* **2000**, *133*, 67–71.
[184] Serpone, N. *J. Photochem. Photobiol. A* **1997**, *104*, 1–12.
[185] Ökte, A. N., Resat, M. S., Inel, Y. *J. Photochem. Photobiol. A* **2000**, *134*, 59–70.
[186] Zhang, T., Oyama, T., Horikoshi, S., Hidaka, H., Zhao, J., Serpone, N. *Sol. Energy Mater. Sol. Cells* **2002**, *73*, 287–303.
[187] Liptákova, B., Báhidský, M., Hronec, M. *Appl. Catal. A* **2004**, *263*, 33–38.
[188] Yamaguchi, S., Sumimoto, S., Ichihashi, Y., Nishiyama, S., Tsuruya, S. *Ind. Eng. Chem. Res.* **2005**, *44*, 1–7.
[189] Dong, T., Li, J., Huang, F., Wang, L., Tu, J., Torimoto, Y., Li, M. S. Q. *Chem. Commun.* **2005,** 2724–2726.
[190] Molinari, R., Poerio, T., Argurio, P. *Catal. Today* **2006**, *118*, 52–56.
[191] Comoretto, L., Chiron, S. *Sci. Total Environ.* **2005**, *349*, 201–210.
[192] Gómez, M. J., Martínez Bueno, M. J., Lacorte, S., Fernández-Alba, A. R., Agüera, A. *Chemosphere* **2007**, *66*, 993–1002.
[193] Bendz, D., Paxéus, N. A., Ginn, T. R., Loge, F. J. *J. Hazard. Mater.* **2005**, *122*, 195–204.

Relevant Website

www.epa.gov – US Environmental Protection Agency: Green Chemistry.

Biographical Sketches

Dr. Angela Caruso was born in Lamezia Terme, Calabria (Italy). She received her degree in pharmaceutical chemistry and technology cum laude in 2004, and the PhD degree in chemical and materials engineering in 2009 under the supervision of Prof. Raffaele Molinari. She has been working at the Department of Chemical and Materials Engineering of the University of Calabria since 2003.

Her research is mainly focused on the development of photocatalytic membrane reactors for partial and total oxidation reactions of organic compounds in water.

Prof. Leonardo Palmisano was born in Termini Imerese (Palermo, Italy) in 1950. He has been a full professor of chemistry in the Department of Chemical Engineering of Processes and Materials of the University of Palermo since 2000. His scientific activity has been mainly focused on the field of heterogeneous photocatalysis and many collaborations have been undertaken all over the world. His scientific production consists of papers published in international journals (more than 200), contributions in proceedings of national and international conferences (around 250), and chapters of books (around 30). He has been invited as a visiting researcher or visiting professor in Spain, UK, Germany, and Japan and he is a member of the Italian Chemical Society, American Chemical Society, and fellow of the Royal Society of Chemistry (FRSC). He has been the editor of the book titled *Processi e metodologie per il trattamento delle acque* (translation: *Processes and Methodologies for Waste Water Treatment*), is coauthor of the didactical book titled *Fondamenti di Chimica* (EDISES), also translated in Spanish as *Fundamentos de Química*, Ariel Ciencia, Barcellona (Spain). Moreover, he is a referee for many international journals.

Prof. Raffaele Molinari was born in Italy in 1953. He has a degree in chemical engineering. He has been a full professor of chemistry, Faculty of Engineering – University of Calabria since 2006; a coordinator of the Doctorate School Chemical Engineering and Materials, University of Calabria since 2007; an associate researcher at ITM-CNR (Rende, CS, Italy) since 1996; a member of the Interuniversity Consortium Chemistry for the Environment (INCA) since 1994; and member in the Directive Council since 2001. Between 1987 and 1988, he was a visiting research associate – Department of Chemical Engineering, North Carolina State University (USA). He is currently a professor at schools and formation courses, nationals, and internationals, as well as a referee for international journals. He is a member of the Italian Chemical Society (SCI), the European Membrane Society (EMS), and the North American Membrane Society (NAMS). He is responsible or coresponsible for some bilateral projects with Egypt and Morocco and for the European Course COMETT held twice at the University of Calabria during 1993–94. He is also responsible for various research projects. His research activity focuses on catalytic membrane reactors; specific interactions combined with membrane separation (supported liquid membranes; complexation – ultrafiltration); and energy analyses on membrane processes. He has published more than 130 papers on books and journals, has an N.1 Italian patent to his credit, has more than 160 contributions on congress proceedings, and more than 90 oral communications at seminars, schools, and congresses.

3.08 Biocatalytic Membranes and Membrane Bioreactors

R Mazzei, E Drioli, and L Giorno, Institute of Membrane Technology, ITM-CNR, University of Calabria, Rende (CS), Italy

3.08.1	Introduction	195
3.08.2	Membrane Bioreactors	197
3.08.2.1	Membrane Bioreactors with Biocatalyst Recycled in the Retentate Stream	197
3.08.2.2	Membrane Bioreactors with Biocatalyst Confined in the Membrane Module Space	199
3.08.3	Biocatalytic Membrane Reactors	199
3.08.3.1	Biocatalytic Membrane Reactors Using Entrapped Enzyme within the Membrane Thickness	200
3.08.3.2	Biocatalytic Membrane Reactors Using Enzymes Gelified on the Membrane Surface	202
3.08.3.3	Biocatalytic Membrane Reactors Using Enzyme Chemically Bound to the Membrane	202
3.08.3.3.1	Enzyme adhesion to the membrane by weak bonds	202
3.08.3.3.2	Enzyme adhesion to the membrane by strong bond	202
3.08.3.4	Biocatalytic Membrane Reactors Using Enzyme Immobilized by Site-Specific Method	205
3.08.3.5	Kinetics of Biocatalytic Membrane Reactor where Transport Occurs by Diffusion	205
3.08.3.5.1	Enzyme immobilized on the surface	205
3.08.3.5.2	Enzyme immobilized into the porous matrix	206
3.08.4	Biocatalytic Membranes and Membrane Bioreactor Applications	206
3.08.4.1	Biocatalytic Membranes and Membrane Bioreactors in Pharmaceutical Applications	207
3.08.4.2	Biocatalytic Membranes and Membrane Bioreactors in Food Applications	207
3.08.4.3	Submerged Membrane Bioreactors in Water Treatment and Other Emerging Applications	208
3.08.5	Conclusions	209
References		209

Glossary

Biocatalytic membrane Membrane which exhibits catalytic properties.

Biocatalytic membrane reactor Reactor configuration in which the membrane is involved in the biocatalytic transformation and promotes mass transport.

Immobilized enzyme Enzyme attached to an inert material such as membrane.

Site-specific immobilization Specific strategy to attach the enzyme in a controlled way. The strategies to orientate the immobilization are based on gene fusion, post-translational modification, site-direct mutagenesis, etc.

Submerged membrane module In this configuration the membrane is immersed into the bulk phase.

Submerged membrane reactor Membrane bioreactor with submerged module.

3.08.1 Introduction

Membrane bioreactors are combined processes in which a biochemical conversion (by action of a catalyst of biological origin) and a physical separation process are simultaneously carried out.

The catalytic action of enzymes is extremely efficient and selective compared with traditional chemical catalysts; the enzymes demonstrate higher reaction rates, milder reaction conditions, and greater stereospecificity. The use of biocatalysts for large-scale production is an important research topic because it enables biotransformations to be integrated into productive reaction cycles.

The most common membrane bioreactor configurations can be classified under two major types

(**Figure 1**): (1) the ones where the membrane controls the mass transport in and out from the reactor bulk and has an indirect effect on the reaction itself (i.e., the reaction occurs in a place different than the membrane, which affects the reaction basically by removing products, adding reagents, retaining the catalyst in the reaction bulk phase, etc.) and (2) the ones where the reaction takes place at the membrane level and therefore has a direct effect on the reaction in addition to governing the mass transport through itself. The latter type is more specifically termed biocatalytic membrane reactor (or catalytic membrane bioreactor) to underline the catalytic properties of the membrane, which are promoted by catalysts of biological origin.

It is also worth mentioning that, this being a growing research field, various new terminologies are being continuously introduced to indicate specific reactor types developed. For example, they can be found in the open literature and are often named on the basis of components used, including solvents, membrane material and/or configuration, coupled membrane separation process, and membrane module position with respect to the processing bulk (side stream or submerged). Therefore, terms such as multiphase enzyme membrane reactor; organic/water biphasic (or two-separate phase) catalytic membrane bioreactor; polymeric (or inorganic) enzyme-loaded membrane reactor; capillary, hollow-fiber or flat-sheet membrane bioreactor; ultrafiltration membrane bioreactor; and cell recycle membrane bioreactor (or fermentor) and submerged membrane bioreactors (SMBRs). However, most of them can be reconducted to the more general cases distinguished by the biocatalyst position with respect to the membrane (catalyst located at the membrane level or compartmentalized in the bulk phase externally to the membrane structure).

The configuration where the membrane performs a separation process while the reaction occurs in the bulk phase of a tank reactor is currently the most exploited on a productive scale. This is because it has been relatively easier to integrate two well-known unit operations (such as a tank reactor and a pressure-driven membrane separation process) and enhancing overall process performance while still benefiting from independent control of parameters.

Biocatalytic membrane reactors represent a more intensified system, as they can perform reaction and separation in the same membrane unit. However, the current still-limited knowledge of mechanisms occurring at the nanoscale within the biocatalyst-loaded membrane microenvironment and how to control/

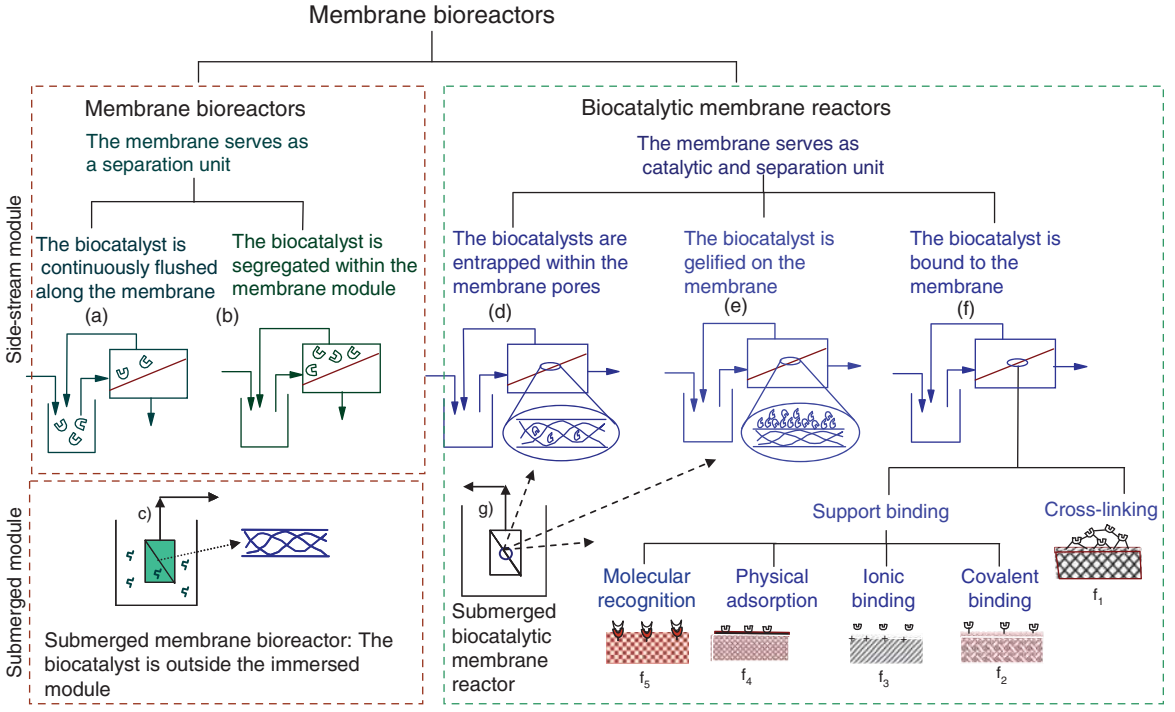

Figure 1 Schematic classification of biocatalytic membranes and membrane bioreactors using side stream (a, b, d, e, f) or submerged module (c, g). The binding illustrated in f_1 to f_5 apply also to submerged biocatalytic membrane reactor.

govern/guide them from a macroscopic level is an obstacle to the exploitation of biocatalytic membrane reactors on a productive scale. Molecular modeling studies are expected to promote more insights in the field. The need of highly precise, selective, clean, safe, and energy-saving processes will drive the development of this technology beyond the current applications.

SMBR in wastewater treatment is probably the most representative example of a relatively new technology that has been driven by new challenges and political strategies (including shortage of water, stringent regulations, and research incentives) and has reached a developing stage (and even approaching to a mature stage) in a couple of decades.

SMBRs for wastewater treatment are discussed elsewhere (chapter 4.07). In this chapter, the configuration of bioreactors and biocatalytic reactors using the module immersed or submerged in the reaction tank is discussed in relation to production and processing of valuable compounds other than water.

3.08.2 Membrane Bioreactors

Membrane bioreactors, where the membrane controls the mass transport while it does not take part in the reaction, have several intrinsic advantages that make them a possible alternative system when compared with other, more conventional bioreactors. One of the main advantages is the possibility to reuse the biocatalyst in a continuous system, which contributes to increase productivity and likely the economic viability of the process. Another important advantage is the continuous selective removal of the products from the reaction media, or vice versa, the controlled supply of reagent to the catalytic reaction environment.

Membrane bioreactors may display additional advantages in multistep reactions. In such cases, if the membranes exhibit some selectivity toward the products, an enrichment of the product that is less rejected can be obtained in the outlet process stream. On the other hand, if a product is rejected by the membrane, it can be concentrated inside the system.

3.08.2.1 Membrane Bioreactors with Biocatalyst Recycled in the Retentate Stream

In the case in which the membrane acts only as a separation unit, the biocatalyst can be continuously flushed along the membrane or confined within the membrane module, that is, in the shell or lumen space. In the first case, a common example is represented by the case where the initial solution contains both the enzyme and the substrate, and the product is separated from the feed solution (**Figure 2(a)**). This type of reactor is based on the combination of a traditional continuously stirred tank reactor (CSTR) with a separation unit (the membrane plant).

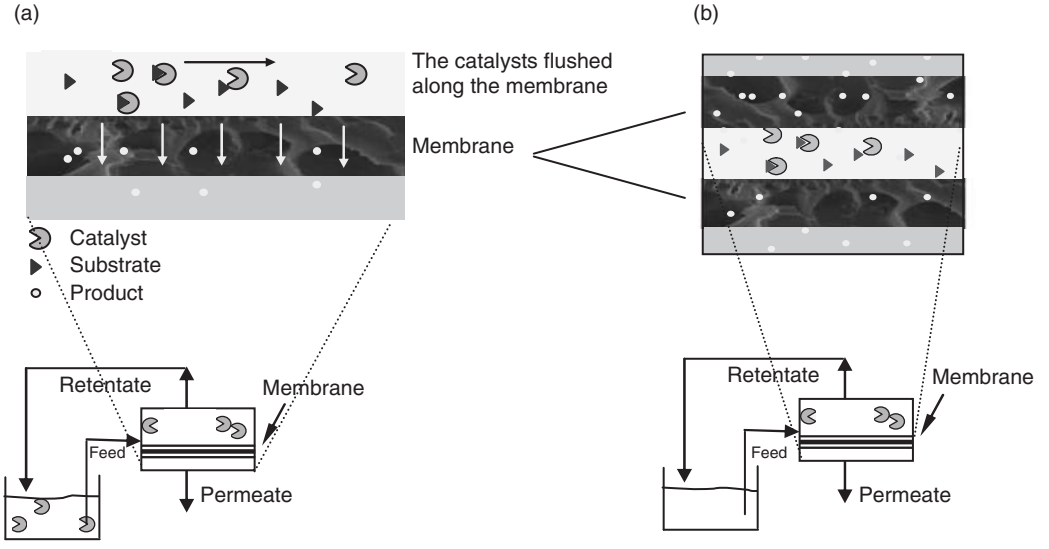

Figure 2 Schematic representation of membrane bioreactors in which membrane works as a separation unit: (a) ultrafiltration (UF) membrane coupled with a continuous stirred tank reactor (CSTR); (b) membrane segregated enzyme reactor (MSER).

The reactor works as a CSTR, but the product either passes through the membrane unit where the enzyme is retained and recycled back into the reactor or remains confined in the membrane module.

An appropriate membrane separation is used to keep larger components in the reaction vessel (i.e., enzyme and macromolecular substrates) and remove low-molecular-weight molecules (i.e., product and inhibitor). The biocatalyst is immobilized by the fact that it is compartmentalized by the membrane in the reaction vessel. This allows continuous processing with the biocatalyst suspended in a homogeneous solution. Direct contact between the substrate and biocatalyst is achieved with limited or no diffusional resistance.

The most common separation process used in this kind of setup is ultrafiltration (UF). Both dead-end continuous stirred UF cells with flat membranes and cross-flow UF through tubular membrane modules have been widely investigated.

Concentration polarization phenomena severely affect the performance of the separation process where the membrane is used only as a separation media; then it is necessary to control the polarization layer on the membrane-pressurized side by means of reactor fluid dynamics and appropriate module design. These reactors are especially suitable for enzymatic systems for which a homogeneous catalyst distribution is particularly important, such as cofactor-requiring mono- and multi-enzyme systems.

Enzyme activity is usually not constant with time. Physicochemical changes in enzyme structure, thermal denaturation, and microbial contamination cause enzyme activity to continuously decrease with time. When enzymes or cells are compartimentalized in UF devices, biocatalyst losses can even occur due to the wrong choice of membrane chemical and morphology properties. It is conventional to measure the enzyme stability in terms of its half-life time ($t_{1/2}$), that is, the time at which enzyme activity is reduced to half its initial value. It can be calculated from the following equations:

$$K_d = \frac{2.303}{\vartheta}\log\frac{A_{E_0}}{A_{E_\vartheta}} \quad t_{1/2} = \frac{0.693}{K_d} \tag{1}$$

where K_d is the enzyme deactivation constant; ϑ is the operation time; A_{E_0} is the initial enzyme activity, or product mass per unit time and reaction volume; and A_{E_ϑ} is the enzyme activity at time ϑ.

Biotransformations by means of enzymes in continuous processes need careful consideration of enzyme activity decay as a function of time in order to correctly assess reactor performance.

The membrane bioreactor in the CSTR/UF configuration is useful for several types of reactions where a typical immobilized enzyme would not be effective. These include cases where the substrate has a high molecular mass and/or it needs high transport properties to efficiently contact the biocatalyst, or the biocatalyst itself is a cell in the growing phase.

Continuous membrane fermentors (or cell-recycle membrane fermentors) belong to these types of examples (**Figure 3**). Here, microporous membranes are used to separate the fermentation broth from the product stream, thus retaining viable cells in the fermentor [1, 2].

The CSTR at steady state works in time-invariant condition with no accumulation at the steady state. Therefore, the balance equation at the steady state becomes

Rate of A IN by flow − Rate of A OUT by flow
+ Rate of production of A by reaction
= Rate of accumulation of mass of A

$$(FC_A)_{IN} - (FC_A)_{OUT} + \nu_r \cdot V = 0 \tag{2}$$

From this, the reaction rate can be determined as

$$v_r = \frac{F(C_{A0} - C_{A1})}{V} \tag{3}$$

where v_r is the reaction rate (mmol cm^{-3} min^{-1}), F the permeate flow rate (cm^{3}min^{-1}), C_f the feed concentration (mmol cm^{-3}), C_p the permeate concentration (mmol cm^{-3}), and V the volume (cm^3).

If the catalyst is an enzyme, the reaction is described by the following chemical equation

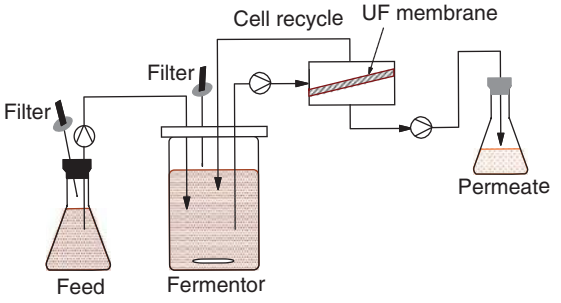

Figure 3 Continuous membrane fermentor apparatus with ultrafiltration cell-recycle system.

$$E+S \underset{k_{-1}}{\overset{k_1}{\rightleftharpoons}} ES \underset{k_{-2}}{\overset{k_2}{\rightleftharpoons}} E+P \qquad (4)$$

The mathematical model that describes the kinetic behavior of enzymes is the Michaelis–Menten equation:

$$V_0 = \frac{V_{max}[S]}{K_m + [S]} \qquad (5)$$

where V_o is the initial reaction rate, V_{max} the maximum reaction rate, K_m the Michaelis–Menten (M–M) constant, and $[S]$ the substrate concentration. Rearranging the M–M equation in linear form, the Lineweaver–Burk equation is obtained. This is a graphical method to directly estimate K_m and V_{max}:

$$\frac{1}{V_0} = \frac{K_m}{V_{max}}\frac{1}{S} + \frac{1}{V_{max}} \qquad (6)$$

If $\frac{1}{V_0}$ versus $\frac{1}{[S]}$ data are plotted, a straight line is obtained, where the intercept to the y-axis is $\frac{1}{V_{max}}$ and the slope is $\frac{K_m}{V_{max}}$.

In the CSTR/UF system, the enzyme works as free homogeneously distributed molecule in the bulk phase and these equations are applied to identify the intrinsic kinetic properties of the biocatalyst.

In addition to product removal, the membrane can also be used to control the supply of reagent molecules. For example, extractive membrane bioreactors were used to permeate organic molecules across the membrane into the biological active reactors [3, 4]. Ion-exchange membrane bioreactors were used to transport ionic compounds through nonporous ion-exchange membranes into a biological active compartment [5, 6]. The advantage of this mode of operation is that biomass performance is not negatively affected by the wastewater pH and composition. In addition, biomass catabolites are not released into the treated water.

3.08.2.2 Membrane Bioreactors with Biocatalyst Confined in the Membrane Module Space

In this configuration, the catalyst is confined in a particular place in the membrane module space (within the hollow-fiber lumen or within the shell surrounding the outer surface of the fibers; **Figure 2(b)**); it is not recirculated in the effluent stream while low-molecular-weight products and inhibitors are removed through the membrane. The system was also termed membrane segregated enzyme reactor (MSER). However, nowadays, this term is less used.

The reactor volume is represented by the space of the module containing the enzyme, which therefore represents the balance region.

The development of hollow fibers with diameters down to about 100 μm makes possible tube-and-shell reactors with a high surface-to-volume ratio.

Bioreactors with compartmentalized cells or microsomes functioning as a bioartificial pancreas or extracorporeal detoxification devices are of high interest for therapeutic applications. The evaluation of stability and catalytic properties of the immobilized system must take into account possible pH differences between the inner core of the fiber, where the reaction takes place, and the bulk of the feed solution.

The choice of reactor configuration depends on the properties of the reaction system. For example, bioconversions for which homogeneous catalyst distribution is particularly important are optimally performed in a reactor with the biocatalyst compartmentalized by the membrane in the reaction vessel.

3.08.3 Biocatalytic Membrane Reactors

In a biocatalytic membrane reactor (the membrane is involved in the biocatalytic transformation and promotes mass transport), in addition to the separation, the membrane also represents the catalytic unit. The different kinds of biocatalytic membrane reactor configuration depend on which way the complex biocatalyst–membrane is prepared.

Immobilized biocatalysts have widespread applications in areas such as organic synthesis, pollution control, and for diagnostic purposes [8, 9, 10, 7, 11]. The selection of the membrane to be used in enzymatic membrane reactors should take into account the size of the (bio)catalyst(s), substrates(s), and products(s) as well as the chemical properties of the species in solution and of the membrane itself. An important parameter to be used in this selection is the solute rejection coefficient, which should be 0 for the product to facilitate permeation, and should be 1 for the enzyme to insure a complete retention of the catalyst inside the reaction system. The selectivity is normally associated with a discrimination based on size exclusion.

Immobilization eliminates the need to separate an enzyme from the product solution and allows these expensive compounds to be reused. In addition, the thermal stability, pH stability, and storage stability of an enzyme may be increased as a result of immobilization. Very often, it has been observed that a decrease of catalytic activity was associated with the increase of catalytic stability. However, it has been demonstrated that this inverse relationship is not a general rule and that if the proper microenvironment conditions are used, immobilized enzyme can maintain native kinetic properties while increasing catalytic stability [12, 13].

The catalyst can be entrapped within the membrane, gelified on the membrane, or bound to the membrane (**Figures 1(d)–1(g)**).

3.08.3.1 Biocatalytic Membrane Reactors Using Entrapped Enzyme within the Membrane Thickness

Biocatalytic membranes can be obtained by entrapment. This method of immobilization is based on the localization of an enzyme within the membrane. It is done in such a way as to retain protein while allowing penetration of the substrate. It can be obtained during membrane preparation process by phase inversion. As an alternative, it can be obtained by cross-flow filtration of an enzyme solution from the sponge to the thin layer having pore size smaller than the enzyme so as to block it within the membrane thickness (**Figure 4**). Asymmetric hollow fibers can provide suitable support for enzyme entrapment.

The amount of biocatalyst loaded, its distribution and activity through the support, and its lifetime are very important parameters to properly orientate the development of such systems. The amount of immobilized protein can be determined by the mass balance between initial and final solutions [14]. Studies have demonstrated that through this type of immobilization, enzyme-loaded membranes are obtained with uniform distribution along the membrane length and thickness [15, 16]. A combined qualitative method [17] merging the classical *in situ* detection of enzyme activity and Western blot analysis was applied for the first time to the capillary asymmetric polysulfone membrane reactor to determine simultaneously the enzyme (β-glucosidase) spatial distribution through the membrane thickness and along the membrane module and its activity after the immobilization through observation via light microscopy.

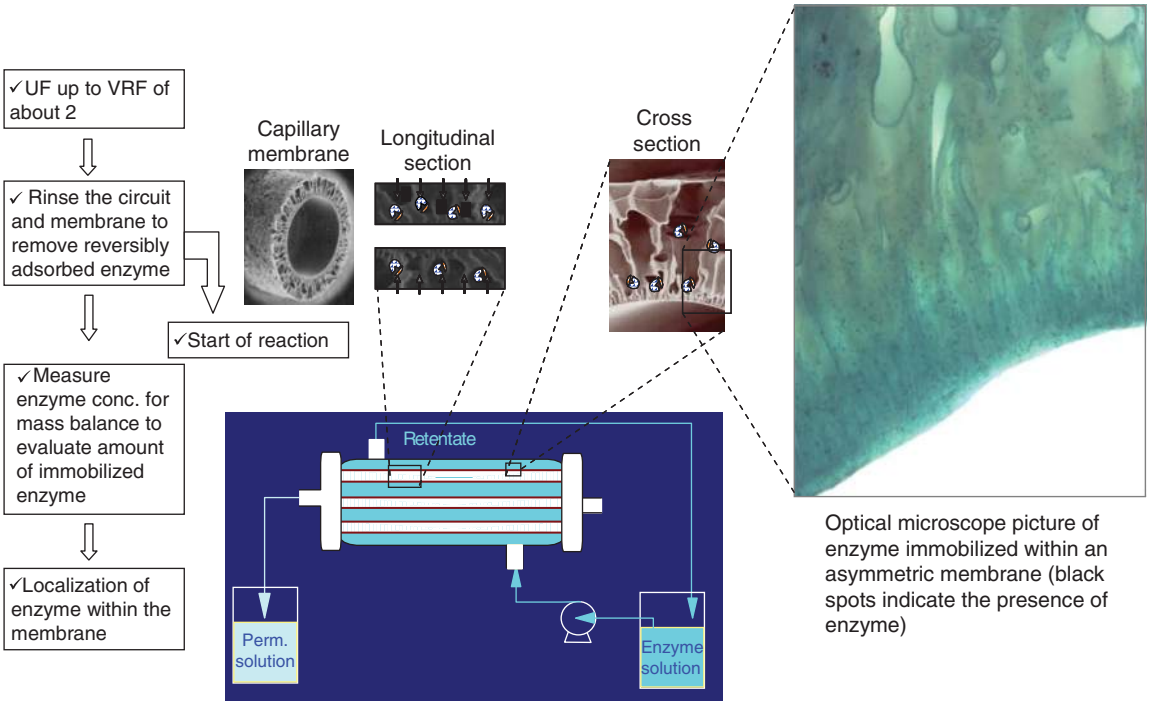

Figure 4 Entrapment of enzyme in asymmetric capillary membrane by cross-flow ultrafiltration from shell to lumen.

Transport of the substrate and product through the enzyme-loaded membrane is an important parameter governing biocatalytic membrane reactor performance.

When the substrate is transported through the membrane by convection, such as when it is permeated under a pressure gradient, the residence time is an important factor to be optimized.

The residence time (τ) of substrate solutions is obtained as

$$\tau = \frac{F}{V} \tag{7}$$

where F is the flow rate ($1\,s^{-1}$) through the membrane and V the reactor volume (l).

Under these conditions, membrane micropores containing the immobilized enzyme can be considered as continuous microreactors working in parallel. The overall reactor volume is represented by the membrane void volume. The reaction rate equation can be derived by the balance equation at steady state (**Figure 5**). In these conditions, no accumulation is present and the reaction rate can be determined according to Equation (3).

For well-controlled convective flow patterns, constant reagent concentration fed to the reactor volume and homogeneous mixing within it (promoted by fluid dynamics through the pores) can be obtained. Such conditions permit to measure kinetic properties, which can be assimilated to the intrinsic ones, that is, they result in the same environment as for enzyme free in solution in a stirred tank reactor [2, 13].

For all cases where the mentioned conditions are not fulfilled, such as when transport occurs by diffusion, different appropriate assumptions need to be considered [18].

The conversion degree of catalytic membrane bioreactors, where the enzyme is present only within the micropores can be calculated as follows:

$$\text{Conversion} = \frac{C_f - C_p}{C_f} \tag{8}$$

where C_f and C_p are the concentration of the substrate in the feed permeate solution, respectively. C_f is constant as a function of time.

It is worth nothing that, if some enzyme molecules are present also on the membrane surface (in addition to those within the pores), it is necessary to take into account the conversion of the substrate in the retentate solution.

In this case, the total conversion is calculated as

$$\text{Conversion} = \frac{(C_r - C_p) + (C_{fi} - C_r)}{C_{fi}} \tag{9}$$

where C_r and C_{fi} are the substrate concentration in the retentate and initial feed solution, respectively.

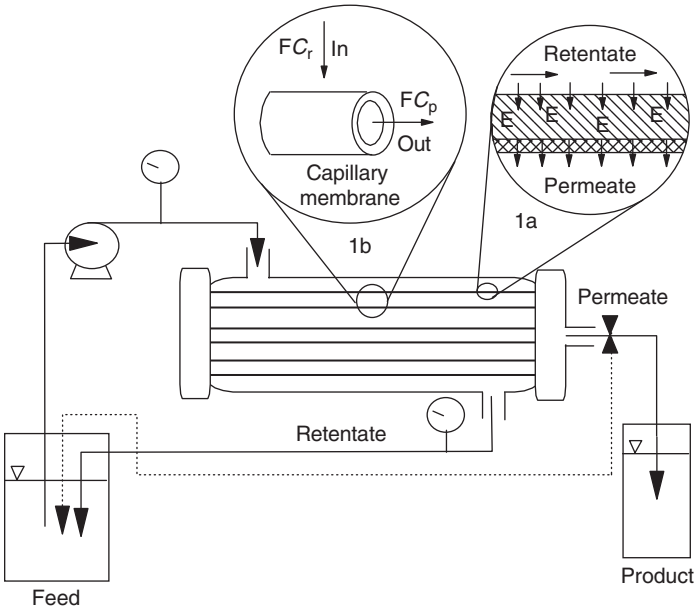

Figure 5 Schematic representation of the membrane reactor volume at which level the balance equation is derived when the solution transport occurs by convection and reagent and product can freely pass through it.

3.08.3.2 Biocatalytic Membrane Reactors Using Enzymes Gelified on the Membrane Surface

Catalytic membranes using enzymes gelified on the membrane surface have also been prepared. The gelification of the biocatalyst on the membrane is based on one of the main drawbacks of membrane processes: concentration polarization phenomena and subsequent protein precipitation upon reaching a critical concentration at the membrane interface. Another disadvantage of this system is the reduction of the specific activity due to mass transport limitations. This type of immobilization is used when direct contact of immobilized enzyme with the substrate solution cannot be achieved otherwise (i.e., the large substrate molecules cannot penetrate within the membrane structure). However, it has the disadvantage of protein leakage during the operation time.

3.08.3.3 Biocatalytic Membrane Reactors Using Enzyme Chemically Bound to the Membrane

Biocatalysts can be attached to the membrane by chemical and biochemical interactions, that is, by physical absorption, ionic binding, covalent linking and cross-linking, and molecular recognition. Interactions can be random as well as directed to specific sites.

3.08.3.3.1 Enzyme adhesion to the membrane by weak bonds

Adhesion of an enzyme onto a solid membrane matrix by weak interactions, such as physical adsorption (or physisorption) promoted by van der Waals forces, is probably the simplest way of preparing immobilized enzymes.

Adsorption relies on nonspecific interaction between the enzyme and the surface of the membrane and is a consequence of surface energy. A major advantage of adhesion by weak interactions as a general method of immobilizing (or heterogenizing) enzymes is that usually no reagents and only a minimum of activation steps are required. As a result, it is less expensive, easy to carry out, and tends to be less disruptive to the enzymatic protein than covalent attachment. In fact, the adhesion of the enzyme to the membrane is mainly obtained by hydrogen bond and van der Waals forces. In this respect, the method bears the greatest similarity to the situation found in biological membranes *in vivo* and has been used to model such systems.

Because of the weak bonds involved, desorption of the protein resulting from changes in temperature, pH, ionic strength, or even the mere presence of substrate is often observed. Another disadvantage can be represented by the adsorption of other proteins or substances during reactor operation. This may alter the properties of the immobilized enzyme or, if the substance adsorbed to the membrane is a substrate for the enzyme, the substrate availability may decrease depending on the surface mobility of enzyme and substrate.

This type of immobilization is particularly suitable when interface proteins are used. For example, lipases and esterases adsorbed on hydrophobic polymeric membranes, such as polypropylene, were used in a two-separate phase membrane reactor showing higher stability and selectivity compared to protein immobilized in hydrophilic membranes [19]. A schematic of the reactor system is illustrated in **Figure 6**.

The adsorption of lipases to the membrane is a function of membrane hydrophobicity and protein concentration. Its adsorption is quite stable to changes of pH and temperature and enzyme removal from the membrane may be obtained by protein hydrolysis with sodium hydroxide.

3.08.3.3.2 Enzyme adhesion to the membrane by strong bond

The most stable method of immobilization is the formation of a covalent bond between the enzyme and the support matrix. When trying to select the type of reaction by which a given protein should be attached, the choice is limited by the fact that the binding reaction must be performed under conditions that do not cause enzyme denaturation with consequent loss of enzymatic activity, and that the moieties of the active site must not be directly involved in the linkage.

The functional groups of proteins suitable for covalent binding under mild conditions include (**Figure 7**) (1) the alpha amino groups of the chain and the epsilon amino groups of lysine and arginine, (2) the alpha carboxyl group of the chain end and the beta and gamma carboxyl groups of aspartic and glutamic acids, (3) the phenol ring of tyrosine, (4) the thiol group of cysteine, (5) the hydroxyl groups of serine and threonine, (6) the imidazile group of histidine, and (7) the indole group of tryptophan [20, 21]. To prevent modification of enzymatic

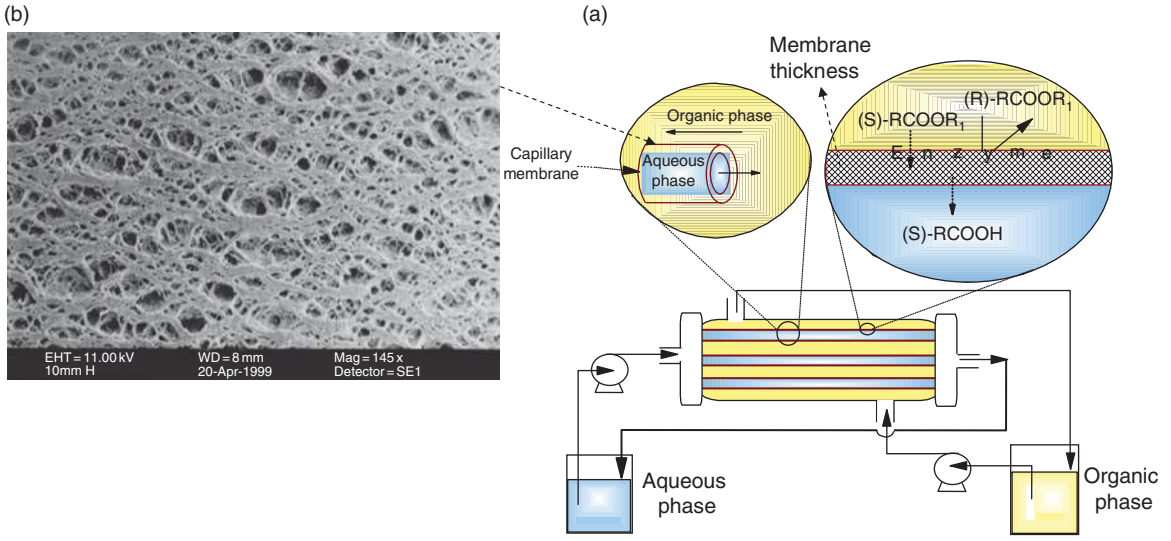

Figure 6 (a) Schematic of a two-separate phase enzyme membrane reactor with este substrate in the organic phase and produced acid in the aqueous phase; (b) scanning electron microscopic (SEM) picture of the external surface of polypropylene membrane

activity or complete inactivation of the immobilized protein, it is important that the catalytic functional groups of the enzyme are not involved in the covalent linkage to the support.

Unfortunately, many of the reactive groups suitable for covalent bond are often also situated in the active center of the enzyme. This problem can sometimes be overcome by the immobilization in presence of molecules that interact with the active site and protect it during the immobilization procedure, such as the substrate [22] or competitive inhibitor of the enzyme [23, 24].

In general, the covalent bond has the advantage of being very stable; therefore, no leakage of enzyme occurs in devices prepared using this method. This may only represent a limit in replacing the deactivated enzyme for subsequent use of the membrane support.

The method is widely used in the preparation of highly selective single-use devices (such as biosensors).

Immobilization of enzymes can be also achieved by intermolecular cross-linking of the protein, either to other protein molecules or to functional groups on to an insoluble support matrix. Cross-linking an enzyme to itself is both expensive and insufficient, as some of the protein material will inevitably be acting mainly as a support, resulting in relatively low specific enzymatic activity (i.e., catalytic activity normalized by the mass of protein). Generally, cross-linking is best used in conjunction with one of the less stable methods (such as gelification, adsorption, etc.).

It is possible, in some cases, to increase the number of reactive residues of an enzyme in order to increase the yield of immobilized enzyme and to provide alternative reaction sites to those essential for enzymatic activity. The wide variety of binding reactions, and membranes with functional groups capable of covalent coupling, or being activated to give such groups, makes this a generally applicable method of immobilization, even if very little is known about the protein structure or active site of the enzyme to be coupled.

In the literature, there are various routes to carry enzyme immobilization creating a bound on supports. The principal strategies are based on chemical grafting or molecular recognition on porous supports.

The sites involved in this chemistry, including carboxylic acid, hydroxyls, and amino or quaternary ammonium groups, are created on the surface of porous material by various means such as the direct chemical surface treatment or the plasma or ultraviolet (UV) activation.

The reactive sites thus created allow the attachment of the enzyme by use of coupling reagents such as tosyl chloride, dicyclohexylcarbodiimide, and glutaraldehyde.

The immobilization by ionic binding, consisting of the attraction of a charged enzyme moiety to the

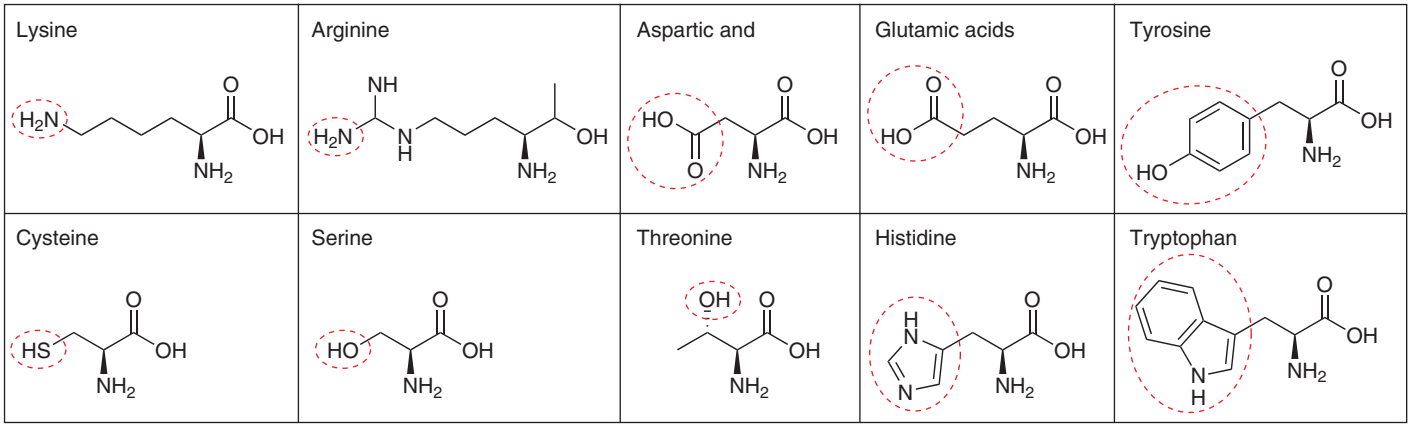

Figure 7 Functional groups of amino acids suitable for covalent binding.

support that has opposite charge, represents a stable attachment, depending on the number of interactions between a single enzyme macromolecule and the membrane support. For this immobilization, membranes with negatively or positively charged groups are used.

3.08.3.4 Biocatalytic Membrane Reactors Using Enzyme Immobilized by Site-Specific Method

Here, we underline some of the specific strategies aiming at attaching enzymes to membranes in a controlled way, avoiding the active site which may no longer be accessible after immobilization. For these purposes, improvement can be achieved by introducing a spacer molecule. Good steric accessibility of active sites can be obtained by oriented immobilization of glycoprotein enzymes through their carbohydrate moieties [25, 26].

Various approaches are developed in order to accommodate site-specific immobilization of enzymes with different structural characteristics, as gene fusion to incorporate a peptidic affinity tag at the N- or C- terminus of the enzyme; post translational modification to incorporate a single biotin moiety on enzymes; and site-directed mutagenesis to introduce unique cysteine molecules to enzymes [27].

A small number of reactions have been designed to couple with functional groups other than the amino and phenolic residues on the protein. Aminoethyl cellulose has been coupled to the carboxylic acid residues of enzymatic protein in the presence of carbodiimide, and thiol residues of a protein have been oxidatively coupled to the thiol groups of a cross-linked copolymer of acrylamide and *N*-acryloyl-cystein [20, 21].

Approaches aiming at creating bio-compatible environments include modifying the surface of polymeric membranes by attaching functional groups such as sugars, polypeptides, and then to adsorb the enzymes.

Another method considered to be of bio-mimetic inspiration and which was shown to be efficient for enzyme attachment consists in using the very strong and specific interaction of the small protein avidin for the biotin [9, 11, 28]. The tetrameric structure of avidin permits itself to interact with four different molecules of biotin at the same time. Various proteins and enzymes could be easily biotinylated, and this mode of enzyme grafting has already been used for production of electrodes as well as for membranes made up of conducting fibers.

3.08.3.5 Kinetics of Biocatalytic Membrane Reactor where Transport Occurs by Diffusion

The kinetic reaction for an immobilized enzyme where transport occurs by diffusion is usually represented as follows:

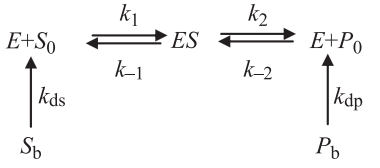

where S_0 and P_0 are the concentration of the substrate and product near the immobilized enzyme, and S_b and P_b are the concentrations of substrate and product in the bulk phase. The constants, k_{ds} and k_{dp}, are related to the diffusion of substrate from the bulk to the enzyme and of the product from the enzyme to bulk phase; these constants take into account diffusion phenomena near the enzyme–membrane wall. In fact, the substrate and the product have two different and opposite concentration gradients through the immobilized enzyme matrix. The concentration of the substrate in the bulk phase decreases near the support due to diffusion phenomena continuing its decrease near the enzyme matrix. An opposite behavior of concentration gradient is observed for the product; near the enzyme matrix, the product concentration is high due to reaction, while it decreases far from the support, arriving at a steady state in the bulk solution.

3.08.3.5.1 Enzyme immobilized on the surface

For the enzyme immobilized on the surface, a stationary film also termed the Nerst diffusion layer, is formed, attached to the enzyme–membrane surface. This layer limits the diffusion of the substrate and, for this reason, the concentration of the substrate in the bulk solution decreases near the immobilized enzyme matrix.

At the steady state, at the interface, the mass transfer of the substrate is balanced from the reaction and consequently from the substrate consumption. In

this case, the Michaelis–Menten equation takes into account the different substrate concentration in the bulk solution and near the surface:

$$\mathcal{J}_s = k_s(S_0 - S) = \frac{V_{max}[S]}{K_m + [S]}$$

In this equation, S and S_0 are the substrate concentration in the bulk and at the immobilized enzyme interface, respectively, and k_s is the mass transfer coefficient.

The ratio between the maximum reaction rate and maximum mass transfer rate is given by the Damköhler number:

$$Da = \frac{V_{max}}{k_s S_0}$$

If $Da << 1$, the transfer rate is larger than the reaction rate, and this means that the system works at a low mass transfer resistance. This is the case known as reaction-limited regime. In this system, the following equation

$$V_{kin} = \frac{V_{max}[S]_b}{K_m + [S]_b}$$

can be assumed.

If $Da >> 1$, the reaction rate is larger than the mass transfer; this is the case known as diffusion-limited regime and $V_{diff} = k_s\,[S]_b$.

The Damköhler number is also the ratio between V_{max}/K_m and k_s, V_{max}/K_m is also the slope of $1/V_0$ versus $1/K_m$, and k_s is the slope of V_{diff} versus S_b.

The mass transfer influence on the reaction is represented by the factor η:

$$\eta = \frac{\text{Observed reaction rate}}{\text{Rate observed without mass trasfer resistance}}$$

If η is ≤ 1, the mass transfer resistance is high and this causes a reduction of the observed activity of the catalyst. The relationship between Da and η is that when Da approaches zero, η approaches 1.

3.08.3.5.2 Enzyme immobilized into the porous matrix

To calculate the observed substrate conversion through an enzyme-loaded support immobilized into the internal surface, it is necessary to take into account the concentration profile within the diffusion layer.

Besides substrate diffusivity in the bulk phase, the diffusion rate through a porous support is influenced by several factors. The effective diffusion coefficient is described by

$$D_{eff} = D_{S_0}\frac{\varepsilon_p}{\tau}\frac{K_p}{K_r}$$

where ε_p is the porosity (or area of support/area of pores), and τ is the tortuosity (the geometry of the pore is not tubular; diffusion occurs changing direction continuously). The tortuosity factor can assume a value in a range of 1.4–7; K_p/K_r is the restricted diffusion roughly estimated as $[1 - r_{substrate}/r_{pore}]^4$, that takes into account the dimension of the pore in relation to the dimension of the substrate; that can have a similar dimension and lead to a situation of restricted diffusion.

The influence of diffusion within porous catalysts upon reaction kinetic was studied in 1930 [3]; this effect was studied on a planar membrane with an immobilized enzyme uniformly distributed. Combining the steady-state diffusion equation with the applicable kinetics rate expression gives

$$D_{eff}\frac{d^2[S]}{dx^2} - \frac{V_{max}[S]}{K_m + [S]} = 0$$

D_{eff} is the effective diffusivity; this means that at the steady state the substrate diffusion rate, through a porous matrix, is equal to the rate conversion.

In addition, in an immobilized system it is possible to evaluate if the reaction is limited by kinetics or mass transport by the Thiele modulus ϕ, given by

$$\phi = L\left(\frac{V_{max}}{D_{eff}K_m}\right)^{1/2}$$

which has the meaning of a reaction rate/diffusion rate.

3.08.4 Biocatalytic Membranes and Membrane Bioreactor Applications

The technological problems associated with the development of biocatalytic membranes on large scale are connected to the need for enzymes having expensive cofactors, low water solubility of substrates, and low enzyme resistance to membrane cleaning agents. However, the several advantages that this technology offers on comparing it with traditional procedures drive their development, especially for production of high value-added components.

In the following paragraphs, the most common examples of biocatalytic membranes and membrane bioreactors patented and whose robustness was proven at industrial application are reported. In **Table 1**,

Table 1 Immobilized biocatalyst in biotechnology applications

Immobilized biocatalyst	*Application*	*References*
β-Galactosidase	Production of oligosaccarides	[30]
Glucose isomerase	Conversion of D-glucose to D-fructose	[31]
Thermolisyn	Production of aspartame	[32]
E coli	Production of L-aspartic acid	[33]
Pseudomonas dacunahe	Production of L-alanin	[34]
Pectinases	Hydrolysis of proteins to improve processability	[35, 36]
Glucosidases	Aroma enhancement in food	[37]
Laccase	Improve processability in wine making	[38]
Trypsin	Production of casein bioactive peptide	[39]
Lactococcus lactis, Lactobacillus dalbruekii	Production of lactic acid	[40, 41]
Fructosil transferase	Production of fructooligosaccarides	[42, 43]
Acetyl transferase	Production of baccatin III	[44]
Protease	Hydrolysis of caroteno-proteins	[45]
Lipase	Production of optically pure enantiomers. Production of diltiazem. Production of lovastatin	[12, 46, 47]
β-Glucosidase	Production of antioxidant molecules	[13]

the immobilized biocatalyst used in food and pharmaceutical applications are reported.

3.08.4.1 Biocatalytic Membranes and Membrane Bioreactors in Pharmaceutical Applications

In literature, many varied works are present regarding the development of a membrane bioreactor for the production of amino acids, antibiotics, anticancer and anti-inflammatory drugs, vitamins, and optically pure enantiomers and antioxidants [47, 48, 24].

Some examples have also been developed at the industrial scale such as the production of amino acids, commercialized by Degussa Company [48] in Germany, the sandwich bioreactor commercialized by Kao Corporation in Japan for the hydrolysis of triglycerides, or the production of cyclodextrins from starch by using hollow-fiber membrane bioreactor commercialized by Nitto Electric [49]. Another example of plant production was developed by Sepracor Inc. in the early 1990s. The system was a full scale multiphase/extractive enzyme membrane reactor plant used in the production of diltiazem chiral intermediate. The system represented an example of integrated and intensified two-separate-phase reactor, in which the biocatalytic membrane has the double role of compartmentalizing the biocatalyst, keeping two phases in contact and separate at the same time [46, 47]. The process was run for several years with modules of 60 m^2 of active membrane area. Another application at the technical scale is the production of L-amino acids from a racemic mixture using the immobilized amino acylase [48].

3.08.4.2 Biocatalytic Membranes and Membrane Bioreactors in Food Applications

One of the first cases on the use of membrane bioreactor in food sector was the production of milk with low lactose content [49]. Nowadays, the hydrolysis of lactose (present in whole milk or cheese whey) by the use of membrane bioreactors is an effective technique running on a large scale.

The intolerance to milk is caused not only due to the presence of lactose, but also because some people cannot digest high-molecular-weight proteins (higher than 5 kDa). The new approach to produce low allergenic fresh milk with improved properties compared to the reconstituted powder milk currently used is to hydrolyze the proteins by membrane bioreactor technology. The advantage of using this technology is that the membrane bioreactor can be designed so as to remove protein fragments equal to or lower than 5 kDa through a membrane of appropriate cutoff. In order to achieve high efficiency, the hydrolytic step should be part of an integrated system where up- and downstream milk is taken into account. Membrane bioreactors are also used to valorize the coproduct of the cheese-making processes, by recovering and reusing compounds present in waste streams.

The other important applications in the food sector include reduction of viscosity of fruit juice

by hydrolyzing pectins, treatments of musts and wine by the conversion of polyphenolic compounds and antocyanes, and the removal of peroxides from diary products.

A more recent application of membrane bioreactor in the food sector is promoted by the industrial demand in the production of functional food and nutraceuticals, and alternative food or food ingredients that confer health benefit. Other applications at technical scale are the production of L-aspartic acid [33], the synthesis of dipeptide Aspartame™ [32], the production of L-alanine by Tanabe Seiyaku [34], the production of fructose-concentrated syrups [31], and the production of L-malic acid with *Brevibacterium ammoniagenes* entrapped in polyacrilamide [50].

3.08.4.3 Submerged Membrane Bioreactors in Water Treatment and Other Emerging Applications

Submerged membrane bioreactors (SMBRs) are one of the membrane operations that, in the last decades, have received much attention worldwide for the treatment of wastewater at the industrial level.

The reason for this lies in the increase of the demand for potable water and on the increase of domestic and industrial wastewater discharges linked to the population growth. In addition, more restrictive legislation toward environmental care, forces industries to minimize the input of energy and water.

The potentialities of the technology lie on the low energy input, long-term operation without cleaning, and less dependence on variation of rheology behavior with concentration; the main constraint is in the high membrane area due to low fluxes linked to the small transmembrane pressure.

The combination of bioreactors and membrane technology enables an innovative and effective treatment process. Conventional wastewater technology is characterized by large wastewater volumes. They generally use open basins and need high surface and long hydraulic retention time of wastewater flows. In conventional activated sludge processes, the purification stage (aeration tank) and the separation of the biomass from the purified waste water (settling tank) are carried out separately and independently of each other. Large basin volumes are necessary for the aeration tank and the final clarifier. The biomass concentration in the aeration tank usually tends to be in the range of only 3–5 $g_{dry\ weight}\,l^{-1}$.

The membrane bioreactor combines biological treatment with membrane separation. The treated water is separated from the purifying bacteria (active sludge) by a process of membrane filtration rather than in a settling tank. Only the treated effluent passes through the membrane; the effluent is then pumped out, whilst the sludge is recovered. The sedimentation in the final clarifier is then replaced by the implementation of a membrane filtration process, which not only allows to separate the biomass from the water, but also the quality of the purified water is considerably improved. The use of microfiltration membranes with pore sizes usually between 0.1 and 0.4 μm ensures the complete retention of suspended matter and leads to a considerable reduction of the amount of bacteria in the outflow of the sewage plant.

Compared with conventional wastewater technology membrane bioreactors have a short hydraulic retention time and high biomass concentrations. In addition, because of the compact way in which they are constructed, membrane bioreactors have a relatively low surface area requirement.

SMBRs employ membrane module cassettes made of bundle of hollow fibers or flat-sheet membrane panels. The cassettes are vertically immersed within a tank containing wastewater and activated sludge and are aerated by a bubble system from the bottom of the units. The aeration serves to activate the sludge and to control concentration polarization and fouling at the membrane level as it generates an upward cross-flow over the membrane. In addition, it ensures effective tank mixing and even distribution of the biomass. The biomass can work at very high level of concentration, which enables a low tank volume and a long sludge age to be utilized; this substantially reduces sludge production. The treated effluent is removed from the membrane units using gravity head (typically 1–1.2 m), or a pumped suction operation can be utilized.

Currently, research interests are devoted toward (1) different configurations of membranes for biomass separation in bioreactors, (2) use of novel and low-cost membrane materials as barrier technologies in membrane bioreactor (MBR) systems, (3) impact of specific mode of bioreactor operation on biomass production and separation in MBRs, and (4) new operating strategies to minimize fouling of membranes in MBR systems.

The development of SMBR technology is also emerging in other fields, including biofuel, pharmaceutical, food, and biotechnology. The concept of

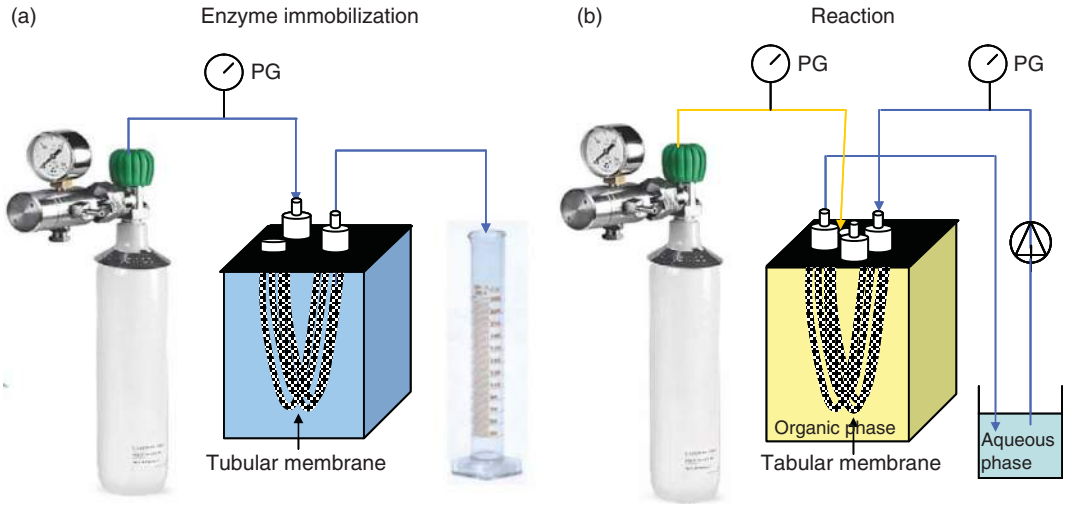

Figure 8 Schematic representation of a submerged biocatalytic membrane bioreactor; (a) immobilization step by filtration, (b) reaction step in two separate phase system.

submerged membrane module to assist either hydrolysis or synthesis of esters for biofuel and biotechnological purposes is investigated in our laboratories. In particular, their development in integrated membrane systems is studied. In this system, submerged biocatalytic membrane reactors can be used to carry out hydrolysis or esterification reactions (**Figure 8**), while SMBRs contribute to the purification of effluents and their recycling into the production system. Other membrane operations, including microfiltration (MF), UF, nanofiltration (NF), membrane contactors and membrane emulsification are combined to promote separation, purification, concentration, and formulation.

The synergistic integration of membrane operations will be among the key strategies to enhance processes precision and efficiency, with maximization of mass and energy conversion into valuable goods while preventing and minimizing waste production. This means, in other words, achieving advanced technology able to face the challenges of sustainable industrial production.

3.08.5 Conclusions

The membrane bioreactor technology has intrinsic characteristics such as efficiency, operational simplicity and flexibility, high selectivity and permeability for bioconversion and transport for specific components, low energy requirements, good stability, environmental compatibility, and easy control and scale-up. These properties make the technology very interesting for the application for the development of a sustainable industrial production.

Except for wastewater treatment, membrane bioreactors are at an emerging-exploratory stage. However, the increasing need of precise processes is favoring a growing interest toward alternative controlled biomimicking routes. This will certainly promote an increase of research efforts in biocatalytic membranes and membrane bioreactor fields. The converging of advanced technologies, including molecular modeling, systems engineering, and systems biology applied to membrane engineering will play a crucial role in advancing the technology and its application in various fields.

References

[1] Taniguchi, M., Kotani, N., Kobayashi, T. *J. Ferm. Technol.* **1987**, *65*, 179.
[2] Giorno, L., Drioli, E., Carvoli, G., Cassano, A., Donato, L. *Biotechnol. Bioeng.* **2001**, *72*(1), 77–84.
[3] Livingston, A. G., Arcangeli, J.-P., Boam, A. T., Zhang, S., Maragon, M., Freita dos Santos, L. M. *J. Membr. Sci.* **1998**, *151*, 29–44.
[4] Splendiani, A., Nicolella, C., Livingston, A. G. *Biotechnol. Bioeng.* **2003**, *83*(1), 8–19.
[5] Velizarov, S., Crespo, J. G., Reis, M. A. *Biotechnol. Prog.* **2002**, *18*, 296–302.
[6] Crespo, J. G., Velizarov, S., Reis, M. A. *Curr. Opin. Biotechnol.* **2004**, *15*, 463–468.
[7] Butterfield, D. A. *Biofunctional Membranes*; Plenum: New York, 1996.

[8] Drioli, E., Giorno, L. *Biocatalytic Membrane Reactors: Application in Biotechnology and Pharmaceutica Industry*; Taylor & Francis: London, 1999.
[9] Amounas, M., Innocent, C., Cosnier, S., Seta, P. *J. Membr. Sci.* **2000**, *176*, 169–176.
[10] Amounas, M., Magne, V., Innocent, C., Dejean, E., Seta, P. *Enzyme Microb. Technol.* **2002**, *31*, 171–178.
[11] Rios, G. M., Belleville, M., Paolucci-Jeanjean, D. *Trends Biotechnol.* **2007**, *25*, 242–246.
[12] Giorno, L., D'Amore, E., Mazzei, R., *et al. J. Membr. Sci.* **2007**, *295*, 95–101.
[13] Mazzei, R., Giorno, L., Mazzuca, S., Drioli, E. *J. Membr. Sci.* **2009**, *339*, 215–223.
[14] Giorno, L., Molinari, R., Drioli, E., Bianchi, D., Cesti, P. *J. Chem. Technol. Biotechnol.* **1995**, *64*, 345.
[15] Crespo, J. P. S. G., Trotin, M., Hough, D., Howell, J. A. *J. Membr. Sci.* **1999**, *155*, 209–230.
[16] Liu, Z. M., Dubremez, J., Richard, V., Yang, Q., Xu, Z. K., Seta, P. *J. Membr. Sci.* **2005**, *267*, 2–7.
[17] Mazzuca, S., Giorno, L., Spadafora, A., Mazzei, R., Drioli, E. *J. Membr. Sci.* **2006**, *285*, 152–158.
[18] Nagy, E. Immobilization of Enzymes on Electrodes. In *Membranes Operations: Innovative Separations and Transformations*Drioli, E., Giorno, L., Eds.; Wiley-VCH: Weinheim, 2009; Chapter 21, pp 309–332.
[19] Li, N., Giorno, L., Drioli, E. *Ann. N. Y. Acad. Sci.* **2003**, *984*, 436–452.
[20] Goel, M. K. Immobilized Enzymes. 1994 http://www.rpi.edu/dept/chem-eng/Biotech-Environ/IMMOB/goel2nd.htm (accessed February 2010).
[21] Nunes, G. S., Marty, J. Immobilization of Enzyme on Electrodes. In *Methods in Biotechnology: Immobilization of Enzymes and Cells*, 2nd edn.;Guisan, J. M., Ed.; Humana: Totowa, NJ, 2006; Chapter 21, p 239.
[22] Jiang, H., Zou, H., Wang, H., Ni, J., Zhang, Q., Zhang, Y. *J. Chromatogr. A* **2000**, *903*, 77–84.
[23] Xie, S., Svec, F., Fréchet, J. M. J. *Biotechnol. Bioeng.* **1999**, *62*, 30.
[24] Charcosset, C. *Biotechnol. Adv.* **2006**, *24*, 482–492.
[25] Turková, J. *J. Chromatogr. B: Biomed. Sci. Appl.* **1999**, *722*, 11S–31S.
[26] Křenková, J., Foret, F. *Electrophoresis* **2004**, *25*, 3550.
[27] Butterfield, D. A., Bhattacharyya, D., Daunert, S., Bachas, L. *J. Membr. Sci.* **2001**, *181*, 29–37.
[28] Rosano, C., Arosio, P., Bolognesi, M. *Biomol. Eng.* **1999**, *16*, 5–12.
[29] Bailey, J. E., Ollis, D. F. *Biochemical Engineering Fundamentals*; McGraw-Hill: New York, 1986; p 97.
[31] Carasik, W., Carrol, J. O. *Food Technol.* **1983,** 85–91.
[32] Chibata, I., Tosa, T., Sato, T. *Appl. Microbiol.* **1974**, *27*, 878–885.
[32] Oyama, K. *J. Chem. Soc.* **1991,** 11.
[34] Takamatsu, S. *Appl. Microbiol. Biotechnol.* **1982**, *15*, 147–149.
[35] Alkorta, I., Garbisu, G., Llama, M. J., Serra, J. L. *Process Biochem.* **1998**, *33*, 21–28.
[36] Giorno, L., Donato, L., Drioli, E. *Fruit Process.* **1998**, *8*, 239–241.
[37] Gallifuoco, A., D'Ercole, L., Alfani, F., Cantarella, M., Spagna, G., Pifferi, P. G. *Process Biochem.* **1998**, *33*, 163–168.
[38] Duran, N., Rosa, M. A., D'Annibale, A., Gianfreda, L. *Enzyme and Microbial Technology* **2002**, *31*, 907–931.
[39] Qi, H. Z. Patent No. CN1546682, 2004.
[40] Kamoshita, Y., Ohashi, R., Suzuki, T. *J. Ferm. Bioeng.* **1998**, *85*, 422–427.
[41] Shiraldi, C., Adduci, V., Valli, V., *et al. Biotechnol. Bioeng.* **2003**, *82*, 213–222.
[42] Nishizawa, K., Nakajima, M., Nabetani, H. *Biotechnol. Bioeng.* **2000**, *68*, 92–97.
[43] Hicke, H.-G., Becker, M., Paulke, B.-R., Ulbricht, M. *J. Membr. Sci.* **2006**, *282*, 413–422.
[44] Frense, D., Lisicki, D., Pflieger, C., Lauckner, G. Device and Method for Enzimatically Producing Baccatin III. Pat. No. WO40066353, 21 July 2005.
[45] Guerrero, L. M. I. Enzymatic Process for Obtaining Astaxanthin and Protein from Fermented Shrimp Residue. Pat. No MXPA02012838, 27 April 2004.
[46] Lopez, J. L., Matson, S. L. *J. Membr. Sci.* **1997**, *125*, 189–211.
[47] Giorno, L., Drioli, E. *Trends Biotechnol.* **2000**, *18*, 339–348.
[47] Yang, W., Cicek, N. *Ilg, J. J. Membr. Sci.* **1997**, *270*, 201–211.
[47] Matson, S. L. Method for Resolution of Stereoisomers in Multiphase and Extractive Membrane Reactors. Pat. No. DK481889, 1 December 1989.
[48] Sato, T., Tosa, T. *Optical Resolution of Aminoacids by Aminoacylase in Industrial Application of Immobilized Biocatalyst;* Tanaka, T., Tosa, T., Kobayashi, T., Eds. Marcel Dekked: New York, 1993; pp 3–14.
[48] Wandrey, C. *Chem. Record* **2004**, *4*, 254–265.
[49] Nam, C. H., Furusaki, S. *Adv. Biochem. Eng./Biotechnol.* **1991**, *44*, 27–64.
[49] Pastore, M., Morisi, F. *Methods Enzymol.* **1976**, *44*, 822–830.
[50] Tanaka, I., Tosa, T., Kobayashi, T., Eds. *Industrial Application of Immobilized Biocatalysts*; Marcel Dekker: New York, 1993; pp 53–55.

Biographical Sketches

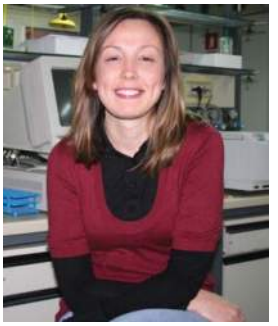

Rosalinda Mazzei is a researcher contractor at the Institute on Membrane Technology, ITM-CNR, Italy. She works in ITM-CNR since 2003. Her research experiences include membrane bioengineering, biocatalytic membrane reactors, membrane bioseparation and bioconversion and membrane emulsification.

Enrico Drioli is full professor at the School of Engineering of the University of Calabria. He has been professor of chemistry and electrochemistry at the School of Engineering of the University of Naples, dean of the School of Engineering of the University of Calabria, director of the Institute on Membranes and Chemical Reactors of the National Research Council, and director of the Institute on Membrane Technology of Consiglio Nazionale delle Ricerche (CNR).

His main research activities focus on membrane science and engineering; membranes in artificial organs; integrated membrane processes; membrane preparation and transport phenomena in membranes; membrane distillation and membrane contactors; and catalytic membrane and catalytic membrane reactors.

He received the following awards and honors: Doctorate Honoris Causa from the University of Paul Sabatier of Toulouse; International Cooperation Honor Award given by the Membrane Industry Association of China for his special dedication to the International Cooperation between China and Europe in the field of membrane and science technology; guest professor in the Environment and Safety Engineering Department at the Jiangsu Polytechnic University, China; honorary member of the A. V. Topchiev Institute of Petrochemical Synthesis at the Russian Academy of Sciences, Moscow; Doctorate Honoris Causa in Chemistry and Chemical Technology from the Russian Academy of Science; and honorary professor at the China Northwest University in Xi'an, Shaanxi, People's Republic of China.

He is involved in many international societies and scientific committees. Currently, he is member of various editorial boards and international advisory boards as well as chairman of the Working Party on Membranes of the European Federation of Chemical Engineering.

He is author of more than 530 scientific papers and 18 patents in the field of membrane science and technology.

Lidietta Giorno is a membrane biotechnologist with background in biological science, chemical technologies, and new materials. Her research experiences include membrane bioengineering, biocatalytic membrane reactors, integrated membrane systems for bioseparations and bioconversions, downstream processing based on molecular separation, membrane chirotechnology, and membrane emulsifier. She has been involved in membrane science and engineering research and development for almost 20 years.

She is a director of the Institute on Membrane Technology of the National Research Council of Italy, ITM-CNR and is involved in research cooperations at European and international level. She worked abroad in the USA at Sepracor Inc. (1992); in The Netherlands at ATO-DLO (1994); and in France, at The University of Compiegne (1997 and 2000). She is a visiting professor at Tianjin University of Science and Technology, China, since 2008.

Lidietta Giorno is a co-author of three books and some 70 peer reviewed scientific papers in international journals. She is an editorial board member of scientific journals, a member of the referee pool of scientific journals and research agencies, and a member of international committees and several scientific societies.

She has served on the European Membrane Society Council for two mandates and is currently the president of the EMS Council and editor of the *EMS Membrane Newsletter*.

3.09 Hollow Fiber Membrane Bioreactor Technology for Tissue Engineering and Stem Cell Therapy

H Ye and Z F Cui, University of Oxford, Oxford, UK

M J Ellis, University of Bath, Bath, UK

H Macedo and A Mantalaris, Imperial College London, London, UK

3.09.1	Introduction	213
3.09.2	HFMB for 3D Tissue Engineering	213
3.09.3	Artificial Functional Organs	215
3.09.3.1	Bioartificial Liver	215
3.09.3.2	Bioartificial Kidney	216
3.09.3.3	Bioartificial Pancreas	217
3.09.4	HFMB for Stem Cell Culture	217
3.09.5	Development of Biodegradable Hollow Fiber Membrane	217
3.09.6	Mathematical Modeling	220
3.09.7	Future Opportunities	223
References		223

3.09.1 Introduction

Hollow fiber membrane modules have had many applications, such as filtration, extraction, and oxygenation, in numerous industrial processes for many years. As bioreactors, they are extensively used for enzyme reactions and cell/bacteria/yeast culture. The concept of a hollow fiber membrane bioreactor (HFMB) used in cell culture is shown in **Figure 1**.

The hollow fiber membranes are contained in an external shell (normally in the shape of a cylinder). The cells can be attached to the outer surface of the membranes, or more commonly maintained in the extracapillary space (ECS). Nutrients flow in the lumen of the fibers and can diffuse out through the pores of the fiber wall to feed the cells. Also, the metabolic waste produced by cells can permeate back into the fibers and be carried away.

HFMBs have been used to culture a variety of mammalian cell lines since their inception by Knazek [1]. HFMBs for mammalian cell cultures are mainly used to produce expensive biochemicals such as vaccines [2], interferons [3], hormones [4], growth factors [5], viruses [6], and monoclonal antibodies [7] and to act as artificial organs [8, 9].

There are many advantages which HFMBs offer over other culture methods. HFMBs have high surface-to-volume ratios of around $30\,cm^2/cm^{-3}$ [10], thus giving the potential to grow cells to high densities. The continuous supply of uniform liquid and gaseous nutrients and removal of metabolic wastes provide a stable microenvironment for cells. The selective permeability property can protect cell culture from the immune system in artificial organ applications and to facilitate the recovery in biological product manufacture [11]. Cells are subject to low shear forces due to their separation from the nutrient flow in the fiber lumen.

More recently, HFMB found its application in the area of regenerative medicine. Generally speaking, regenerative medicine includes either engineered functional tissues or therapeutic quantities of cells. Tissue engineering applications aim at developing functional tissues from cells in combination with a suitable matrix to support and accelerate regenerative healing, while cell therapy only transplants required type and amount of cells into the defect site. This chapter presents a summary on the application of HFMBs in regenerative medicine, as an enabling technology to support three-dimensional (3D) tissue culture and to expand stem cells.

3.09.2 HFMB for 3D Tissue Engineering

New developments in the tissue engineering field are extensive. Almost all tissues and organ systems are under consideration and some tissues are already

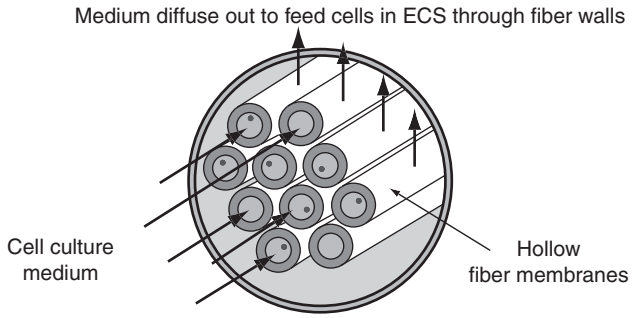

Figure 1 Schematic diagram of hollow fiber membrane bioreactor.

available commercially or under clinical trial [12]. However, currently only avascular (cartilage) or thin sheets of tissues (skin) are capable of being successfully engineered [13]. The mass of 3D tissue, especially dense tissue, that may be produced *in vitro* is very limited [14]. To develop a 3D tissue, the problems of oxygen and nutrient supply to the cells and waste removal from these cells, particularly in the center of the construct, must be addressed. Biological angiogenesis is the primary requirement for generation of an appreciable mass of most tissues, but initiation and control of angiogenesis remains a major technical challenge to tissue engineering. An engineering solution to applying oxygen and essential nutrients to the growing tissue *in vitro* is to use HFMBs with the hollow fiber membrane network mimicking the blood capillary system.

However, using the conventional HFMB, tissue structures could not be produced because of the lack of the necessary 3D scaffolds for cell attachment and proliferation. *In vivo*, cells are supported and maintained by extracellular matrix (ECM) and a similar environment will be required for cells to form 3D tissue structures *in vitro*. A major difference between the design of HFMBs to be used for growing cells and that for producing engineered tissues lies in the inclusion of biomaterial scaffolds in the latter to allow the growth of 3D structures.

The concept of an HFMB for growing bone tissue is shown in **Figure 2** as an example. The original idea stems from how blood is supplied to compact human bone. Compact bones consist of closely packed cylindrical osteons with blood vessels going through in the center. A hollow fiber can play similar role of a blood vessel when growing bone *in vitro*. The hollow fibers are embedded parallel to each other into some scaffolding materials and the whole construct is contained in an external housing. Cells are seeded throughout the scaffolds and the nutrients flowing in the fiber lumen can diffuse out through the porous walls of the hollow fibers to feed cells. The cell metabolic waste can also permeate back into the fiber lumen and be brought away. In this manner, cells can get adequate supply of nutrients relatively independent of their position in the scaffolds. In addition, the local accumulation of metabolic waste is avoided so that a chemostat environment is ensured which is very beneficial to cell growth.

In a proof-of-concept study, it was shown that rat bone marrow stem cells (rBMSCs) cultured in the

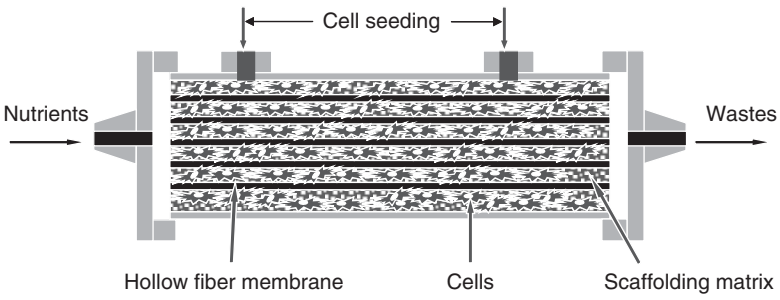

Figure 2 Schematic diagram of HFMB for tissue engineering. The hollow fiber membranes are embedded parallel to each other within scaffolding materials and the whole construct is contained in an external housing. Cells are seeded outside the hollow fiber membranes and the nutrients flowing in the fiber lumen can diffuse out through the porous walls of the hollow fibers to feed cells. The cell metabolic waste can also permeate back into the fiber lumen and be brought away.

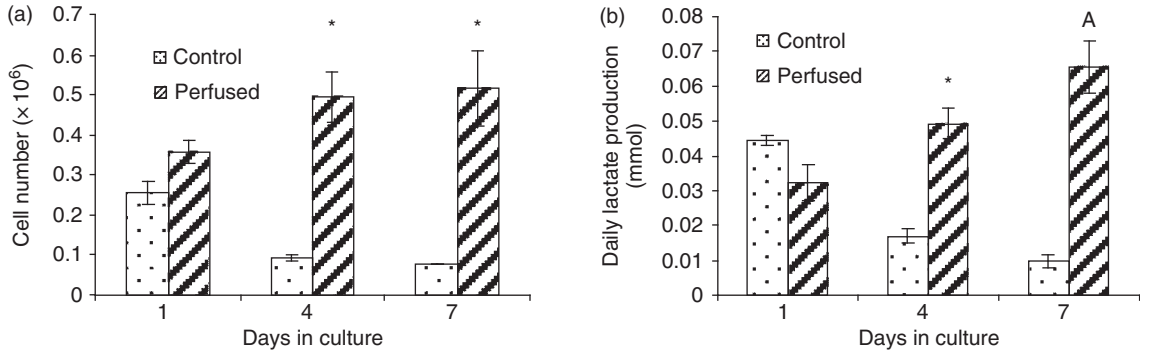

Figure 3 Cell proliferation in HFMBs: (a) calculated cell number estimated by Alamar Blue™ Assay of control and perfused groups and (b) daily lactate production in the culture medium of control and perfused groups ($^*p < 0.05$) [15].

perfused HFMBs had significantly higher viability and proliferation rate than the ones in static (nonperfused) HFMBs [15] (**Figure 3**). For each biological assay performed (lactate production, cell viability, and cell proliferation), it was observed that, while there were no significant differences at day 1, there was significantly improved cell survival and proliferation in the perfused bioreactors at later time points (day 4 and 7). This was confirmed by the light and electron microscopic examination showing increased numbers of intact cells invading the ECM in the perfused samples compared to the cell debris observed within the nonperfused samples. These observations are consistent with that continuous perfusion providing a more efficient supply of nutrients and also a stable pericellular microenvironment compared to the nonperfusion where diffusion from the outer surface will be a limiting factor.

In the follow-on study, HFMBs were proved to have supplied desirable long-term culture environment for rBMSCs seeded into 3D porous polycaprolactone (PCL) scaffold. rBMSCs proliferated and differentiated in the HFMBs and formed bone-like tissue after implantation into nonobese diabetic/severe combined immunodifficient (NOD/SCID) mice (**Figure 4**).

3.09.3 Artificial Functional Organs

3.09.3.1 Bioartificial Liver

Liver transplantation is currently the only mode of treatment for patients in acute liver failure who are not responding to supportive therapy [16]. Various liver support devices have been developed to stabilize the patients while they wait for suitable donors and act as a bridge to transplantation. A bioartificial liver (BAL) is a synthetic system that, with the inclusion of hepatocytes, can perform specific tasks closer to the *in vivo* performances. HFMB can fulfill the design requirements of BAL, that is, the cells used in the device be given an anchorage substrate and isolated from the host immune system. Hollow fiber membranes provide some degree of anchorage for hepatocytes and this may be supplemented by ECM materials, such as collagen. In addition, the membrane isolates xenogeneic hepatocytes from immune system. In addition to immunoisolation, membranes can also provide protection from viral transmission. Concerns have been expressed regarding the possibility of xenozoonotic retroviral infection of patients treated with a BAL using porcine hepatocytes. In a hollow fiber-based BAL, cells can be cultured either inside or outside of the hollow fibers.

According to Legallais *et al.* [8], BALs based on HFMB perfusion bioreactors can accommodate larger amount of cells than their perfusion bioreactor counterparts, on an extent of 10–100-fold, depending on the overall geometry of the design. This pinpoints the relative importance that has been given to the hollow-fiber-type design. A review on the different materials, up-to-date at the time, used in the design of HFMB for hepatocytes cultures concluded that polysulfone (PS) represented the best material, of all tested, in terms of facilitation of cell attachment and maintenance of cellular integrity and metabolic activity [8].

Some authors highlight the limitations of hollow fibers as long-term solutions for the culture of hepatocytes [17]. The membrane, while can separate cells from immune system, does reduce diffusion of nutrients and oxygen to the cells. In addition, their tendency to foul by adsorption of plasma proteins or

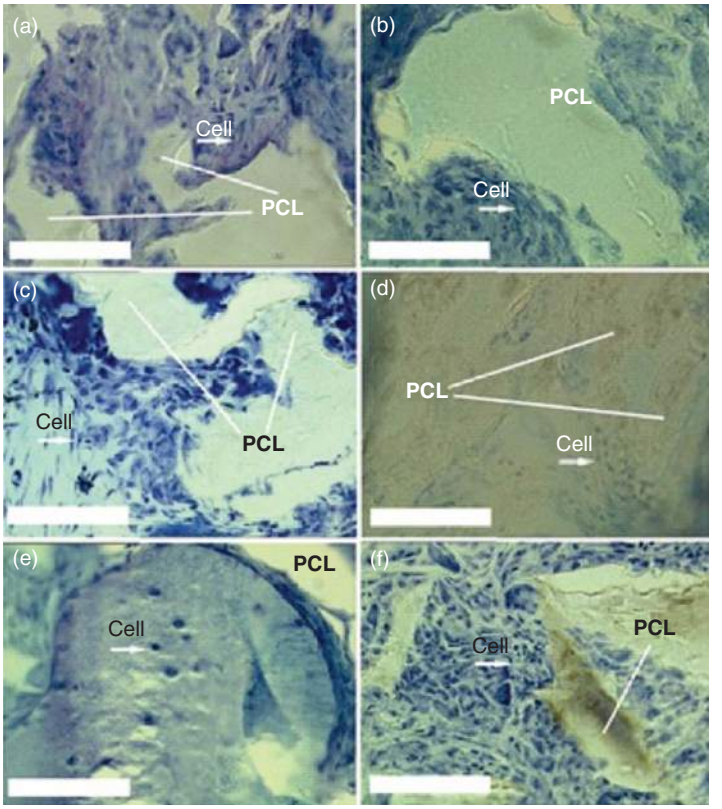

Figure 4 Photomicrographs of toluidine blue staining of representative tissue sections of bioconstructs (rBMSCs + PCL scaffolds) (a, c, e) and PCL scaffolds alone (b, d, f) implanted in NOD/SCID mice. (a, b) Two weeks after implantation; (c, d) 4 weeks after implantation; (e, f) 8 weeks after implantation. Bar = 100 μm.

the development of biofilms, which further increases the resistance to mass transport, was pointed out as a major drawback of this geometry [18].

3.09.3.2 Bioartificial Kidney

The treatment for patients with acute or chronic renal failure using dialysis or hemofiltration is still suboptimal with high morbidity and mortality. Poor outcomes may be due to the fact that these therapies substitute for the small solute clearance function of the kidney but do not replace the lost reclamation, metabolic, and endocrine functions of this organ [19]. The success of HFMB-based extracorporeal liver-assist devices and encapsulated islets of Langerhans to treat liver failure and diabetes mellitus has provoked the application of HFMBs in renal replacement therapy, especially with the proven success of hemodialysis and hemofiltration in which hollow fiber membrane cartridges are employed.

The bioartificial renal tubule-assist device (RAD) of a single renal tubule by using hollow fiber membrane has been achieved [20]. Scale-up from a single hollow fiber to a multifiber RAD has also proceeded and utilizes both porcine and human renal proximal tubule cells grown along the inner surface of PS immunoisolating hollow fibers [21, 22]. These hollow fibers are packaged in bioreactor cartridges with membrane surface areas as large as 0.7 m^2 resulting in a device containing up to 2.5×10^9 cells. *In vitro* studies of these RADs have demonstrated their retention of differentiated active vectorial transport of sodium, bicarbonate, glucose, and organic anions. In preclinical and clinical studies, this bioartificial kidney has consistently demonstrated excellent safety with reduction in mortality and mobility [23]. The RAD with human cells also demonstrated functional and metabolic performance for up to 24 h of use in patients [24].

The current version of the RAD in clinical trials is large and requires an extracorporeal circuit with peristaltic pumps to provide driving pressure for hemofiltration. Nevertheless, the cell therapy component in a bioartificial kidney will supply some functions of a healthy kidney that dialysis strategies simply do

not. The combination of cell therapy with solute clearance could be a viable renal replacement therapy that confers dialysis independence to the patient [25].

3.09.3.3 Bioartificial Pancreas

The concept of bioartificial pancreas (BAP) is quite similar to that of BAL and kidney. A BAP is to protect transplanted islets from graft rejection by an artificial membrane permeable to glucose and insulin but impermeable to immunoglobulins and cells of the host's immune system. HFMB has been used both as intravascular and extravascular BAP devices. Intravascular devices are implanted as an artery-to-vein (AV) shunt in the recipient's body and are usually made of tubular hollow fiber membranes [26]. The lifetime of intravascular BAP is usually much shorter than extravascular one mainly due to the presence of blood coagulation in the fibers [27]. Extravascular devices are mainly implanted in the peritoneal cavity, but have also been implanted in other regions, for example, the subcutaneous tissue site.

3.09.4 HFMB for Stem Cell Culture

Autologous and allogeneic stem cell transplantation have attracted much attention over the last two decades as variable therapeutic options for treating those diseases for which modern medicine previously could offer little hope. Stem cells are unique in that they have the capacity for self-renewal and are capable of forming at least one, and sometimes many, specialized cell types. The promise of stem cells for clinical therapy, however, has been limited because the number of stem cells that can be obtained directly from tissue/organ is inadequate. For example, although umbilical cord blood represents a rich source of transplantable hematopoietic stem cells (HSCs) that can be easily obtained from tissue normally discarded at birth, cells obtained from a single cord blood collection, more often than not, contain too few HSCs to ensure the hematological engraftment of an adult patient [28, 29]. One way to overcome the above-mentioned limitation is to expand stem cell numbers *in vitro* (outside the body). Stem cells are sensitive to changes in culture conditions and prone to differentiate into other cell types. Thus, well-controlled culture condition is paramount in stem cell expansion. The inadequacies of current culture protocols using tissue-culture flasks, roller bottles, or gas-permeable bags are related to their multistep procedures. By such methods, the primary progenitor cells must endure the enzymatic treatment, physical dissociation, the force of centrifugation; in addition, the vessel has to be opened to the environment for frequent cell transfer and re-suspension, exposing the cultures to the risk of contamination. HFMB could be adopted for expanding stem cells due to its relatively homogeneous culture environment, low shear stress on cells, large surface area, and easy control through external operational manipulation.

Yamazoe and Iwata [30] demonstrated that dopaminergic neurons were effectively induced from embryonic stem (ES) cells enclosed in semi-permeable hollow fiber membranes by maintaining them in PA6 conditioned medium. It suggested that differentiation of ES cells in HFMB is a promising approach to realize cell therapy of Parkinson's disease.

The application of HFMB also provided a solution for many of the difficulties associated with hematopoietic stem cell gene transfer [31]. It was shown that $CD34^+$ progenitors could be cultured and transduced in an HFMB without losing CD34 identity while maintaining viability. Much higher transduction efficiencies were achieved in primary colony-forming cells derived from the HFMB compared with traditional gas-permeable bags.

3.09.5 Development of Biodegradable Hollow Fiber Membrane

The ultimate goal for tissue engineering is to develop implantable functional tissues/organs to replace defected ones. Ideally, what are left in the human body should only be cells/tissues, but not other synthetic materials. In the case of HFMB, as the hollow fiber membranes form part of the engineered tissue, they should be made of biodegradable materials, and hence eventually replaced by body's own blood vessel ingrowth into the engineered tissues following the implantation.

Poly(lactide-co-glycolide) (PLGA) is a common synthetic biodegradable polymer used for scaffold fabrication in tissue engineering , as it has been approved for application as a suture material, a number of orthopedic devices, including interference screws, and for drug delivery. A number of cell types have been successfully cultured on the PLGA membranes (flat sheet and hollow fibers), including human bone-derived cells (HBDC) [32], human mesenchymal stromal cells (hMSCs) [33], rat MSC (**Figure 5**), rat pancreatic cells, and liver cells transdifferentiated from the pancreatic cells on the PLGA–PVA.

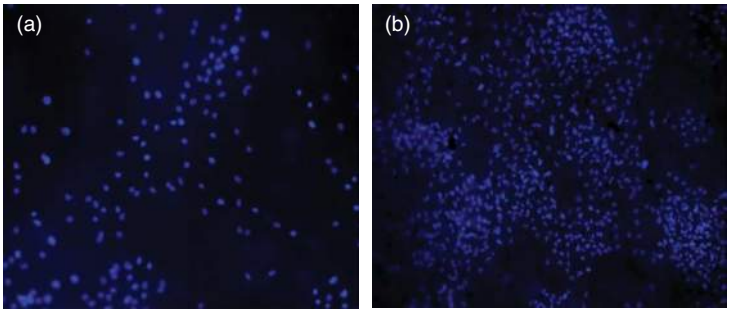

Figure 5 Hoechst staining of mesenchymal stem cells seeded on PLGA (a) and on 5% PVA-PLGA flat sheets (b) after 24 h seeding. 100× magnification.

The fabrication process of hollow fiber membranes is demonstrated in **Figure 6**. In this scheme, the spinning dope, consisting of a viscous, degassed, and filtered polymer solution (20–40% polymer by weight), is pumped into a coaxial tube, jet spinneret. The polymer content is usually close to the precipitation point. The thread line emerging from the spinneret is quickly stabilized by an internal quench (coagulating) medium (nonsolvent liquid or gas) as it emerges from the jet orifice. The nascent hollow thread is further stabilized in a quench bath. At this point, the fiber has sufficient mechanical integrity to pass over guides and rollers under moderate tension. In most commercial production lines, the spinning rate is 10–1000 m min^{-1} and is governed by the spinning method, dope compositions, and the morphological and dimensional requirements. Therefore, dope compositions and spinning conditions are sought that result in the establishment of the hollow fiber immediately on emergence from the orifice. Residual quenching liquid and solvent are usually removed by some sort of a washing step prior to use [34].

The polymer chemistry, the thermodynamic interaction of the polymer, solvent and nonsolvent, the rheology of the spinning dope, and the setup of the spinning apparatus all influence the morphology and therefore the physical, chemical, and mass transport characteristics of the hollow fiber membrane. A few examples of the parameter that proved key in fabricating the PLGA hollow fiber membranes are discussed in the following.

Solvent selection. There are many potential solvents that will dissolve PLGA and that have been used for scaffold preparation by various techniques. Examples of such solvents (and the techniques for which they have been used) include: methylene chloride [35] and methyl chloride [36] (for high-temperature extrusion and dip coating); glacial acetic acid (for low temperature and pressure injection moulding [37, 38]); chloroform (for extrusion, dip coating and film casting, with either solvent evaporation or by immersion precipitation [39–46]) (**Table 1**).

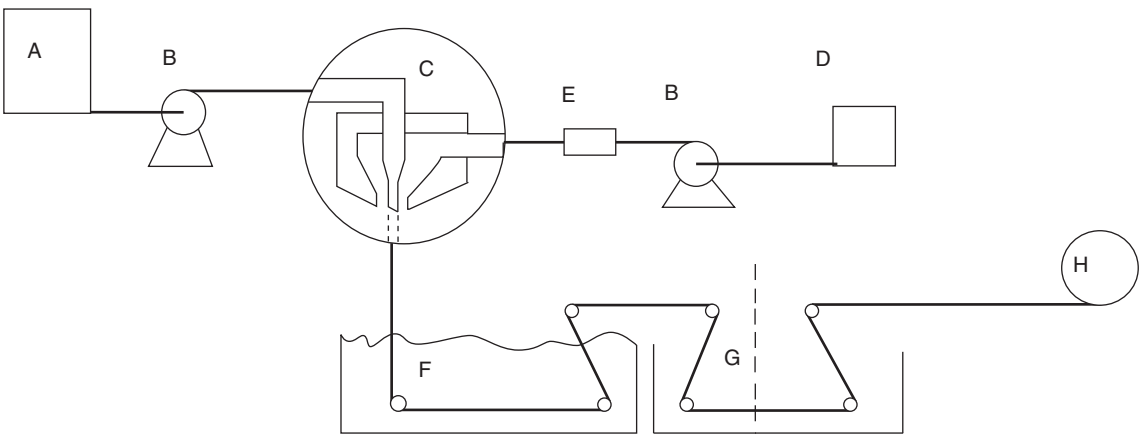

Figure 6 Schematic of dry-jet wet spinning employing tube-in-orifice spinneret. A: bore injection medium (liquid, gas, or suspended solids); B: pump; C: spinneret; D: polymer spinning solution; E: micrometer dope filter; F: coagulation cooling bath; G: quench bath; and H: collection pool.

Table 1 Properties of solvents commonly used in PLGA scaffold preparation

	Chloroform	*Methyl chloride*	*Dioxane*	*NMP*
Toxicity	Irritant and probable carcinogen Can be fatal on ingestion or inhalation	Irritant and probable carcinogen Known mutogen	Irritant and probable carcinogen	Skin, eye, and respiratory irritant
Volatility	Volatile	Volatile	Volatile	Nonvolatile at STP[a]
Flammability		Highly flammable	Highly flammable	
Misciblity water	Not miscible	Slightly soluble in water[52]	Miscible	Miscible

[a] STP is standard temperature pressure; 273 K and 1 atm.
Data from Oxford University MSDS (2009) Material Safety Data Sheet. http://msds.chem.ox.ac.uk/#MSDS (accessed 25 August, last update 30 October). unless otherwise stated [61].

Due to their nature, many solvents are harmful and hazardous. Volatile solvents not only increase the chance of user exposure but can also affect the solution composition as a function of time. Chloroform and methyl chloride are poorly miscible with water so are of no use in a ternary system where water is used as the nonsolvent. In comparison, *N*-methyl pyrrolidone (NMP) is considered relatively harmless and has been used in animal models and shown to increase bone formation [47]. Dioxane and NMP are common solvents for hollow fiber preparation so data are relatively easy to obtain on the solvent–water interactions which are important for predicting and assessing the hollow fiber structure and performance.

When a solvent–nonsolvent combination with a high mutual affinity is used, instantaneous demixing occurs and a porous membrane will be obtained. If the combination has low mutual affinity, delayed demixing will proceed and a dense, nonporous membrane will form. Dioxane-water and NMP-water both have high mutual affinities so porous structures are expected to form. Chloroform and methylene chloride cannot be paired with water, but methanol, ethanol, or propanol are suitable nonsolvent alternatives. Still, the mutual affinity is low and a nonporous structure will result [34]. For cell culture, the membrane should all easy mass transfer of all the molecules, i.e. there should be no size exclusion. The range of molecular weights will be dependent on the media composition, and this size range can be determined using HPLC. Typically molecules up to 150 kDa [50] must be able to permeate, but in some systems molecules can be up to 300 kDa, when undefined serum is used. While there may be complex membrane-protein and protein-protein interactions, and the shape of the protein is also a factor in determining mass transfer, a rough estimate of the necessary pore size can be found by considering the fact that a 1000 kDa molecule will have an approximate size of 0.1mm [51]. It should also be noted that the maximum pore size should be 5 micrometer as cells can enter spaces larger than this which will cause pore blockage

Spinning dope viscosity. The viscosity of the solution will affect the shear experienced in the spinneret and will influence the structure. It is also necessary to have a solution with a viscosity that is low enough to allow the solution to flow, but high enough to hold the solution together until precipitation has occurred. The viscosity range used for spinning varies between groups; Eenink *et al.* [53] selected spinning dopes with viscosities in the range 20–100 Pa s, whereas Tai *et al.* [54] found that viscosities between 8 and 15 Pa s were ideal. In the study by Eenink *et al.* [53], a minimum polymer concentration of 10% (w/w) was regarded as necessary to obtain a suitable hollow fiber. Below this concentration, there would not be enough polymer to form a continuous structure. Polymer concentration can affect the porosity of the membrane. A higher volume fraction of polymer will give a less porous structure. A higher initial concentration means a higher concentration at the film interface so leading to a less porous top layer, which will reduce the flux [34]. It can be observed that the PLGA chemistry (e.g., poly lactic acid (PLA):poly glycolic acid (PGA) ratio, PLA isomer, and molecular weight and stereochemistry) as well as the solvent (**Figure 7**) affected the viscosity. A 20% w/w PLGA (50:50 to 100:0 PLA:PGA) in NMP spinning dope was selected as the most suitable polymer concentration when using rac-lactide (50:50 *l*-PLA: *d*-PLA) [52].

Improving hydrophilicity and permeability. The surface properties and porosity of the hollow fiber membranes are important to the identified applications. The hydrophobic nature of PLGA can be problematic for cell seeding. As much as 70% ethanol is a suitable prewetting solution; however, ethanol acts as a

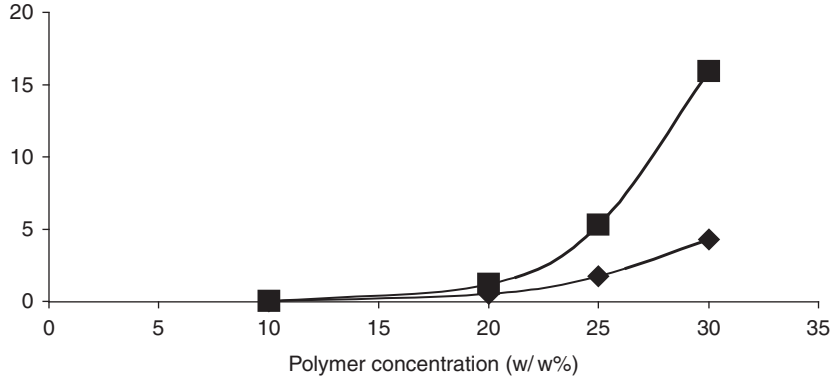

Figure 7 Viscosity of PLGA (50:50) in NMP (diamonds) and dioxane (squares). Readings were taken at 25 °C [51].

plasticizer for PLGA and causes shrinking [55] so great care must be taken during the prewetting process which should be carried out before fixing in the bioreactor. Sterilization can be done also using 70% ethanol or using an antibiotic–antimycotic solution [56]. The easiest approach to using PLGA membranes is not to dry them out, that is, use them soon after spinning, although for long-term use of batches this is acknowledged as impractical. To overcome this, poly vinyl alcohol (PVA) can be added to spinning dope.

Addition of PVA to spinning dope. Blended PVA–PLGA flat sheets fabricated by a melt-molding particulate-leaching method have been shown to be more hydrophilic than control PLGA scaffolds [57], and the same effect has been seen using PVA in PLGA spinning dopes: hollow fiber membranes were fabricated by wet spinning using 20% w/w polymer (75:25 PLA:PGA) in NMP with the addition of 5% PVA w/v. Contact angle measurements indicated an increase of hydrophilicity of the PLGA–PVA fibers (62° for PLGA and 50° for PLGA–PVA), and the PLGA–PVA membranes were observed to sink in water and cell culture media, unlike PLGA fibers which float, giving further indication of their hydrophilicity. The addition of PVA to the PLGA solution resulted in an increase in mean pore size (0.54 for PLGA and 1.1 μm for PLGA–PVA). The mechanical test conducted on the PLGA–PVA fibers showed that the tensile strength was lower than that of the PLGA membranes; addition of PVA resulted in a decrease in the Young's modulus (109 ± 2.5 MPa for PLGA and 75 ± 9.5 MPa for PLGA–PVA). Water flux was calculated at steady state for these membranes as $\mathcal{J} = 700\,\mathrm{l\,h^{-1}\,m^{-2}}$. A BSA in water solution ($250\,\mu\mathrm{g\,ml^{-1}}$) was used to evaluate protein permeation; the BSA permeate concentration reached steady state after about 2.5 h at the feed concentration of $250\,\mu\mathrm{g\,ml^{-1}}$.

3.09.6 Mathematical Modeling

These initial findings have proved the concept of using HFMB for tissue engineering and indicated that implantable amount of bone tissue could be grown by using HFMBs in the future. However, it has also become necessary to develop a theoretical framework that elucidates the uncertain quantitative relationships between the cell environment and tissue behavior in order to guide the design of effective bone tissue engineering protocols. These may include, for example, a framework to analyze the flow and transport behavior in relation to tissue and nutrient (solute) properties, and the reaction rates in a changing tissue environment. The available experimental results need to be placed within a consistent and coherent theoretical framework. This can then help in interpreting the obtained results and direct further experimental work in an appropriate manner. It should also be noted that due to the nature of the HFMB system used for growing tissue (i.e., sterile operating conditions and relatively small dimension compare to industrial processes), it does not allow precise online monitoring of most variables of interest. Instead, a mathematical model can be used to determine these variables.

There has been many attempts of mathematical modeling for the development of hollow fiber-immobilized enzyme and hollow fiber ultrafiltration systems [58–60]. Radial and axial profiles were generated from these models in addition to plots of the effective reactor length as a function of the conversion and the radial Thiele modulus.

While the mathematical framework of an HFMB for cell culture would not be radically different from the above applications, the results are inapplicable to cell culture systems, due to the large differences in cell kinetics and feed flow rates [11]. Also, while the development of mathematical models for cell culture

applications derived from those of enzyme reactors, the two model systems have different objectives. The enzymatic system is to maximize conversion of substrate as the cell culture system is to prevent substrate depletion.

The simplest model is a diffusion-limited bioreactor in which convection in the fiber membrane and ECS is neglected. This assumption is realistic in the case where the HFMB is constructed of relatively low-molecular-weight cutoff (nominally <30 kDa) ultrafiltration membranes, or the cell annulus is of tissue-like density. For the HFMBs used for tissue engineering, a porous scaffold is always included in the ECS; thus, the diffusion-limited model is applicable.

In a Krogh cylinder model, Ye *et al.* were able to show axial and radial concentration profiles of glucose and oxygen in an HFMB used to grow 3D bone tissue (**Figure 8**) [61]. In the concentration profiles shown in **Figure 8**, it can be observed that under the current operating conditions, the glucose and oxygen were sufficient for cell growth throughout the whole bioreactor domain. The model can be used to study how important parameters influenced the substrate concentration in the HFMB. For example, **Figure 9** shows the radial concentration profiles of glucose and oxygen for different cell densities in the region of cellular matrix. As evident, the drop in

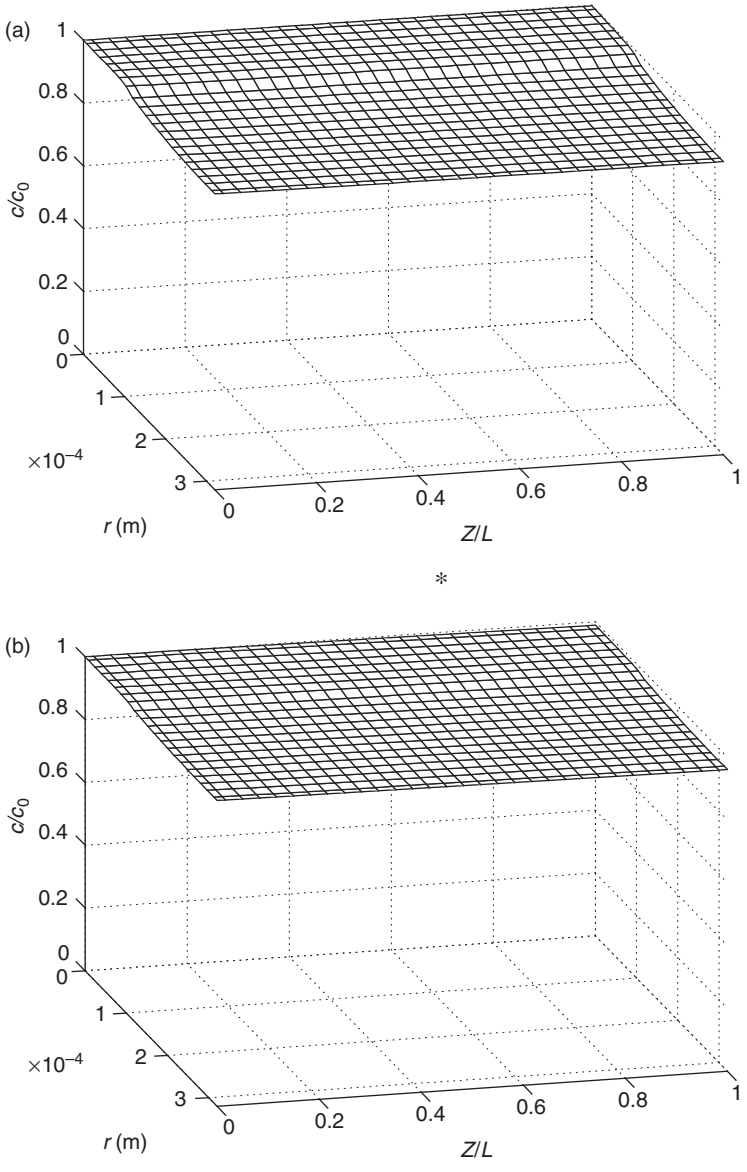

Figure 8 Concentration profiles for glucose (a) and oxygen (b) in HFMB [61].

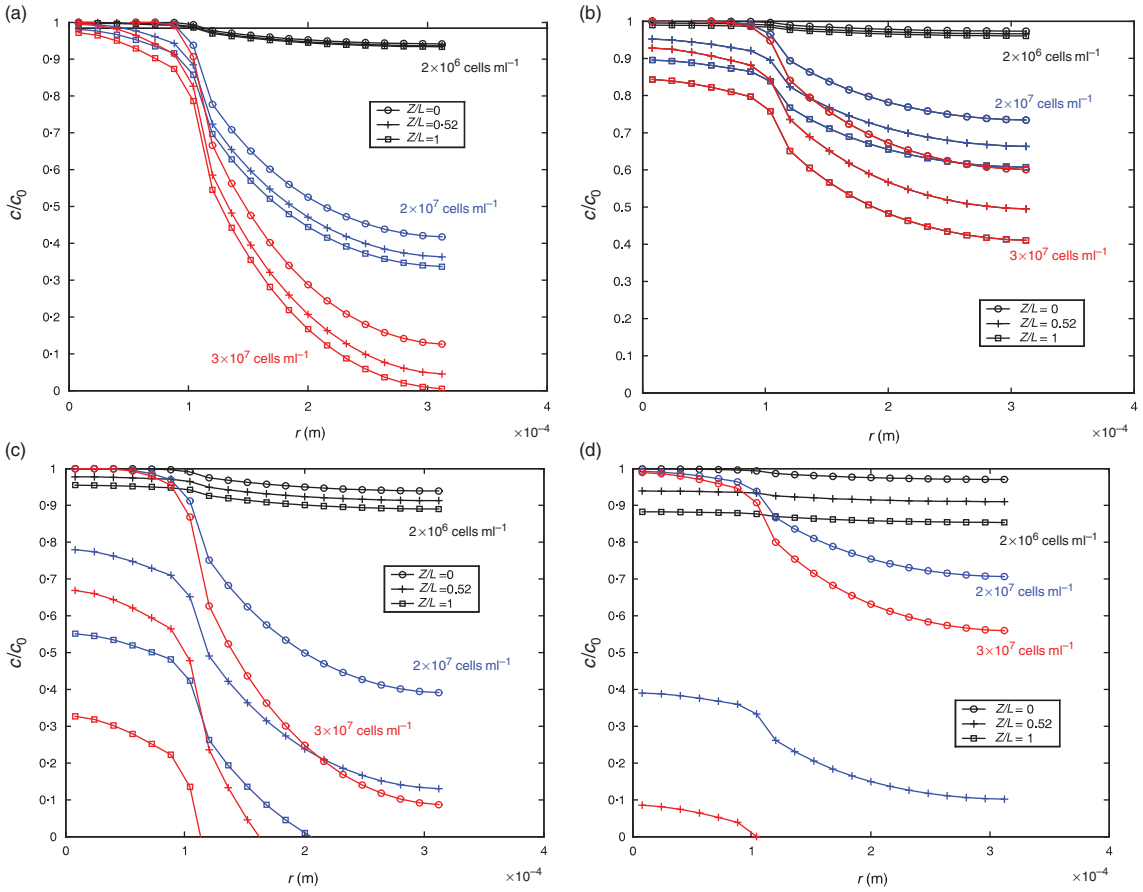

Figure 9 Radial concentration profiles of glucose and oxygen at different cell densities and fiber length. Panels (a) and (b) show the radial concentration profiles of glucose and oxygen, respectively, at different cell densities with fiber length = 0.03 m; panels (c) and (d) show the radial concentration profiles of glucose and oxygen, respectively, with fiber length = 0.3 m. $Z/L = 0$: inlet; $Z/L = 0.52$: near middle; $Z/L = 1$: outlet [61].

axial concentration is larger with higher cell densities for both glucose and oxygen. **Figures 9(a)** and **9(b)** (fiber length = 0.03 m) indicate that for a cell density of 2×10^6 cells ml^{-1} (the cell seeding density used in the laboratory experiments [15]), the radial substrate concentration in the cellular matrix remains higher than approximately 90% of the inlet substrate concentration. However, if the cell density increases to a larger number, glucose concentration drops faster than those for oxygen concentration. It suggests that under the current operating conditions, glucose may be the limiting substrate for the growth of bone tissues in HFMB. This is because when the cell number increases, they may be deprived of glucose first in some part of the bioreactor. Although the radial concentration of glucose drops faster than oxygen at the same cell density, the axial concentration difference between the inlet and outlet is larger for oxygen than that for glucose (**Figures 9c and 9d**). This implies that with a longer fiber length, oxygen could become the limiting substrate for cells.

With the developed mathematical model, the influences of some important operating parameters, such as cell density, medium flow rate, cellular matrix thickness, and properties of hollow fiber membranes, and scaffolding materials, on the substrate concentration distribution in the HFMB could be analyzed. The model will help define the scales at which the HFMBs are not mass transfer limited. It is a much more efficient and cost-effective procedure to assess effects of bioreactor geometries and operating conditions on nutrient transport behavior when compared with building and testing HFMB prototypes.

3.09.7 Future Opportunities

Hollow fiber membrane bioreactors have shown their advantages in various applications outlined in this chapter and beyond. Although the concept has been proved, detailed research and development are needed to translate the laboratory research into clinical applications.

Functional hollow fiber membranes. The surface properties and functions of the hollow fiber membranes are critical to the stem cell expansion, as stem cells require surface niche for their proliferation (and controlled differentiation). Hollow fibers with encapsulated growth factors or functional molecules for controlled release would be useful. For tissue engineering application, tunable degradation rate would be highly desirable.

Hollow fiber membranes made of natural biopolymers. As natural biopolymers offer outstanding advantages in cell adhesion, biocompatibility, and possible interactions with cells, hollow fiber membranes made of such materials can easily find their application. Possible natural polymer candidates include collagen, alginate, chitosan, etc. New fabrication methods may need to be developed.

3D soft tissue development. Hollow fiber membrane network to mimic human capillaries is ideal for the engineering of 3D soft tissues for the treatment of lost tissues due to trauma or cancer. Culture of tissues of multiple cell types and their integration into the host need to be properly addressed.

Disposable device. For stem cell expansion, it is important to develop hollow fiber membrane devices which are standardized, presterilized and prepacked, and good manufacture practice (GMP) complied. With such devices, cell expansion, harvest, and implantation can all be done in a clinically relevant setting.

References

[1] Knazek, R. A. *Fed. Proc.* **1974**, *33*, 1978–1981.
[2] Prilliman, K., Lindsey, M., Zuo, Y., Jackson, K. W., Zhang, Y., Hildebrand, W. *Immunogenetics* **1997**, *45*, 379–385.
[3] Nachman, M. *J. Chromatogr.* **1992**, *597*, 167–172.
[4] Hussain, A., Zimmerman, C. A., Boose, J. A., *et al. J. Clin. Endocrinol. Metab.* **1996**, *81*, 1184–1188.
[5] Liu, J. J., Chen, B. S., Tsai, T. F., *et al. Cytotechnology* **1991**, *5*, 129–139.
[6] Ratner, P. L., Cleary, M. L., James, E. *J. Virol.* **1978**, *26*, 536–539.
[7] Yazaki, P. J., Shively, L., Clark, C., *et al. J. Immunol. Methods* **2001**, *253*, 195–208.
[8] Legallais, C., David, B., Dore, E. *J. Membr. Sci.* **2001**, *181*, 81–95.
[9] Delaunay, C., Darquy, S., Honiger, J., Capron, F., Rouault, C., Reach, G. *Artif. Organs* **1998**, *22*, 291–299.
[10] Knazek, R. A., Gullino, P. M., Kohler, P. O., Dedrick, R. L. *Science* **1972**, *178*, 65–66.
[11] Tharakan, J. P., Gallagher, S. L., Chau, P. C. *Adv. Biotechnol. Proc.* **1988**, *7*, 153–184.
[12] Stock, U. A., Vacanti, J. P. *Annu. Rev. Med.* **2001**, *52*, 443–451.
[13] Marler, J. J., Upton, J., Langer, R., Vacanti, J. *Adv. Drug Delivery Rev.* **1998**, *33*, 165–182.
[14] Freed, L. E., Vunjak-Novakovic, G. *Adv. Drug Delivery Rev.* **1998**, *33*, 15–30.
[15] Ye, H., Xia, Z., Ferguson, D. J., Triffitt, J. T., Cui, Z. *J. Mater. Sci. Mater. Med.* **2007**, *18*, 641–648.
[16] Wu, F. J., Peshwa, M. V., Cerra, F. B., Hu W.-S. *Tissue Eng.* **1995**, *1*, 29–40.
[17] Flendrig, L. M., te Velde, A. A., Chamuleau, R. A. *Artif. Organs* **1997**, *21*, 1177–1181.
[18] Ishihara, K., Hasegawa, T., Watanabe, J., Iwasaki, Y. *Artif. Organs* **2002**, *26*, 1014–1019.
[19] Humes, H. D. *Semin. Nephrol.* **2000**, *20*, 71–82.
[20] MacKay, S. M., Funke, A. J., Buffington, D. A., Humes, H. D. *ASAIO J.* **1998**, *44*, 179–183.
[21] Humes, H. D., MacKay, S. M., Funke, A. J., Buffington, D. A. *Kidney Intl.* **1999**, *55*, 2502–2514.
[22] Humes, H. D., Buffington, D. A., MacKay, S. M., Funke, A. J., Weitzel, W. F. *Nat. Biotechnol.* **1999**, *17*, 451–455.
[23] Tumlin, J., Wali, R., Williams, W., *et al. J. Am. Soc. Nephrol.* **2008**, *19*, 1034–1040.
[24] Humes, H. D., Weitzel, W. F., Bartlett, R. H., *et al. Kidney Intl.* **2004**, *66*, 1578–1588.
[25] Fissell, W. H., Fleischman, A. J., Humes, H. D., Roy, S. *Transl. Res.* **2007**, *150*, 327–336.
[26] Monaco, A. P., Maki, T., Ozato, H., *et al. Ann. Surg.* **1991**, *214*, 339–360; discussion 361.
[27] Silva, A. I., de Matos, A. N., Brons, I. G., Mateus, M. *Med. Res. Rev.* **2006**, *26*, 181–222.
[28] Broxmeyer, H. E., Hangoc, G., Cooper, S., *et al. Proc. Natl. Acad. Sci. U.S.A.* **1992**, *89*, 4109–4113.
[29] Wagner, J. E., Broxmeyer, H. E., Byrd, R. L., *et al. Blood* **1992**, *79*, 1874–1881.
[30] Yamazoe, H., Iwata, H. *Biomaterials* **2006**, *27*, 4871–4880.
[31] Pan, D., Stroncek, D. F., Whitley, C. B. *J. Gene Med.* **2004**, *6*, 1293–1303.
[32] Ellis, M. J., Chaudhuri, J. B. *Biotechnol. Bioeng.* **2008**, *101*, 369–377.
[33] Morgan, S. M., Tilley, S., Perera, S., *et al. Biomaterials* **2007**, *28*, 5332–5343.
[34] Mulder, M. *Basic Principles of Membrane Technology*, 2nd edn.; Kluwer: Dordrecht, 1992.
[35] Widmer, M. S., Gupta, P. K., Lu, L., *et al. Biomaterials* **1998**, *19*, 1945–1955.
[36] Luciano, R. M., de Carvalho Zavaglia, C. A., de Rezende Duek, E. A. *Artif. Organs* **2000**, *24*, 206–208.
[37] Hadlock, T., Sundback, C., Hunter, D., Cheney, M., Vacanti, J. P. *Tissue Eng.* **2000**, *6*, 119–127.
[38] Sundback, C., Hadlock, T., Cheney, M., Vacanti, J. *Biomaterials* **2003**, *24*, 819–830.
[39] Yoshimoto, H., Shin, Y. M., Terai, H., Vacanti, J. P. *Biomaterials* **2003**, *24*, 2077–2082.
[40] Wan, A. C., Mao, H. Q., Wang, S., Leong, K. W., Ong, L. K., Yu, H. *Biomaterials* **2001**, *22*, 1147–1156.
[41] Wang, S., Wan, A. C., Xu, X., *et al. Biomaterials* **2001**, *22*, 1157–1169.
[42] Kivalo, M., Siren, V., Raitta, C., Immonen, I. *J. Mater. Sci. Mater. Med.* **1999**, *10*, 53–58.

[43] Ishaug, S. L., Crane, G. M., Miller, M. J., Yasko, A. W., Yaszemski, M. J., Mikos, A. G. *J. Biomed. Mater. Res.* **1997**, *36*, 17–28.
[44] Ishaug, S. L., Payne, R. G., Yaszemski, M. J., Aufdemorte, T. B., Bizios, R., Mikos, A. G. *Biotechnol. Bioeng.* **1996**, *50*, 443–451.
[45] Ishaug-Riley, S. L., Crane, G. M., Gurlek, A., *et al. J. Biomed. Mater. Res.* **1997**, *36*, 1–8.
[46] Ishaug-Riley, S. L., Crane-Kruger, G. M., Yaszemski, M. J., Mikos, A. G. *Biomaterials* **1998**, *19*, 1405–1412.
[47] Miguel, B. S., Ghayor, C., Ehrbar, M., Jung, R. E., Zwahlen, R. A., Hortschansky, P., Schmoekel, H. G., Weber, F. E. *Tissue Engineering Part A* **2009**, *15*, 2955–2963.
[48] Kumar, S., Wittmann, C., Heinzle, E. *Biotechnol. Lett.* **2004**, *26*, 1–10.
[49] Planchamp, C., Vu, T. L., Mayer, J. M., Reist, M., Testa, B. *J. Pharm. Pharmacol.* **2003**, *55*, 1181–1198.
[50] Ellis, M. J., Chaudhuri, J. B. *Biotechnol. Bioeng.* **2007**, *96*, 177–187.
[51] Sadek, P. C. *The HPLC Solvent Guide*; Wiley: New York, 1996.
[52] Eenink, M. J. D., Feijen, J., Olijslager, J., Albers, J. H. M., Rieke, J. C., Greidanus, P. J. *J. Control. Release* **1987**, *6*, 225–247.
[53] Tai, C. C., Perrera, S. P., Crittenden, B. D. Development of Adsorbent Hollow Fibres. In *7th World Congress of Chemical Engineering*, Glasgow, UK, 2005.
[54] Lu, L., Peter, S. J., Lyman, M. D., *et al. Biomaterials* **2000**, *21*, 1837–1845.
[55] Shearer, H., Ellis, M. J., Perera, S. P., Chaudhuri, J. B. *Tissue Eng.* **2006**, *12*, 2717–2727.
[56] Oh, S. H., Kang, S. G., Kim, E. S., Cho, S. H., Lee, J. H. *Biomaterials* **2003**, *24*, 4011–4021.
[57] Lewis, W., Middleman, S. *AIChE J.* **1974**, *20*, 1012.
[58] Rony, P. R. *Biotechnol. Bioeng.* **1971**, *13*, 431.
[59] Waterland, L. R., Michaels, A. S., Robertson, C. R. *AIChE J.* **1974**, *20*, 50–59.
[60] Ye, H., Das, D. B., Triffitt, J. T., Cui, Z. F. *J. Membr. Sci.* **2006**, *272*, 169–178.
[61] Material Safety Data Sheet. http://msds.chem.ox.ac.uk/#MSDS (accessed 25 August, last update 30 October).

Biographical Sketches

Hua Ye studied at the Dalian University of Technology in China and earned a BEng in chemical engineering in 1998. She was awarded her DPhil in biochemical engineering (in tissue engineering, 2005) at the University of Oxford . In the same year, she joined the Department of Chemical Engineering at the Imperial College London as a postdoctoral fellow. Currently, she is a Research Councils UK (RCUK) academic fellow in tissue engineering and stem cell technologies at the University of Oxford. Her research interests include stem cell bioprocessing (expansion and differentiation) and bioreactors for tissue engineering.

Professor Zhanfeng Cui is the Donald Pollock professor of chemical engineering, University of Oxford since the Chair was established in 2000. He is the founding director of the Oxford Centre for Tissue Engineering and Bioprocessing (OCTEB).

He was educated in China and received his BSc from the Inner Mongolia University of Technology (1982) and MSc (1984) and PhD (1987) from the Dalian University of Technology. After a postdoctoral experience at the Strathclyde University in Scotland, he joined the Edinburgh University as a lecturer in chemical engineering (1991). He then held academic appointments at the Oxford Engineering Science Department as university lecturer (1994-98) and reader (1999-2000). He was a visiting professor of Georgia Institute of Technology, USA (1999), the Brown Intertec visiting professor to the University of Minnesota, USA (2004), and a Chang-Jiang visiting professor to the Dalian University of Technology, China (2005). He is a chartered engineer, a chartered scientist, and a fellow of the Institution of Chemical Engineers. In 2009, he was awarded the degree of DSc by the Oxford University to recognize his research achievement. His research interests include tissue engineering and stem cell technologies, and bioseparation and bioprocessing, and membrane science and technology. Along with his co-workers, he has published over 120 articles in refereed journal papers and filed seven patent applications in the last five years. He was the academic founder of Zyoxel Limited, an Oxford University subsidiary in 2009.

Marianne J. Ellis graduated with a degree in Chemical & Bioprocess Engineering in 2001, followed by a PhD in Tissue Engineering in 2005 from the Department of Chemical Engineering, University of Bath. She spent one year working as a postdoctoral researcher before being appointed as a lecturer in the Department, in 2005. She is also a Board Member of the Bath Centre for Regenerative Medicine. From her early work, designing poly(lactide-co-glycolide) membrane-scaffolds, she has developed an interest in the entire process of tissue engineering, from sourcing the raw materials for scaffold fabrication, to fabricating scaffolds, to how the end user will work with a tissue engineered system. The research involves studying the chemical, physical and biological micro-environment at the scaffold surface and macro-environment of the bioreactor. She also has a keen interest in sustainable technology with a view to developing tissue engineering constructs using low carbon footprint methods.

Hugo M. Macedo graduated in chemical engineering in 2006 from the New University of Lisbon (Portugal), where he was awarded a PhD scholarship by the Portuguese Fundação para a Ciênciae Tecnologia. Hugo's main interests range from research and development of bioreactors for stem cell bioprocessing to entrepreneurship. Currently, he is a PhD student in tissue engineering at the Imperial College London in the cross-disciplinary field between membrane and stem cell technologies.

A. Mantalaris is a reader heading the Biological Systems Engineering Laboratory (BSEL) in the Centre for Process Systems Engineering at the Department of Chemical Engineering at the Imperial College London. His research interests lie in bioprocess/tissue engineering, focusing on applied stem cell bioprocessing. He has developed novel 3D bioreactors and novel bioprocesses that integrate embryonic stem cell culture. He has over 60 publications in journals, 10 book chapters, and holds three US patents. In 2008, he co-edited a book titled *Advances in Tissue Engineering.* BSEL has won the best student poster award at Tissue Engineering Society International in Florida in 2003, the Junior Moulton Award by the IChemE for best paper in 2004, the Young Investigator Award at the 7th International Conference on Cellular Engineering in Seoul in 2005, the Rector's Research Excellence Award in 2006, the Live Demo Award at ISCAS for the 'Intelligent stem cell culture systems' in 2007, and the first prize at the 65th Annual Meeting of the Hellenic Association of Orthopaedics Surgery and Traumatology in 2009. Mantalaris is on the editorial boards of *Tissue Engineering* and *Stem Cells International,* a member of the MRC Stem Cell User Liaison Committee, and teaches at the Rice University summer course on advances in tissue engineering.

3.10 Membrane Approaches for Liver and Neuronal Tissue Engineering

S Morelli, S Salerno, A Piscioneri, M Rende, C Campana, and L De Bartolo, Institute on Membrane Technology, ITM-CNR, at University of Calabria, Rende (CS), Italy

3.10.1	**Introduction**	229
3.10.2	**Membranes for Liver Tissue Regeneration**	230
3.10.2.1	Cell Source	231
3.10.2.2	Culture System	233
3.10.2.3	Bioreactor	233
3.10.2.4	Membrane BAL Systems in Clinical Evaluation	236
3.10.2.5	Membrane BAL system in Preclinical and *In Vitro* Evaluation	237
3.10.2.6	Novel Membrane Biohybrid System for Liver Regeneration	239
3.10.3	**Membranes for Neuronal Tissue Regeneration**	240
3.10.3.1	Clinical Approaches for Treating Nerve Injuries	241
3.10.3.2	Bioengineering Strategies for Nerve Repair	241
3.10.3.2.1	Guidance therapies	241
3.10.3.2.2	Tissue response to bridging devices	242
3.10.3.3	Membranes Used in *In Vivo* Neuronal Regeneration	245
3.10.4	**Conclusions**	247
References		248

3.10.1 Introduction

Restoration and replacement of damaged tissue have greatly progressed and contributed significantly to surgery in the twentieth century. Especially, tissue reconstruction is still one field of important research, since the goal of producing perfect artificial tissue has not been achieved. The difficulties encountered in repairing or replacing severely damaged tissue may be resolved through a process called tissue engineering. Tissue engineering is a rapidly emerging field that combines the established disciplines of engineering, biology, and medicine with the goal of fabricating biological substitutes that restore, maintain, or improve tissue function [1]. It has the potential to produce a bioartificial organ and tissue substitutes that can grow with the patient. This should lead to a permanent solution to the damaged organ or tissue without the need for supplementary therapies, thus making it a cost-effective treatment in the long term [2]. Although initially targeted for applications in regenerative medicine, a novel application of this technology has been to generate experimental model systems for studying biological mechanisms and testing the efficacy of potential therapies. In particular, this very promising technique involves the *in vitro* seeding and attachment of human cells onto a material. These cells then proliferate, migrate, and differentiate into the specific tissue while secreting the extracellular matrix (ECM) components required to create the tissue. It is evident, therefore, that the choice of material is crucial to enable the cells to behave in the required manner to produce specific tissues and organs. Different materials have been proposed to support cells and promote their differentiation and proliferation toward the formation of a new tissue.

The design and selection of a biomaterial is a critical step in the development of scaffolds for tissue engineering. Generally, the ideal biomaterial should be nontoxic, biocompatible, promoting favorable cellular interactions and tissue development, while possessing adequate mechanical and physical properties. In addition, it should be biodegradable and bioresorbable to support the reconstruction of a new tissue without inflammation [3].

During the 1960s and the 1970s, a first generation of materials was developed for use inside the human

body. These early biomaterials must have been used to achieve a suitable combination of physical properties that match those of the replaced tissue with a minimal toxic response in the host. In 1980, there were more than 50 implanted devices in clinical use made from 40 different materials [4]. A common feature of most of the materials was their biological inertness.

By the mid-1980s bioactive materials which had begun to be clinically used in a variety of orthopedic and dental applications were developed [5]. Another advance in these bioactive materials was the development of resorbable biomaterials that exhibited clinically relevant controlled chemical breakdown and resorption. Improvements in these bioinert, bioactive, and resorbable biomaterials are limited because all biomaterials used for repair or restoration of the body represent a compromise – living tissue can respond to changing physiological loads or biochemical stimuli, but synthetic materials cannot. This limits the lifetime of artificial body parts. Recently, the next third-generation biomaterials were designed to stimulate specific cellular response at the molecular level. The separate concepts of bioactive materials and resorbable materials were converged. Molecular modification of resorbable polymer systems elicits specific interactions with cell integrins and thereby direct cell proliferation, differentiation, and ECM production and organization.

Polymeric materials have greatly contributed to the development of bioactive and biodegradable materials. Polymethylmethacrylate (PMMA) was the first synthetic polymer introduced for medical use. Other polymers used are, for example, polyethylene (PE) in catheters and drainage tubes [6]; polytetrafluoroethylene (PTFE) as vascular graft material [7]; polyvinylchloride (PVC) in medical tubing, polyglycol lactide (PGL) in absorbable suture thread, polylactide (PLA) in bone screw, polyurethane (PU) in pulsative blood-flowing arterial vascular reconstruction [8]; and polydimethylsiloxane (PDMS) in catheters, drainage tubing, and insulation for a pacemaker lead. This latter polymer owing to its oxygen permeability is used in membrane oxygenators. Its exceptional flexibility and stability has been applied to produce finger joints, heart valves, breast implants, nasal implants, etc.

Besides, synthetic material components of ECM, such as collagen, laminin, elastin, and fibronectin, have been used as matrices for tissue engineering and as vehicles for cell delivery. Collagen has been widely used as a scaffold and carrier for cells in tissue engineering and regenerative medicine, particularly in soft-tissue applications such as skin [9]. Carbohydrate polymers have been utilized not only in hydrogels for drug delivery but also in tissue engineering [10].

Progress in both membrane and cell culture technology has also greatly contributed to the success of artificially engineered tissue. It was demonstrated that polymeric membranes are attractive for their characteristics of selectivity, stability, and biocompatibility in the use of biohybrid systems for cell culture. In particular, semipermeable membranes act as supports for the adhesion of anchorage-dependent cells and allow the specific transport of metabolites and nutrients to cells and the removal of catabolites and specific products [11–13].

In tissue-engineered constructs, the surface and transport properties of the membranes play an important role in the promotion of cell adhesion, proliferation, and viability. The material surface properties, such as chemical composition, hydrophilicity/hydrophobicity, charge, free energy, and roughness, affect cell adhesion through the modulation of proteins secreted by cells or contained in the physiological liquids.

Novel strategies aimed at improving cell–biomaterial interactions have been proposed: the development of new biocompatible and cytocompatible materials and modification of surface chemistry including grafting of functional groups, and immobilization of molecules leaving the bulk properties unaltered.

In this chapter, we review the membrane bioartificial systems developed for tissue engineering. Particular attention is given to the recent achievements in liver and neuronal tissue engineering.

3.10.2 Membranes for Liver Tissue Regeneration

Each year 30 000 people die of end-stage liver disease in the United States, with an estimated annual cost of $9 billion dollars [14]. Liver transplantation is the only established successful treatment for end-stage liver disease, and currently there are 100 524 people on the waiting list for a donor organ and of those, there are 16 005 candidates awaiting a liver transplant (based on United Network for Organ Sharing Organ Procurement and Transplantation Network, UNOS

OPTN, data as of 6 November 2008). In 2006, there were 6649 liver transplants performed in the United States and 1935 died while waiting for a liver transplant due to organ shortage [15]. The European Liver Transplant Registry (ELTR) has cumulated data concerning 75 530 transplantations in 67 848 patients from 136 centers in 23 countries from May 1968 to June 2007 [16]. Cirrhosis is the most frequent indication for transplantation in Europe, followed by cholestatic disease, primary liver tumors, and acute hepatic failure [17].

Liver failure is potentially reversible because of liver regeneration [18], so considerable work has been done over many years to develop effective liver-support devices. Various nonbiological approaches, such as hemodialysis, hemoperfusion, and plasmapheresis, have limited success because of insufficient replacement of the synthetic and metabolic functions of the liver in these systems [19, 20]. On the other hand, extracorporeal biological treatment, including whole-liver perfusion, liver-slice perfusion, and cross-hemodialysis, have shown some beneficial results, but they are difficult to implement in a clinical setting [21]. For these reasons, many researchers have developed various extracorporeal biohybrid artificial liver (BAL) systems. Generally, a BAL system consists of functional liver cells supported by an artificial cell culture material. In particular, it incorporates hepatocytes into a bioreactor in which the cells are immobilized, cultured, and induced to perform the hepatic functions by processing the blood or plasma of liver-failure patients. The BAL system acts as a bridge for the patients until a donor organ is available for transplantation or until liver regeneration [22]. The development of a BAL system involves many design considerations. It must provide: (1) an adhesion support to the cells; (2) adequate mass transfer of oxygen, nutrients, and toxic substances from blood or plasma of patients to the cell compartments and proteins, catabolites, and other specific compounds produced by cells from the cell compartment to the blood or plasma; (3) immunoprotection of cells; and (4) biocompatibility. BAL devices are classified by the cell source, the type of culture system for the hepatocytes, and the configuration of the bioreactor (**Table 1**).

3.10.2.1 Cell Source

The choice of the cellular component plays a critical role in the performance of a BAL device. Cells inside must retain their differentiated functions. Primary xenogeneic hepatocytes and human cell lines have been used in the development of BAL.

In particular, due to a lack of human-organ availability, the current main source of hepatocytes for bioartificial systems is xenogeneic material. Primary porcine hepatocytes, for example, which can be obtained in large quantities, have been widely used as the cell source for hybrid artificial livers. Porcine hepatocytes exhibit biotransformation functions, synthesis of urea, albumin, and other proteins, and are activated by growth factors that also activate human cells [23].

Although the cells are easily obtained in large quantities and demonstrate the same qualities and therapeutic effects of human hepatocytes, this type of cell source carries the risk of xenogeneic infections and lack of metabolic compatibility [24]. An alternative approach is to use human immortalized hepatocyte cell lines which have the necessary functional and survival characteristics [25, 26]. The advantages of using established cell lines include the ability to culture large quantities of cells for an extended period of time and the ability to control the degree of hepatocyte function that is displayed [27, 28]. However, because these cells are cancerous in nature, it is important to maintain safe handling practices when considering the possibility of using these cells clinically.

Stem cells have been suggested as interesting cell sources. Stem cells, found in sources such as bone marrow, are the most flexible cells in terms of being undetermined in their pathway and expressing a remarkable ability to differentiate into a desired cell type. Hepatic progenitor cells that are in the liver are often distinguished as primary or small hepatocytes. These cells can differentiate into other functional cells of the liver. Primary hepatocytes are harvested via perfusion and are the precursor cells to mature hepatocytes. Primary human hepatocytes are very difficult to culture, and human cells that are obtained via perfusion do not survive beyond several divisions [29]. In addition, not only are human hepatocytes difficult to maintain in culture, they also do not perform normal functions or undergo differentiation [30]. To sum up, the problems are the limitations in the supply of human hepatocytes, the possible infection in porcine hepatocytes, and tumorigenesis in cell lines and gene-transferred hepatocytes. A preservation method is necessary when using human liver cells as the cell source for a bioartificial liver. The preference for progressive freezing is indicated by a report that compared stepwise freezing with

Table 1 Characteristics of membrane BAL systems in clinical evaluation

References	*Bioartificial system*	*Bioreactor configuration*	*Membrane*	*Cell source*	*Cell capacity*	*Culture technique*	*Cell position*	*Level of development*
Matsumara *et al*., 1987 [47]	Kiil dyalizer bioartificial liver	Plate	Cellulose (MWCO 20 kDa)	Primary rabbit hepatocytes	1×10^{10}	Suspension	Dalysate compartment	First clinical report
Margulis *et al*., 1989 [48]		Cartridge	Polyvinyl chloride	Porcine hepatocytes	4×10^{7}	Suspension	Shell	Phase II clinical trials
Sussman *et al*.,1992 [49]	ELAD Amphioxus cell Technology	Hollow fiber	Cellulose acetate (MWCO = 70 kDa)	Human cell line (C3A)	2×10^{11}	Aggregates	Shell	Phase I clinical trial
Demetriou *et al*., 1995 [50]	Hepat Assist Circe Biomedical	Hollow fiber	Polysulfone membranes (pore size 0.2 μm)	Cryopreserved porcine hepatocytes	5×10^{9}	Microcarrier-attached irregular aggregates	Shell	Phase II/III clinical trial
Gerlach *et al*., 1994 [51]	LLS Charite, Humboldt Univ. Germany	Hollow fiber	Polyamide (MWCO=100 kDa) Polyethersulfone (MWCO=80 kDa) Silastic polypropylene (0.2 μm pore size)	Pig primary hepatocytes–endothelial cells	2.5×10^{9}	Aggregates	Shell	Phase I
Patzer *et al*., 2002 [52]	BLSS Excorp Medical Inc.	Hollow fiber	Cellulose acetate (MWCO=100kDa)	Porcine primary hepatocytes	70–120 g	Collagen gel entrapped	Shell	Phase I/II clinical trials
Flendrig *et al*., 1997 [53]	AMC-BAL Univ. Amsterdam	Spirally wound	Nonwoven polyester matrix, polypropylene membranes (pore size 0.2 μm)	Pig primary liver cells	1×10^{10}	Small aggregates	Shell/on the nonwoven polyester matrix	Phase I
Ding *et al*., 2003 [54]	BAL TECA Corp.	Hollow fiber	Polysulfone (MWCO=100 kDa)	Swine hepatocytes	1×10^{10}	Aggregates	Shell	Phase 0

progressive freezing as the freezing method following precultivation of adult liver cells separated from the removed liver [31].

3.10.2.2 Culture System

Hepatocytes are involved in many important liver functions: blood detoxification; bile secretion; protein, steroid, or fat metabolism; and vitamin, iron, or sugar storage. This multifunctionality implies a great number of biological parameters, which are difficult to reproduce *in vitro* to maintain all the functionalities of the hepatocytes. Moreover, primary cultured hepatocytes rapidly lose liver-specific functions when maintained under standard *in vitro* culture conditions. To overcome such limitations in hepatocyte *in vitro* culture, many strategies to restore and maintain normal hepatic structure and function have been developed, such as the use of protein-coated culture dishes [32], collagen sandwich [33], coculture with other liver-derived or nonliver types of cells [34]. Implantable systems utilizing microcarriers, microcapsules, or aggregates have also been developed. Other established culture models have also been able to promote prolonged hepatocyte survival and metabolic function *in vitro*. These models include the use of porous membranes in a flat configuration, such as the modified polyetheretherketone (PEEK-WC) membrane [35], polyvinyl formal (PVF) resin [36], and poly(D,L-glycolic-co-lactic acid) PGLA foam [37], hepatic multicellular aggregates (spheroids) in suspension culture [38], in microstructured scaffolds [39], and in pores of porous matrices like polyurethane foam (PUF) [40] as well as entrapment of hepatic cells in coated alginate beads [41].

3.10.2.3 Bioreactor

A hybrid liver-support device is one of the most complex bioreactors, considering the several functions a liver performs. Its design is to ensure: the rapid detoxification of neural and hepatic toxins; the return of liver-specific hepatotrophic factors, as well as liver-specific coagulation factors, back into the patient's blood; and the maintenance of liver-cell detoxification and synthetic functions until liver-tissue regeneration. On the basis of these considerations, an efficient culture device must be designed considering the following important design criteria: (1) to use a sufficient number of differentiated hepatocytes that can maintain the long-term functions; (2) to reduce mass-transfer resistances and eliminate substrate limitations so that the device can function at maximum efficiency; and (3) to minimize the dead volume in the device, thereby reducing plasma-dilution effects in the patient. The ideal bioreactor design would maximize mass transfer to the hepatocytes, thereby allowing nutrients, including oxygen, and toxins from the patient's blood or plasma to reach the hepatocytes. The treated blood or plasma, including metabolites and synthetic products, would then be returned to the patient's circulation. To achieve this task a large surface area is important for cell adhesion. An ideal device should integrate efficient mass transport, scalability, and maintenance of hepatocyte functions. One of the most promising bioreactors is the membrane bioreactor. Membranes with suitable molecular weight cut-off (MWCO) have been proven to provide an effective immunoisolation barrier to immunocompetent species present in the patient's blood. Thus, xenogenic or allogenic implants may be used without the need of immunosuppression therapy. Membranes also permit the transport of nutrients and metabolites to cells and the transport of catabolites and specific metabolic products to blood. In the case of anchorage-dependent cells, they offer high surface area available for cell attachment and culture. In these bioreactor designs, mass transfer is determined by the MWCO or pore diameter and occurs by diffusion and/or convection in response to existing transmembrane concentration or pressure gradients. Some bioreactors use membranes with MWCO ranging from 70 to 100 kDa that allow the transport of serum albumin but exclude proteins with high molecular weight (MW) such as immunoglobulins and cells (**Table 1**). The advantage in using these membranes is that they provide immunoprotection. Other bioreactors use microporous membranes with large pore diameter (0.2 μm) that allows the free passage of plasma proteins, toxins, and clotting factors between blood or plasma and cells, but they exclude the passage of cells (**Table 1**). The advantage in using a membrane with large pore diameter is that it increases the fluid convection in order to improve mass-transfer conditions. Polymeric membranes with different morphologies and chemical–physical properties have been used in BAL devices [42]. The majority of extracorporeal BALs use cellulose and polysulfone derivatives (**Tables 1** and **2**). Morphological properties (e.g., pore size, pore-size distribution, and roughness) and physico-chemical properties (e.g., surface charge, wettability, and

Table 2 Membrane BAL systems in *in vitro* and preclinical tests

References	*Bioartificial system*	*Bioreactor configuration*	*Membrane material*	*Cell source*	*Bioreactor cell capacity*	*Culture technique*	*Cell position*
Hu *et al*., 1997 [55]	Liver × 2000	Hollow fiber	Polysulfone (MWCO 100 kDa)	Porcine hepatocytes	1×10^8	Gel entrapment	Lumen
Shiraha *et al*., 1996 [56]	BAL	Hollow fiber	Polysulfone (pore size 0.2 μm). Agarose microcapsule	Rat hepatocytes, HepG2	9×10^7	Multicellular spheroids	Extrafiber space
Naka *et al*., 1999 [57]	BLSS	Hollow fiber	Polyethylene (Plasma Flo) (0.3 μm pore size)	Porcine hepatocytes	5.4×10^9	Entrapment	Extrafiber space
De Bartolo *et al*., 2000 [11]	FMB-BAL	Flat	Polyterafluoroethylene and polycarbonate (pore size 0.2 μm)	Pig hepatocytes	1×10^{10}	Sandwich	Between flat membranes
Nagaki *et al*., 2001 [58]	BAL	Hollow fiber bioreactor	Polyolefin fiber 0.4 μm pore size	Rat hepatocytes, HepG2	2×10^7	Entrapment	Extrafiber space
Roy *et al*., 2001 [64]	Flat-plate	Microchannel bioreactor	Polyurethane membrane dense	Rat hepatocytes	2×10^6	Monolayer	Over the surface
Jasmund *et al*., 2002 [59]	Oxy-HFB	Crosswise hollow fiber	Polyethylene (pore size 0.2 μm) polypropylene	Pig liver cells	$1–5 \times 10^9$	Aggregate	Extrafiber space
Mizumoto and Funatsu, 2004 [61]	LLS HALLS	Hollow fiber Multicapillary	Polyethylene coated with EVAL hollow fiber polyurethane foam and capillary	Porcine hepatocytes	0.5–100 g	Organoids spheroids	Extrafiber space
Curcio *et al*., 2007 [62]	RWMS	Flat	Fluorocarbon dense membrane	Rat hepatocytes	$7.5–9 \times 10^5$	Spheroids	Over the surface
Schmtmeier *et al*., 2006 [63]	Minibioreactor	Flat	Polyterafluoroethylene membrane dense	Porcine hepatocytes	6×10^6	Monolayer	Over the surface
Sauer *et al*., 2004 [65]	Slide reactor	Hollow fiber	Polyethersulfone membranes (pore size 0.2 μm)	Human hepatoma cells	8×10^4	Aggregates	Between hollow fibers
Pless *et al*., 2006 [66]	Microchannel bioreactor	Flat-plate	Polyurethane membrane dense	Rat hepatocytes	2×10^6	Monolayer	Over the surface

Ostrovidov *et al*., 2004 [67]	PDMS microbioreactor	Flat	Polydimethylsiloxane and polyester membrane (pore size 0.4 μm)	Rat hepatocytes	5×10^5	Monolayer	Over the surface
Ye *et al*., 2006 [68]	LSS	Hollow fiber	Cellulose acetate membrane PMB-30 modified (MWCO 100 kDa)	RTH33 cell line	2×10^6	Monolayer	Extracapillary space
De Bartolo *et al*., 2007 [69]	Multibore fiber bioreactor	Multibore capillary	Modified polyethersulfone (pore size 0.2 μm)	Human hepatocytes	7.5×10^6	Small aggregates	Lumen
Lu *et al*., 2005 [70]	PVDF-hollow fiber	Hollow fiber	Polyvinylidene difluoride (pore size 0.5 μm)	Rat hepatocytes	5×10^7	Aggregates	Extracapillary space
Memoli *et al*., 2007 [71]	Membrane bioreactor	Flat	Galactosylated polyethersulfone (pore size 0.1 μm)	Human hepatocytes	4.7×10^7	Small aggregates	Over the surface

surface free energy) affect both the adhesion and metabolic functions of hepatocytes [12, 43].

However, most of the commercial membranes used in liver-cell culture are developed for hemodialysis, in which they are optimized to be inert with blood proteins and cells. As a result, membranes express poor properties with regard to cell interactions and functions. Thus, the development of membranes that are able to favor the adhesion and the expression of liver-specific functions is quite important in the design of a tissue-engineered liver bioreactor. Several strategies have been proposed to improve the cytocompatibility of membranes including the development of new membranes and surface modification by grafting of functional groups (e.g., COOH, NH_2), or by immobilization of biomolecules such as RGD peptide or galactose that interact with cell receptors [44, 45].

Another important issue in bioartificial liver design is the maintenance of sufficient oxygen supply to the hepatocytes. Since hepatocytes are highly metabolic with high oxygen-uptake rates, in order to oxygenate the circulating blood or plasma, some devices incorporate an oxygenator in the bioreactor, while others use an inline oxygenator in the extracorporeal perfusion circuit.

3.10.2.4 Membrane BAL Systems in Clinical Evaluation

Currently, several BAL devices are in various stages of clinical evaluation and are listed in **Table 1**. Many of these devices use hollow fiber membranes (HFMs) as supports for the cultured hepatocytes and as immunoselective barriers between the plasma of the patients and the hepatocytes used in the bioreactor [46].

In 1987, Matsumura *et al.* [47] reported an early clinical trial of a bioartificial liver. The device was developed on the principle of hemodialysis against a suspension of functioning hepatocytes. The liver suspension was placed in a dialysate compartment on one side of a cellulosic semipermeable membrane. The blood flows through a compartment on the opposite side of the membrane (**Table 1**). Later, one of the first large clinical studies was performed by Margulis *et al.* [48] in which 20-ml capsules filled with porcine hepatocytes in suspension were used.

Since the 1990s, several BALs were proposed. Sussman *et al.* developed an extracorporeal liver-assist device (ELAD) in which the human hepatocyte cell line C3A, which is derived from hepatoblastoma cell line (HepG2), is located outside the hollow fiber and blood flows through the lumen of the hollow fibers. A portion of the patient's plasma is ultrafiltrated through a cellulose acetate membrane (70 kDa) and is in direct contact with the C3A cells [49]. This device was commercialized by Amphioxus Cell Technologies.

A hollow fiber device that uses cryopreserved porcine hepatocytes attached to collagen-coated dextran microcarriers that are called Hepatic Assist was developed by Demetriou *et al.* In this system, hepatocytes are loaded into the extracapillary space and patient plasma flows through the capillary lumina of membranes with a pore size of 0.2 µm. This size is sufficiently small to block the passage of whole cells [50]. Plasma first passes through an activated charcoal column and then flows through the lumen of the hollow fibers.

A more complex system was proposed by Gerlach *et al.* The liver-support system (LSS) or the modular extracorporeal liver system (MELS) consists of a bioreactor with four interwoven independent capillary membrane systems that serve different functions. The cells are cultured on the outer surface and among the capillaries. Each fiber type exhibits a different function: silastic membranes for oxygen supply and removal of carbon dioxide, polyamide fiber for the plasma inflow, polyethersulfone (PES) fiber for plasma outflow, and hydrophilic polypropylene membranes for sinusoidal endothelial coculture [51]. With this capillary array, decentralized metabolite and gas exchange with small gradients are possible. Due to independent plasma inflow and plasma outflow compartments, decentralized perfusion of cells between these capillaries is achieved. Additional functions could be integrated into the module.

The BLSS is a hollow fiber device that uses porcine hepatocytes embedded in a collagen matrix. This system uses cellulose acetate hollow fibers with a 100-kDa MWCO containing greater than 70 g of primary porcine hepatocytes embedded in a collagen matrix. The patient's blood is perfused through the capillary lumina [52]. In the circuit, a flowing nutrient stream directly perfuses the hepatocytes providing specific nutrients.

The Academic Medical Center Bioartificial Liver (AMC-BAL) developed by Flendrig *et al.* [53] uses a three-dimensional, spirally wound, nonwoven polyester matrix for hepatocyte attachment with integrated hollow fibers for oxygen delivery to the cells. In contrast with the other systems, the

AMC-BAL uses direct contact between the patient's plasma and the matrix-attached hepatocyte to improve bidirectional mass transfer.

Another BAL system that is currently in clinical testing is a bioreactor from TECA Corp. in which a polysulfone membrane with MWCO of 100 kDa compartmentalizes porcine hepatocytes [54].

3.10.2.5 Membrane BAL system in Preclinical and *In Vitro* Evaluation

Several BAL systems have been evaluated preclinically in *in vitro* experiments and in large-animal models of liver failure.

In the Liverx2000 system of Hu *et al.* [55], the hepatocytes are suspended in a collagen gel and injected into the lumen of a hollow fiber with a MWCO of 100kDa and the extracapillary compartment is perfused with a recirculating medium. The flow of the medium through the luminal space provides hepatocyte nutrients (**Table 2**).

A bioartificial liver-support system consisting of a hollow fiber cartridge using encapsulated multicellular spheroids of rat hepatocytes was developed by Shiraha *et al.* The spheroids, formed in a positively charged polystyrene dish, were encapsulated into microdroplets of agarose that contained about 9×10^7 rat hepatocytes. The medium was circulated in a closed circuit in which the cartridge was inserted [56].

Several alternative device configurations have advanced to the stage of large-animal, preclinical evaluation. Naka *et al.* have developed a system using primary porcine hepatocytes that is similar to the BLSS. The differences are in the use of microporous polysulfone HFMs in the hepatocyte bioreactor and perfusion of plasma through the bioreactor. The system has shown some efficacy in support of ischemic pig liver-failure model [57].

The flat-membrane bioreactor (FMB) developed by De Bartolo *et al.* consists of primary porcine hepatocytes cultured between semipermeable flat membranes. This is a reproducible model with total hepatectomy in pigs, suitable in testing the safety and efficacy of the liver-support system. Isolated hepatocytes were cultured within an ECM between oxygen-permeable flat-sheet membranes in the FMB. In particular, both sides of the outside shell are constituted of PTFE membranes permeable to oxygen, carbon dioxide, and aqueous vapor, which allow direct oxygenation of the cells adhering to the surface and to the medium overlying the cells. Porcine hepatocytes are maintained in a three-dimensional coculture with nonparenchymal cells. A microporous polycarbonate membrane separates the medium from the cell compartment. The FMB maintained stable cell-specific functions and is a safe and efficient device [11].

Nagaki *et al.* developed a hybrid liver-support system which consists of plasma perfusion through porous hollow fiber modules inoculated with 10 billion porcine hepatocytes entrapped in a basement membrane matrix, Engelbreth–Holm–Swarm (EHS) gel. This system was applied to pigs with ischemic liver failure. It was demonstrated that the use of a BAL support device in combination with a hollow fiber module and hepatocytes entrapped in EHS gel has potential advantages for clinical use in patients with hepatic failure [58].

An oxygenating hollow fiber bioreactor (OXY-HFB) BAL system was developed by Jasmund *et al.* [59] and it consists of oxygenating and integral heat-exchange fibers with a simple design. Primary liver cells are seeded on the surface of the fibers in the extrafiber space. Oxygen requirements are supplied and temperature is controlled via the fibers. Plasma from the patient is perfused through the extrafiber space and brought into direct hepatocellular contact.

The liver lobule-like structure module (LLS) BAL system has many hollow fibers that act as blood capillaries and are regularly arranged close to each other [60]. Hepatocytes are inoculated by a centrifugal force in the outer space of the hollow fibers. The multicapillary PUF module used as a BAL system consists of a cylindrical PUF block with many capillaries in a triangular arrangement to form a flow channel [61]. The hepatocytes in the foam pores formed spheroids with a diameter of 100–150 μm.

Based on the use of a gas-permeable membrane, a rotating-wall gas-permeable membrane system was developed by Curcio *et al.*, and used for the formation and culture of hepatocyte spheroids. Microgravity conditions were obtained in rotating-wall systems in which hepatocyte aggregates were formed by cells protected from gravitational forces and acceleration. Owing to the high O_2 permeability of the rotating-wall membrane system, the viability and functions of the cells improved with respect to a polystyrene (PS) rotating-wall system [62].

Schmitmeier *et al.* developed a new small-scale bioreactor with the hepatic sandwich model. It is of the same dimension as the conventional 24-well cell-cultivation plate where the bottom is replaced

by the gas-permeable PTFE membrane. Compared to hepatocytes cultured in conventional systems, primary porcine hepatocytes exhibited stronger liver-specific capacity and remained in a differentiated state in the small-scale bioreactor over a cultivation period of 17 days. This *in vitro* model could serve as a tool to predict the liver response to newly developed drugs [63].

Pless *et al.* evaluated primary human liver cells in bioreactor cultures for extracorporeal liver support on the basis of urea production. In particular, the long-term course of 47 bioreactor cultures of hepatocytes over a culture period of 21 days was investigated. The bioreactors based on the design developed by Gerlach *et al.* consist of three interwoven hollow fiber capillary bundles, forming four compartments, and integrated into a PU housing. Two of the bundles are made of hydrophilic PES membranes with a pore size of 0.5 μm, serving for medium supply during stand-by or for plasma perfusion during clinical application. The third bundle consists of hydrophobic multilaminate HFMs and was perfused with a mixture of air and CO_2 supplying the cells with oxygen and carbon dioxide [64].

A simple hollow fiber-based bioreactor that is suitable for light microscopy was developed by Sauer *et al.* [65] to evaluate cell–cell and cell–membrane interactions. The SlideReactor offers a cell compartment separated from a medium inflow and outflow compartment. Due to its simple design and the use of materials available in most laboratories, SlideReactor is a simple and valuable tool to evaluate the cell-to-cell and cell-to-hollow-fiber interaction and enables the comparison of different types or arrangement of hollow fibers, for example, for use in bioreactor-based ELADs, or analysis of the influence of medium supplements on the cell viability and tissue integrity.

A flat-plate microchannel bioreactor with an internal membrane oxygenator was designed to improve oxygen supply to the cells. The hepatocytes are attached to a glass substrate and are in direct contact with the perfusing medium. A PU gas-permeable membrane separates the liquid compartment from the oxygenating gas compartment. This design allows oxygen delivery to the hepatocytes to be decoupled from the medium flow, thereby allowing oxygen delivery and flow to be studied independently. Hepatocytes with oxygen-dependent functional heterogeneity may exhibit optimal function in this bioreactor [66].

Ostrovidov *et al.* [67] developed two types of membrane-incorporating microbioreactors to improve the maintenance of primary rat hepatocytes: one with a commercially available polyester membrane and the other with a PDMS membrane. These microbioreactors closely mimic the *in vivo* liver architecture and revealed to be promising tools toward future application in drug screening or liver-tissue engineering [67].

Ye *et al.* presented a bifunctional cellulose acetate (CA) HFM bioreactor modified with 2-methacryloyloxyethyl phosphorylcholine (MPC) copolymers (PMB30 (MPC-co-n-butyl methacrylate) (BMA) and PMA30 (MPC-co-methacrylic)) for preparing a novel liver assist HFM bioreactor. A CA/PMB-PMA30 HFM modified asymmetrically on the inner and outer surface with PMB30 and PMA30 was prepared successfully. The modified HFM has good hemocompatibility and antifouling property on the other surface due to the modification effect of the MPC copolymer [68].

De Bartolo *et al.* [69] developed a multibore fiber bioreactor as an *in vitro* liver-tissue model to study disease, drugs, and therapeutic molecules alternative to animal experimentation. This bioreactor, owing to the membrane configuration, combines the advantage of having seven compartments represented by seven capillaries arranged in one single fiber with high stability and mechanical resistance. Human hepatocytes were cultured in the intraluminal compartment of the multibore fiber bioreactor. The morphological, physico-chemical, and transport properties of the multibore fiber membranes favor cell adhesion and ensure sufficient oxygenation process, nutrient feeding, end-product removal, and distribution of fluid molecules inside the cell environment.

Membrane bioreactors using specific adhesive substrates such as galactosylated membranes were developed in order to improve the adhesion and specific functions of liver cells. A galactosylated polyvinylidene difluoride hollow fiber bioreactor provided specific adhesion and showed an enhanced albumin production of rat hepatocytes [70]. Recently, a flat bioreactor using galactosylated-PES membrane promoted the long-term maintenance of differentiated functions of human hepatocytes outside of the body [71]. This human hepatocyte bioreactor was applied to study interleukin-6 (IL-6) effects on the production of acute phase proteins and gave evidence that IL-6 downregulated the gene expression and synthesis of fetuin-A by primary

human hepatocytes. The human hepatocyte bioreactor behaves like the *in vivo* liver, reproducing the same hepatic acute-phase response that occurs during the inflammation process.

3.10.2.6 Novel Membrane Biohybrid System for Liver Regeneration

In the last few years, several studies have demonstrated that semipermeable synthetic membranes can be used for the development of biohybrid systems for liver cell cultures. We demonstrated that the morphological and physico-chemical properties of membranes, such as surface free-energy parameters, affect cell adhesion and specific metabolic functions of hepatocytes [12, 72]. Polymeric membranes are able to support the long-term maintenance of metabolic and biotransformation functions of isolated human hepatocytes in a biohybrid system [35, 73]. Moreover, surface modification by plasma process and the immobilization of biomolecules, such as RGD and galactose, on membrane surface improve cell adhesion and the maintenance of differentiated functions [44, 45, 74–79].

In the recent past, the *in vitro* use of membrane biohybrid systems including bioreactor systems contributed to provide important information about the effect of various drugs, such as diclofenac (DIC), rofecoxib, and paracetamol, whose effects are not completely known, on the specific functions of human hepatocytes [69, 71, 80, 81]. A novel biohybrid system constituted by a modified PEEK-WC and PU membrane and human hepatocytes was developed by De Bartolo *et al.*, as an *in vitro* system able to reproduce all liver functions to be used for drug testing and toxicity alternative to animal experimentation. In this system, human hepatocytes showed polygonal shape and intercellular junctions with the neighboring cells formed a structure that is close to the *in vivo* liver architecture (**Figure 1**).

This system was used to investigate the effect of a triterpene, ursolic acid (UA), on the specific metabolic functions of human hepatocytes. UA is a pentacyclic triterpene acid which is widely distributed in medical herbs and plants [82] and it possesses antibacterial, antiviral, hepatoprotective, and immunomodulatory activity [83]. In particular, the protective effects on the liver cells in the presence of toxic concentrations of the drug were investigated. Membranes were prepared from a polymeric blend of PEEK-WC or poly(oxa-1,4-phenylene-oxo-1,4-phenylene-oxa-1,4-phenylene-3,3-(isobenzofurane-1,3-dihydro-1-oxo)-diyl-1,4-phenylene) and PU by inverse-phase technique using the direct immersion–precipitation method. Therefore to obtain information about the mechanism whereby UA reduces drug toxicity, we investigated the effect of UA on the specific functions of human hepatocytes cultured on PEEK-WC–PU membranes in presence of the anti-inflammatory drug DIC at a concentration (700 μM) that is known to be toxic. The hepatoprotective effect of UA was evaluated on the liver-specific functions, such as urea synthesis, using DIC at toxic concentration (700 μM) in the presence of UA (100 μg ml^{-1}) (**Figure 2**). The ability of human hepatocytes cultured on the PEEK-WC–PU membrane system to synthesize urea was maintained for the whole culture period of 24 days. In the presence of DIC, urea synthesis decreased dramatically whereas administration of DIC with UA showed less drastic effects on the metabolic functions. It is interesting to note that when the two substances are simultaneously supplied, hepatocytes synthesize urea with a rate that lies between the rates when treated alone with either of them.

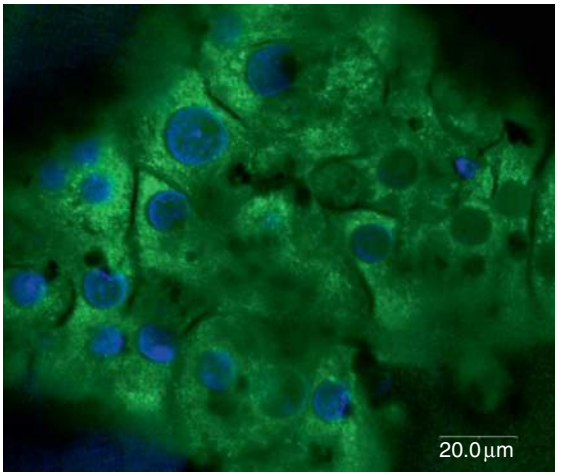

Figure 1 Confocal image of human hepatocytes on PEEK-WC–PU membranes immunostained for actin (green). DAPI (blue) counterstaining was used to detect nuclei. Scale bar 20 μm.

These results demonstrated that the biohybrid PEEK-WC–PU system is able to reproduce liver functions *in vitro* and therefore it can be used as model system for drug testing and toxicity as well as for studying metabolic diseases and therapeutic molecules.

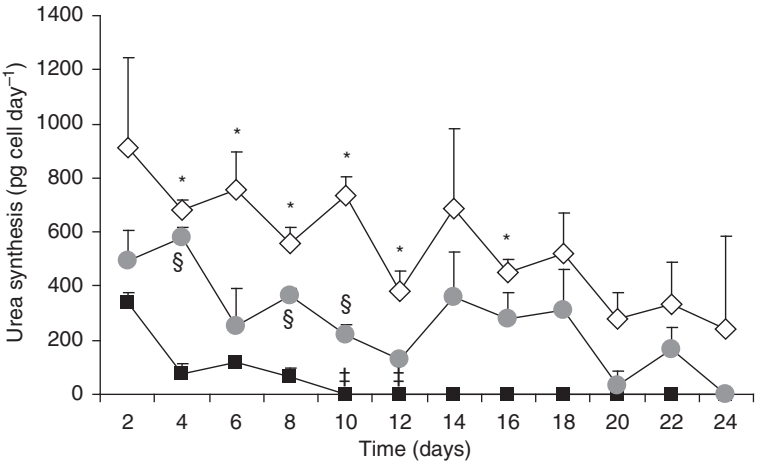

Figure 2 Urea synthesis of human hepatocytes cultured in biohybrid PEEK-WC–PU system for 24 days and treated with: (◇) ursolic acid (UA) (100 μg ml^{-1}); (■) diclofenac (DIC) (700 μM); (●) ursolic acid–diclofenac association (UA + DIC). The values are the mean of six experiments ± standard deviation. On fourth day of culture: $^{*}p < 0.05$ vs. DIC; §$p < 0.05$ vs. DIC. On sixth day of culture: $^{*}p < 0.05$ vs. DIC. On eighth day of culture: $^{*}p < 0.05$ vs. DIC; §$p < 0.05$ vs. DIC. On tenth day of culture: $^{*}p < 0.05$ vs. DIC; §$p < 0.05$ vs. DIC; ‡$p < 0.05$ vs. UA + DIC. On twelfth day of culture: $^{*}p < 0.05$ vs. DIC; ‡$p < 0.05$ vs. UA + DIC. On sixteenth day of culture: $^{*}p < 0.05$ vs DIC.

3.10.3 Membranes for Neuronal Tissue Regeneration

In the tissue-engineering strategies to repair all body parts, neuronal repair stands out. The nervous system consists of the central nervous system (CNS) which includes the brain and the spinal cord and the peripheral nervous system (PNS), which is composed of cranial, spinal, and autonomic nerves that connect to the CNS. The functional unit of the nervous system is the neuron that has a cell body and dendrites and axons. The dendrites serve as antennae to receive signals from the surroundings or other neurons whereas the axon that is longer than the dendrite is engaged in transporting impulses from the cell body to dendrites of other neurons through synapses [84]. Electrical impulses can also pass from axon to axon, axon to soma, or from dendrite to dendrite. Injury to the nervous system caused by mechanical, thermal, or ischemic factors can impair various nervous system functions such as memory, cognition, language, and voluntary movement. CNS injury may result in death or permanent disability.

In the United States alone, more than 3 million cases of traumatic brain injury are reported annually. These patients include anyone who has fallen, especially someone older than 64 years; a person who has been in a motor vehicle accident; someone with a gunshot wound or violence-related injury; or an adolescent or young adult who has a sports-related injury. Approximately 400 000 Americans suffer from neurological symptoms associated with multiple sclerosis (MS). Furthermore, over 5 million people in the United States and Europe alone suffer from the dementia associated with Alzheimer's disease. About 450 000 people in the United States live with spinal cord injury (one in 670), and there are about 11 000 new spinal cord injuries every year (one in 30 000) [85].

While in PNS injury the several axons can re-extend and reinnervate with a functional recovery, a rare return of damages, structures, and functions is observed following injuries to the CNS. Owing to the profound impact of CNS damage, extensive studies have been carried out aimed at facilitating CNS repair. Many strategies have been developed to facilitate axonal reinnervation and to direct their outgrowth. Various devices using synthetic and biological substrates are being developed as biomaterial bridges for peripheral nerve grafts. In particular, membranes in tubular configuration act as a guidance channel to protect the regenerating axons in the lumen from the external environment. The membrane reduces the infiltration of fibrous tissue and provides a conduit for the diffusion of neurotrophic factors and allows the selective transport of molecules between the lumen and the surrounding environment.

Current attempts are focused on seeking new biomaterials, new cell sources, as well as novel

designs of tissue-engineered neuronal bridging devices, to generate safer and more efficacious nervous-tissue repairs.

3.10.3.1 Clinical Approaches for Treating Nerve Injuries

For peripheral nerve injury, one of the current clinical treatments for nerve transaction is surgical end-to-end reconnection, which involves the suturing of individual fascicles within the nerve cable. End-to-end repair, however, is only effective if the nerve ends are directly adjacent and can be reconnected without causing tension. If the injury creates a gap in the nerve, autologous nerve grafts or autografts are used. For longer nerve gaps, this approach is not used because any tension introduced in the nerve cable would inhibit the regeneration while an autologous nerve graft from other donor sites is used. This technique has the disadvantage of the loss of function at the donor site and the need for multiple surgeries. There are a few devices that are now Food and Drug Administration (FDA) approved for relatively short nerve defects, including Integra Neurosciences Type I collagen tube (NeuraGen Nerve Guide) [86] and SaluMedica's SaluBridge Nerve Cuff [87]. However, these treatments are reserved for small defects (several millimeters) and do not address larger peripheral nerve injuries.

For CNS injury, and particularly spinal cord injury, clinical treatment is less promising. If bone fragments exist near the site of injury, then surgery may be performed to reduce any risk of secondary injury. Anti-inflammatory drugs, such as methylprednisone, are often also administered to reduce swelling and secondary injury [88]. Unfortunately, there is currently no treatment available to restore nerve function.

3.10.3.2 Bioengineering Strategies for Nerve Repair

Bioengineering efforts are focused on creating a permissive environment for regeneration and providing a seamless interface between the CNS and the PNS. Many researchers are presently focusing efforts on creating physical or chemical pathways for regenerating axons. These devices include physical or mechanical guidance cues, cellular components, and biomolecular signals, as reviewed individually below. Future therapies will incorporate multiple cues into unique devices that more closely mimic native nerve. They will also be interactive and programmable, and thus capable of seamless communication with surrounding tissues.

3.10.3.2.1 Guidance therapies

The growth of cells and tissue is strongly influenced by environmental cues. In particular, topographical features, such as that created by cells, matrix proteins, and surface texture on biomaterials, influence cell and tissue growth. This phenomenon is termed as contact guidance. The physical guidance of axons is a vital component of nerve repair. Since the 1960s, when Millesi *et al.*[89] pioneered microsurgical techniques to accurately align nerve fascicles in the direct resection of nerve ends, with improved functional outcomes, the need for physical guidance has been acknowledged as an essential element in nerve regeneration. The nerve guides or nerve-guidance channels serve to direct axons sprouting from the proximal nerve end, provide a conduit for the diffusion of growth factors secreted by the injured nerve ends, and reduce the infiltration of scar tissue. Past research in this area has focused either on existing natural or on synthetic materials; however, none of the materials studied to date have matched or exceeded the performance of the nerve autograft. As a result, researchers are now focusing on the combination of materials and desired biomolecules to create new composite materials that can actively stimulate nerve regeneration. Matrices are incorporated into the lumen of the guidance channel to enhance the organization of the regeneration environment and provide topographic-guidance cues via aligned textures, and biological-guidance cues by patterned biomolecules, to facilitate unidirectional outgrowth of the regenerating axons [90–96]. Cells [97], ECM molecules [98], or growth factors [99] can be incorporated into the tube to assist axonal sprouting and outgrowth. Among the variety of tubular structures used for guidance channels, semipermeable HFMs appear to be a favorable guide to regenerate neuronal tissue. The most promising results were observed with a minichannel entubulation device in which Schwann cells were seeded into a semipermeable nondegradable HFM made of a random copolymer of acrylonitrile and vinylchloride (PAN–PVC) with an outer diameter comparable to that of the hemisected part of the right spinal cord [97, 100, 101]. A large number of both myelinated and nonmyelinated regenerating axons were discovered in the midpoint of the channel and some of the regenerating axons were able to traverse the

bridge–host interface and reenter the host CNS environment. These axons terminated as button-like structures in the gray matter. In order to confirm the efficacy of the minichannel design on CNS axon regeneration, further evaluations of functional recovery and synaptic reconnections are necessary.

Topographic cues such as the surface microgeometry of the guidance channels and the morphology of the intraluminal matrices within the nerve-bridging device may represent key elements in the successful guidance of regenerating axons. In fact, unoriented ECM materials allow little nerve regeneration [102].

3.10.3.2.2 Tissue response to bridging devices

In a tissue-engineered construct, the response of tissue depends on the properties of the materials and the cells [103]. Material properties, including morphological, structural, mechanical, physicochemical [104], and electrical properties [105], affect tissue response. The cells within the construct interact with the material directly via physical contact or indirectly via the diffusion of cell-secreted soluble factors.

In the case of a typical tissue-engineered neuronal bridging device, the properties of the material components relevant to the tissue response include the surface microgeometry [106], the MWCO [107], the electrical properties [108], possibly the bioactive factors that are loaded and sustainedly released through the channel wall, and the degradation rate for biodegradable materials [109].

Axon guidance by concentration gradients of soluble guidance cues has been extensively studied *in vitro*. The modification of the surface with neuronal trophic factors has been found to elicit neuronal regeneration. The patterning of materials with chemical cues, such as ECM proteins (e.g., laminin, fibronectin, and RGD peptide), has been evaluated in the neurite outgrowth. Neurons from rat brainstem and cortices adhered to surfaces coated with laminin. DRG neurite attachment was found to be dependent on fibronectin strip width (30 μm). Hippocampal neurons adhered to and extended neurites on the pattern of poly-L-lysine and laminin. Electric fields in the form of voltage gradients have been observed to polarize the nervous system along the rostral–caudal axis during the development ($5–18\,mV\,mm^{-1}$) and direct nerve growth and accelerate wound healing in the rat cornea (+40 mV/0.5 mm) [110]. Cues in three dimensions, such as matrigel, collagen, as well as polymer synthetic polymer-based scaffolds, support longer neurites than in bidimensional culture systems. Topographical cues influence nerve growth and regeneration. The influence of topographical features on neuronal cell adhesion and differentiation has been studied using patterned adhesive areas that provide only a fraction of the surface for cell adhesion while the rest is cell repellent or using contact-guidance cues in combination with nerve growth factors or electric field [111–113]. Neurons have the ability to respond to topographical features in their microenvironment and they have been shown to adhere, migrate, and orient their axons to navigate surface features such as grooves in substrates at micro- and nanoscales. Topographical guidance of neurite outgrowth has been explored *in vitro* with well-defined micropatterned substrates. Topographic guidance of neurites' outgrowth has been explored *in vitro* with culture substrate containing etches, microchannels, nanotubes, or microgrooves [114–118]. Mahoney *et al.* [119] studied the effects of microchannels of 20–60 μm in width and 11 μm in depth on PC-12 cell cultures. Neurites were directed along the axis of the grooves with microchannels of 20–30 μm being most effective at neurite directions. Other authors found an optimal surface with roughness in the range of 50 nm for the attachment of primary neurons isolated from the substantia nigra [120].

De Bartolo *et al.* [121] showed that hippocampal neurons exhibited a different morphology in response to varying the properties of the membrane surface. Indeed, cells grown on the smoother membranes such as fluorocarbon (FC) and PES membranes displayed a large number of neurites with consequent formation of bundles. The density of axonal network increases the neurites to become more elaborate and highly branched on the smoother surfaces (**Figure 3**). As a consequence, while a very complex network was formed on these membranes, cells tend to, instead, form aggregates and most of the processes are developed inside the pores of the membranes when rougher PEEK-WC surfaces were used. Aebischer *et al.* [106] observed that smooth inner walls of polymeric channels induced the formation of discrete nerve cables with a number of myelinated axons within an organized fibrin matrix in contrast with the rough inner walls that elicited the formation of scattered nerve fascicles in an organized fibrin matrix.

Zhang *et al.* fabricated HFMs with unidirectional aligned grooves parallel to the hollow-fiber long axis

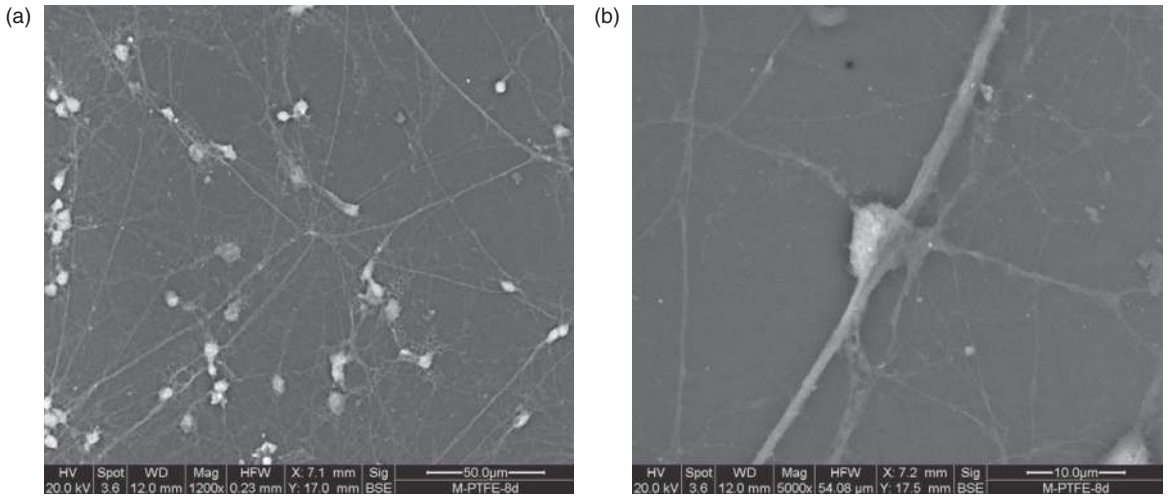

Figure 3 Micrographs of hippocampal neurons after 8 days of culture on (a) modified fluorocarbon (FC) membrane and (b) different magnification.

on the inner surfaces from both nondegradable and biodegradable natural and synthetic polymers. HFM guidance channels with aligned grooves on the inner surfaces may allow enhanced orientation and directional outgrowth of regenerating axons [122]. Both surface and transport properties of the membranes play an important role in neuronal regeneration: the surface microgeometry of the membrane inner wall affects the orientation of the axonal growth, and the MWCO of the membrane affects axonal regeneration by governing the mass transfer of molecules between the controlled regenerating environment within the channel lumen and the external environment [107]. In **Table 3**, the main studies with neuronal cells using membrane systems are reported.

The MWCO of the membrane can be adjusted to allow diffusion of nutrients, waste products, and the external humoral factors that are beneficial to regeneration across the membrane–tissue interface, excluding the transport of immunocompetent species and molecules. Polyvinyl alcohol (PVA) and polyethylene-co-vinylalcohol (EVAL) membranes were used for culture of neural stem cells isolated from embryonic cerebral cortex. Single neural stem cells seemed to remain dormant on the EVAL. Conversely, the development of cell clusters at low density allowed the differentiation of cells into neurons and astrocytes [123]. The physico-chemical properties of the membrane surface are also important in the interactions with cells. Manwaring *et al.* cultured cells derived from meningeal tissue on surfaces with different wettability: PAN–PVC, polyethylene vinyl acetate (PEVAC), polypropylene (PP) PS, and Tecoflex (TECO). The hydrophilic materials supported the highest level of cell attachment while the hydrophobic materials supported less cell adhesion [124]. Other studies demonstrated that PC-12 cells are a differentiated neuronal phenotype with a long neurite on polyethylene surface with moderate wettability [125].

Chang *et al.* studied the effect of membranes made of a polymeric blend of polyethyleneimine (PEI) and EVAL with different concentrations of PEI on the behavior of granule neuronal cells. The addition of PEI at increasing concentrations resulted in a change in wettability properties of the membranes with contact angle ranging from 23 to 85°. An increased cell viability was observed on membrane surface at 57.8° [126].

In understanding the interactions between microfabricated synthetic interfaces and cells, Lopez *et al.* investigated microfabricated nanoporous silicon membranes modified with collagen and laminin on the survival, proliferation, and differentiation of PC-12 cells. The modification of the membrane with collagen was important to improve the adhesion of cells [127].

The tubular membrane can be engineered to allow adsorption of the bioactive factors to the channel walls during the fabrication process, which could be released within the lumen to favor nerve regeneration. Previous studies reported enhanced nerve regeneration *in vivo* under the effect of growth factors

Table 3 Characteristics of membranes *in vitro* neuronal regeneration

Reference	*Membrane*	*Configuration*	*Matrices*	*Membrane properties*	*Cells*	*Effect*
Li *et al*., 1999 [129]	Polyacrylonitrile polyvinylchloride copolymer	Hollow fiber	Macroporous cellulosic microcarriers	Hydrogel	PC-12 L-dopa secreting and C2C12 CNTF secreting	Cell proliferation, dopa and CNTF secretion
Manwaring *et al*., 2001 [124]	Glass, CA, PES, PAN-PVC, PS, PP, PEVAC	Flat	-	Contact angle ranging from 35 to 95°	Dorsal root ganglion and cerebellar granule neurons	Cell proliferation on CA, PAN–PVC, PEVAC and glass
Broadhead *et al*., 2002 [130]	Copolymer of acrylonitrile and vinylchloride	Hollow fiber	-	Cut-off 40,150 kDa	PC-12	Proliferation and maintenance of viability
Lee *et al*., 2003 [125]	Polyethylene	Flat	Corona treated	Wettability gradient surfaces	PC-12	Longer neurites on surface with contact angle of 55°
Zhang *et al*., 2005 [122]	Aromatic polyether-based polyurethane, Poly DL-lactide-coglicolide	Hollow fiber	Poly-L-lysine and laminin	Grooves on the lumen of width of 38.5–91 μm	Dorsal root ganglion	High rate of neurite outgrowth on textured inner surface
Young *et al*., 2005 [123]	Polyvinyl alcohol and polyethylene-co-vinyl alcohol	Flat	-	Dense structure	Cerebral cortical stem cells	Differentiation in neurons/strocytes and prolifertaion
Lopez *et al*., 2006 [127]	Silicon	Flat	Laminin and collagen	Pore size ranging from 20 to 50 nm	PC-12	The modification of collagen increases cell survival and functionality
Chang *et al*., 2007 [126]	Polyethyleneimine-polyethylenevinylalcohol	Flat	-	Contact angle 23.2–84.9°	Rat cerebellar granule neurons	Increased cell viability on surface with 57.8°
De Bartolo *et al*., 2008 [121]	Fluorocarbon, polyethersulfone, modified polyetheretherketone	Flat	Poly-L-lysine	Roughness ranging from 6 to 200 nm	Hippocampal neurons	Surface with Ra up to 50 nm favored the formation of longer neurites and BDNF secretion

or neurotrophic factors released from the walls of the guidance channels [128].

Both nonbiodegradable materials, such as silicon, PE, PVC, polyvinylidenedifluoride, and PTFE, and biodegradable materials, such as collagen, chitosan, polycaprolactone, and polyglycolic acid, have been used to realize tube as nerve-guidance channels for repairing transected nerves. Particularly semipermeable HFMs seeded with fetal spinal cord cells have been shown to markedly promote axonal growth across a gap in adult-rat spinal cord. Zhang *et al.* used semipermeable HFMs with highly aligned textures on the inner surface in order to promote the dorsal root ganglion regeneration. Aromatic polyether PU was used as nondegradable and poly-DL-lactide-coglycolide was employed as a degradable polymer. The presence of grooves with heights of 38.5–91 μm allowed the regeneration of neurites that were aligned and parallel to the direction of the grooves [96].

Asymmetric HFMs of PAN–PVC were used to encapsulate PC-12 cells secreting dopa and C2C12-secreting ciliar neurotrophic factor (CNTF) supported the proliferation of cells and the secretion of specific factors [129]. PAN–PVC membranes with structural properties have been used for PC-12 cells by Broadhead *et al.* [130]. The encapsulated cell biomass, the number of proliferating cells, and the quantity of dopamine released increased as a function of increasing HFM diffusive permeability. In this respect, membrane permeability plays a dual role by regulating the size of the cell mass that generates the product and by being able to restrict the diffusion of the product across the membrane into the surrounding environment. Unlike biomass size, the percentage of viable cells was independent of membrane permeability.

The use of biodegradable materials in guidance channels offers the advantage of timely disappearance from the implantation site without an additional surgical intervention once the regeneration process is completed and further allows connection of the regenerated axons with the host circuitry. The important characteristics of a biodegradable guidance channel include minimal tissue response following implantation, *in vivo* degradation at a rate that matches with the regeneration process, nontoxic and readily excreted degradation products, and the absence of toxic residual chemicals that may be contained in their preparation [109].

For most of the biodegradable materials that are well tolerated in the CNS, such as polylactic, polyglycolic acid and their various copolymers [131–133], polyanhydrides [134], hydrogels [135], and poly(phosphoester) [136], the tissue inflammatory response generally becomes stabilized and resolved as a function of material degradation. Biodegradable materials formulated into microspheres were designed for controlled drug delivery at a CNS tissue site.

3.10.3.3 Membranes Used in *In Vivo* Neuronal Regeneration

Synthetic HFMs can be used to repair nerve transaction. Transplantation of porous tubes in poly(2-hydroxyethyl methacrylate-co-methyl methacrylate) was performed by Reynolds *et al.* [137], following a spinal cord transaction surgery in order to improve locomotor functions in rat (**Table 4**).

Semipermeable membranes are also used for the cell encapsulation in order to immunoisolate the cells from the host by being permeable to molecules smaller than certain sizes, but restricting the passage of larger molecules, such as antibodies and complement components, from entering the membrane lumen and interacting directly with the encapsulated cells [138]. One of the applications of HFMs with encapsulated cells is with regard to implantation in the CNS for treatment of Parkinson's disease. Parkinson's disease is a neurological disease characterized by the progressive loss of dopaminergic neurons, in the substantia nigra pars compacta, which are important to motor control. A treatment strategy under development involves the implantation of encapsulated dopamine-secreting cells, with the purpose being to alleviate at least some of the symptoms of Parkinson's disease through the targeted delivery of dopamine. There are also other nervous system disorders where the delivery of missing factor(s), for example, neurotransmitters, neurotrophic factors, or enzymes, might compensate for a disease-caused deficiency and thus alleviate symptoms. Although approaches such as the use of pumps or slow-release polymer systems could be employed, the use of encapsulated secretory cells is a particularly attractive one for chronic implant therapies since the supply will last as long as the cells survive. There are two methods of encapsulation: micro- and macroencapsulation [138]. For macroencapsulation, cells are usually suspended in a matrix within an HFM. The open ends of the hollow fiber are sealed, thereby forming a capsule within which cells reside. In this case, the relatively thick fiber membrane represents a large diffusion distance for

Table 4 *In vivo* applications of membranes in neuronal regeneration

Reference	*Membrane*	*Configuration*	*Matrices*	*Membrane properties*	*Cells*	*Effect*
Benvensite *et al*., 1987 [139]	Diaflo	Microdialysis tube	-	50 kDa		Cellular reaction to implant
Winn *et al*., 1989 [140]	PAN–PVC	Capsules	-		Giant cells	Immunoisolation form xenograft
Aebischer *et al*., 1989 [107]	Polysulfone	Tubes	-	MWCO 10 and 100 kDa	Sciatic nerve	Regeneration of peripheral nerve with 10 kDa MW cut-off membrane
Li *et al*., 1999 [129]	Polyacrylonitrile polyvinylchloride copolymer	Hollow fiber	Macroporous cellulosic microcarriers	Hydrogel	PC-12 L-dopa secreting and C2C-12 CNTF secreting	Cell proliferation *in vitro* and *in vivo* and release of L-dopa and CNTF
Sajadi *et al*., 2006 [141]	Polyethersulfone	Fiber	Polyvinylalcohol	Inner diameter 500 μm	MDX-12 secreting GDNF	Regeneration of nigrostrial dopaminergic fibers
Reynolds *et al*., 2008 [137]	Poly-2-hydroxyethyl methacrylate-co-methyl methacrylate	Tube	-	Dense structure		Improvement of locomotion function after spinal transection
Xue *et al*., 2001 [142]	Alginate-polylysine-alginate	Microcapsules	Polylysine	Diameter 100–300 μm	Bovine chromaffin cells	Reversion of behavioral deficits in hemiparkinsonian rats
Kim *et al*., 2004 [143]	Alginate	Microcapsule	Poly-L-lysine	Diameter 100–300 μm	Chromaffin cells	Maintenance of cell viability after implantation and analgesic effect

the release of catecholamine. This limit can be overcome by microcapsules. The thin membrane and spherical shape result in a high surface-to-volume ratio that facilitates transmembrane diffusion and enhances cell viability. A disadvantage of the microcapsules is that they are fragile and cannot be retrieved easily.

One of the first studies concerning the implantation of HFMs was that of Benveniste, who implanted a Diaflo HFM microdialysis tube in the rat hippocampus and studied the cellular reaction. Hypertrophic astrocyte processes invaded the spongy fiber wall 3 days after and late collagen deposits and occasional granuloma were formed. This study represents an initial attempt toward understanding the CNS tissue response to an HFM device [139]. Later, Winn *et al.* [140] encapsulated cells in a PAN–PVC HFM implanted into an adult male rat's right parietal cortex. A layer of reactive astrocytes mixed with other inflammatory cells including macrophages and microglia enveloped the membrane with some of the cells penetrating into the fiber wall. However, the response was benign due to a consistent absence of necrosis at or around the implant–brain interface over time.

Semipermeable polysulfone tubular membranes with MWCO ranging from 100 to 1000 kDa were used in transacted hamster sciatic nerve model to support nerve regeneration in the absence of a distal nerve stump by Aebischer *et al.* [107]. The MWCO of the tubular membrane affected the outcome of regeneration. Only membranes with MWCO of 100 kDa supported the regeneration of well-differentiated peripheral nervous tissue containing a significant number of myelinated axons.

Li *et al.* [129] used asymmetric hollow fiber membranes of PAN–PVC copolymer to encapsulate PC-12 cells secreting L-dopa and dopamine attached to macroporous cellulosic microcarriers. PC-12 cells on microcarriers were embedded in polyethylene oxide (PEO) or agarose within hollow fiber devices. Devices were implanted into rodent striatum for 4 weeks and assayed for catecholamine release. Proliferation control is attained by embedding cell-containing microcarriers in nonmitogenic hydrogels.

Glial-cell line derived neurotrophic factor (GDNF) was encapsulated in HFMs of PES previously filled with PVA cylindrical matrix and the fiber ends sealed with acrylic-based glue. The implantation of encapsulated cells by PES fibers in animal models of Parkinson's disease [141] leads to improvement of movement associated with striatal reinnervation of dopaminergic fibers.

Microcapsules made of alginate–polylysine–alginate have been used by Xue *et al.* [142], to encapsulate bovine chromaffin cells that have been implanted into the brain of hemiparkinsonian rats. The results of this study show great promise in the application of adrenal autograft tissue for the treatment of Parkinson's disease. Bovine chromaffin cells have also been encapsulated in microcapsules of alginate with 100–300 μm diameter covered by poly-L-lysine and implanted in the subarachnoid space of rats. The microcapsules reduced the symptoms of pain. The cells were morphologically normal and retained their functionality [143].

3.10.4 Conclusions

With the recent advances in the field of biomaterials, particularly in membrane systems, there is much promise of working toward functional tissue-engineered constructs. Many strategies are being developed to realize tailored synthetic and biodegradable membrane systems that are compatible with human cells and tissues. The preclinical development stage of some of these membrane systems demonstrates their potentiality in the tissue engineering field. Bioartificial membrane systems could not only have a role in the replacement of injured organ or tissue but also accelerate the development of new drugs that may cure patients as an alternative to animal experimentation. Many problems encountered with testing potential drugs can be overcome and redesigned on a quicker time scale and at lower cost utilizing a system that can effectively act as a functioning liver. Considering the multidisciplinary nature of tissue engineering, it is important for clinicians, basic scientists, and engineers to collaborate and explore all areas of possibilities in order to realize new advancements toward the creation of an entire organ.

Acknowledgments

The authors acknowledge the European Commission through the Livebiomat project STRP NMP3-CT-013653 in the FP6 and the Italian Ministry of University and Research (MIUR) through the PRIN 2007SCPN4C_003 research project.

References

[1] Langer, R., Vacanti, J. P. *Science* **1993**, *260*, 920–926.
[2] Patrick, C. W., Mikos, A. G., McIntire, L. V. Prospects of Tissue Engineering. In *Frontiers in Tissue Engineering*; Patrick, C. W., Mikos, A. G., McIntire, L. V., Eds.; Elsevier: Oxford, 1998; pp 3–11.
[3] Kim, B. S., Baez, C. E., Atala, A. *World J. Urol.* **2000**, *18*, 2–9.
[4] Hench, L. L. *Science* **1980**, *208*, 826.
[5] Yamamuro, T. In *CRC Handbook of Bioactive Ceramics*; Yamamuro, T., Hench, L. L., Wilson, J., Eds.; CRC Press: Boca Raton, FL, 1990; Vol. 2, p 89.
[6] Chinn, J. A., Sauter, J. A. *J. Biomed. Mater. Res.* **1998**, *39*, 130–136.
[7] Bujan, J., Garcia-Honduvilla, N. *J. Biomed. Mater. Res.* **1998**, *39*, 32–38.
[8] Kim, Y. H., Park, K. D. *Biomater. Res.* **1997**, *1*, 34–37.
[9] Patino, M. G., Neiders, M. E., Andreana, S., Noble, B., Cohen, R. E. *J. Oral Implantol.* **2002**, *28*, 220–225.
[10] Coviello, T., Matricardi, P., Marianecci, C., Alhaique, F. *J. Control. Release* **2007**, *119*, 5–24.
[11] De Bartolo, L., Jarosch-Von Schweder, G., Haverich, A., Bader, A. *Biotechnol. Prog.* **2000**, *16*, 102–108.
[12] De Bartolo, L., Morelli, S., Bader, A., Drioli, E. *Biomaterials* **2002**, *23*, 2485–2497.
[13] Unger, R. E., Huang, Q., Peters, K., Protzer, D., Paul, D., Kirkpatrick, C. J. *Biomaterials* **2005**, *26*, 1877–1884.
[14] Asonuma, K., Gilbert, J. C., Stein, J. E., Tekada, T., Vacanti, J. P. *J. Pediatr. Surg.* **1992**, *27*, 298–301.
[15] United Network for Organ Sharing, http://www.unos.org (accessed November 2009).
[16] European Liver Transplant Registry, http://www.eltr.org (accessed November 2009).
[17] Adam, R., McMaster, P., O'Grady, J. G., *et al. Liver Transplant.* **2003**, *9*, 1231–1243.
[18] Michalopoulos, G. K., DeFrances, M. C. *Science* **1997**, *276*, 60–66.
[19] Opolon, P. *Artif. Organs* **1979**, *3*, 354–360.
[20] Knell, A. J., Dukes, D. C. *Lancet* **1976**, *2*, 402–403.
[21] Stockman, H. B., Hiemstra, C. A., Marquet, R. L., Ijzermans, J. N. *Ann. Surg.* **1973**, *231*, 460–470.
[22] Strain, A. J., Neuberger, J. M. *Science* **2002**, *295*, 1005–1009.
[23] te Velde, A. A., Ladiges, N. C. J. J., Flendrig, L. M., Chamuleau, R. A. F. M. *J. Hepatol.* **1995**, *23*, 184–192.
[24] Pasher, A., Sauer, I. M., Neuhaus, P. *Int. J. Artif. Organs* **2002**, *25*, 1006–1012.
[25] Kono, Y., Yang, S., Letarte, M., Roberts, E. A. *Exp. Cell Res.* **1995**, *221*, 478–485.
[26] McCloskey, P., Edwards, R. J., Tootle, R., Selden, C., Roberts, E., Hodgson, H. J. *J. Hepatol.* **1999**, *31*, 841–851.
[27] Allen, J. W., Bhatia, S. N. *Tissue Eng.* **2002**, *8*, 725–737.
[28] Nyberg, S. L., Remmel, R. P., Mann, H. J., Peshwa, M. V., Hu, W., Cerra, F. B. *Ann. Surg.* **1994**, *220*, 59–67.
[29] Mitaka, T., Kojima, T., Mizuguchi, T., Mochizuki, Y. *Biochem. Biophys. Res. Commun.* **1995**, *214*, 310–317.
[30] Mitaka, T., Mizuguchi, T., Sato, F., Mochizuki, C., Mochizuki, Y. *J. Gastroenterol. Hepatol.* **1998**, *13*, S70–S77.
[31] Alexandre, E., Viollon-Abadie, C., David, P., *et al. Cryobiology* **2002**, *44*, 103–113.
[32] Jauregui, H. O., McMillian, P. N., Driscoll, J., Naik, S. *In Vitro Cell. Develop. Biol.* **1986**, *22*, 13–22.
[33] Dunn, C. Y., Tompkins, R. G., Yarmush, M. L. *Biotechnol. Prog.* **1991**, *7*, 237–245.
[34] Sakai, Y., Ichikawa, K., Sakoda, A., Suzuki, M. *Cytotechnology* **1996**, *21*, 243–252.
[35] De Bartolo, L., Morelli, S., Gallo, M. C., *et al. Biomaterials* **2005**, *26*, 6625–6634.
[36] Miyoshi, H., Okawa, K., Ohshima, N. *J. Biomater. Sci. Polym. Edn.* **1997**, *9*, 227–237.
[37] Ranucci, C. S., Moghe, P. V. *Tissue Eng.* **1999**, *5*, 407–420.
[38] Yamada, K., Kamihira, M., Ijima, S. *Biochem. Eng. J.* **2001**, *8*, 135–143.
[39] Eschbach, E., Chatterjee, S. S., Noldner, M., *et al. J. Cell Biochem.* **2005**, *95*, 243–255.
[40] Nakazawa, K., Matsushita, T., Funatsu, K. *Cytotechnology* **1997**, *24*, 235–242.
[41] Joly, A., Desjardins, J. F., Fremond, B., *et al. Transplantation* **1997**, *63*, 795–803.
[42] Demetriou, A. A., Arnaout, W. S., Backfish, G., Moscioni, A. D. In *Artificial Liver Support*, 2nd edn.; Brunner, G., Mito, M., Eds.; Springer: Berlin, 1993; pp 283–295.
[43] De Bartolo, L., Catalano, G., Della Volpe, C., Drioli, E. *J. Biomater. Sci., Polym. Edn.* **1999**, *10*, 641–655.
[44] De Bartolo, L., Morelli, S., Lopez, L. C., *et al. Biomaterials* **2005**, *26*, 4432–4441.
[45] De Bartolo, L., Morelli, S., Rende, M., *et al. J. Nanosci. Nanotechnol.* **2006**, *6*, 2344–2353.
[46] Arnaout, W. S., Moscioni, A. D., Barbout, R. L., Demetriou, A. A. *J. Surg. Res.* **1990**, *48*, 379–382.
[47] Matsumara, K. N., Guevara, G. R., Huston, H., *et al. Surgery* **1987**, *101*, 99–103.
[48] Margulis, M. S., Erukhimov, E. A., Andreiman, L. A., *et al. Res. Surg.* **1990**, *2*, 99–102.
[49] Sussman, N. L., Chong, M. G., Koussayer, T., *et al. Hepatology* **1992**, *16*, 60–65.
[50] Demetriou, A. A., Rozga, J., Podesta, L., *et al. Scand. J. Gastroenterol.* **1995**, *208*, 111–117.
[51] Gerlach, J. C., Encke, J., Hole, O., Muller, C., Ryan, C. J., Neuhaus, P. *Transplantation* **1994**, *58*, 594–988.
[52] Patzer, J. F., Mazariegos, G. V., Lopez, R. *Am. Coll. Surg.* **2002**, *195*, 299–310.
[53] Flendrig, L. M., la Soe, J. W., Jorning, G. G., *et al. J. Hepatol.* **1997**, *26*, 1379–1392.
[54] Ding, Y. T., Qiu, Y. D., Chen, Z., *et al. World J. Gastroenterol.* **2003**, *9*, 829–832.
[55] Hu, W. S., Friend, J. R., Wu, F. J., *et al. Cytotechnology* **1997**, *23*, 29–38.
[56] Shiraha, H., Koide, N., Hada, H., *et al. Biotechnol. Bioeng.* **1996**, *50*, 416.
[57] Naka, S., Takeshita, K., Yamamoto, T., Tani, T., Kodama, M. *Artif. Organs* **1999**, *23*, 822–828.
[58] Nagaki, M., Miki, K., Kim, Y., *et al. Dig. Dis. Sci.* **2001**, *46*, 1046–1056.
[59] Jasmund, L., Langsch, A., Simmoteit, R., Bader, A. *Biotechnol. Prog.* **2002**, *18*, 839–846.
[60] Lee, D. H., Yoon, H. H., Park, J. K. *Korean Chem. Eng. Res.* **2004**, *42*, 129–138.
[61] Mizumoto, H., Funatsu, K. *Artif. Organs* **2004**, *28*, 53–57.
[62] Curcio, E., Salerno, S., Barbieri, G., De Bartolo, L., Drioli, E., Bader, A. *Biomaterials* **2007**, *28*, 5487–5497.
[63] Schmitmeier, S., Langsch, A., Jasmund, I., Bader, A. *Biotechnol. Bioeng.* **2006**, *95*, 1198–1206.
[64] Roy, P., Baskaran, H., Tilles, A. W., Yarmush, M., Toner, M. *Ann. Biomed. Eng.* **2001**, *29*, 947–955.
[65] Sauer, I. M., Scwartlander, R., Schmid, J., *et al. Artif. Organs* **2005**, *29*, 264–267.
[66] Pless, G., Steffen, I., Zeilinger, K., *et al. Artif. Organs* **2006**, *30*, 686–694.
[67] Ostrovidov, S., Jiang, J., Sokai, Y., Fujii, T. *Biomed. Microdev.* **2004**, *6*, 279–287.
[68] Ho Ye, S., Watanable, J., Takai, M., Iwasaki, Y., Ishihara, K. *Biomaterials* **2006**, *27*, 1955–1962.

[69] De Bartolo, L., Morelli, S., Rende, M., *et al. Macromol. Biosci.* **2007**, *7*, 671–680.
[70] Lu, H. F., Lim, W. S., Zhang, P. C., *et al. Tissue Eng.* **2005**, *11*, 1667–1677.
[71] Memoli, B., De Bartolo, L., Favia, P., *et al. Biomaterials* **2007**, *28*, 4836–4844.
[72] De Bartolo, L., Morelli, S., Bader, A., Drioli, E. *J. Mater. Sci. – Mater. Med.* **2001**, *12*, 959–963.
[73] De Bartolo, L., Morelli, S., Rende, M., Gordano, A., Drioli, E. *Biomaterials* **2004**, *25*, 3621–3629.
[74] De Bartolo, L., Morelli, S., Piscioneri, A., *et al. Biomol. Eng.* **2007**, *24*, 23–26.
[75] Morelli, S., Salerno, S., Rende, M., *et al. J. Membr. Sci.* **2007**, *302*, 27–35.
[76] Hersel, U., Dahmen, C., Kessler, H. *Biomaterials* **2003**, *24*, 4385–4415.
[77] Lopina, S. T., Wu, G., Merrill, E. W., Griffith, C. L. *Biomaterials* **1996**, *17*, 559–569.
[78] Lu, H. F., Lim, W. S., Tang, Z. Q., *et al. Biomaterials* **2003**, *24*, 4893–4903.
[79] Ying, L., Yin, C., Zhuo, R. X., *et al. Biomacromolcules* **2003**, *4*, 157–165.
[80] De Bartolo, L., Morelli, S., Giorno, L., *et al. J. Membr. Sci.* **2006**, *278*, 133–143.
[81] De Bartolo, L., Salerno, S., Giorno, L., *et al. Catal. Today* **2006**, *118*, 172–180.
[82] Sohn, K. H., Lee, H. Y., Chung, H. Y., Young, H. S., Yi, S. Y., Kim, K. W. *Cancer Lett.* **1995**, *94*, 213–218.
[83] Novotny, L., Vachalkova, A., Biggs, D. *Neoplasma* **2000**, *48*, 241–246.
[84] Bahr, M., Bonhoeffer, F. *Trends Neurosci.* **1994**, *17*, 473–479.
[85] Centers for Disease Control and Prevention, http://www.cdc.gov (accessed November 2009).
[86] Archibald, S. J., Shefner, J., Krarup, C., Madison, R. D. *J. Neurosci.* **1995**, *15*, 4109–4123.
[87] Lundborg, G., Dahlin, L., Dohi, D., Kanje, M., Terada, N. *J. Hand Surg. (Br.)* **1997**, *22*, 299–303.
[88] McDonald, J. W. *Sci. Am.* **1999**, *281*, 64–73.
[89] Millesi, H., Ganglberger, J., Berger, A. *Chir. Plast.* **1967**, *3*, 47.
[90] Ferrari, F., De Castro Rodrigues, A. D., Malvezzi, C. K., Dal Pai Silva, M., Padovani, C. R. *Anat. Rec.* **1999**, *256*, 227–232.
[91] Guest, J. D., Rao, A., Olson, L., Bunge, M. B., Bunge, R. P. *Exp. Neurol.* **1997**, *148*, 502–522.
[92] Jones, D. G., Redpath, C. M. *Clin. Anat.* **1998**, *11*, 263–270.
[93] King, V. R., Henseler, M., Brown, R. A., Priesley, J. V. *Exp. Neurol.* **2003**, *182*, 383–398.
[94] Li, Y., Field, P. M., Raisman, G. *J. Neurosci.* **1998**, *18*, 10514–10524.
[95] Stokols, S., Tsuzynski, M. H. *Biomaterials* **2004**, *25*, 5839–5846.
[96] Zhang, N., Yan, H., Wen, X. *Brain Res. Rev.* **2005**, *49*, 48–64.
[97] Chau, C. H., Shum, D. K., Li, H., *et al. FASEB J.* **2004**, *18*, 194–196.
[98] Dowsing, B. J., Hayes, A., Bennet, T. M., Morison, W. A., Messina, A. *Muscle Nerve* **2000**, *23*, 1356–1364.
[99] Iannotti, C., Li, H., Lu, X., Wirthlin, L., Xu, X. M. *Exp. Neurol.* **2003**, *183*, 379–393.
[100] Xu, X. M., Guenard, V., Kleitman, N., Bunge, M. B. *J. Comp. Neurol.* **1995**, *351*, 145–160.
[101] Xu, X. M., Zhang, S. X., Li, H., Bunge, M. B. *Eur. J. Neurosci.* **1999**, *11*, 1723–1740.
[102] Chamberlain, L. J., Yannas, I. V., Hsu, H. P., Strichartz, G., Spector, M. *Exp. Neurol.* **1998**, *154*, 315–329.
[103] Schmidt, C. E., Leach, J. B. *Annu. Rev. Biomed. Eng.* **2003**, *5*, 293–347.
[104] Chesmel, K. D., Black, J. J. *Biomed. Mater. Res.* **1995**, *29*, 1089–1099.
[105] Borgens, R. B. *Neuroscience* **1999**, *91*, 251–264.
[106] Aebischer, P., Guenard, V., Valentini, R. F. *Brain Res.* **1990**, *531*, 211–218.
[107] Aebischer, P., Guenard, V., Brace, S. *J. Neurosci.* **1989**, *9*, 3590–3595.
[108] Valentini, R. F., Sabatini, A. M., Dario, P., Aebischer, P. *Brain Res.* **1989**, *480*, 300–304.
[109] Maquet, V., Martin, D., Scholtes, F., *et al. Biomaterials* **2001**, *22*, 1137–1146.
[110] Song, B., Zhao, M., Forrester, J., McCaig, C. *J. Cell Sci.* **2004**, *117*, 4681–4690.
[111] Gomez, N., Lu, Y., Chen, S., Schmidt, C. E. *Biomaterials* **2007**, *28*, 271.
[112] Dowell-Mesfin, N. M., Abdul-Karim, M. A., Turner, A. M. P., *et al. J. Neural. Eng.* **2004**, *1*, 78.
[113] Schmidt, C. E., Shastri, V. R., Vacanti, J. P., Langer, R. *Proc. Natl. Acad. Sci. USA* **1997**, *94*, 8948.
[114] Ahmed, I., Liu, H. Y., Mamiya, P. C., *et al. J. Biomed. Mater. Res.* **2006**, *76*, 851.
[115] Yang, F., Murugan, R., Wang, S., Ramakrishna, S. *Biomaterials* **2005**, *26*, 2603.
[116] Lovat, V., Panzarotto, D., Lagostena, L., *et al. Nano Lett.* **2005**, *5*, 1107.
[117] Norman, J., Desai, T. *Ann. Biomed. Eng.* **2006**, *34*, 89.
[118] Li, G. N., Hoffman-Kim, D. *Tissue Eng.* **2008**, *14*, 33.
[119] Mahoney, M. J., Chen, R. R., Tan, J., Saltzman, W. M. *Biomaterials* **2005**, *26*, 771.
[120] Fan, Y. W., Cui, F. Z., Chen, L. N., Zhai, Y., Xu, Q. Y., Lee, I. S. *Appl. Surf. Sci.* **2002**, *187*, 213.
[121] De Bartolo, L., Rende, M., Morelli, S., *et al. J. Mem. Sci.* **2008**, *325*, 139–149.
[122] Zhang, N., Zhang, C., Wen, X. *J. Biomed. Mater. Res.* **2005**, *75A*, 941–949.
[123] Young, T.-H., Hung, C.-H. *Biomaterials* **2005**, *26*, 4291–4299.
[124] Manwaring, M. E., Biran, R., Tresco, P. A. *Biomaterials* **2001**, *22*, 3155–3168.
[125] Lee, S. J., Khang, G., Lee, Y. M., Lee, H. B. *J. Colloid Interface Sci.* **2003**, *259*, 228–235.
[126] Chang, K.-Y., Chen, L.-W., Young, T.-H., Hsieh, K.-H. *J. Polym. Res.* **2007**, *14*, 229–243.
[127] Lopez, C. A., Fleischman, A. J., Roy, S., Desai, T. A. *Biomaterials* **2006**, *27*, 3075–3083.
[128] Terris, D. J., Toft, K. M., Moir, M., Lum, J., Wang, M. *Arch. Otolaryngol. Head Neck Surg.* **2001**, *127*, 294–298.
[129] Li, R. H., Williams, S., White, M., Rein, D. *Tissue Eng.* **1999**, *5*, 453–465.
[130] Broadhead, K. W., Biran, R., Tresco, P. A. *Biomaterials* **2002**, *23*, 4689–4699.
[131] Cao, X., Schoichet, M. S. *Biomaterials* **1999**, *20*, 329–339.
[132] Emerich, D. F., Tracy, M. A., Ward, K. L., *et al. Cell Transplant.* **1999**, *8*, 47–58.
[133] Gautier, S. E., Oudega, M., Fragoso, M., *et al. Biomed. Mater. Res.* **1998**, *42*, 642–654.
[134] Dang, W., Daviau, T., Brem, H. *Pram. Res.* **1996**, *13*, 683–691.
[135] Tsai, E. C., Dalton, P. D., Schoichet Tator, C. H. J. *Neurotrauma* **2004**, *21*, 789–804.
[136] Wang, S., Wan, A. C., Xu, X., Gao, S., Mao, H. Q., Leong, H. W., Yu, H. *Biomaterials* **2001**, *22*, 1157–1169.

[137] Reynolds, L. F., Bren, M. C., Wilson, B. C., Gibson, G. D., Shoichet, M. S., Murphy, R. J. L. *Spinal Cord* **2008**, *46*, 58–64.
[138] Uludag, H., De Vos, P., Tresco, P. A. *Adv. Drug Delivery Rev.* **2000**, *42*, 29–64.
[139] Benveniste, H., Diemer, N. H. *Acta Neuropathol.* **1987**, *74*, 234–238.
[140] Winn, S. R., Aebischer, P., Galletti, P. M. *J. Biomed. Mater. Res.* **1989**, *23*, 31–44.
[141] Sajadi, A., Bansadoun, J. C., Schneider, B. L., Lo Bianco, C., Aebischer, P. *Neurobiol. Dis.* **2006**, *22*, 119–129.
[142] Xue, Y., Gao, J., Xi, Z., *et al. Artif. Organs* **2001**, *25*, 131–135.
[143] Kim, Y. M., Jeon, Y. H., Jin, G. C., Lim, J. O., Baek, W. Y. *Artif. Organs* **2004**, *28*, 1059–1066.

Biographical Sketches

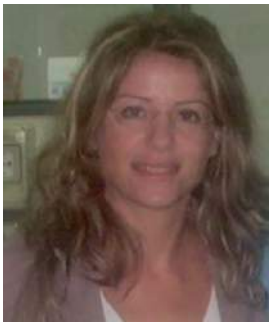

Dr. Sabrina Morelli, PhD
Researcher

Dr. Simona Salerno
Temporary research associate

Antonella Piscioneri
Ph.D. student

Maria Rende
Ph.D. student

Carla Campana
Ph.D. student

Loredana De Bartolo, PhD, is responsible for several national and European research projects and is the author of more than 60 papers published in international journals in the field of membranes, biomaterials, and artificial organs. She is currently the founding member of the European Federation on Regenerative Medicine.

3.11 Separation and Purification of Stem and Blood Cells by Porous Polymeric Membranes

A Higuchi, National Central University, Taoyuan, Taiwan (R.O.C.)

3.11.1	**Introduction**	254
3.11.2	**Blood-Cell Separation**	255
3.11.2.1	Leukocyte-Removal Filter	256
3.11.2.2	LCAP Using Leukocyte-Removal Filter	259
3.11.2.3	Therapeutic Mechanism of LCAP through the Filters	261
3.11.3	**Stem-Cell Separation**	261
3.11.3.1	HSCs and Blood	262
3.11.3.1.1	Separation of HSCs and blood cells by membranes	262
3.11.3.1.2	Separation of HSCs by several surface-modified membranes	265
3.11.3.2	Separation of MSCs/Mesenchymal Progenitor Cells	268
3.11.3.2.1	Flow-cytometric analysis of mesenchymal cells	269
3.11.3.2.2	Cell separation through PU membranes	269
3.11.3.2.3	Cell separation through various porous membranes	272
3.11.4	**Concluding Remarks**	273
References		273

Glossary

CD Cluster of differentiation, a protocol used for the identification and investigation of cell surface molecules present on cells. Hematopoietic stem cells and T helper cell generally express CD34 ($CD34^+$ cell) and CD4 ($CD4^+$ cell), respectively.

c-Myc One of the genes of transcription factors relating to pluripotency of cells.

Ficoll–Hypaque or Ficoll–Paque method Isolation method for mononuclear cells in the blood by density centrifugation.

Fluorescence-activated cell sorting (FACS) Flow cytometry is a technique for counting and examining various kinds of cells by suspending them in a stream of fluid and passing them by an electronic detection apparatus. The antibody conjugated with fluorescence for the surface marker of cells binds to the targeted cells with specific binding between the antibody and the surface marker of the cells, and allows the detection of the targeted cells from the fluorescent signals in FACS. The targeted cells can be separated by applying the electrical field from the electrical charging plate in FACS.

Klf4 One of the genes of transcription factors relating to pluripotency of the cells.

Leukocytapheresis (LCAP) Leukocyte removal from the blood for clinical therapy by the filtration of blood through the leukocyte removal filters.

Magnetic cell selection system (MACS) This is one of the cell separation methods, in which magnetic beads attaching a monoclonal antibody that binds to the targeted cells are mixed with cell solution. The magnetic beads attaching the monoclonal antibody that binds to the targeted cells are separated by magnetic force to collect the specific marked cells.

Oct-3/4 One of the genes of transcription factors relating to pluripotency of the cells.

Permeation ratio (%) It is defined as $(N_p/N_f) \times 100$, where N_p and N_f are the number of cells in the permeate and feed solutions, respectively.

PSL Therapy with prednisolone (corticosteroid) administration.

Recovery ratio (%) This is defined as $(N_r/N_f) \times 100$ where N_r and N_f are the number of cells in the permeate solution after the permeation of human serum albumin (HSA) solution and in the feed solutions, respectively.

Scrapie prion Scrapie is a fatal, degenerative disease that affects the nervous systems of animals. It is one of the several transmissible

spongiform encephalopathies (TSEs), which are related to bovine spongiform encephalopathy (BSE or mad cow disease) and chronic wasting disease of deer. Similar to other spongiform encephalopathies, scrapie is caused by a prion.

SOX2 One of the genes of transcription factors relating to pluripotency of the cells.

α_P Separation factor for permeation defined as the relative permeation ratio of KUSA-A1 cells divided by that of H-1/A cells.

Nomenclature

r pore diameter of membrane (μm)

α_P separation factor

3.11.1 Introduction

Cell separation is a key technology in the isolation of cells from tissue and the transplantation of blood cells or mesenchymal stem cells (MSCs). Techniques such as centrifugation [1–3], fluorescence-activated cell sorting (FACS) [4], magnetic cell selection [5–8], affinity column chromatography [9–11], and membrane filtration [12–17] are typically employed for cell separation. The centrifugal separation of cells is a typical method employed to separate platelets, leukocytes, mononuclear cells, red blood cells (RBCs), and nonblood cells from blood. The centrifugal technology is frequently used to separate specific cells from tissue or organ samples in tissue-engineering experiments. For example, hepatocytes were isolated from collagen-digested liver followed by the centrifugation for the separation between hepatocytes and nonparenchymal liver cells. An initial step in the isolation of endothelial progenitor cells involves centrifugation processes of blood samples through a Ficoll density gradient to isolate mononuclear cells [2]. However, the centrifugation method is not suitable for the separation of cells with similar characteristics, such as T and B cells or $CD34^+$ cells and mononuclear cells. Furthermore, it is not applicable for the clinical application on bedside because of too noisy and too big and heavy instrument on bedside.

The most highly purified cellular preparations are obtained using FACS in conjunction with a fluorescently labeled antibody as the cell-surface marker. Figure 1 shows schematic mechanism of cell analysis

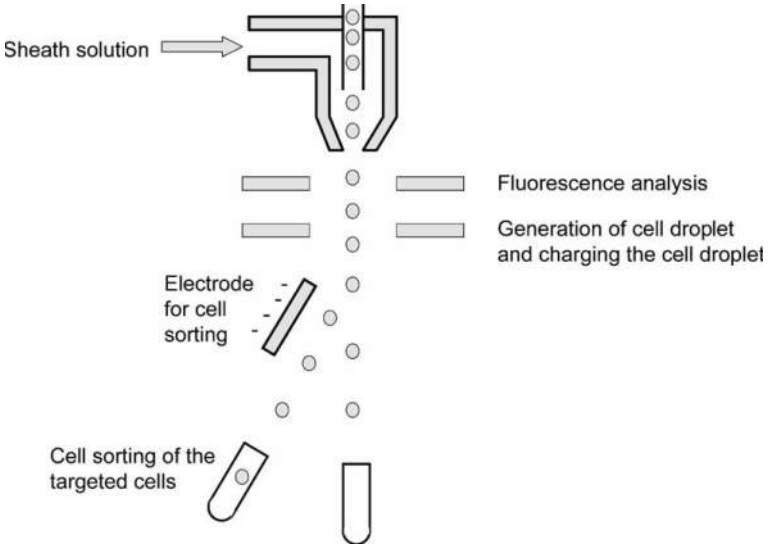

Figure 1 Mechanism of cell analysis and sorting in fluorescence-activated cell sorting (FACS).

and sorting in FACS. Flow cytometry is a technique for counting and examining various kinds of cells by suspending them in a stream of fluid and passing them by an electronic detection apparatus. It allows simultaneous multiparametric analysis of the physical and/or chemical characteristics of up to thousands of particles per second. The antibody conjugated with fluorescence for the surface marker of cells binds to the targeted cells with specific binding between the antibody and the surface marker of the cells, and allows the detection of the targeted cells from the fluorescent signals in FACS. The targeted cells can be separated by applying the electrical field from the electrical charging plate in FACS.

However, FACS cannot be applied to clinical applications because of difficulties with sterility and the excessive time requirements for the purification of sufficient quantities of specific cells (such as $CD34^+$ cells). Furthermore, FACS cannot be used directly from tissue or organ samples (e.g., blood sample), and it needs pretreatment using another cell separation method, such as centrifugation, before usage of FACS. The other problem is that an expensive antibody conjugated with fluorescent probe is necessary to bind to the targeted cells to detect the cells by FACS.

A magnetic cell selection system (MACS, Isolex magnetic cell selection system, Baxter healthcare or CliniMACS, Miltenyi Biotec) is a sophisticated cell separation method, in which magnetic beads attaching a monoclonal antibody as the cell-surface marker are mixed with cells from tissue suspension samples, peripheral blood, umbilical cord blood, or bone marrow [5–8]. **Figure 2** shows the schematic mechanism of the separation method by an MACS. The magnetic beads attaching the monoclonal antibody are separated by magnetic force to collect the specific marked cells. However, the MACS also needs to use an expensive antibody conjugated with magnetic beads to bind to the targeted cells for the detection of the cells. Both cell-separation methods using FACS and MACS are not applicable if the antibodies to the specific markers on the surface of the targeted cells have not been established.

Cell separation through membrane filtration was recently reported by several researchers [12–22]. Here, we discuss the recent development of blood-cell separation and stem-cell separation by the membrane filtration method from different cell sources such as blood and tissue cell samples in the following sections.

3.11.2 Blood-Cell Separation

Blood is a living tissue composed of several blood cells in plasma. The cellular elements of RBCs, platelets, and white blood cells make up 45% of the volume of whole blood. Another 55% is plasma, which contains 7–8% of the plasma proteins and

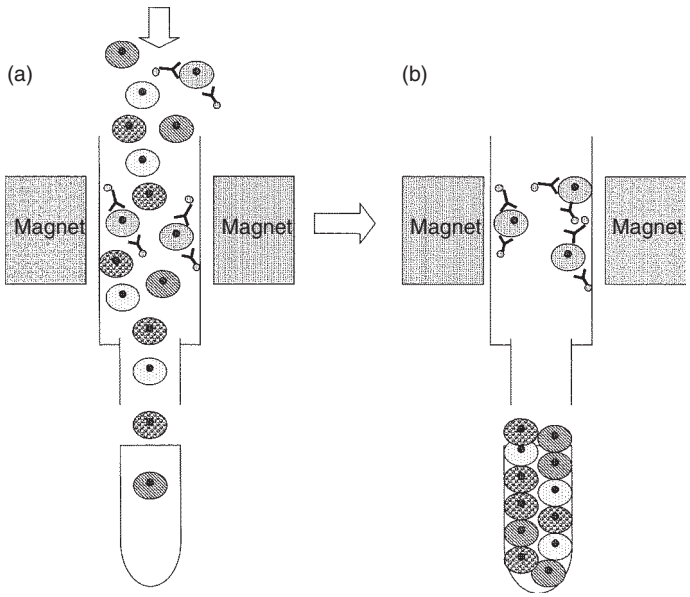

Figure 2 Schematic mechanism of the separation method of cells by a magnetic cell selection system. (a) During permeation of cell solution. (b) After permeation of cell solution.

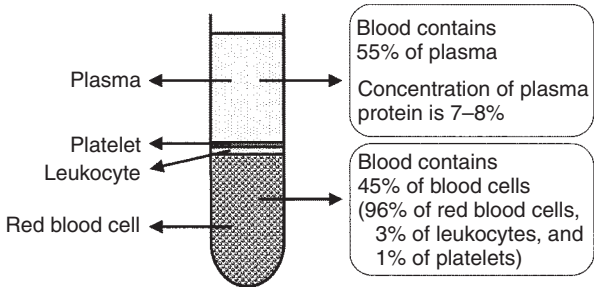

Figure 3 Blood components.

92–93% of water (**Figure 3**). Blood for transplantation is typically passed through membrane filters to eliminate leukocytes, which function to prevent infection by viruses (such as the human immunodeficiency virus and the hepatitis C virus), and to avoid side effects originating from leukocytes [12, 13]. Compared with other cell-separation methods, the membrane filtration is simple and inexpensive, and sterility is easy to maintain during the process. We discuss the recent development of leukocyte-removal filters and clinical therapy of blood filtration using leukocyte-removal filter (leukocytapheresis (LCAP)) in the following sections.

3.11.2.1 Leukocyte-Removal Filter

Blood transfusion-related adverse reactions have been reported to be caused by leukocytes in blood products. It is desirable to reduce leukocytes in blood samples and drugs as possible. In the recent years, blood-component therapy is widely used to replace whole blood transfusions due to the improvement of transfusion techniques. RBC concentrates and platelet concentrates are the most frequently transfused blood components [12, 13, 21]. Blood-component therapy can not only reduce waste of blood resources, but also provide benefits to more patients from a donor blood unit [23].

It has been reported that white blood cells (leukocytes) generate many adverse reactions during blood-transfusion therapy, which are grafted versus host disease (GVHD), platelet refractoriness, nonhemolytic febrile transfusion reaction, and infection of viruses, such as human T-lymphotropic virus (HTLV), cytomegalovirus (CMV), and human immunodeficiency virus (HIV) [24–26]. **Table 1** summarizes side effects of transfusion caused by contamination of leukocytes. It was found that most of the viruses infect specific type of leukocytes, such as granulocytes, monocytes, lymphocytes, lymphocytes-B, T helper cell ($CD4^+$ cell), and T-cell suppressor/cytotoxic cells ($CD8^+$ cell). HTLV-1 and HIV mainly infect T helper cell [27–30], while CMV mainly infects granulocytes, monocytes, and lymphocytes. GVHD was mainly generated by T helper cell and T-cell suppressor/cytotoxic cells ($CD8^+$ cell) [31]. In addition, a possible transmission of scrapie prion was reported to be mediated by B cells [21, 32].

Table 1 Specific infection of virus or protein to leukocytes and side effect of transfusion caused by contamination of leukocytes[a]

Disease	*Cause of virus or protein*	*Infected blood cells*
AIDS	HIV	T-helper cells
Herpes	CMV	Granulocytes, monocytes, and lymphocytes
Herpes	EBV	B cell
Leukemia	HTLV-1	T-helper cell ($CD4^+$ cell)
NHFTR	IL-1, IL-8 (protein)	Granulocytes, monocytes
Allo-immunization		Macrophage, B cell
CJD	Prion (protein)	B cell
GVHD		T helper cells, T-cell suppressor/cytotoxic cells ($CD8^+$ cell)

[a] AIDS, acquired immune deficiency syndrome; NHFTR, nonhaemolytic febrile transfusion reactions; CJD, Creutzfeldt–Jakob disease; GVHD, graft versus host disease; HIV, human immunodeficiency virus; CMV, cytomegalovirus; HTLV-1, human T-lymphotropic virus; EBV, Epstein-Barr virus.

Table 2 Commercially available leukocyte-removal filters[a]

Filter name	*Production company*	*Base materials*	*Morphology*
Sepacell R-500A	Asahi Kasei Medical	PET	NW
Sepacell PLX-5A	Asahi Kasei Medical	PET	NW
Imugard IIIRC	Termo	PU	S
Imugard IIIPL	Termo	PU	S
Pall RCXL2	Pall	PBT	NW
LeukoGard RS	Pall	NA	NA
Pall RC400	Pall	NA	NA
Fresenius Biofil02	Fresenius	NA	NA
Nipro CF-2	Nipro	Polyester	NW
Sitafilter	Nipro	NA	NA

[a] PET, poly(ethylene terephthalate); PBT, poly(butylene terephthalate); PU, polyurethane; NW, nonwoven fabric; S, sponge structure made from salt leaching method.
NA, not available.

Therefore, removal of leukocytes in RBC and platelet concentrates as well as whole blood component are essential to prevent the adverse effect of contaminated leukocytes [23, 33]. Leukocytes can be removed using a filter comprised of nonwoven fabric or sponge materials as a filter medium. **Table 2** summarizes commercially available leukocyte-removal filters. The mechanism of leukocyte removal on the filters comprised of nonwoven fabric is based on the adsorption of leukocytes, while that comprised of sponge materials is based on the sieving effect and adsorption.

Filtration methods have several advantages compared to other methods of removing leukocytes such as centrifugation. Virus contamination is lower in blood components during the process in the filtration method than in the centrifugation method due to the mild operation and the ease of operation under sterilized conditions. The filtration method does not require a special apparatus such as centrifugation equipment, and provides high leukocyte removal from the blood components.

It is also reported that leukocyte depletion using the filters reduces the risk of reintroduction of hepatocellular carcinoma cells during liver transplantation or an intracellular parasite of monocytes transmissible by transfusion [34, 35].

Vries *et al.* [36] investigated clinical efficacy and biocompatibility of leukocyte- and fat-removal filters during cardiac surgery, because activated leukocytes and fat particles are associated with organ injury in patients after a cardiac surgery, and the effects of activated leukocytes and fat particles on the injuries of lungs, brain, and kidneys in patients have been reported [36–39]. Leukocyte depletion as well as fat particles by means of filtration were proposed as a method to reduce this organ injury [40–42]. Most clinical filtration procedures are currently performed during a cardiopulmonary bypass (CPB) with its concomitant hemodilution. Vries *et al.* [36] measured the leukocyte and fat-removal properties and the biocompatibility of three different filters (i.e., two leukocyte removal filters and fat-removal filter) using residual heart–lung machine blood. They determined the circulating leukocyte and platelet acid concentration after the filters. They also investigated free hemoglobin, plasma elastase, and complement C5–9 to assess the biocompatibility of the filters [36]. The total leukocyte counts and fat particles were higher after the lipid removal filter compared to the leukocyte-removal filters, which means leukocyte-removal filters effectively remove leukocyte and fat particles. They concluded that the leukocyte-removal filters were superior to the fat-removal filter both in leukocyte and in fat removal. A clear mechanism for filtering leukocytes has not been determined, but most scientists consider the size and depth of the filter material important [43–46].

Leukocyte-removal filters were typically made of polyurethane (PU) foaming membranes where the pore was made by salt leaching method and nonwoven fabric. The typical scanning electron microscopy (SEM) pictures of those leukocyte-removal filters are shown in **Figure 4**. The pore structure of both filters is found to be completely different, although the pore size of those filters was almost the same from capillary flow porometer measurements. The mechanism of leukocyte removal (i.e., separation of leukocyte

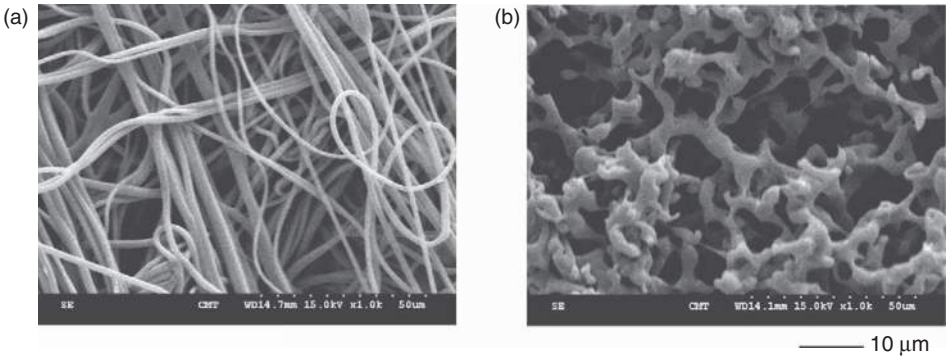

Figure 4 Typical SEM pictures of leukocyte removal filters made of nonwoven fabric (a) and polyurethane forming membranes (b).

from plasma and other blood cells) in leukocyte-removal filters is mainly based on leukocyte adsorption on the filters. The adsorption of leukocytes was affected significantly by filter materials, pore structure, and pore size [47].

Umegae *et al.* [48] and Shirokaze [47] investigated the effect of fiber diameters on leukocyte-removal rate using filters made of nonwoven fabric. They found that the leukocyte removal rate increased with the decrease of fiber diameter of nonwoven fabric. Leukocyte-removal rate increased when the fiber of nonwoven fabric is less than 10 μm, especially less than 3 μm [47, 48]. This can be explained by the increase in surface area with the decrease in fiber diameter of nonwoven fabric.

Filter media can control interactions with blood cells through hydrophilic/hydrophobic treatment of filter materials or through a surface coating with charged substances [23]. Nishimura [49] investigated leukocyte retention by means of hydrophilicity and surface charge. A filter material was coated with vinyl monomers containing amine functional groups and nonionic hydrophilic vinyl monomers. Pall and Gsell [50] prepared a leukocyte-removal filter having surface with acryl/methacrylic acid and a hydroxyl/carboxyl functional group. Carbohydrates and polysaccharides are also used to induce adhesion of leukocytes on the leukocyte-removal filters [51, 52]. Hiraide [51] reported leukocyte-removal rates through nonwoven fabric coated with hydroxyapatite.

Currently, commercially available leukocyte-removal filters (membranes) are applied after blood is centrifuged and separated into RBCs, platelets, and plasma. However, direct removal of leukocytes from whole blood without the centrifugation procedure has not yet been achieved using leukocyte-removal filters. This is thought to be because adhesion of platelets to the membrane surface causes considerable loss of platelets in the whole blood passed through the leukocyte-removal filters. A high recovery of platelets and RBCs, as well as a high removal ability of leukocytes, is necessary for whole blood filters for leukocyte removal. Therefore, coating (surface) materials as well as filter (membrane) materials must be adequately designed to successfully construct whole blood filters for leukocyte removal [21].

Only a few researchers have investigated whole blood filters for leukocyte removal [21, 53–56]. Paunovic *et al.* [53] investigated leukocyte reduction from whole blood using leukocyte-removal filters composed of multiple layers of microporous PU membranes. Direct removal of leukocytes from whole blood was confirmed to show higher reduction of leukocytes as well as higher recovery of the three blood components (RBCs, platelets, and plasma) as compared with the current technique that involves treatment of each component (RBCs, platelets, and plasma) after separation by centrifugation to remove the leukocytes [21, 53–56]. The mechanism of leukocyte removal has been explained by a mechanical sieving effect of the cells through the leukocyte-removal filters, while low platelet adhesion to the surface of the filters resulted in high platelet permeation through the filters. This was thought to be achieved by the biocompatibility of PU on the surface of the filters. However, it has not yet been clarified how the surface properties of the leukocyte removal filters affect leukocyte removal and platelet permeation through the filters.

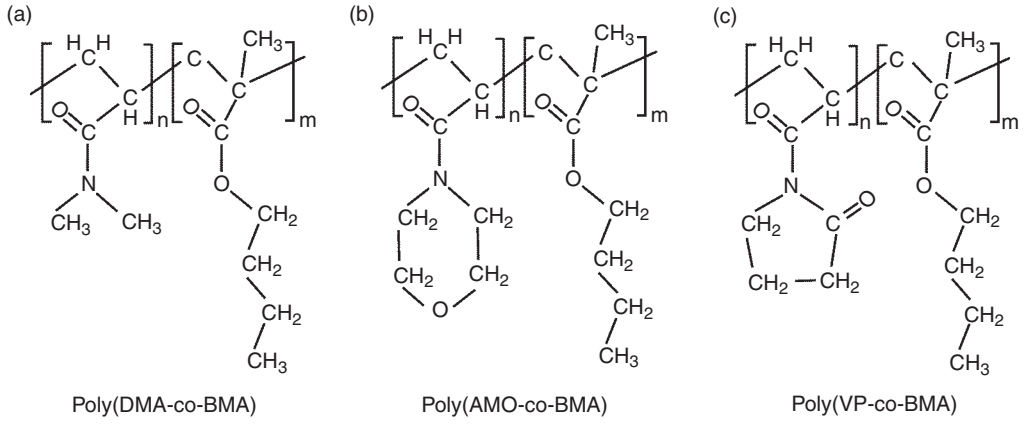

Figure 5 Chemical scheme of copolymers, poly(*N,N′*-dimethylacrylamide-co-buthylmethacrylate) [poly(DMA-co-BMA)], poly(*N*-acryloylmorpholine-co-buthylmethacrylate) [poly(AMO-co-BMA)], and poly(*N*-vinylpyrrolidone-co-buthylmethacrylate) [poly(VP-co-BMA)] for coating filters used to remove leukocytes from whole blood [21].

Natori and Higuchi *et al.* [21] synthesized three types of amphiphilic copolymers using *n*-butylmethacrylate (BMA) as a hydrophobic monomer, and each of *N,N′*-dimethylacrylamide (DMA), *N*-acryloylmorpholine (AMO), and *N*-vinylpyrrolidone (VP) as hydrophilic comonomers for coating filters used to remove leukocytes from whole blood (see **Figure 5**). The influence of the amphiphilic property of the resulting filters, which were composed of nonwoven fabrics coated with the above copolymers, on leukocyte removal and platelet permeation through the filters from whole blood was investigated. The platelet permeation ratio through hydrophobic noncoated filters was only 0.2%, because platelets in whole blood adhered easily to the hydrophobic filter material [21]. However, filters coated with poly(AMO-co-BMA) of high AMO content showed a much higher platelet permeation ratio (nearly 90%). Further, the filters coated with poly(DMA-co-BMA) also showed high permeation ratios of platelets (more than 78%) over a broad range of DMA content in the copolymer. On the other hand, the coated filters showed a slightly higher permeation ratio of leukocytes than did the noncoated filters, resulting from the increase in hydrophilicity of the surface of the filters. Moreover, the coating of the amphiphilic copolymers on the surface of the nonwoven fabrics affected the pore size of the filters, affecting the permeation ratio of leukocytes more strongly than that of platelets. They found that the coated filters effectively improved platelet permeation through the filters, with a slight increase in the permeation ratio of leukocytes [21].

The investigation of the effect of surface properties of the filters on the leukocyte removal through the filters is necessary to further develop leukocyte-removal filters which will be available commercially.

3.11.2.2 LCAP Using Leukocyte-Removal Filter

LCAP using a leukocyte-removal filter was performed in the treatment of systemic lupus erythematosus (SLE) in 1986 [47, 57]. Based on this trial, LCAP using the leukocyte-removal filter has been tried widely as a treatment for autoimmune or inflammatory diseases in rheumatology, gastroenterology, and neurology. The filter was recognized to have immunosuppressive and anti-inflammatory effects in the studies applied to rheumatoid arthritis [58], and erythematosus [59]. The targets of clinical trials of LCAP using a leukocyte-removal filter have been spread to another autoimmune-related and inflammatory diseases such as ulcerative colitis (UC), Crohn's disease, and rapidly progressive glomerulonephritis [47].

UC is a chronic inflammatory disease of the rectum and colon, which is characterized by abdominal pain, diarrhea, hematochezia, fever, and anemia. The administration of corticosteroids is a typical treatment in bringing about a clinical remission [60, 61]. However, corticosteroids are not always effective even in doses over 1 mg kg^{-1} day^{-1}, while the long-term use of corticosteroids often causes serious side effects such as hormonal disturbance, growth retardation, liver dysfunction, glaucoma,

peptic ulcer, and psychological problems. Alternative treatment for active UC requires to avoid the clinical problems associated with corticosteroid therapy. In the recent years, LCAP and granulocytapheresis (GCAP) using a leukocyte-removal filter have been found effective in patients with inflammatory bowel disease [60, 62, 63].

Especially, a multicenter randomized controlled study of UC proved the high efficient improvement for the patients treated by LCAP using a leukocyte-removal filter [47].

Figure 6 shows a schematic representation of the LCAP method using leukocyte-removal filter. The saline solution with anticoagulant (e.g., nafamostat mesilate) should be circulated in the circuit before LCAP treatment. During the treatment, blood of a patient is drawn from a cubital or femoral vein into the circulation circuit of LCAP through the filter using a pump. The blood proceed to flow through the circuit and is returned to the corresponding vein of the patient's other arm or leg. Typically, 2–3 l of blood is processed in a single 1-h session at a flow rate of 30–50 ml min^{-1}. Anticoagulant should be injected continuously into the circuit to prevent coagulation. This process is basically the same as the widely used direct hemoperfusion-type adsorption therapy and is performed using a general extracorporeal treatment unit. Usually, LCAP is performed once a week for 5 weeks as intensive therapy and approximately once a month as maintenance therapy [47].

Adsorption of leukocytes on the filters made of polyester nonwoven fabric was reported to be dependent on the viscosity of the cells [64, 65]. Monocytes have the highest surface viscosity, followed by granulocytes among the leukocytes. Lymphocytes have relatively lower viscosity. The removal rate of blood-cell components in a clinical test was reported for 14 patients suffering from UC where 3 l of blood was processed by LCAP in 1-h treatment with the flow rate of blood set at 50 ml min^{-1} through the leukocyte-removal filter [66]. It was found that monocytes and granulocytes were removed almost 100% during treatment, while lymphocytes were removed approximately 64% at 15 min after the start of the treatment. The removal rate of lymphocyte decreased with increase of time and reached 20% at the end of the treatment (1 h). The high performance of platelet removal was found where removal rate of platelets was approximately 93% at 15 min after the start of the treatment and approximately 46% at the end of the treatment [66].

The number of leukocytes in the peripheral blood of a UC patient decreased to about 40% of its initial count after 30 min of LCAP treatment. However, the leukocyte number generally increased gradually even if the treatment was continued to remove leukocytes [47, 63]. It was reported that the number of leukocytes increased to 170% of its initial number in the peripheral blood even after the LCAP therapy was completed [47, 63, 67]. However, the excess

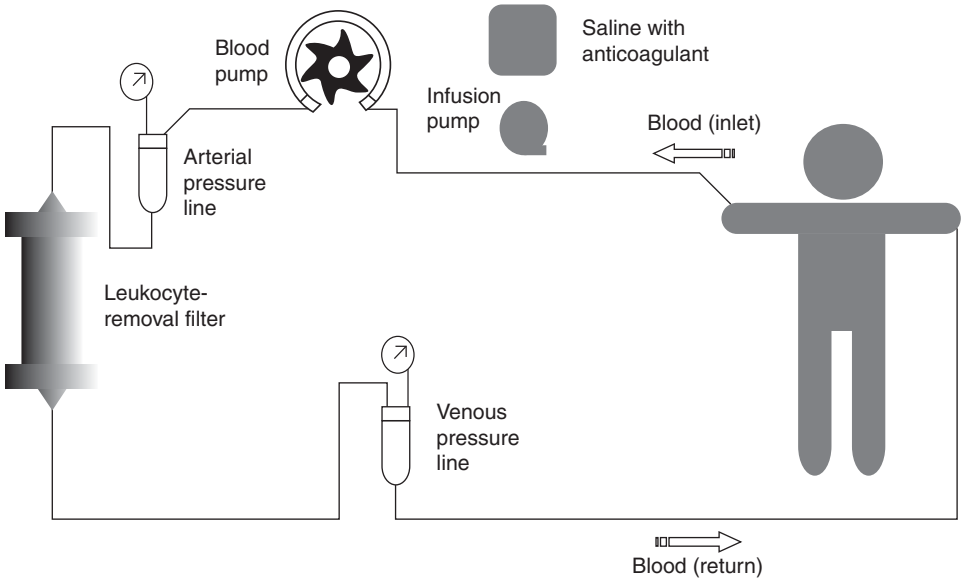

Figure 6 Schematic representation of leukocytapheresis method using leukocyte-removal filter.

number of leukocytes returned to the initial value the next day. Therefore, these phenomena were explained by the homeostatic maintenance control system to keep the constant number of leukocytes in the peripheral blood [47, 63, 67]. The key point of LCAP treatment through the leukocyte-removal filter is that aged and/or activated leukocytes and platelets were removed from a patient's blood.

The Research Committee of Inflammatory Bowel Disease (IBD Research Committee) under the auspices of the Ministry of Health and Welfare of Japan conducted a randomized controlled study on patients with moderate or severe UC from 1994 to 1998 [47]. The patients were separated into two groups, that is, the prednisolone (PSL) (therapy with prednisolone (corticosteroid) administration) group and the LCAP (therapy using leukocyte-removal filter) group [68]. Statistically significant improvement during the intensive therapy was observed in about 70% of the group of LCAP therapy using leukocyte-removal filter, which was substantially higher than in the group of therapy with corticosteroid administration. The incidence rate of the adverse effects in the group of LCAP therapy using leukocyte removal filter was also reported to be lower than in the PSL group [47].

Ueki *et al.* reported the clinical effectiveness of LCAP therapy using leukocyte-removal filter administered to 25 rheumatoid arthritis patients with the American College of Rheumatology (ACR) core set for 4 weeks after the three sessions of LCAP treatment [47, 67]. The average score of tender and swollen joints was reported to decrease significantly. As many as 16 of the 25 patients (64%) were reported to achieve an ACR 20% response that indicates overall improvement with LCAP treatment [67]. Hidaka *et al.* evaluated the efficacy of LCAP in drug-resistant rheumatoid arthritis with an ACR core set at 1 week after the termination of the treatment in a randomized double-blind controlled trial. It was reported that 19 of 24 patients (79%) in the group of LCAP therapy using leukocyte-removal filter achieved an ACR 20% response, although the patients in the sham apheresis group did not show any overall improvement [47, 69].

3.11.2.3 Therapeutic Mechanism of LCAP through the Filters

Several effective mechanisms were proposed for LCAP through leukocyte-removal filter, and are discussed as follows.

It was reported that several leukocytes, that is, lymphocytes and monocytes, infiltrate the mucous membrane of the large intestine in a UC patient. The tissues are damaged by inflammatory cytokines secreted by the leukocytes due to secretion of cytokines and active biomolecules by activated leukocytes. Activated leukocytes easily adhere to vascular endothelial cells and migrate to the mucous membrane of the large intestine when blood flows near the local inflammation site. Therefore, the removal of the leukocytes from the peripheral blood of a patient can safeguard the mucous membrane of the large intestine from leukocytes attack and hence decrease inflammation reaction in the patient [47, 70].

Immune profiles of lymphocytes of UC patients treated with LCAP were reported by Noguchi *et al.* [71]. They found that $CD4^+DR^+$ cells increased and $CD4^+DR^-$ cells decreased in the blood filtered through the leukocyte-removal filter compared to the peripheral blood. Furthermore, the interleukin (IL)-4 production was extensively increased by the filter-passed lymphocytes. It was suggested that the redistributed T lymphocytes producing IL-4 may be one of the factors leading to remission and curing at the local inflammatory sites. The leukocyte-removal filter also removes platelets at a high rate during LCAP treatment. It is also known that the activated oxygen was secreted by the leukocytes, which were stimulated by the activated platelets in the peripheral blood of UC patients [72]. Therefore, the removal of activated platelets results in the inhibition of the production of activated oxygen and relieving symptoms of inflammation.

3.11.3 Stem-Cell Separation

Stem cells are characterized by the ability to renew themselves through mitotic cell division and differentiate into a diverse range of specialized cell types. Stem cells are defined as the cells having characteristics of self-renewal capacity, and long-term viability, which can produce at least one type of highly differentiated descendant. The two broad types of mammalian stem cells are: embryonic stem cells that are isolated from the inner cell mass of blastocysts and adult stem cells that are found in adult tissues. Recently, induced pluripotent stem (iPS) cells were developed by Yamamiya *et al.*, which are artificially derived from a nonpluripotent cell (i.e., adult somatic cell) by inducing a forced

expression of certain genes such as Oct-3/4, SOX2, c-Myc, and Klf4 [73–75]. In a developing embryo, stem cells can differentiate into all of the specialized embryonic tissues. In adult organisms, stem cells and progenitor cells act as a repair system for the body, replenishing specialized cells, also maintain the normal turnover of regenerative organs, such as skin, blood, or intestinal tissues. Stem cells can now be grown and transformed into specialized cells with characteristics consistent with cells of various tissues such as osteoblasts, chondrocytes, adipocytes, nerves, or muscles through cell culture. Highly plastic adult stem cells from a variety of sources, including umbilical cord blood and bone marrow, are routinely used in medical therapies. Here, we summarize the purification and isolation of hematopoietic stem cells (HSCs) and MSCs by the membrane filtration method.

3.11.3.1 HSCs and Blood

HSCs are multipotent stem cells that give rise to all the blood cell types, including myeloid (monocytes and macrophages, neutrophils, basophils, eosinophils, erythrocytes, megakaryocytes/platelets, dendritic cells) and lymphoid lineages (T cells, B cells, and NK cells) (see **Figure 7**). The hematopoietic tissue contains cells with long-term and short-term regeneration capacities and committed multipotent, oligopotent, and unipotent progenitors. We discuss the HSC separation from peripheral and umbilical cord blood through porous polymeric membranes by the filtration method in the following sections.

3.11.3.1.1 Separation of HSCs and blood cells by membranes

Blood cell separation is an important technology for the transplantation of blood cells and HSCs. More than 500 ml of cryopreserved $CD34^+$ cells (HSCs) are used in conventional unpurified mononuclear transplantation procedures, whereas the amount of magnetically purified and concentrated $CD34^+$ needed is only 3–10 ml [76, 77]. This reduction in the required cell volume leads to reduced side effects, which include headache and irregular blood pressure, and which are attributed to the cryopreservant, dimethyl sulfoxide, as well as to broken blood cells in the cryopreserved blood [5, 76].

Purification of $CD34^+$ cells (HSCs) from peripheral blood and umbilical cord blood is reported to reduce the contamination of myeloma cells in graft. This leads to improved patient survival and prevents acute or chronic graft-versus-host disease (GVHD), which is due to decreased T cell number [78]. There is also a large demand for T and B cell separation in the therapy and diagnosis of autoimmune disease and cancer [79–82]. Specific T cell selection (separation), which has the ability of graft-versus-leukemia (GVL) effect but does not have the ability of GVHD will enable the clinical application of lymphocyte therapy, because the T cells responsible for GVL and GVHD may be different [83].

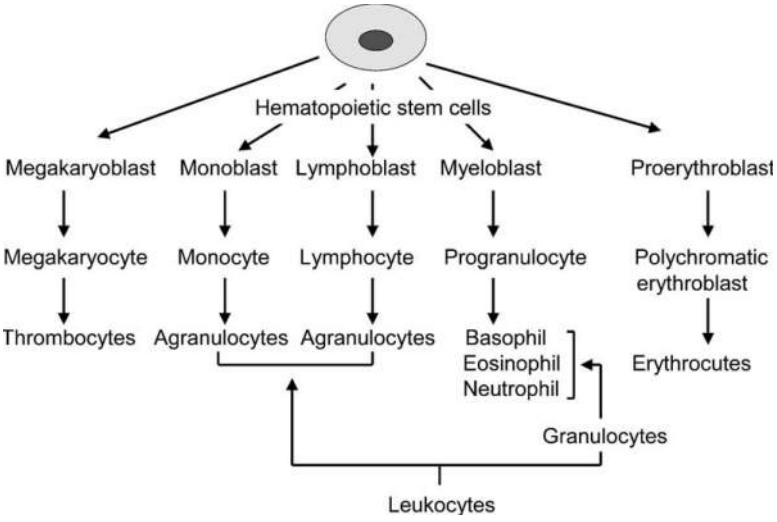

Figure 7 HSCs are multipotent stem cells that give rise to all the blood cell types including myeloid (monocytes and macrophages, neutrophils, basophils, eosinophils, erythrocytes, megakaryocytes/platelets, dendritic cells) and lymphoid lineages (T cells, B cells, and NK cells).

Blood cell separation is typically performed by centrifugation, fluorescence activated cell sorting (FACS) [83], magnetic cell selection [5–8], or membrane filtration. The centrifugal separation of blood cells is a well-known method to separate platelets, leukocytes, and RBCs, but this method does not work well for the separation of cells with similar characteristics, such as T and B cells or $CD34^+$ cells and mononuclear cells. The most highly purified cellular preparations are obtained by FACS in conjunction with a fluorescently labeled antibody for cell-surface marker. However, this cannot be used for clinical applications because of difficulties with sterility and the excessive time needed to purify sufficient quantities of $CD34^+$ cells.

An alternative to these methods is to use a MACS (e.g., Isolex magnetic cell selection system, Baxter healthcare or CliniMACS, Miltenyi Biotec), in which magnetic beads attaching an anti-CD34 monoclonal antibody are mixed with cells from peripheral blood, umbilical cord blood, or bone marrow. The magnetic beads attaching anti-CD34 monoclonal antibody are separated by magnetic force to collect the $CD34^+$ cells. Mobilized autologous apheresis by magnetic cell selection has been reported to result in a 91.7% purification of $CD34^+$ cells with a 55% recovery [5].

Yamaguchi *et al.* [84] and Koizumi *et al.* [85] reported the efficient purification of $CD34^+$ cells (HSCs) using a nylon fiber syringe system along with magnetic cell selection. After the isolation of mononuclear cells from the peripheral blood by density centrifugation in Ficoll–Hypaque, a nylon-fiber syringe filter was used to deplete adhering cells [84]. The cells were further purified using magnetic $CD34^+$ selection. This resulted in a >90% pure $CD34^+$ cell preparation with an 86% yield [84].

Stem cell separation from peripheral blood was investigated using unmodified and surface-modified PU membranes with various functional groups by Higuchi *et al.* [15–19]. Reaction scheme to prepare the surface-modified PU membranes is shown in **Figure 8**.

Higuchi *et al.* [15–19] investigated the permeation of HSCs through the surface-modified and unmodified PU membranes. Only viable cells were measured using 7-amino-actinomycin D (7AAD) dying method, because the dead and apoptotic cells dyed with 7-amino-actinomycin D were stronger than viable cells. **Figure 9** shows the permeation ratio of $CD34^+$ cells through the surface-modified and unmodified PU membranes. The permeation ratio was less than 5% for the surface-modified and unmodified PU membranes where the permeation ratio is defined as

$$\text{Permeation ratio } (\%) = (N_p/N_f) \times 100 \qquad (1)$$

where N_p and N_f are the number of cells in the permeate and feed solutions, respectively [15–19]. This indicates that the $CD34^+$ cells adhere to the membranes stronger than RBCs, platelets, T cells, and B cells (see **Figure 10**). The adhesion of blood cells to the PU membranes appeared to increase in the following order: RBCs < platelets < T cells < B cells < $CD34^+$ cells.

Human serum albumin (HSA) solution was passed through the PU membranes as a rinsing (recovery) solution after permeation of blood. **Figure 9** also shows the recovery ratio of $CD34^+$ cells. The recovery ratio of $CD34^+$ cells was the highest after

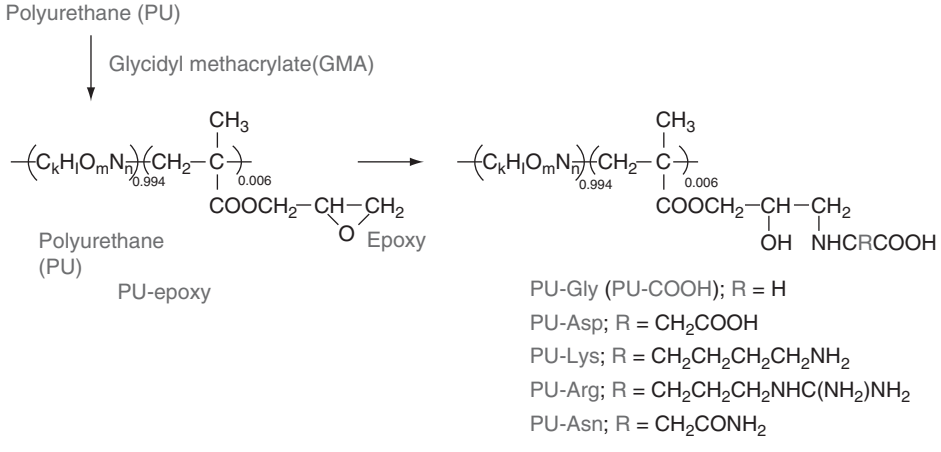

Figure 8 Reaction scheme of the surface-modified PU foaming membranes [18].

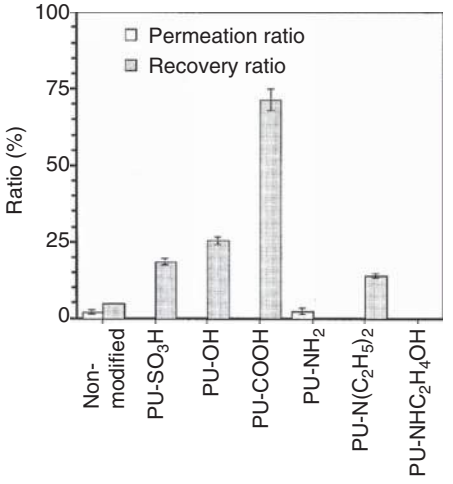

Figure 9 Permeation and recovery ratio of $CD34^+$ cells through unmodified and surface-modified PU membranes after permeation of peripheral blood [15].

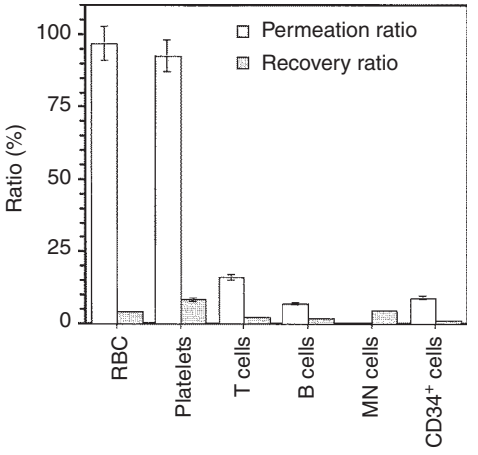

Figure 10 Permeation and recovery ratio of RBCs, platelets, T cells, B cells, $CD34^+$ cells, and MN cells through unmodified PU membranes after permeation of peripheral blood [15].

permeation of HSA solution through PU membranes grafted with polymer segments having carboxylic acid (PU-COOH, see **Figure 8**) membranes where the recovery ratio is defined as

$$\text{Recovery ratio } (\%) = (N_r/N_f) \times 100 \qquad (2)$$

where N_r is the number of cells in the permeate solution after the permeation of HSA solution [15–19]. This result was unexpected because the PU-SO_3H membranes allowed the highest recovery of T and B cells (see **Figure 11**) and because the PU-SO_3H membranes were expected to give the

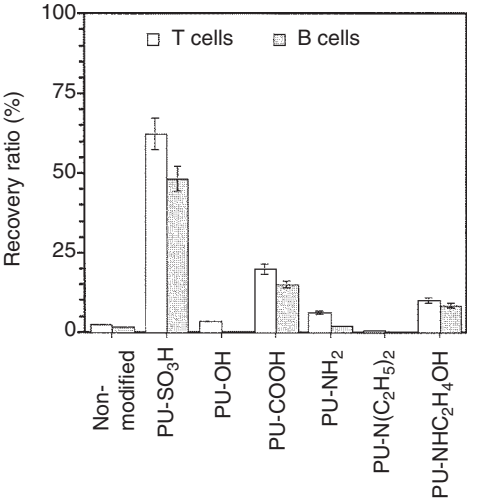

Figure 11 Recovery ratio of T and B cells through nonmodified and surface-modified PU membranes after permeation of peripheral blood and recovery solution of HSA solution [15].

highest recovery of $CD34^+$ cells before HSA permeation. Therefore, it appears that not only the pore structure and surface charge but also the specific functional group on the membrane surface can regulate the attachment and detachment of specific cells [15].

Finally, Higuchi *et al.* [15] examined the permeation and recovery ratio of several blood cell types through the unmodified PU and PU-COOH (**Figure 12**). $CD34^+$ cells were mainly recovered in

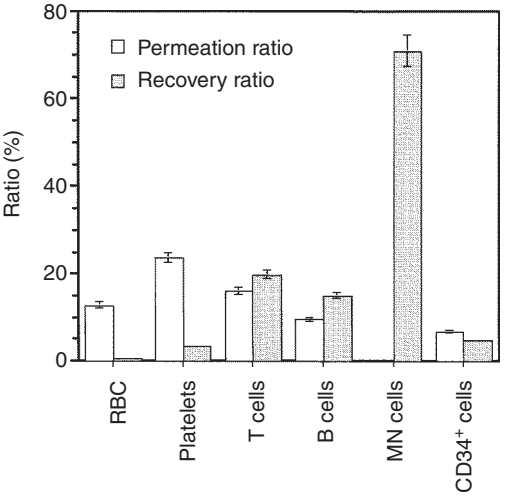

Figure 12 Permeation and recovery ratio of RBCs, platelets, T cells, B cells, $CD34^+$ cells, and MN cells through PU-COOH membranes after permeation of peripheral blood [15].

the permeate of the PU-COOH membranes (**Figure 12**), whereas both RBCs and platelets could preferentially permeate through the unmodified PU membranes (**Figure 10**). In contrast, $CD34^+$ cells could not permeate through the unmodified membranes (**Figure 10**). The permeation and recovery ratios of mononuclear cells were found to be less than 10% [15].

After permeation of peripheral blood followed by HSA, the ratio of $CD34^+$ cells to mononuclear cells in the permeate was enhanced at least 11-fold. We conclude that the surface-modified PU membranes display different permeation and recovery ratios for specific cell types depending on the functional groups (nanosegments) attached to the membranes.

In conjunction with PU-COOH membranes, passing HSA solution to detach adhered cells allowed the isolation of $CD34^+$ cells and reduction of mononuclear cells in the permeate solution. This process may also be useful as a preliminary step in the purification of $CD34^+$ cells by magnetic cell selection (e.g., Isolex™ magnetic cell selection or CliniMACS™) because reduction of mononuclear cells is essential for obtaining high purity and yield of these cells by magnetic cell selection [84, 85].

3.11.3.1.2 Separation of HSCs by several surface-modified membranes

Pluronic, a polyethylene oxide (PEO)–polypropylene oxide (PPO)–PEO triblock copolymer, exhibits amphiphilic properties, and undergoes self-assembly into micelles as well as a lyotropic liquid crystal gel phase due to its hydrophilic PEO and hydrophobic PPO blocks [86–89]. Pluronic F127 can reversibly interconvert at 30 °C from a soluble form at <30 °C to a liquid crystal form at >30 °C in aqueous solution. From these observations, Higuchi *et al.* [20] developed pluronic (PL)-coated (15PL-coated PU and 30PL-coated PU) and pluronic-immobilized PU (PU-PL) foaming membranes for use in temperature-controlled cell separation from blood, based on the fact that pluronic segments are dehydrated at 37 °C and hydrated at 4 °C. Reaction scheme for the preparation of pluronic-immobilized PU foaming membranes is shown in **Figure 13** [20]. Hyaluronic acid (HA)-coated PU foaming (5HA-coated PU) membranes were also prepared for HSC separation in their studies [20], because HA binds to HA-binding proteins and CD44 on the cells [90, 91]. PU-COOH membranes were also evaluated for HSC separation, because the most highly purified $CD34^+$ cells (highest recovery ratio of $CD34^+$ cells divided by recovery ratio of RBCs) were obtained using PU-COOH membranes with $r = 5.2$ μm compared with other surface-modified membranes investigated in their previous study [15, 22]. Unmodified membranes were used as a control in experiments on HSC separation.

The amount of coating on pluronic-coated and HA-coated membranes was obtained by comparing the weight of the membranes before and after coating. The coating amount was estimated to be 5–15 mg cm^{-2} (i.e., 10.5 mg cm^{-2} on 15PL-coated PU, 15.1 mg cm^{-2} on 30PL-coated PU, and 4.9 mg cm^{-2} on 5HA-coated PU) [20]. The surface morphology of unmodified PU was slightly different from that of 30PL-coated PU membranes from SEM observation. Thicker fibrils were observed on 30PL-coated PU membranes compared with those on unmodified PU membranes due to the thick coating of pluronic on the membranes.

Blood permeation through unmodified PU, 15PL-coated PU, 30PL-coated PU, 5HA-coated PU, PU-PL, and PU-COOH membranes was investigated at 37 °C.

Figure 14 shows the permeation ratio of RBCs, platelets, lymphocytes, and $CD34^+$ cells through unmodified and modified PU membranes. RBCs were observed to pass preferentially through all membranes except 5HA-coated PU. The high permeation ratio of RBCs could be explained by the easily deformable character of RBCs due to their lack of nuclei.

Platelets were also able to pass through unmodified PU, pluronic-coated PU, and PU-COOH membranes (permeation ratio >50%). A high permeation ratio of platelets was observed through unmodified and modified PU membranes except for HA-coated, and pluronic-immobilized membranes in the investigation. Pluronic and HA on the membranes may have tended to hinder permeation of platelets through the membranes. Very little permeation (<20% permeation ratio) of lymphocytes and $CD34^+$ cells was observed through unmodified and modified PU membranes. This was thought to be because $CD34^+$ cells and lymphocytes adhere to surfaces more strongly than other blood cells. Forraz *et al.* [92] reported that primitive hematopoietic stem and progenitor cells expressed cell-adhesion molecules (CD162 and CD164) abundantly, causing them to adhere to membrane surfaces. A low permeation ratio through 5HA-coated PU was explained by noting that HA binds

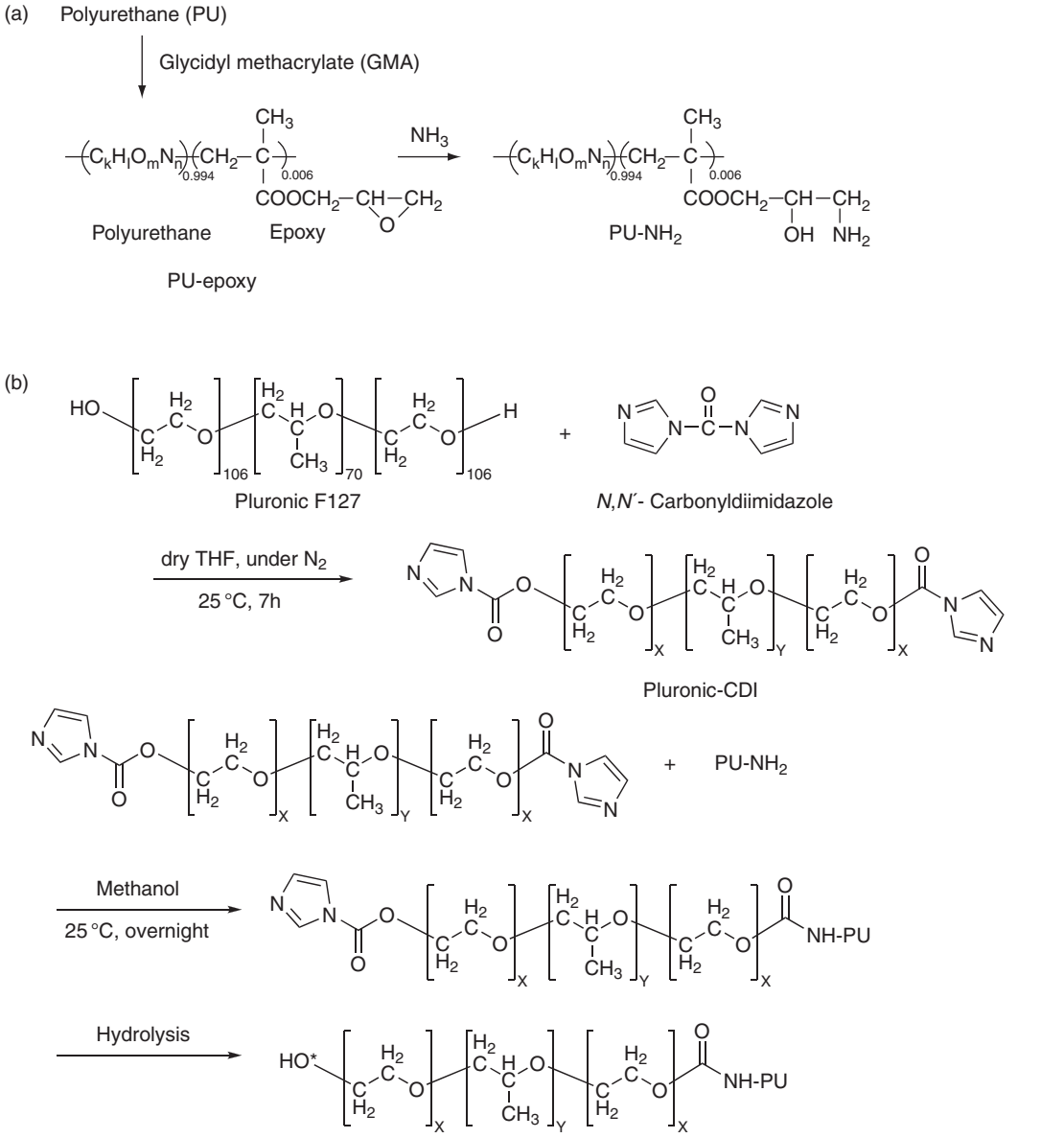

Figure 13 Reaction scheme of PU-NH_2 membranes (a), and CDI-activated pluronic F127 and immobilization of CDI-activated pluronic F127 on the PU-NH_2 membranes (b) [20].

to HA-binding proteins and CD44 on the cells [90, 91]. Most blood cells tended to bind to the surface of 5HA-coated PU membranes.

HSA solution was passed through the unmodified and modified PU membranes as a rinsing solution at 4 °C following permeation of blood at 37 °C. **Figure 15** shows the recovery ratio of RBCs, platelets, lymphocytes, and $CD34^+$ cells through unmodified PU, 15PL-coated PU, 30PL-coated PU, 5HA-coated PU, PU-PL, and PU-COOH membranes [20].

Recovery ratios of RBCs, platelets, and lymphocytes through unmodified and modified PU membranes were found to be <15% in **Figure 15**. The low recovery ratio of RBCs through unmodified and modified PU membranes was attributed to the high permeation ratio of RBCs through all membranes except 5HA-coated membranes, because a few RBCs remained to be bound on the membranes after permeation of blood. The recovery ratios of lymphocytes were low because they adhered strongly to the membranes.

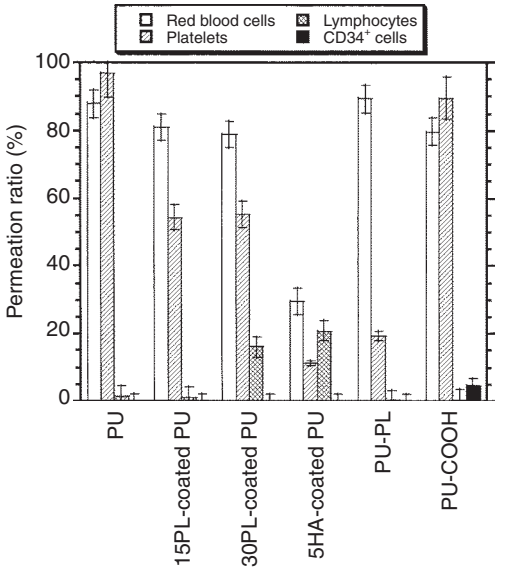

Figure 14 Permeation ratios of RBC, platelets, lymphocytes, and $CD34^+$ cells through unmodified PU, 15PL-coated PU, 30PL-coated PU, 5HA-coated PU, PU-PL, and PU-COOH membranes after permeation of peripheral blood at 37 °C [20].

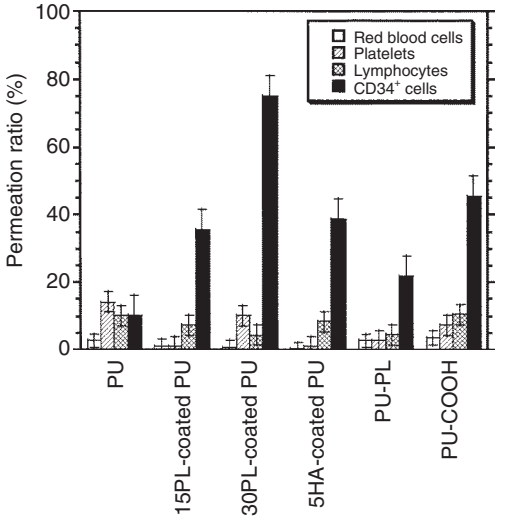

Figure 15 Recovery ratios of RBCs, platelets, lymphocytes, and $CD34^+$ cells through unmodified PU, 15PL-coated PU, 30PL-coated PU, 5HA-coated PU, PU-PL, and PU-COOH membranes after permeation of peripheral blood at 37 °C and 0.5 wt.% of HSA solution subsequently at 4 °C [20].

$CD34^+$ cells passed through the modified membranes when the recovery solution was permeated through the membranes after blood. The recovery ratio of $CD34^+$ cells through pluronic-coated membranes increased with increasing coating amount. This was because of the increase in water solubility of pluronic at low temperatures, as described above. The rather low (42%) recovery ratio of $CD34^+$ cells through 30PL-coated PU membranes when the recovery solution was permeated through the membranes at 37 °C instead of 4 °C supports the explanation. The recovery ratio of $CD34^+$ cells through 30PL-coated PU membranes was higher than that through PU-COOH membranes, the highest among membranes in **Figure 15**.

Several types of surface-modified PU membranes were also prepared by Higuchi *et al.* [19]. PU membranes modified with arginine (PU-Arg) and lysine (PU-Lys) had zwitterionic groups, whereas PU membranes modified with glycine (PU-Gly), asparagine (PU-Asn), and aspartate (PU-Asp) had negatively charged carboxylate groups (**Figure 8**). PU-Gly is PU-COOH membrane [15, 93, 94]. Experiments on the purification of $CD34^+$ cells from peripheral blood were carried out using several types of these surface-modified PU membranes, and the permeation and recovery ratios of $CD34^+$ cells through these membranes are shown in **Figure 16** [19].The recovery ratio of $CD34^+$ cells from membranes with zwitterionic groups (PU-Arg and PU-Lys) was found to be less than for PU-Gly (PU-COOH) membranes. In their previous study [84], it was reported that the recovery ratio of $CD34^+$ cells was less than 20% through membranes modified with positively charged groups on their surfaces.

The presence of the carboxylate groups on the surface-modified PU membranes led to weak electrostatic repulsions between cells and membranes because of the negatively charged surfaces of these cells. The zwitterionic groups on PU-Arg and PU-Lys membranes caused them to have a higher surface potential than PU-COOH membranes, and might therefore have led to the lower recovery ratios of $CD34^+$ cells through the former membranes than through the latter. PU-COOH membranes showed the highest recovery ratio of $CD34^+$ cells, higher than for other negatively charged membranes such as PU-Asp and PU-Asn.

HSCs as well as several other stem and progenitor cells are found in bone marrow [95, 96] and umbilical cord blood [97, 98]. Most current research on the use of stem cells in tissue engineering has focused on the development of tissues and organs from specific stem cells [96, 98]. Safe and simple separation and purification of specific stem or MSCs from bone marrow or umbilical cord blood are essential for this application.

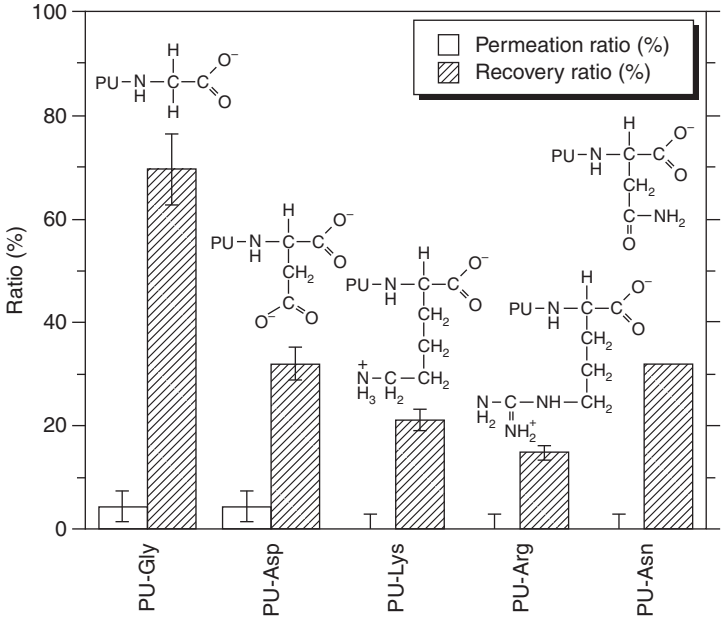

Figure 16 Permeation and recovery ratio of $CD34^+$ cells through surface-modified PU membranes after permeation of peripheral blood [18].

Membrane separation can provide a more sanitary and simple isolation of these cells than FACS, MACS, or other separation methods.

Forraz *et al.* [92] reported that negative-isolated cells, which depleted umbilical cord blood mononuclear cells from blood cells expressing mature hematopoietic markers (glycophorin A, CD2, CD3, CD7, CD16, CD33, CD38, CD45, and CD56), lineage-negative cells, enriched long-term culture-initiating cells. The lineage-negative cells maintained and expanded more primitive hematopoietic stem and progenitor cells than $CD34^+$ and $CD133^+$ cells, and expressed higher levels of the cell-adhesion molecule CD162 (expression ratio (ER) = 16.0%) and CD164 (ER = 96.7%) involved in hematopoietic progenitors forming bone marrow than CD34 (ER = 14.4%) and CD133 (ER = 7.0%) [92]. Therefore, primitive hematopoietic stem and progenitor cells tend to adhere to PU membrane surfaces, due to their expression of these cell-adhesion molecules on their surfaces.

$CD34^+$ cells were efficiently recovered (85% recovery ratio) through PU-COOH membranes in a process using 20 wt.% aqueous dextran as the recovery solution [20]. This indicated that dextran solution was preferable to HSA and bovine serum albumin (BSA) solutions during the recovery process.

3.11.3.2 Separation of MSCs/ Mesenchymal Progenitor Cells

MSCs and mesenchymal progenitor cells (MPCs) have the potential to differentiate into bone, cartilage, or fat [99, 100]. Thus, MSCs and MPCs are thought to be promising materials for regenerative medicine and gene therapies. MSCs have already been used in the clinical application to repair or regenerate somatic tissues, such as bone defects [101] and infarcted heart [102, 103]. Furthermore, several researchers suggested that MSCs might be used to regenerate other cells or tissues, such as neurons [104], retina [105], β-cell [106], and hepatocytes [99, 107]. Gene transfer into MSCs mediated by retrovirus [108], adenovirus [109], or lentivirus vectors [110] has also been investigated. Human MSCs can be obtained from various tissues, such as bone marrow [100, 111], adipose tissue [112], placenta [113, 114], amniotic fluid [115], umbilical cord blood [116, 117], etc. MSCs and MPCs are generally isolated by repeated passage of adherent cells derived from a particular tissue of interest, followed by analysis of the ability of such cells to differentiate into mesenchymal lineages [99].

Purification and isolation of specific mesenchymal stem or progenitor cells will be necessary to obtain bone-marrow stromal cells for use in clinical applications in future. For example, it is necessary to

generate cardiomyocytic progenitors from marrow stroma for the treatment of heart failure by cell transplantation into damaged myocardia. Thus, a method is needed for the separation and isolation of specific mesenchymal cells from bone-marrow stromal cells. Cell separation can be accomplished by centrifugation [1, 118], FACS [9], magnetic cell selection [6–9], affinity chromatography [10, 11], or membrane filtration [12, 13, 15] as discussed in Section 3.11.1. Of these methods, membrane filtration method is a good candidate for the purification of mesenchymal cells because it is simple and inexpensive and because it is easy to maintain sterility during the filtration process. In fact, it is already discussed in the previous section that HSCs could be purified by filtration through chemically modified 5-μm-pore PU membranes.

In this section, we introduce one of the examples in the separation between mesenchymal stem and progenitor cells, that is, two types of marrow stromal cells – osteoblast cell line (KUSA-A1) and preadipocyte cell line (H-1/A) [17].

3.11.3.2.1 Flow-cytometric analysis of mesenchymal cells

KUSA-A1 osteoblasts and H-1/A preadipocytes, two mesenchymal cell lines, were incubated with fluorescent probes (Cell Tracker Orange™ and Cell Tracker Green™, respectively) to allow their independent detection before and after permeation through porous polymeric membranes. The numbers of KUSA-A1 and H-1/A cells in the mixed cell solution were determined from flow-cytometric scattergrams at 575 nm for KUSA-A1 cells and 525 nm for H-1/A cells. These values are close to those of phycoerythrin (PE) and fluorescein isothiocyanate (FITC), which are used for conventional cell counting of specific cells [17]. **Figure 17(a)** shows the flow-cytometric scattergrams for the KUSA-A1 (osteoblasts) and H-1/A (preadipocytes) cells. The fluorescence intensities at 525 and 575 nm for the two cell types were significantly different. The forward and side light scattering intensities, shown in **Figure 17(b)**, indicate that both cell types have a broad size distribution, although KUSA-A1 cells are mostly smaller than H-1/A cells. Furthermore, the flow-cytometric scattergrams of KUSA-A1 cells and H-1/A cells (forward light scattering intensity vs. side light scattering intensity and fluorescence intensity at 525 vs. 575 nm) were found to be identical in single- and mixed-cell solutions (data not shown). Thus, cell aggregates did not appear to be formed when KUSA-A1 cells and H-1/A cells were mixed together in a culture medium [17].

3.11.3.2.2 Cell separation through PU membranes

The differences in the cell sizes and shapes suggested that KUSA-A1 and H-1/A cells can be separated by using porous polymeric membranes. This possibility was examined with the use of a variety of membrane types. **Figure 18** shows an SEM image of the surface of the porous polymeric membranes tested in this study. A regular screen pore morphology was found on the surface of nylon-net filters (**Figure 18(b)**) and silk screens (**Figures 18(e)** and **18(f)**), whereas a specific pore morphology was not found on the surface of nonwoven fabrics (**Figures 18(c)** and **18(d)**). Furthermore, a deformed open pore structure was found on the surface of the PU membranes (**Figure 18(a)**) [17].

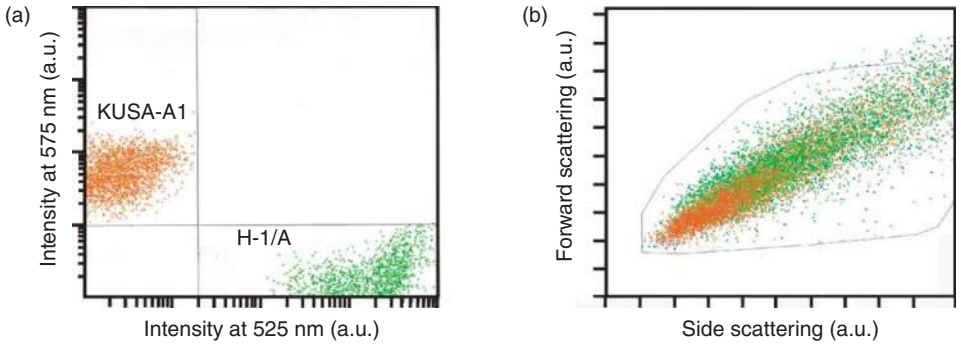

Figure 17 Flow-cytometric scattergrams of mixed solution of KUSA-A1 cells (orange dots) and H-1/A cells (green dots), each having a cell density of 50 000 cells ml^{-1} in the fluorescent intensity at 575 nm and 525 nm (a) and in the light intensity of forward scattering and side scattering (b). (Color figure can be viewed in the online issue of Reference 17.)

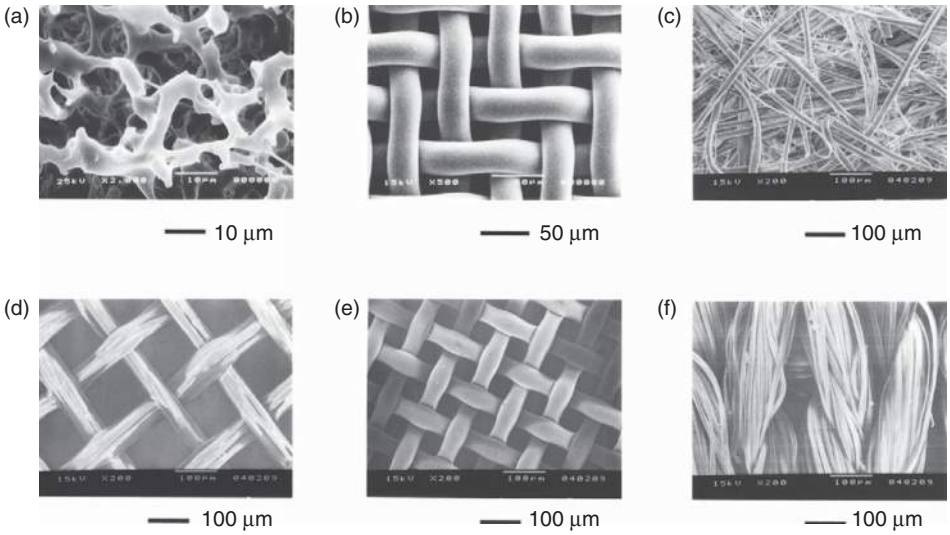

Figure 18 Scanning electron micrographs of the membrane surfaces of (a) unmodified polyurethane (PU) membranes, (b) nylon-net filter, (c) nonwoven fabrics made of acrylonitrile, (d) nylon + polyester, (e) silk screens made of silk (mesh size 150), and (f) silk screens made of Tetron™ (mesh size 250) [17].

The permeation of cells through PU and surface-modified PU membranes was investigated first, because a previous study showed that HSCs can be recovered from peripheral blood with the use of surface-modified PU (PU-COOH) membranes [15]. The permeation of KUSA-A1 cells, H-1/A cells, and a mixture of the two cell types through PU and surface-modified PU membranes (pore size = 12 μm) at 25 °C were examined. **Table 3** shows the permeation ratio through the membranes with a suspension of a single-cell type (50 000 cells ml^{-1}) used as the feed solution. The table also shows the results obtained when the feed solution was a mixture of the two cell types. A relatively low (<5%) permeation ratio through PU and surface-modified PU membranes was found with either a single-cell solution or a mixed-cell solution. Because open pore volume of the membrane interior in PU and surface-modified PU membranes is calculated as 0.506 ml (i.e., $1.25 \times 1.25 \times 3.14 \times 0.12 \times 0.86$ cm) and the total cell volume permeated through the membranes is approximately calculated as 3.375×10^{-4} ml in a mixed-cell solution (i.e., 6 ml × 50 000 cells $ml^{-1} \times 2 \times (7.5 \times 10^{-4} \times 7.5 \times 10^{-4} \times 7.5 \times 10^{-4} \times 4/3$ cm)) in this study, the low permeation ratio is not due to the overloading of the cells permeated through the membranes. The low permeation ratio through PU and surface-modified PU membranes is due to the high degree of cell adhesion on the membranes and a complicated pore structure of the membranes [17].

Table 3 Permeation ratio (*P*) and recovery ratio (*R*) of KUSA-A1 cells and H-1/A cells through PU, PU-SO_3H, and PU-COOH membranes after permeation of single-cell solution and mixed-cell solution at the cell density of 50 000 cells ml^{-1} and 25 °C [17]

Membrane	*P(KUSA-A1) (%)*	*P(H-1/A) (%)*	*R(KUSA-A1) (%)*	*R(H-1/A) (%)*
Single-cell permeation				
PU	4.25	1.6	6.1	8.0
PU-SO_3H	1.4	0.5	5.9	7.1
PU-COOH	0.1	0.1	4.5	4.6
Mixed-cell permeation				
PU	1.2	0.15	2.0	1.9
PU-SO_3H	0	0.1	3.5	3.4
PU-COOH	0	0	5.9	6.8

Data from Higuchi, A., Shindo, Y., Gomei, Y., Mori, T., Uyama, T., Umezawa, A. *J. Biomater. Sci. Polym. Ed. Part B – Appl. Biomater*. **2005**, *74*, 511–519.

The permeation ratio of both KUSA-A1 and H-1/A cells through PU membranes was found to be higher than that through PU-SO_3H and PU-COOH membranes. The surface modification of PU-SO_3H and PU-COOH membranes may cause the decreased pore size of the surface-modified membranes compared to the unmodified PU membranes. The permeation ratio, when the feed solution contained a single-cell type, was found to be higher than the permeation ratio when it was a mixed-cell solution through PU and surface-modified PU membranes. Although flow-cytometric analysis suggested that coagulation or interaction does not occur between KUSA-A1 and H-1/A cells (data not shown), some coagulation or interaction between KUSA-A1 and H-1/A cells that was not detected from flow-cytometric analysis might lead to a decrease of the permeation ratio in the mixed-cell solution compared to the permeation ratio in the single-cell solution. It was also found that the permeation ratio for KUSA-A1 cells was higher than for H-1/A cells, which is consistent with the relatively smaller size of KUSA-A1 cells, as shown in **Figure 17(b)** [17].

There was extensive adhesion of the KUSA-A1 and H-1/A cells to the membrane surface from an SEM image of the PU membrane surface after the permeation of KUSA-A1 or H-1/A cells. The high adhesiveness of the cells may explain their low permeation ratios through the PU membranes [17].

Next, the effect of passing an HSA solution through the membranes following permeation of the single-cell or mixed-cell solutions was examined. **Table 3** shows that the recovery ratio of KUSA-A1 and H-1/A cells following this treatment was higher than the permeation ratio. However, the recovery ratio was still below 10% through any of the PU membranes. Slightly higher recovery ratio through the PU and PU-SO_3H membranes in a mixed feed solution was found when compared to that in a single-cell type. On the other hand, no significant difference in the recovery ratio was found between feed solutions containing a single-cell type or a mixture of cell types through PU-COOH membranes [17].

Next, the flow-cytometric analysis of the permeate solution of KUSA-A1 and H-1/A cells and also that of the recovery solution following filtration through PU membranes were examined. **Figure 19(a)** shows the forward versus side light scattering intensity in the permeate solution after permeation of the cells through PU membranes. Both smaller sized KUSA-A1 and H-1/A cells passed through the PU membranes. Therefore, KUSA-A1 cells have a higher permeation ratio than H-1/A cells, because KUSA-A1 cells are typically smaller than H-1/A cells (see **Figure 17**) [17].

Figure 19(b) shows the results of recovery solution following subsequent permeation of HSA solution. The pattern of the scattergram in the recovery solution (**Figure 19(b)**) was identical to that of the feed solution (**Figure 17(b)**), even though the numbers of both KUSA-A1 cells and H-1/A cells were significantly lower in the recovery solution. Thus, there is no significant separation of KUSA-A1 and H-1/A cells in the recovery solution following permeation with HSA solution [17].

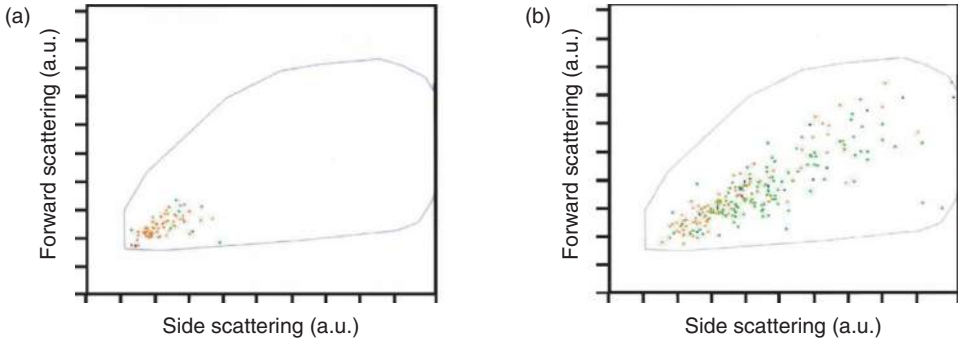

Figure 19 Flow-cytometric scattergrams of KUSA-A1 cells (orange dots) and H-1/A cells (green dots) in the relationship between forward light scattering intensity and side light scattering intensity in the permeate solution after permeation of mixed cells of KUSA-A1 cells (orange dots) and H-1/A cells (green dots) through the PU membranes at (a) the cell density of each 50 000 cells ml^{-1} and (b) following subsequent permeation of HSA solution. (Color figure can be viewed in the online issue of Reference 17.)

3.11.3.2.3 Cell separation through various porous membranes

The separation of KUSA-A1 and H-1/A cells by several porous membranes, including uncoated nylon-net filters, fibronectin- or collagen-coated nylon-net filters, nonwoven fabrics made of acrylonitrile or a combination of nylon and polyester, silk screen No. 150 made of silk or Tetron™, and silk screen No. 250 made of Tetron™, were also examined [17]. **Table 4** summarizes the permeation ratio through these membranes with the use of a feed solution containing a mixture of KUSA-A1 and H-1/A cells. With the use of the nylon-net filter and fibronectin-coated nylon-net filter, the permeation ratio for KUSA-A1 cells was higher than for H-1/A cells. This is mainly due to the smaller cell size of the KUSA-A1 cells as detected in the forward and side light scattering intensities shown in (**Figure 17(b)**). In addition, a high cell permeation ratio was also found with the use of silk screens made of silk or Tetron™. This was because silk screens have a larger pore size than the nylon-net filter and PU membranes (see **Figure 18**). A relatively good separation factor for permeation (α_P), defined as the relative permeation ratio of KUSA-A1 cells divided by that of H-1/A cells, was obtained when the mixed-cell solution was passed through the nylon-net filter ($\alpha_P = 1.8$) or fibronectin-coated nylon-net filter ($\alpha_P = 1.5$) membranes, whereas a separation was not obtained when the nonwoven fabrics or silk screens were used. Overall, the results suggest that the pore size of nylon-net filter was optimal for producing a sieving effect [17].

The effect of passing the HSA solution through the porous polymeric membranes after permeation of the cell mixture was also assessed. As summarized in **Table 4**, the recovery ratio of both KUSA-A1 and H-1/A cells was relatively low (<20%) for all of the membranes. This is caused by the high adhesiveness of the mesenchymal cells and their high permeation ratio. Analysis of the recovery solution shows that there was no effective separation of KUSA-A1 and H-1/A cells. This is probably due to the fact that the KUSA-A1 and H-1/A cells are both mesenchymal cells and have similar characteristics (i.e., adhesiveness) [17].

The above results show that a separation of cells with similar characteristics, such as different types of MPCs (i.e., osteoblasts and preadipocytes), can be obtained in the permeate solution, but not in the recovery solution following membrane filtration. The main factor in this separation is the sieving effect of cells through the porous membranes. Therefore, prior to separation, flow cytometry should be carried out to confirm that the cells to be separated have different sizes. Separation factor ($\alpha_P = 1.8$) and a high permeation ratio were achieved when a mixed-cell solution was passed through a nylon-net filter with an 11-μm pore size, whereas an extremely low permeation ratio (<5%) of both cell types was found with the use of surface-modified or unmodified PU foaming membranes with a 12-μm pore size. It was also found that the nylon-net filter had screen-like pore structure, whereas the PU membranes had a deformed open pore structure. This indicates that not only the pore

Table 4 Permeation ratio (*P*) and recovery ratio (*R*) of KUSA-A1 cells and H-1/A cells through PU, nylon-net filter [nylon (a)], nylon-net filter coated with fibronectin [nylon (b)] and collagen [nylon (c)], nonwoven fabrics made of acrylonitrile [nonwoven (a)], nylon and polyester [nonwoven (b)], and silk screens made of silk [silk screen (a), mesh size 150] and Tetron™ [silk screen (b), mesh size 150 and silk screen (c), mesh size 250] after permeation of mixed-cell solution at the cell density of 50 000 cells ml^{-1} and 25 °C [17]

Membrane	*P(KUSA-A1) (%)*	*P(H-1/A) (%)*	*R(KUSA-A1) (%)*	*R(H-1/A) (%)*
PU	1.2	0.15	2.5	1.0
Nylon (a)	57.0	32.0	15.0	17.5
Nylon (b)	77.0	53.0	9.5	6.5
Nylon (c)	38.5	37.0	7.0	6.5
Nonwoven (a)	47.0	42.0	15.0	14.0
Nonwoven (b)	49.0	45.0	17.0	16.0
Silk screen (a)	99.0	99.5	3.0	3.5
Silk screen (b)	99.0	99.5	2.0	1.5
Silk screen (c)	98.0	97.0	3.0	2.5

Data from Higuchi, A., Shindo, Y., Gomei, Y., Mori, T., Uyama, T., Umezawa, A. *J. Biomater. Sci. Polym. Ed. Part B – Appl. Biomater.* **2005**, *74*, 511–519.

size but also the pore morphology are important for membrane-based cell separation [17].

3.11.4 Concluding Remarks

We discussed the recent development of blood-cell separation and stem-cell separation by membrane filtration method through surface-modified membranes from different cell sources such as blood and tissue cell samples. The exact surface marker for primitive hematopoietic stem and progenitor cells remains unclear currently. Isolating such cells by membrane filtration of umbilical cord or bone marrow is thought to be more effective than magnetic bead or flow-cytometry sorting methods, because cell separation in membrane filtration is based not only on cell size, but also on the intensity of cell adhesion to the membrane surface. Of all the methods, membrane separation is likely to provide the most sanitary and simple isolation of stem and progenitor cells [20].

Even a small degree of enrichment, such as the separation factor of 1.8, is also considered effective in the transplantation of mesenchymal cells in clinical applications although clinical trials using the enriched-cell type of mesenchymal cells have not yet been performed. In conclusion, cell separation between MPCs through porous polymeric membranes was shown to be possible. This technology will contribute to the future clinical application of cell transplantation into the damaged tissue of patients.

One of the drawbacks of separation of stem cells by the membrane filtration method is the relatively low selectivity compared to FACS and MACS methods using specific antibodies. The development of surface-modified membranes immobilized nanosegments having specific interaction between nanosegments and stem cells (e.g., CS-1 oligopeptides for HSCs, N-cadherin for MSCs, E-cadherin for ES cells, and CD133 for cancer stem cells) might be necessary in future.

References

[1] Edwards, M., Twin, J., Wilkinson, S. *ANZ J. Surg.* **2002**, *72*, 655–659.
[2] Aoki, M., Yasutake, M., Murohara, T. *Stem Cells* **2004**, *22*, 994–1002.
[3] Asahara, T., Murohara, T., Sullivan, A., *et al. Science* **1997**, *275*, 965–967.
[4] Juan, G., Hernando, E., Cordon-Cardo, C. *Cytometry* **2002**, *49*, 170–175.
[5] Gryn, J., Shadduck, R. K., Lister, J., Zeigler, Z. R., Raymond, J. M. *J. Hematother. Stem Cell Res.* **2002**, *11*, 719–730.
[6] Carreras, E., Saiz, A., Marin, P., *et al. Haematologica* **2003**, *88*, 306–314.
[7] Domingo, J. C., Mercadal, M., Petriz, J., De Madariaga, M. A. *J. Microencapsul.* **2001**, *18*, 41–54.
[8] Comella, K., Nakamura, M., Melnik, K., *et al. J. Cytometry* **2001**, *45*, 285–293.
[9] Kikuchi, A., Karasawa, M., Tsuruta, T., Kataoka, K. *J. Colloid Interface Sci.* **1993**, *158*, 10–18.
[10] Kataoka, K., Sakurai, Y., Hanai, T., Maruyama, A., Tsuruta, T. *Biomaterials* **1988**, *9*, 218–224.
[11] Ohba, H., Bakalova, R., Moriwaki, S., Nakamura, O. *Cancer Lett.* **2002**, *184*, 207–214.
[12] Komai, H., Naito, Y., Fujiwara, K., Takagaki, Y., Noguchi, Y., Nishimura, Y. *Perfusion* **1998**, *13*, 27–34.
[13] Muller-Steinhardt, M., Hennig, H., Kirchner, H., Schlenke, P. *Transfusion* **2002**, *42*, 153–158.
[14] Yasutake, M., Sumita, M., Terashima, S., Tokushima, Y., Nitadori, Y., Takahashi, T. A. *Vox Sang.* **2001**, *80*, 101–105.
[15] Higuchi, A., Yamamiya, S., Yoon, B. O., Sakurai, N., Hara, M. *J. Biomed. Mater. Res.* **2004**, *68A*(1), 34–42.
[16] Higuchi, A., Tsukamoto, Y. *J. Biomed. Mater. Res.* **2004**, *71A*(3), 470–479.
[17] Higuchi, A., Shindo, Y., Gomei, Y., Mori, T., Uyama, T., Umezawa, A. *J. Biomater. Sci. Polym. Ed. Part B – Appl. Biomater.* **2005**, *74*, 511–519.
[18] Higuchi, A., Yang, S.-T., Li, P.-T., *et al. J. Appl. Polym. Sci.* **2009**, *114*, 671–679.
[19] Higuchi, A., Yang, S.-T., Li, P.-T., *et al. J. Membr. Sci.* **2009**, *339*, 184–188.
[20] Higuchi, A., Sekiya, M., Gomei, Y., *et al. J. Biomed. Mater. Res. Part A* **2008**, *85A*, 853–861.
[21] Natori, S. H., Gomei, Y., Higuchi, A. *J. Biomed. Mater. Res. Part B – Appl. Biomater.* **2006**, *78B*, 318–326.
[22] Higuchi, A., Iizuka, A., Gomei, Y., *et al. J. Biomed. Mater. Res.* **2006**, *78A*, 491–499.
[23] Kim, E. J., Yeo, G. D., Pai, C. M., Kang, I.-K. *J. Biomed. Mater. Res.* **2009**, *90B*, 849–856.
[24] Brittingham, T. E., Chapli, H. *J. Am. Med, Assoc.* **1957**, *165*, 819–825.
[25] Payne, R. *Vox Sang.* **1957**, *2*, 233–241.
[26] Brozovic, B. *The Role of Leukocyte Depletion in Blood Transfusion Practice*; Blackwell Scientific Publications: Oxford, 1987.
[27] Levine, A., Liebman, H. The Acquired Immunodeficiency Syndrome (AIDS). In *Williams' Hematology*; Beutler, E., Lichtman, M., Coller, B., Kipps, T., Eds.; McGraw-Hill: New York, 1995; pp 975–997.
[28] Hjelle, B. Transfusion-Transmitted HTLV-I and HTLV-II. In *Principles of Transfusion Medicine,* 2nd edn.; Rossi, E. C., Simon, T., Moss, G., Gould, S., Eds.; Williams and Wilkins: Baltimore, MD, 1996; pp 709–716.
[29] Gulter, K., Luban, N. Transfusion-Transmitted Cytomegalovirus and EBV Disease. In *Principles of Transfusion Medicine,* 2nd edn.; Rossi, E. C., Simon, T., Moss, G., Gould, S., Eds.; Williams and Wilkins: Baltimore, MD, 1996; pp 717–732.
[30] Pollock, J., Presti, R., Paetzold, S., Virgin, H. *Virology* **1997**, *227*, 168–179.
[31] Kondo, K., Xu, J., Macarski, E. *Proc. Natl. Acad. Sci. U.S.A.* **1996**, *93*, 11137–11142.
[32] Klein, M., Frigg, R., Flechsig, E., *et al. Nature* **1997**, *390*, 687–690.
[33] Diepenhorst, P., Spokholt, R., Prins, H. K. *Vox Sang.* **1972**, *23*, 308–320.

[34] Gwak, M. S., Lee, K. W., Kim, S. Y., *et al. Liver Transpl.* **2005**, *11*, 331–335.
[35] Cardo, L. J., Salata, J., Harman, R., Mendez, J., Weina, P. J. *Transfusion* **2006**, *46*, 896–902.
[36] Vries, A. J. de., Vermeijden, W. J., Gu, Y. J., Hagenaars, J. A., van Oeveren, W. *Artif. Organs* **2006**, *30*, 452–457.
[37] Zanardo, G., Michielon, P., Paccagnella, A., *et al. J. Thorac. Cardiovasc. Surg.* **1994**, *107*, 1489–1495.
[38] Moody, D. M., Brown, W. R., Challa, V. R., Stump, D. A., Reboussin, D. M., Legault, C. *Ann. Thorac. Surg.* **1995**, *59*, 1304–1307.
[39] Tonz, M., Mihaljevic, T., von Segesser, L. K., Fehr, J., Schmid, E. R., Turina, M. I. *Chest* **1995**, *108*, 1551–1556.
[40] Gu, Y. J., de Vries, A. J., Boonstra, P. W., van Oeveren, W. J. *Thorac. Cardiovasc. Surg.* **1996**, *112*, 494–500.
[41] Tang, A. T. M., Alexiou, C., Hsu, J., Sheppard, S. V., Haw, M. P., Ohri, S. K. *Ann. Thorac. Surg.* **2002**, *74*, 372–377.
[42] Kaza, A. K., Cope, J. T., Fiser, S. M., *et al. Ann. Thorac. Surg.* **2003**, *75*, 555–559.
[43] de Vries, A. J., Gu, Y. J., Douglas, Y. L., Post, W. J., Lip, H., van Oeveren, W. *Eur. J. Cardiothorac. Surg.* **2004**, *25*, 261–266.
[44] Ramirez, G., Romero, A., Garcia-Vallejo, J. J., Munoz, M. *Transfusion* **2002**, *42*, 66–75.
[45] Smit, J. J., de Vries, A. J., Gu, Y. J., van Oeveren, W. *J. Lab. Clin. Med.* **2000**, *135*, 238–246.
[46] Pietersz, R. N., Steneker, I., Reesink, H. W. *Transfus. Med. Rev.* **1993**, *7*, 17–24.
[47] Shirokaze, J. *Therap. Apher.* **2002**, *6*, 261–266.
[48] Umegae, M., Nishimura, T., Kuroda, T., Kato, H. *Jpn. J. Artif. Organs* **1988**, *17*, 413–416.
[49] Nishimura, T., Mizoguchi, Y. Filter Medium for Selectively Removing Leukocytes. US Pat. 49,36,998, 1990.
[50] Pall, D. B., Gsell, T. C. Device and Method for Separating Leukocytes from Platelet Concentrate. US Pat. 48,80,548, 1989.
[51] Hiraide, T. *Sen-I Gakkai.* **1993**, *49*, 417–421.
[52] Ikada, Y. *Biomaterials* **1994**, *15*, 725–736.
[53] Paunovic, D., van der Meer, P., Kjeldsen-Kragh, J., *et al. Transfusion* **2004**, *44*, 1197–1203.
[54] Larsson, S., Gulliksson, H., Paunovic, D. *Transfusion* **2001**, *41*, 534–539.
[55] Natori, S. H., Kurita, K. *Polym. Adv. Technol.* **2007**, *18*, 263–267.
[56] Natori, S. H., Kurita, K. *J. Biomed. Mater. Res. Part B* **2007**, *81B*, 419–426.
[57] Tsuda, H., Yokoyama, M., Sato, M., Yamagata, J., Hashimoto, H., Hirose, S. *Jpn. J. Artif. Organs* **1986**, *15*, 1637–1640.
[58] Matsuda, T., Isumihara, T., Gotanda, M., Niimura, T. *Ther. Plasmapher.* **1987**, *7*, 73–78.
[59] Hashimoto, H. *Med. Immunol.* **1985**, *10*, 61–68.
[60] Kawasaki, Y., Suzuki, J., Suzuki, S., Suzuki, H. *J. Pediatr. Gastroenterol. Nutr.* **2004**, *39*, 422–425.
[61] Jewell, D. P., Snook, J. A. Immunology of Ulcerative Colitis and Crohn's Disease. In *Inflammatory Bowel Disease*; Allan, R. N., Keighley, M. R., Alexander-Williams, J., Hawkins, C., Eds.; Churchill Livingstone: London, 1990; pp 127–146.
[62] Sawada, K., Ohnishi, K., Fukui, S., *et al. J. Gastroenterol.* **1995**, *30*, 322–329.
[63] Sawada, K., Ohnishi, K., Kosaka, T., *et al. Therap. Apher. Dial.* **1997**, *1*, 207–211.
[64] Sunny, D. *Transfus. Med. Rev.* **1993**, *12*, 65–77.
[65] Sunny, D. Mechanism of Leukocyte Removal by Filtration. In *Leukocyte-Depleted Blood Products*; Lane, T. A., Myllyla, G., Eds.; Current Studies in Hematology and Blood Transfusion; Karger: Basel, 1994; Vol. 60, pp 123–133.
[66] Sugi, K. *BIO Clinica* **1997**, *12*, 339–342.
[67] Ueki, Y., Yamasaki, S., Kanamoto, Y., *et al. Rheumatology* **2000**, *39*, 165–171.
[68] Shimoyama, T., Sawada, K. Prospective Multicenter Randomized Trial for Treatment of Ulcerative Colitis by Leukocytapheresis with Leukocyte Removal Filter. In *Annual Report of the Research Committee of Inflammatory Bowel Disease*; Ministry of Health and Welfare of Japan: Tokyo, 1998; pp 126–129.
[69] Hidaka, T., Suzuki, K., Matsuki, Y., *et al. Arthritis Rheum.* **1999**, *42*, 431–437.
[70] Sawada, K., Ohnishi, K., Kosaka, T., *et al. Internal Med.* **1996**, *77*, 287–292.
[71] Noguchi, M., Hiwatashi, N., Hayakawa, T., Toyota, T. *Ther. Apher.* **1998**, *2*, 109–114.
[72] Sugimura, K., Suzuki, K., Hasegawa, K., *et al. Influence to Active Oxygen Productivity of Granulocyte by Activated Platelet of Ulcerative Colitis Patient. In Annual Report of the Research Committee of Inflammatory Bowel Disease*; Tokyo: Ministry of Health and Welfare of Japan, 1999; pp 93–97.
[73] Takahashi, K., Yamanaka, S. *Cell* **2006**, *126*, 663–676.
[74] Okita, K., Ichisaka, T., Yamanaka, S. *Nature* **2007**, *448* (7151), 313–317.
[75] Takahashi, K., Tanabe, K., Ohnuki, M., *et al. Cell* **2007**, *131*, 861–872.
[76] Hohno, Y., Takagami, Y. Basics of Transplantation of $CD34^+$ Cells: Purification Methods. In *New Trends in Hematopoietic Stem Cell Transplantation*; Harada, M., Katoh, S., Sanada, Y., Eds.; Nanoudo: Tokyo, 1998; pp 151–160.
[77] Cancelas, J. A., Querol, S., Canals, C., *et al. J. Hematother.* **1995**, *4*, 531–538.
[78] Preti, R. A., Lazarus, H. M., Winter, J., *et al. Cytotherapy* **2001**, *3*, 85–95.
[79] Tsuruta, T. *Adv. Polym. Sci.* **1996**, *126*, 1–51.
[80] Maruyama, A., Tsuruta, T., Kataoka, K., Sakurai, Y. *J. Biomed. Mater. Res.* **1998**, *22*, 555–571.
[81] Kataoka, K., Okano, T., Sakurai, Y., *et al. Makromol. Chem. Rapid Commun.* **1982**, *3*, 275–279.
[82] Nabeshima, Y., Tsuruta, T., Kataoka, K., Sakurai, Y. *J. Biomater. Sci. Polym. Ed* **1989**, *1*, 85–98.
[83] Sanada, Y. Transplantation of Hematopoietic Cells: General Theory. In *New Trends in Hematopoietic Stem Cell Transplantation*; Harada, M., Katoh, S., Sanada, Y., Eds.; Nanoudo: Tokyo, 1998; pp 1–7.
[84] Yamaguchi, M., Sawada, K., Sato, N., Koizumi, K., Sekiguchi, S., Koike, T. *Bone Marrow Transplant.* **1997**, *19*, 373–379.
[85] Koizumi, K., Nishio, M., Endo, T., *et al. Bone Marrow Transplant.* **2000**, *26*, 787–793.
[86] Higuchi, A., Aoki, N., Yamamoto, T., *et al. J. Biomed. Mater. Res. Part A* **2006**, *79A*, 380–392.
[87] Wanka, G., Hoffmann, H., Ulbricht, W. *Macromolecules* **1994**, *27*, 4145–4159.
[88] Shishido, S. M., Seabra, A. B., Loh, W., Ganzarolli de Oliveira, M. *Biomaterials* **2003**, *24*, 3543–3553.
[89] Higuchi, A., Aoki, N., Yamamoto, T., *et al. Biomacromolecules* **2006**, *7*, 1083–1089.
[90] Amemiya, K., Nakatani, T., Saito, A., Suzuki, A., Munakata, H. *Biochim. Biophys. Acta* **2005**, *1724*, 94–99.
[91] Zhu, H., Mitsuhashi, N., Klein, A., *et al. Stem Cells* **2006**, *24*, 928–935.
[92] Forraz, N., Pettengell, R., McGuckin, C. P. *Stem Cells* **2004**, *22*, 100–108.
[93] Ahmed, N., Vogel, B., Rohde, E., *et al. Int. J. Mol. Med.* **2006**, *18*, 233–240.

[94] Lara, O., Tong, X., Zborowski, D. M., Farag, S. S., Chalmers, J. J. *Biotechnol. Bioeng.* **2006**, *94*, 66–80.
[95] Fuchs, E., Segre, J. A. *Cell* **2000**, *100*, 143–155.
[96] Kohyama, J., Abe, H., Shimazaki, T., *et al. Differentiation* **2001**, *68*, 235–244.
[97] Rogers, I., Casper, R. F. *Hum. Reprod. Update* **2003**, *9*, 25–33.
[98] Kakinuma, S., Tanaka, Y., Chinzei, R., *et al. Stem Cells* **2003**, *21*, 217–227.
[99] Sudo, K., Kanno, M., Miharada, K., *et al. Stem Cells* **2007**, *25*, 1610–1617.
[100] Pittenger, M. F., Mackay, A. M., Beck, S. C., *et al. Science* **1999**, *284*, 143–147.
[101] Horwitz, E. M., Gordon, P. L., Koo, W. K. K., *et al. Proc. Natl. Acad. Sci. U.S.A.* **2002**, *99*, 8932–8937.
[102] Perin, E. C., Dohmann, H. F., Borojevic, R., *et al. Circulation* **2003**, *107*, 2294–2302.
[103] Strauer, B. E., Brehm, M., Zeus, T., *et al. Circulation* **2002**, *106*, 1913–1918.
[104] Sugaya, K. *Int. Rev. Cytol.* **2003**, *228*, 1–30.
[105] Zhang, J., Shan, Q., Ma, P., Jiang, Y., Chen, P., Wen, J, *Sci. China Ser. C Life Sci.* **2004**, *47*, 241–250.
[106] Chang, C. F., Hsu, K. H., Chiou, S. H., Ho, L. L. T., Fu, Y. S., Hung, S. C. *J. Biomed. Mater. Res. Part A* **2008**, *86A*, 1097–1105.
[107] Chapel, A., Bertho, J. M., Bensidhoum, M., *et al. J. Gene Med.* **2003**, *5*, 1028–1038.
[108] Vanderbyl, S., MacDonald, G. N., Sidhu, S., *et al. Stem Cell* **2004**, *22*, 324–333.
[109] Tsuda, H., Wada, T., Ito, Y., *et al. Mol. Ther.* **2003**, *7*, 354–365.
[110] Zhang, X. Y., La Russa, V. F., Reiser, J. *J. Virol.* **2004**, *78*, 1219–1229.
[111] Colter, D. C., Sekiya, I., Prockop, D. J. *Proc. Natl. Acad. Sci. U.S.A.* **2001**, *98*, 7841–7845.
[112] Zuk, P. A., Zhu, M., Ashjian, P., *et al. Mol. Biol. Cell* **2002**, *13*, 4279–4295.
[113] Chen, L., He, D. M., Zhang, Y. *Cell. Mol. Biol. Lett.* **2009**, *14*, 528–536.
[114] Barlow, S., Brooke, G., Chatterjee, K., *et al. Stem Cells Develop*. **2008**, *17*, 1095–1107.
[115] Pan, H. C., Chin, C. S., Yang, D. Y., *et al. Neurochem. Res.* **2009**, *34*, 1304–1316.
[116] Hou, L., Cao, H., Wang, D., *et al. Int. J. Hematol.* **2003**, *78*, 256–261.
[117] Lee, M. W., Yang, M. S., Park, J. S., Kim, H. C., Kim, Y. J., Choi, J. *Int. J. Hematol*. **2005**, *81*, 126–130.
[118] Vij, R., Brown, R., Shenoy, S., *et al. Bone Marrow Transplant.* **2000**, *25*, 1223–1228.

Biographical Sketch

Akon Higuchi is a chair professor in the Department of Chemical and Materials Engineering, National Central University. He is also a researcher in the Department of Reproduction, National Research Institute for Child Health and Development, Tokyo, Japan. He is a consultant for two venture companies in Japan. He was born in Tokyo and obtained his BSc, MSc, and PhD degrees from the Tokyo Institute of Technology. He was a professor at Seikei University during 1993–2007. He chaired and organized several sessions in international meetings such as Pacifichem, Annual North American Membrane Society Meeting (NAMS), Annual Meeting of American Chemical Society (ACS), and International Congress on Membranes and Membrane Processes (ICOM). His research topics include biomedical engineering using polymeric membranes, stem cell culture on materials having nanosegments, stem cell purification through membranes, and DNA engineering. He is a member of the editorial boards of several journals. His favorite sports are skiing and jogging.